

R. Landolfo
R. Zandonini
editors



This book collects the main outcomes of the research activity carried out within the line "Steel and Steel-Concrete Composite Structures" of the ReLUIS project 2014-2016 (Italian Civil Protection research project), which was chaired by Raffaele Landolfo and Riccardo Zandonini. Ten research units were involved in the scientific programme coming from the following Universities: Napoli "Federico II", Salerno, Pisa, Sannio, Marche, Campania "Luigi Vanvitelli", Chieti-Pescara "G. d'Annunzio", Trento, Trieste and Genova. The research line was mainly devoted to the development of innovative approaches for the design of steel and steel-concrete composite buildings. Starting from the outcomes achieved during the previous ReLUIS project, novel results were obtained in the last years that are herein presented considering the four main investigated area, which are: steel and steel composite beam-to-column joints, conventional steel and steel-composite buildings, non-conventional steel buildings, steel and steel-composite bridges.

Steel and steel-concrete composite structures in seismic area:
advances in research and design
The Research Project RP3 of the ReLUIS-DPC 2014-2018
Activity carried out during years 2014-2016

Steel and steel-concrete composite structures in seismic area: advances in research and design

The Research Project RP3 of the ReLUIS-DPC 2014-2018
Activity carried out during years 2014-2016

Raffaele Landolfo
Riccardo Zandonini
editors



ISBN 978-88-89972-74-8



Steel and steel-concrete
composite structures in seismic area:
advances in research and design

The Research Project RP3 of the ReLUIS-DPC 2014-2018

Activity carried out during years 2014-2016

Raffaele Landolfo, Riccardo Zandonini
editors



ISBN 978-88-89972-74-8

© 2018 DoppiaVoce
Napoli
www.doppiaVoce.it

Tutti i diritti riservati.
È vietata ogni riproduzione.

Opera in libero accesso, secondo i termini indicati nel sito www.doppiaVoce.it.

CONTENTS

<i>Foreword</i>	V
SECTION 1 – STEEL JOINTS	
Seismic design and testing of extended stiffened end-plate beam-to-column joints	3
<i>Raffaele Landolfo, Mario D’Aniello, Roberto Tartaglia, Silvia Costanzo</i>	
Seismic design of full-strength full-ductility extended end plate beam-to-column joints	25
<i>Vincenzo Piluso, Gianvittorio Rizzano, Massimo Latour, Antonella Bianca Francavilla</i>	
Standard beam-to-column joints	57
<i>Gianfranco De Matteis, Giuseppe Brando, Elisabetta D’Alessandro</i>	
Reversible steel joint for seismic-resistant structures	93
<i>Margherita Pongiglione, Chiara Calderini, Mario D’Aniello, Raffaele Landolfo</i>	
SECTION 2 – STEEL-CONCRETE COMPOSITE JOINTS	
The guidelines for the design of steel-concrete composite joints in seismic areas	105
<i>Claudio Amadio, Marco Fasan, Maria Rosaria Pecce, Giuseppe Logorano</i>	
SECTION 3 – CONVENTIONAL MULTI-STOREY BUILDINGS	
Concentric braced frames: global and local numerical studies on the seismic behaviour of steel multistory bracing systems by refined FEM analyses	135
<i>Beatrice Faggiano, Antonio Formisano, Luigi Fiorino, Vincenzo Macillo, Carmine Castaldo, Federico M. Mazzolani, Raffaele Landolfo</i>	
Progressive collapse risk assessment of seismic designed steel moment frames	175
<i>Massimiliano Ferraioli, Alberto Mandara, Angelo Lavino</i>	
The guidelines for the design of steel-concrete composite moment resisting frames in seismic areas	211
<i>Claudio Amadio, Marco Fasan, Maria Rosaria Pecce, Giuseppe Logorano</i>	
SECTION 4 – CONVENTIONAL ONE-STOREY BUILDINGS	
Seismic vulnerability analysis of single-storey industrial buildings	247
<i>Francesco Morelli, Raffaele Laguardia, Andrea Piscini, Marco Faggella, Rosario Gigliotti, Walter Salvatore</i>	
Single-storey steel industrial buildings: design strategies evaluation based on economic and environmental analyses	269
<i>Chiara Calderini, Riccardo Berardi, Sara Rossi</i>	
SECTION 5 – NON-CONVENTIONAL BUILDINGS: STICK BUILT SYSTEMS	
Non-conventional building: stick-built systems – methodologies for prediction of shear wall response	291
<i>Raffaele Landolfo, Maria Teresa Terracciano, Bianca Bucciero, Tatiana Pali, Vincenzo Macillo, Ornella Iuorio, Luigi Fiorino</i>	

Non-conventional building: stick-built systems – design by testing	319
<i>Nadia Baldassino, Martina Bernardi, Riccardo Zandonini</i>	
SECTION 6 – NON-CONVENTIONAL BUILDINGS: SHEAR PANEL SYSTEMS	
Shear panel systems	353
<i>Gianfranco De Matteis, Giuseppe Brando</i>	
SECTION 7 – NON-CONVENTIONAL BUILDINGS: HYBRID SYSTEMS	
Design procedure for failure mode control of hybrid MRF-EBF systems	393
<i>Rosario Montuori, Elide Nastri, Vincenzo Piluso</i>	
Seismic-resistant steel frames with reinforced concrete infill walls	429
<i>Andrea Dall'Asta, Graziano Leoni, Francesco Morelli, Walter Salvatore, Alessandro Zona</i>	
SECTION 8 – BRIDGES	
Seismic behaviour of steel-concrete composite bridge decks	451
<i>Luigino Dezi, Sandro Carbonari, Andrea Dall'Asta, Fabrizio Gara, Lucia Minnucci</i>	

FOREWORD

The seismic design of steel buildings is a process in rapid and continuous evolution. This advancement implies that, when adopting steel materials, practitioners should be able to tackle effectively the issues related to a wide range of structural typologies as well as of innovative technological solutions, which are the fruitful result of the synergy between industrial and scientific research worlds. The current project ReLUIs – Italian Civil Protection – incorporates a specific line on “Steel and Steel-Concrete Composite Structures” aimed both to enhance the design rules provided by the existing codes for conventional structural typologies and to provide rules for innovative structural typologies. The research activities in the period 2014-2016 stemmed directly from the results obtained in the previous ReLUIs – Italian Civil Protection research project (2010-2013). The research studies were carried out by ten Research Units (RUs), working in synergy on the following thematic areas:

- (i) Steel and steel composite beam-to-column joints: design guidelines were developed for joints typically used in seismic-resistant moment frames;
- (ii) conventional steel and steel-composite buildings: the rules for concentrically braced structures were revised in order to improve the overall ductility and to avoid the premature failure of the columns;
- (iii) non-conventional steel buildings: design guidelines for the use of both cold-formed profiles in residential buildings and hybrid systems in multistorey buildings (e.g. MRF-EBF dual systems and steel frames infilled with reinforced concrete walls) were developed;
- (iv) steel and steel-composite bridges: the practical issues related to the local and global seismic response of steel-concrete composite bridge decks were investigated.

The detailed list of research tasks in charge of each RUs is summarised in the Table hereinafter.

Table 1. Research units and related tasks.

Research Unit	Affiliation	Research Coordinator	Task
UNINA	University of Naples “Federico II”	Raffaele Landolfo	<ul style="list-style-type: none"> • Steel joints • Conventional multi-storey buildings • Non-conventional buildings: stick-built systems
UNISA	University of Salerno	Vincenzo Piluso	<ul style="list-style-type: none"> • Steel joints
UNIFI	University of Pisa	Walter Salvatore	<ul style="list-style-type: none"> • Conventional one-storey buildings
UNISANNIO	University of Sannio	Marisa Pecce	<ul style="list-style-type: none"> • Conventional multi-storey buildings
UNIVPM	Marche Polytechnic University	Luigino Dezi	<ul style="list-style-type: none"> • Bridges
UNICAMP	University of Campania “Luigi Vanvitelli”	Alberto Mandara	<ul style="list-style-type: none"> • Conventional multi-storey buildings
UNICH	University of Chieti-Pescara	Gianfranco De Matteis	<ul style="list-style-type: none"> • Steel joints • Non-conventional buildings: shear panel systems
UNITN	University of Trento	Riccardo Zandonini	<ul style="list-style-type: none"> • Non-conventional buildings: stick-built systems
UNITS	University of Trieste	Claudio Amadio	<ul style="list-style-type: none"> • Conventional multi-storey buildings
UNIGE	University of Genoa	Chiara Calderini	<ul style="list-style-type: none"> • Steel joints • Steel-concrete composite joints • Conventional one-storey buildings

On the basis of this distribution list, this book is organized in eight sections as follows:

- Section 1 devoted to steel joints;
- Section 2 devoted to steel-concrete composite joints;
- Section 3 devoted to conventional multi-storey buildings;
- Section 4 devoted to conventional one-storey buildings;
- Section 5 devoted to non-conventional buildings: stick-built systems;
- Section 6 devoted to non-conventional buildings: shear panel systems;
- Section 7 devoted to non-conventional buildings: hybrid systems;
- Section 8 devoted to bridges.

As Coordinators of the research line “Steel and Steel-Concrete Composite Structures” within the 2014-2018 ReLUIIS – Italian Civil Protection research project, on behalf of all RUs we gratefully acknowledge the Italian Department of Civil Protection for the financial support.

Raffaele Landolfo
Riccardo Zandonini

SECTION 1

STEEL JOINTS

SEISMIC DESIGN AND TESTING OF EXTENDED STIFFENED END-PLATE BEAM-TO-COLUMN JOINTS

Raffaele Landolfo ^a, Mario D’Aniello ^b, Roberto Tartaglia ^c, Silvia Costanzo ^d

^a *University of Naples Federico II, Naples, Italy, landolfo@unina.it*

^b *University of Naples Federico II, Naples, Italy, mdaniel@unina.it*

^c *University of Naples Federico II, Naples, Italy, roberto.tartaglia@unina.it*

^d *University of Naples Federico II, Naples, Italy, silvia.costanzo@unina.it*

ABSTRACT

This chapter describes the main aspects related to the design of extended stiffened bolted end-plate joints. Bolted extended stiffened end-plate beam-to-column joints are widely used in moment resisting steel frames. The characterization of strength, stiffness and ductility of this type of joints is crucial in order to evaluate the global seismic response of steel structures. The literature provides several models able to predict the mechanical behaviour of the joints as well as the European Codes. Nevertheless, in EN1993:1-8 the influence of the rib stiffeners on both strength and stiffness of this type of joints is not clearly accounted for. Therefore, the requirements provided by current codes are examined and discussed at the light of recent research outcomes in order to harmonize the design rules. Moreover, design assumptions specifically conceived for seismic resistant extended endplate reinforced by rib stiffeners are discussed and experimentally validated.

KEYWORDS

Beam-to-column joints, seismic design, hierarchy criteria, experimental test, ductility.

1 INTRODUCTION

Extended stiffened (ES) end plate bolted connections are popular among European steel fabricating industries and widely used in European practice as moment-resistant joints in low and medium rise steel frames, especially thanks to the simplicity and the economy of fabrication and erection. Indeed, these types of connection are characterized by a limited use of welds, being solely the end-plate and some stiffeners shop-welded to the beam, which allows keeping down the cost and guaranteeing good quality control. Then, the end plate-beam assembly is field-bolted to the column flange, thus shortening the construction time.

Bolted endplate beam to column connections have been widely studied in the last fifty years (Sherbourne 1961, Douty and Mc Guire 1965, Nair et al. 1974, Mann and Morris 1979, Frye and Morris 1975, Agerskov 1977, Krishnamurthy 1978, Whittaker and Walpole 1982, Witteveen et al. 1982, Korl et al. 1990, Ysai and Popov 1990, Aggarwal 1994, Ghobarah et al 1992, Jaspert 1997, Adey et al 1998, Sumner et al 2000, Adey et al 2000, Wang et al 2001, Bjorhovde 2004, Guo et al 2006, Shi et al 2007). The former design criteria have been developed by (Sherbourne 1961, Douty and Mc Guire 1965, Nair et al. 1974, Mann and Morris 1979, Agerskov 1977), which schematized the behaviour of endplate connections by

means of an analogy with T-stub connections. More recently, methods based on refined yield line analysis have been suggested, in which the currently accepted design procedures of end-plate connections have been derived (Jaspart 1997, Beg et al. 2004, Gioncu et al. 2005, Girao Coelho 2004, Weynand et al. 1995).

ES joints can be designed to be either full or partial strength and full or semi-rigid. The experimental and theoretical evidence showed that this type of joint can effectively behave as full strength. Conversely, a full rigid behaviour could not be obtained in several cases. Therefore, ES bolted joints can be easily conceived as semi-rigid joints, which results in an additional savings in the gravity load system.

Moreover, in moment resisting frames subjected to seismic loads the use of semi-rigid joints can lead to lighter structures thanks to lower design forces due to increase of fundamental periods related to the increase of lateral flexibility (Elnashai and Elghazouli 1994).

However, it can be arguable that after Northridge and Kobe earthquakes semi-rigid connections have been considered as viable alternatives to welded connections for seismic resisting buildings, providing similar or superior seismic performance compared to full rigid connections (Leon 1995). Indeed, those seismic events showed that fully welded joints can be severely prone to premature brittle failure (Leon 1995). In USA, after Northridge earthquake, recommendations for seismic design of extended stiffened bolted beam-to-column joints were developed within the SAC project and published as a series of FEMA documents and then incorporated into the AISC341 and AISC358. These seismic provisions require that beam-to-column connections should be designed with sufficient strength to guarantee the formation of plastic hinge into the beam and located close to the protruding part of the connection away from the column face. This design philosophy aims having a strong column, a strong connection, and a weak beam.

In European code EN1993:1-8 (hereinafter also referred as Eurocode 3 or EC3) requirements for calculating the strength and stiffness of extended plate bolted joints have been provided on the basis of T-stub yield line theory, but the influence of the rib stiffeners on both strength and stiffness of ES joints is not properly addressed. Moreover, specific provisions for seismic design of joints are missing. With this regard, according to Eurocodes the joints can be designed either full-strength or partial-strength as respect to the connected beams. These two different performance objectives may significantly modify the dissipative behaviour of seismic resistant MRFs. Indeed, in case of full strength joints plastic hinge should form in beams, while in case of partial strength joints the plastic deformation should concentrate in the connections. The former design strategy needs to guarantee that joints have flexural overstrength larger than connected beams. Unfortunately, owing to the variability of steel strength and to the actual post-yield flexural overstrength of steel beams, these connections could not have enough overstrength. In EN 1998-1 (hereinafter also referred as EC8), the minimum required joint overstrength is equal to $1.1 \times \gamma_{ov} \times M_{b,pl,Rd}$ (being $M_{b,pl,Rd}$ the beam plastic moment and γ_{ov} the ratio between the mean over the characteristic yield stress, generally assumed equal to 1.25) and it could be largely overcome in many cases. In addition, it is necessary to give effective rules to control the behaviour of column web panel for either full strength or weak dissipative web panel.

Concerning partial strength joints, this design criterion requires that joints should have sufficient rotation capacity to guarantee the formation of global mechanism. At the present time, EN 1993-1-8 provides models to compute the strength and the stiffness of connections but no rules are available to predict the joint rotation capacity. The joint rotational response depends on the deformation behaviour of each component constituting the joint (e.g. end plate in bending, beam in tension, panel zone, bolts, etc.). Therefore, EN 1993-1-8 intends that the partial strength joint could have sufficient monotonic rotation capacity if designed

concentrating the plastic deformations into those components providing high ductility (e.g. the end plate in bending), while the brittle components (as the bolts and welds) should behave elastically. This criterion is sufficient for joints designed for gravity and wind loads. Regarding the seismic loading, EC8 refers to EC3 for the design and verification of members and connections and in case of semi-rigid and/or partial strength dissipative joints requires the following conditions:

- the joints should have a rotation capacity consistent with the global deformations;
- members framing into the joints should behave in a stable manner at the ultimate limit state;
- the effect of joint deformations on global drift should be taken into account using either nonlinear static pushover analysis or non-linear dynamic time history analysis.

In addition, the joint should guarantee a rotation capacity at least equal to 0.035 rad for high ductility class (DCH) structures and 0.025 rad for medium ductility class (DCM) structures (provided that designed using a behaviour coefficient q larger than 2). The cyclic rotation capacity should be ensured without degradation of strength and stiffness greater than 20%. Finally, the column web panel shear deformation should contribute lesser than 30% of the total rotation capacity.

Since no requirements and rules are provided to obtain this type of performance, EC8 requires design supported by specific experimental testing, resulting in impractical solutions within the typical time and budget constraints of real-life projects. As an alternative to design supported by testing, the code allows using analytical approaches based on experimental studies or prescribes to find existing data on experimental tests performed on similar connections in literature. It is clear that this procedure is unfeasible from the designer's point of view. As it can be easily recognized US practice addresses this issue in a more pragmatic way providing standard joints that are pre-qualified for seismic resistance (AISC358-16). This approach has a great interest for the European steelwork industry. Unfortunately, US design practice and usual ranges of steel profiles are quite far from those usually adopted in Europe. Thus, the rules and requirements given by AISC358-16 are not directly applicable to European context. The above considerations are general for all types of both welded and bolted joints. However, each joint typology is characterized by specific criticism which needs further investigation. In the light of these remarks, the study presented in this Chapter focuses to develop seismic design criteria of ES bolted end-plate beam-to-column joints, in line with EC3 philosophy. Therefore, based on a critical review of the state of the art the main aspects characterizing the joint performance have been identified and experimental tests have been carried out to validate the developed criteria.

The present chapter is organized into two main parts. The design criteria and relevant rules are discussed in the first part, while the experimental tests in the second.

2 DESIGN OF STIFFENED EXTENDED ENDPLATE JOINTS

2.1 Generality

According to EN1993:1-8, the prediction of rotational behaviour of connections (in terms of both strength and stiffness) can be carried out using the components method. This methodology consists in identifying each source of strength and deformability that is modelled as a mechanical spring (namely the "component"). The appropriate combination of all components allows deriving the stiffness and resistance properties of the joint; the assembling is based on the simulated distribution of internal forces.

In the proposed approach, the joint behaviour has been classified on the basis of both the connection and the column web panel strength. Regarding the former aspect, in the present

study two different levels of connection-to-beam moment capacity ratio have been considered:

- Full strength connection: plastic deformations should occur only in the beam, while the connection should behave elastically; the connection is designed to provide a moment capacity at least 1.5 times larger than that of the connected beam.
- Equal strength connection: plastic deformations may contemporary occur both in the connection zone and in the connected beam, namely the connection strength is equal to the beam strength.

For what concerns the column web panel, the joints have been designed considering strong web panel joints, namely the column web panel behave elastically, while the first nonlinear event is reached in the connection zone and/or in the connected beam (depends on the weakest component)

In order to control the joint mechanism, in the proposed design procedure, the joint should be designed considering separately the following three main parts:

- Connection zone
- Column web panel zone
- Beam zone

Each zone has been individually designed according to specific assumptions and then simply capacity design criteria have been applied, in order to obtain different joint configurations compliant to the different performance criteria previously defined.

Differently from EN1993:1-8, the number of bolt-rows in tension is not defined by using equilibrium conditions of the internal forces, but it has been fixed a-priori according to what observed in the preliminary finite element results for different joint configurations. Preliminary analyses showed that the bolt-rows above the beam flange and the one below are always active in tension; lower bolt-rows have been assumed not-active (namely in compression).

For each performance criterion and with reference to the joint configuration (external or internal) the design of specimens has been carried out in order to meet the following capacity design requirements:

Full-strength TS Joints:

$$M_{wp,Rd} \geq M_{con,Rd} > M_{con,Ed} \quad (1)$$

Equal-strength TS Joints:

$$M_{wp,Rd} \geq M_{con,Rd} = M_{con,Ed} \quad (2)$$

- $M_{wp,Rd}$ is the flexural strength corresponding to the strength of column web-panel;
- $M_{con,Rd}$ is the contribution of connection zone to the joint bending strength;
- $M_{con,Ed}$ is the joint design moment, evaluated for the different strength-performance levels
- Joint configuration: exterior joint with strong web panel (TS)
- Connection strength: full strength (F), equal strength (E)

It is worth to specify that in exterior joint configuration, the column web panel is designed to be over-strong respect to the connection zone, while the interior joint configurations is designed in order to obtain a balanced web panel (i.e. the first nonlinear event is reached concurrently in the column web panel, in the connection zone and in the beam section at the end of the rib). This different criterion is explained considering that larger demand on the column web panel is experienced by internal joints due to anti-symmetrical moments in the seismic design situation; thereby, the shear force acting in the column web panel in the X joint configurations is about two times larger than those experienced in T-joint configurations.

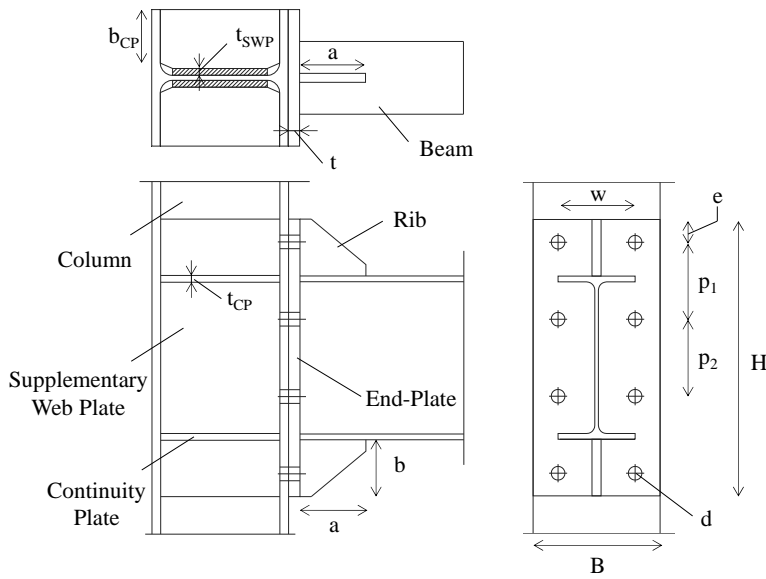


Figure 1. Extended stiffened end plated beam to column joint: main geometric properties.

2.2 Evaluation of joint design moment at the column face

The design moment $M_{j,Ed}$ has been calculated at the column face and, depending on the Full-strength connection:

$$M_{con,Ed,F} = \gamma_{sh} \cdot \gamma_{ov} \cdot (M_{B,Rd} + V_{B,Ed} \cdot s_h) \quad (3)$$

Equal-strength connection:

$$M_{con,Ed,F} = (M_{B,Rd} + V_{B,Ed} \cdot s_h) \quad (4)$$

Where:

$M_{B,pl,Rd}$ is the plastic flexural strength of the connected beam.

s_h is the distance between the column face and the tip of the stiffener;

$V_{B,Ed}$ is the shear force corresponding to the occurring of the plastic hinge in the connected beam; it is given by:

$$V_{B,Ed} = V_{B,Ed,M} + V_{B,Ed,G} \quad (5)$$

Where:

$V_{B,Ed,M}$ is the contribution due to the formation of the plastic hinge, taken as:

$$V_{B,Ed,M} = \frac{2 \cdot M_{B,pl,Rd}}{L_h} \quad (6)$$

$V_{B,Ed,G}$ is the contribution due to the gravitational loads;

L_h is the approximate distance between plastic hinges;

γ_{ov} is overstrength factor due to the material randomness, assumed equal to 1.25;

γ_{sh} is the strain hardening factor according to AISC358-10; it is given as:

$$\gamma_{sh} = \frac{f_y + f_u}{2 \cdot f_y} \leq 1.20 \quad (7)$$

In the current design procedure, the strain hardening factor has been assumed equal to 1.20, based on both the provisions of AISC358-16 and the preliminary results of test numerical simulations.

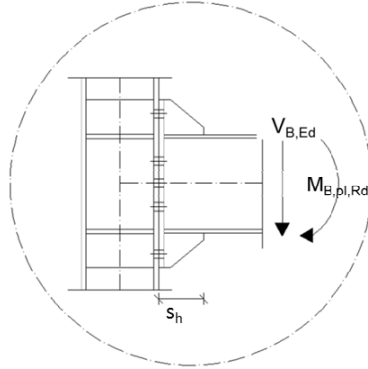


Figure 2. Evaluation of design moment for stiffened extended endplate joints.

2.3 Design of the connection zone

The strength of connection zone can be calculated according to component method, but for each bolt row the following contributions have been disregarded:

- column web panel in shear
- beam flange and web (and rib) in compression.

This choice is motivated by the fact that the distribution of internal forces is not known a-priori and also change with the joint rotation (from elastic to plastic range). Hence, the interaction between column and beam cannot be effectively accounted for. Design and verification of both components (column web panel in shear and beam + rib in compression) has been carried out separately.

The presence of the rib stiffeners is not properly addressed in EN1993:1-8. Therefore, analytical and semi-empirical formulations, found in literature and validated by own-made numerical simulations, have been implemented in the calculation of stiffened joints. The additional design assumptions accounting for the presence of the rib stiffeners are summarized hereinafter.

In particular, the design and verification of rib elements have been carried out according to the model provided by Lee et al. (2002, 2005); the main idea is based on the observation that force transfer mechanism in the ribs can be represented by an equivalent strut model (see Figure 3).

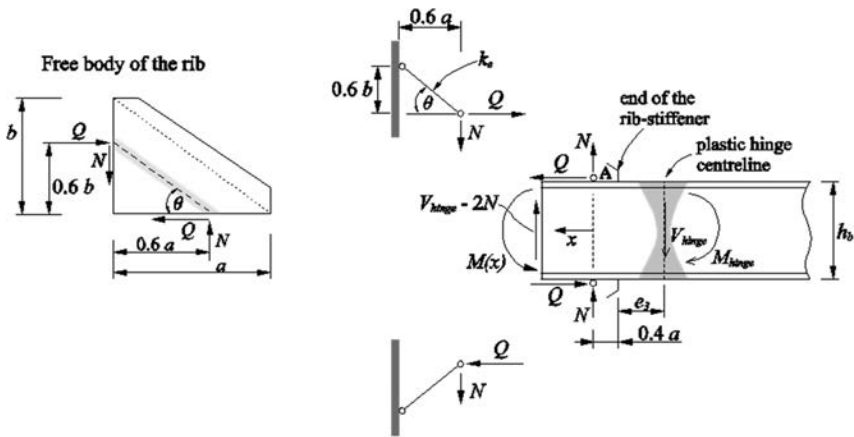


Figure 3. Equivalent strut model proposed by Lee (2002) and Lee et al. (2005).

The Equivalent strut area, A_e , is defined as

$$A_e = \eta_e \cdot h_e \cdot t, \tag{8}$$

Where:

η_e is defined as equivalent strut area factor;

t is the rib thickness;

h_e is a span perpendicular to the strut line (Figure 4) defined as:

$$h_e = \frac{ab - c^2}{\sqrt{(a-c)^2 + (b-c)^2}} \tag{9}$$

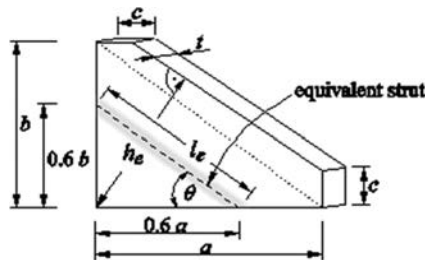


Figure 4. Definition of rib geometry with equivalent strut as defined in Lee (2002).

The rib stiffeners have been designed to behave elastically bearing the normal force N (see Eq. 10) and total shear force Q (see Eq. 11) at the beam/column-rib interface:

$$N = \left(\frac{b}{a}\right) \cdot Q \tag{10}$$

$$Q = \frac{\frac{(0.21a+0.51L')ad_b}{I_b}}{\frac{1}{\eta} \frac{(0.6)\sqrt{(a^2+b^2)}\sqrt{(a-c)^2+(b-c)^2}}{(ab-c^2)t} + \frac{(0.18b+0.30d_b)(ad_b)}{I_b}} \cdot V_{pd} \quad (11)$$

In addition, EN1993:1-8 does not provide specific equations to calculate the effective length of the equivalent t-stub model for the bolt row(s) above the tension flange in the stiffened zone. In the current procedure such effective lengths have been computed on the basis of instructions given by the Green Book P398, which is based on English BS EN 1993-1-8 and its UK National Annex. In this document, the effective lengths for the bolt rows belonging to the rib stiffener (for both one-bolt row-up and two-bolt rows-up configurations) are obtained considering the circular and non-circular yielding patterns shown in Figure 5:

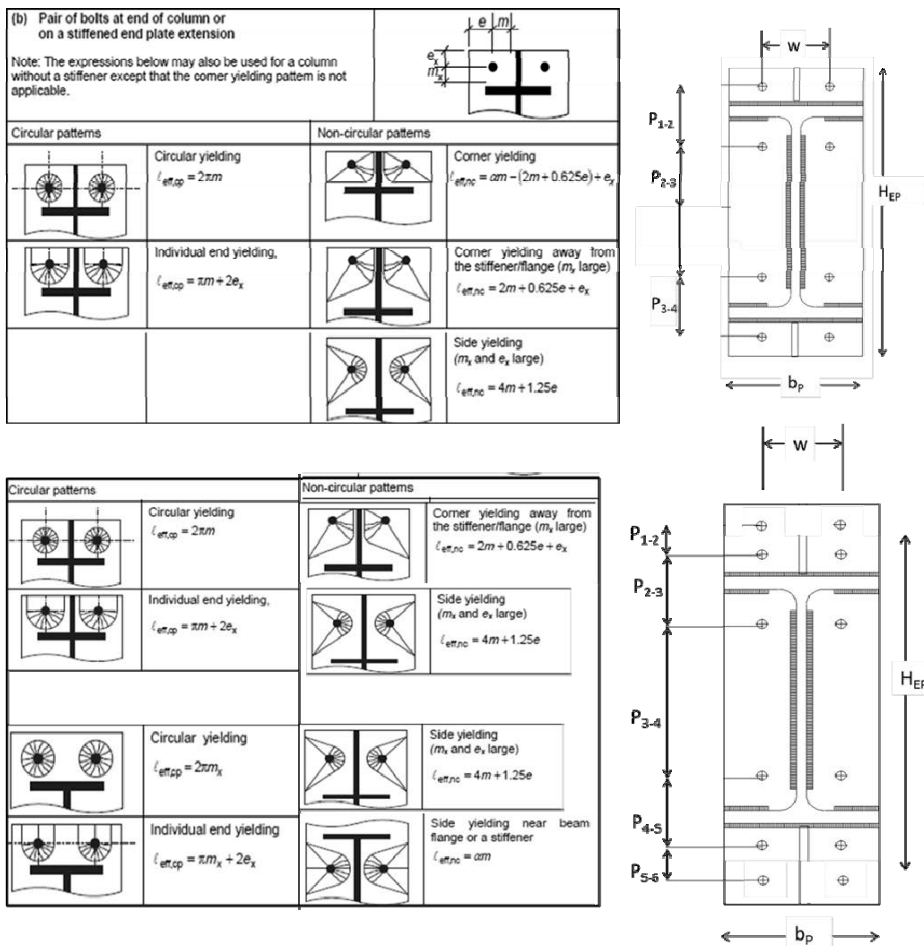


Figure 5. Effective lengths for bolts on a stiffened end plate extension according to British Standard.

Another important aspect is the position of the compression centre. For joint types covered by EN 1993-1-8 provisions, the compression centre is located at the centre of beam's bottom flange; in the current design procedure, owing the presence of the rib stiffeners, the centre of compression is assumed to be shifted at the centroid of the section made of the rib and the rib. This assumption is consistent with results obtained from own-made preliminary numerical analyses and also with experimental and numerical results carried out by Abidelah et al. (2012). In this study, the Authors concluded that "...the compression centre of the analytical model is better situated at the centroid of the Tee represented by the stiffener and the beam flange".

2.4 Rules to enhance the ductility of the connection

Strength, stiffness and ductility are strictly related to the components of the joint, which fall on two categories, i.e. ductile and brittle. Therefore, the joint ductility depends on the type of failure mode and the corresponding plastic deformation capacity of the activated component. The joint ductility is strictly dependent on the ductility of the equivalent T-stubs at each bolt row in tension, whose behaviour deserves some considerations. Figure 6 concisely depicts the dependency of failure mode on geometric properties and end-plate to bolt strength ratio. Indeed, in abscissa it is reported β that is the ratio between the flexural strength of the plates, or column flanges, ($M_{pl,Rd}$) and the axial strength of the bolts ($F_{t,Rd}$), while the vertical axis reports the ratio η between the T-stub strength (F) over $F_{t,Rd}$. As it can be observed, the strength for mode 1 in case of non-circular pattern depends on the ratio $v = n/m$, where m is the distance between the bolt axis and the flange-to-web expected location of the plastic hinge, and n is the minimum of the distance between the edge of the flange and the bolts axis or $1.25m$.

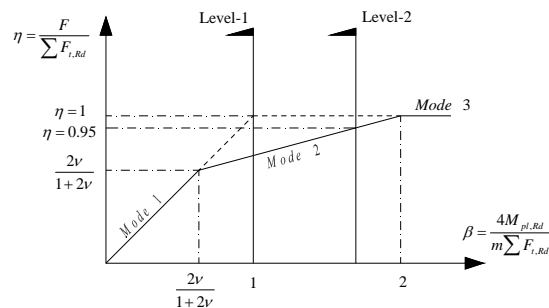


Figure 6. T-Stub resistance and corresponding mechanism according to EN1993:1-8.

Therefore, in line with EC3, in order to avoid brittle collapse (i.e. mode 3) two possible ductility criteria can be adopted, namely:

Level-1: $\beta \leq 1$ this condition imposes either a failure mode I or failure mode II (but very close to mode I), which provide very high ductility.

Level-2: $\beta < 2$ and $\eta \leq 0.95$, this condition imposes a failure mode II with limited ductility, but avoiding brittle failure.

It should be noted that the level of ductility to be guaranteed depends on the design performance objectives. Indeed, it is crucial providing the larger ductility for Equal and Partial strength, less for Full strength joints. Also according to the Eurocode 3, the joint

rotation capacity should be checked if M_{jrd} is less than $1.2 M_{B,pl,rd}$ and two alternative ways can be pursued: 1) performing experimental tests; 2) controlling the thickness t of either end-plate or column flange, provided that the joint design moment resistance is governed by those components, which should satisfy the following inequality:

$$t \leq 0.36d \sqrt{\frac{f_{ub}}{f_y}} \quad (12)$$

where d is the nominal bolt diameter, f_y is the yield strength of the relevant basic component and f_{ub} is the bolt ultimate strength.

Eq. (12) theoretically complies with the ductility Level-1 depicted in Fig. 6. Indeed, it is based on the assumption that bolted joints have sufficient rotation capacity if the resistance of each individual bolt ($F_{t,Rd}$) is greater than the resistance ($F_{p,Rd}$) of the connected plates (end-plate or flange) in order to prevent premature failure of the bolts. The EC3 design resistance of a bolt in tension is given as follows:

$$F_{t,Rd} = \frac{0.9A_s f_{ub}}{\gamma_{M2}} \quad (13)$$

where A_s is the tensile stress area of the bolt and γ_{M2} is the relevant partial safety factor (recommended equal to 1.25).

In addition, according to the EN 1993-1-8, the maximum design resistance of a plate occurs in the case of a circular mechanism, which leads calculating the following strength:

$$F_{p,Rd} = \frac{\pi t^2 f_y}{\gamma_{M0}} \quad (14)$$

where t is the plate thickness and γ_{M0} is the relevant partial safety factor (recommended equal to 1).

As it can be easily recognized Eqs. 12 and 14 assume perfectly plastic behaviour of steel plates. However, the ductility Level-1 for seismic resistant Partial strength joints should be expressed accounting for both the random variability of plate material and its relevant strain hardening, so that the following inequality can be used:

$$F_{t,Rd} \geq \gamma \cdot F_{p,Rd} = \gamma_{ov} \cdot \gamma_{sh} \cdot F_{p,Rd} \quad (15)$$

The overstrength factor γ in Eq. (15) can be taken equal to 1.5, since the Eurocode recommended value for γ_{ov} is equal to 1.25, the value for γ_{sh} given by Eq. (7) is equal to 1.2 for European mild carbon steel, and the recommended partial safety factor γ_{M0} is equal to 1.0. Thus, rearranging the inequality (15) with Eq. (12), the ductility condition accounting for capacity design criteria can be expressed as following:

$$t \leq \frac{0.42 \cdot d}{\sqrt{\gamma_{ov} \cdot \gamma_{sh}}} \cdot \sqrt{\frac{\gamma_{M0} \cdot f_{ub}}{\gamma_{M2} \cdot f_y}} \leq 0.30 \cdot d \cdot \sqrt{\frac{f_{ub}}{f_y}} \quad (16)$$

Regarding full and equal strength joints, even though either no or poor ductility should be respectively exploited, a local hierarchy criterion is advisable in order to avoid undesirable failure mode in the brittle components due to material variability. Hence, in line with ductility Level-2, the strength of bolts should satisfy the following inequality:

$$F_{t,Rd} \geq \gamma_{ov} \cdot F_{p,Rd} \quad (17)$$

Eq. (17) can be rearranged and after some algebraic manipulations it provides a similar criterion as given by Eq. (12).

It is important to highlight that all criteria previously described require that failure of welds has to be unquestionably avoided, because of their brittle collapse mechanism.

2.5 Choice of the type of high-strength pre-loadable bolts

The type of pre-loadable bolts to be used for the prequalified joints has been also investigated. With this regard, in Europe both HV and HR assemblies can be used for high strength pre-loadable bolts, but their tensile failure mode is significantly different (D'Aniello et al. 2016, 2017), namely nut stripping in the first case (see Fig. 7a,b) and tensile tearing in the second (see Fig. 7d,e). It is also interesting to observe that in both types of bolts the low-cycle fatigue resistance inversely increases with the diameter, namely being larger for the smaller diameters (see Fig. 7c,f). This feature can be explained considering that larger size of the crests (which increase with the diameter of the shank) of the threaded zone corresponds to an increase of the stress concentration.

Considering that the shear resistance is kept once the nut stripping is activated, HV bolts were used to qualify the joints.

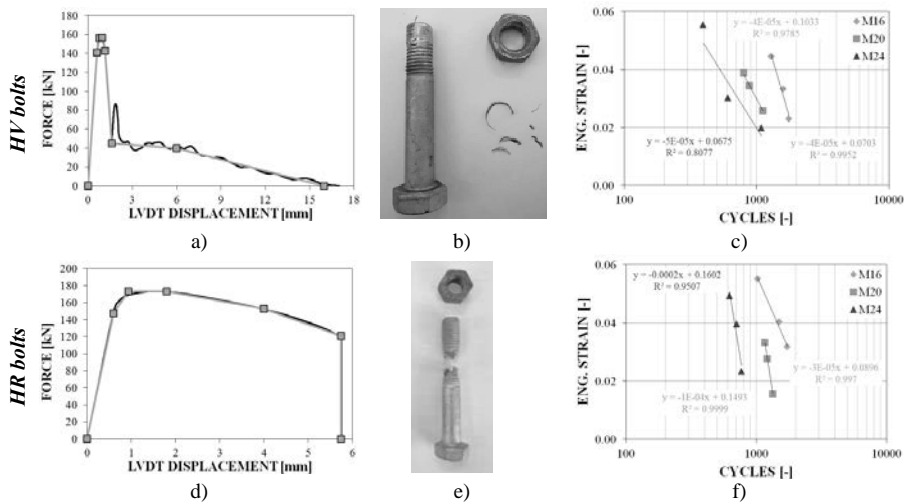


Figure 7. HV vs. HR bolts: force – displacement, failure mode and low-cycle fatigue resistance.

2.6 Design of column web panel zone

Preliminary numerical results showed that, owing to the presence of the rib stiffeners and the shifting of the compression centre, the portion of the column web panel engaged in shear is larger than in the unstiffened joints. Thereby, the design shear force has been calculated accounting for this aspect according to the following equation:

$$V_{wp,Ed} = \frac{\sum M_{j,Ed}}{z_{wb}} - V_C \quad (18)$$

Where:

$\sum M_{j,Ed}$ is the sum of bending moments in the beam at the column face.

z_{wp} is the distance between the middle of the upper continuity plate and the 0.6 of the height of the lower rib stiffener (see Figure 8 and Figure 9)

V_c is the shear force in the column.

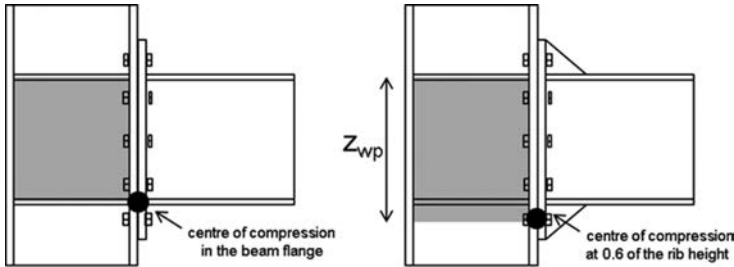


Figure 8. Influence of the rib stiffener on the shear web panel area.

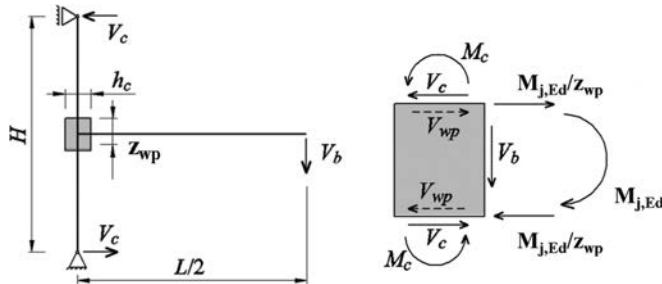


Figure 9. Evaluation of shear design force on the web panel.

The design plastic shear resistance $V_{wp,Rd}$ of column web panel computed according to EN1993-1-8; Clause 6.2.6.1(2) is given by:

$$V_{wp,Rd} = \frac{0.9 \cdot A_w \cdot f_y}{\sqrt{3} \cdot \gamma_{M0}} + \Delta V \quad (19)$$

Where ΔV is the contribution to the web panel shear resistance due to the plastic hinges occurring in the beam flanges or continuity plates (see Figure 10).

According to the present design procedure, for both full and equal strength connections, the contribution ΔV has been neglected in order to avoid any yielding phenomena in the column. Indeed this mechanism can occur for very large rotations, for which yielding is expected to be already occurred. In addition, it should be also noted that in presence of additional web plates, the shear area A_v has been defined as the sum of column shear area, and the full area of additional web plates.

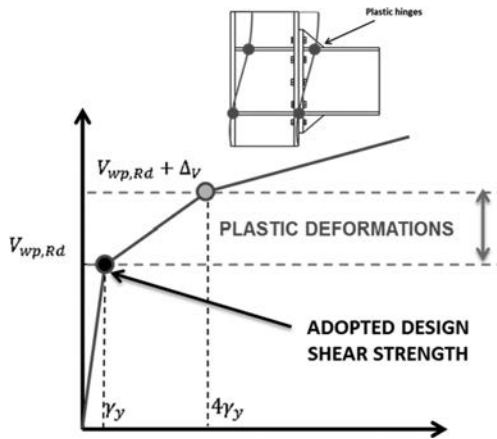


Figure 10. Shear strength evaluation for web panel zone.

2.7 Design of welds

All design considerations discussed in the previous Sections require that the failure of welds should be avoided. Apart from the calculation of strength that should comply with EN1993:1-8, the joint details should be conceived by adopting the most appropriate type of weld depending on the component that must be connected and its relevant plastic engagement. Unfortunately, the current version of EN1993:1-8 does not provide specific details for seismic resistant joints. Hence, the designer is free to select the type of weld base material and details that are nominally able to withstand the design forces, but this approach does not guarantee the fulfilment of the design performance objectives. On the contrary, US practice based on qualification procedure given by AISC 358-10 limits subjective choices by imposing specific details to guarantee the design objectives. In light of this observation, it is reasonable to extend the types of weld details given by AISC 358 to European ES joints, except for the material properties and the welding procedures. Thereby, as recommended by AISC 358, full penetration weld (FPW) are considered for rib stiffeners, because of the large stress concentration and strain demand developing by the rib strut mechanism. FPWs are also used for beam flange to end-plate splices with reinforcing fillet welds (FW) according to AISC 358 provisions. This choice is crucial to ensure the appropriate T-Stub mechanism in the connection zone where the larger demand is expected. On the other hand, beam web to end-plate welds can be FWs, since low strain demand is expected.

The details for continuity plates (CPs) to column welds depend on the design criterion adopted for column web panel strength. Indeed, if the column web panel is designed to resist forces neglecting the contribution $V_{wp,add,Rd}$ (e.g. for both full and equal strength joints) no plastic engagement is expected for CPs and fillet welds can be used. On the contrary, if the contribution $V_{wp,add,Rd}$ is accounted for (e.g. for partial strength joints), FPWs should be used in order to avoid brittle failure due to their large plastic engagements.

Finally, FPWs are considered for connecting the vertical edges of additional web plates to the column and also plug welds (PW) to prevent the buckling or separation of the lapped parts.

3 EXPERIMENTAL TESTS

3.1 Features of the tested joints

Two specimens have been designed for testing, namely i) full strength and ii) equal strength extended stiffened end-plate joints. The dimensions of beam (i.e. 7000 mm) and column (i.e. 3500 mm) are extracted from a set of low- and medium-rise MRFs designed according to EN 1998-1 [7]. The beam-to-column configurations is the follows: IPE450 (beam) – HEB 340 (column).

The geometry of the specimens is reported in Table 1, while the details are reported in Figures 11 and 12.

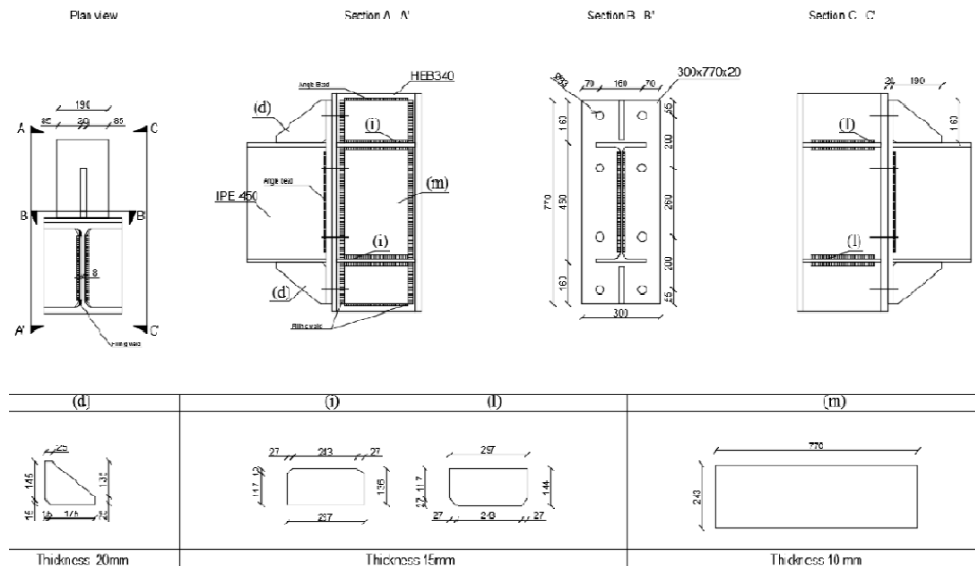


Figure 11. Geometry of the ES-E specimen.

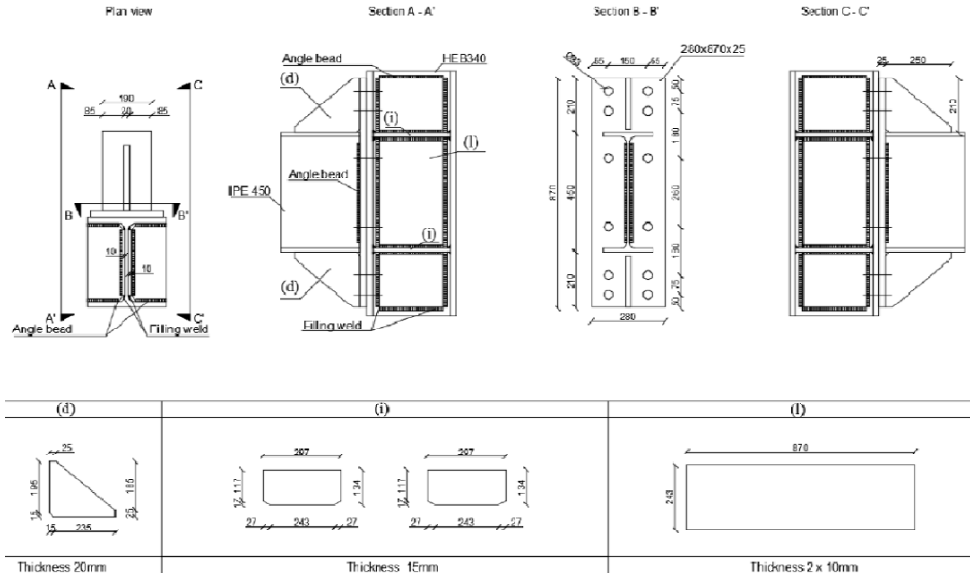


Figure 12. Geometry of the ES-F specimen.

Table 1. Geometric properties of the investigated ES joints (see Fig. 1 for the meaning of symbols).

Joint ID	End-Plate		Rib		Bolt diameter	Bolt spacing				Continuity plates		Supplementary web plate		
	H	B	t	b		a	d	e	w	p_1	p_2	b_{CP}	t_{CP}	Side
	mm	mm	mm	mm	mm	mm	mm	mm	mm	mm	mm	mm	-	mm
ES1-F	870	280	25	210	250	30	50	150	90	155	234	15	2	16
ES1-E	770	300	20	160	190	30	55	150	200	260	234	15	1	8

3.2 Test Setup

The test setup of University of Naples is presented in Figure 13; it is suitable for both internal and external joints. The connections will be tested horizontally; the size of specimens is 3.75 m for columns and about 3.5 m for the beams (depending on the column size).

Both column ends have been designed to be pinned and restrained with cylindrical hinges placed at a distance of 3.4 m; additional restraints have been provided in order to avoid lateral-torsional buckling in the beams. Two actuators are located at the tips of the beams; additional stiffeners have been provided for the beams at the actuators location.

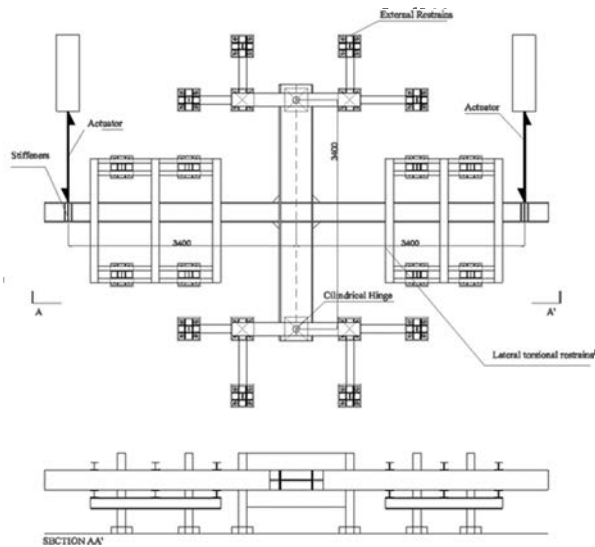


Figure 13. Test set-up at the University of Naples Federico II.

The specimen dimensions, the jack capacity and the jack stroke have been checked to confirm that they can respond to the test requirements, i.e. (1) the specimens should be failed with significant post-yielding deformations; and (2) the beam and the column lengths should be realistic in order to obtain the actual transfers of forces at the joint level. To check the jack capacity, a possible over-strength of the material has been considered: $1,25 \times 510 \text{ N/mm}^2$ has been assumed as ultimate strength for the actual S355 steel. With respect to the deformation requirement, a rotation of about $60 - 70 \text{ mrad}$ at the joint level (extracting the deformations associated to the beam and the column deformations) could be reached during the tests.

For what concerns the measuring instrumentation, displacement transducers will be used to record the deformation of the specimens during the tests. The transducer locations are shown in Figure . With this distribution of displacement transducers, the key deformations that are necessary to characterize the joint behaviour can be derived, in detail:

- Transducers 1 e 2 have been located at the cylindrical hinges in order to measure the column rigid rotation;
- Transducers 3 e 4 have been located along the column length in order to evaluate the displacement due to the column elastic rotation;
- The panel zone rotation is given by transducers 5-6 diagonally fixed on the panel at the level of continuity plates
- Transducers 7 is located at the endplate upper tip in order to evaluate eventually slip of the endplate.
- The joint rotation is measured by transducers 8-9 fixed at the ribs tip.
- Transducers 10-11 are located in the beam zone where the plastic hinge is expected in order to appreciate eventually plastic rotation of the beam.

In order to measure the girder displacements, two wire transducers have been located at beam ends as shown in Figure 14.

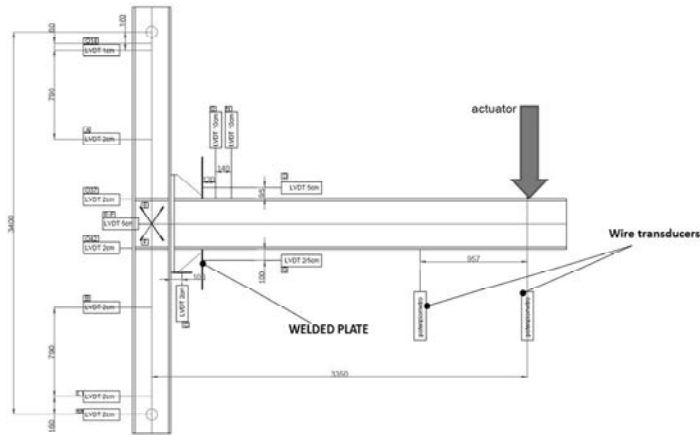


Figure 14. Instrumentation planned by the University of Naples Federico II.

3.3 Loading procedure

Parameters used to control the tests on beam to column joints are interstorey drift θ of test assembly and bending moment M at the column centreline. It should be noted that test control parameters θ and M are used primarily for load application, relating directly to lateral displacement at the tip of the column δ and actuator force F which are usually used to control a test. Additional measurements and parameters are used in order to characterize response of the specimen.

The parameters used to control the tests are the joint rotation θ and bending moment M , defined as follows (see Figure 15):

$$\theta = \delta / L_{\text{beam}}$$

$$M = F \cdot L_{\text{beam}}$$

Where:

θ is the joint rotation;

M is the bending moment at the column centerline;

δ is the deformation of the beam to column joint assembly, defined as the lateral displacement at the tip of the beam; eventually sources of deformability due to support displacements are deducted.

L_{beam} is beam length to column centerline;

F is force applied at the tip of the beam.

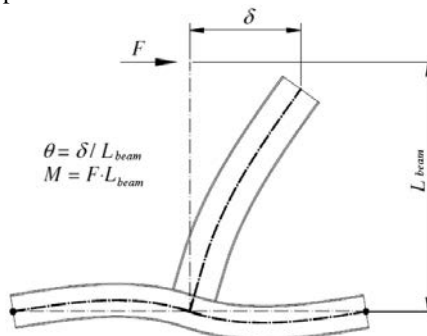


Figure 15. Parameters for beam to column joints tested applying the force at the tip of the beam.

A quasi-static loading should be used in the tests. Loading rate should be small enough so that strain rate effects do not affect the results. It should be noted that apparently the loading rate to be used in test on beam-to-column joints is not properly addressed in current codes.

EN ISO 6892-1 (2009) provides the following values for tensile tests:

in the elastic range: 6-6.60 MPa/s (if stress control is used);

at yielding plateau: $\dot{\epsilon} = 0.00025 - 0.0025s^{-1}$ (if strain control is used);

The adopted loading protocol is the ANSI/AISC 341-16 procedure is prescribed in absolute values of interstorey drift θ as follows (see Figure 16)

- cycles at $\theta=0.00375$ rad;
- cycles at $\theta=0.005$ rad;
- cycles at $\theta=0.0075$ rad;
- cycles at $\theta=0.01$ rad;
- 2 cycles at $\theta=0.015$ rad;
- 2 cycles at $\theta=0.02$ rad;
- 2 cycles at $\theta=0.03$ rad;
- 2 cycles at $\theta=0.04$ rad.

Continue loading at increments of $\theta=0.01$ rad, with two cycles of loading at each step. The loading has been continued until the assembly exhibits complete failure, characterized by the loss of load resistance.

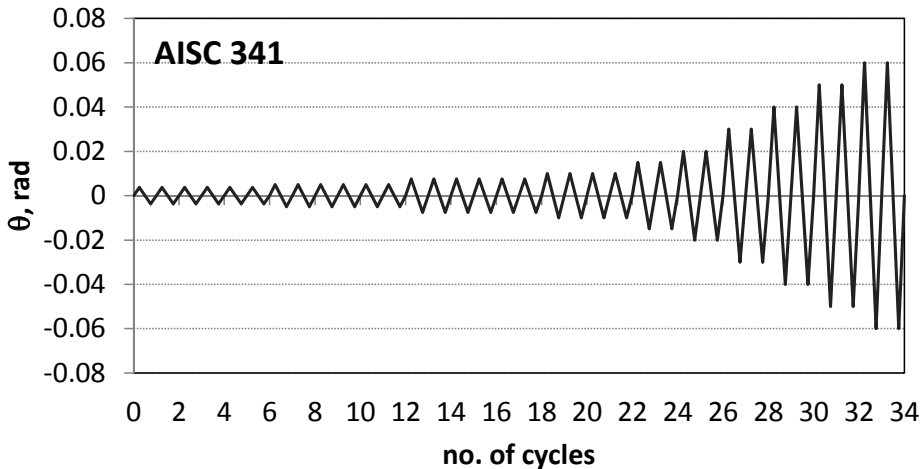


Figure 16. ANSI/AISC 341-16 (2016).

3.4 Test Results

Both specimens exhibited the expected performance. In particular, the full-strength joints showed the formation of plastic hinge into the beam only and no damage was observed in the rest of the joint. Figure 17a shows the response curves highlighting the contributions of beam, connection and column web panel, while the failure mode is depicted in Figure 17b.

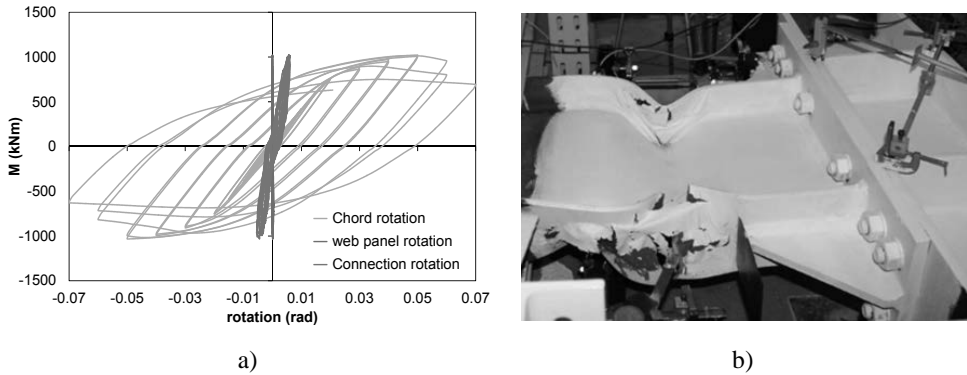


Figure 17. Experimental response of ES-F specimen: a) moment rotation curve; b) failure mode.

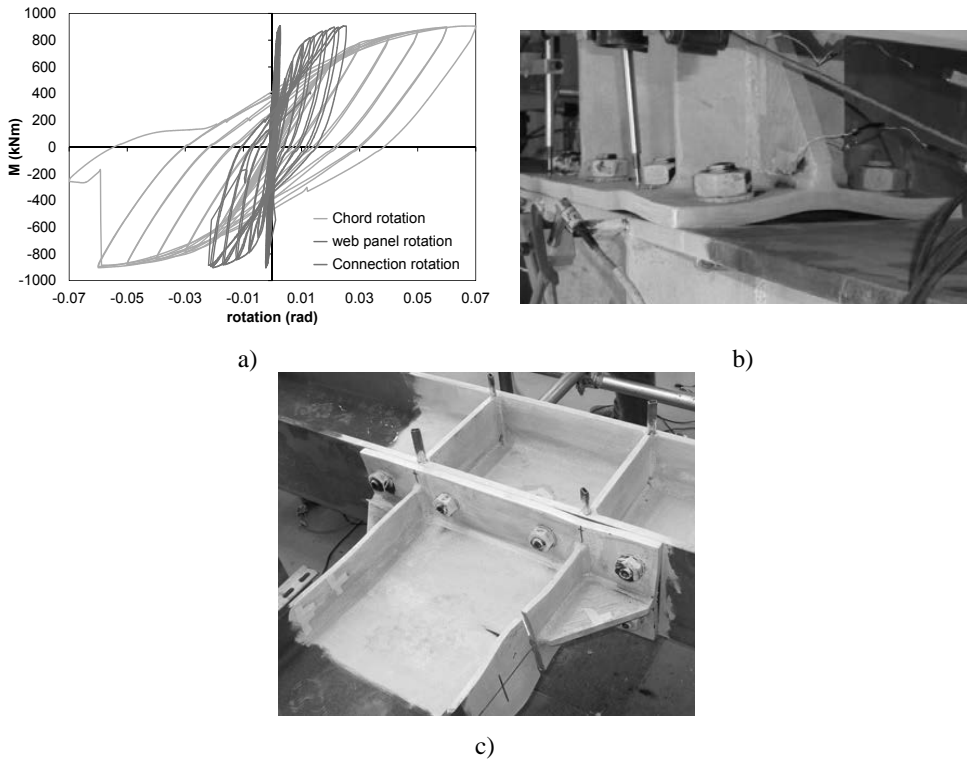


Figure 18. Experimental response of ES-E specimen: a) moment rotation curve; b,c) failure mode.

The experimental response of the equal strength joints, namely ES-E specimen, confirms the design performance criteria. Indeed, the failure mode is characterized by plastic deformations in the connection (mode 1 for each bolt row) and some plastic bending into the beam flanges that occurs after the 4% of chord rotation. Figure 18a shows the response curves highlighting the contributions of beam, connection and column web panel, while the failure mode is depicted in Figures 18b and c.

4 CONCLUSIONS

The design criteria and related requirements for bolted extended stiffened end-plate beam-to-column joints have been investigated and critically discussed on the basis of a parametric study based on finite element analyses. In particular, a capacity design procedure has been proposed to control the joint response for different performance levels.

Based on this study, the following conclusions can be drawn:

- The presence of rib stiffeners substantially increases the strength and the stiffness of end-plate joints. The yield line pattern is significantly affected by the rib and the effective lengths given by the Green Book are suitable to predict the yield strength of ES connections.
- Differently from extended unstiffened connections, the centre of compression is not located into the mid thickness of the beam flange in compression, but it is shifted below, thus increasing the lever arm.
- The centre of compression can be conservatively assumed into the centroid of the T section of the compressed zone, namely the section made of the beam flange and the rib stiffener at end-plate face, thus confirming the findings by Abidelah et al. (2012).
- Calculating the bending strength of ES joints considering the compression center located in the beam flange leads to a conservative design of the joints and higher material consumption. In particular, considering the actual position of center of compression is beneficial for the design of the column web panel. Indeed, lower design shear forces can be considered thus reducing the need to use supplementary web plates.
- The ductility criterion of EN1993:1-8 has been revised in light of Eurocode 8 philosophy and a novel design equation has been derived to avoid mode 3 and to enforce ductile behaviour of ES joints by controlling the maximum thickness of the end-plate related to the diameter of bolts.
- The contribution of bolt rows below the symmetry axis of the connection can be neglected without affecting the prediction of strength.
- Experimental tests confirmed the effectiveness of the proposed design rules.

5 ACKNOWLEDGEMENTS

The research leading to these results has received funding from the European Union's Research Fund for Coal and Steel (RFCS) research programme under grant agreement n° RFSR-CT-2013-00021.

The Authors thank also the financial support of the RELUIS project "Linea di Ricerca Acciaio e Composte Acciaio-Calcestruzzo" 2014-2015, 2015-2016 and 2016-2017.

6 REFERENCES

- Abidelah A., Bouchaïr A., Kerdal D.E. (2012) "Experimental and analytical behavior of bolted end-plate connections with or without stiffeners". *Journal of Constructional Steel Research* 76, 13–27.
- Adey B. T., Grodin G. Y., Chenye J. J. R. (1998). "Extended endplate moment connections under cyclic loading". *Journal of Constructional Steel Research*, 46(1–3), 435–436.
- Adey B. T., Grondin G. Y., Cheng J. J. R. (2000). "Cyclic loading of end plate moment connections". *Canadian Journal of Civil Engineering*, 274, 683–701.

- Agerskov H. (1977). "Analysis of bolted connections subject to prying". *Journal of Structural Engineering*, Div. ASCE, 103(11): 2145–2163.
- Aggarwal A. K. (1994). "Comparative test on endplate beam-to-column connections". *Journal of Constructional Steel Research*, 30, 151–175.
- ANSI/AISC 341-16 (2016). "Seismic Provisions for Structural Steel Buildings". American Institute of Steel Construction.
- ANSI/AISC 358-16 (2016). "Prequalified Connections for Special and Intermediate Steel Moment Frames for Seismic Applications".
- Beg D., Zupanè E., Vayas I. (2004). "On the rotation capacity of moment connections". *Journal of Constructional Steel Research*, 60, 601–620.
- Bjorhovde R. (2004). "Deformation considerations for connection performance and design". *Proceedings of the Fifth International ECCS/AISC Workshop on Connections in Steel Structures: Innovative Steel Connections* (Eds.: F.S.K. Bijlaard, A.M. Gresnigt and G.J. van der Vegte), Amsterdam, 11–20.
- Cassiano D., D'Aniello M., Rebelo C. (2017) "Parametric finite element analyses on flush end-plate joints under column removal". *Journal of Constructional Steel Research*, 137: 77–92.
- Ciutina A. L., Dubina D. (2008). "Column Web Stiffening of Steel Beam-to-Column Joints Subjected to Seismic Actions". *Journal of Structural Engineering*, 134(3), 505–510.
- D'Aniello M., Tartaglia R., Costanzo S., Landolfo R. (2017). "Seismic design of extended stiffened end-plate joints in the framework of Eurocodes". *Journal of Constructional Steel Research*, 128, 512–527. doi: 10.1016/j.jcsr.2016.09.017
- D'Aniello M., Cassiano D., Landolfo R. (2016). "Monotonic and cyclic inelastic tensile response of European preloadable gr10.9 bolt assemblies". *Journal of Constructional Steel Research*, 124, 77–90.
- D'Aniello M., Cassiano, D., and Landolfo, R. (2017) "Simplified criteria for finite element modelling of European preloadable bolts". *Steel and Composite Structures, An International Journal*, 24(6): 643–658.
- Douty R. T., McGuire W. F. (1965). "High strength bolted moment connections". *Journal of structural division, ASCE*, 91(4), 101–128.
- Elnashai A., Elghazouli A.Y. (1994). "Seismic behaviour of semi-rigid steel frames". *Journal of Constructional Steel Research*, 29, 149–174.
- EN 1993-1-8, Design of steel structures - Part 1-8: Design of joints
- EN 1998-1, Design of structures for earthquake resistance - Part 1: General rules, seismic actions and rules for buildings
- FEMA (2000a), FEMA-350, "Recommended Seismic Design Criteria for New Steel Moment Frame Buildings", Federal Emergency Management Agency, Washington, DC.
- FEMA (2000b), FEMA-353, "Recommended Specifications and Quality Assurance Guidelines for Steel Moment Frame Construction for Seismic Applications", Federal Emergency Management Agency, Washington, DC.
- Frye M. J., Morris G. A. (1975). "Analysis of flexibility connected steel frames". *Canadian Journal of Civil Engineering*, 2(3), 280–291.
- Ghobarah A., Korol R. M., Osman A. (1992). "Cyclic behavior of extended end-plate joints." *Journal of Constructional Steel Research*, 118(5), 1333–1353.
- Gioncu V., Mateescu G., Petcu D., Anastasiadis A. (2000). "Prediction of available ductility by means of local plastic mechanism method: DUCTROT computer program". *Chapter 2.1 in Moment Resistant Connections of Steel Frames in Seismic Areas* (Ed.: F Mazzolani), E&FN Spon, 95–146.
- Girão Coelho A.M. (2004). "Characterization of the ductility of bolted end plate beam-to-column steel connections". PhD Thesis, University of Coimbra.
- Guo B.; Gu Q., Liu F. (2006) "Experimental Behavior of Stiffened and Unstiffened End-Plate Connections under Cyclic Loading". *Journal of Structural Engineering*, 132(9), 1352–1357.
- Jaspert J.P. (1997). "Contributions to recent advances in the field of steel joints – column bases and further configurations for beam-to-column joints and beam splices". Professorship Thesis, University of Liège.

- Korol R. M., Ghobarah A., Osman A. (1990). "Extended endplate connections under cyclic loading: behavior and design". *Journal of Constructional Steel Research*, 16(4), 253–280.
- Krishnamurthy N. (1978). "A fresh look at bolted endplate behaviour and design". *Eng. J.*, 15(2), 39–49.
- Kukreti A. R., Ghassemieh M., Murray T. M. (1990). "Behavior and design of large capacity moment endplates". *Journal of Structural Engineering*, 116(3), 809–828.
- Lee C-H. "Seismic Design of Rib-Reinforced Steel Moment Connections based on Equivalent Strut Model". *Journal of Structural Engineering*, ASCE, Vol. 128, No. 9, September 1, 2002.
- Lee C.-H. Jung J.-H., Oh M.-H., Koo E.-S. "Experimental Study of Cyclic Seismic Behavior of Steel Moment Connections Reinforced with Ribs". *Journal of Structural Engineering*, ASCE, Vol. 131, No. 1, January 1, 2005
- Leon R.T. (1995). "Seismic Performance of Bolted and Riveted Connections. Background Reports: Metallurgy, Fracture Mechanics, Welding, Moment Connections and Frame System Behavior", Report No SAC-95-09, FEMA-288 / March 1997, Federal Emergency Management Agency, Washington, DC.
- Nair, R. S., Birkemoe, P. C., and Munse, W. H. (1974). "High strength bolts subject to tension and prying". *Journal of Structural Engineering*. Div. ASCE, 100(2), 351–372.
- Mann, A. P., and Morris, L. J. (1979). "Limit design of extended endplate connections". *Journal of Structural Engineering*, Div. ASCE, 105(3), 511–526.
- Murray T.M. and Kukreti A.R. (1988). "Design of 8-Bolt Stiffened Moment End Plates". *Engineering Journal*, AISC, Second Quarter, 45-52.
- P-398. "Joints in Steel Construction: Moment-Resisting Joints to Eurocode 3". The Steel Construction Institute and The British Constructional Steelwork Association, 2013.
- Sherbourne, A. N. (1961). "Bolted beam-to-column connections". *Journal of Structural Engineering*, 39(6), 203–210.
- Shi Y., Shi G., Wang Y. (2007) "Experimental and theoretical analysis of the moment–rotation behaviour of stiffened extended end-plate connections". *Journal of Constructional Steel Research*, 63, 1279–1293.
- Shi G., Shi Y., Wang Y. (2007) "Behaviour of end-plate moment connections under earthquake loading". *Engineering Structures* 29, 703–716.
- Sumner E.A., Murray T.M. (2004) "Extended End-Plate Moment Connections Seismic and Wind Applications. Design Guide 4", 2nd Edition, American Institute of Steel Construction, Inc.
- Sumner E.A., Mays T.W., Murray T.M. (2000). "Cyclic testing of bolted moment end-plate connections". Research report SAC/BD-00/21. CE/VPI-ST 00/03. Blacksburg (VA): Department of Civil and Environmental Engineering, Virginia Polytechnic Institute and State University; 2000.
- Tartaglia R., D'Aniello M. (2017). "Nonlinear performance of extended stiffened end plate bolted beam-to-column joints subjected to column removal". *Open Civil Engineering Journal*, 11 (Suppl-1, M6): 369-383.
- Tsai K. C., Popov E. P. 1990. "Cyclic behavior of end-plate moment connections." *Journal of Structural Engineering*, 116(11), 2917–2930.
- Wang Y., Zhang H. Y., Li H. J. (2001). "Experimental research on semi-rigid steel beam-to-column joints under cyclic loading". *Proc., 6th Pacific Structural Steel Conf., Vol. 2*, Beijing, 800–807.
- Weynand K., Jaspert J.P., Steenhuis M. (1995). "The stiffness model of revised Annex J of Eurocode 3". *Proceedings of the Third International Workshop on Connections in Steel Structures III, Behaviour, Strength and Design* (Eds.: R Bjorhovde, A Colson and R Zandonini), Trento, 441–452
- Whittaker D., Walpole W. R. (1982). "Bolted endplate connections for seismically designed steel frames." Research Rep. No. 82-11, Dept. of Engineering, Univ. of Canterbury, New Zealand.
- Witteveen J., Stark J. W., Bijloord, F. S., and Zoetemeijer, P. (1982). "Welded and bolted beam-to-column connections". *Journal of Structural Engineering*, Div. ASCE, 108(2), 433–455.
- Zoetemeijer P. "Semi-rigid bolted beam-to-column connections with stiffened column flanges and flush-end plates". In: Howlett JH, Jenkins WM, Stainsby R, editors. *Joints in structural steelworks*. London: Pentech Press; 1981. p. 2.99–2.118.
- Zoetemeijer P. (1990). "Summary of the research on bolted beam-to-column connections". Report 25-6-90-2, Faculty of Civil Engineering, Stevin Laboratory – Steel Structures, Delft University of Technology.

SEISMIC DESIGN OF FULL-STRENGTH FULL-DUCTILITY EXTENDED END PLATE BEAM-TO-COLUMN JOINTS

Vincenzo Piluso^a, Gianvittorio Rizzano^a, Massimo Latour^a,
Antonella Bianca Francavilla^a

^a *University of Salerno, Italy, v.piluso@unisa.it, g.rizzano@unisa.it, mlatour@unisa.it,
afrancavilla@unisa.it*

ABSTRACT

The analysis and modelling of the ultimate behaviour of the beam-to-column connections is certainly one of the most studied topics in the field of steel structures. In particular, seismic design of steel frames is commonly carried out to assure the dissipation of the seismic input energy in the so-called “dissipative zones” which have to be properly detailed in order to assure wide and stable hysteresis loops. Once avoided the yielding of columns, beam-to-column joints play a role of paramount importance. In fact, beam-to-column joints can be designed either as Full Strength (FS) or Partial Strength (PS). In the first case, the seismic input energy is dissipated by means of plastic cyclic excursions of the beam ends. In the second case, dissipation requires the plastic engagement of ductile joint components. This work addresses the design criteria to be adopted to assure a full-strength full-ductility behaviour of Unstiffened Extended End-Plate (U-EEP) beam-to-column joints. The validation of the design procedure is accomplished by three-dimensional finite element analyses with ABAQUS 6.13 software. Finally, in order to clarify the design procedure in detail, a worked numerical example concerning the design of an external joint is handed out.

KEYWORDS

Full strength connections, extended endplate, ductility

1 INTRODUCTION

Within the analysis of steel structures, the modelling of the ultimate behaviour of beam-to-column joints is one of the most studied topic. As well known, before the introduction of the concept of semi-rigidity [1,2], steel frame design was accomplished by properly considering a limit assumption regarding the joint behaviour. Depending on the beam-to-column joint typology, it can be either assumed that all the ends of the members converging in the joint are subjected to the same rotation and the same displacements or assumed that the joints are able to permit free rotations. The first case leads to continuous frames, while the second one to pinned frames. The application of the semi-rigidity concept has required the development of a general methodology working out in detail the provision of the rotational stiffness and the flexural resistance of joints. This resulted in a strong effort, in Europe more than in United States, which has led to the complete definition and codification of the component method [3,4]. This allows the analysis of actual semi-continuous structural systems, starting from the geometrical and mechanical properties of beam-to-column joints.

The component method is essentially based on mechanical models constituted by the assembling of spring elements modelling the joint components. The non-linearity of the joint moment-rotation response is obtained starting from the inelastic constitutive laws adopted for the components. The method is suitable for the modelling of any kind of joint provided that the components are properly identified and their constitutive law is deservedly modelled.

Even though some authors have already investigated some aspects related to the prediction of the plastic deformation capacity [5-8] and of the cyclic behaviour of connections [9-13] past experimental and theoretical researches have often focused their attention mainly on the prediction of the stiffness and resistance of joint components. Therefore, the prediction of the plastic deformation capacity of connections is still an open research field whose primary aim is devoted to the prediction of the plastic rotation capacity of partial strength connections.

Moreover, it cannot be denied that the classification of beam-to-column joints as full-strength or as partial-strength is too simplistic, because it is rigorous only in the pure theoretical case in which both the joint and the connected member exhibit a perfectly plastic behaviour. As soon as the distinction between the joint and the connection is made (Figure 1), allowing the definition of the joint as the combination in series of the connection and the panel zone of the column web, also the concept of beam-joint system becomes noticeable, being constituted by the combination in series of the beam-to-column joint and the beam end.

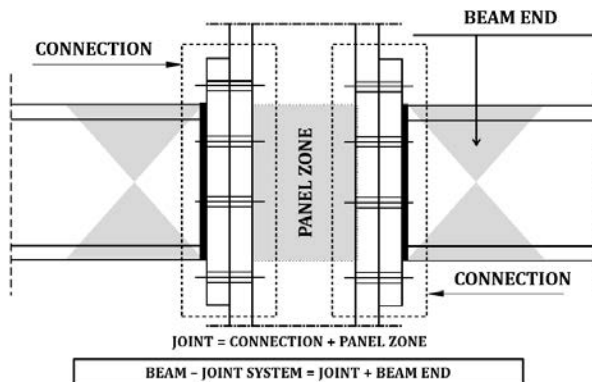


Figure 1. Beam-joint system.

This concept is of primary importance under the point of view of yielding location and, therefore, for seismic design purposes. This statement can be easily explained considering a tri-linear modelling of the moment-rotation curve of both the beam-to-column joint and the beam end (Figure 2). In fact, generally the plastic rotation supply Θ_{pu} of the beam-joint system can be regarded as the sum of two contributions: the plastic rotation of the beam-to-column joint φ_p and the plastic rotation provided by the beam end ϑ_p . Therefore, an accurate evaluation of the moment-rotation curve of the beam-to-column joint is required, because the plastic rotation provided by the beam end is strictly dependent on the flexural resistance that the beam-to-column joint is able to develop [14].

Concerning beam-to-column joint, $M_{j,y}$ is the value of the bending moment leading to first yielding, $M_{j,p}$ is the conventional plastic moment defining the knee of the moment-rotation curve according to Eurocode 3, $M_{j,u}$ is the theoretical ultimate flexural resistance of the beam-to-column joint. Regarding the beam, sM_{pb} is the bending moment corresponding to the occurrence of local buckling of the beam compressed flange.

The parameter s is the non-dimensional buckling stress depending on the width-to-thickness ratios of the plate elements constituting the beam section and on the longitudinal stress gradient. Starting from the analysis of the experimental data [15,16], by means of a multiple regression analysis, Mazzolani and Piluso [17] defined the following empirical relationship:

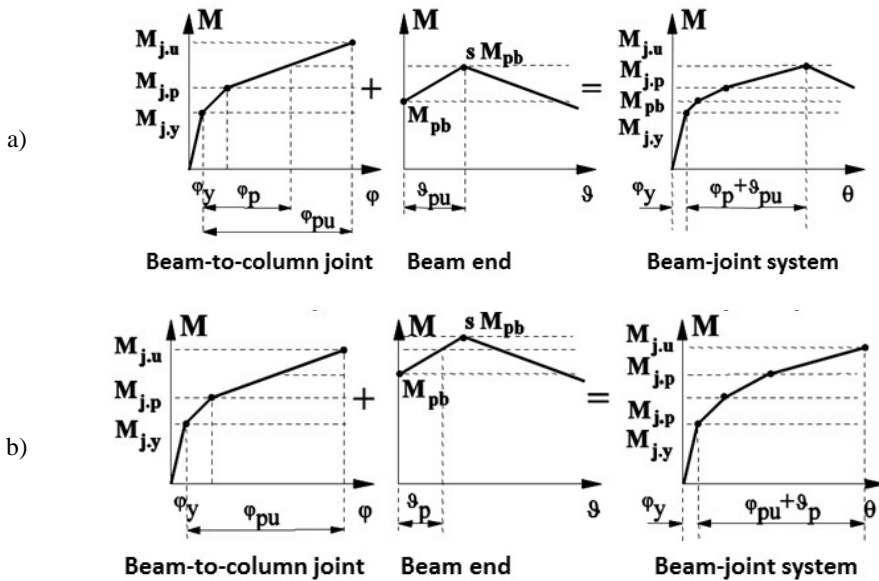
$$s = \frac{1}{0.546321 + 1.632533\lambda_f^2 + 0.062124\lambda_w^2 - 0.602125\frac{b_f}{L_e} + 0.001471\frac{E}{E_h} + 0.007766\frac{\varepsilon_h}{\varepsilon_y}} \leq \frac{f_u}{f_y} \quad (1)$$

where λ_f and λ_w are, respectively, the normalized slenderness parameters of the flange and of the web equal to:

$$\lambda_f = \frac{b_f}{2 t_f} \sqrt{\frac{f_{ym.f}}{E}} \quad \text{and} \quad \lambda_w = \frac{d_w}{2 t_w} \sqrt{\frac{f_{ym.w}}{E}} \quad (2)$$

where b_f is the flange width, t_f is the flange thickness, d_w is the compressed part of the beam web, t_w is the web thickness, L_e is the shear length of the beam, E is the Young modulus, E_h is the hardening modulus, ε_y is the strain corresponding to yielding and ε_h is the strain corresponding to the end of the yield plateau.

Four significant cases can arise [14] (Figure 2):



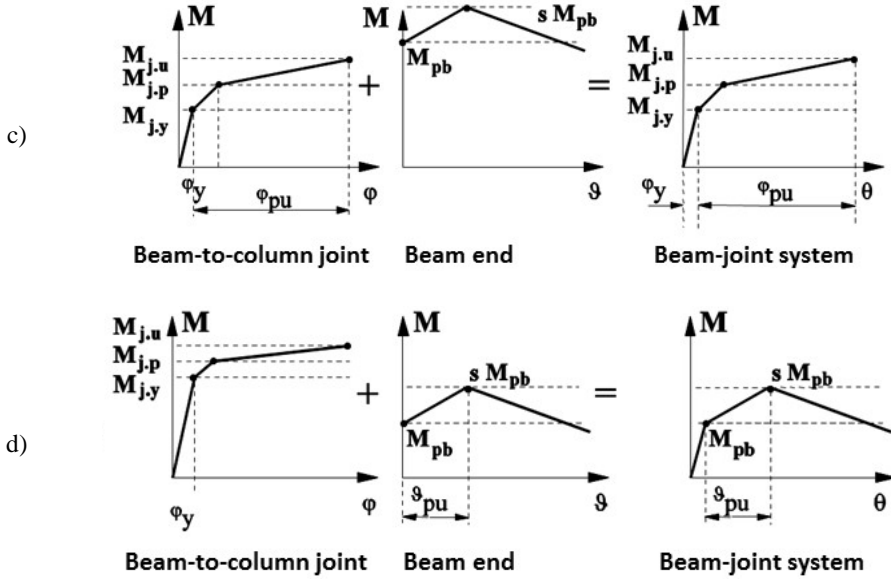


Figure 2. Plastic rotation supply of the beam-joint system [14].

a) $M_{j,u} \geq s M_{pb}$

In this case the ultimate resistance of the beam-to-column joint allows the complete exploitation of the beam plastic reserves, so that:

$$\vartheta_p = \vartheta_{pu} \quad \text{and} \quad \varphi_p \leq \varphi_{pu} \quad (3)$$

where ϑ_{pu} is the ultimate plastic rotation of the beam and φ_{pu} is the theoretical value of the ultimate plastic rotation of the beam-to-column joint.

Therefore, the plastic rotation supply of the beam-joint system is given by the sum of the beam plastic rotation supply and a part, for $M_{j,u} > s M_{pb}$, or the total value, for $M_{j,u} = s M_{pb}$, of the plastic rotation supply of the beam-to-column joint. As the plastic rotation supply of the beam-joint system is greater than the plastic rotation capacity of the connected beam, the beam-to-column joints can be defined as full-strength full-ductility.

b) $M_{pb} \leq M_{j,u} < s M_{pb}$

In this case, even though the beam end can be engaged in plastic range, the ultimate resistance of the beam-to-column joint is not sufficient to completely exploit the beam plastic reserves, so that:

$$\vartheta_p < \vartheta_{pu} \quad \text{and} \quad \varphi_p = \varphi_{pu} \quad (4)$$

Therefore, the plastic rotation supply of the beam-joint system is given by the sum of the plastic rotation supply of the joint and of a part of that of the connected beam. The beam-to-column joint can be defined as full-strength (because $M_{j,u} > M_{pb}$), but cannot be defined “a priori” as full-ductility, because the plastic rotation capacity of the beam-joint system is strictly dependent on the contribution (φ_{pu}) due to the beam-to-column joint.

c) $M_{j,u} \leq M_{pb}$

In this case, the ultimate resistance of the beam-to-column joint is not sufficient to engage the beam in plastic range, so that:

$$\vartheta_p = 0 \quad \text{and} \quad \varphi_p = \varphi_{pu} \quad (5)$$

Therefore, the ultimate plastic rotation of the beam-joint system is coincident with the plastic rotation of the beam-to-column joint. The beam-to-column joint can be defined as partial-strength. Nothing can be said, a priori, about on the degree of restoration of rotation capacity, because the plastic rotation capacity of the beam-joint system is strictly dependent on φ_{pu} .

d) $M_{j,y} > sM_{pb}$

In this case, the elastic flexural resistance is sufficient to completely exploit the plastic reserves of the beam, so that:

$$\vartheta_p = \vartheta_{pu} \quad \text{and} \quad \varphi_p = 0 \quad (6)$$

Consequently, the plastic rotation of the beam-joint system is equal to the plastic rotation of the beam end. The beam-to-column joint can be referred as full-strength full-ductility. The difference with respect to case a) is that the beam-to-column joint remains in elastic range ($\varphi_p = 0$).

Regarding the evaluation of the plastic rotation of the beam end, simple relations are available in literature [18-21]. In addition, the plastic rotation of the beam-to-column joints can be determined starting to the knowledge of the plastic deformation of each component, through an advanced modelling of their force-displacement law (up to the ultimate displacement). In fact, the plastic displacement occurring at the tensile flange level is equal to the sum of the ultimate displacement of the weakest component and of the contributions of the other components. The resulting plastic rotation is given by the ratio of that such plastic displacement and the level arm [14].

2 CAPACITY DESIGN OF BEAM-TO-COLUMN JOINTS

The seismic design of beam-to-column joints is traditionally aimed to assure that yielding occurs at the beam ends of the connected beam where the dissipation of the earthquake input energy is expected relying on wide and stable hysteresis loops. To this aim, Eurocode 8 [22] requires that the degree of overstrength required is guaranteed in case of full penetration butt welds or satisfying, in case of other joint typologies, the following relationship:

$$M_{j,Rd} > 1.1 \cdot \gamma_{ov} \cdot M_{b,Rd} \quad (7)$$

where $M_{j,Rd}$ represents the joint design resistance, $M_{b,Rd}$ the plastic moment of the connected beam and γ_{ov} is an overstrength factor accounting for the random variability of the steel yield strength, while the coefficient 1.1 covers the effects of material strain hardening. Eurocode 8 recommends the use of $\gamma_{ov} = 1.25$; conversely, the Italian code [23] suggests a joint overstrength coefficient depending on the steel grade ($\gamma_{ov} = 1.20$ for S235, $\gamma_{ov} = 1.15$ for S275 and $\gamma_{ov} = 1.10$ for S355).

One of the causes of significant and premature joint damage during the seismic events of Northridge and Kobe can be recognised in the use of design criteria not able to assure a sufficient degree of overstrength to allow the full development of the beam plastic rotation capacity. In fact, regarding the overstrength which the beam is able to exhibit, due to strain hardening, it depends on the width-to-thickness ratios of flanges and web. As a consequence, the joint overstrength needed to assure the full-strength requirement is strictly related to the

behavioural class of the beam section (i.e. ductile, compact, semi-compact and slender). It means that, decreasing the width-to-thickness ratios of flanges and web, the plastic deformation capacity of the beam increases, but this beneficial effect could be vanished if the beam-to-column joint does not possess the overstrength required by the simultaneous increase of the beam ultimate resistance. In addition, also the influence of random material variability both on the beam flexural resistance and the beam-to-column joint moment resistance has to be properly accounted for.

Only a few studies concerning the influence of random material variability on the behaviour of steel connections are available [24-27]. In particular, it has been proposed [24] to formulate the design requirement for full-strength and full-ductility joints by means of a probabilistic approach calibrated on the basis of the results coming from Monte Carlo simulations [28], including both the random material variability of the plate elements and that of bolt properties [29].

A simplified approach to account for the influence of random material variability is herein proposed by assuming an overstrength factor $\gamma_{ov,rm}$ equal to the ratio between the average value of the yield strength of beam flanges $f_{ym,bf}$ and the nominal yield strength $f_{y,b}$. Conversely, the amount of overstrength due to the development of strain-hardening up to the occurrence of local buckling is taken into account directly considering the width-to-thickness ratios of beam flanges and web. Therefore, the ultimate beam flexural resistance at the plastic hinge location is evaluated as:

$$M_{b,u} = \gamma_{ov,rm} \cdot \gamma_{ov,sh} \cdot \gamma_{M0} \cdot M_{b,p} \quad (8)$$

where:

$$M_{b,p} = \frac{Z_b \cdot f_{y,b}}{\gamma_{M0}} \quad (9)$$

being Z_b the plastic modulus of the beam section and γ_{M0} the partial safety factor.

The average yield strength of beam flanges is evaluated accounting for the influence of the flange thickness t_{bf} , so that:

$$\gamma_{ov,rm} = \frac{f_{ym,bf}}{f_{y,b}} = \frac{f_0 - \beta t_{bf}}{f_{y,b}} \quad (10)$$

where the parameters f_0 and β depend on the steel grade (Table 1).

Table 1. Mechanical properties of the material.

Steel classes	f_0 [MPa]	β [MPa/mm]	$\frac{E}{E_h}$	$\frac{\epsilon_h}{\epsilon_y}$
S 235	313.4	2.254	37.5	12.3
S 275	323.3	0.910	42.8	11.0
S 355	444.2	2.987	48.2	9.8

The coefficient $\gamma_{ov,sh}$ accounting for the influence of strain hardening is given by $\gamma_{ov,sh} = s$ [17], where s is the parameter given by Eq. (1).

3 DESIGN PROCEDURE FOR FULL-STRENGTH FULL-DUCTILITY JOINTS

Starting from the average ultimate resistance of the beam provided by Eq. (8), a design procedure aiming to the development of full-strength full-ductility joints is proposed and discussed with reference to extended end-plate joints with four bolts in tension. The end-plate is unstiffened. The design goal is accomplished by properly applying the basic principles of "capacity design" at component level, considering all the joint components defined by Eurocode 3 within the framework of the "component method".

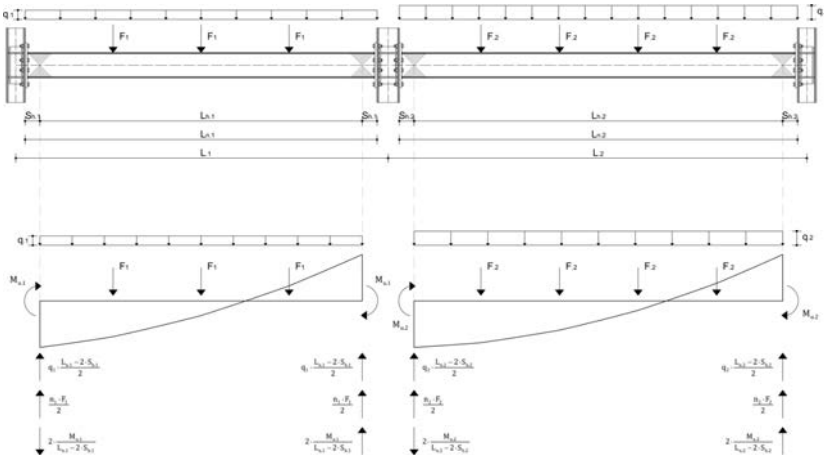


Figure 3. Reference structural scheme considering seismic actions from left to right.

In particular, the proposed procedure starts from the identification of the maximum internal actions which the fully yielded and strain-hardened beam is able to transmit to the joint. The reference structural scheme is depicted in Fig. 3. By denoting with i the left end joint and with j the right end joint for each beam and considering seismic actions from left to right, the shear action occurring at the plastic hinge locations are given by:

$$\begin{aligned}
 V_{bu.i}^{(1)} &= \frac{q_1 L_{h1}}{2} + \frac{n_{F1} F_1}{2} - \frac{2 M_{bu.1}}{L_{h1}} & V_{bu.j}^{(1)} &= \frac{q_1 L_{h1}}{2} + \frac{n_{F1} F_1}{2} + \frac{2 M_{bu.1}}{L_{h1}} \\
 V_{bu.i}^{(2)} &= \frac{q_2 L_{h2}}{2} + \frac{n_{F2} F_2}{2} - \frac{2 M_{bu.2}}{L_{h2}} & V_{bu.j}^{(2)} &= \frac{q_2 L_{h2}}{2} + \frac{n_{F2} F_2}{2} + \frac{2 M_{bu.2}}{L_{h2}}
 \end{aligned}
 \tag{11}$$

where the vertical loads are those occurring in the seismic load combination ($G_k + \psi_2 Q_k$) according to Eurocode 8, L_h is the distance between the two plastic hinges, F are the concentrated forces due to the secondary beams and n_F is the number of these forces. The parameter s_h , i.e. the distance between the plastic hinge and the column flange, is taken equal to the beam height.

On the basis of the maximum moment which the beams are able to transmit given by Eq. (8), the bending moment M_{cf} and shear action V_{cf} at the column flange can be evaluated as follows:

- in the case of external joint i of beam 1:

$$M_{cf.i}^{(1)} = M_{bu.1} - V_{bu.i}^{(1)} \cdot S_{h1} - \frac{q_1 S_{h1}^2}{2} \quad V_{cf.i}^{(1)} = V_{bu.i}^{(1)} + q_1 S_{h1} \quad (12)$$

- in the case of internal joint j of beam 1:

$$M_{cf.j}^{(1)} = M_{bu.1} + V_{bu.i}^{(1)} \cdot S_{h1} + \frac{q_1 S_{h1}^2}{2} \quad V_{cf.j}^{(1)} = V_{bu.j}^{(1)} + q_1 S_{h1} \quad (13)$$

- in the case of internal joint i of beam 2:

$$M_{cf.i}^{(2)} = M_{bu.2} - V_{bu.i}^{(2)} \cdot S_{h2} - \frac{q_2 S_{h2}^2}{2} \quad V_{cf.i}^{(2)} = V_{bu.i}^{(2)} + q_2 S_{h2} \quad (14)$$

- in the case of external joint j of beam 2:

$$M_{cf.j}^{(2)} = M_{bu.2} + V_{bu.i}^{(2)} \cdot S_{h2} + \frac{q_2 S_{h2}^2}{2} \quad V_{cf.j}^{(2)} = V_{bu.j}^{(2)} + q_2 S_{h2} \quad (15)$$

Obviously, the analysis is repeated for the case of seismic actions from left to right and the most severe internal actions are considered.

Regarding the design of column web panel stiffeners, they have to be designed considering the maximum shear action occurring when the beams are in the ultimate conditions.

- In the case of panel zone of external joint i of first bay:

$$V_{wp.Ed} = \frac{M_{cf.i}^{(1)}}{d_{b1} - t_{bf.1}} - \frac{V_{c1} + V_{c2}}{2} \quad (16)$$

- In the case of panel zone of internal joint:

$$V_{wp.Ed} = \frac{M_{cf.j}^{(1)}}{d_{b1} - t_{bf.1}} + \frac{M_{cf.i}^{(2)}}{d_{b2} - t_{bf.2}} - \frac{V_{c1} + V_{c2}}{2} \quad (17)$$

- For the external panel zone j of the beam 2:

$$V_{wp.Ed} = \frac{M_{cf.j}^{(2)}}{d_{b2} - t_{bf.2}} - \frac{V_{c1} + V_{c2}}{2} \quad (18)$$

In the case of extended end plate connections with four bolts in tension, according to Eurocode 3, a simplified model can be adopted to design the tension zone by means on an equivalent T-stub whose lever arm is equal to $d_b - t_{bf}$ (Fig. 4).

According to this model, the design of all the joint components has to guarantee the transmission, at the beam flanges' levels, of a compression force C_u and of a tensile force T_u given by:

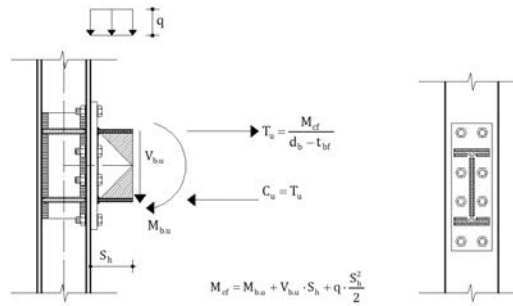


Figure 4. Simplified model for the design of the tension zone.

$$T_u = C_u = \frac{M_{cf}}{d_b - t_{bf}} \quad (19)$$

Starting from the knowledge of T_u and C_u values occurring when the beam plastic hinges have attained their ultimate flexural resistance, all the geometrical details of the connecting elements can be designed by means of the resistance formulations provided by Eurocode 3 for the joint components. To this aim, a specific sequence of design operations or resistance checks of the joint components has to be followed:

Step 1: Evaluation, by means of Eq. (8), of the average (because of random material variability) ultimate moment $M_{b,u}$ which the fully yielded and strain-hardened beam is able to transmit.

Step 2: Calculation of bending moment M_{cf} and shear action V_{cf} at the column flange and evaluation of compression force C_u and tensile force T_u to be transmitted at the beam flanges' levels.

Step 3: Design of the bolt diameter accounting for the combined action of shear and tension.

Step 4: Design of throat thickness of welds connecting the end-plate to the beam flange and design of throat thickness of welds connecting the end-plate to the beam web assuming that they have to transmit a bending moment proportional to the plastic modulus of the beam web alone.

Step 5: Design of the end-plate thickness according by modelling the tension zone by means of an equivalent T-stub and assuming that the distance m between the bolt axis and the yield line located close to the beam flange is equal to the minimum allowed by the code, $m=1.2 d_0$ with d_0 equal to the diameter of the hole; the width of the end-plate can be defined considering code requirements concerning the bolt spacing and the edge distances.

Step 6: Check of the resistance of the column web in shear and design of supplementary web plates if needed. Eurocode 3 introduces a limitation about the thickness of the supplementary plates. In particular, the shear area A_{vc} may be increased no more than $b_s t_{vc}$. If a further supplementary web plate is added on the other side of the web, no further increase of the shear area is allowed. The proposed method does not take into account such limitation.

Step 7: Check of the resistance of the column web in tension and in compression; if needed continuity plates are added and/or supplementary web plates are extended to cover also tension and compression zones.

Step 8: Check of the resistance of the column flange in bending; if not satisfied, backing plates can be adopted to increase the resistance of the equivalent T-stub modelling the column flange in bending, provided that type 1 mechanism occurs, otherwise (type 2 mechanism) the increase of the bolt diameter is needed and the procedure has to be repeated starting from step 3.

4 DESIGN EXAMPLES AND FINITE ELEMENT MODELLING

Reference is made to the layout depicted in Figure 5.

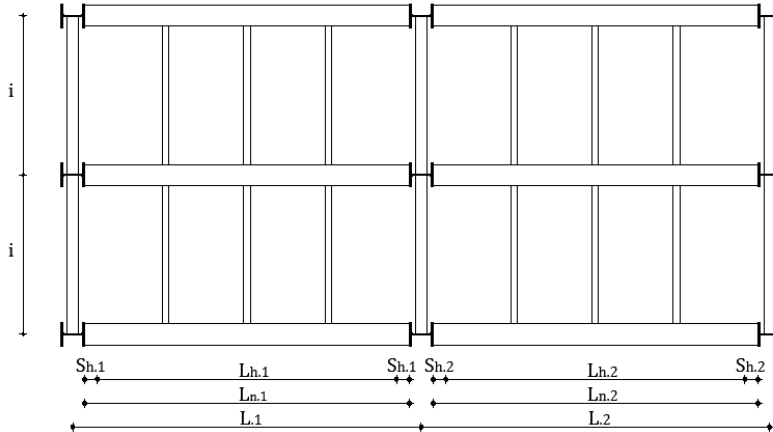


Figure 5. Building plan layout of study cases.

Three different solutions have been designed with reference to the external joint of the longitudinal inner frame by varying the geometry of the structure. In Table 2, the input data for the three cases analysed are summarized.

Table 2. Input data of case studies.

Study case	Beam section	Column section	Beam steel grade	Column steel grade	Plates steel grade	Bolt class	q [kN/m]	F [kN]	n_F	L_n [mm]
A	IPE 600	HEM 320					1.25	65	3	8641
B	IPE 450	HEM 260	S235	S355	S275	10.9	1.00	45	3	6232
C	IPE 220	HEM 200					0.75	30	3	3800

For the sake of simplicity the detailed calculations are not reported here and the main results obtained both with the proposed and with the EC8 design procedures are directly summarized in Table 3. Nevertheless, in order to clarify the proposed design method one of the cases, namely the case A, is described in detail in a worked example reported in Annex. From Table 3 it can be observed that the most important difference occurs for the case study C, i.e. in the case with the smallest beam size, where the design bending moment according to the proposed design procedure is about the 36.4% greater than the one required according to Eurocode 8. This difference reduces to the 26.5% for study case B and to 23.6% for study case A. It is worth to observe that this difference, in two cases out of three, exceeds the value of the partial safety factor $\gamma_{M2}=1.25$ suggested by EC8 for the design of bolts and welds and, therefore, it is expected that, in these cases, the EC8 design procedure may fail.

Table 3. Design solutions for analysed study cases.

	Study case A		Study case B		Study case C	
	Proposal approach	Eurocode 8 approach	Proposal approach	Eurocode 8 approach	Proposal approach	Eurocode 8 approach
$\gamma_{ov,rm}$	1.15	1.25	1.24	1.25	1.25	1.25
$\gamma_{ov,sh}$	1.28	1.10	1.26	1.10	1.30	1.10
$M_{cf}[kNm]$	1336	1081	663	524	120	88
$V_{cf}[kN]$	405	353	278	239	107	93
$T_u[kN]$	2299	1860	1524	1203	571	417
$d_b[mm]$	36	33	30	27	20	16
$a_f[mm]$	29	23	22	18	14	11
$a_w[mm]$	10	10	9	8	6	5
$t_{ep}[mm]$	55	45	45	35	25	20
$t_s[mm]$	5	-	5	-	5	-
$t_{cp}[mm]$	20	20	15	15	10	10
$a_{cp}[mm]$	8	8	6	6	4	4
$F_{(Rd.1)}/T_u$	2.79	3.56	2.94	3.73	1.67	2.29
$F_{(Rd.2)}/T_u$	1.18	1.39	1.22	1.41	1.03	1.08

In order to evaluate the accuracy of the examined design criteria, numerical simulations by means of advanced finite element models have been performed using ABAQUS 6.13 software. Since the behaviour of the analysed connections is strongly affected by in-plane and out-of-plane deformations, by contacts between the connecting elements and the profiles of column and beam and by geometrical and material non linearities, the finite element model has been developed adopting a three-dimensional approach based on the following steps: geometrical characterization of the components, definition of material properties, definition of the interactions between the elements, definition of the boundary conditions and choice of the elements and size of the mesh, calibration and application of a proper initial imperfection model.

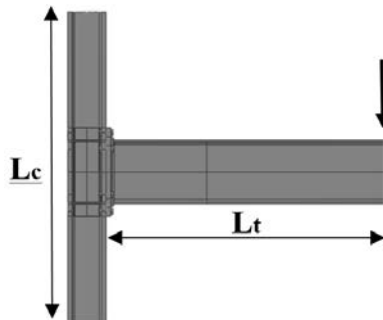


Figure 6. Analysed structural scheme.

The simulation has been performed considering the scheme depicted in Fig. 6, restrained with a hinge at the bottom end of the column and a roller with horizontal axis at the top end of the column. The beam end is loaded with a vertical force inducing in the joint a combination of shear and bending consistent with the actions arising in the reference scheme under seismic loads. To this aim, the length of the beam has been assumed equal to M_{cf}/V_{cf} , thus assuring that when the design bending resistance is attained also the corresponding shear action is achieved. The length of the column has been assumed equal to 3500 mm, i.e. the interstorey height of the sample building.

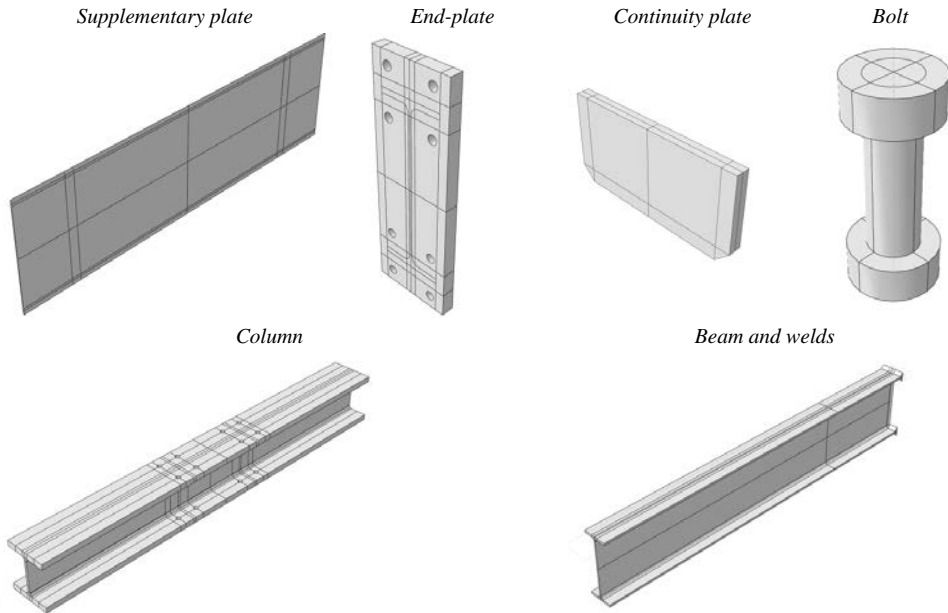


Figure 7. Components of the finite element model.

Regarding the *geometrical definition* of the components, the model is made up of seven repetitive elements: the column, the beam, the end plate, the bolts, the continuity plates and the additional supplementary web plates (Figure 7). The *material properties* of the plate elements and of the profiles have been described by means of an elastic-plastic isotropic model by adopting a quadrilinear true stress-true strain law (Figure 8a). The parameters for different constructional steels are given in Table 2.

The behaviour of the material of the bolts has been modelled using a simplified tri-linear model (Figure 8b) based on the yield and ultimate nominal strength according to the bolt class. The strain corresponding to the ultimate resistance and the ultimate strain have been evaluated by means of the following relationships: $\varepsilon_m = A_r$ [%] and $\varepsilon_u = \ln(1/1-Z)$, where A_r is elongation at fracture and Z is the necking ratio given by the ratio between the original cross-sectional area and the minimum cross-sectional area after fracture. The values provided by the manufacturer [30] have been adopted.

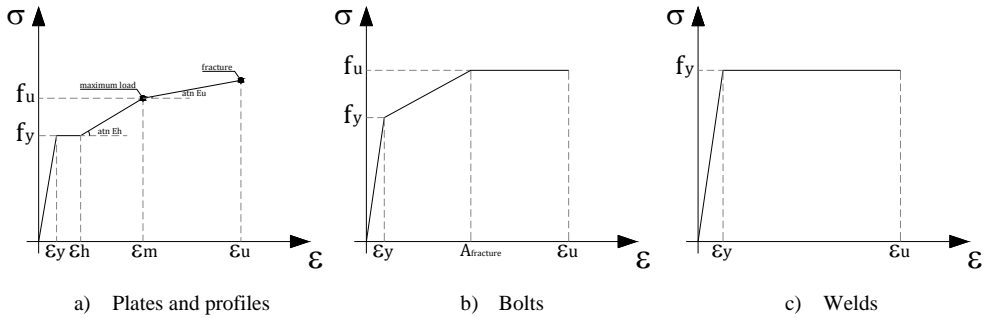


Figure 8. Material constitutive laws.

The welds have modelled by means of a bilinear elastic-perfectly plastic law (Figure 8c) with yield strength and ultimate strain defined according to [31].

Regarding the value of the yield strength of all the components, consistently with the design approach which accounts the influence of random material variability considering the average yield strength of the beam flanges, the average value of the yield strength has been adopted for the beam component, while for all others components the nominal characteristic value has been assumed.

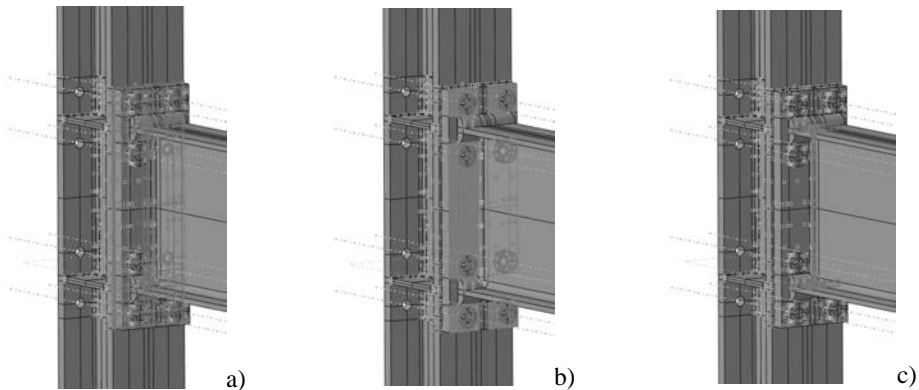


Figure 9. Definition of the contacts: a) end-plate/column flange; b) bolt head/end-plate; c) end-plate/beam end.

All the *interactions* between the different elements have been defined using the surface-to-surface contact formulation with finite sliding. In particular, the following interactions have been defined (Figure 9): between the end-plate and the column flange, between the bolt head and the end-plate, between the bolt shank and the plate hole, between the bolt shank and the column flange hole, between the end-plate and the beam end. In the normal direction a "hard contact" has been used, while in the tangential direction a friction coefficient equal to 0.20 has been adopted.

Where there was the need to link the rigid kinematic mechanisms of the section to those of a point externally restrained, the constraints have been modelled by introducing at the end of the section of the members a central node and "coupling internal constraints" (Figure 10a).

In order to simulate the application of an axial force, at the top of the column an external pressure equal to 30% of the yield strength of the material has been applied (Figure 10b).

Regarding the *finite element type*, in order to reduce the computational efforts, eight-node brick elements with reduced integration and first order approximation (C3D8R) have been adopted. The end part of the beam close to the column where local buckling phenomena are expected, for a length equal to 2.5 times the beam height, has been modelled with non linear eight-node brick elements with full integration (C3D8). Such elements, as also reported in [32], are particularly accurate for analysis where buckling effects are significant.

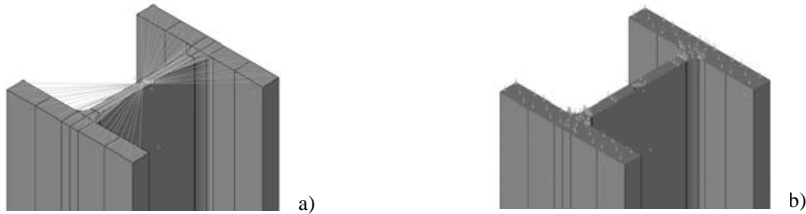


Figure 10. a) Coupling internal constrains; b) application of external pressure.

Preliminarily, a sensitivity analysis has been performed in order to determine the *mesh dimension*. The parameters that could influence the results are the number of the elements in the thickness of the plates, the dimension of the mesh of the bolts and the dimension of the elements where the local buckling is expected. In order to obtain accurate results, the following “meshing” procedure has been applied: where local buckling is expected the maximum dimension of the elements has been taken as 20 mm, the plates with elements whose dimension is at least 30 mm and with 2 elements in the thickness, the bolts have been divided using elements with minimum dimension equal to 6 mm with a deviation factor equal to 0.1.

In addition, *geometrical imperfections* have been introduced according to the requirements of EN10034 [34], by using a distorted shape of the joint similar to the 1st buckling mode preliminarily evaluated by means of an elastic buckling analysis. The calibration of the distortion of the model has been performed based on the maximum value of the angular distortion of the flanges of steel profiles given by EN 1090-2 [35]. The model finalized to the execution of the “linear buckling analysis” is depicted in Figure 11.

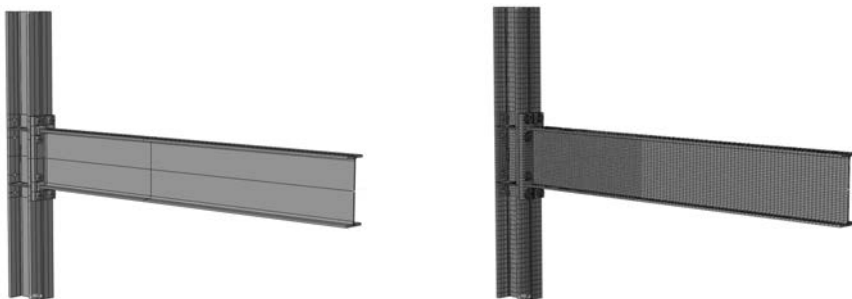


Figure 11. ABAQUS Model.

The results of the buckling analyses are reported in Figure 12 representing the first four buckling modes. In particular, because of the application of the load downwards, the first and the third buckling mode involve the combined buckling of the bottom flange and the

compressed part of the web. Similarly, the second and the fourth mode provide the buckling of the upper flange of the profile when the load is applied upward. Therefore, as the analyses developed in this paper are referred to monotonic downward loading conditions, an imperfection pattern proportional to first buckling mode has been introduced.

Following this approach, the proportionality coefficient $k_{1^{st}mode}$ for scaling the "buckling eigenmode" has been determined as the ratio between the 80% [33] of the maximum manufacturing tolerance (equal to 2% of the width of the flange [34]) and the sum of the beam flange tip displacements δ_f in the buckled configuration:

$$k_{1^{st}mode} = \frac{0.8 \times 0.02 \times b_f}{2 \times \delta_f} \quad (20)$$

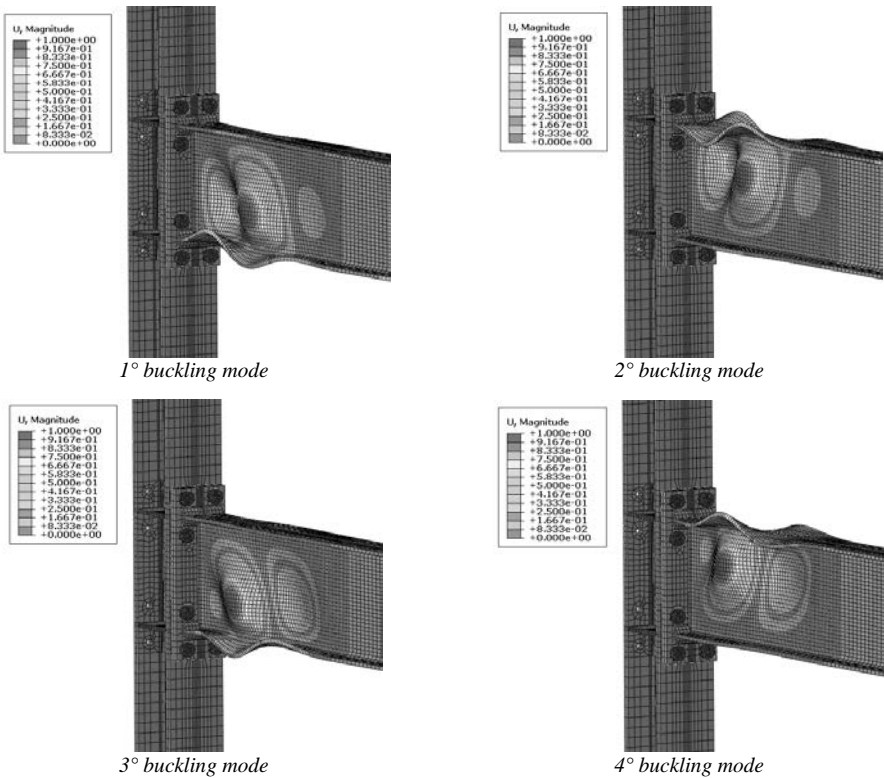


Figure 12. buckling modes of beam-to-column joints.

According to the design criteria adopted, it is expected that plastic deformations are mainly located at the beam end. Conversely, the connection components are expected to be subjected to very limited yielding. In fact, it should be noted that, even if the joints have been designed to attain full strength, limited yielding of joint components has to be expected because the formulas used for design, as suggested by Eurocode 3, are based on the definition of design plastic resistances rather than on elastic design resistances.

The finite element model has been validated through comparison with some experimental tests collected from technical literature. Specimens from two different experimental campaigns have been considered: a set of tests on full-strength connections described in [36] and a group of tests on partial-strength extended end-plate connections reported in [37]. The first group of data regards cases where the plastic engagement is mainly concentrated in the beam and it is used to check the model accuracy when the moment-rotation response of the beam-joint system is governed by the local buckling of the beam flange in compression. Conversely, the second group of data regards partial strength connections in which several joint components undergo plastic deformations. These data are used to check whether or not the FE model is able to reproduce accurately the response of the joint.

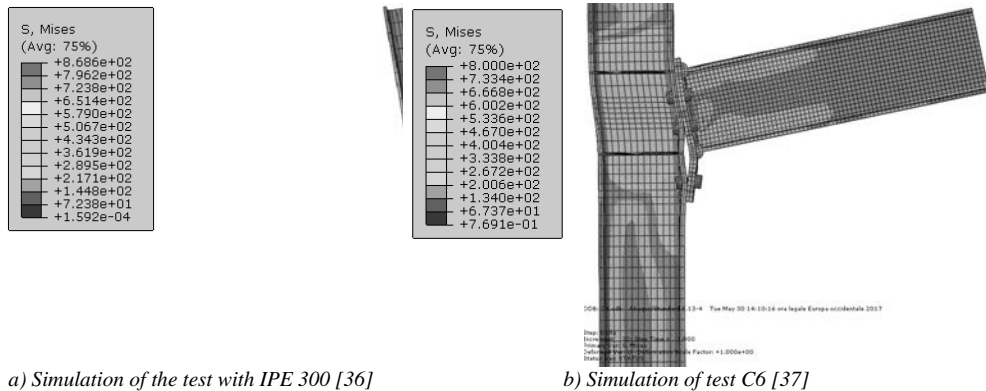


Figure 13. Examples of the developed validation FE models.

In particular, among the reference data of the first group [36], two cases have been selected, one regarding a connection fastening an IPE 300 beam, another regarding a HEB 240 profile, both made of S275 steel. These tests are non-uniform bending tests carried out under monotonic loading conditions. Conversely, among the data of the second group [37] four specimens of external beam-to-column joints have been selected, namely those identified in the original manuscript [37] as C5, C6, C7 and C8. They concern extended end-plate joints fastening rather shallow beams (UB 25.4) to columns with a relatively thin flange (UC 46.2). In these tests, the connection and the members are made of an Australian steel grade with nominal yield stress equal to 250 MPa and M20 or M16 bolts made up of a steel grade equivalent to the European 8.8 class. The connections are realized with a typology similar to that considered in this paper, namely with extended end-plate and two internal bolt rows. Case by case, the plates have thickness equal to 16 or 20 mm. The results of the validation study are summarized in Figs.13-15 and they evidence the good agreement between FE models and tests in all the considered cases. As it is possible to verify easily from the moment-rotation diagrams the model demonstrates to be able to follow with high accuracy the experimental results during the whole loading process, simulating accurately both the initial strain-hardening and the softening branch arising after the development of local buckling phenomena.

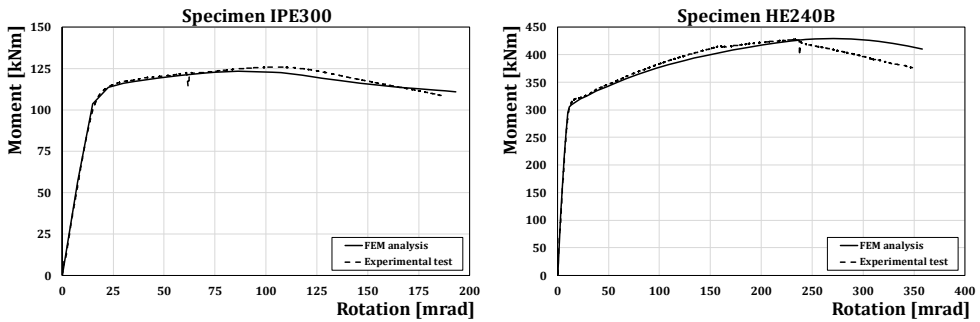


Figure 14. Comparison between experimental results [36] and finite element simulation.

In a similar way, the FE model proves to be able to simulate accurately the moment-rotation response of extended end-plate connections (cases C5-C8) when the joint components are engaged in plastic range (Fig.15). In particular, in the four considered cases the components mainly engaged in plastic range are the end-plate and column flange in bending, the shear panel and the bolts in tension and shear. Some minor yielding of the beam end is also occurring in all the considered cases.

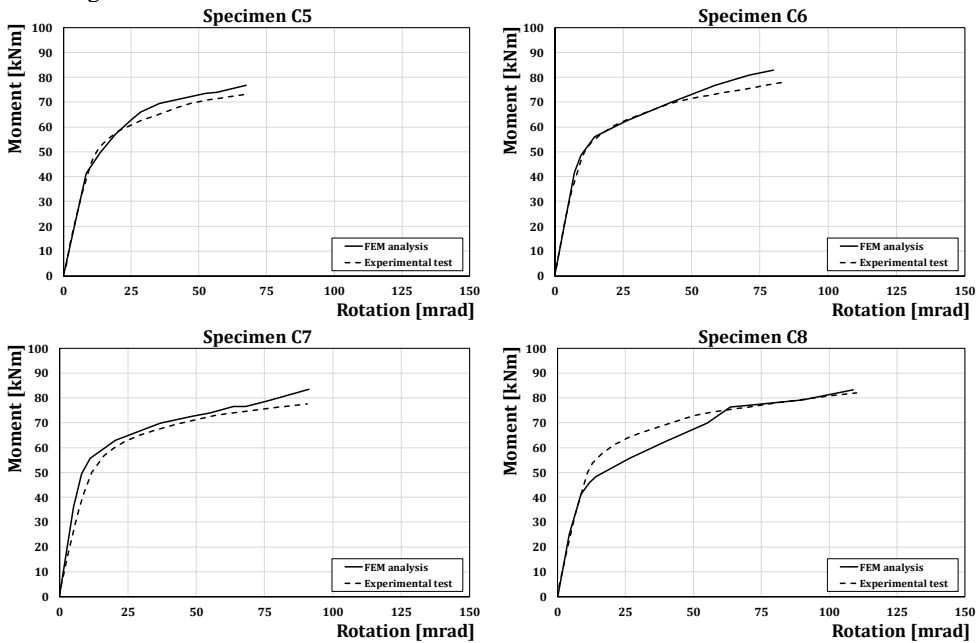


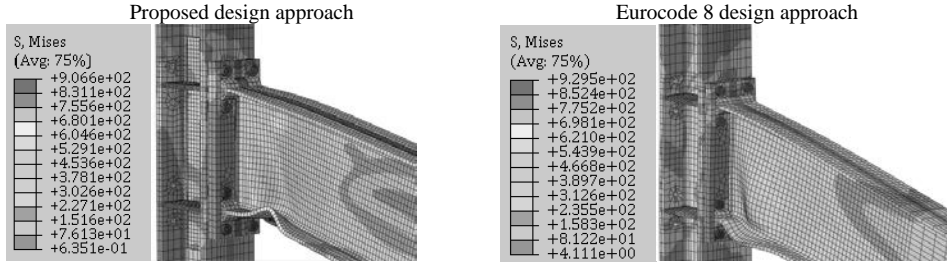
Figure 15. Comparison between experimental results [37] and finite element simulation.

5 RESULTS OF FINITE ELEMENT SIMULATIONS

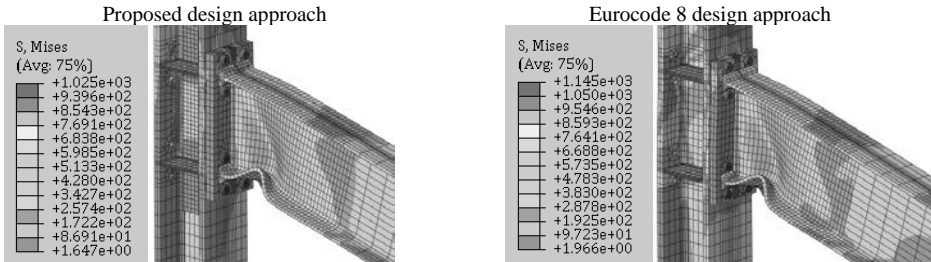
From the overall point of view, as expected, FE analyses showed in almost all the cases the concentration of the plastic deformations at the beam end where the plastic hinge,

characterized by the development of plastic local buckling of the compressed beam flange and out-of-plane buckling of the web, occurred.

STUDY CASE A: IPE 600 BEAM – HEM 320 COLUMN



STUDY CASE B: IPE 450 BEAM – HEM 260 COLUMN



STUDY CASE B: IPE 220 BEAM – HEM 200 COLUMN

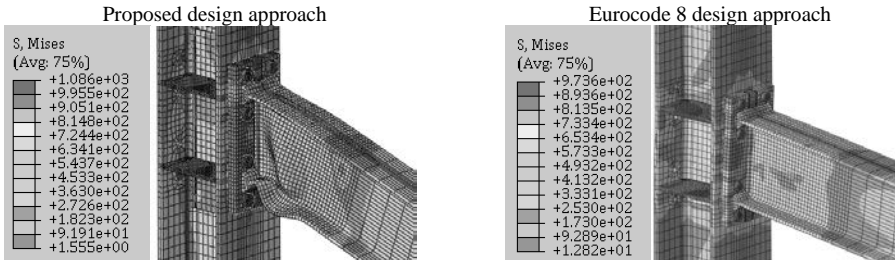


Figure 16. Ultimate behaviour of the analysed joints (Von Mises stresses).

The moment-rotation curves of the beam-joint system for all the analysed cases are represented in Figs. 17-19. The curves have been obtained, in all cases, by multiplying the force applied at the end of the cantilever for L_t (Fig.6) and dividing the displacement evaluated in the same point for the same length.

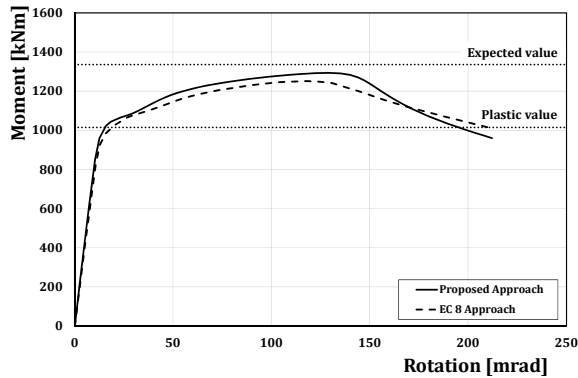


Figure 17. Moment-rotation curves (case A).

The curves reported in in Fig.17 are referred to study case A. As expected, after the initial linear behaviour, at the attainment of the plastic resistance of the section, they provide a non-linear response characterized by the increase of the bending moment, due to the material strain-hardening which continues up to the attainment of the local buckling of the beam compressed flange. The achievement of the maximum bending moment corresponds to the complete development of local buckling. The following softening branch is due to the post-buckling behaviour. In the two cases (EC8 and proposed procedure), as it is possible to check easily from the figure, the values are very similar and, in particular, equal to 1293 kNm (proposed approach) and 1251 kNm (EC8). These values are a little bit lower than the design value, evaluated at the column flange level, equal to 1336 kNm. Such scatter, with respect to the design value, is very low being less than 7%. It is mainly related to the accuracy of the empirical relationship (1) for evaluating $\gamma_{ov.sh} = s$.

With reference to the case study B, the shape of the moment-rotation curve is analogous to the previous case and the values of the moment corresponding to the complete development of local buckling of the beam flange are equal to 662 kNm and 666 kNm in case of the joint designed according to the proposed approach and to Eurocode 8, respectively. These values of the bending moment are practically equal to the design value (663 kNm) confirming the accuracy of the formulations used to predict the overstrength factor s (Figure 18).

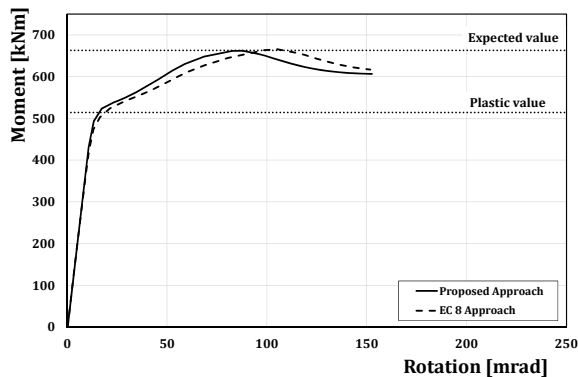


Figure 18. Moment-rotation curves (case B).

Similarly, in the study case C (Fig. 19) the local buckling is achieved in correspondence of a bending moment equal to 115 kNm and 113 kNm, respectively, in case of the joint designed according to the proposed approach and to Eurocode8. These values are slightly lower (about 7% and 8%, respectively) than the design value (equal to 123 kNm). In this case, regarding the ultimate rotation, it is useful to underline that the joint designed according to Eurocode 8, because of an abrupt drop of the flexural resistance, shows a rotation supply (131 mrad) significantly less than the one of the joint designed according to the capacity design criteria proposed.

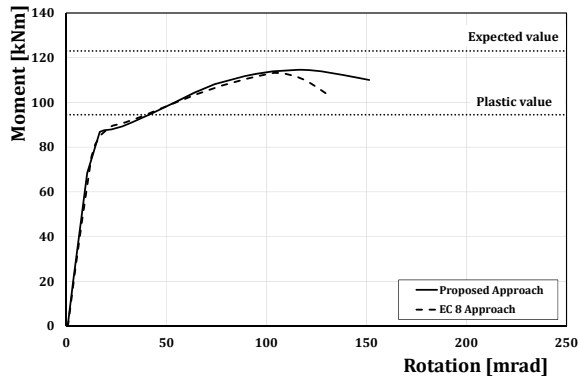


Figure 20. Moment-rotation curves (case C).

This difference is due to the brittle failure of the bolts connecting the end-plate to the column flange.

As a conclusion, the comparison between the moment-rotation curves of the joints designed according to the capacity design criteria herein proposed with those designed according to the EC8 provisions, shows that the differences can be very important, especially concerning the failure mode, in those cases where EC8 underestimation of the amount of strain-hardening leads to the bolt failure (case C), undermining significantly the rotation capacity of the beam-joint system. Even though such brittle behaviour is out of the design philosophy of EC8, it has been shown that it can actually occur because of the actual overstrength of the connected member, which can be significantly underestimated by the 1.10 factor adopted by EC8 (as reported in the 4th column of Table 3). It is important to underline that such brittle failure of the bolts may happen even if they are usually oversized adopting a partial safety factor equal to 1.25, according to EC3.

In any case, due to the fact that the EC8 procedure for connections is not completely rationally addressed, aside from the possible activation of undesired failure modes, in many cases, it also happens that the plastic engagement of the joint components is significant. This means that, in case of severe seismic events, the repair of many parts of the connection has to be accounted for. Conversely, the beam overstrength is more rationally considered by the use of the capacity design criteria proposed, so that all the joint components are sized for actions assuring a negligible plastic engagement.

In order to quantify the damage of the joints' components, a damage parameter defined as the ratio between the equivalent plastic deformation (PEEQ) evaluated at the achievement of the rotational capacity of the beam-joint system and the elastic deformation has been considered. To this scope, all the components have been isolated and the corresponding deformation maps

have been tracked in order to determine the value of the equivalent plastic deformation summarized, as summarized in the Tables 4-6.

Table 4. Damage to joint components expressed as PEEQ and NPEEQ (NPEEQ=PEEQ/ε_y) – study case A.

	Study case A			
	Proposal approach		Eurocode8 approach	
	PEEQ	NPEEQ	PEEQ	NPEEQ
Beam	0.3577	319.65	0.3577	319.65
Welds	0.0101	5.57	0.0696	38.46
End-Plate	0.0016	1.25	0.0205	15.68
Column	0.0062	3.65	0.0260	15.35
Supplementary plate	0.0007	0.43	-	-
Bolts	0.0177	4.12	0.2719	63.44
Continuity plate	0.0000	0.00	0.0000	0.00

With reference to the case study A (IPE 600 beam and HEM 320 column), the results provided in Tables 4-6 point out that the level of yielding occurring in the connection components is very limited when the beam-to-column joint is designed according to the criteria herein proposed, achieving a maximum value of 5.57 in the welds; conversely, the use of Eurocode 8 design criteria leads to a normalised PEEQ equal to 63.44 in the bolts and 38.46 in the welds.

Table 5. Damage to joint components expressed as PEEQ and NPEEQ (NPEEQ=PEEQ/ε_y) – study case B.

	Study case B			
	Proposal approach		Eurocode8 approach	
	PEEQ	NPEEQ	PEEQ	NPEEQ
Beam	0.8000	714.89	0.9600	857.87
Welds	0.0100	5.53	0.0431	23.82
End-Plate	0.0070	5.35	0.0180	13.75
Column	0.0061	3.61	0.0270	15.97
Supplementary plate	0.0010	0.59	-	-
Bolts	0.0116	2.71	0.0921	21.49
Continuity plate	0.0000	0.00	0.0000	0.00

Even in the study case B (IPE 450 beam and HEM 260 column), the maximum normalized PEEQ occurs in the welds and is equal to 5.53 for the design procedure proposed while, in case of Eurocode 8, yielding leads to maximum values of normalised PEEQs equal to 23.82 and 21.49 in the bolts and in the welds, respectively.

Table 6. Damage to joint components expressed as PEEQ and NPEEQ (NPEEQ=PEEQ/ε_y) – study case C.

	Study case C			
	Proposal approach		Eurocode8 approach	
	PEEQ	NPEEQ	PEEQ	NPEEQ
Beam	0.9665	863.68	0.1902	169.97
Welds	0.0756	41.78	0.0540	29.84
End-Plate	0.0016	1.22	0.0231	17.64
Column	0.0041	2.43	0.0370	21.89
Supplementary plate	0.0016	0.95	-	-
Bolts	0.0012	0.28	0.5053	117.90
Continuity plate	0.0000	0.00	0.0037	2.83

Finally, in study case C (IPE 220 beam and HEM 200 column), the maximum normalized PEEQs in the joint components occurs in the welds and is equal to 41.78 in the case of the design procedure herein proposed while, in case of Eurocode 8, it occurs in the bolts in tension and is equal to 117.90. Also in this case, damage is highly concentrated at the end of the connected beam even though the bolts achieve their ultimate capacity in case of the joint designed according to Eurocode 8.

It is important to point out that, even though these PEEQ values have been derived with reference to monotonic loading conditions, they give an important information about the strain concentrations occurring in the joint components. These concentrations are of paramount importance as soon as cyclic loading conditions are considered revealing the probable failure mode.

6 CONCLUSIONS

In this paper, rigorous capacity design criteria have been suggested to assure the development of full-strength full-ductility behaviour of beam-to-column joints. The criteria suggested have been applied and validated by means of FE simulations with reference to unstiffened extended end-plate connections. In particular, three different external beam-to-column joints have been designed, according to both the criteria proposed and to Eurocode 8, and their performances have been compared. The validation of the design criteria has been made by means of three-dimensional finite element analyses, carried out by ABAQUS 6.13 software.

The results obtained, on one hand, have confirmed the accuracy of the design approach and, on the other hand, have pointed out some criticisms of EC8 design criteria. In fact, EC8 provisions do not rationally account for the overstrength due to the beam strain-hardening. In particular, in some cases, the underestimation of the overstrength due to strain hardening is not compensated by the partial safety factor commonly applied in bolt design, thus leading to the brittle failure of the bolts. For the same reason, some joint components are significantly engaged in plastic range when EC8 design criteria are applied so that the resulting behaviour is characterized by a significant sharing of yielding between the connected beam end and such joint components.

The effectiveness of the design criteria herein proposed has been demonstrated comparing the damage level of the joints' components. The results obtained shows that, in case of connections designed according to the criteria proposed, the damage is conspicuously concentrated at the end of the beam which constitutes the main dissipative zone while all the connection's elements practically remain elastic, or only with very limited yielding. Conversely, in case of joints designed according to Eurocode 8, the joint components are significantly engaged in plastic range achieving high strain levels, certainly beyond the yield limit. The developed analyses have demonstrated that following EC8 design procedure, the welds may be engaged in plastic range with deformations up to 38.46 times the yield strain and, in a similar way, the bolts may fail or, in general, undergo severe damages.

ANNEX A: WORKED DESIGN EXAMPLE

Seismic design of beam-to-column joints needs the knowledge of the gravity loads acting on the beams in the seismic load combination, the beam and column sections and the material properties. The design is aimed to the evaluation of the required bolt diameter, throat thickness of fillet welds, end-plate thickness, continuity plate thickness and, if needed,

thickness of supplementary web plates. Many relationships are needed to develop all the design steps. Therefore, in order to clarify the proposed procedure, a worked design example is herein shown in detail, with reference to the external joint corresponding to study case A, whose input data are given in Table 2.

Step 1 - Evaluation of the average ultimate moment which the fully yielded and strain hardened beam is able to transmit:

The distance between the plastic hinge and the column flange is:

$$s_h = \frac{d_b}{2} = \frac{600}{2} = 300 \text{ mm}$$

The clear length of the beam is $L_n = 9000 - 359 = 8641 \text{ mm}$ and the distance between the plastic hinges is $L_h = L_n - 2s_h = 8641 - 600 = 8041 \text{ mm}$.

The nominal plastic moment of the beam (steel grade S235) is equal to $M_{b,p} = 786 \text{ kNm}$.

Considering the beam flange thickness, the overstrength coefficient $\gamma_{ov.rm}$ accounting for the random variability of the material is given by (see Table 1):

$$\gamma_{ov.rm} = \frac{f_{ym.bf}}{f_{y.b}} = \frac{f_0 - \beta t_{bf}}{f_{y.b}} = \frac{313.4 - 2.254 \times 19}{235} = \frac{270.57}{235} = 1.15$$

The average value of the yield stress of the web is equal to:

$$f_{ym.bw} = f_0 - \beta t_{bw} = 313.4 - 2.254 \times 12 = 286.35 \text{ MPa}$$

The normalized slenderness parameters of flange and web are equal to:

$$\bar{\lambda}_f = \frac{b_{bf}}{2 t_{bf}} \sqrt{\frac{f_{ym.bf}}{E}} = \frac{220}{2 \cdot 19} \sqrt{\frac{270.57}{210000}} = 0.208$$

$$\bar{\lambda}_w = \frac{d_{bw}}{2 t_{bw}} \sqrt{\frac{f_{ym.w}}{E}} = \frac{562}{2 \cdot 12} \sqrt{\frac{286.35}{210000}} = 0.865$$

The beam shear length is equal to $L_e = L_h/2 = 8041/2 = 4020.5 \text{ mm}$.

The overstrength coefficient accounting for the influence of strain hardening is:

$$\begin{aligned} \gamma_{ov.sh} &= \\ &= \frac{1}{0.5463 + 1.6325 \cdot 0.208^2 + 0.0621 \cdot 0.865^2 - 0.6021 \frac{220}{4020.5} + 0.0015 \cdot 37.5 + 0.0078 \cdot 12.3} \\ &= \\ &= 1.28 \end{aligned}$$

Therefore, the average value of the ultimate moment $M_{b,u}$ which can be transmitted by the fully yielded and strain-hardened beam is given by:

$$M_{b,u} = 1.15 \cdot 1.28 \cdot 1.05 \cdot 786 \cong 1214 \text{ kNm}$$

With reference to the external joint, the value of the shear action at the plastic hinge axis in the ultimate condition is equal to:

$$V_{bu} = \frac{q L_h}{2} + \frac{n_F F_d}{2} + \frac{2 M_{bu}}{L_h} = \frac{1.25 \cdot 8.041}{2} + \frac{3 \cdot 65.00}{2} + \frac{2 \cdot 1214}{8.041} \cong 404.6 \text{ kN}$$

Step 2 - Calculation of bending moment and shear action at the column flange and evaluation of compression force and tensile force to be transmitted at the beam flanges' levels:

The flexural and shear action, respectively M_{cf} and V_{cf} , at the column flange are given by:

$$M_{cf} = M_{bu} + V_{bu} \cdot s_h + \frac{q s_h^2}{2} = 1214 + 404.6 \cdot 0.3 + \frac{1.25 \cdot 0.3^2}{2} \cong 1336 \text{ kNm}$$

$$V_{cf} = 404.6 + 1.25 \cdot 0.30 \cong 405 \text{ kN}$$

Consequently, the compression/tensile force to be transmitted at the beam flanges' level is obtained as:

$$T_u = C_u = \frac{M_{cf}}{d_b - t_{bf}} = \frac{1336000}{600 - 19} \cong 2299 \text{ kN}$$

Step 3 - Design of the bolt diameter:

For the design of the diameter of the bolts in tension side the following actions have to be considered:

$$F_{t,Ed} = \frac{T_u}{n_b} = \frac{2299}{4} = 574.75 \text{ kN} \quad F_{v,Ed} = \frac{V_{cf}}{2 n_b} = \frac{405}{2 \cdot 4} = 50.6 \text{ kN}$$

Therefore, according to Eurocode 3, the check under combined shear and tension lead to determine a first minimum value of the resistant area of the bolts. In particular, for 10.9 class:

$$A_{res} \geq \frac{\gamma_{M2}}{f_{tb}} \left(\frac{F_{v,Ed}}{\alpha_v} + \frac{F_{t,Ed}}{1.26} \right)$$

$$= A_{res} \geq \frac{1.25}{1000} \left(\frac{50600}{0.5} + \frac{574750}{1.26} \right) \cong 696.69 \text{ mm}^2$$

According to Eurocode 3, in any case, the resistant area of the bolts has to be greater than the value determined considering only the tension action:

$$A_{res} \geq \frac{\gamma_{M2} F_{t,Ed}}{0.9 f_{tb}} = \frac{1.25 \cdot 574750}{0.9 \cdot 1000} \cong 798.26 \text{ mm}^2$$

Consequently, bolts M36 have been chosen.

Step 4 - Design of the welds:

According to Eurocode 3, the design of the welds has been carried out considering the throat thickness of the fillet weld in its actual position.

With reference to the welds connecting the flange beam to the end-plate, the length of the both internal and external fillets has been assumed as:

$$l_f = b_{bf} - 2 \cdot r_b - t_{bw} = 220 - 2 \cdot 24 - 12 = 160 \text{ mm}$$

Therefore the required throat thickness of the weld is:

$$a_f \geq \frac{T_u}{\sqrt{2} \cdot l_f} \frac{\beta_w \gamma_{M2}}{f_{tk}} = \frac{2299000 \cdot 0.80 \cdot 1.25}{160\sqrt{2} \cdot 360} = 28.23 \text{ mm} \rightarrow a_f = 29 \text{ mm}$$

The welds connecting the web beam and the end-plate have to be able to transmit the shear action V_{cf} and the ultimate flexural action $M_{w,u}$ that the web flange transmits:

$$M_{w,u} = \gamma_{ov.rm} \cdot \gamma_{ov.sh} \cdot \gamma_{M0} \cdot M_{w,p} = 1.15 \cdot 1.28 \cdot 1.05 \cdot 212.07 \cong 327.77 \text{ kNm}$$

The length of the fillets is:

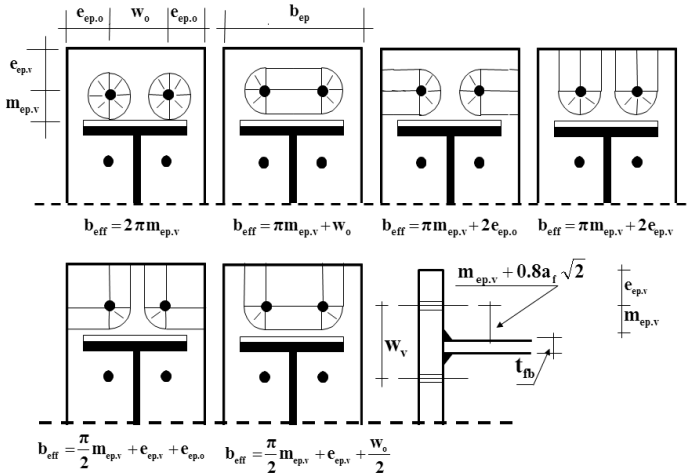
$$l_w = d_{bw} - 2 r_b = 562 - 2 \cdot 24 = 514 \text{ mm}$$

and the thickness results to be:

$$a_w \geq \frac{\beta_w \gamma_{M2}}{f_{tk}} \frac{1}{l_w} \sqrt{\frac{8 M_{w,u}^2}{l_w^2} + \frac{3}{4} V_{cf}^2} = \frac{0.8 \cdot 1.25}{360} \frac{1}{514} \sqrt{\frac{8 (327.77 \cdot 10^6)^2}{514^2} + \frac{3}{4} (405 \cdot 10^3)^2} \cong 9.92 \text{ mm} \rightarrow a_w = 10 \text{ mm}$$

Step 5 – Design of the end-plate:

Considering the design criteria already adopted for the bolts, failure mechanism type 3 can be excluded. Therefore, only the resistance formulations for mechanism type 1 and mechanism type 2 have to be considered to check the equivalent T-stub modelling the end-plate in bending. It is assumed that the distance m between the bolt axis and the plastic hinge located close to the beam flange is equal to the minimum technologically compatible, $m=1.2 d_0$ being d_0 the diameter of the bolt hole. In addition, the width of the plate is defined on the basis of the code requirements for bolt spacing and of technological conditions.



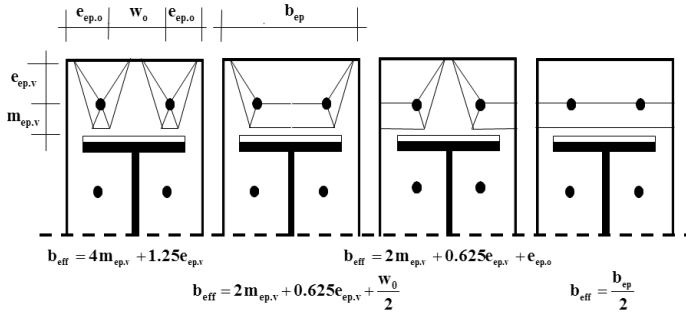


Figure 17. Determination of the effective length for a single bolt row on the basis of the possible collapse mechanisms.

The horizontal distance between the bolts w has to satisfy the following limitations:

$$w_{\min} \cong t_{cw} + 2 r_c + 1.8 d_0 = 21 + 2 \cdot 27 + 1.8 \cdot 37.5 = 142.5 \text{ mm}$$

$$w_{\max} = b_{cf} - 2.4 d_0 = 309 - 2.4 \cdot 37.5 = 219 \text{ mm}$$

According to the above limitations, the bolt spacing is taken equal to $w_0 = 170 \text{ mm}$. Regarding the width of the end-plate, it should be greater than:

$$b_{ep} = \max\{w + 2.4 d_0; b_{bf}\} = \max\{170 + 2.4 \cdot 37.5; 220\} = 260 \text{ mm}$$

and, anyway, smaller than the width of the column that is equal to 309 mm, consequently the width of the end plate is taken equal to 280mm.

As a consequence, the horizontal distance between the bolt axis and the edge of the plate $e_{ep,0}$ is:

$$e_{ep,0} = \frac{b_{ep} - w_0}{2} = \frac{280 - 170}{2} = 55 \text{ mm}$$

For the evaluation of the effective length of the equivalent T-stub, taken $m_x = e_x = 1.2d_0 = 45 \text{ mm}$, it results:

$$b_{eff,ep,1} = \min\{2\pi m_x; \pi m_x + w; \pi m_x + 2e_{ep}\} = \min\{282.6; 311.3; 251.3\} = 251.3 \text{ mm}$$

which accounts for the circular patterns and:

$$\begin{aligned} b_{eff,ep,2} &= \min\{4m_x + 1.25e_x; e_{ep} + 2m_x + 0.625e_x; 0.5w + 2m_x + 0.625e_x\} = \\ &= \min\{4 \cdot 45 + 1.25 \cdot 45; 45 + 2 \cdot 45 + 0.625 \cdot 45; 0.5 \cdot 170 + 2 \cdot 45 + 0.625 \cdot 45\} = \\ &= \min\{236.25; 173.12; 203.12\} = 203.12 \text{ mm} \end{aligned}$$

which accounts for non-circular patterns.

Definitely, the effective length of the equivalent T-stub is:

$$b_{eff,ep} = \min\{b_{eff,1}; b_{eff,2}; 0.5 b_{ep}\} = \min\{251.3; 203.12; 0.5 \cdot 280\} = 140 \text{ mm}$$

The thickness of the end-plate required to avoid the collapse of the equivalent T-stub according to type-1 mechanism is:

$$F_{1,Rd} = 2 \frac{b_{eff} t_{ep}^2 f_{y,ep}}{m \gamma_{M0}} = T_u \rightarrow$$

$$t_{ep.1} = \sqrt{\frac{m_x T_u \gamma_{M0}}{2 \cdot b_{eff,ep} \cdot f_{y,ep}}} = \sqrt{\frac{45 \cdot 2299000 \cdot 1.05}{2 \cdot 140 \cdot 275}} \cong 37.56 \text{ mm}$$

Similarly, to avoid the collapse of the equivalent T-stub according to type-2 mechanism the required end-plate thickness is:

$$F_{2,Rd} = 2 \frac{\frac{f_{y,ep} b_{eff} t_{ep}^2}{\gamma_{M0}} + 2 F_{t,Rd} n}{m + n} = T_u \rightarrow$$

$$t_{ep.2} = \sqrt{\frac{2 \gamma_{M0}}{b_{eff,ep} f_{y,ep}} \left[\frac{T_u (m_x + e_x)}{2} - 2 F_{t,Rd} e_x \right]} =$$

$$= \sqrt{\frac{2 \cdot 1.05}{140 \cdot 275} \left[\frac{2299000 (45 + 45)}{2} - 2 \cdot 588240 \cdot 45 \right]} \cong 52.50 \text{ mm}$$

Therefore, the thickness of the end-plate has been assumed equal to 55mm.

Step 6 - Check of the resistance of the column web in shear and design of supplementary web plates if needed:

The shear resistant area of the column section is given by:

$$A_{vc} = A - 2 b_{cf} t_{cf} + (t_{cw} + 2r_c)t_{cf} = 31200 - 2 \cdot 309 \cdot 40 + (21 + 2 \cdot 27) \cdot 40$$

$$= 9480 \text{ mm}^2$$

The resistance of the column web panel, without continuity and/or supplementary plates, is:

$$V_{wp,Rd} = \frac{0.9 \cdot A_{vc} \cdot f_{y,cw}}{\sqrt{3} \cdot \gamma_{M0}} = \frac{0.9 \cdot 9480 \cdot 355}{\sqrt{3} \cdot 1.05} \cong 1665 \text{ kN}$$

Since continuity plates in the both compression and tension zones have been considered, the plastic shear resistance of the column web panel is incremented by the contribution due to the resistant mechanism activated by the continuity plates.

The plastic moment of the column flange is given by:

$$M_{pl.cf,Rd} = \frac{b_{cf} t_{cf}^2 f_{y,c}}{4 \gamma_{M0}} \frac{1}{1.05} = \frac{309 \cdot 40^2 \cdot 355}{4} \frac{1}{1.05} \cong 41.79 \text{ kNm}$$

Therefore the contribution due to the additional resistant mechanism activated by the continuity plates results:

$$V_{wp,add,Rd} = \frac{4 \cdot M_{pl.cf,Rd}}{d_s} = \frac{4 \cdot 41.79}{0.581} = 287.7 \text{ kN}$$

where d_s is the distance between the centrelines of the stiffeners.

The total resistance of the column web panel is:

$$V_{wp,Rd,tot} = V_{wp,Rd} + V_{wp,add,Rd} = 1665 + 287.7 \cong 1953 \text{ kN}$$

Whereas the shear resistance of the column web panel is lower than the action transmitted by the beam in its ultimate conditions, supplementary web plates are needed whose width is taken equal to:

$$b_{s,max} = d_{cw} - 2r_c = 279 - 2 \cdot 27 = 225 \text{ mm}$$

According to Eurocode 3, the resistance of the material constituting the supplementary plates has to be the same of the column; the thickness of the stiffeners results to be:

$$t_s \geq \frac{\sqrt{3} \cdot \gamma_{M0} (T_u - V_{wp,add,Rd})}{0.9 \cdot b_s \cdot f_{y,wc}} - \frac{A_{vc}}{b_s} = \frac{\sqrt{3} \cdot 1.05 \cdot (2299000 - 287700)}{0.9 \cdot 225 \cdot 355} - \frac{9480}{225} \cong 9.76 \text{ mm}$$

Consequently, it is possible to use a couple of supplementary plates whose thickness is 5 mm or a single supplementary web plate whose thickness is equal to 10 mm.

Step 7 - Check of the resistance of the column web in tension and in compression.

Since continuity plates have been considered in the evaluation of the shear resistance of the column web panel, their design is required. The transverse stiffeners can be designed according to two possible approaches. The first approach requires that the action transmitted from the beam flanges in their ultimate conditions, equal to T_u , is absorbed relying exclusively on the tensile/compression resistance of continuity plates, neglecting the resistance of the column web. The second approach allows the reduction of the thickness of the continuity plates, taking advantage of the contribution due to the resistance of the column web.

In accordance to the latter, the resistance of the column web in compression and the resistance of the continuity plates have to be determined; the former is given by:

$$F_{cwc,Rd} = b_{eff,cwc} (t_{cw} + t_{s,tot}) \cdot \frac{f_{y,cw}}{\gamma_{M0}} = \frac{546.02 (21 + 10) 355}{1.05} \cong 5723 \text{ kN}$$

where $b_{eff,cwc}$ is the effective length of the column web given by:

$$b_{eff,cwc} = t_{fb} + 2\sqrt{2} a_f + 5(t_{fc} + r_c) + 2 t_{ep} = 19 + 2\sqrt{2} \cdot 29 + 5(40 + 27) + 2 \cdot 40 \cong 546.02 \text{ mm}$$

and $t_{s,tot} = 10 \text{ mm}$ is the thickness of the supplementary web plates.

Obviously, if $F_{cwc,Rd} \geq T_u$ it is possible to evaluate the possibility of omitting the continuity plates. In such a case, it is necessary to check again the resistance of column web in shear according to Step 6.

Subsequently, the welds have been designed:

$$a_{cp} \geq \frac{\beta_w t_{cp} f_{y,cp}}{\sqrt{2} f_{tk}} = \frac{0.85 \cdot 20 \cdot 275}{\sqrt{2} \cdot 430} \cong 7.68 \text{ mm} \quad \rightarrow \quad a_{cp} = 8 \text{ mm}$$

Step 8 - Check of the resistance of the column flange in bending:

In bolted connections, an equivalent T-stub in tension may be used to model the design resistance of the column flange in bending. As highlighted for the end-plate in bending, failure mode according to mechanism type-3 can be excluded because of the design criterion adopted for the bolts. Therefore, the design resistances for mechanism type-1 and type-2 have to be evaluated. In particular, the following equation has to be considered:

$$F_{1,Rd} \geq T_u \quad F_{2,Rd} \geq T_u$$

where:

$$F_{1,Rd} = 2 \frac{b_{eff} t_{cf}^2 f_{y,cf}}{m \gamma_{M0}} \quad \text{and} \quad F_{2,Rd} = 2 \frac{\frac{f_{y,cf} b_{eff} t_{cf}^2}{2} + 2 F_{t,Rd} n}{m + n}$$

in which b_{eff} is the effective length of the equivalent T-stub corresponding to a single bolt row, t_{cf} is the thickness of the column flange, m is the distance between the bolt line and the plastic hinge arising at the T-stub stem, n is the distance between the bolt line and the end of the plate where the contact forces are concentrated and $f_{y,cf}$ is the yield resistance of the column flange.

With reference to Fig. 18a it is possible to define:

$$m_c = \frac{w - t_{wc} - 1.6 r_c}{2} = \frac{170 - 21 - 1.6 \cdot 27}{2} = 52.9 \text{ mm}$$

while the horizontal distance between the bolt axis and the edge of the column flange is:

$$e = \frac{b_c - w}{2} = \frac{309 - 170}{2} = 69.5 \text{ mm}$$

The vertical distance between the first and second bolt rows is:

$$w_v = 2 (m + 0.8 a_f \sqrt{2} + t_{fb}/2) = 2 (45 + 0.8 \cdot 29 \sqrt{2} + 19/2) = 174.62 \text{ mm}$$

In presence of continuity plates whose fillet welds have a throat thickness equal to 8 mm, it results:

$$m_2 = \frac{w_v - t_{cp} - 1.6 a_{cp} \sqrt{2}}{2} = \frac{174.62 - 20 - 1.6 \cdot 8 \sqrt{2}}{2} = 68.26 \text{ mm}$$

According to Eurocode 3 the effective length, in presence of transverse stiffeners, is given by:

$$b_{eff} = \min\{2\pi m_c; \alpha \cdot m_c\} = \min\{2\pi \cdot 52.9; 5.93 \cdot 52.9\} \cong 313.7 \text{ mm}$$

where the parameter α has been determined considering the geometrical parameters λ_1 and λ_2 :

$$\lambda_1 = \frac{m_c}{m_c + e} = \frac{52.9}{52.9 + 69.5} = 0.43 \quad \lambda_2 = \frac{m_2}{m_c + e} = \frac{68.26}{52.9 + 69.5} = 0.57$$

by means the abacus in Fig. 18b:

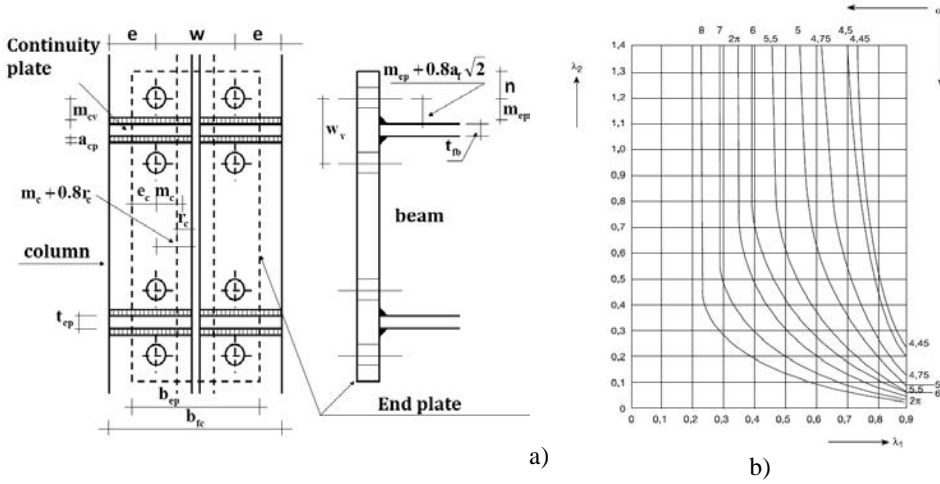


Figure 18. Column flange: a) geometrical properties; b) abacus.

Thereafter, the design resistances for mechanisms type-1 and type-2 are given by:

$$F_{1,Rd} = 2 \frac{f_{y.cf} b_{eff.cf} b t_{cf}^2}{m_c} \frac{1}{\gamma_{M0}} = 2 \frac{355 \cdot 313.7 \cdot 40^2}{52.9} \frac{1}{1.05} \cong 6416 \text{ kN} \geq T_u$$

$$F_{2,Rd} = 2 \frac{f_{y.cf} \frac{b_{eff.cf} b t_{cf}^2}{2} + 2 F_{t,Rd} n}{m_c + n} \frac{1}{\gamma_{M0}} = 2 \frac{355 \frac{313.7 \cdot 40^2}{2} + 2 \cdot 588240 \cdot 55}{52.9 + 55} \frac{1}{1.05} \cong 2715 \text{ kN} \geq T_u$$

where $n = \min\{e; e_{ep}; 1.25m_c\} = \min\{69.5; 55; 1.25 \cdot 52.9\} = 55 \text{ mm}$.

Since the both design resistances are greater than the action T_u , derived by means of capacity design principles, the check of the column flange in bending is satisfied.

7 REFERENCES

- [1] J.P. Jaspart: "Étude de la semi-rigidité des noeuds poutre-colonne et son influence sur la résistance et la stabilité des ossatures en acier" PhD Thesis, University of Liège, Liège, 1991.
- [2] F. Mazzolani and V. Piluso: "An attempt of codification of semirigidity for seismic resistant steel structures", Third international workshop on connections in steel structures, Trent, 28-31 May, 1992.
- [3] CEN (2005): "Eurocode 3: Design of Steel Structures – Part 1-8: Design of Joints", EN 1993-1-8.
- [4] D.B. Moore, F. Wald (ed.): "Design of Structural connections to Eurocode 3 – Frequently Asked Questions", Building Research Establishment Ltd, Watford, 2003, ISBN 80-01-02838-0, Project Continuing Education in Structural Connections, No. CZ/00/B/F/PP-134099, Leonardo Da Vinci, Programme.
- [5] Latour, M. and Rizzano, G., (2013b), "A Theoretical Model for Predicting the Rotational Capacity of Steel Base Joints", Journal of Constructional Steel Research, 91, pp. 88-99.
- [6] Latour, M., Piluso, V. and Rizzano, G., (2014d), "Rotational Behaviour of Comon Base Plate Connections: Experimental Analysis and Modelling", Engineering Structures, pp. 14-23.

- [7] Girao Coelho, A. M., Bijlaard, F. & Simoes Da Silva, L., (2004), "Experimental Assessment of the Ductility of Extended End Plate Connections" *Engineering Structures*, 26, pp. 1185-1206.
- [8] Beg, D., Zupancic, E. & Vayas, I., (2004), "On the Rotation Capacity of Moment Connections", *Journal of Constructional Steel Research*, 60, pp. 601-620.
- [9] Piluso, V., Rizzano, G. (2008), "Experimental analysis and modelling of bolted T-stubs under cyclic loads", *Journal of Constructional Steel Research*, Vol. 64, pp. 655-669.
- [10] Iannone, F., Latour, M., Piluso, V. & Rizzano, G., (2011), "Experimental Analysis of Bolted Steel Beam-to-Column Connections: Component Identification", *Journal of Earthquake Engineering*, 15(2), pp. 214-244.
- [11] Latour, M., Piluso, V. and Rizzano, G., (2011a), "Experimental Analysis of Innovative Dissipative Bolted Double Split Tee Beam-to-Column Connections", *Steel Construction*, June, 4(2), pp. 53-64.
- [12] Hu, J., Leon, R. and Park, T., (2012), "Mechanical Models for the Analysis of Bolted T-stub Connections under Cyclic Loads", *Journal of Constructional Steel Research*, 78, pp. 45-57.
- [13] Bravo, M. and Herrera, R., (2014) "Performance under cyclic load of built-up T-stubs for Double T moment connections. *Journal of Constructional Steel Research*, Volume 103, pp. 117-130.
- [14] C. Faella, V. Piluso and G. Rizzano: "Structural Steel Semirigid Connections", CRC Press, Boca Raton, Ann Arbor, London, Tokyo. ISBN 0-8493-7433-2, 1999.
- [15] U.Kuhlmann: "Definition of Flange Slenderness Limits on the Basis of Rotation Capacity Values", *Journal of Constructional Steel Research*, pp. 21-40, 1989.
- [16] B. Kato: "Rotation Capacity of H-section members as determined by local buckling", *Journal of Construction Steel Research*, 13, 95-109, 1989.
- [17] F.M. Mazzolani and V. Piluso: "Evaluation of the rotation capacity of steel beams and beam-column", 1st COST C1 Workshop, Strasbourg, 28-30 October, 1992.
- [18] B. Kato: "Rotational Capacity of steel members subject to Local Buckling", *9th World Conference on Earthquake Engineering*, Vol. IV, paper 6-2-3, August 2-9, Tokyo-Kyoto, 1988.
- [19] Y.E. Yee and R.E. Melchers: "Moment-rotation curves for bolted connections", *Journal of Structural Engineering*, ASCE, Vol. 112, Issue 3, pp. 615-635, 1986.
- [20] B. Kato: "Deformation Capacity of Steel Structures", *Journal of Constructional Steel Research*, pp. 33-94, N.17, 1990.
- [21] A. Girao Coelho: Characterization of the ductility of bolted extended end plate beam-to-column steel connections. PhD Thesis: Universidade de Coimbra, 2004.
- [22] CEN, EN 1998-1-1. Eurocode 8: Design of structures for earthquake resistance - Part 1: General rules, seismic actions and rules for buildings, *European committee for standardization*, 2005.
- [23] Ministero delle Infrastrutture: "Norme tecniche per le costruzioni", NTC2008, 2008.
- [24] V. Piluso and G. Rizzano: "Random material variability effects on full-strength end-plate beam-to-column joints", *Journal of constructional steel research*, vol.63, 2007.
- [25] G.L. Tucker and R.M. Bennet: "Reliability Analysis of Partially Restrained Steel Connections", *Journal of Structural Engineering*, ASCE, Vol. 116, No. 4, April, pp. 1090-1101, 1990.
- [26] R.M. Bennett and F.S. Najem-Clarke: "Reliability of Bolted Steel Tension Members", *Journal of Structural Engineering*, ASCE, Vol.113, No. 8, pp. 1865-1872, 1987.
- [27] H. Gervásio, L. Simões da Silva and L. Borges: "Reliability assessment of the post-limit stiffness and ductility of steel joints", *Third European Conference on Steel Structures*, Coimbra, 2002, September 19-20, 2002.
- [28] R.Y. Rubinstein: "Simulation and the Monte Carlo method", John Wiley & Sons, 1981.
- [29] J.W. Fisher, T.V. Galambos, G.L. Kulak and M.K. Ravindra: "Load and resistance factor design criteria for connection", *ASCE annual Convention & Exposition*, Chicago, October 16-20, 1978.
- [30] Gruppo Fontana, Catalogo Tecnico: Prescrizioni Tecniche, 2004.
- [31] BS-EN-ISO 2560. Welding consumables: covered electrodes for manual metal arc welding of non-alloy and fine grain steels, Classification, 2009.
- [32] O.S. Bursi and J.P. Jaspart: "Calibration of a finite Element model for isolated bolted end-plate steel connections", *Journal of Constructional Steel Research* 44, 224-262, 1997.

- [33] CEN, EN 1993-1-5. Eurocode 3: Design of steel structures - Part 1-5: Plated structural elements, *European committee for standardization*, 2007.
- [34] CEN, EN 10034. Structural steel I and H sections – Tolerances on shape and dimensions, *European committee for standardization*, 1993.
- [35] CEN, EN 1090-2. Execution of steel structure and aluminium structure: Technical requirements for steel structures. Annex G: Test to determine slip factor, 2008.
- [36] M. D'Aniello, R. Landolfo, V. Piluso and G. Rizzano: “Ultimate behavior of steel beams under non-uniform bending”, *Journal of Constructional Steel Research*, 78, 144-158, 2012.
- [37] A.K. Aggarwal: “Comparative Tests On Endplate Beam-To-Column Connections”, *Journal of Constructional Steel Research*, 30, 151-175, 1994.

STANDARD BEAM-TO-COLUMN JOINTS

Gianfranco De Matteis ^a, Giuseppe Brando ^b, Elisabetta D'Alessandro ^b

^a *Department of Architecture and Industrial Design, University of Campania "L. Vanvitelli", Aversa, Italy, gianfranco.dematteis@unicampania.it*

^b *Department of Engineering and Geology, University "G. d'Annunzio" of Chieti-Pescara, Pescara, Italy, giuseppe.brando@unich.it*

ABSTRACT

This Chapter describes the research activities carried out at the University of Campania and the University of Chieti-Pescara within the ReLuis Project in the period 2014-2016, focused on the behaviour of steel beam-to-column joints. Nowadays steel beam-to-column joints can be classified and calculated according to the rules set out by Eurocode 3 (EN 1993-1-8, 2005), based on the so called "component method". However, due to the complexity of the method, as well as its scarce attitude to be used in a design key, the designers are often discouraged to fulfil its application.

In the light of this premise, this Chapter describes two tools developed in order to overcome the above difficulties: *i*) an automatic procedure allowing an easy-to-use application of the component method for the evaluation of both stiffness and strength of beam-to-column joints, enabling also to plot the moment-rotation curve describing the joints behaviour; *ii*) Design Charts for design purposes to set joint details according to the required structural performance. The above practical tools should help to achieve the positive goal for promoting the component method among Italian designers, so to go beyond the current unsatisfactory practice.

KEYWORDS

Beam-to-Column Joints, Components Method, Moment-Rotation Curve, Joint Classification, Design charts, EC3.

SYMBOLS

E	Young modulus	A	Cross section
A_v	Cross Section Shear area	h	Section depth
d_w	Web depth	t_f	Flange thickness
t_w	Web thickness	s	Root radius
t_p	Plate thickness	b_p	Plate depth
w	Spacing between centres of bolts measured perpendicular to the load	e_p	Spacing from the centre of a bolt hole to the plate end part measured perpendicular to the load

e_f	Spacing from the centre of a bolt hole to the flange end part measured perpendicular to the load	d_{v1}	Distance from the centre of compression to the first bolt-row
d_{v2}	Distance from the centre of compression to the second bolt-row	p	Spacing between centres of bolts measured in the direction of load transfer
z	Level arm	n	Number of bolts
r	Bolt-row number	$l_{eff,cp}$	Effective length of an equivalent T-stub (circular patterns)
$l_{eff,nc}$	Effective length of an equivalent T-stub (non circular patterns)	b_{eff}	Effective width for a brace member to chord connection
$F_{t,Rd}$	Design resistance of a bolt	$F_{c,wc,Rd}$	Design transverse compression resistance of column web
$F_{c,fb,Rd}$	Design compression resistance of beam web and flange	$V_{wp,Rd}$	Design plastic shear resistance of column web
$F_{T,Rd}$	Design tension resistance of a T-stub	$F_{t,wc,Rd}$	Design transverse tension resistance of column web
$F_{t,wb,Rd}$	Design tension resistance of beam web	$F_{ti,Rd}$	Design tension resistance of bolt-row i in tension
$M_{j,Rd}$	Design moment resistance of the joint	$M_{pl,Rd}$	Design plastic moment resistance
S_j	Rotational stiffness of the joint	k_i	Stiffness coefficient for basic joint component i
k_{wc}	Reduction factor for interaction with shear	μ	Stiffness ratio
w	Reduction factor for possible effects of interaction with shear	β	Transformation parameter
ρ	Reduction factor for plate buckling	ϕ	Rotation capacity of the joint (rad)
α	Slenderness coefficient		

1 INTRODUCTION

Beam-to-column joints play a key role in the structural response of steel Moment Resisting Frames (MRFs), strongly influencing their performance and manufacturing processes costs

(Weynand et al., 1998). Hence, the prediction of the connections mechanical behaviour is a factor that cannot be neglected, both in the design stage and in the safety assessment phase.

Many experimental and numerical studies were developed in the past and nowadays the main mechanisms determining the strength and the stiffness of metal beam-to-column joints are well identifiable. Tests under both monotonic and cyclic loads for investigating the significance of the main geometrical and mechanical parameters (beam size, end plate thickness, bolt layout, etc.) were carried out by several researchers (Adey et al., 2000; De Matteis et al., 2000; He et al., 2010; Maali et al., 2016), also considering unconventional joint configurations (Jordão et al., 2013) or stressing on specific components (Rahiminia et al., 2013; El-Tawil, 2000; Kosarieh and Danesh, 2016). These experimental tests represented the basis for developing highly non linear FEM models (for instance Bursi and Jaspart, 1997; De Matteis et al., 2009; Sui et al., 2013; Chen et al., 2016) that were used to carry out parametric analyses (Augusto et al., 2017; Ma et al., 2016; Mansouri and Saffari, 2014; Hedayat et al., 2016). Such analyses allowed to provide useful design formulations and to put into evidence the variability of the joint response depending on some specific geometric features.

With reference to the use of beam-to-column joints in seismic prone zone, several additional research studies were developed in recent years in order to provide information concerning the ductility of some specific components (Takatsuka et al., 2014; Shi et al., 2017). Moreover, the same methodologies used for studying steel beam-to-column joints were also used for other types of joints, such as column base (Tsavdaridis et al., 2016; Kaziolas et al., 2013; Kavinde et al., 2012) or composite joints (Li et al., 2017).

In the past, in order to practise hand-calculation methodologies, designers were used to model beam-to-column joints by idealized schematizations, given by perfectly flexible hinges or, alternatively, by infinitely rigid connections (Diaz et al., 2011). Nonetheless, this type of procedure appears to be too much simplistic and approximate, as it does not allow to evaluate the joint contribution to the deformability and strength of the whole structure.

On the contrary, it is necessary to account for both the linear and the non linear behaviour of joints especially in the case of MRFs. To this purpose, the most procedure is based on experimental analyses, but they might be too much expensive for the common design practice (Faella et al., 2000) and they are usually reserved to research and to special applications (Kosarieh and Danesh, 2016), for which specific economic resources are available.

Over the last decades, extensive researches, aimed at providing simplified tools for steel joints calculation, were carried out, with the result that today it is possible to compute the actual flexural behaviour of joints through the evaluation of their real stiffness and strength. This type of effort led to a substantial evolution of Codes and Provisions, with the introduction of a new model of "semi-rigid / partial strength" beam-to-column joint, which offers the possibility to contemplate a special class of MRF defined as semi-continuous.

One of the available procedures for a reliable modelling of steel joints is the so called "Component Method", currently adopted by EC3-Part 1.8 (EN 1993-1-8, 2005). According to this method, the joint is schematized as an assemblage of "components", which are idealized by independent springs characterized by elasto-plastic or rigid-plastic behaviours. Each component is characterised by its own strength and stiffness, working either in tension, compression or shear (Jaspart, 2000). Therefore, this procedure can be applied to a great variety of joints, bolted or welded, provided that force-deformation response of each component is available.

The application of the method is articulated into three simple steps: 1) Decomposition of the joint into basic components; 2) evaluation of the stiffness and strength of each component; 3)

assemblage of the components for the determination of the global joint mechanical behaviour. The final result consists in a moment-rotation curve plotted on the basis of the flexural stiffness and the maximum strength that the joint is able to offer.

However, although the steps that have to be implemented appear clear and simple, the complexity of the calculation required for the evaluation of some components, as well as the high variability of possible joint types, depending on the geometrical and mechanical parameters characterizing the different parts, make the method very laborious and not easy to be implemented. For this reason, it is convenient resorting to easier approaches, especially in the step of selecting the type of joints that more suitably allows to satisfy certain structural requirements.

Based on the above remarks, the present study aims at providing specific design charts that allow to define the geometrical and mechanical features of steel beam-column joints able to ensure minimum performance requirements in terms of flexural strength and stiffness. To this purpose, an automatic tool for an easy-to-use application of the component method has been developed. Then, the proposed tool is employed for performing an extensive parametric analysis of two bolt rows end plate beam-to-column steel joints by which the design charts are drawn out.

The Chapter is organized in three main parts:

- 1) introduction and validation of the automatic tool;
- 2) parametric analysis for the evaluation of the influence of the main parameters on the global behaviour of the joint;
- 3) development of design charts that allow to identify the geometrical-mechanical features to be assigned to the joint in order to satisfy minimum predefined performance requirements.

2 COMPONENT METHOD COMPUTERIZATION

2.1 General

An automatic tool for the application of the component method has been developed. It is applicable to any type of beam-to-column joint, even if, for presentation purpose, only an application to a single way beam-to-column steel joint with extended end-plate (Fig. 1a) is provided in this Section. This is characterized (Fig. 1b) by a HE 200A column transverse section, a IPE 240 beam transverse section, a 10mm thick extended end-plate that is connected to the column flange by means of M16 bolts. A steel grade S275 has been considered for the members and the connecting plates and a class 8.8 has been assumed for the bolts.

The tool was written in a visual basic editor that was interfaced to the excel software of Microsoft Office. Therefore the interface of the proposed automatic tool is a spreadsheet that allows to manage easily all the parameters included in the formulations provided by EC3-Part 1.8. It is articulated into three sections.

The first, shown in Fig. 2, is organized in order to enable the input of geometrical and mechanical features characterising all the basic components. In addition it is possible to select conveniently the values of some coefficients contemplated in the EC3-Part 1.8 formulations, for instance the reduction factor for interaction with shear k_{wc} (EC3-Part 1.8 §6.2.6.2), the slenderness coefficient α (EC3-Part 1.8 §6.2.6.5) and the transformation parameter β (EC3-Part 1.8 §5.3). Also, it is possible to account for the presence of stiffeners or other

strengthening elements that can be applied to the joint and may influence the component behaviour.

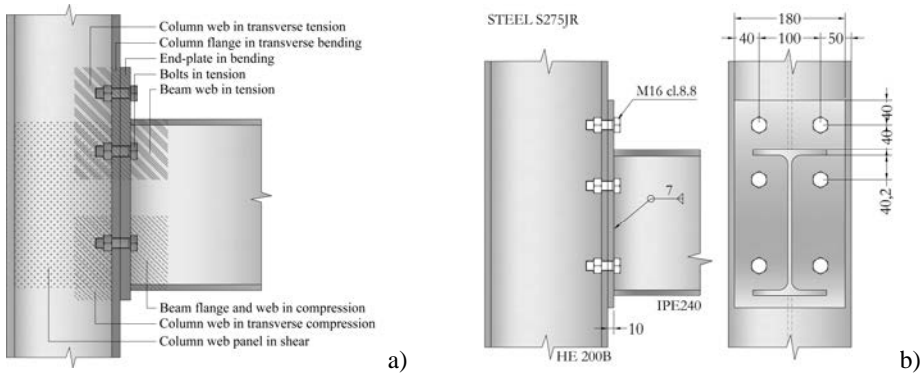


Figure 1. a) Basic components and b) geometric characteristics of the considered bolted extended end-plate beam-to-column joint.

COLUMN			
SECTION	HEA200		
Yield strength	275	$f_{y,wc}$	N/mm^2
Cross section	538.3	A	mm^2
Section depth	190	h	mm
Web depth	134	d_{wc}	mm
Flange thickness	10	t_f	mm
Flange width	200	b_f	mm
Web thickness	6.5	t_{wc}	mm
Root radius	18	r_{wc}	mm
Distance from the centre of compression to the first bolt-row	265.10	d_{c1}	mm
Distance from the centre of compression to the second bolt-row	185.10	d_{c2}	mm
Reduction factor	1	k_{sc}	§6.2.6.2

BEAM			
SECTION	IPE240		
Yield strength	275	$f_{y,wb}$	N/mm^2
Cross section	391.2	A	mm^2
Section depth	240	h	mm
Web depth	199.4	d_{wb}	mm
Flange thickness	9.8	t_f	mm
Flange width	120	b_f	mm
Web thickness	6.2	t_{wb}	mm
Root radius	15	r_{wb}	mm
Flange fillet weld trough thickness	7	a_f	mm
Web fillet weld trough thickness	7	a_w	mm
Beam length	6000	L_b	mm

PLATE			
Yield strength	275	$f_{y,wp}$	N/mm^2
Plate thickness	10	t_p	mm
Plate depth	180	b_p	mm
Orientation spacing between centres of bolts	100	w	mm
Spacing between the top of column flange and the first bolt-row	30	m_1	mm
Spacing between the bottom of column flange and the second bolt-row	40.2	m_2	mm
Orientation spacing from centre of bolt hole to plate-flange end part	50	e_p/e_f	mm
Vertical spacing from centre of bolt hole to plate end part	40	e_p	mm
	32.35	e_w	mm
	22.08	e_{w2}	mm
	28.98	e_{w1}	mm
Slenderness coefficient	7.5	α	§6.2.6.3 Fig.6.11

Figure 2. Graphic interface for inputting joint data.

All the input data can be easily set through the use of drop-down menus, by which the user is guided to make the necessary choices. Only the data that are bold type can be set by the user, whereas the other parameters are derived.

In the second section, the spreadsheet provides directly the strength and the stiffness coefficients k_{idi} that will be recalled in eq. (2), of each component, according to the formulation provided by EC-Part 1.8.

2.2 Definition of joint components

With reference to extended end-plate beam-to-column joints which are here considered as an example, the relevant components are: "column web panel in shear", "column web in transverse compression", "column web in transverse tension", "column flange in bending", "end-plate in bending", "beam flange and web in compression", "beam web in tension" and "bolts in tension".

The behaviour of the tension zone of the joint is ruled by the following components: "column flange in bending", "end-plate in bending", "column web in tension", "beam web in tension", "bolts in tension".

▪ Flange and end-plate in bending

For both the "flange in bending" with "bolt in tension" and the "end-plate in bending" with "bolt in tension" components, T-stub models, characterized by proper effective lengths are considered. These are calculated using yield lines with circular or non-circular patterns, according to the formulations proposed by Zoetemeijer (1990). The strengths of these components are those ones of the representative T-stubs, each one evaluated as the minimum tensile strength associated to the three different failure mechanisms shown in Figure 3, for which EC3 provides formulations according to an hypothesis of elastic perfectly plastic behaviour of the base material. They are "Complete flange yielding", "Flange yielding and bolts failure", "Bolts failure".

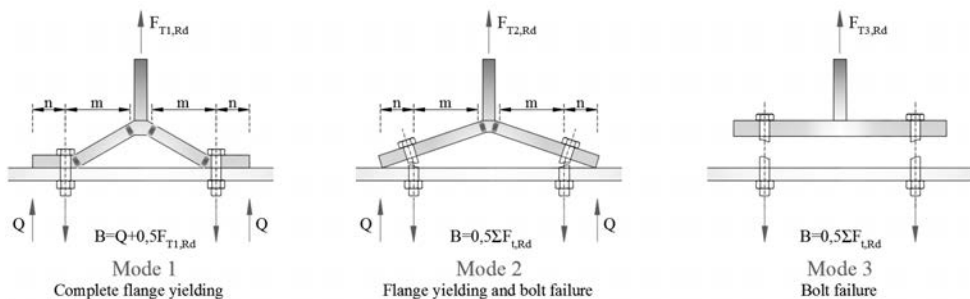
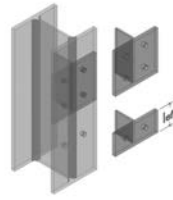


Figure 3. T-stub failure modes.

According to the requirements EC3-Part 1.8, the components based on the T-Stub models, the minimum strengths among the ones obtained considering bolts rows working individually, are calculated in the spreadsheet as shown in Figures 5 and 6, for external and inner rows respectively. For bolt rows working in group, strength and stiffness coefficients are given in Figure 4.

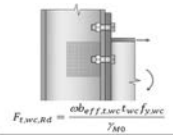
DESIGN RESISTANCE GROUP OF BOLT-ROW			
Column flange in traverse bending			
Distance from the centre of compression to the first bolt-row	265.1	d_1	mm
Distance from the centre of compression to the second bolt-row	185.1	d_2	mm
Distance from the second bolt-row to the first	80	p_1	mm
Mid-distance from the second bolt-row to the first	80	p_2	mm
Effective length end bolt-row (circular patterns)	181.58	$l_{ef,fp}$	mm
Effective length end bolt-row (non-circular patterns)	129.29	$l_{ef,nc}$	mm
Effective length inner bolt-row (circular patterns)	168.00	$l_{ef,ip}$	mm
Effective length inner bolt-row (non-circular patterns)	80.00	$l_{ef,inc}$	mm
Effective length inner bolt-row for stiffened flange (c.p.)	181.58	$l_{ef,ip,ss}$	mm
Effective length inner bolt-row for stiffened flange (n.c.p.)	192.93	$l_{ef,inc,ss}$	mm
Effective length 1 (circular patterns)	209.70	l_{e1}	mm
Effective length 2 (non-circular patt.)	209.70	l_{e2}	mm
Design tension resistance of a bolt	99432	$F_{t,Rd}$	N
Number of bolts	4	n	
Design plastic moment resistance 1	1373056	$M_{p1,Rd}$	Nmm
Design plastic moment resistance 2	1373936	$M_{p2,Rd}$	Nmm
Stiffness coefficient	5.57	k_1	
Mode 1	109728	$F_{T1,Rd}$	N
Mode 2	237943	$F_{T2,Rd}$	N
Mode 3	361728	$F_{T3,Rd}$	N
Column web in traverse tension			
Effective length	209.70	$l_{ef,w}$	mm
Effective thickness for stiffened column	6.5	$t_{w,eff}$	mm
Shear area	1808	A_w	mm ²
Reduction factor for possible effects of shear	0.76	α	§6.2.6.2 Tab.6.3
Transformation parameter	1	β	§5.3 Tab.5.4
Stiffness coefficient	7.12	k_2	
Design resistance	278721	$F_{t,w,Rd}$	N



$$F_{T1,Rd} = \frac{4M_{p1,Rd}}{m}$$

$$F_{T2,Rd} = \frac{2M_{p2,Rd} + n \sum F_{t,Rd}}{m + n}$$

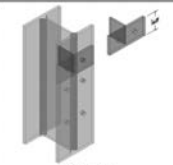
$$F_{T3,Rd} = \sum F_{t,Rd}$$



$$F_{t,w,Rd} = \frac{\alpha l_{ef,w} t_{w,eff} f_{y,w}}{\gamma_{M0}}$$

Figure 4. Evaluation of strength and stiffness coefficients for the components modelled by T-stub: bolt-row in tension working in group.

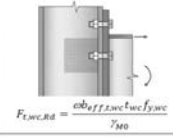
BENDING AND TENSION			
DESIGN RESISTANCE INDIVIDUAL BOLT-ROW (End bolt row)			
Column flange in traverse bending			
Effective length (circular patterns)	203.16	$l_{ef,fp}$	mm
Effective length (non-circular patterns)	179.40	$l_{ef,nc}$	mm
Effective length for stiffened flange (circular patterns)	181.58	$l_{ef,ip,ss}$	mm
Effective length for stiffened flange (non-circular patterns)	192.93	$l_{ef,inc,ss}$	mm
Effective length 1 (circular patterns)	179.40	l_{e1}	mm
Effective length 2 (non-circular patt.)	179.40	l_{e2}	mm
Design tension resistance of a bolt	99432	$F_{t,Rd}$	N
Number of bolts	2	n	
Design plastic moment resistance 1	1174643	$M_{p1,Rd}$	Nmm
Design plastic moment resistance 2	1174643	$M_{p2,Rd}$	Nmm
Stiffness coefficient	6.77	k_1	
Mode 1	145242	$F_{T1,Rd}$	N
Mode 2	133465	$F_{T2,Rd}$	N
Mode 3	198864	$F_{T3,Rd}$	N
Column web in traverse tension			
Effective length	179.40	$l_{ef,w}$	mm
Effective thickness for stiffened column	6.5	$t_{w,eff}$	mm
Shear area	1808	A_w	mm ²
Reduction factor for possible effects of shear	0.81	α	§6.2.6.2 Tab.6.3
Transformation parameter	1	β	§5.3 Tab.5.4
Stiffness coefficient	6.09	k_2	
Design resistance	240042	$F_{t,w,Rd}$	N
End-plate in bending			
Effective length (circular patterns)	138.66	$l_{ef,fp}$	mm
Effective length (non-circular patterns)	90.00	$l_{ef,nc}$	mm
Effective length 1 (circular patterns)	90.00	l_{e1}	mm
Effective length 2 (non-circular patt.)	90.00	l_{e2}	mm
Design tension resistance of a bolt	99432	$F_{t,Rd}$	N
Number of bolts	2	n	
Design plastic moment resistance 1	589286	$M_{p1,Rd}$	Nmm
Design plastic moment resistance 2	589286	$M_{p2,Rd}$	Nmm
Stiffness coefficient	3.00	k_3	
Mode 1	196752	$F_{T1,Rd}$	N
Mode 2	124203	$F_{T2,Rd}$	N
Mode 3	198864	$F_{T3,Rd}$	N
Beam web in tension			
Effective length	90.00	l_{ef}	mm
Stiffness coefficient	∞	k_4	
Design resistance	146143	$F_{t,w,Rd}$	N



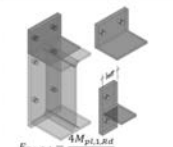
$$F_{T1,Rd} = \frac{4M_{p1,Rd}}{m}$$

$$F_{T2,Rd} = \frac{2M_{p2,Rd} + n \sum F_{t,Rd}}{m + n}$$

$$F_{T3,Rd} = \sum F_{t,Rd}$$



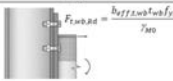
$$F_{t,w,Rd} = \frac{\alpha l_{ef,w} t_{w,eff} f_{y,w}}{\gamma_{M0}}$$



$$F_{T1,Rd} = \frac{4M_{p1,Rd}}{m}$$

$$F_{T2,Rd} = \frac{2M_{p2,Rd} + n \sum F_{t,Rd}}{m + n}$$

$$F_{T3,Rd} = \sum F_{t,Rd}$$



$$F_{t,w,Rd} = \frac{\beta l_{ef} w}{\gamma_{M0}}$$

Figure 5. Evaluation of strength and stiffness coefficients for the components modelled by T-stub: first bolt-row in tension working individually.

DESIGN RESISTANCE INDIVIDUAL BOLT-ROW (Inner bolt row)			
Column flange in traverse bending			
Effective length (circular patterns)	283.16	$L_{ef,fp}$	mm
Effective length (non-circular patterns)	179.40	$L_{ef,nc}$	mm
Effective length for stiffened flange (circular patterns)	283.16	$L_{ef,fp,2s}$	mm
Effective length for stiffened flange (non-circular patterns)	242.63	$L_{ef,nc,2s}$	mm
Effective length 1 (circular patterns)	179.40	L_{e1}	mm
Effective length 2 (non-circular patt.)	379.40	L_{e2}	mm
Design tension resistance of a bolt	99432	$F_{t,Rd}$	N
Number of bolts	2	n	
Design plastic moment resistance 1	1174643	$M_{pl1,Rd}$	Nmm
Design plastic moment resistance 2	1174643	$M_{pl2,Rd}$	Nmm
Stiffness coefficient	4.77	k_1	
Mode 1	145242	$F_{t,Rd1}$	N
Mode 2	132465	$F_{t,Rd2}$	N
Mode 3	188964	$F_{t,Rd3}$	N
Column web in traverse tension			
Effective length	179.40	$L_{ef,nc}$	mm
Effective thickness for stiffened column	6.8	$t_{w,eff}$	mm
Shear area	1809	A_w	mm ²
Reduction factor for possible effects of shear	0.81	ω	§6.2.6.2 Tab.6.3
Transformation parameter	1	β	§3.3 Tab.5.4
Stiffness coefficient	6.06	k_1	
Design resistance	246942	$F_{t,w,Rd}$	N
End-plate in bending			
Effective length (circular patterns)	182.00	$L_{ef,fp}$	mm
Effective length (non-circular patterns)	217.35	$L_{ef,nc}$	mm
Effective length 1 (circular patterns)	182.00	L_{e1}	mm
Effective length 2 (non-circular patt.)	217.35	L_{e2}	mm
Slenderness coefficient	7.5	α	§6.2.6.5 Fig.6.11
Design tension resistance of a bolt	99432	$F_{t,Rd}$	N
Number of bolts	2	n	
Design plastic moment resistance 1	1191847	$M_{pl1,Rd}$	Nmm
Design plastic moment resistance 2	1423145	$M_{pl2,Rd}$	Nmm
Stiffness coefficient	6.97	k_2	
Mode 1	164470	$F_{t,Rd1}$	N
Mode 2	144331	$F_{t,Rd2}$	N
Mode 3	188964	$F_{t,Rd3}$	N
Beam web in tension			
Effective length	182.00	L_{ef}	mm
Stiffness coefficient	6	k_1	
Design resistance	295528	$F_{t,w,Rd}$	N

Figure 6. Evaluation of strength and stiffness coefficients for the components modelled by T-stub: second bolt-row in tension working individually.

▪ Column web in transverse tension and compression

The resistance of the "column web in transverse tension", as well as the "column web in transverse compression", are also calculated in the spreadsheet, considering the reduction factors ω (EC3-Part 1.8 §6.2.6.2 Tab 6.3) accounting for the interaction with the shear acting on the column web panel.

The strength of the compression zone (Figure 7) is offered by the weakest component between the "column web in transverse compression" and the beam web and flange in compression. For the resistance of the "column web in transverse compression" component, the reduction factor for plate buckling ρ (EC3-Part 1.8 §6.2.6.2) is considered, depending on the plate slenderness $\bar{\lambda}_p$.

Also, the aforementioned reduction factors accounting for the interaction with shear ω (EC3-Part 1.8 §6.2.6.2 Tab 6.3), is accounted for.

Moreover, the strength is multiplied by the reduction factor k_{wc} (EC3-Part 1.8 §6.2.6.2) when the maximum longitudinal compressive stress in the column web, due to axial force and bending moment acting on the column, exceed the 70% of the yield strength. In fact, the interaction of local stresses derived from column axial force can decrease the strength of the basic components and can produce the failure of "column web panel in compression" for crushing or buckling (Brando et al., 2015).

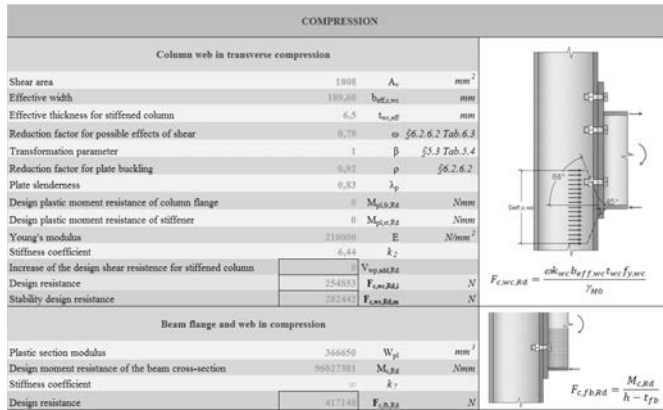


Figure 7. Evaluation of strength stiffness coefficients for compression zone basic components.

▪ **Column web in shear**

For the "column web in shear" component, the strength relies on the hypothesis that a uniform stress distribution develops in the column web panel. In addition, the spreadsheet allows to calculate the increment of strength also in the presence of web transverse stiffeners (Figure 8).

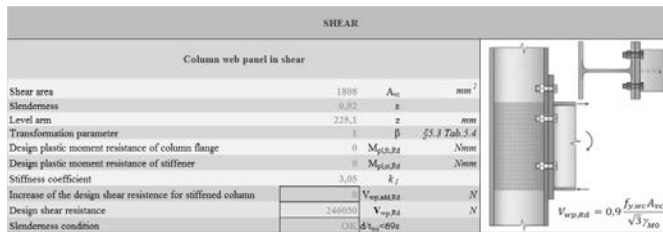


Figure 8. Evaluation of strength stiffness coefficients for the column web panel in shear.

2.3 **Evaluation of joint behaviour**

In the third section, the spreadsheet gives the value of the flexural strength ($M_{j,Rd}$) and stiffness ($S_{j,ini}$) of the whole joint (Figure 9).

▪ **Evaluation of flexural strength**

In case of bolted end-plate connections, the flexural strength is calculated as follows (eq. 1):

$$M_{j,Rd} = \sum_r h_r F_{tr,Rd} \tag{1}$$

where $F_{tr,Rd}$ is the effective design resistance of the bolt row r , whereas h_r is the distance of bolt row r from the centre of compression.

The sum expressed in eq. (1) considers that the numbering of the single bolt-rows starts from the farthest to the closest with respect to the centre of compression. Each bolt row is considered individually and its effective design tension resistance $F_{tr,Rd}$ is calculated as the smallest value of the design tension resistance of the components "column web in tension", "column flange in bending", "end-plate in bending", "beam web in tension". The sum in eq.

(1) concludes when the sum of the effective strength of the considered individual bolt rows exceeds the design resistance of those bolt rows taken as a group.

Nonetheless, when the sum of $F_{tr,Rd}$ exceeds the strength of the "column web panel in shear", properly divided by the aforementioned factor ω that accounts for the shear-moment interaction, of the "column web in transverse compression", of the beam "flange and web in compression", the flexural strength of the joint is given by the minor strength calculated for these components multiplied for the relative lever arm.

The evaluation of the maximum bending moment $M_{j,Rd}$ that the joint can support allows a classification in terms of strength. In detail, the joint is classified as (i) "hinge" when the ratio m between $M_{j,Rd}$ and the resistance of the weakest connected element is up to 25%, (ii) "full strength" when $M_{j,Rd}$ is greater than the resistance of the weakest connected element ($m \geq 1$) and (iii) "partial strength" in all the other cases. In case of "full strength" joints, when the ratio between the joint strength and strength of the connected element is higher than 1.20, it is not necessary to implement a rotation control in a structural analysis.

▪ Evaluation of flexural stiffness

For the evaluation of the initial elastic flexural stiffness $S_{j,in}$ of the joint, the spreadsheet accounts for eq. (2), as specified by the EC3-Part 1.8:

$$S_{j,in} = \frac{E \cdot z^2}{\mu \cdot \sum_i k_{idi}} \quad (2)$$

where

k_{idi} is the stiffness coefficient of each component;

z is the lever arm of the whole joint, given in EC3-Part 1.8 §6.2.7.1 Fig 6.15

μ is a coefficient which assumed equal to 1.

The stiffness value obtained by Eq. (2) characterizes the linear behaviour of the joint and leads to classify it as a "hinge", "semi-rigid" or "rigid" joint according to the indications that EC3-Part 1.8 provides in alternative way owing to the fact that the main structure is a moment resisting or a braced frame. In particular, the joint is classified as "rigid" if $S_{j,in} \geq k_b EI_b / L_b$, where I_b and L_b are the second moment of area and the length of the beam, k_b is equal to 8 for braced frames and 25 for moment resisting frames; the above inequality is to be considered valid whether in every storey $(I_b \cdot L_c) / (I_c \cdot L_b) \geq 0,1$, where I_c and L_c are the second moment of area and the length of the column. On the other hand, the joint is classified as "hinge" if $S_{j,in} \leq 0,5 k_b EI_b / L_b$, "semi-rigid" for all other joints. The information related to the joint classification, in terms of strength or stiffness, are also provided as shown in Figure 9.

▪ Moment-Rotation curve definition

As a final step, the spreadsheet provides the moment rotation (M- ϕ) curve to be assumed for the considered joint. As prescribed by EC3, a linear behaviour - with the constant stiffness given by eq. (2) - is assumed up to a moment value $M_{j,Ed} \leq 2/3 M_{j,Rd}$. Instead, for $2/3 M_{j,Rd} < M_{j,Ed} \leq M_{j,Rd}$ the tangent stiffness of the curve is still given by eq (2), in which μ is provided by the following expression (eq. 3):

MOMENT RESISTANCE			
Distance from the centre of compression to the first bolt-row	265,1	d_{c1}	mm
Distance from the centre of compression to the second bolt-row	185,1	d_{c2}	mm
Mid-distance from the bolt-row to the centre of compression	225,1	d_c	mm
Design tension resistance of the first bolt-row in tension	110273	$F_{t1,Rd}$	N
Design tension resistance of the second bolt-row in tension	63010	$F_{t2,Rd}$	N
Design moment resistance	3995120	$M_{j,Rd}$	Nmm
ROTATION CAPACITY			
Stiffness ratio	1	μ	§6.3.1
Coefficient	2,7	Ψ	§6.3.1 Tab.6.8
Level arm	225	z	mm
Effective stiffness coefficient for bolt-row 1	1,01	$k_{st,r,1}$	
Effective stiffness coefficient for bolt-row 2	1,27	$k_{st,r,2}$	
Equivalent level arm	227,8	z_{eq}	mm
Equivalent stiffness coefficient	2,21	k_{st}	
Rotational stiffness	11382591870	$S_{j,R}$	Nmm
Classification of joint by strength			
Plastic column modulus	429480	$W_{pl,c}$	mm ³
Plastic beam modulus	366650	$W_{pl,b}$	mm ³
Design plastic moment of the column	112482857	$M_{pl,Rd,c}$	Nmm
Design plastic moment of the beam	96027381	$M_{pl,Rd,b}$	Nmm
	0,41	η	m
Classification of joint by stiffness			
Moment of inertia of the beam	38920000	$I_{b,eq}$	mm ⁴
Beam length	6000	$L_{b,eq}$	mm
Nominally pinned limit	681100000		Nmm
Partial-strength limit	34055000000		Nmm

Figure 9. Evaluation of the resistance and the flexural elastic stiffness of the joint.

$$\mu = \left(\frac{1.5 \cdot M_{j,Ed}}{M_{j,Rd}} \right)^\psi \tag{3}$$

where ψ is a coefficient that depends on the type of connection and that in case of bolted flanged connection is equal to 2.7. It is useful to note that once the maximum strength $M_{j,Rd}$ is attained, a null stiffness is considered.

In Fig. 10, the moment rotation curve obtained from the spreadsheet for the extended end-plate beam-to-column joint considered in this paper as a matter of example is shown.

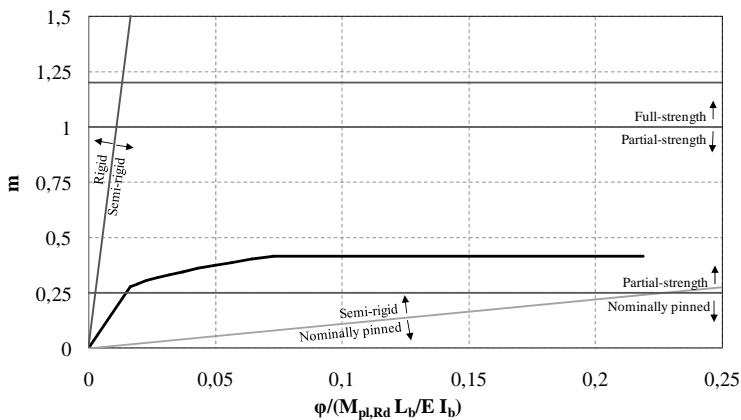


Figure 10. Moment-rotation curve of the considered beam-to-column joint obtained through the application of the proposed automatic tool.

3 VALIDATION OF THE AUTOMATIC PROCEDURE

For validation purpose, the previously presented automatic procedure has been applied checking the results of two beam-to-column joints that were already dealt with by Abidelah et al. (2012) and Prinz et al. (2014). The flexural performances of the specimens proposed by these Authors were studied by experimental tests and were evaluated by the application of the components method, according to the EC3 formulations.

The tested specimen of Abidelah et al. (2012) is an extended end-plate beam-to-column joint, where the end-plate is bolted to the column by two tension bolts rows and one bolt row arranged in the compression part, for a total number of six bolts M16, class 8.8. The column profile has a standardized transversal section HE120A, while the beam has a standardized section IPE240. The end plate has a thickness of 15 mm. Fillet welds with a throat thickness of 6 mm were used to connect the beam to the end-plate. The geometrical features of the joint are described in Figure 11.a. A S235 steel grade was used as base material for the beam, the column, and end-plate, with nominal yield ($f_{y,n}$) and ultimate ($f_{u,n}$) strengths of 235 and 360 MPa, respectively. It should be noted that the real mechanical characteristics were always higher than the nominal ones, according to the results of some tensile tests carried out on coupons cut from the flange and web of the beam and column, as reported in Table 1.

Table 1. Mechanical properties of the steel specimens studied by Abidelah et al. (2012).

Component	Yield stress $f_{y,n}$ (MPa)	Ultimate stress $f_{u,n}$ (MPa)
Beam web	343	456
Beam flange	356	480
Column web	345	456
Column flange	338	435
Endplate	310	44
Bolt	893	1010

As shown in Figure 11.b, the moment-rotation curve obtained by the automatic procedure proposed in Section 2 perfectly fits the results obtained by Abidelah et al. (2012) through the implementation of the component method and well approximates the behaviour observed by experimental tests.

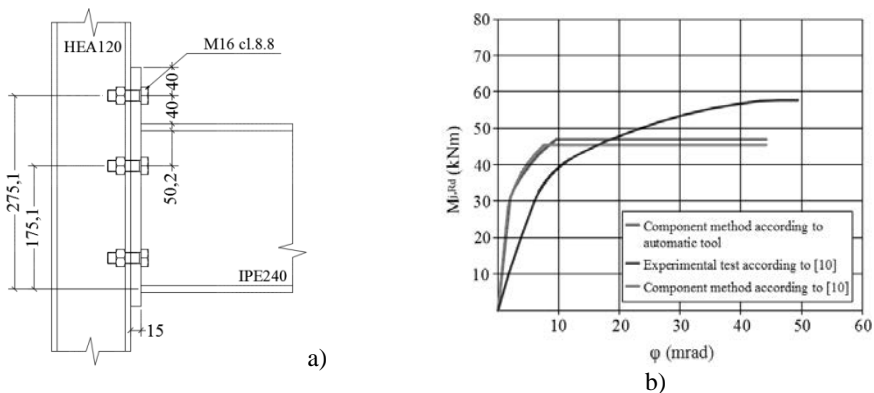


Figure 11. a) Geometry of the joint tested by Abidelah et al. (2012); b) validation of the proposed automatic tool with the results obtained by test and by the numerical application of the component method, as reported in Abidelah et al. (2012).

It is to be considered that the revealed discrepancies with respect to the experimental tests are due to the fact that EC3 procedure is quite conservative, as it does not consider the material hardening and the randomness related to the mechanical features of the base material, which can produce a significant overstrength of the joint.

Prinz et al. (2014) tested two extended end-plate beam-to-column joints shown in Figure 12a and Figure 13a. They were characterized by an end-plate connected to the column flanges by two tension bolt rows and one bolt row in the compression zone of the joint, for a total number of six bolts M20, class 10.9. Column profiles HE300A and HE300B standardized sections were considered for the first and for the second specimen, respectively. For both the tested joints, a beam standardized section HE300B and a 30mm thick end plate were adopted. The nominal and real mechanical features of the elements that form the tested specimens are reported in Table 2.

Table 2. Mechanical properties of the steel specimens studied by Prinz et al. (2014)

Material grade	Element	Yield stress (MPa)	Ultimate stress (MPa)
S235 JR+M	HE300 A	353	433
S235 JR+M	HE300 B	353	433
S355 J2+N	Endplate	366	538

In the following, in order to apply the component method application, the nominal mechanical features are employed. As shown in Figure 12.b and Figure 13.b, the moment-rotation curve obtained by the automatic procedure applying the nominal values of the mechanical features fits perfectly the curve obtained by the component method application.

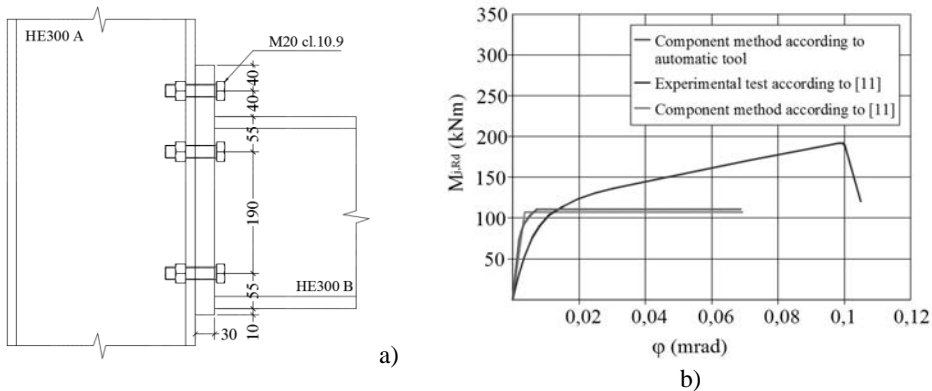


Figure 12. a) Geometrical characteristics of the first joint studied by Prinz et al. [10]; b) validation of the proposed automatic tool with the results obtained by test and by the numerical application of the component method, as reported in Prinz et al. (2014).

4 PARAMETRIC ANALYSIS

With reference to the joint typology described in Figure 1, in order to identify the geometric parameters influencing its strength and the stiffness, the proposed automatic calculation tool has been used in order to carry out a wide parametric analysis. The following features have been varied: *i*) sections of the connected elements (all European standardized HE –A, B and

M- section profiles ranging from HE100A to HE600M), end-plate thickness (10 mm, 20 mm, 30 mm, 40 mm), bolt grades and diameters (grade 8.8 for bolts diameter 16 mm and 22 mm, grade 10.9 for bolts diameter 18 mm and 24 mm). In the whole, 103.968 different type of specimens have been investigated. The outcomes of these analyses have represented the basis for the Design Charts shown in Figure 5.

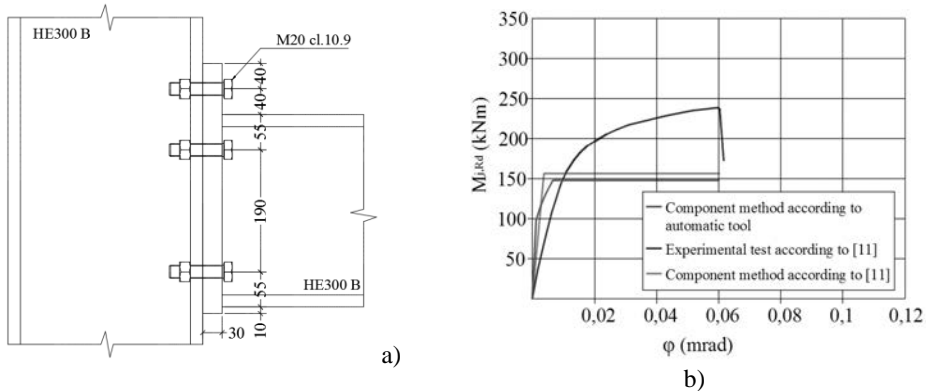


Figure 13. a) Geometrical characteristics of the second joint studied by Prinz et al. [10]; b) validation of the proposed automatic tool with the results obtained by test and by the numerical application of the component method, as reported in Prinz et al. (2014).

As a matter of example, the flexural strengths and corresponding stiffness values of 11,552 typologies, those ones characterized by HE-B sections only for both beams and columns, are reported in Figure 14 (for M24- 10.9 bolts), Figure 15 (M22- 8.8 bolts), Figure 16 (M18- 10.9 bolts) and Figure 17 (M16-8.8 bolts).

It is possible to observe that for joined profiles of reduced sections with relatively thick flanges, for example for HE100B beams coupled to HE120B columns, bolts grade and diameter do not influence the joint strength. In fact, for plate thickness lower than 20 mm, the component that undergoes failure is the end plate in bending, that experiences a mode-1 failure mechanism (full plasticity of the T-stub flange). On the contrary, for end plate thicker than 20 mm, the component that rules the strength is the column web in transverse compression-tension. On the other hand, the implemented analyses evidenced that for the above sections, but with thinner flanges (HE100A and HE 120A) the weaker component, for thick end-plate, is the column flange in bending.

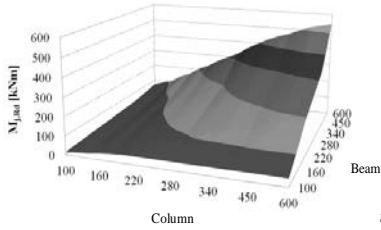
For beam and column sections of medium size, for example for HE260B beams coupled to HE300B columns, bolt diameter and grade influence the strength of the joint as, for end-plate thicker than 10 mm, they are involved in mode 2 mechanisms of the T-stub models used for the end plate strength definition or for the column flange in bending.

Contrarily, for large sections profiles, for example for HE500B beams coupled to HE600B columns, joints strength is greatly influenced by the bolt grade and diameter, while the thickness of the end-plate play a role for thickness lower than 30 mm. In particular, for bolt diameters of 16 mm and 18 mm, the weaker component is the end plate that experience a mode 1 T-stub mechanism. On the contrary, for an end plate thickness of 20 mm, a failure mode 2 can be observed, while for a plate of 30 mm, only bolts undergo failure (mode 3). Instead, for bolts diameters of 22 mm or 24 mm, the transition from failure mode 1 to failure

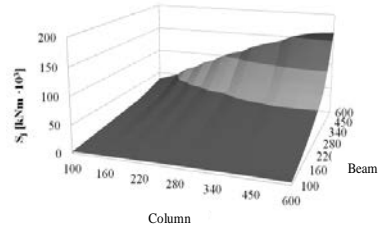
mode 2 occurs for a plate thickness of 20 mm, whereas the transition from failure mode 2 to failure mode 3 is observed for an end plate thickness of 30 mm.

Anyway, with the bolt configuration shown in Figure 1b, for bolt diameter higher than 24 mm, end-plate with thickness higher than 30 mm are not involved in failure mechanisms.

$t_p = 40\text{ mm}$

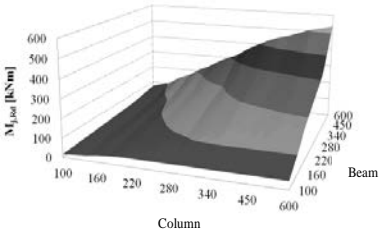


a)

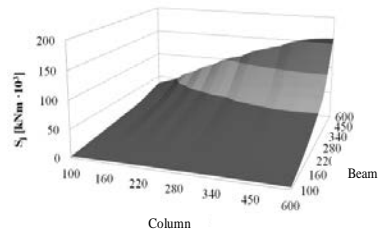


b)

$t_p = 30\text{ mm}$

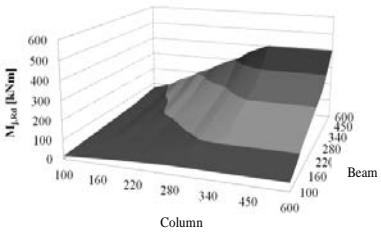


c)

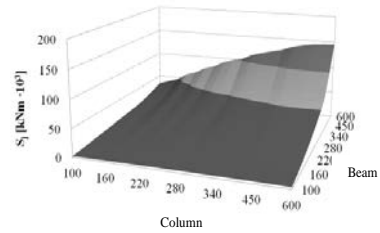


d)

$t_p = 20\text{ mm}$

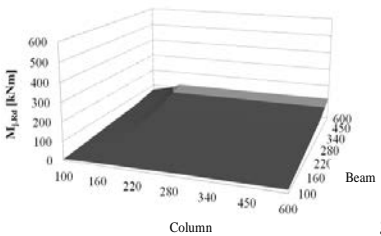


e)

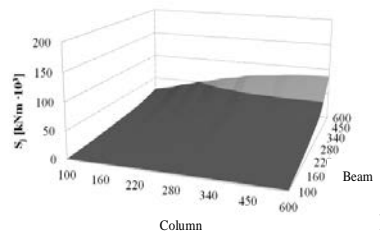


f)

$t_p = 10\text{ mm}$



g)



h)

M_{Rd} [kNm] ■ 0-100 ■ 100-200 ■ 200-300 ■ 300-400 ■ 400-500 ■ 500-600

S_f [kNm · 10³] ■ 0-50 ■ 50-100 ■ 100-150 ■ 150-200

Figure 14. Resisting moment and stiffness of flange connections for different of end plate thicknesses t_p (bolts M24 cl.10.9).

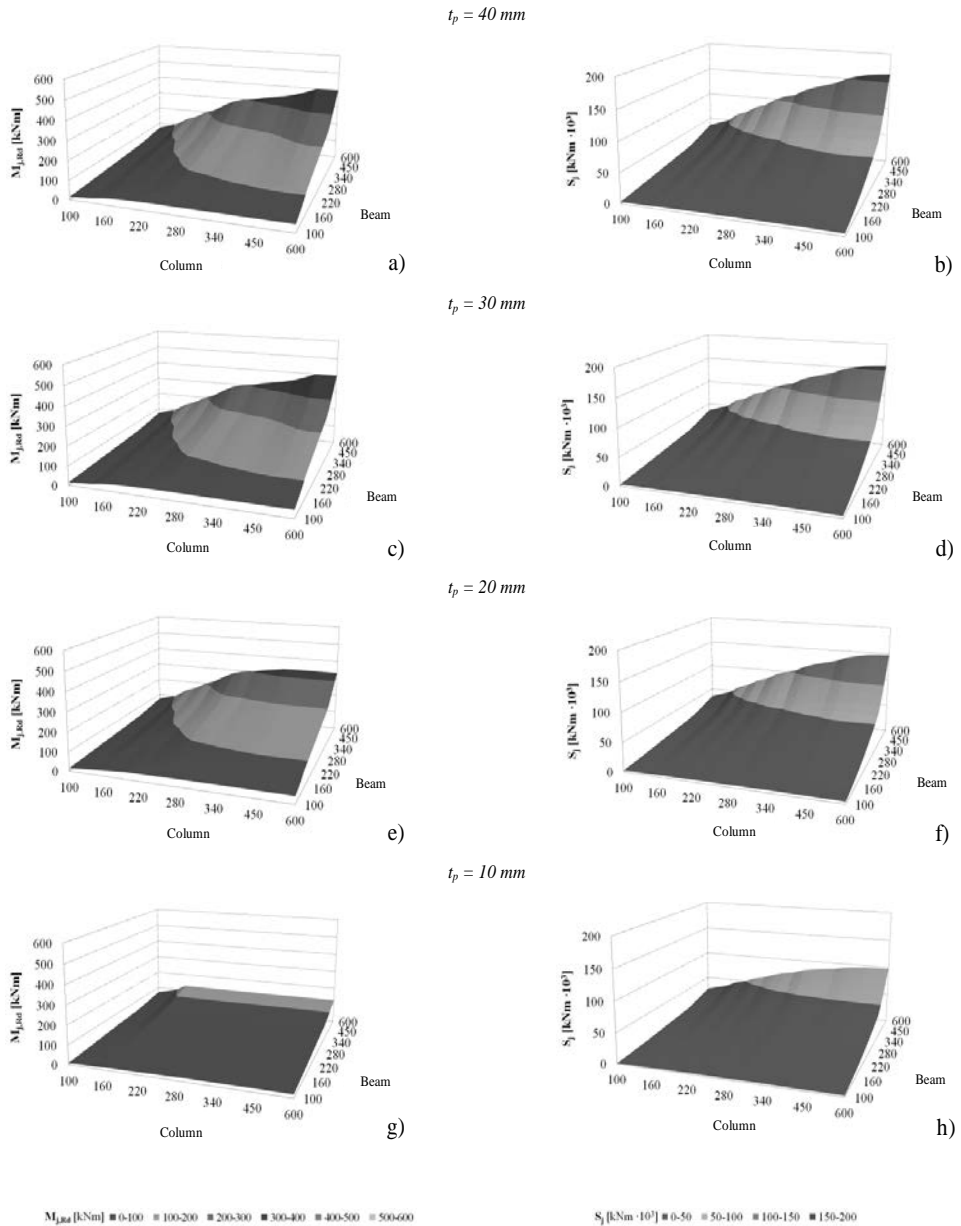
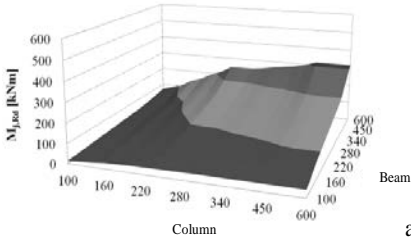
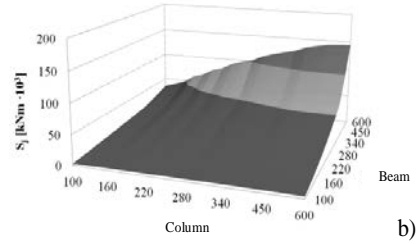


Figure 15. Resisting moment and stiffness of flange connections for different end plate thicknesses t_p (bolts M22 cl.8.8).

$t_p = 40 \text{ mm}$

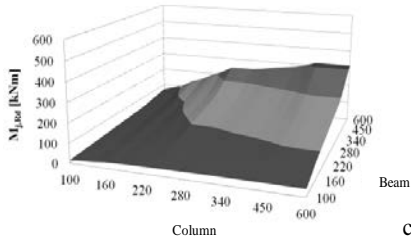


a)

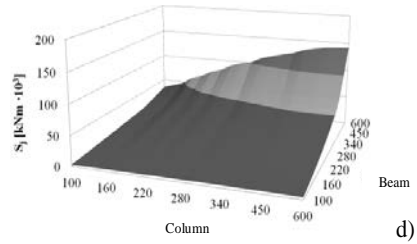


b)

$t_p = 30 \text{ mm}$

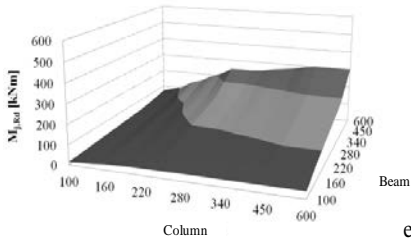


c)

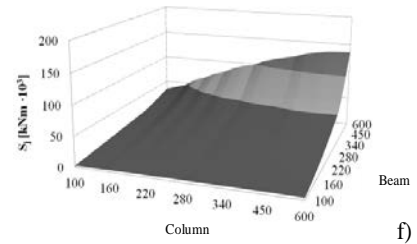


d)

$t_p = 20 \text{ mm}$

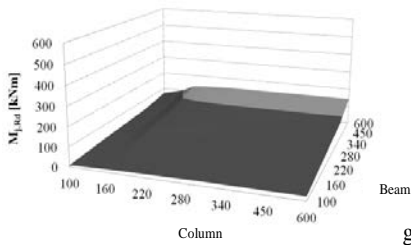


e)

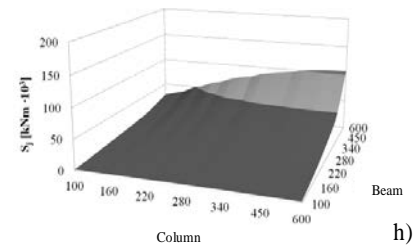


f)

$t_p = 10 \text{ mm}$



g)



h)

M_{Rd} [kNm] ■ 0-100 ■ 100-200 ■ 200-300 ■ 300-400 ■ 400-500 ■ 500-600

S_j [kNm · 10³] ■ 0-50 ■ 50-100 ■ 100-150 ■ 150-200

Figure 16. Resisting moment and stiffness of flange connections for different end plate thicknesses t_p (bolts M18 cl.10.9).

5 DESIGN CHARTS

The results of the parametric analyses described in the previous Section allowed to define design charts. These are proposed at the end of the Chapter for a typical bolted end plate beam-to-column joint with or without stiffeners.

Once that the target performance of the joint is established, in terms of resisting moment $M_{j,Rd}$, expressed as a percentage (25%, 50%, 75%, 100% and 120%) of the plastic moment of the weakest connected member (beam or column), the charts give back, for a wide selection of couple of beam and column sections, the design parameters listed below:

- Bolt diameter d_b
- Bolt Grade c_{l_b}
- End Plate thickness t_p
- Thickness of possible required plate to be welded to the column web i_r, t_{wc}
- Thickness of possible required plate to be welded to the beam flanges i_r, t_{fb}
- Thickness of possible required plate to be welded to the beam web i_r, t_{wb}
- Thickness of possible required column backing plate i_r, t_{wb} .

Moreover, the chart give back a relative stiffness coefficient k ($[m^{-1}]$) expressed as follows:

$$\tilde{k} = \frac{S_{j,in}}{E \cdot I_b} \quad (4)$$

Where $S_{j,in}$ is given in eq (2). This coefficient allows to classify the joint also in terms of stiffness.

6 CONCLUSIONS

In this Chapter an operational tool for the automatic implementation of the component method for the evaluation of steel beam-to-column joints flexural response is presented. It is a spreadsheet that accounts for all the formulations provided, for each component, by Eurocode 3 and which is characterized by an easy-to-use graphic interface that allows a feasible manageability of both the input and the output data.

As a main output of the proposed automatic procedure, the non linear moment-rotation curve of the treated joint is given, which is a useful element to classify the joint, as well as to carry out analysis of moment resisting frames.

The given automatic tool has been validated on the basis of other experimental and numerical studies existing in literature. As it accurately follows the procedure given by Eurocode 3, it is affected by some weaknesses concerning both the ultimate strength, that is usually underestimated, and the stiffness that can be overestimated. For this reason, some corrective factors could be introduced in a future version of the tool.

The convenience of adopting the proposed automatic tool is proven by the results obtained by the implementation of a parametric analysis that allowed to define some design charts to be used for the optimal selection of beam-column joints able to guarantee pre-established minimum performance requirements in terms of flexural strength and stiffness. The charts, given at the end of this Chapter, give important information that can support the designer in the best choice of a beam-to-column joint to be adopted for a steel moment resisting frame.

		BEAM																				
		HEA 100	HEA 120	HEA 140	HEA 160	HEA 180	HEA 200	HEA 220	HEA 240	HEA 260	HEA 280	HEA 300	HEA 320	HEA 340	HEA 360	HEA 400	HEA 450	HEA 500	HEA 550	HEA 600		
HEA 100	$f_{t,red}$																					
	$f_{c,red}$																					
HEA 120	$f_{t,red}$																					
	$f_{c,red}$																					
HEA 140	$f_{t,red}$																					
	$f_{c,red}$																					
HEA 160	$f_{t,red}$																					
	$f_{c,red}$																					
HEA 180	$f_{t,red}$																					
	$f_{c,red}$																					
HEA 200	$f_{t,red}$																					
	$f_{c,red}$																					
HEA 220	$f_{t,red}$																					
	$f_{c,red}$																					
HEA 240	$f_{t,red}$																					
	$f_{c,red}$																					
HEA 260	$f_{t,red}$																					
	$f_{c,red}$																					
HEA 280	$f_{t,red}$																					
	$f_{c,red}$																					
HEA 300	$f_{t,red}$																					
	$f_{c,red}$																					
HEA 320	$f_{t,red}$																					
	$f_{c,red}$																					
HEA 340	$f_{t,red}$																					
	$f_{c,red}$																					
HEA 360	$f_{t,red}$																					
	$f_{c,red}$																					
HEA 400	$f_{t,red}$																					
	$f_{c,red}$																					
HEA 450	$f_{t,red}$																					
	$f_{c,red}$																					
HEA 500	$f_{t,red}$																					
	$f_{c,red}$																					
HEA 550	$f_{t,red}$																					
	$f_{c,red}$																					
HEA 600	$f_{t,red}$																					
	$f_{c,red}$																					

Fig. A-2 Design Chart for HE-A section (Partial Strength joints with $M_{j,red} < 0.50 M_{pl,R}$)

COLUMN

$N_{1,3d} > 0.75M_{pl,R1}$	BEAM																		
	HEA 100	HEA 120	HEA 140	HEA 160	HEA 180	HEA 200	HEA 220	HEA 240	HEA 260	HEA 280	HEA 300	HEA 320	HEA 340	HEA 360	HEA 400	HEA 450	HEA 500	HEA 600	
HEA 100	ck	ck	ck	ck	ck	ck	ck	ck	ck	ck	ck	ck	ck	ck	ck	ck	ck	ck	ck
HEA 120	ck	ck	ck	ck	ck	ck	ck	ck	ck	ck	ck	ck	ck	ck	ck	ck	ck	ck	ck
HEA 140	ck	ck	ck	ck	ck	ck	ck	ck	ck	ck	ck	ck	ck	ck	ck	ck	ck	ck	ck
HEA 160	ck	ck	ck	ck	ck	ck	ck	ck	ck	ck	ck	ck	ck	ck	ck	ck	ck	ck	ck
HEA 180	ck	ck	ck	ck	ck	ck	ck	ck	ck	ck	ck	ck	ck	ck	ck	ck	ck	ck	ck
HEA 200	ck	ck	ck	ck	ck	ck	ck	ck	ck	ck	ck	ck	ck	ck	ck	ck	ck	ck	ck
HEA 220	ck	ck	ck	ck	ck	ck	ck	ck	ck	ck	ck	ck	ck	ck	ck	ck	ck	ck	ck
HEA 240	ck	ck	ck	ck	ck	ck	ck	ck	ck	ck	ck	ck	ck	ck	ck	ck	ck	ck	ck
HEA 260	ck	ck	ck	ck	ck	ck	ck	ck	ck	ck	ck	ck	ck	ck	ck	ck	ck	ck	ck
HEA 280	ck	ck	ck	ck	ck	ck	ck	ck	ck	ck	ck	ck	ck	ck	ck	ck	ck	ck	ck
HEA 300	ck	ck	ck	ck	ck	ck	ck	ck	ck	ck	ck	ck	ck	ck	ck	ck	ck	ck	ck
HEA 320	ck	ck	ck	ck	ck	ck	ck	ck	ck	ck	ck	ck	ck	ck	ck	ck	ck	ck	ck
HEA 340	ck	ck	ck	ck	ck	ck	ck	ck	ck	ck	ck	ck	ck	ck	ck	ck	ck	ck	ck
HEA 360	ck	ck	ck	ck	ck	ck	ck	ck	ck	ck	ck	ck	ck	ck	ck	ck	ck	ck	ck
HEA 400	ck	ck	ck	ck	ck	ck	ck	ck	ck	ck	ck	ck	ck	ck	ck	ck	ck	ck	ck
HEA 450	ck	ck	ck	ck	ck	ck	ck	ck	ck	ck	ck	ck	ck	ck	ck	ck	ck	ck	ck
HEA 500	ck	ck	ck	ck	ck	ck	ck	ck	ck	ck	ck	ck	ck	ck	ck	ck	ck	ck	ck
HEA 600	ck	ck	ck	ck	ck	ck	ck	ck	ck	ck	ck	ck	ck	ck	ck	ck	ck	ck	ck

Fig. A.3 Design Chart for HE-A section (Partial Strength joints with $N_{1,3d} > 0.75 M_{pl,R1}$)

NW1103

		M _{r,0} > 1.0 M _{p,0} RC										RH-AM									
		HEA 100	HEA 120	HEA 130	HEA 160	HEA 180	HEA 200	HEA 220	HEA 240	HEA 260	HEA 280	HEA 300	HEA 320	HEA 340	HEA 360	HEA 400	HEA 450	HEA 500	HEA 550	HEA 600	
HEA 100	fr-rc																				
	fr-rc																				
HEA 120	fr-rc																				
	fr-rc																				
HEA 140	fr-rc																				
	fr-rc																				
HEA 160	fr-rc																				
	fr-rc																				
HEA 180	fr-rc																				
	fr-rc																				
HEA 200	fr-rc																				
	fr-rc																				
HEA 220	fr-rc																				
	fr-rc																				
HEA 240	fr-rc																				
	fr-rc																				
HEA 260	fr-rc																				
	fr-rc																				
HEA 280	fr-rc																				
	fr-rc																				
HEA 300	fr-rc																				
	fr-rc																				
HEA 320	fr-rc																				
	fr-rc																				
HEA 340	fr-rc																				
	fr-rc																				
HEA 360	fr-rc																				
	fr-rc																				
HEA 400	fr-rc																				
	fr-rc																				
HEA 450	fr-rc																				
	fr-rc																				
HEA 500	fr-rc																				
	fr-rc																				
HEA 550	fr-rc																				
	fr-rc																				
HEA 600	fr-rc																				
	fr-rc																				

COLUMN

Fig. A.4 Design Chart for HE-A section (Full Strength) joints with M_{r,0} > 1.0 M_{p,0}

COLUMN		BEAM																				
		HEA 100	HEA 120	HEA 140	HEA 160	HEA 180	HEA 200	HEA 220	HEA 240	HEA 260	HEA 280	HEA 300	HEA 320	HEA 340	HEA 360	HEA 400	HEA 450	HEA 500	HEA 500	HEA 600		
HEA 300	$M_{pl,Rd} > 1.2M_{pl,Rd}$																					
	$M_{pl,Rd} > 1.2M_{pl,Rd}$																					
HEA 320	$M_{pl,Rd} > 1.2M_{pl,Rd}$																					
HEA 340	$M_{pl,Rd} > 1.2M_{pl,Rd}$																					
HEA 360	$M_{pl,Rd} > 1.2M_{pl,Rd}$																					
HEA 400	$M_{pl,Rd} > 1.2M_{pl,Rd}$																					
HEA 450	$M_{pl,Rd} > 1.2M_{pl,Rd}$																					
HEA 500	$M_{pl,Rd} > 1.2M_{pl,Rd}$																					
HEA 550	$M_{pl,Rd} > 1.2M_{pl,Rd}$																					
HEA 600	$M_{pl,Rd} > 1.2M_{pl,Rd}$																					

Fig. A.5 Design Chart for HE-A section (Full) Strength joints with $M_{pl,Rd} > 1.2 M_{pl,Rd}$

		BEAM																			
		HEB 100	HEB 120	HEB 140	HEB 160	HEB 180	HEB 200	HEB 220	HEB 240	HEB 260	HEB 280	HEB 300	HEB 320	HEB 340	HEB 360	HEB 400	HEB 450	HEB 500	HEB 550	HEB 600	
HEB 100	$f_{t,red}$	M12	0	M12	2																
	$f_{c,red}$	8.8	0	8.8	0	8.8	0	8.8	0	8.8	0	8.8	0	8.8	0	8.8	0	8.8	0	8.8	0
HEB 120	$f_{t,red}$	M12	0	M12	1	M12	6														
	$f_{c,red}$	8.8	0	8.8	0	8.8	0	8.8	0	8.8	0	8.8	0	8.8	0	8.8	0	8.8	0	8.8	0
HEB 140	$f_{t,red}$	M12	0	M12	0	M12	0	M12	8												
	$f_{c,red}$	8.8	0	8.8	0	8.8	0	8.8	0	8.8	0	8.8	0	8.8	0	8.8	0	8.8	0	8.8	0
HEB 160	$f_{t,red}$	M12	0	M12	0	M12	0	M12	8	M12	18										
	$f_{c,red}$	8.8	0	8.8	0	8.8	0	8.8	0	8.8	0	8.8	0	8.8	0	8.8	0	8.8	0	8.8	0
HEB 180	$f_{t,red}$	M12	0	M12	0	M12	0	M12	0	M12	0	M12	0	M12	0	M12	0	M12	0	M12	0
	$f_{c,red}$	8.8	0	8.8	0	8.8	0	8.8	0	8.8	0	8.8	0	8.8	0	8.8	0	8.8	0	8.8	0
HEB 200	$f_{t,red}$	M12	0	M12	0	M12	0	M12	0	M12	0	M12	0	M12	0	M12	0	M12	0	M12	0
	$f_{c,red}$	8.8	0	8.8	0	8.8	0	8.8	0	8.8	0	8.8	0	8.8	0	8.8	0	8.8	0	8.8	0
HEB 220	$f_{t,red}$	M12	0	M12	0	M12	0	M12	0	M12	0	M12	0	M12	0	M12	0	M12	0	M12	0
	$f_{c,red}$	8.8	0	8.8	0	8.8	0	8.8	0	8.8	0	8.8	0	8.8	0	8.8	0	8.8	0	8.8	0
HEB 240	$f_{t,red}$	M12	0	M12	0	M12	0	M12	0	M12	0	M12	0	M12	0	M12	0	M12	0	M12	0
	$f_{c,red}$	8.8	0	8.8	0	8.8	0	8.8	0	8.8	0	8.8	0	8.8	0	8.8	0	8.8	0	8.8	0
HEB 260	$f_{t,red}$	M12	0	M12	0	M12	0	M12	0	M12	0	M12	0	M12	0	M12	0	M12	0	M12	0
	$f_{c,red}$	8.8	0	8.8	0	8.8	0	8.8	0	8.8	0	8.8	0	8.8	0	8.8	0	8.8	0	8.8	0
HEB 280	$f_{t,red}$	M12	0	M12	0	M12	0	M12	0	M12	0	M12	0	M12	0	M12	0	M12	0	M12	0
	$f_{c,red}$	8.8	0	8.8	0	8.8	0	8.8	0	8.8	0	8.8	0	8.8	0	8.8	0	8.8	0	8.8	0
HEB 300	$f_{t,red}$	M12	0	M12	0	M12	0	M12	0	M12	0	M12	0	M12	0	M12	0	M12	0	M12	0
	$f_{c,red}$	8.8	0	8.8	0	8.8	0	8.8	0	8.8	0	8.8	0	8.8	0	8.8	0	8.8	0	8.8	0
HEB 320	$f_{t,red}$	M12	0	M12	0	M12	0	M12	0	M12	0	M12	0	M12	0	M12	0	M12	0	M12	0
	$f_{c,red}$	8.8	0	8.8	0	8.8	0	8.8	0	8.8	0	8.8	0	8.8	0	8.8	0	8.8	0	8.8	0
HEB 340	$f_{t,red}$	M12	0	M12	0	M12	0	M12	0	M12	0	M12	0	M12	0	M12	0	M12	0	M12	0
	$f_{c,red}$	8.8	0	8.8	0	8.8	0	8.8	0	8.8	0	8.8	0	8.8	0	8.8	0	8.8	0	8.8	0
HEB 360	$f_{t,red}$	M12	0	M12	0	M12	0	M12	0	M12	0	M12	0	M12	0	M12	0	M12	0	M12	0
	$f_{c,red}$	8.8	0	8.8	0	8.8	0	8.8	0	8.8	0	8.8	0	8.8	0	8.8	0	8.8	0	8.8	0
HEB 400	$f_{t,red}$	M12	0	M12	0	M12	0	M12	0	M12	0	M12	0	M12	0	M12	0	M12	0	M12	0
	$f_{c,red}$	8.8	0	8.8	0	8.8	0	8.8	0	8.8	0	8.8	0	8.8	0	8.8	0	8.8	0	8.8	0
HEB 450	$f_{t,red}$	M12	0	M12	0	M12	0	M12	0	M12	0	M12	0	M12	0	M12	0	M12	0	M12	0
	$f_{c,red}$	8.8	0	8.8	0	8.8	0	8.8	0	8.8	0	8.8	0	8.8	0	8.8	0	8.8	0	8.8	0
HEB 500	$f_{t,red}$	M12	0	M12	0	M12	0	M12	0	M12	0	M12	0	M12	0	M12	0	M12	0	M12	0
	$f_{c,red}$	8.8	0	8.8	0	8.8	0	8.8	0	8.8	0	8.8	0	8.8	0	8.8	0	8.8	0	8.8	0
HEB 550	$f_{t,red}$	M12	0	M12	0	M12	0	M12	0	M12	0	M12	0	M12	0	M12	0	M12	0	M12	0
	$f_{c,red}$	8.8	0	8.8	0	8.8	0	8.8	0	8.8	0	8.8	0	8.8	0	8.8	0	8.8	0	8.8	0
HEB 600	$f_{t,red}$	M12	0	M12	0	M12	0	M12	0	M12	0	M12	0	M12	0	M12	0	M12	0	M12	0
	$f_{c,red}$	8.8	0	8.8	0	8.8	0	8.8	0	8.8	0	8.8	0	8.8	0	8.8	0	8.8	0	8.8	0

Fig. A-6 Design Chart for IHE-B section (Partial Strength joints with $M_{j,Rd} < 0.25 M_{pl,Rd}$)

NR11010

$M_{1,act} \geq 0.75 M_{p,0.80}$		BEAM																			
		HEB 100	HEB 120	HEB 140	HEB 160	HEB 180	HEB 200	HEB 220	HEB 240	HEB 260	HEB 280	HEB 300	HEB 320	HEB 340	HEB 360	HEB 400	HEB 450	HEB 500	HEB 550	HEB 600	
HEB	$f_{t,act}$																				
100	$f_{t,act}$																				
	$f_{t,act}$																				
HEB	$f_{t,act}$																				
120	$f_{t,act}$																				
	$f_{t,act}$																				
HEB	$f_{t,act}$																				
140	$f_{t,act}$																				
	$f_{t,act}$																				
HEB	$f_{t,act}$																				
160	$f_{t,act}$																				
	$f_{t,act}$																				
HEB	$f_{t,act}$																				
180	$f_{t,act}$																				
	$f_{t,act}$																				
HEB	$f_{t,act}$																				
200	$f_{t,act}$																				
	$f_{t,act}$																				
HEB	$f_{t,act}$																				
220	$f_{t,act}$																				
	$f_{t,act}$																				
HEB	$f_{t,act}$																				
240	$f_{t,act}$																				
	$f_{t,act}$																				
HEB	$f_{t,act}$																				
260	$f_{t,act}$																				
	$f_{t,act}$																				
HEB	$f_{t,act}$																				
280	$f_{t,act}$																				
	$f_{t,act}$																				
HEB	$f_{t,act}$																				
300	$f_{t,act}$																				
	$f_{t,act}$																				
HEB	$f_{t,act}$																				
320	$f_{t,act}$																				
	$f_{t,act}$																				
HEB	$f_{t,act}$																				
340	$f_{t,act}$																				
	$f_{t,act}$																				
HEB	$f_{t,act}$																				
360	$f_{t,act}$																				
	$f_{t,act}$																				
HEB	$f_{t,act}$																				
400	$f_{t,act}$																				
	$f_{t,act}$																				
HEB	$f_{t,act}$																				
450	$f_{t,act}$																				
	$f_{t,act}$																				
HEB	$f_{t,act}$																				
500	$f_{t,act}$																				
	$f_{t,act}$																				
HEB	$f_{t,act}$																				
550	$f_{t,act}$																				
	$f_{t,act}$																				
HEB	$f_{t,act}$																				
600	$f_{t,act}$																				
	$f_{t,act}$																				

A.8 Design Chart for HE-B section (Partial Strength joints with $M_{1,act} \geq 0.75 M_{p,0.80}$)

$M_{pl,Rd} \geq 1.0 M_{pl,Rd}$		BEAM																		
		HEB 100	HEB 120	HEB 140	HEB 160	HEB 180	HEB 200	HEB 220	HEB 240	HEB 260	HEB 280	HEB 300	HEB 320	HEB 340	HEB 360	HEB 400	HEB 450	HEB 500	HEB 550	HEB 600
HEB 100	d_f																			
	$R_{t,c}$																			
HEB 120	d_f																			
	$R_{t,c}$																			
HEB 140	d_f																			
	$R_{t,c}$																			
HEB 160	d_f																			
	$R_{t,c}$																			
HEB 180	d_f																			
	$R_{t,c}$																			
HEB 200	d_f																			
	$R_{t,c}$																			
HEB 220	d_f																			
	$R_{t,c}$																			
HEB 240	d_f																			
	$R_{t,c}$																			
HEB 260	d_f																			
	$R_{t,c}$																			
HEB 280	d_f																			
	$R_{t,c}$																			
HEB 300	d_f																			
	$R_{t,c}$																			
HEB 320	d_f																			
	$R_{t,c}$																			
HEB 340	d_f																			
	$R_{t,c}$																			
HEB 360	d_f																			
	$R_{t,c}$																			
HEB 400	d_f																			
	$R_{t,c}$																			
HEB 450	d_f																			
	$R_{t,c}$																			
HEB 500	d_f																			
	$R_{t,c}$																			
HEB 550	d_f																			
	$R_{t,c}$																			
HEB 600	d_f																			
	$R_{t,c}$																			

Fig. A.9 Design Chart for HE-B section (Full Strength joints with $M_{pl,Rd} \geq 1.0 M_{pl,Rd}$)

COLUMN

$M_{pl,Ed} > 1.0 M_{pl,Rk}$		BEAM																	
		HEB 100	HEB 120	HEB 140	HEB 160	HEB 180	HEB 200	HEB 220	HEB 240	HEB 260	HEB 280	HEB 300	HEB 320	HEB 340	HEB 360	HEB 400	HEB 450	HEB 500	HEB 600
HEB 100	$\frac{d_h}{t_w}$ $\frac{d_h}{t_{flk}}$																		
HEB 120	$\frac{d_h}{t_w}$ $\frac{d_h}{t_{flk}}$																		
HEB 140	$\frac{d_h}{t_w}$ $\frac{d_h}{t_{flk}}$																		
HEB 160	$\frac{d_h}{t_w}$ $\frac{d_h}{t_{flk}}$																		
HEB 180	$\frac{d_h}{t_w}$ $\frac{d_h}{t_{flk}}$																		
HEB 200	$\frac{d_h}{t_w}$ $\frac{d_h}{t_{flk}}$																		
HEB 220	$\frac{d_h}{t_w}$ $\frac{d_h}{t_{flk}}$																		
HEB 240	$\frac{d_h}{t_w}$ $\frac{d_h}{t_{flk}}$																		
HEB 260	$\frac{d_h}{t_w}$ $\frac{d_h}{t_{flk}}$																		
HEB 280	$\frac{d_h}{t_w}$ $\frac{d_h}{t_{flk}}$																		
HEB 300	$\frac{d_h}{t_w}$ $\frac{d_h}{t_{flk}}$																		
HEB 320	$\frac{d_h}{t_w}$ $\frac{d_h}{t_{flk}}$																		
HEB 340	$\frac{d_h}{t_w}$ $\frac{d_h}{t_{flk}}$																		
HEB 360	$\frac{d_h}{t_w}$ $\frac{d_h}{t_{flk}}$																		
HEB 400	$\frac{d_h}{t_w}$ $\frac{d_h}{t_{flk}}$																		
HEB 450	$\frac{d_h}{t_w}$ $\frac{d_h}{t_{flk}}$																		
HEB 500	$\frac{d_h}{t_w}$ $\frac{d_h}{t_{flk}}$																		
HEB 600	$\frac{d_h}{t_w}$ $\frac{d_h}{t_{flk}}$																		

COL:100

Fig. A.10 Design Chart for HE-B section (Full Strength joints with $M_{pl,Ed} > 1.0 M_{pl,Rk}$)

$M_{j,pc} \geq 1.0 M_{j,pc}$		HEM																			
		HEM 100	HEM 120	HEM 140	HEM 160	HEM 180	HEM 200	HEM 220	HEM 240	HEM 260	HEM 280	HEM 300	HEM 320	HEM 340	HEM 360	HEM 400	HEM 450	HEM 500	HEM 600		
HEM 100	$f_{t,pc}$	M12	M12	M14	M14	M16	M16	M18	M18	M20	M20	M22	M22	M24	M24	M26	M26	M28	M28	M30	
HEM 140	$f_{t,pc}$	8.8	10.5	16.9	1																
HEM 180	$f_{t,pc}$	2.58	3	4	M16	23															
HEM 240	$f_{t,pc}$	8.8	10.9	16.9	1	8.8	1														
HEM 300	$f_{t,pc}$	2.17	3	4	M16	5															
HEM 360	$f_{t,pc}$	M12	M12	M14	M14	M16	M16	M18	M18	M20	M20	M22	M22	M24	M24	M26	M26	M28	M28	M30	M30
HEM 400	$f_{t,pc}$	8.8	10.9	16.9	1	8.8	1														
HEM 450	$f_{t,pc}$	2.97	3	4	M16	7															
HEM 500	$f_{t,pc}$	8.8	10.9	16.9	1	8.8	1														
HEM 600	$f_{t,pc}$	2.44	3	4	M16	5															
HEM 100	$f_{t,pc}$	M12	M12	M14	M14	M16	M16	M18	M18	M20	M20	M22	M22	M24	M24	M26	M26	M28	M28	M30	M30
HEM 140	$f_{t,pc}$	8.8	10.9	16.9	1	8.8	1														
HEM 180	$f_{t,pc}$	2.44	3	4	M16	5															
HEM 240	$f_{t,pc}$	8.8	10.9	16.9	1	8.8	1														
HEM 300	$f_{t,pc}$	2.17	3	4	M16	5															
HEM 360	$f_{t,pc}$	M12	M12	M14	M14	M16	M16	M18	M18	M20	M20	M22	M22	M24	M24	M26	M26	M28	M28	M30	M30
HEM 400	$f_{t,pc}$	8.8	10.9	16.9	1	8.8	1														
HEM 450	$f_{t,pc}$	2.97	3	4	M16	7															
HEM 500	$f_{t,pc}$	8.8	10.9	16.9	1	8.8	1														
HEM 600	$f_{t,pc}$	2.44	3	4	M16	5															
HEM 100	$f_{t,pc}$	M12	M12	M14	M14	M16	M16	M18	M18	M20	M20	M22	M22	M24	M24	M26	M26	M28	M28	M30	M30
HEM 140	$f_{t,pc}$	8.8	10.9	16.9	1	8.8	1														
HEM 180	$f_{t,pc}$	2.44	3	4	M16	5															
HEM 240	$f_{t,pc}$	8.8	10.9	16.9	1	8.8	1														
HEM 300	$f_{t,pc}$	2.17	3	4	M16	5															
HEM 360	$f_{t,pc}$	M12	M12	M14	M14	M16	M16	M18	M18	M20	M20	M22	M22	M24	M24	M26	M26	M28	M28	M30	M30
HEM 400	$f_{t,pc}$	8.8	10.9	16.9	1	8.8	1														
HEM 450	$f_{t,pc}$	2.97	3	4	M16	7															
HEM 500	$f_{t,pc}$	8.8	10.9	16.9	1	8.8	1														
HEM 600	$f_{t,pc}$	2.44	3	4	M16	5															

Fig. A.14 Design Chart for HE-M section (Full Strength joints with $M_{j,pc} \geq 1.0 M_{j,pc}$)

NONI/OO

$M_{1,0.03} > 1.2M_{1,0.02}$		BEAM																			
		HEM 100	HEM 120	HEM 140	HEM 150	HEM 160	HEM 180	HEM 200	HEM 220	HEM 240	HEM 260	HEM 280	HEM 300	HEM 320	HEM 340	HEM 360	HEM 400	HEM 450	HEM 500	HEM 600	
HEM 100	$f_{t,c}$	10.5	17	10.9	20																
	$f_{t,t}$	34	6	37	6																
HEM 120	$f_{t,c}$	2.14	0	1.84	3																
	$f_{t,t}$	10.9	17	10.9	20																
HEM 140	$f_{t,c}$	3.2	3	3.7	6																
	$f_{t,t}$	10.9	17	10.9	20																
HEM 160	$f_{t,c}$	2.9	1	3.5	5																
	$f_{t,t}$	10.9	17	10.9	20																
HEM 180	$f_{t,c}$	2.8	0	3.3	4																
	$f_{t,t}$	10.9	17	10.9	20																
HEM 200	$f_{t,c}$	2.69	0	2.17	0	1.53	5														
	$f_{t,t}$	10.9	17	10.9	20																
HEM 220	$f_{t,c}$	2.6	0	2.14	0	1.6	0														
	$f_{t,t}$	10.9	17	10.9	20																
HEM 240	$f_{t,c}$	2.6	0	2.14	0	1.6	0														
	$f_{t,t}$	10.9	17	10.9	20																
HEM 260	$f_{t,c}$	2.63	0	2.24	0	1.65	1	1.56	3												
	$f_{t,t}$	10.9	17	10.9	20																
HEM 280	$f_{t,c}$	2.51	0	2.65	0	1.86	0	1.54	0	1.26	1										
	$f_{t,t}$	10.9	17	10.9	20																
HEM 300	$f_{t,c}$	2.3	0	2.6	0	1.90	0	1.37	0	1.29	0										
	$f_{t,t}$	10.9	17	10.9	20																
HEM 320	$f_{t,c}$	2.92	0	2.71	0	1.91	0	1.59	0	1.41	0										
	$f_{t,t}$	10.9	17	10.9	20																
HEM 340	$f_{t,c}$	2.3	0	2.5	0	3.1	0	3.2	0	3.7	0										
	$f_{t,t}$	10.9	17	10.9	20																
HEM 360	$f_{t,c}$	3.12	0	3.14	0	3.16	0	3.18	0	3.2	0										
	$f_{t,t}$	10.9	17	10.9	20																
HEM 400	$f_{t,c}$	2.3	0	2.5	0	2.9	0	3.1	0	3.5	0										
	$f_{t,t}$	10.9	17	10.9	20																
HEM 450	$f_{t,c}$	2.3	0	2.5	0	2.9	0	3.1	0	3.5	0										
	$f_{t,t}$	10.9	17	10.9	20																
HEM 500	$f_{t,c}$	2.89	0	2.70	0	1.94	0	1.82	0	1.35	0										
	$f_{t,t}$	10.9	17	10.9	20																
HEM 550	$f_{t,c}$	2.66	0	2.47	0	1.80	0	1.51	0	1.26	0										
	$f_{t,t}$	10.9	17	10.9	20																
HEM 600	$f_{t,c}$	2.35	0	2.36	0	1.73	0	1.45	0	1.22	0										
	$f_{t,t}$	10.9	17	10.9	20																
	$f_{t,c}$	2.3	0	2.5	0	2.9	0	3.1	0	3.5	0										
	$f_{t,t}$	10.9	17	10.9	20																
	$f_{t,c}$	2.45	0	2.30	0	1.66	0	1.40	0	1.17	0										
	$f_{t,t}$	10.9	17	10.9	20																

Fig. A.15 Design Chart for HT-M section (Pull Strength) joints with $M_{1,0.02} > 1.0 M_{1,0.03}$

7. REFERENCES

- Abidelah A, Bouchaïr A and Kerdal DE (2012) Experimental and analytical behavior of bolted end-plate connections with or without stiffeners. *Journal of Constructional Steel Research* 76: pp. 13–27.
- Adey B.T., Grondin G.Y. and Cheng J.J.R., (2000) Cyclic loading of end plate moment connections, *Canadian Journal of Civil Engineering*, 27(4): pp.683-701
- Augusto, H., Simões da Silva, L., Rebelo, C., Castro, J.M. (2017). Cyclic behaviour characterization of web panel components in bolted end-plate steel joints. *Journal of Constructional Steel Research*, 133, pp. 310-333.
- Brando G, Sarracco G and De Matteis G (2015) Strength of aluminium column web in tension. *Journal of Structural Engineering-ASCE*. 141 (7), July 2015, Article number 4014180 CID: 04014180, (doi: [http://dx.doi.org/10.1061/\(ASCE\)ST.1943-541X.0001138](http://dx.doi.org/10.1061/(ASCE)ST.1943-541X.0001138)).
- Bursi, O.S., Jaspert, J.P. (1997). Calibration of a Finite Element Model for Isolated Bolted End-Plate Steel Connections. *Journal of Constructional Steel Research*, 44 (3), pp. 225-262.
- Chen, X., Shi, G. (2016). Finite element analysis and moment resistance of ultra-large capacity end-plate joints. *Journal of Constructional Steel Research*, 126, pp. 153-162.
- De Matteis, G., Mandara, A., Mazzolani, F.M. (2000). T-stub Aluminium Joints: the Influence of Behavioural Parameters. *Computers and Structures*, Vol. 78, No. 1-3, 311-327.
- De Matteis, G., Brescia, M., Formisano, A., Mazzolani, F.M. (2009). Behaviour of welded aluminium T-stub joints under monotonic loading. *Computer & Structures*, vol. 87, Issues 15-16, 990-1002.
- Díaz C, Pascual M, Mariano V and Osvaldo MQ (2011) Review on the modelling of joint behaviour in steel frames. *Journal of Constructional Steel Research*, 67:5, pp. 741-758.
- El-Tawil, S. (2000). Panel zone yielding in steel moment connections. *Engineering Journal*, 37 (3), pp. 120-131.
- EN 1993-1-8 (2005). "Eurocode 3: Design of steel structures - Part 1-8: Design of joints" .Authority: The European Union Per Regulation 305/2011, Directive 98/34/EC, Directive 2004/18/EC.
- Faella C, Piluso V and Rizzano G (2000) *Structural Steel Semirigid Connections*. CRC Press, Florida, ISBN 0-8493-7433-2.
- He, J., Yoda, T., Takaku, H., Liu, Y., Chen, A., Iura, M. (2010). Experimental and numerical study on cyclic behaviour of steel beam-to-column joints. *International Journal of Steel Structures*, 10 (2), pp. 131-146.
- Hedayat, A.A., Saffari, H., Jazebi, E. (2016). Investigation of the effective parameters on the strength and ductility of the welded flange plate connections. *Asian Journal of Civil Engineering*, 17 (1), pp. 15-42.
- Jaspert JP (2000) General report: session on connections. *Journal of Constructional Steel Research*, 55, pp. 69-89.
- Jordão, S., Simões Da Silva, L., Simões, R. (2013). Behaviour of welded beam-to-column joints with beams of unequal depth. *Journal of Constructional Steel Research*, 91, pp. 42-59.
- Kanvinde, A.M., Grilli, D.A., Zareian, F. (2012). Rotational stiffness of exposed column base connections: Experiments and analytical models. *Journal of Structural Engineering*, 138 (5), pp. 549-560.
- Kaziolias, D.N., Efthymiou, E., Zygomalas, M., Baniotopoulos, C.C. (2013). On the separation zones in aluminium base-plate connections. Numerical simulation and laboratory testing. *Lecture Notes in Applied and Computational Mechanics*, 56 LNACM, pp. 293-308.
- Kosariéh, A.H., Danesh, F. (2016). Effects of panel zone yielding on seismic behavior of welded-flange-plate connections. *Bulletin of Earthquake Engineering*, 14 (10), pp. 2805-2825.
- Li, R., Samali, B., Tao, Z., Kamrul Hassan, M. (2017). Cyclic behaviour of composite joints with reduced beam sections. *Engineering Structures*, 136, pp. 329-344.
- Liu, Z.Q., Xue, J.Y., Peng, X.N., Gao, L. (2015). Cyclic test for beam-to-column abnormal joints in steel moment-resisting frames *Steel and Composite Structures*, 18 (5), pp. 1177-1195.
- Ma, H., Ren, S., Fan, F. (2016). Experimental and numerical research on a new semi-rigid joint for single-layer reticulated structures. *Engineering Structures*, 126, pp. 725-738.

- Maali, M., Kılıç, M., Aydın, A.C. (2016). Experimental model of the behaviour of bolted angles connections with stiffeners. *International Journal of Steel Structures*, 16 (3), pp. 719-733.
- Mansouri, I., Saffari, H. (2014). A new steel panel zone model including axial force for thin to thick column flanges. *Steel and Composite Structures*, 16 (4), pp. 417-436.
- Prinz GS, Nussbaumer A, Borges L and Khadka S (2014) Experimental testing and simulation of bolted beam-column connections having thick extended endplates and multiple bolts per row. *Engineering Structures* 59: pp. 434-447.
- Rahiminia, F., Namba, H. (2013). Joint panel in steel moment connections, Part 1: Experimental tests results. *Journal of Constructional Steel Research*, 89, pp. 272-283.
- Shi, G., Chen, X., Wang, D. (2017). Experimental study of ultra-large capacity end-plate joints. *Journal of Constructional Steel Research*, 128, pp. 354-361.
- Sui, W.-N., Sun, X., Wang, Z.-F., Li, G.-C. (2013). Research on design method and mechanical performance of the irregular joint with different beam depths. *Gongcheng Lixue/Engineering Mechanics*, 30(SUPPL.1), pp. 83-88.
- Takatsuka, K., Suita, K., Tanaka, T., Umeda, T. (2014). Effect of beam section size and connection detail on deformation capacity :Deformation capacity of welded beam-to-column connection subjected to repeated plastic strain Part 4. *Journal of Structural and Construction Engineering*, 79 (696), pp. 315-321.
- Tsavdaridis, K.D., Shaheen, M.A., Baniotopoulos, C., Salem, E. (2016).Analytical approach of anchor rod stiffness and steel base plate calculation under tension. *Structures*, 5, pp. 207-218.
- Weynand, K., Jaspert, J.-P., Steenhuis, M. (1998). Economy studies of steel building frames with semi-rigid joints. *Journal of Constructional Steel Research*, 46 (1-3), p. 85.
- Zoetemeijer P (1990) Summary of the research on bolted beam-to-column connections. Report 25-6-90-2, Delft University of Technology, Technology, Faculty of Civil Engineering, Stevin Laboratory—Steel Structures.

REVERSIBLE STEEL JOINT FOR SEISMIC-RESISTANT STRUCTURES

Margherita Pongiglione ^a, Chiara Calderini ^b, Mario D’Aniello ^c,
Raffaele Landolfo ^d

^a *University of Genoa, Genoa, Italy, margheritapongiglione@gmail.com*

^b *University of Genoa, Genoa, Italy, chiara.calderini@unige.it*

^c *University of Naples “Federico II”, Naples, Italy, mario.daniello@unina.it*

^d *University of Naples “Federico II”, Naples, Italy, landolfo@unina.it*

ABSTRACT

In the paper, the design of a novel seismic-resistant steel connection, which can be easily repaired and deconstructed at the same time, is presented. In the joint, all the bolt-holes and welds are placed off the structural profiles; instead, they are “clamped” by ad-hoc designed friction-based bolted splices. This way, the joint uses friction strength to resist the serviceability actions, but dissipates by friction hysteresis under the design seismic forces. At the same time, in case that the structure needed to be repaired, relocated or reused, the clamps could be easily removed and the structural elements promptly repaired, transported or reused.

KEYWORDS

Resilience, Sustainable structures, Steel joint; dissipative connections.

1 INTRODUCTION

Seismic-resistant steel structures are generally designed to withstand seismic-induced forces by dissipating energy thanks to the plastic deformations occurring into ductile zones without collapsing (Tenchini *et al.*, 2014; Cassiano *et al.*, 2016; D’Aniello *et al.*, 2017). However, these structures should also be economically repaired in order to avoid further economic and environmental impacts. On the other hand, buildings whose life span very likely depends on economic and technological factors can also be deconstructable, in order to have them disassembled and reused at their end-of-life, rather than demolished and disposed of (Pongiglione *et al.*, 2017).

Nowadays, strategies for reducing repair costs and maximizing a building’s post-seismic-event operability have been developed (Piluso *et al.*, 2014; Latour *et al.*, 2014, Latour *et al.*, 2015; Ioan *et al.*, 2016). In particular, this objective can be achieved by limiting the damage into specific parts (i.e. “dissipative fuses”), where the earthquake’s energy can be dissipated leaving the rest of the structure intact. After major seismic-events, these “fuses” can be replaced rather quickly and economically.

In line with this strategy, it is possible to conceive fully deconstructable and reusable buildings. This approach is named “Design for Disassembly” (or DfD). Research on DfD is today at its early stages and mainly focused on connections detailing, as connections removal is the most crucial part in the disassembly process of steel structures.

The purpose of this work is to adopt the DfD approach to complement the latest seismic design strategies, with the overall objective of integrating sustainability and resilience

approaches. In particular, this work is concerned with the design a novel seismic-resistant steel connection, which can be easily repaired and deconstructed at the same time. The purpose of the proposed connection is to allow moment-resisting steel frames for a prompt repair, in case of hazardous events, or for integral disassembly, in case that the structural system needs to be adapted, relocated, or even disposed of.

2 JOINT DESIGN

2.1 Geometrical Features

The examined joint has been conceived to comply with the main DfD principles from Crowther (2000) which reflect on the following criteria for steel structures (Pongiglione *et al.*, 2017):

- “To reduce the number of bolts” (with respect of traditional connections): the smaller the number of bolts to unbolt, the faster the disassembly process;
- “To use the same type of bolts”: the fewer the disassembly tools, the faster the disassembly process;
- “The joint should be adaptable to different structural members”: the more adaptable, the more reusable the connection;
- “To reduce the holes in the structural members, increasing their reusability”: too many holes require patching the holes, when not cutting off the bolted part;
- “To be easily accessible for the disassembly operation”: a non-accessible connection cannot be disconnected at all;
- “To be reversible, since its disassembly produces no damage on it”;
- “To be easily assembled” (so that DfD and assembly are not in conflict).

In order to comply with all these requirements, the proposed joint was conceived without using welds and/or holes for both column and beam, which are connected together by means of a set of specifically designed connecting devices and clamps as shown in Figure 1. As it can be observed, this joint consists of two diagonals (element 3 in Figure 1) and two stiffened seat connections (element 6 in Figure 1) The diagonals, which are connected to elements 1 and 2 by means of a pin (element 4 in Figure 1), serve to increase the lever arm, thereby reducing the entity of the horizontal forces acting on the structural elements. The seat connections are meant to transfer the beam shear load to the column.

The connections between seats, diagonals, beam and column are obtained by means of “ad-hoc” designed friction-based bolted splices or “clamps” (element 5 in Figure 1). These clamps consist in steel plates that are paired up by means of high-strength preloaded bolts. This way it was possible to place all the bolt-holes and welds off the structural profiles.

In order to prevent the clamps from opening as a consequence of the tightening of bolts, a set of turnbuckles were inserted in order to keep the plates clamping the structural profiles. The turnbuckles consist in two bolt shanks (element 8 in Figure 1) that are screwed into a pipe (element 7 in Figure 1), tapped with right hand threaded on one end and left hand on the other end. This allows for adjusting their total length and for proper tensioning. Furthermore, steel spacers (element 9 in Figure 1) have been placed between the paired plates.

Whether reusability is ensured by the use of the beam clamps, resilience and reparability are obtained through the clamps that dissipate by friction hysteresis under the design seismic forces.

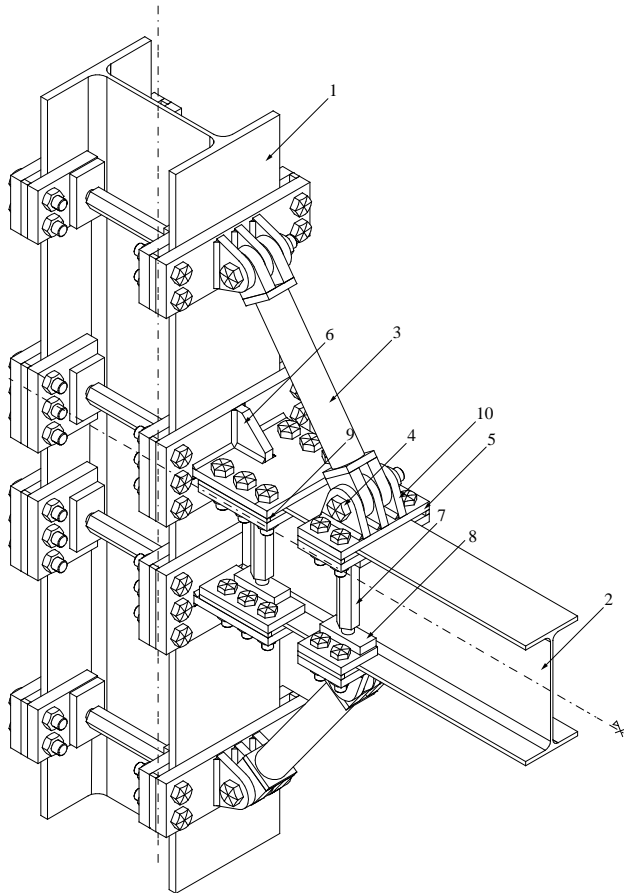


Figure 1. 3D view of the designed connection.

2.2 Performance levels and acceptance criteria

This connection is conceived to behave as rigid for serviceability limit state (SLS), and to allow beam-to-column relative rotation at ultimate limit state (ULS) by means of the relative slip between the beam flanges and the bolted clamps. In addition, the rational application of capacity design rules allows preserving all structural components (at both local and global level) from damage. This objective can be obtained following three main design phases. This first phase is the design of the friction resisting connections at beam flange for the actions due to ULS loading combinations. The slip strength should be calibrated in order to guarantee adequate strength, which should be sufficiently lower than the strength of the connected beam.

The second phase corresponds to the design of the other clamped connections that are non-dissipative. These connections will be designed to resist without slipping for the maximum calculated forces, which will be properly magnified to account for the variability of both friction coefficient and clamping forces.

The third phase corresponds to the design of columns and the remaining parts of the frames (e.g. column to column splice, base connections, etc.) that could be designed to be stable and elastic under the maxima effects developed by the dissipative friction connections.

The dissipative connections are expected to guarantee a rotation capacity equal to 0.04 radians. Hence, the clamps must be detailed accordingly. No slip can be accepted in the remaining clamped connections.

3 FINITE ELEMENT SIMULATIONS

3.1 Generality

The geometry of the proposed connections differs from the traditional beam-to-column joints commonly used in practice. In order to characterize the behavior of the novel components of the joint, a set of preliminary finite element (FE) analyses was performed to identify the main collapse mechanism and to determine if this mechanism is consistent with the overall goals of reparability and reusability.

The first assembly of components that has been analyzed consists in the beam clamps (shown in yellow in Figure 2). This assembly was analyzed with the objective to determine whether the clamps are able to transfer the design force to the beam before the slippage occurs.

The second assembly consists in the column clamps subject to a perpendicular design force (shown in green in Figure 3). This assembly was analysed with the goal to investigate the behaviour of the most critical components identified through the Component Method: the end-plate and the column flange in transverse bending.

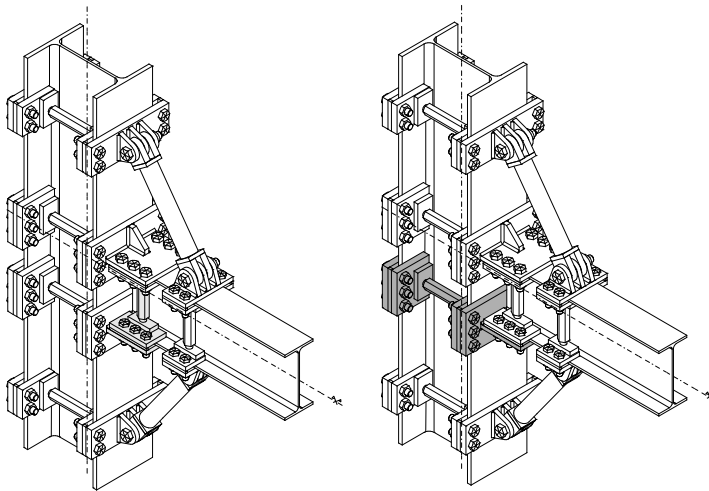


Figure 2. Beam (left) and column (right) clamps assembly.

3.2 Modelling assumptions

Finite element analyses were carried out using ABAQUS 6.14. The material non linearity was considered applying a true stress-true strain curve coming from coupon tests performed during experimental tests (D'Aniello *et al.*, 2017, Cassiano *et al.*, 2017). Geometrical non linearity were properly accounted for. C3D8I element (i.e. 8-node linear brick, incompatible mode) was adopted for meshing of all parts constituting the joint, i.e. column, beam, plates, bolts and welds (Tartaglia and D'Aniello, 2017). Three type of contact were introduced in the FE model:

- "Hard" contact: to model the normal contacts;
- Coulomb friction with friction coefficient equal to 0.3 for tangential behaviour;
- "Surface-to-surface" interaction: to model the contacts between adjacent surfaces.

The material of European high strength bolts is modelled as described by D'Aniello *et al.* (2016, 2017).

3.3 Numerical analyses of beam clamps

Three different design versions of the clamps were investigated under two loading conditions: the bolt tightening; the beam slip. As shown in Figure 4, the three design versions consist in: a) clamps with no spacers; b) clamps with shims; and c) clamps with steel spacers (in Figure 7 8). In this case, a half model was used to take advantage of symmetry.

Boundary conditions are the same in all three versions: the top of the half turnbuckles and the top the half beam are vertically restrained. The bottom clamp is fully restrained in correspondence of the red dot, in Figure 4.

Contact interaction were defined between:

- the top clamps and the beam;
- the bottom clamps and the beam;
- the bolts (head, nut, and shank) and the clamps (bolt-hole included);
- the turnbuckles' plates and the top clamps;
- the spacers or the shims (when present) and the clamps.

Each analysis ended when both the bolts and the turnbuckles were fully preloaded. Turnbuckles' preloading was assigned by applying an axial compressive displacement to the top of each half-bar.

The three design versions were compared in terms of equivalent plastic strain (expressed in %), deformation (the deformed shape is plotted together with the equivalent plastic strain, with a scale factor equal to 3) and Von Mises Stress (expressed in MPa).

As it can observe from Figure 5, the "no spacers" option is the only that produces a plasticization, while the "shims" and the "spacers" options don't lead to a permanent strain. Also, the "no spacers" option is the one that produces the largest stress state (the Von Mises stress reaches 790 MPa in the bolts and in the turnbuckles) and the largest deformation.

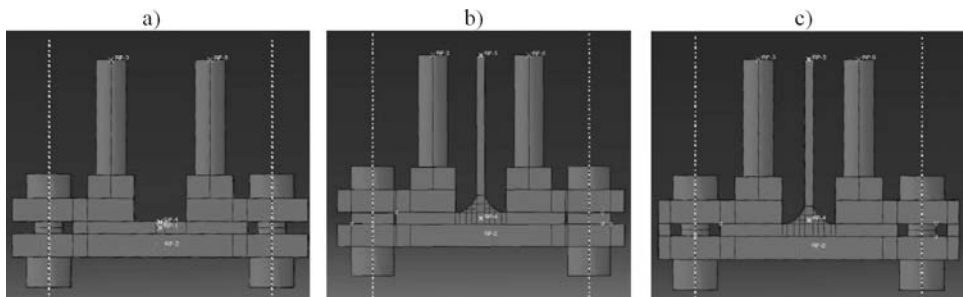


Figure 4. Clamps assembly: clamps with no spacers (a), clamps with shims (b), and clamps with steel spacers (c).

The "shims" option produces a smaller deformation than the "no spacers" option, but the stress state is still high (the Von Mises stress reaches 725 MPa in the bolts and in the turnbuckles).

The “spacers” option is the one that undergoes the smallest deformation (almost invisible from Figure 5) and the lowest stress state (the Von Mises stress reaches 392 MPa in the bolts). For these reasons, the “spacers” option was judged the best one and the following analyses on the beam clamps and on the column clamps assemblies will implement it.

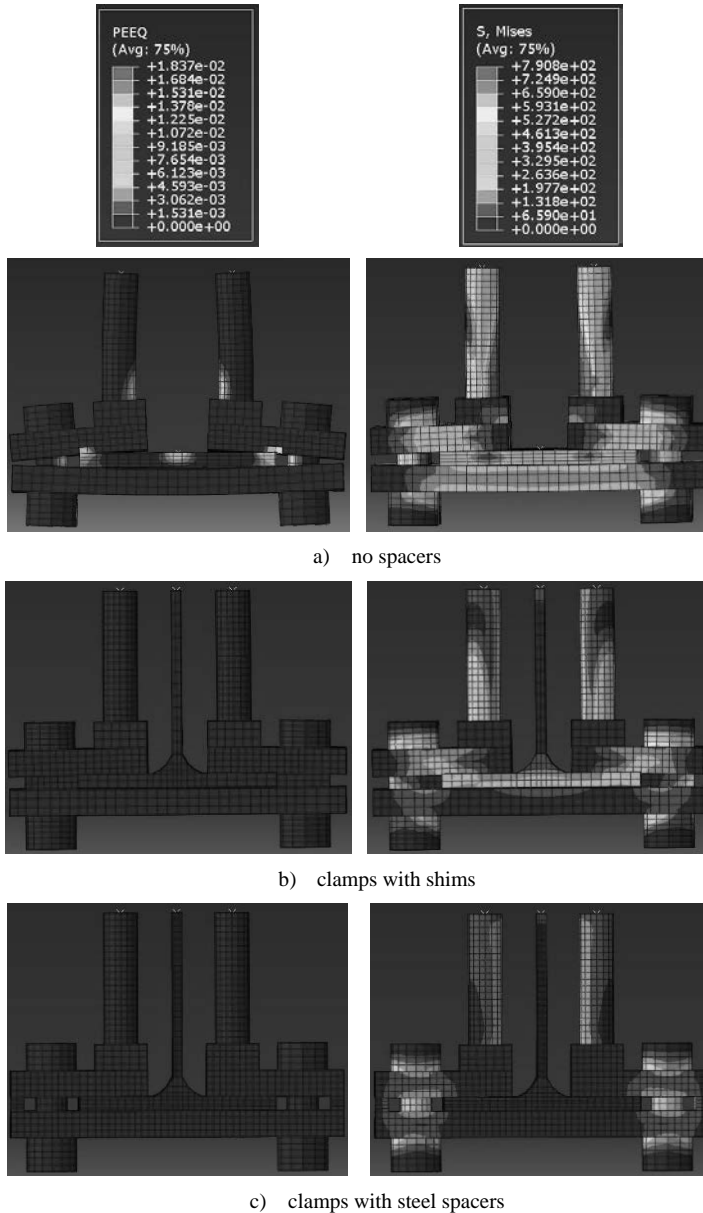


Figure 5. Equivalent plastic strain expressed in % on the left (deformation scale factor = 3) and Von Mises Stress expressed in MPa in the investigated configurations.

Once the most efficient configuration was chosen, a monotonic analysis was run on the beam clamps assembly. Keeping the boundary conditions and contact interactions of the preliminary analysis, a monotonic horizontal displacement was applied the beam web in the point p_b , as shown in Figure 6.

The response curve of the beam clamps under slip loading is shown in Figure 7. By plotting the reaction force F_b of point p_b as a function of its horizontal displacement d_b , it was possible to calculate the maximum force $F_{b,max}$ that the clamps are able to transfer to the beam before slipping and to compare $F_{b,max}$ to the design force $F_{h,Ed}$.

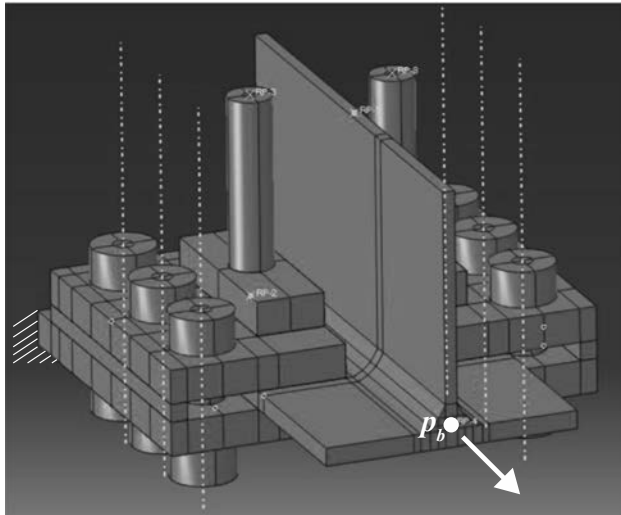


Figure 6. Beam clamps: monotonic analysis.

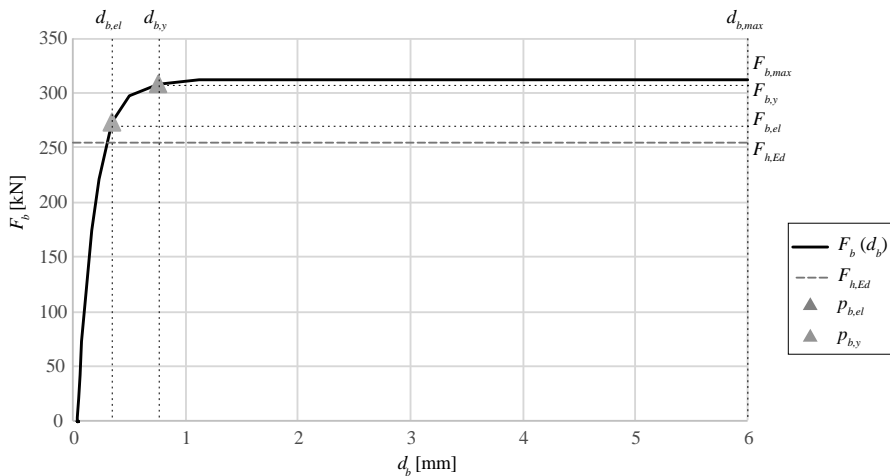


Figure 7. Force-displacement graph of the reaction force F_b of point p_b as a function of its horizontal displacement d_b and comparison with the design force $F_{h,Ed}$.

3.4 Numerical analyses of column clamps

The boundary and loading conditions of the models consider one side of the column as fully restrained, while a horizontal tensile displacement d_c applied to point p_c , on the flange that is welded to the clamp (in Figure 8). Turnbuckles' preloading was assigned by applying a compressive force to an internal surface of the turnbuckle's bar.

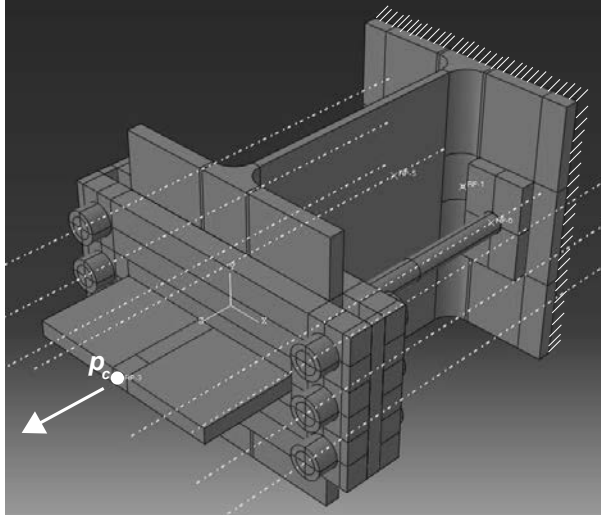


Figure 8. Column clamps: model assembly.

Once determined the most appropriate mesh size, the assembly shown in Figure 8 was tested under a monotonic load.

By plotting the reaction force F_c of point p_c as a function of its horizontal displacement d_c , it was possible to calculate the value of the reaction force at the yield point $F_{c,y}$, that is when the first plasticization occurs, and to compare $F_{c,y}$ to the design force $F_{h,Ed}$ (Figure 9).

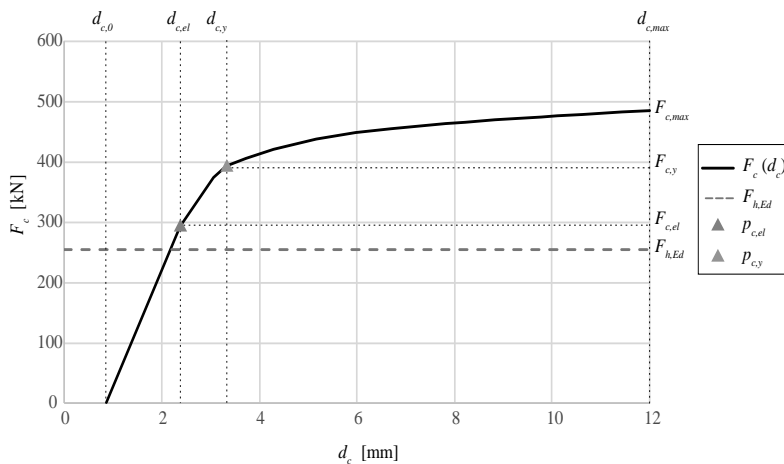


Figure 9. Force-displacement graph of the reaction force F_c of point p_c as a function of its horizontal displacement d_c and comparison with the design force $F_{h,Ed}$.

The failure mode is mostly characterized by plastic deformation of the column flange at the rolling radius, see Figure 9. This implies that the design criteria are effective. Because the column clamps are designed to be elastic and therefore stronger than the connected columns in order to avoid plastic deformations into the clamps that are the unique elements that guarantee the connection between beam and column.

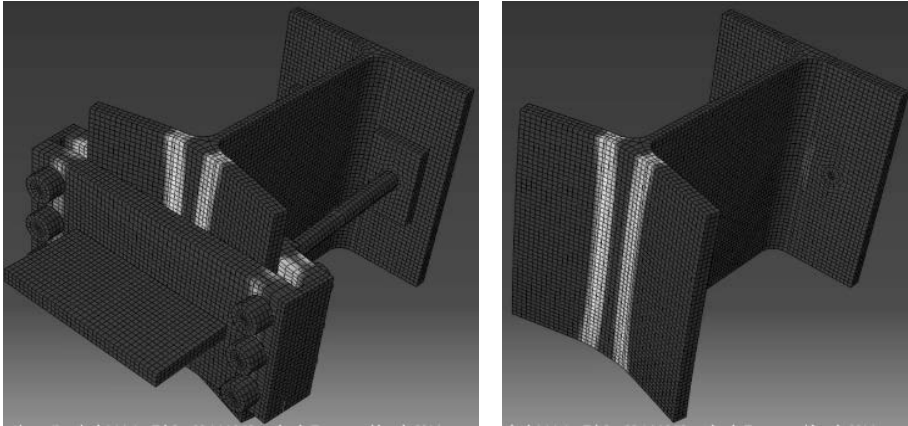


Figure 9. Failure mode of the column clamp.

4 CONCLUSIONS

The numerical study described in this paper was mostly devoted to investigate the behaviour of the main components of a novel beam-to-column joint, which has been specifically conceived for low-to-moderate seismic areas as fully deconstructable and reusable according to the philosophy of “Design for Disassembly” (or DfD). The preliminary results show that the system can profitably work. Further experimental and numerical research is necessary to characterize the overall and local response as well as the design rules.

Preliminary structural analysis focused on the clamps, which are the most crucial part in making this connection work. However, the entire connection assembly should be analyzed. This analysis would be essential to determine the actual connection’s capacity, expressed by its moment-rotation curve. Further areas of future research may consist in investigating the fire-resistance of the designed clamp. In particular, the structural behavior of the clamps in case of fire needs to be investigated, focusing on the reduction of the slip-factor and the clamping force.

Another aspect worth consideration is the compliance of this novel connection with existing building codes. Yet, existing building codes do not consider the possibility of designing slip-critical connections that have no “shear safety mechanisms”. This is true especially as far as concerns fire safety issues. Yet, according the EN 1993-1-2, slip-critical connections should be considered “as having slipped in fire”, no matter the surface treatment performed on them. Last but not least, future works should assess total fabrication costs of the designed connection and time for assembly/disassembly processes. This assessment would be essential to strengthen the causes of reparability and reusability and the overall idea of pursuing a unique, integrated design solution.

5 REFERENCES

- Cassiano, D., D'Aniello, M., Rebelo, C., Landolfo, R., da Silva, L. 2016. Influence of seismic design rules on the robustness of steel moment resisting frames. *Steel and Composite Structures, An International Journal*, **21(3)**: 479-500.
- Cassiano, D., D'Aniello, M., Rebelo, C., 2017. Parametric finite element analyses on flush end-plate joints under column removal. *Journal of Constructional Steel Research*, **137**: 77–92.
- Crowther, P., 2000. Developing guidelines for designing for deconstruction. In Proc., Deconstruction – Closing the Loop, Building Research Establishment (BRE), Watford, United Kingdom.
- D'Aniello, M., Tartaglia, R., Costanzo, S., Landolfo, R., 2017. Seismic design of extended stiffened end-plate joints in the framework of Eurocodes, *Journal of Constructional Steel Research*, **128**, 512–527
- D'Aniello, M., Cassiano, D., Landolfo, R., 2016. Monotonic and cyclic inelastic tensile response of European preloadable GR10.9 bolt assemblies, *Journal of Constructional Steel Research*, **124**: 77–90.
- D'Aniello, M., Cassiano, D., Landolfo, R., 2017. Simplified criteria for finite element modelling of European preloadable bolts. *Steel and Composite Structures, An International Journal*.
- EN 1998-1, Design of structures for earthquake resistance - Part 1: General rules, seismic actions and rules for buildings.
- Ioan, A., Stratan, A., Dubina, D., Poljansek, M., Molina, F. J., Taucer, F., Pegon, P., Sabau, G., 2016. Experimental validation of re-centering capability of eccentrically braced frames with removable links, *Engineering Structures*, **113**, 335-346
- Latour, M., Piluso, V., Rizzano, G., 2014. Experimental Analysis on Friction Materials for Supplemental Damping Devices, *Construction and Building Materials*, **65**, 159-176.
- Latour, M., Piluso, V., Rizzano, G., 2015. Free from damage beam-to-column joints: Testing and design of DST connections with friction pads, *Engineering Structures* **85**, 219–233.
- Piluso, V., Montuori, R., Troisi, M., 2014. Innovative structural details in MR-frames for free from damage structures, *Mechanics Research Communications* **58** 146-156.
- Tenchini, A., D'Aniello, M., Rebelo, C., Landolfo, R., da Silva, L.S., Lima, L. 2014. Seismic performance of dual-steel moment resisting frames. *Journal of Constructional Steel Research*, **101**: 437-454
- Tartaglia, R., D'Aniello, M., 2017. Nonlinear performance of extended stiffened end plate bolted beam-to-column joints subjected to column removal. *The Open Civil Engineering Journal*, **11**: 3-15.
- Pongiglione, M., Calderini, C., Guy, G.B. 2017 A new demountable seismic-resistant joint to improve industrial building reparability. *International Journal of Disaster Resilience in the Built Environment* **8(3)**.

SECTION 2

STEEL-CONCRETE COMPOSITE JOINTS

THE GUIDELINES FOR THE DESIGN OF STEEL-CONCRETE COMPOSITE JOINTS IN SEISMIC AREAS

Claudio Amadio ^a, Marco Fasan ^b, Maria Rosaria Pecce ^c, Giuseppe Logorano ^d

^a *University of Trieste, Trieste, Italy, amadio@units.it*

^b *University of Trieste, Trieste, Italy, mfasan@units.it*

^c *University of Sannio, Benevento, Italy, pecce@unisannio.it*

^d *University of Sannio, Benevento, Italy, logorano@unisannio.it*

ABSTRACT

The behaviour of steel and steel-concrete composite joints has been thoroughly studied in the last decades, with focus on their influence on the global response of framed structures. Nevertheless, especially as far as composite steel-concrete structures are concerned, there are no well-established design guidelines to optimize choices and adequately design composite joints. For this purpose, the Guidelines for the seismic design of steel-concrete composite framed structures and the non-linear analysis and the Guidelines for the seismic design of steel-concrete composite joints were developed within the RELUIS 2014-16 project, financed by the ‘Dipartimento di Protezione Civile’ (Department of Civil Protection). This paper highlights the main issues that need to be addressed with regards to the seismic design of the beam to column joints and frames belonging to steel-concrete structures, discussing rules reported within codes, as well as modelling approaches. The provisions that are referred to this paper are the ‘Norme Tecniche per le Costruzioni’ (NTC2008) and the Eurocode 4 [EN 1994-1-1:2004] as far as the general rules to be applied to the design of a composite structure are concerned, and the Eurocode 8 [EN 1998-1:2004] as regards the specific rules to be applied.

KEYWORDS

Composite joints, Steel-concrete frames, slab mechanisms, slab-column interactions.

1 INTRODUCTION

This paper focuses on the main issues affecting the modelling and design of steel-concrete composite structures in seismic areas, with focus on the evaluation of joints behavior. Indications for the design of seismic-resistant composite frames and structural joints have recently been collected in specific Guidelines developed under the ReLUIIS Project 2014-16. The regulations referred to this note are the Italian building code (NTC2008) and the Eurocode 4 [EN 1994-1-1: 2004] as regards the general rules to be applied in the design of a composite structure and the Eurocode 8 [EN 1998-1: 2004] for the specific rules to be applied in seismic areas. Specifically, the different resistant mechanisms that might occur in the concrete slab at the beam-to-column intersection are discussed. Moreover, a design procedure of the slab able to assure a high ductility of the node is described. Finally, the stiffness and resistance of the basic composite components are defined to determine the moment-rotation curve of a composite joint, either welded or bolted.

2 STEEL-CONCRETE COMPOSITE FRAMES

The behaviour of a steel-concrete composite frame under seismic actions can be very complex, and attention must be given to the nodal behaviour that can be influenced by multiple parameters, such as:

- the sign of the bending moment, the moment-rotation curve is asymmetric;
- the type of steel joint (welded, with extended end-plate, with cleats etc.);
- the presence or not of a concrete cantilever edge strip;
- the node position inside the frame (interior or exterior);
- a bracing system if present.

In a moment resisting frame, the slab is usually in contact with the column (see Figure 1); in this case, interactions between the slab and the column can arise, with the development of different strut-and-tie resistant mechanisms that form between the longitudinal and transverse rebars and the concrete in compression.

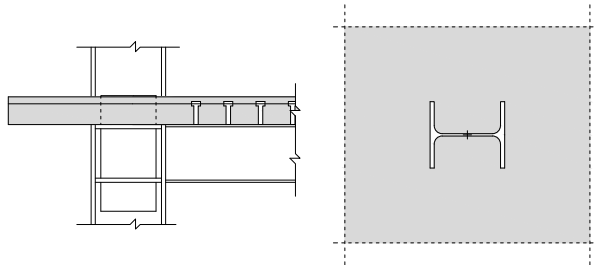


Figure 1. Typical steel-concrete compound joint (slab in contact with the column).

These interactions significantly affect the joint response in terms of ductility, stiffness, and resistance, and therefore a careful evaluation is required to ensure that the principle of hierarchy of resistances is satisfied (Amadio *et al.*, 2016, 2017a).

A design alternative that allows to ignore the composite action near the node is to disconnect the slab, i.e. to avoid, through suitable construction details, the slab-column interactions. Generally, the following arrangements are necessary (Chaudhari *et al.*, 2015) (Seek and Murray, 2008):

- shear studs should not be placed in the beam for a distance from the column face of 1.5 times the height of the composite beam;
- a 2 to 3 centimetres gap between the column and the slab must be made to avoid direct contact and thus the formation of struts;
- the longitudinal rebars must be interrupted at the column.

As for Eurocode 8, interactions can be avoided if the slab is “*totally disconnected from the steel frame in a circular zone around a column of diameter $2b_{eff}$, with b_{eff} being the larger of the effective widths of the beams connected to that column*”.

However, the construction details required to disconnect the slab still need to be studied in depth, particularly as regards the possibility of maintaining the continuity of the longitudinal rebars to realize, through the use of hinged steel joints, composite beams that behave like continuous on multiple supports under vertical loads, and at the same time transfer only shear forces to the column (Amadio *et al.*, 2017b).

In the case of steel-concrete composite structures, the possible construction typologies are numerous. In fact, they vary according to the static scheme that the structure assumes under

the action of horizontal and vertical loads, and hence depending on the type of joint. Based on the structural system that opposes the horizontal forces (earthquake, wind, imperfections, etc.), two macro categories are identified:

- braced composite structures;
- moment resisting composite structures.

Below, the main construction choices available for both cases are briefly described.

2.1 Braced structures

The bracing system is considered effective if:

- its stiffness K_{brace} is much greater than that of the frame K_{frame} (usually at least $K_{brace} > 5 K_{frame}$);
- the seismic base shear V_b is absorbed mainly by the bracing system (for example $V_{b, brace} > 80\% V_b$).

It is thus clear that a correct evaluation of the joint influence is also required when designing braced structures; when adopting this structural typology, it is appropriate to “isolate” the slab to build pinned frames and entrust the entire horizontal action to the bracing system. For this purpose, some of the possible design choices are:

- pinned beams: the slab is disconnected from the column by means of a gap and there is no rebar continuity between two consecutive spans (Figure 2);

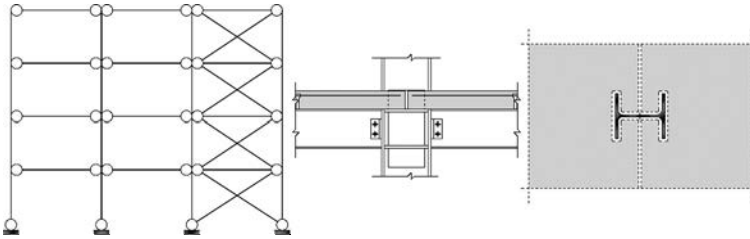


Figure 2. Braced frame with pinned beams.

- Continuous beams and pinned columns: the slab is still disconnected but the longitudinal rebars are continuous. The beam behaves as continuous on multiple supports and the negative bending moments at the node are self-balanced (Figure 3);

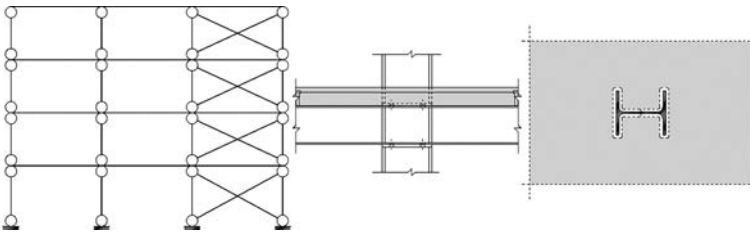


Figure 3. Braced frame with continuous beams and pinned columns.

- Frame with disconnected slab and cleated steel joints: the cleats transmit only shears forces to the column while continuity of longitudinal rebars keeps the beam running as a continuous on multiple supports under the action of vertical loads (Figure 4).

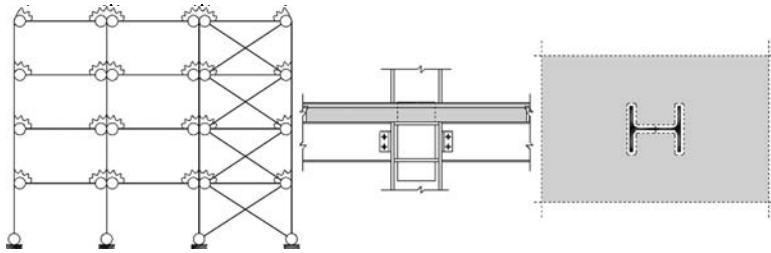


Figure 4. Braced frame with web cleats connection.

2.2 Moment-Resisting Frames (MRF)

In MRF both vertical and horizontal loads are entrusted to the framed system, therefore the connections must be able to transfer the bending moments. Two solutions can be adopted for the slab detailing:

- Slab disconnected from the column (isolated slab): only steel components offer resistance at the beam-column (Figure 5a);
- Slab in contact with the column: it is necessary to evaluate the slab-column interactions (Figure 5b).

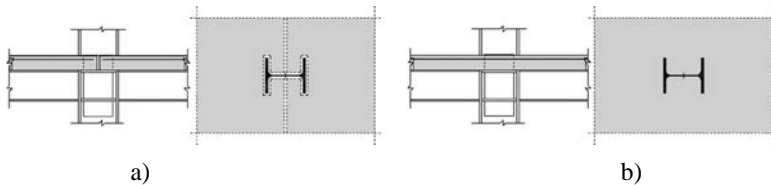


Figure 5. MRF composite structure: Isolated slab (a), Slab in contact (b).

In both cases, the role played by the joint and dissipations near the nodal zone are fundamental to evaluate the structural response (Fasan, 2013), (Pecce and Rossi, 2015). This aspect is deepened in the “*Linee guida per la progettazione sismica di nodi composti acciaio-calcestruzzo*” (Amadio *et al.*, 2016).

3 COMPOSITE JOINTS

In steel-concrete composite joints interactions between the slab and the column lead to creation of different strut-and-tie mechanisms between the rebars in tension (both longitudinal and transversal) and the concrete in compression in contact with the column.

Such interactions significantly affect the joint ductility, stiffness, and resistance, and it is therefore necessary to carefully evaluate them to ensure the principle of hierarchy of resistance is satisfied. At beam-column intersection, depending on the node configuration, several mechanisms can be present simultaneously. In these cases, the maximum compression force that can be transmitted from the slab to the column is given by the sum of the resistances of the individual mechanisms.

3.1 Resistant mechanisms of the slab

3.1.1 Mechanism 1: direct contact between the slab and the column flange

Mechanism 1 consists in a compressed strut in direct contact with the column flange (Figure 6), as proposed in the Eurocode 8, the maximum transmitting force is:

$$F_{Rd,1} = b_b d_{eff} (0.85 f_{ck} / \gamma_c) \quad (1)$$

Where b_b represents the bearing width of the concrete of the slab (equal to the width of the column or that of any plate used to increase the contact area), d_{eff} the effective depth of the slab (equal to its thickness in the case of solid slabs or to the thickness of the slab over the ribs in the case of a slab with a sheet steel), f_{ck} and γ_c the compressive characteristic resistance and the concrete safety coefficient. This mechanism is present either with slab in compression (positive bending moment) or in tension (negative bending moment) (see Figure 6).

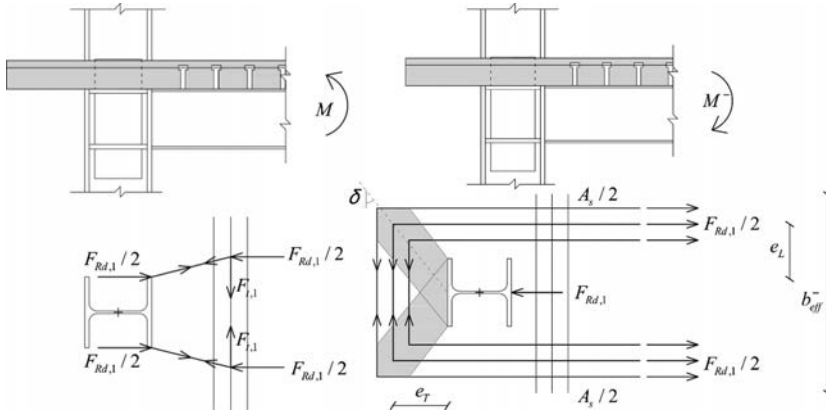


Figure 6. Mechanism 1: a) Positive bending moment; b) Negative bending moment.

- Slab in compression

When the slab is in compression (Figure 6a), the force $F_{Rd,1}$ spreads along the beam for a length almost equal to b_{eff}^+ and generates a transversal force $F_{t,1}$ which can be calculated as (Plumier *et al.*, 1998) (Figure 7):

$$F_{t,1} = \frac{F_{Rd,1}}{2} \tan \alpha = \frac{F_{Rd,1}}{4} \frac{(b_{eff}^+ - b_b)}{b_{eff}^+} \quad (2)$$

Since $b_{eff}^+ = 0.15l$, it follows:

$$F_{t,1} = 0.25 b_b d_{eff} 0.85 \frac{f_{ck}}{\gamma_c} \frac{0.15l - b_b}{0.15l} = A_T (f_{yk,T} / \gamma_s) \quad (3)$$

where A_T represent the transversal rebars area, therefore the mechanism 1 transmit the maximum force if in the slab is placed a total rebar area of:

$$A_T = 0.25b_b d_{eff} \frac{0.15l - b_b}{0.15l} \left(\frac{0.85f_{ck} / \gamma_c}{f_{yk,T} / \gamma_s} \right) \tag{4}$$

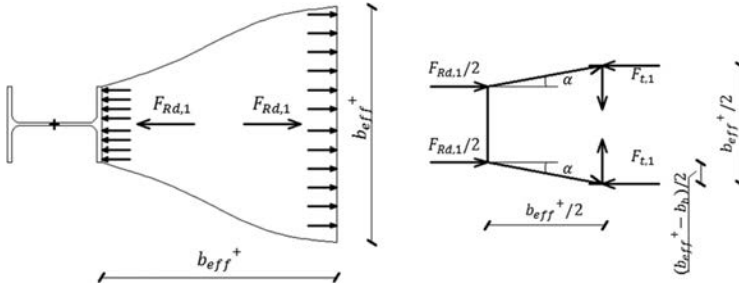


Figure 7. Spread of the concentrated force due to mechanism 1.

- Slab in tension

The longitudinal rebars behave like ties and, depending on the nodal configuration, concrete struts might appear in contact with the column on the opposite side (see Figure 6b). To obtain a ductile behaviour the longitudinal rebars should yield before the concrete crushing, hence:

$$A_{s,1} \leq \frac{F_{Rd,1}}{f_{yd,1}} = b_b d_{eff} \left(\frac{0.85f_{ck} / \gamma_c}{f_{yk,1} / \gamma_s} \right) \tag{5}$$

3.1.2 Mechanism 2: inclined concrete struts in contact with the column sides

This mechanism, as proposed in the Eurocode 8, consists in inclined concrete struts in contact with the column sides. The maximum transmissible force is:

$$F_{Rd,2} = 0.7h_c d_{eff} (0.85f_{ck} / \gamma_c) \tag{6}$$

Where h_c represents the height of the column. The presence of this mechanism depends on the node configuration.

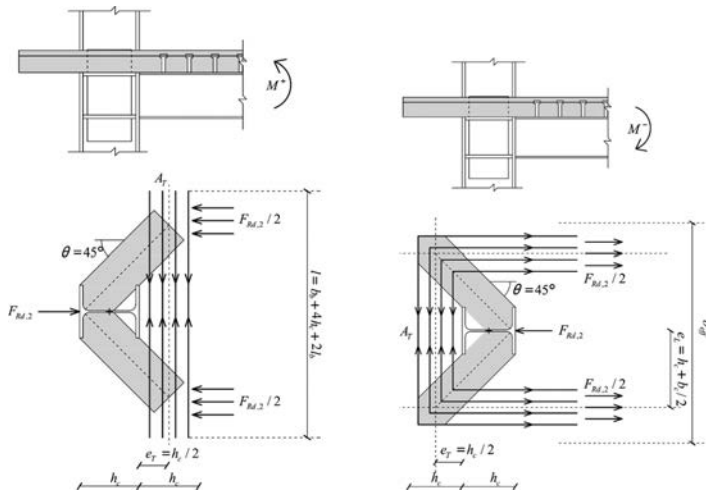


Figure 8. Mechanism 2: a) Positive bending moment; b) Negative bending moment.

- Slab in compression (Figure 8a)

In this case the longitudinal rebars do not participate in the activation of the mechanism. On the contrary, the transversal rebars need to be properly designed. Assuming an inclination angle of the struts $\theta = 45^\circ$ and a concrete resistance $0.7f_{cd}$, the maximum resistance of each strut is:

$$F_{c,2} = 0.7b_0d_{eff} (0.85f_{ck} / \gamma_c) = 0.7h_c / \sqrt{2}d_{eff} f_{cd} \quad (7)$$

Where b_0 is the width of the strut. The compressive concrete strength has been reduced to consider the presence of transversal tractions. The maximum force transmissible by mechanism 2 is obtained by finding the resultant of the two struts:

$$F_{Rd,2} = 2 \frac{F_{c,2}}{\sqrt{2}} = 0.7h_c d_{eff} (0.85f_{ck} / \gamma_c) \quad (8)$$

The force in the steel tie is equal to $F_{Rd,2}/2$, therefore the total area of transversal rebars needed is:

$$A_{T,2} \geq \frac{F_{Rd,2}}{2(f_{yk,T} / \gamma_s)} = 0.35h_c d_{eff} \left(\frac{0.85f_{ck} / \gamma_c}{f_{yk,T} / \gamma_s} \right) \quad (9)$$

Following this design (suggested by EC8), the concrete crushes before the transversal rebar yielding is reached. However, to increase the ductility the rebars should yield before reaching the crushing of struts. This condition can be achieved dimensioning the transversal rebars as follows (Amadio *et al.*, 2017a):

$$A_{T,2} \leq \frac{F_{Rd,2}}{2(f_{yk,T} / \gamma_s)} = 0.35h_c d_{eff} \left(\frac{0.85f_{ck} / \gamma_c}{f_{yk,T} / \gamma_s} \right) \quad (10)$$

Following the last case, the maximum force transmissible by mechanism 2 become:

$$F_{Rd,2} = 2A_{T,2} f_{yk,T} / \gamma_s \quad (11)$$

- Slab in tension (Figure 8b)

When the slab is subject to a negative moment, mechanism 2 balances the tension of the longitudinal rebars (Figure 8b). In this case the inclined struts appear on the opposite side to the application of the stress. The maximum force transmissible by each strut should be expressed as a function of its inclination angle θ . Assuming a concrete compressive strength of $0.7f_{cd}$ it can be evaluated as:

$$F_{c,2} = 0.7b_0d_{eff} (0.85f_{ck} / \gamma_c) = 0.7(h_c \sin \theta) d_{eff} f_{cd} \quad (12)$$

The maximum force transmissible by mechanism 2 is obtained by finding the resultant of the two struts:

$$F_{Rd,2} = 2F_{c,2} \cos \theta = 1.4h_c d_{eff} (0.85f_{ck} / \gamma_c) \sin \theta \cos \theta \quad (13)$$

To achieve the yield of the longitudinal reinforcement before the concrete crushing, the maximum rebars area should be determined as:

$$A_{s,2} \leq \frac{F_{Rd,2}}{2(f_{yk,l} / \gamma_s)} = 1.4h_c d_{eff} \sin \theta \cos \theta \left(\frac{0.85f_{ck} / \gamma_c}{f_{yk,l} / \gamma_s} \right) \quad (14)$$

3.1.3 Mechanism 3: struts in contact with the studs of transversal beam

The maximum transmissible force by this mechanism is:

$$F_{Rd,3} = nP_{Rd} \quad (15)$$

with n number of studs present along the transverse beam for a length equal to the effective width and P_{Rd} the shear strength of the single stud.

When the slab is in tension, to achieve the yield of the longitudinal reinforcement before the concrete crushing, the maximum rebars area should be determined as:

$$A_{s,3} \leq \frac{F_{Rd,3}}{f_{yd,l}} \quad (16)$$

3.2 Basic composite joint components and ductility criteria

To evaluate the strength and stiffness of a joint using the component method, it is necessary to identify the basic components that affect its behaviour, characterizing their stiffness k_i and resistance $F_{Rd,i}$. As mentioned above, besides the steel components, a steel-concrete composite joint is influenced:

- by the longitudinal reinforcement placed in the slab;
- by the interactions between the concrete slab and the steel parts.

Consequently, in addition to the bare steel components (defined in EC3 1-8), it is necessary to consider other components: the longitudinal rebars in tension and the concrete slab in compression (as well as to modify the "standard" components influenced by the presence of the concrete).

3.2.1 Longitudinal steel reinforcement in tension

- *Resistance*

Both in an interior joint or in an exterior joint the traction that could be present in the longitudinal rebars is balanced by the strut-and-tie mechanisms occurring in the side of the column opposite to the traction (mechanisms 1 and 2). For an elastic internal joint stressed on both sides, the distribution of stresses within the slab is shown in Figure 9 where the bending moment of the left side $M_{Ed,l}$ is expressed as a function of the bending moment present on the right side $M_{Ed,r}$ (suppose in this case $M_{Ed,r} < M_{Ed,l}$, considering the sign) through the transformation parameter β defined as (neglecting the shear effect):

$$\beta_r = 1 - \frac{M_{Ed,l}}{M_{Ed,r}} \quad (17)$$

$$\beta_l = \frac{M_{Ed,r}}{M_{Ed,l}} - 1 \quad (18)$$

In which the bending moments have positive sign when they compress the slab and negative when they tend the slab.

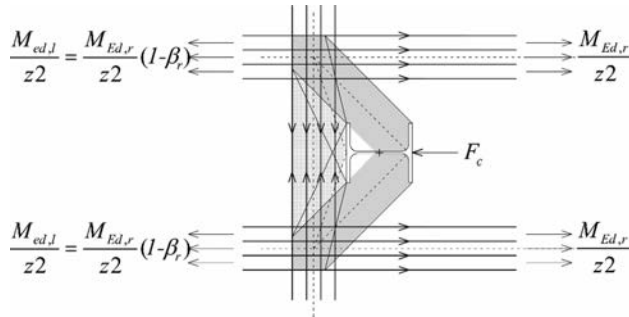


Figure 9. Elastic force distribution in a composite joint ($M_{Ed,r} < M_{Ed,l}$).

The difference between the forces present in the slab (see Figure 9, where z represents the internal lever arm) due to the different value of the internal bending moments acting on the left and right side of the joint generates a compression force F_c which is transmitted to column through the development of the struts. In the state of maximum exploitation of mechanisms 1 and 2 (Figure 10), the traction on the right-hand side ($F_{t,r}$) and left ($F_{t,l}$) of the joint are obtained by imposing the force equilibrium on the basis of the resistances of the mechanisms present in the slab:

$$F_{t,r} = \frac{\sum F_{Rd,i}}{\beta_r} \tag{19}$$

$$F_{t,l} = \frac{\sum F_{Rd,i} (1 - \beta_r)}{\beta_l} = \frac{\sum F_{Rd,i}}{\beta_l} \tag{20}$$

An upper limit to this force is represented by the strength of the armature A_s present in the slab within the effective width at negative bending moment b_{eff} . The maximum tension force transmitted by the slab, defined as the basic component "longitudinal steel reinforcement in tension", is thus:

$$F_{t,slab,Rd}^r = \min \left(\frac{\sum F_{Rd,i}}{\beta_r}; A_s^r f_{yd} \right) \geq 0 \tag{21}$$

$$F_{t,slab,Rd}^l = \min \left(\frac{\sum F_{Rd,i}}{\beta_l}; A_s^l f_{yd} \right) \geq 0 \tag{22}$$

Where A_s^r represents the rebars area on the right side of the joint and A_s^l the one on the left side.

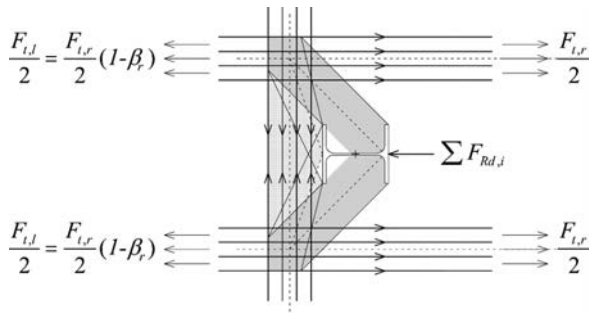


Figure 10. Maximum exploitation condition ($M_{Ed,r} < M_{Ed,l}$).

When the joint is stressed by negative moments, the formation of the mechanisms 1 and 2 is guaranteed only if the rebars in tension can be anchored over the column (cantilever or internal joint). Also when the negative bending moments are equal on both sides ($M_{Ed,r} = M_{Ed,l}$) the mechanisms are not activated because the forces in the slab are in equilibrium. In this case the parameter β is equal to zero and the components " *longitudinal steel reinforcement in tension* " are:

$$F_{t,slab,Rd}^r = A_s^r f_{yd} \quad (23)$$

$$F_{t,slab,Rd}^l = A_s^l f_{yd} \quad (24)$$

Therefore, the basic component "*longitudinal rebars in tension*" is a function not only of the rebars placed on the slab but also of the nodal configuration (presence or not of different mechanisms) and of the bending moments (via the parameter β). It makes sense to evaluate this component exclusively on the joint side where a negative bending moment is applied. In general, to check the joint resistance, this component should be determined for each load combination. On the other hand, in an external joint, being one bending moments equal to zero, the maximum tolerable traction is independent of β and is equal to:

$$F_{t,slab,Rd}^r = \min\left(\sum F_{Rd,i}; A_s^r f_{yd}\right) \geq 0 \quad (25)$$

$$F_{t,slab,Rd}^l = \min\left(\sum F_{Rd,i}; A_s^l f_{yd}\right) \geq 0 \quad (26)$$

Under seismic loading, in order to provide adequate ductility to the joint, it would be desirable to achieve the yield of the longitudinal reinforcement before the concrete crushing. This condition is assured if, for each seismic load combination, the following inequalities are applied:

$$A_s^r \leq \left| \frac{\sum F_{Rd,i}}{\beta_r f_{yd}} \right| \quad (27)$$

$$A_s^l \leq \left| \frac{\sum F_{Rd,i}}{\beta_l f_{yd}} \right| \quad (28)$$

- *Stiffness*

The stiffness coefficient is defined by EC4 [§EC4 1-1 A.2.1.1], it can be expressed in the form:

$$k_{s,r,slip} = \frac{A_{sl}}{l_r} k_{slip} \quad (29)$$

Parameter l_r represents the "effective length" of the reinforcement, defined in the eurocode depending on the node configuration and loading condition. The values of this parameter suggested in the Eurocode are shown in Table 4 (§EC4-1-1 prospectus A1).

Table 1. Effective length of the longitudinal reinforcement.

Nodal Configuration	Stresses	Effective Length
Exterior Joint		$l_r = 3.6h_c$
Interior Joint	$M_{Ed,r} = M_{Ed,l}$	$l_r = h_c / 2$
	$M_{Ed,r} > M_{Ed,l}$	<ul style="list-style-type: none"> Joint with $M_{Ed,r}$: $l_r = h_c \left(\frac{1+\beta}{2} + k_\beta \right)$ $k_\beta = \beta (4.3\beta^2 - 8.9\beta + 7.2)$ Joint with $M_{Ed,l}$: $l_r = h_c \left(\frac{1-\beta}{2} \right)$

Other formulations have been proposed by various authors. In particular, according to Gil and Bayo (2007), the effective length is independent from the bending moments and is:

- For external joint:

$$l_r = \frac{h_c}{2} + 0.8z \quad (30)$$

- For interior joints:

$$l_r = 2(h_c + z) \quad (31)$$

where z represents the distance between the axis of the lower flange of the steel beam and the centre of gravity of the reinforcement (internal lever arm).

The k_{slip} stiffness factor considers the effect of the shear deformation of connectors. Its formulation is due to Aribert (1995):

$$k_{slip} = \frac{1}{1 + \frac{E_s (A_{sl} / l_r)}{k_{sc}}} \quad (32)$$

Where:

$$k_{sc} = \frac{Nk_{sc}}{v - \left(\frac{v-1}{1+\xi} \right) \frac{h_s}{d_s}} \quad (33)$$

$$v = \sqrt{\frac{(1+\xi) Nk_{sc} d_s^2 l}{E_s I_s}} \quad (34)$$

$$\xi = \frac{E_a I_a}{d_s^2 E_{sl} A_{sl}} \quad (35)$$

and:

h_s is the distance between the centre of gravity of the longitudinal reinforcement and the centre of compression;

d_s is the distance between the centre of gravity of the longitudinal reinforcement and the centre of gravity of the steel section;

I_a is the moment of inertia of the steel beam;

l is the length of the beam subjected to negative bending moment (conventionally the 15% of the span length);

N is the number of studs distributed over the length l ;

k_{sc} is the stiffness of a single stud.

3.2.2 Concrete slab in compression

- *Resistance*

Under seismic loading, positive bending moment on one side and negative on the other side of the joint might occur. For each load combination that involves this behaviour, it is necessary to evaluate the positive resistant moment of the joint and hence to define the "concrete slab in compression" basic component. This component, defined as $F_{c,slab,Rd}$, is determined by evaluating the force equilibrium at the joint from the knowledge of the basic component "longitudinal reinforcement in tension" $F_{t,slab,Rd}$ and the sum of the resistances of Mechanisms $\Sigma F_{Rd,i}$ (Figure 11):

$$F_{c,slab,Rd}^r = \sum F_{Rd,i} - F_{t,slab,Rd}^l \quad (36)$$

$$F_{c,slab,Rd}^l = \sum F_{Rd,i} - F_{t,slab,Rd}^r \quad (37)$$

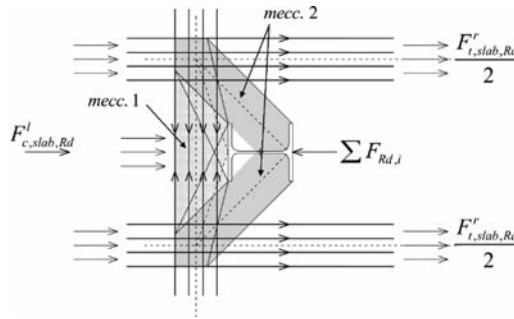


Figure 11. Stresses distribution due to seismic action.

The component $F_{c,slab,Rd}$ can be derived directly from equations 19 and 20. In seismic conditions, the stressing bending moments can assume opposite sign and consequently the transformation factor β_r assumes a positive value greater than one. By replacing this value in equations 19 and 20, the forces on the right and left side of the column have the same direction (one induces traction and the other compression). However, such equations are valid only until $F_{t,slab,Rd}$ is governed by the resistance of the mechanisms. To consider also the possibility that $F_{t,slab,Rd}$ is governed by the reinforcement resistance $F_{c,slab,Rd}$ is then defined by equations 36 and 37.

$F_{c,slab,Rd}$ is a function of the longitudinal reinforcement in tension. Therefore, it is also a function of β and must be evaluated for each load combination that provides a positive bending moment at the beam-to-column intersection (on the side where that moment acts).

- *Stiffness*

Codes currently give no indications on the stiffness of the slab mechanisms. It can be assumed equal to (Amadio *et al.*, 2014):

$$k_c = k_{c,1} + k_{c,2} \quad (38)$$

This stiffness coefficient is defined from the stiffness of mechanisms 1 and 2 acting in parallel. The coefficients $k_{c,1}$ and $k_{c,2}$ of the mechanisms are respectively (Amadio *et al.*, 2010) (Bella, 2009):

- Mechanism 1:

The stiffness coefficient is calculated by considering a strut length of h_c (Figure 12). Under this hypothesis, the stiffness coefficient of mechanism 1 is calculated as:

$$k_{c,1} = \frac{A_c E_{cm}}{h_c E_s} = \frac{(b_p h_c) E_{cm}}{h_c E_s} \quad (39)$$

Where E_{cm} is the concrete elastic modulus whereas E_s the steel ones.

- Mechanism 2:

with reference to Figure 13, the stiffness coefficient of the mechanism 2 can be set as:

$$k_{c,2} = \frac{2}{\frac{1}{k_t \left(\frac{l_y}{l_x}\right)^2} + \frac{1}{k_p \left(1 + \left(\frac{l_y}{l_x}\right)^2\right)}} = \frac{2}{\frac{1}{k_t} + \frac{1}{2k_p}} \quad (40)$$

Where the stiffness coefficient of the single strut k_p and tie k_t is assumed:

$$k_t = \frac{A_T}{l_y} = \frac{A_T}{1.5h_c} \quad (41)$$

$$k_p = \frac{A_p}{\sqrt{l_x^2 + l_y^2}} \frac{E_{cm}}{E_s} = \frac{0.7h_c d_{eff}}{\sqrt{1.5h_c^2 + 1.5h_c^2}} \frac{E_{cm}}{E_s} \quad (42)$$

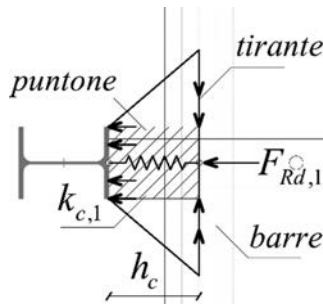


Figure 12. Mechanism 1.

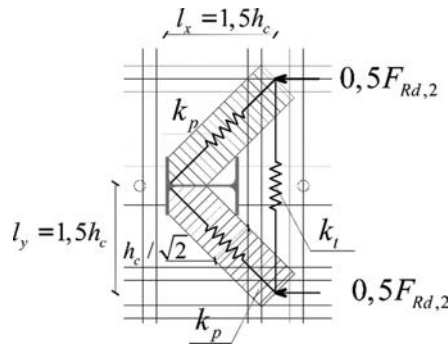


Figure 13. Mechanism 2.

3.3 Design of the slab according to EC8

The possible nodal configurations in the case of exterior or interior joint are described in the following, reporting their behaviour according to the bending moments and the necessary checks to ensure the hierarchy of resistance between the beam and the joint.

3.3.1 External joint

The possible configurations that an external composite joint (located on the perimeter of a three-dimensional frame) may have and the design of the slab are summarized in Table 2. As shown in 3.2.2, the maximum compressive force transmitted through the slab in an external joint is given, depending on the nodal configuration, by the sum of the resistances of the various mechanisms since $F_{t,slab,Rd}$ is equal to zero. Considering the case where an external edge strip is present and the absence of a transverse beam (construction detail "b" of Table 2), the maximum compression force is given by mechanisms 1 and 2:

$$F_{Rd,1} + F_{Rd,2} = (b_b + 0.7h_c)d_{eff}(0.85f_{ck} / \gamma_c) \quad (43)$$

This condition corresponds to an effective connection width of:

$$b_{eff,conn}^+ = b_b + 0.7h_c \quad (44)$$

Such width corresponds to the maximum effective width at a positive moment for such node configuration. It is thus noted that the maximum compressive force that can be transmitted by the connection at the level of the slab is the same of that transmitted by the beam.

This means that to achieve an overstrength of the joint with respect to the beam, unless there are very short spans, the transverse beam must be introduced (construction detail "c" in Table 2), choosing appropriately the number of connectors n to fit within the effective width.

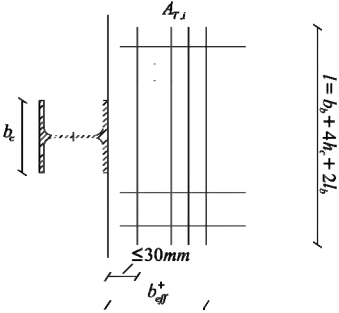
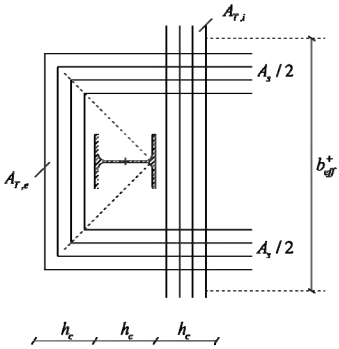
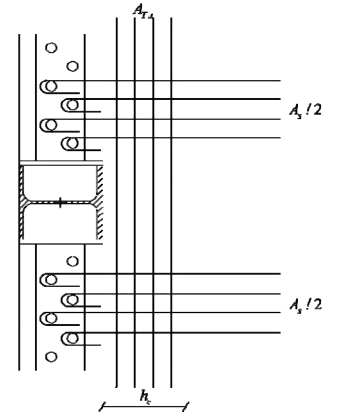
3.3.2 Interior joint

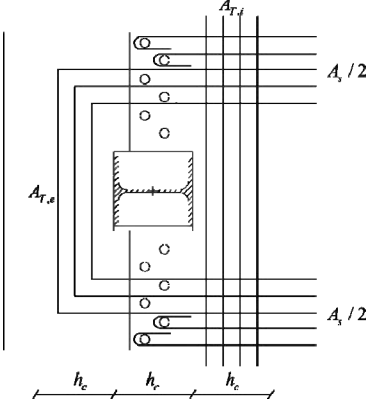
The possible configurations that an interior composite joint can assume, the design of the slab and the hierarchy checks are summarized in Table 3.

An interior joint subjected to an earthquake can experience at the same time a positive bending moment on one side that generates within the slab a tensile force F_{st} and from a negative bending moment on the other side that generates within the slab a compression force F_{sc} . In an interior node, it is therefore necessary to consider the interaction between the connections on both sides of the column due to the continuity of the slab and the longitudinal

reinforcement. In particular, the negative resistant moment on one side depends on the ability of the concrete to resist compression stresses on the other side.

Table 2. Slab design for an external joint.

Nodal Configuration	Slab design
<p>a) No transversal beam; No cantilever edge strip</p> 	$F_{c,slab,Rd} = \sum F_{Rd,i} = F_{Rd,1}$ $F_{t,slab,Rd} = 0$ $A_T = A_{T,1} \geq 0.25b_b d_{eff} \frac{0.15l - b_b}{0.15l} \left(\frac{0.85f_{ck}}{f_{yk,T}} / \gamma_s \right)$
<p>b) Edge strip beam, No transversal beam</p> 	$F_{c,slab,Rd} = \sum F_{Rd,i} = F_{Rd,1} + F_{Rd,2}$ $F_{t,slab,Rd} = \min \left[(A_{s1} + A_{s2}) f_{yd}; (F_{Rd,1} + F_{Rd,2}) \right]$ $A_{T,i} = A_{T,1} + A_{T,2}$ $A_{T,e} \geq \frac{A_{sl}}{2}$
<p>c) Transversal beam, No edge strip</p> 	$F_{c,slab,Rd} = \sum F_{Rd,i} = F_{Rd,1} + F_{Rd,2} + F_{Rd,3}$ $F_{t,slab,Rd} = \min \left[A_{s3} f_{yd}; \sum F_{Rd,i} \right]$ $A_{T,i} = A_{T,1} + A_{T,2}$

Nodal Configuration	Slab design
<p>d) Transversal beam, edge strip</p> 	$F_{c,slab,Rd} = \sum F_{Rd,i} = F_{Rd,1} + F_{Rd,2} + F_{Rd,3}$ $F_{t,slab,Rd} = \min \left[(A_{s1} + A_{s2} + A_{s3}) f_{yd}; \sum F_{Rd,i} \right]$ $A_{T,i} = A_{T,1} + A_{T,2}$ $A_{T,e} \geq \frac{A_{s1} + A_{s2}}{2}$

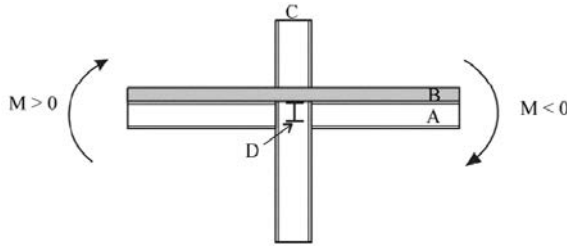


Figure 14. Interior joint subjected to seismic loading.

The direct consequence of this consideration is that the forces F_{sc} and F_{st} can only be equilibrated by mechanisms 1 and 2 and, when the transverse beam is present, by the mechanism 3. In seismic conditions, the joint can at most be stressed by the bending resistant moments on each side. Under these assumptions the compressive and tensile forces on the slab assume their maximum value which is equal to:

$$F_{sc} = b_{eff}^+ d_{eff} (0.85 f_{ck} / \gamma_c) \quad (45)$$

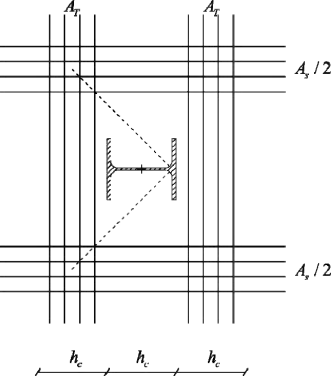
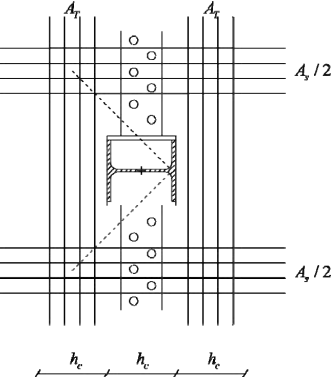
$$F_{st} = A_{sl} (f_{yk,l} / \gamma_s) \quad (46)$$

Where A_{sl} represents the longitudinal reinforcement placed within b_{eff}^- . Such forces must be equilibrated by the mechanisms. To ensure that such forces can be transferred, the maximum compressive force transmitted by the mechanisms should be greater than the sum of the forces F_{sc} and F_{st} . To prevent the concrete crushing and to ensure that the failure occurs with the yield of the reinforcement of the slab on one side and with the yield of the lower flange of the steel beam on the other side, it is necessary to verify that:

- In absence of transversal beam:

$$1.2(F_{sc} + F_{st}) \leq F_{Rd,1} + F_{Rd,2} \quad (47)$$

Table 3. Slab design for an interior joint.

Nodal Configuration	Slab design
<p>a) No transversal beam</p> 	<p>1) $M_{Ed,r} \neq M_{Ed,l}$, both negative</p> $F_{t,slab,Rd}^r = \min \left(\frac{F_{Rd,1} + F_{Rd,2}}{\beta_r}; A_s^r f_{yd} \right)$ <p>2) $M_{Ed,r} = M_{Ed,l}$, both negative</p> $F_{t,slab,Rd}^r = A_s^r f_{yd}; F_{t,slab,Rd}^l = A_s^l f_{yd}$ <p>3) $M_{Ed,r}$ negative and $M_{Ed,l}$ positive</p> $F_{c,slab,Rd}^l = F_{Rd,1} + F_{Rd,2} - F_{t,slab,Rd}^r$ $F_{t,slab,Rd}^r = \min \left(\frac{F_{Rd,1} + F_{Rd,2}}{\beta_r}; A_s^r f_{yd} \right)$ <p>4) $M_{Ed,r}$ positive and $M_{Ed,l}$ negative</p> $F_{c,slab,Rd}^r = F_{Rd,1} + F_{Rd,2} - F_{t,slab,Rd}^l$ $F_{t,slab,Rd}^l = \min \left(\frac{F_{Rd,1} + F_{Rd,2}}{\beta_l}; A_s^l f_{yd} \right)$ <p>5) For every case</p> $A_T = A_{T,1} + A_{T,2}$ $1.2(F_{sc} + F_{st}) \leq F_{Rd,1} + F_{Rd,2}$
<p>b) Edge strip beam, No transversal beam</p> 	<p>1) $M_{Ed,r} \neq M_{Ed,l}$, both negative</p> $F_{t,slab,Rd}^r = \min \left(\frac{F_{Rd,1} + F_{Rd,2} + F_{Rd,3}}{\beta_r}; A_s^r f_{yd} \right)$ <p>2) $M_{Ed,r} = M_{Ed,l}$, both negative</p> $F_{t,slab,Rd}^r = A_s^r f_{yd}; F_{t,slab,Rd}^l = A_s^l f_{yd}$ <p>3) $M_{Ed,r}$ negative and $M_{Ed,l}$ positive</p> $F_{c,slab,Rd}^l = F_{Rd,1} + F_{Rd,2} + F_{Rd,3} - F_{t,slab,Rd}^r$ $F_{t,slab,Rd}^r = \min \left(\frac{F_{Rd,1} + F_{Rd,2} + F_{Rd,3}}{\beta_r}; A_s^r f_{yd} \right)$ <p>4) $M_{Ed,r}$ positive and $M_{Ed,l}$ negative</p> $F_{c,slab,Rd}^r = F_{Rd,1} + F_{Rd,2} + F_{Rd,3} - F_{t,slab,Rd}^l$ $F_{t,slab,Rd}^l = \min \left(\frac{F_{Rd,1} + F_{Rd,2} + F_{Rd,3}}{\beta_l}; A_s^l f_{yd} \right)$ <p>5) For every case should be checked:</p> $A_T = A_{T,1} + A_{T,2}$ $1.2(F_{sc} + F_{st}) \leq F_{Rd,1} + F_{Rd,2} + F_{Rd,3}$

- With transversal beam:

$$1.2(F_{sc} + F_{st}) \leq F_{Rd,1} + F_{Rd,2} + F_{Rd,3} \quad (48)$$

In the latter, the struts are activated by compression of the concrete on the studs due to the application of a positive bending moment, so the number of studs involved in mechanism 3 is evaluated by considering the effective width under positive bending b_{eff}^+ . In seismic area, the effective width used to evaluate the resistant positive bending moment of an internal joint is equal to $b_{eff}^+ = 0.15l$. Considering that in design practice $b_b = b_c \cong h_c$ and that on average $h_c \cong 0.05l$, it results:

$$b_{eff,conn}^+ = b_b + 0.7h_c \cong 1.7h_c \cong 0.085l \ll b_{eff}^+ = 0.15l \quad (49)$$

Therefore, an overstrength of the joint with respect to the beam is possible only in the presence of:

- oversize of the column in very short spans;
- mechanism 3.

It follows that it is usually necessary to introduce the transverse beam and appropriately selecting the number of connectors n to be placed within the effective width.

3.4 Moment-rotation curve

The behaviour of a joint is described by its moment-rotation curve (Fasan, 2013), (Pecce and Rossi, 2015), which depends on the stiffness and resistance of its basic components. Generally steel-concrete composite joints are non-symmetric and therefore their active components are function of the bending moment (Figure 15). A composite joint is hence characterized by a different moment-rotation curve according to the sign of the bending moment.

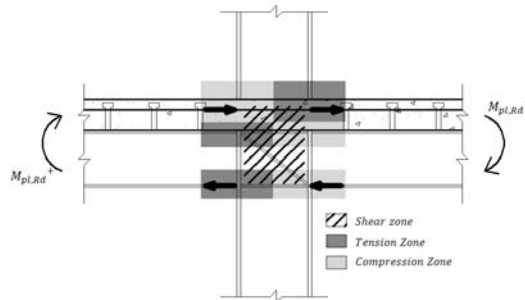


Figure 15. Interior joint subjected to seismic loading.

Generally, for each row of basic components, it is possible to obtain its effective strength through equilibrium considerations between the various resistances. The basic components are a function of the node type. The joint resistant moment is equal to the product between the effective strength $F_{r,Rd}$ that can be developed, each with its own sign, and their arm h_r with respect to a point belonging to the joint:

$$M_{j,pl,Rd} = \sum_{i=1}^r F_{i,Rd} h_r \quad (50)$$

Stiffness is also asymmetrical. In general, to obtain the moment-rotation curve, a basic mechanical model needs to be defined. The following describes the procedure to be used to

design and verify welded and bolted joints. For more details on the component method and other node types refer to EC3 1-8. The general steps to follow are:

- Identification of active components in the tension, shear and compression;
- Identifying the strength and stiffness of each component;
- Assembling the components and defining the moment-rotation curve of the joint via equilibrium considerations;
- Verification of welds (beam-to-column welds in the case of welded joints and between the plate and the beam in the case of bolted joints);
- Checks of bolts resistance.

Bolts, welds, plate and column flange are seized to transfer the stresses deriving from hierarchy criteria. The basic components of a welded and bolted joint with extended end-plate are listed in Table 4 and Table 5 respectively. The procedures to be followed for the determination of the resistant moment differ according to the moment sign.

Table 4. Basic components for a welded composite joint.

Zone	Basic Component	Resistance	Stiffness
Tension	Column flange in transverse bending [§EC3 1-8 6.2.6.4]	$F_{fc,Rd}$	-
	Column web in transverse tension [§EC3 1-8 6.2.6.3]	$F_{t,wc,Rd}$	k_3
	Longitudinal reinforcement in tension [sec. 3.2.1]	$F_{t,slab,Rd}$	$k_{s,r,slip}$
Compression	Column web in transverse compression [§EC3 1-8 6.2.6.2]	$F_{c,wc,Rd}$	k_2
	Concrete slab in compression [sec. 3.2.2]	$F_{c,slab,Rd}$	k_c
	Beam flange and web in compression [§EC3 1-8 6.2.6.7]	$F_{c,fb,Rd}$	-
Shear	Column web panel in shear [§EC3 1-8 6.2.6.1]	$V_{wp,Rd}$	k_1

Table 5. Basic components for an extend end plate bolted composite joint.

Zone	Basic Component	Resistance	Stiffness
Tension	Bolts in tension [§EC3 1-8 Table 3.4]	$F_{t,Rd}$	k_{10}
	Bolts in shear [§EC3 1-8 Table 3.4]	$F_{v,Rd}$	k_{11}
	Bolts in bearing [§EC3 1-8 Table 3.4]	$F_{b,Rd}$	k_{12}
	Punching shear resistance [§EC3 1-8 Table 3.4]	$B_{p,Rd}$	-
	Column web in transverse tension [§EC3 1-8 6.2.6.3]	$F_{t,wc,Rd}$	k_3
	Column flange in transverse bending [§EC3 1-8 6.2.6.4]	$F_{t,fc,Rd}$	k_4
	End-plate in bending [§EC3 1-8 6.2.6.5]	$F_{t,ep,Rd}$	k_5
	Beam web in tension [§EC3 1-8 6.2.6.8]	$F_{t,wb,Rd}$	-
Compression	Longitudinal reinforcement in tension [sec. 3.2.1]	$F_{t,slab,Rd}$	$k_{s,r,slip}$
	Column web in transverse compression [§EC3 1-8 6.2.6.2]	$F_{c,wc,Rd}$	k_2
	Concrete slab in compression [sec 3.2.2]	$F_{c,slab,Rd}$	k_c
Shear	Beam flange and web in compression [§EC3 1-8 6.2.6.7]	$F_{c,fb,Rd}$	-
Shear	Column web panel in shear [§EC3 1-8 6.2.6.1]	$V_{wp,Rd}$	k_1

3.4.1 Negative bending moment

The design negative resistant moment of the joint is obtained from the limitation imposed by the compression resistance at the lower flange. It is assumed that the neutral axis cannot move closer to the slab as the lower flange instability could prevent it (safety criterion). The steps to follow to define the resistant negative moment of a welded joint are:

- a) calculate the resistance of each component;
- b) find the maximum resistance that can be developed at each level, namely:
 - the maximum compressive strength that can be developed at the lower flange of the beam $F_{c1, Rd}$, given by:

$$F_{c1, Rd} = \min(F_{c,wc,Rd}; V_{wp,Rd} / \beta) \quad (51)$$

- maximum tensile strength at the rebars level:

$$F_{t1,max} = \min(F_{t,slab,Rd}; V_{wp,Rd} / \beta) \quad (52)$$

- the maximum tensile resistance that can be developed at the top flange of the beam:

$$F_{t2,max} = \min(F_{t,wc,Rd}; F_{fc,Rd}; V_{wp,Rd} / \beta) \quad (53)$$

the column flange in transverse bending is taken into account only if the joint is not stiffened with continuity plates;

- c) define the effective strength of each level $F_{tr,Rd}$ approaching the flange in compression starting from the farthest point and by interrupting the procedure when the sum of the effective resistances equals the maximum compression resistance $F_{c1,Rd}$.

To perform point c), whether it is a welded joint or a bolted joint with end-plate, the first row in tension is at the level of the rebars. Such resistance shall not exceed maximum compressive strength that can be developed at the lower flange:

$$F_{t1,Rd} = \min(F_{t1,max}; F_{c1,Rd}) \quad (54)$$

In order to obtain a ductile behaviour, the rebars at the beam-to-column intersection should be designed in order to yield before the maximum strength of the mechanisms is reached as described in 3.2.1. Moreover, rebars should yield before the maximum compression strength of the joint $F_{c1, Rd}$ is achieved. This is assured if the following inequality is true:

$$F_{t,slab,Rd} = A_s f_{yd} \leq F_{c1,Rd} \quad (55)$$

The effective strength of the other rows in tension differs depending on whether the joint is welded or bolted with extend end-plate. In welded joints, the second (and last) row in tension is placed at the upper flange of the beam. The direction and intensity of the force that can be developed by this row $F_{t2,Rd}$ is determined by force equilibrium. $F_{t2, Rd}$ in a welded joint can then be set equal to:

$$F_{t2,Rd} = \min(F_{t2,max}; (F_{c1,Rd} - F_{t1,Rd})) \quad (56)$$

In a joint where the ductility criterion expressed in equation 55 is respected, $F_{t2,Rd}$ is always a tensile force or at most null. The procedure described so far can be summarized in Figure 16. With reference to this figure, the negative resistant moment can be set equal to (the centre of the lower flange is chosen as pole but any pole can be used):

$$M_{j,pl,Rd}^- = F_{t1,Rd} h_{t1} + F_{t2,Rd} h_{t2} \quad (57)$$

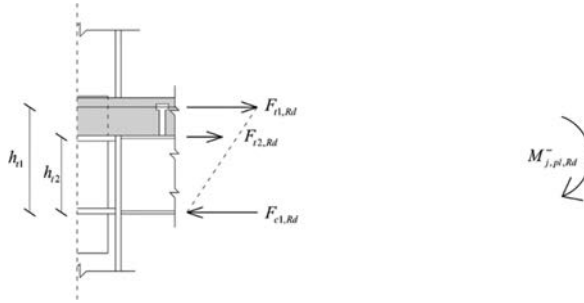


Figure 16. Force distribution in a welded joint under negative moment.

If the joint is bolted, it is necessary to identify the effective resistance of each row in tension $F_{tr,Rd}$, equal to the lower between the resistance of the row taken individually $F_{tr,Rd,alone}$ or as part of a group of bolts $F_{tr,Rd,gr}$ (if this mechanism is possible) (EC3 1-8 6.2.7.2). The following basic components should be considered:

- column web in transverse tension $F_{t,wc,Rd}$;
- column flange in transverse bending $F_{t,fc,Rd}$;
- end-plate in bending $F_{t,ep,Rd}$;
- beam web in tension $F_{t,wb,Rd}$;

The procedure for calculating the maximum effective resistances that can be developed is performed in accordance with point c) and can be summarized as follows:

$$\begin{aligned} -F_{t1,Rd} &= \min(F_{t1,max}; F_{c1,Rd}); \\ -F_{t2,Rd} &= \min(F_{t2,Rd,alone}; (F_{c1,Rd} - F_{t1,Rd})); \\ -F_{t3,Rd} &= \min(F_{t3,Rd,alone}; (F_{t,Rd,gr2-3} - F_{t2,Rd}); (F_{c1,Rd} - F_{t1,Rd} - F_{t2,Rd})); \\ -F_{t4,Rd} &= \min \left(\begin{array}{l} F_{t4,Rd,alone}; (F_{t,Rd,gr3-4} - F_{t3,Rd}); (F_{t,Rd,gr2-3-4} - F_{t2,Rd} - F_{t3,Rd}); \\ (F_{c1,Rd} - F_{t1,Rd} - F_{t2,Rd} - F_{t3,Rd}) \end{array} \right); \\ &\dots; \\ -F_{tm,Rd} &= \dots; \end{aligned} \quad (58)$$

The previous procedure leads to a plastic distribution of effective forces. This distribution can only be developed if the joint has adequate ductility (T-stub failure mode 1 or 2). Otherwise, a linear distribution is required. In particular, if the resistance of a row $F_{tx,Rd}$ exceeds the value $1.9F_{t,Rd}$ (design tension resistance of the bolts), the further rows resistance must be defined using the following inequality:

$$F_{tr,Rd} \leq F_{tx,Rd} \frac{h_r}{h_x} \quad (59)$$

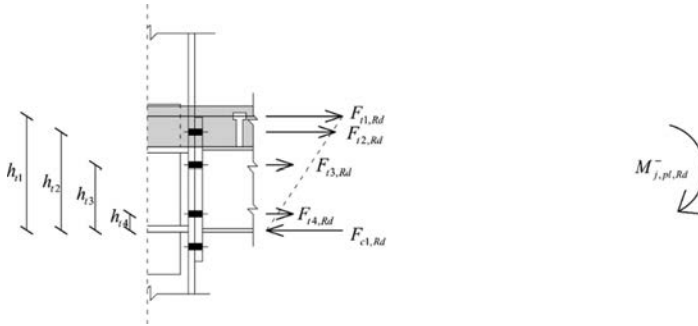


Figure 17. Force distribution in a bolted end-plate joint under negative moment.

Referring to Figure 17, the negative resistant moment is equal to (the centre of gravity of the compressed flange is chosen as the pole):

$$M_{j,pl,Rd}^{-} = F_{t1,Rd}h_{t1} + F_{t2,Rd}h_{t2} + F_{t3,Rd}h_{t3} + F_{t4,Rd}h_{t4} \quad (60)$$

3.4.2 Positive bending moment

When the joint is subject to a positive bending moment the concrete slab is compressed. If there is a full-strength shear connection, this will allow the neutral axis to move towards the metallic components as the moment increases. Thanks to the studs, the instability of the compressed flange is also prevented. Based on these considerations, the positive resistant moment of the joint can be evaluated as follows:

- calculate the resistance of each component;
- find the maximum resistance that can be developed at each level, namely:
 - the maximum compressive strength of the slab $F_{c1,max}$, given by:

$$F_{c1,max} = \min(F_{c,slab,Rd}; V_{wp,Rd} / \beta) \quad (61)$$

- the maximum compressive strength that can be developed at the top flange of the beam $F_{c2,max}$, given by:

$$F_{c2,max} = \min(F_{c,wc,Rd}; V_{wp,Rd} / \beta) \quad (62)$$

- maximum compression strength $F_{c,max}$:

$$F_{c,max} = \min(F_{c1,max} + F_{c2,max}; V_{wp,Rd} / \beta) \quad (63)$$

- the maximum tensile resistance that can be developed at the lower flange of the beam:

$$F_{t1,max} = \min(F_{t,wc,Rd}; F_{fe,Rd}; V_{wp,Rd} / \beta) \quad (64)$$

the column flange in transverse bending is considered only if the joint is not stiffened with continuity plates;

- c) define the effective strength of each level $F_{tr,Rd}$ approaching the flange in compression starting from the farthest point and by interrupting the procedure when the sum of the effective resistances equals the maximum compression resistance $F_{c,max}$;
- d) define, via force equilibrium, the effective compression strength of the concrete slab $F_{c1,Rd}$ and of top flange $F_{c2,Rd}$:

$$F_{c1,Rd} = \min\left(\sum F_{tr,Rd}; F_{c1,max}\right) \quad (65)$$

$$F_{c2,Rd} = \min\left(\sum F_{tr,Rd} - F_{c1,Rd}; F_{c2,max}\right) \quad (66)$$

In a welded joint $\sum F_{tr,Rd}$ coincides with the maximum strength that can be developed at the bottom flange of the beam. Such resistance must not exceed the maximum compressive strength that can be developed:

$$F_{t1,Rd} = \min\left(F_{t1,max}; F_{c,max}\right) \quad (67)$$

The procedure described so far can be summarized in Figure 18. With reference to this figure, the positive resistant moment can be set equal to (the pole is the centre of the lower flange):

$$M_{j,pl,Rd}^+ = F_{c1,Rd} h_{c1} + F_{c2,Rd} h_{c2} \quad (68)$$

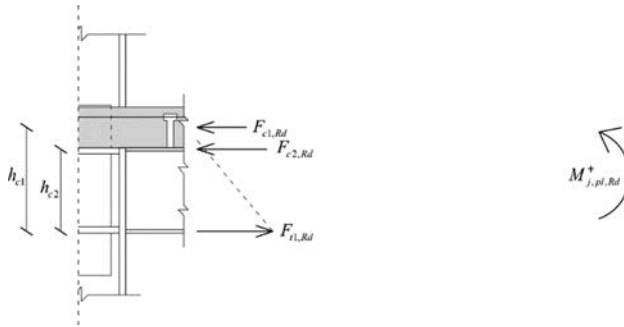


Figure 18. Force distribution in a welded joint under positive moment.

If the joint is bolted, it is necessary to identify the effective resistance of each row in tension $F_{tr,Rd}$, equal to the lower between the resistance of the row taken individually $F_{tr,Rd,alone}$ or as part of a group of bolts $F_{tr,Rd,gr}$ (if this mechanism is possible) (EC3 1-8 6.2.7.2). The following basic components should be considered:

- column web in transverse tension $F_{t,wc,Rd}$;
- column flange in transverse bending $F_{t,fc,Rd}$;
- end-plate in bending $F_{t,ep,Rd}$;
- beam web in tension $F_{t,wb,Rd}$;

The procedure for calculating the maximum effective resistances that can be developed is performed in accordance with point c) and can be summarized as follows:

$$\begin{aligned}
-F_{t1,Rd} &= \min(F_{t1,Rd,alone}; F_{c,max}); \\
-F_{t2,Rd} &= \min(F_{t2,Rd,alone}; (F_{t,Rd,gr1-2} - F_{t1,Rd}); (F_{c,max} - F_{t1,Rd})); \\
-F_{t3,Rd} &= \min \left(\begin{aligned} & \left(F_{t3,Rd,alone}; (F_{t,Rd,gr2-3} - F_{t2,Rd}); (F_{t,Rd,gr1-2-3} - F_{t1,Rd} - F_{t2,Rd}); \right); \\ & (F_{c,max} - F_{t1,Rd} - F_{t2,Rd}) \end{aligned} \right); \\
-F_{t4,Rd} &= \min \left(\begin{aligned} & \left(F_{t4,Rd,alone}; (F_{t,Rd,gr3-4} - F_{t3,Rd}); (F_{t,Rd,gr2-3-4} - F_{t2,Rd} - F_{t3,Rd}); \right); \\ & (F_{c,max} - F_{t1,Rd} - F_{t2,Rd} - F_{t3,Rd}) \end{aligned} \right); \\
&\dots; \\
-F_{tn,Rd} &= \dots;
\end{aligned} \tag{69}$$

Referring to Figure 19, the positive resistant moment is equal to:

$$M_{j,pl,Rd}^+ = F_{c1,Rd} h_{c1} + F_{c2,Rd} h_{c2} - F_{t3,Rd} h_{t3} - F_{t2,Rd} h_{t2} \tag{70}$$

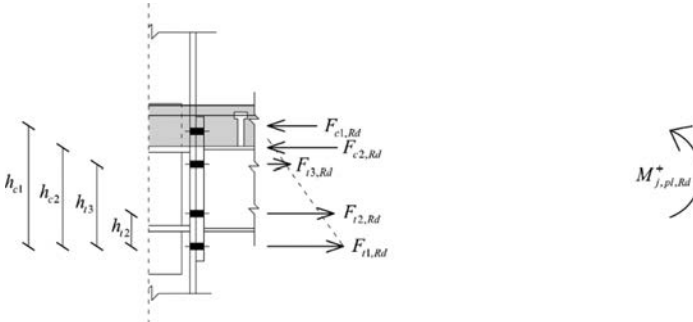


Figure 19. Force distribution in a bolted end-plate joint under positive moment.

3.4.3 Stiffness

The stiffness is generally asymmetrical because, as seen so far, different resistant mechanisms intervene with their rigidities. In general, to obtain the moment-rotation curve, a basic mechanical model needs to be defined. The stiffness of the basic components that affect the moment-rotation curve are reported in Table 4 for a welded joint and Table 5 for a bolted joint with extended end-plate.

The basic mechanical models for a welded joint subjected to negative or positive bending moments are shown in Figure 20 and Figure 22 respectively.

The basic mechanical models for a bolted joint with extend end-plate subjected to negative or positive bending moments are shown in Figure 21 and Figure 23 respectively.

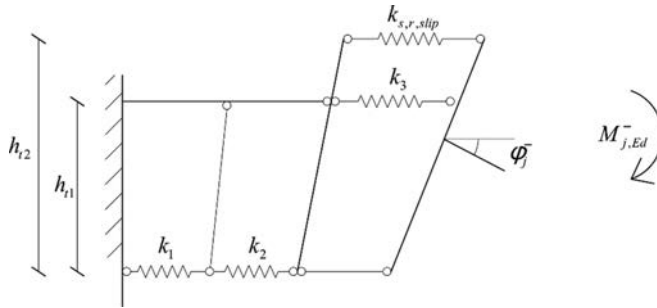


Figure 20. Mechanical model of a welded joint subject to negative moment.

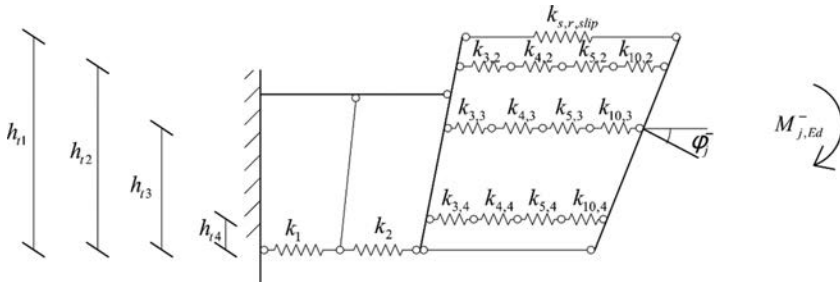


Figure 21. Mechanical model of a bolted joint under negative moment.

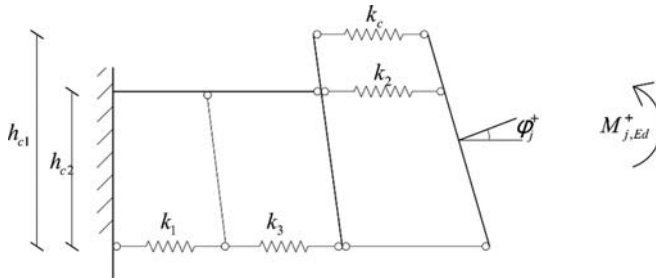


Figure 22. Mechanical model of a welded joint subject to positive moment.

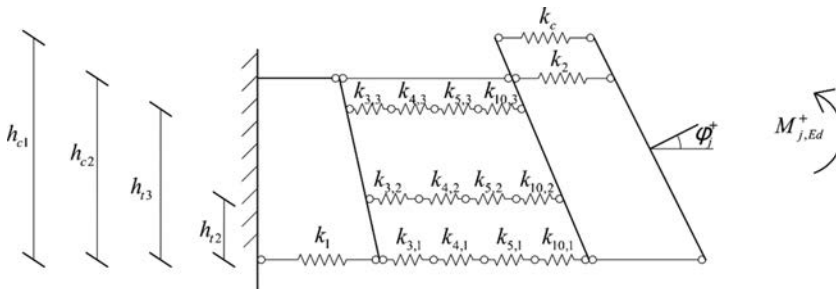


Figure 23. Mechanical model of a bolted joint under positive moment.

The mechanical models could be further simplified defining the effective stiffness of each row. To find it, it is necessary to add in series the springs in the row r (the springs having the same lever arm). Such stiffness may be equal to:

$$k_{eff,r} = \frac{1}{\sum 1/k_{i,r}} \quad (71)$$

Once the basic mechanical models and the effective stiffness are defined, it is possible to determine the joint initial stiffness such as:

$$S_{j,ini} = E \left(-d_{CR} \sum_{r=1}^n k_{eff,r} h_r + \sum_{r=1}^n k_{eff,r} h_r^2 \right) \quad (72)$$

Where d_{CR} represents the distance between the calculation pole and the centre of rotation:

$$d_{CR} = \frac{\sum_{r=1}^n k_{eff,r} h_r}{\sum_{r=1}^n k_{eff,r}} \quad (73)$$

The stiffness is set equal to $S_{j,ini}$ until the urgent moment does not exceed $2/3M_{j,pl,Rd}$. The secant stiffness, which detects the point of intersection between the moment-rotation curve of the joint and the point at which the plastic resistant moment of the joint $M_{j,pl,Rd}$ is reached, is assumed equal to $S_{j,ini}/\mu$. The stiffness ratio μ is defined in EC3 1-8 as:

$$\mu = \left(1.5 \frac{M_{j,Ed}}{M_{j,pl,Rd}} \right)^\psi \quad (74)$$

The coefficient ψ depends on the type of joint. For a welded or bolted end-plate joint it assumes a value of 2.7. Rotations are obtained by dividing the moments for the corresponding stiffness:

$$\varphi_{j,1} = 2/3M_{j,pl,Rd} / S_{j,ini} \quad (75)$$

$$\varphi_{j,2} = M_{j,pl,Rd} / (S_{j,ini} / \mu) \quad (76)$$

The moment rotation curve is hence represented by a trilinear curve as in Figure 24.

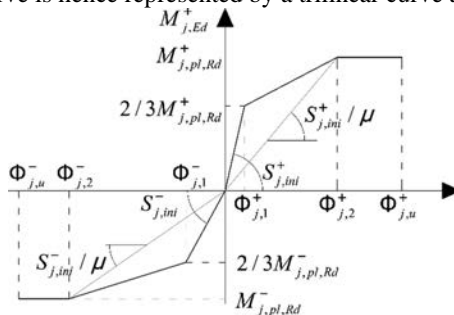


Figure 24. Moment-rotation curve.

4 CONCLUSIONS

This paper briefly presents the main aspects concerning the design and behaviour of composite joints subjected to earthquake loading. It describes in detail the strut-and-tie mechanisms that activate in the slab at the beam-to-column intersection. Depending on the nodal configuration, the main design choices that a designer can perform in the cases of braced or moment-resisting frames are presented. In the latter case, the possibility of eliminating the interactions between the column and the slab solution by suitable construction details has also been highlighted. The information presented herein are shown in guidelines that allows to account for the complexity of the composite action.

ACKNOWLEDGEMENTS

DPC-RELUIS 2014-2016 is gratefully acknowledged for funding the research activity.

REFERENCES

- Amadio C., Akkad N., Fasan M., Noè S. (2014). "Modellazione in campo non lineare delle strutture composte intelaiate acciaio-calcestruzzo in zona sismica- Parte I: Il giunto composto", *Costruzioni metalliche*, 5, pp. 36-42.
- Amadio C., Bedon C., Fasan M., Pecce M. (2017a). "Refined numerical modelling for the structural assessment of steel-concrete composite beam-to-column joints under seismic loads", *Engineering Structures*, 138(1), pp. 394-409, doi: 10.1016/j.engstruct.2017.02.037.
- Amadio C., Bedon C., Fasan M. (2017b). "Numerical assessment of slab-interaction effects on the behaviour of steel-concrete composite joints", *Journal of Constructional Steel Research*, 139, pp. 397-410, doi: 10.1016/j.jcsr.2017.10.003.
- Amadio C., Bella M., Macorini L. (2010). "A macro-model for beam-to-column connections in steel-concrete composite frames", *4th International Conference on Steel & Composite Structures*, Sydney, Australia.
- Amadio C., Pecce M., Fasan M., Logorano G. (2016). "Linee guida per la progettazione sismica di nodi composti acciaio-calcestruzzo", Reluis, Napoli.
- Aribert J. (1995). "Influence of slip of the shear connection on composite joint", *Third International Workshop on Connections in Steel Structures*, University of Trento.
- Bella M. (2009). "Modellazione numerica di strutture sismoresistenti e analisi probabilistica di tipo Montecarlo", *PhD Thesis*, University of Trieste.
- CEN, European Committee for Standardization. (2005a). "Eurocode 3: Design of steel structures - Part 1-8: Design of joints", EN 1993-1-8.
- CEN, European Committee for Standardization. (2005b). "Eurocode 4: Design of composite steel and concrete structures - Part 1-1: General rules and rules for buildings", EN 1994-1-1.
- CEN, European Committee for Standardization. (2005c). "Eurocode 8: Design of structures for earthquake resistance - Part 1: General rules, seismic actions and rules for buildings", EN 1998-1.
- Chaudhari T. D., MacRae G. A., Bull D., Chase G., Hicks S., Clifton G. C., Hobbs M. (2015). "Composite Slab Effects On Beam-Column Subassembly Seismic Performance", *8th International Conference on Behavior of Steel Structures in Seismic Area*, Shanghai, China.
- Fasan M. (2013). "Analisis and modelling of steel-concrete composite structures", Master thesis, University of Trieste, Italy.
- Gil B., Bayo E. (2007). "An alternative design for internal and external semi-rigid composite joints. Part II: Finite element modelling and analytical study", *Engineering Structures*, 30(1), pp. 232-246, doi: 10.1016/j.engstruct.2007.03.010.

- Plumier A., Doneux C., Bouwkamp J., Plumier G. (1998). "Slab design in connection zone of composite frames", *11th European Conference on Earthquake Engineering*, Paris, France.
- Pecce M., Rossi F. (2015). "The experimental behaviour and simple modelling of joints in composite MRFs", *Engineering Structures*, 105(december), pp. 249-263, 10.1016/j.engstruct.2015.09.042 .
- Seek M. W., Murray T. M. (2008). "Seismic Strength of Moment End-Plate Connections with Attached Concrete Slab", *Proceedings of Connections VI, American Institute of Steel Construction*, Chicago.

SECTION 3

CONVENTIONAL MULTI-STOREY BUILDINGS

CONCENTRIC BRACED FRAMES: GLOBAL AND LOCAL NUMERICAL STUDIES ON THE SEISMIC BEHAVIOUR OF STEEL MULTISTORY BRACING SYSTEMS BY REFINED FEM ANALYSES

Beatrice Faggiano, Antonio Formisano, Luigi Fiorino, Vincenzo Macillo,
Carmine Castaldo, Federico M. Mazzolani, Raffaele Landolfo

*Dept. Structures for Engineering and Architecture, University of Naples Federico II, Naples, Italy
faggiano@unina.it, antoform@unina.it, lfiorino@unina.it, vincenzo.macillo@unina.it,
carmine.castaldo@unina.it, fmm@unina.it, landolfo@unina.it*

ABSTRACT

The critical review of the design methodologies given in the Italian and European seismic code for steel Concentrically Braced Frames is the spark for deepening the seismic behaviour of such typical steel seismic resistant structures, aiming at providing more efficient design criteria able to ensure adequate safety under earthquake actions. To this purpose, common structural configurations of CBF are designed through both linear static and dynamic analyses. The design assessment is carried out, evidencing the mutual influence of design criteria on the results of structural sizing and thus the aspects to be deepened for improvement. Seismic performance is then evaluated through both static and dynamic non-linear analyses, relating the design features with the main seismic performance parameters. The analysis of global structural systems is followed by the detailed study of base structural systems like the component braces, both X braces and single diagonal.

KEYWORDS

Steel Concentrically braced frames, Seismic design criteria, Non-linear incremental static and dynamic analyses, Hysteretic behaviour of steel braces, FEM numerical simulation of cyclic tests on single braces.

1 INTRODUCTION

The basic principle for the seismic design of structures is that, in case of earthquake, the loss of human life should be prevented at the cost of sacrificing the structural integrity. The modern anti-seismic limit state design philosophy is based primarily on the exploitation of the structures ability to develop cyclic deformations in plastic range, for dissipating energy generated by earthquakes. To this purpose structures should be designed as sufficiently ductile, allowing a global dissipative behaviour and, therefore, ensuring a certain inelastic displacement corresponding to a predetermined level of damage without reaching the collapse. Seismic analysis should be capable to capture the displacement capacity of a structure and to evaluate both the elastic and post-yielding contributions to the behaviour, aiming at identifying where and how progression of plastic effects is achieved, where and

which are the structural weaknesses, what kind of failure and how it is reached, what is the extent of structural ductility.

In recent years the huge amount of research and advances in the field of seismic engineering, together with the frequent occurrence worldwide of seismic events of high intensity and serious consequences, not last the case of Italy recently stroke by severe earthquakes, has motivated the upgrading of technical codes for constructions. With particular focus on steel structures, a crucial moment for the development of the national seismic design codes was the draft of OPCM 3274 and 3431 (2005) since 2003, which introduced an extensive chapter, in line with Eurocode 8 (EC8), Design of structures for earthquake resistance (EN 1998-1, 2005), with the addition of some noticeable changes with respect to the European standard, integrating the evidences of extensive studies. However these amendments were not included in the technical standards, for the sake of symmetry with EC8 (Mazzolani and Della Corte, 2008). What is more, the Italian NTC2008 (M.D., 2008) had several cuts with respect to EC8, which were partially recovered in the explicative Italian Ministerial Circular (M. C., 2009).

A general outline of the design aspects and applications related to steel CBF structures, among the other steel seismic resistant structures, is presented in Mazzolani et al. (2006), where the modern approach is discussed, evidencing the conformity between the Italian and European codes.

Concentric bracing frames (CBF), as seismic resistant structures, consist of diagonal braces located in the plane of the frame, forming a truss that resist the horizontal actions mainly through axial forces. The presence of the bracing provides to the structure a high elastic stiffness, which allows to satisfy limitations on lateral displacements at the Damage Limit State. The energy dissipation should be entrusted to the formation of plastic fuses in the tensile braces. The specific design goal is to achieve a ultimate global behaviour, involving only the plastic deformation of braces, preventing the failure of beams, columns and connections. Braces in compression are usually designed to buckle, thus, the cyclic inelastic behaviour of CBF is characterised by the degradation of the energy dissipation capacity due to the repetition of the instability of braces. Focusing on a single steel brace, as part of a CBF, it typically buckles globally under compression and yields under tension axial loads. Because of the complex asymmetric inelastic behaviour and the wide range of possible configurations, it is nearly impossible to design the steel braces to achieve a uniform demand-to-capacity ratio along the height of CBFs and, ultimately, avoid local story mechanisms that are associated with concentration of plastic deformations, inducing structural collapse under strong earthquakes.

In the context of performance-based earthquake engineering, also for CBF there is the need to quantify the collapse capacity of structures subjected to extreme earthquakes (Giugliano et al., 2011; Marino, 2014; Faggiano et al., 2014, 2015, 2016) and, taking account of the cyclic deterioration in strength and stiffness of structural components, the stored capacity, once the steel braces failure has occurred, should be evaluated (Formisano et al., 2006; Hines et al., 2009). This topic is investigated by several researchers through both experimental and analytical studies on either single braces, or single story single bay, or multi-storey multispans structural systems, by analysing both local and global behaviour of bracing systems.

Past experimental studies show that the cyclic behaviour of steel braces depends upon numerous geometric and material parameters; the three basic ones are slenderness ratio, boundary conditions and cross-section of profiles (Jain et al., 1978; Black et al., 1980; Tang and Goel, 1989; Tremblay, 2002; Bruneau and Lee, 2005; Fell et al., 2009; Ashwin Kumar et al., 2015). The influence of the cross-section shapes and other member properties on the structural performance, generally estimated in terms of strength, ductility, energy dissipation and mid-length lateral deformation (Goggins et al., 2016), are evaluated. These studies lead to

the development of a wide range of either phenomenological (Ikeda et al., 1984), physical theories (Ikeda and Mahin, 1984; D'Aniello et al., 2015), or fiber-based (Jin et al., 2003; Krishnan, 2010) and detailed finite element models (Huang and Mahin, 2010). For structural systems, overall cyclic response and brace failure mechanisms are investigated (Jiun-Wei and Mahin, 2014) through non-linear static analyses on CBFs with different stories and span lengths, evidencing the great effect of the geometrical configurations on the response modification factors (Jinkoo and Choi, 2005; Moussa and Mahdi, 2010).

The reliable prediction of the dynamic behaviour of CBFs near collapse could be achieved through an accurate representation of the modelling parameters of the steel brace that control global/local instabilities and, ultimately, the fracture attributable to low-cycle-fatigue. For this reason, the need for the utilization of large structural component databases arises (Lignos and Krawinkler, 2011, 2012, 2013). Recently, proposed engineering approaches to trace collapse of structural systems (FEMA P695, 2009) put in evidence the efficiency of refined mathematical representation of structural components within an analytical model.

For CBF structural systems, both Italian and European codes therefore specify design provisions, aiming at obtaining a ductile and dissipative ultimate behaviour by imposing that the yielding of diagonal members occurs before damage and premature failure of beams, columns and connections. Such hierarchy resistance criterion among structural members should be achieved through a simplified procedure, which is implemented starting from a linear analysis of the CBF structure under reduced seismic loads. The simplified procedure provides, among other, a maximum allowable value for the normalised slenderness, in order to ensure satisfactory behaviour under cyclic loading, the definition of a structural overstrength coefficient Ω , defined as the minimum value among the overstrength coefficient Ω_i calculated for each diagonals along the structure, with small variation along the building height, in order to obtain a uniform distribution of plastic demand. With particular reference to CBF-X the use of a static scheme with tension-only (T/O) diagonals for the evaluation of the design forces in the brace members at the Ultimate limit state is indicated together with a minimum allowable value for the normalised slenderness of diagonals in order to avoid overloading of columns in the pre-buckling stage of compressed diagonals. With particular reference to Chevron Braced Frames (CBF-V), specific design requirements are provided for the beam where braces converge. A more rigorous plastic design procedure for CBFs is proposed by Longo et al. (Longo et al., 2008a; 2008b). More recently Marino (2014) has suggested a unified design approach for CBFs.

A wide research activity, aiming at the progressive upgrading and optimization of seismic design rule for constructions, including steel braced structures, is ongoing within the Italian project RELUIS-DPC. In this context, a deep analysis of X and V braced structures is presented in D'Aniello et al. (2010-2015) and in Faggiano et al. (2014; 2015a-c, 2017a-c).

The overview, hereafter presented, on the codification aspects according to the Italian technical Code (NTC08) and the Eurocode 8 evidences some critical issues both in the design process (Section 2, Castaldo et al., 2014; Faggiano et al., 2014, 2015a, b, c, 2017a; Macillo et al., 2014) and in the seismic capacity of structures (Section 3, Castaldo et al., 2014; Faggiano et al., 2014, 2017a, Macillo et al., 2014a, b).

The evaluation of the seismic response is deepened through both non-linear incremental static (ISA, Castaldo et al., 2014; Faggiano et al., 2014; Faggiano et al., 2017a; Macillo et al., 2014a, b) and dynamic analyses (IDA, Faggiano et al., 2017c) of some representative case study structures designed according to current seismic codes. ISAs and IDAs are carried out by means of the softwares SAP2000 (CSI, 2008) and SeismoStruct (Seissoft, 2014). The behaviour factors and collapse mechanisms, as well as the reliability of the Capacity Design criteria, are assessed.

A critical analysis of the design criteria for CBF-X structures is devoted to detect situations where the currently agreed calculation model, which neglects at the ultimate limit state the compression braces, is reliable or not. Hereafter (Sections 4 and 5) reference is made to available tests carried out on both one storey CBF-X frames (Wakabayashi et al., 1970) and single braces (Black et al., 1980). The one storey CBF-X structural FE models are set-up by means of the SeismoStruct software (Seismosoft, 2014; Formisano et al., 2015). Therefore parametric analyses are carried out by varying several geometrical parameters, such as the width-to-height (L/H) shape ratio of the structure, the adimensional slenderness and the cross-section types of braces. Non-linear static seismic analysis are then performed, with the purpose to identify the cases where the influence of the compression brace on the CBF-X behaviour is not negligible. Definitely, ranges of adimensional slenderness for the braces delimiting the possibility to adopt the calculation models based on single tensile diagonals only are identified. Moreover, the inelastic behaviour of braces subjected to reversed cyclic loading is examined (Faggiano et al., 2017c) with reference to the experimental tests by Black et al. (1980) on several braces, with the purpose to evaluate the hysteretic behaviour of axially loaded steel struts, frequently encountered in practice, having different cross-section shapes and slenderness ratios. Tests are reproduced by means of the software ABAQUS CAE 6.13-1 (Klarsson and Soresen, 2008), achieving a reliable FE model as a tool for carrying out a numerical parametric investigation campaign that allows a accurate knowledge on the hysteretic behaviour of brace members belonging to CBF systems. Therefore, the mechanical model of the member, to be implemented in global analysis models, can be optimized and reliable design criteria can be defined.

2 GENERAL REVIEW OF THE DESIGN METHODS FOR CONCENTRIC BRACED FRAMES

2.1 *The NTC2008 design criteria for CBF structures*

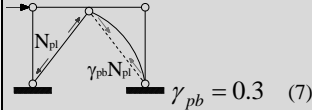
2.1.1 *General aspects*

In Concentrically Braced Frames (CBF), the resistance against seismic actions is provided by the contribution of both tensile and compression braces. The ideal design ultimate condition of a dissipative braced system is the simultaneous buckling of compression bracings and yielding of tensile ones, the braces being the dissipative elements. According to the commonly accepted resistance hierarchy criterion, the other structural elements, such as columns, beams and connections, have to remain in elastic range and, therefore, they should be designed to have an adequate overstrength as respect to braces. In Table 1 the Ultimate Limit State (ULS) design rules for seismic resistant concentric braced systems are summarised.

Firstly, members should be ductile, thus belonging to Class sections 1 or 2, according to the cross section classification defined in Eurocode 3 (EN 1993-1-1, 2005; Formisano *et al.*, 2006) and taken by NTC2008. In order to prevent the untimely collapse of beams and columns, according to the hierarchy design criterion, the code requires to determine the overstrength factor Ω , as in Table 1. This indicates how much the axial force and then the seismic force can exceed the design value until the brace member reaches the complete plasticization. It is not the same for all diagonals, it depending on the distribution of internal forces within the structure and on some sources of oversizing, like the selection of structural members among the standard profiles or the need to provide lateral stiffness for deformability check, further to the imposed limitation of slenderness. The latter condition is particularly strict at the upper stories, giving rise to Ω factors increasing along the height of the structures.

As a consequence, aiming at assuring a distribution in elevation as uniform as possible to promote the yielding of all braces, the difference between the maximum and the minimum values should be limited to 25% (Table 1).

Table 1. NTC08 design criteria for steel CBF structures.

		X-Brace	Chevron Brace
		Class sections 1 or 2; for circular hollow sections: $d/t \leq 36$	
		$N_{Ed}/N_{pl,Rd} \leq 1$ (1)	$N_{Ed}/N_{b,Rd} \leq 1$ (2)
		$1.3 \leq \bar{\lambda} \leq 2$ (3)	$\bar{\lambda} \leq 2$ (4)
Brace		$\Omega = \Omega_{min} = \left\{ \frac{N_{pl,Rdi}}{N_{Edi}} \right\}_{min}$; $\frac{\Omega_{max} - \Omega_{min}}{\Omega_{min}} \leq 1.25$ (5)	
Beam		$N_{Ed} = N_{EdG} + 1.1\gamma_{Rd}\Omega_{min}N_{EdE}$ (6)	 $\gamma_{pb} = 0.3$ (7)
Column		$N_{Ed} = N_{EdG} + 1.1\gamma_{Rd}\Omega_{min}N_{EdE}$ (8)	
q -factor	Ductility Class	High	2.5
		Low	2
<p>where: d and t are diameter and thickness of the circular hollow profile, respectively; N_{Eds}, $N_{pl,Rds}$, $N_{b,Rd}$ are the brace design axial force, plastic resistance, buckling resistance; $\bar{\lambda}$ is the brace normalized slenderness; Ω is the overstrength factor; γ_{Rd} is the steel overstrength factor that is the ratio between the average and the characteristic values of the yielding strength; γ_{pb} is a factor representative of the residual brace strength after buckling; N_{EdG}, N_{EdE} are the axial forces corresponding to non-seismic and seismic loads.</p>			

Moreover, considering that diagonals do not plasticize together at the same level of seismic forces, the Ω factor to be used is assumed as the minimum one, Ω_{min} , corresponding to the first non-linear event, such as the plasticization of the first brace. Once designed the braces and calculated the Ω factor, the capacity design criterion is applied for determining the design forces for beams and columns (Eq. 8, Table 1).

2.1.2 CBF-X

The design of CBF-X is performed by considering only the contribution of braces in tension, assuming that at collapse braces in compression are already buckled and do not provide any bearing capability. With this assumption, tensile braces are designed on the basis of the plastic resistance (Eq. 1, Table 1). Moreover, the normalized slenderness ($\bar{\lambda}$) of diagonals should be limited within a prefixed range (Eq. 3, Table 1), where the upper limit has the aim to avoid excessive distortions due to buckling of braces in compression, which could cause damage to connections or claddings, while the lower limit ensures the validity of the structural model with only active tensile braces as well as restricts the design internal forces in the columns, which are commensurated with the plastic resistance of braces.

The behaviour factor q for dissipative structures is assumed as equal to 4 for both low and high ductility classes. In the ideal condition in which the whole brace in tension is plasticized, ductility and dissipation capability of members would be much greater than how quantified by such q value. However it is not possible to be confident on the ideal behaviour due to the uncertainties related to the behaviour of braces under the seismic cyclic actions. In fact braces undergo alternate states of tension and compression, therefore if the brace in compression buckles, the unstable deformed shape in bending is characterized by localized plastic

deformation, thus the subsequent cycle in tension finds a degraded member, with limited ductile capabilities.

2.1.3 CBF-V

In the CBF-V, the compressed brace provides a contribution to the overall system stability, thus it cannot be neglected. For this reason, both braces are taken into account in the design model. Therefore the design resistance is the buckling strength (Eq. 2, Table 1) and only the upper limit of the normalized slenderness of diagonals is imposed (Eq. 4, Table 1), aiming at avoiding excessive distortions of braces in compression due to buckling, which could cause permanent damage to either connections or non-structural claddings. In addition, beams have to be designed by considering the concentrated force at the middle-span due to the unbalanced force between the plastic resistance of the tensile brace and the residual resistance of the compressed one after buckling, the latter being set equal to 30% of the brace plastic resistance (Eq. 7, Table 1). The beam is therefore subjected to bending moment, shear and axial forces. The behaviour factor q is equal to 2.5 and 2 for High and Low ductility classes, respectively.

2.2 The case study

The study structures have typical configuration and size of a regular building. The reference geometrical scheme, together with the main design features are given in Figure 1.

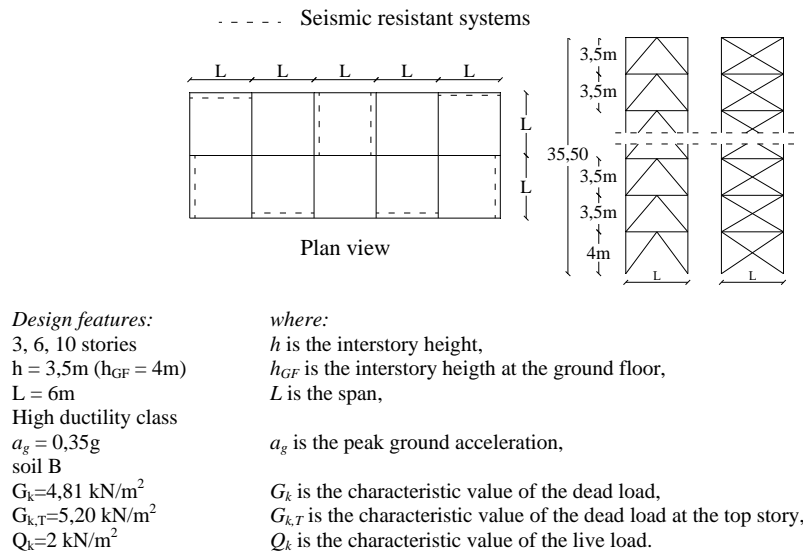


Figure 1. Geometry and design features of the study structures.

For the sake of simplicity, the elastic spectrum is obtained according to the code OPCM 3431 (2005) since seismic parameters are independent from the geographic position, unlike the current NTC2008. Each case study is designed through either the Linear Static (LS) or Linear Dynamic (LD) analyses.

For CBF-X the profiles used for the diagonal members are HE sections; in total 6 case studies are examined. For CBF-V for columns two cross section types are used, namely welded box sections and HE profiles, for beams HE profiles are used; while for braces two cross-section types, namely Circular Hollow Sections (CHS) and HE profiles, are used; in total 12 case

studies are examined.

As far as the Damage Limit State (DLS) is concerned, the limitation of the inter-story drift equal to 1% is considered, corresponding to infill panels not rigidly connected to the main structure.

The results of the design phases in terms of member profiles of the different investigated structures together with the total weight of each member type are provided in Faggiano et al. (2014) for CBF-X and in Faggiano et al. (2015c) for CBF-V.

2.3 Design assessment

2.3.1 CBF-X

The NTC08 design procedure shows a first critical issue in the ambiguity in the use of LD analysis. For CBF-X, the code prescribes that at the ULS only braces in tension resist the seismic forces, while the compressed braces are considered buckled and unable to provide strength. Nevertheless the vibration properties of the structure, i.e. periods and vibration modes, are strictly related to the linear behaviour and they should be determined considering the contribution of both braces in tension and in compression, therefore they cannot be calculated disregarding braces in compression. For this reason, for the structures examined the LD analysis is performed by considering the presence of both braces not only for evaluating the elastic vibration properties, but also for assessing seismic forces in the members. Then, in order to consider the model with only one active diagonal, the design of braces is carried out by assuming the axial forces as the double of the one calculated by the structural model including both diagonals (Fig. 2; Macillo et al., 2014a, b; Faggiano et al., 2014, 2015a, b).

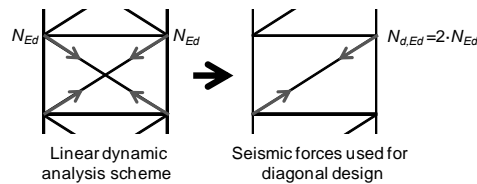


Figure 2. Structural scheme assumed for linear dynamic analysis.

In Table 2, the main design information on the study structures, such as W the structural weight, T the fundamental period of vibration, F_h the design base shear and Ω_{\min} the design overstrength factor, are reported (Macillo et al., 2014a, b; Faggiano et al., 2014, 2015a, b).

The design results show that the CBF-X designed by LS analyses are generally subjected to seismic actions higher than those designed by LDs. This difference is mainly related to the underestimation of the fundamental vibration period through the empirical formula provided by NTC2008 in case of LS. This issue is more evident for taller buildings. For instance, in case of 10s structures, T calculated by the code formula is smaller than T_{LD} , with a consequent increment of the total seismic force. This issue also influences the weight of seismic resistant members, the structural weight of LS structures being higher than the LDs.

Another critical issue observed in the design phase is the difficulty in selecting the brace profiles. In particular, the lower bound 1.3 of $\bar{\lambda}$ strongly limits the HE profiles that can be used, making difficult the selection of the diagonal cross-sections. In addition, the low seismic demand at upper storeys implies oversized bracings with corresponding very high Ω values. This especially occurs at the top storey, where the uniformity of the Ω factor distribution along the structure height is hard to be satisfied (Eq. 3, Table 1). Thus, for the 10s structures examined the top storey is not considered in the Ω check.

Table 2. Design results for CBF-X.

Design Method	N. storeys (s)	W [kN]		T [s]		F_h [kN]		Ω_{\min}	
		CHS	HE	CHS	HE	CHS	HE	CHS	HE
LS	3	37	37	0.30*	0.30*	348	348	2.52	2.52
	6	110	110	0.50*	0.50*	687	687	1.88	1.88
	10	186	186	0.73*	0.73*	781	781	1.44	1.44
LD	3	37	37	0.31	0.31	354	354	2.40	2.40
	6	95	95	0.59	0.59	548	548	1.94	1.94
	10	149	149	1.25	1.25	486	486	1.75	1.75

* $T=C_1H^{3/4}$ with $C_1 = 0.05$, H = total height of the structure

2.3.2 CBF-V

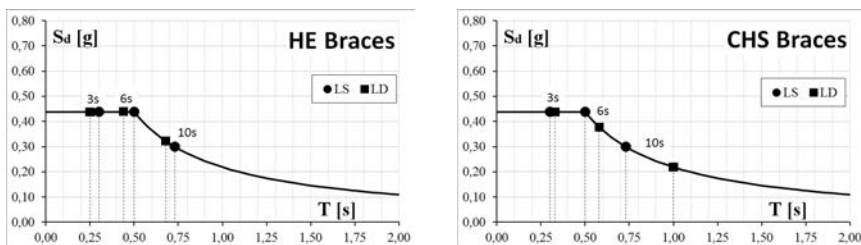
Commonly, the design of columns is conditioned by the gradual cross-section reduction criterion. In fact, strong variation of the cross-section sizes along the building height should be avoided, they being generally a source of localised damage. Moreover the structure story stiffness variation at consecutive floors should be limited, in order to fulfil regularity requirements devoted to assure the achievement of the most uniform state of stress and deformation and in particular plastic hinges distribution along the structure height at the ultimate limit states. Another influencing design aspect is that HE profiles larger than HEB300 are barely able to withstand high axial loads, because, as far as the depth increases, the base is almost constant; thereby, being the increment of second moment of area extremely limited, for profiles larger than HEB300, the axial buckling check is hard to be satisfied. For these reasons, for 10s structures and 6s HE braces structures, the columns are realized with welded square box sections, opportunely reduced along the building height, in order to absorb the high axial loads deriving from the capacity design criterion. Columns are HE profiles for 6s frames in case of CHS braces, as the same for 3s frames, where, due to the limited number of floors, the hierarchy design criterion is not penalising.

In Table 3 the main design information on the study structures are reported (Faggiano et al., 2015a, b; 2017a). In Figure 3 the response spectra with the evidence of T for 3s, 6s and 10s in case of HE braces and CHS braces are shown.

Table 3. Design results for CBF-V.

Design Method	N. storeys	W [kN]		T [s]		F_h [kN]		Ω_{\min}	
		CHS	HE	CHS	HE	CHS	HE	CHS	HE
LS	3	46	63	0.3*	0.3*	549	549	2.15	3.90
	6	159	234	0.5*	0.5*	1085	1085	2.11	4.04
	10	408	722	0.73*	0.73*	1254	1254	2.46	4.43
LD	3	52	71	0.33	0.25	580	588	2.32	4.21
	6	140	215	0.58	0.44	1062	1064	1.86	3.41
	10	309	602	1	0.68	988	1428	2.34	3.70

* $T=C_1H^{3/4}$ with $C_1 = 0.05$, H = total height of the structure

**Figure 3. The LS and LD first periods of vibration T for the study CBF-V.**

In general some observations can be done by comparing on one hand CHS and HE braces structures, on the other hand LS and LD design.

CHS braces structures are lighter than HE braces structures. This is particularly evident for LS 10s buildings, where the adoption of HE braces induces the use of welded double T beam profiles at the lower storeys, due to the high forces transferred by the braces, oversized for the limited availability of standard HE hot-rolled profiles. This limitation does not exist for CHS profiles, which are produced with a large range of cross-sections.

The vibration periods T determined by LD analysis are higher for CHS braces structures than for HE braces structures, in conformity to the previous observation. In the LS design the first vibration period does not depend on the bracing details, it being calculated by means of the simplified formula. Moreover, the T_{LD} , as respect to the T_{LS} is lower for HE braces structures, is higher for CHS braces structures.

In case of 10s and 6s structures the LD design gives rise to lower base shears and weights as respect to the LS design, contrary in case of 3s frames. This trend does not reflect the variation of the first periods of vibration T , due to the influence of the superior modes of vibration, which could provide not negligible additional actions that are ignored by the LS analysis.

Concerning the over-strength factor the following observations can be done:

- High values of Ω_{\min} , ranging from 1.86 to 2.46 and 3.41 to 4.43 for CHS and HE braces structures, respectively, are achieved. These imply a significant increment of design axial forces in the columns according to the capacity design.
- The Ω variation ratio (Eq. 5, Table 1) is always governed by the top storey braces, whose Ω values are generally larger than those at lower storeys. This is due to the use of brace cross-sections, which are subjected to low seismic actions but should contemporary respect the standard slenderness limit. As a consequence, elastic members are oversized, it producing a weight increase.
- In case of HE braces, Ω_{\min} is generally larger than the design behaviour factor q (2.5), what is not acceptable.

2.4 Main remarks

Based on the previous observations possible improvements of the NTC2008-EC8 design criteria for CBF can be related to the following items:

- For CBF-X the design procedure could be clearly stated in agreement with the ULS model with only tensile diagonal active.
- The use of HE profiles for structural members can become more convenient if a wider spectra of cross sections are produced, in order that profiles could best fit all the design requirements in terms of strength and stiffness, reducing the overstrength that alters the effect of the design provisions as respect to the expectations. This could also either avoid the scatter in the geometrical variability of members composed by different parts, as it occurs for columns belonging to high rise buildings, or enhance the efficiency of the capacity design, or simplify the connection among members.
- The simplified formula for the determination of the first period of vibration, necessary in case of LS design, should be better fitted according to the number of floors, taking also into account the structural system type, it being differentiated in case of bracing systems and for type of bracings.
- The top story needs specific design criteria, which balance capacity design and slenderness requirements. Some authors proposed a different approach based on the

reduction of the bracing members section at the ends to obtain $\Omega=1$ (Giugliano *et al.*, 2010, 2011).

- With regards to capacity design, it should be explicitly stated that the overstrength factor Ω should be in any case lower than the design behaviour factor q .

In general, the results briefly presented, in line with the literature references, delineate some important issues and suggestions for improvements, related to the design procedure and structural models. However they require more wide elaborations through further extensive campaign of both experimental and numerical investigations aiming at both optimizing the calculation models and providing simplification to the design methods.

3 THE IMPACT OF CURRENT DESIGN CRITERIA ON THE SEISMIC PERFORMANCE OF CONCENTRIC BRACED STEEL STRUCTURES

3.1 Methodology of analysis

With the aim to assess the seismic response of structures examined, either non-linear incremental static analyses (on both CBF-X and CBF-V structures) and non-linear incremental dynamic analyses (on CBF-V structures) are performed on the case studies given in section 2.2. The most relevant behavioural issues, like the behaviour factor, the failure modes and the effectiveness of the capacity design criteria are evaluated. Based on the results obtained, suggestions for the enhancement of design criteria are presented.

3.2 Numerical modelling issues for CBF

Non-linear static analyses are performed by means of the FE software SAP2000 v. 14.0.0 (CSI, 2008). Members are modelled as beam elements with lumped plasticity, columns are continuous along the total height and both beam-to-column and brace-to-beam connections are hinged. Plastic hinges of beams and columns are modelled by considering the classic elastic-perfectly plastic constitutive law (Mazzolani and Piluso, 1996).

For bracing members, the definition of the behavioural model under seismic actions is still an open issue, due to the complexity of the actual behaviour (D'Aniello *et al.*, 2013, 2014). The force-displacement model assumed in the study is shown in Figure 4a, where every significant limit state point is evidenced (Castaldo *et al.*, 2014; Macillo *et al.*, 2014a, b; Faggiano *et al.*, 2014, 2017a).

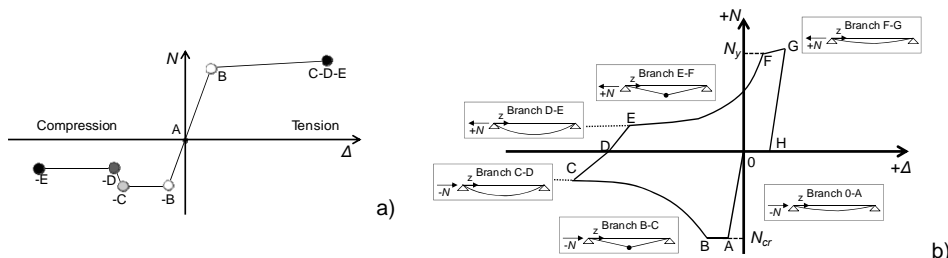


Figure 4. The bracing member behaviour: a) assumed model (Faggiano *et al.*, 2014; 2017a); b) Georgescu model (1996).

It is a simplification of the mathematical model proposed by Georgescu (1996), which is depicted in Figure 4b. The brace ductility is limited according to the simplified approach proposed by Tremblay (Tremblay, 2002). In this way, it is possible to take into account,

although with approximation, the actual behaviour of braces in compression (D'Aniello et al., 2010, 2013, 2015), consisting in the buckling and then post-buckling phases, where a loss of strength and stiffness results in a reduction of the brace dissipative capacity.

In particular, the Georgescu model is based on the following main assumptions (Fig. 4b): under horizontal forces one brace is in compression, the other in tension, the behaviour is initially linear-elastic with the same behaviour in tension and in compression (branch OA); when the compression force attains the buckling resistance, the compressed brace assumes a non-linear behaviour, the force cannot further increase, while lateral displacements grows till a given level at a constant force (branch AB); for larger displacements, the resistance decreases determining the post-critical condition (branch BC). In order to provide a ductility limit for braces, reference is made to the wide experimental campaign performed by Tremblay (2002), including bracing systems with different cross-sections, namely rectangular and circular hollow sections (RHS [4x2x0.125-152x152x9.5]mm, Pipe [4.0x0.226-4.5x0.237]mm), double T profiles (W [6x15.5-8x21]mm), C-profiles side by side ([50x50x6x6]mm). Tremblay proposed a simplified approach in which the total available ductility μ_F is given as a function of the normalised slenderness $\bar{\lambda}$ (Eq. 9):

$$\mu_F = a + b \cdot \bar{\lambda} \quad (9)$$

where a is equal to 2.4,
 b is equal to 8.3,
 $\bar{\lambda}$ is the slenderness.

The ductility μ_F is considered as the sum of the ductility in compression and in tension.

Non-linear incremental dynamic analyses (IDA) are performed by means of the SeismoStruct software (Seismosoft, 2014) on a 2D model (Faggiano et al., 2017b).

The structural members are modelled with distributed inelasticity elements, formulated with a Force-Based approach, accounted for through integration of the material response over the cross-section and integration of the section response along the element length. This model has been proved to be the best fitting one to simulate the seismic response of braced structures ((Filippou and Fenves, 2004; Scott and Fenves, 2006; Fragiadakis and Papadrakis, 2008; Calabrese et al., 2010, D'Aniello et al., 2013, 2015). The numerical integration method is based on the Gauss Lobatto distribution (Abramowitz and Stegun, 1964).

Columns are considered as continuous along the structure total height and hinged beam-to-column and brace-to-beam connections are assumed. In order to well reproduce the behaviour in compression of the brace, an initial camber is introduced (D'Aniello et al., 2013), as an initial out-of-plane imperfection. The latter is computed according to Dicleli and Calik (2008) formulation, which gives the better accuracy (Eq. 11):

$$\Delta_0 = \frac{M_{pb}}{N_b \left(1 + \frac{N_b L^2}{8EI} - \frac{N_b L^2}{\pi^2 EI} \right)} \quad (11)$$

where M_{pb} is the reduced plastic moment,
 N_b is the buckling load,
 E is the elastic modulus of steel,
 I is the second moment of area of the cross-section,
 L is the brace length.

The initial camber of the brace is depicted in Figure 5a, whereas the assumed force-displacement behaviour of diagonal members is shown in Figure 5b (D’Aniello et al., 2012, 2013). The P- Δ effect is taken into account by employing the “dummy” column (Fig. 5c), which is subjected to the gravity load of interior frames not included in the analysis models. This column, which is connected by pinned rigid links, has not any lateral stiffness.

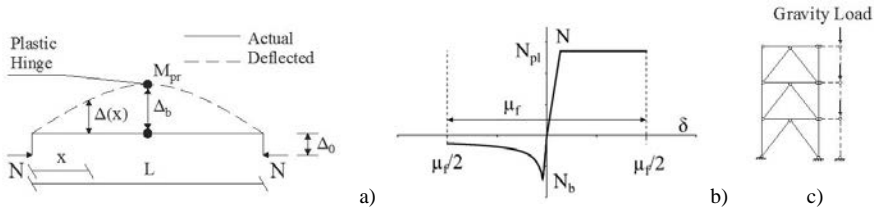


Figure 5. a) Dicleli and Calik’s initial camber; b) Assumed force-displacement behaviour; c) Dummy column.

The bi-linear model is chosen to simulate the steel behaviour. The average value of the steel yield stress, obtained by multiplying the nominal value of the material yield stress by the randomness coefficient γ_{ov} equal to 1.25, is used (MD 14/01/2008).

The Physical-Theory Model (PTM) is adopted to simulate the response of braces. The brace ductility is limited according to the simplified approach proposed by Tremblay (2002, Eq. 9): In this way, it is possible to contemplate, although with some approximations, the actual behaviour of braces: yielding in tension and buckling in compression, where a loss of strength and stiffness results in a reduction of the brace dissipative capacity.

Masses are assumed as lumped into master joints at each storey.

3.3 Behaviour factor evaluation

The behaviour factor q is a coefficient that allows to perform an elastic seismic analysis of the structure, taking into account the inelastic behaviour capabilities. It is a measure of the structural ductility and depends on the type of seismic resistant system. The q factor is used as a reduction coefficient of the elastic spectrum, which characterizes the elastic response at the earthquake site, thus obtaining a design inelastic spectrum. In this way it is possible to perform a seismic structural analysis in elastic field, with reduced seismic actions as respect to those corresponding to the elastic response under the site earthquake, accepting at the ultimate limit state a degree of permanent damage due to inelastic deformation associated to seismic input energy dissipation. Therefore, the q factor represents the ratio between the resistance that the structure has to possess to remain in elastic range, F_e , and the design resistance under earthquake, F_h . The latter is generally slightly lower than the actual structure resistance corresponding to the occurrence of the first non-linear event in the structural system, F_1 , because of the intrinsic design overstrength (Fig. 6a).

With this premises, also the definition of the behaviour factor q is an open issue.

The q factor assumed in the study, in case of incremental static analyses (ISA), is determined, coherently with the previous definitions, according to the following equation 12 (Fig. 6a, Uang, 1991; Castaldo et al., 2014; Macillo et al., 2014a, b; Faggiano et al., 2014, 2017a), where q_Ω and q_μ are the behaviour factor contributions related to overstrength and ductility, respectively; F_1 is the base shear at the first non-linear event, F_h is the design base shear, F_u is the maximum base shear value on the pushover curve, d_y is the displacement corresponding to the conventional elastic limit and d_u is the ultimate displacement.

The q_Ω factor takes into account the structure overstrength, through the ratio F_1/F_h , and the

plastic redistribution capacity through the ratio F_u/F_1 . In particular the q_u factor represents the structure ductility, it being given by the ratio d_u/d_y (for $T^* > T_C$, where T^* is the fundamental period of the equivalent SDOF system and T_C is the limit period between the constant acceleration region and constant velocity region of the design spectrum).

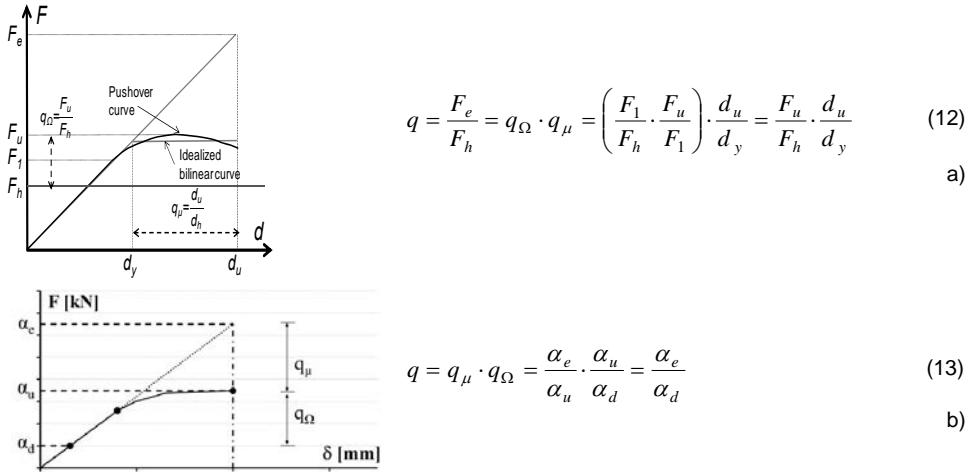


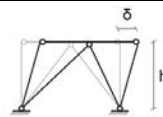
Figure 6. Evaluation of the behaviour factor Incremental a) Static Analysis and b) Dynamic Analysis.

Similarly, in case of incremental dynamic analyses (IDA), the behavior factor is calculated according to the equation 13, as the ratio between the amplification factor corresponding to the collapse condition and the amplification factor corresponding to the design condition (Faggiano et al., 2017b). The application of equations (12, 13) for the definition of the q factor requires another assumption to be made, it being related to the selection of the ultimate condition, which d_u corresponds to.

With regards to the static analysis, two different definitions for the ultimate displacement d_u are considered (Castaldo et al., 2014; Macillo et al., 2014a, b; Faggiano et al., 2014, 2017a, b). In the first case the behaviour factor q corresponds to d_u as the lowest displacement among those corresponding either to the development of a collapse mechanism, or the achievement of the diagonal maximum local ductility of the brace, or the 15% strength loss with respect to the peak force on the pushover curve. In the second case the behaviour factor, namely $q_{2\%}$, corresponds to d_u at the achievement of the interstorey drift equal to 2%, as provided by FEMA 356 (2000) for braced steel structures at Collapse Prevention limit state. In case of IDA, reference is made to different definitions of the ultimate condition, related to different extents of the maximum inter-story drift (FEMA 356, Table 4).

Table 4. Recommended inter-storey drifts at different limit states (FEMA 356).

Limit State	Maximum Drift (%)	$d_r = \delta/h$
Near Collapse	2	
Life Safety	1.5	
Optional*	1.0	
Immediate Occupancy	0.5	



*The so-called *Optional* state ($d_r=1\%$) is not properly a Limit state, but it has been identified anyway for the sake of completeness.

3.4 Seismic performance evaluation

3.4.1 CBF-X

The seismic performance of the structures is evaluated through incremental static analyses (IDA), in terms of collapse modes and behaviour factors, aiming at the evaluation of the accuracy of design assumptions (Macillo et al., 2014a, b; Faggiano et al., 2014).

In Figures 7 and 8 the failure modes (Fig. 7) and pushover curves (Fig. 8) for the investigated CBF-X structures are depicted. In Figure 8 the points reported correspond to the limit states defined in Figure 4a.

The failure modes exhibited by the structures examined always differ from the global mechanism. In particular, the 2% inter-storey drift limit is always attained before the other previously defined ultimate conditions and the crisis is located in a single storey, where the complete yielding of the braces in tension occurs. As a consequence, plastic hinges at the columns ends develop with the loss of load-bearing capacity of the entire structures (Fig. 7 and 8). Nevertheless, for the investigated cases, the collapse occurs after the yielding of a large number of braces, which is more than 60% of the total ones. This means that the applied design criteria allow for a fair dissipative behaviour of the structures investigated.

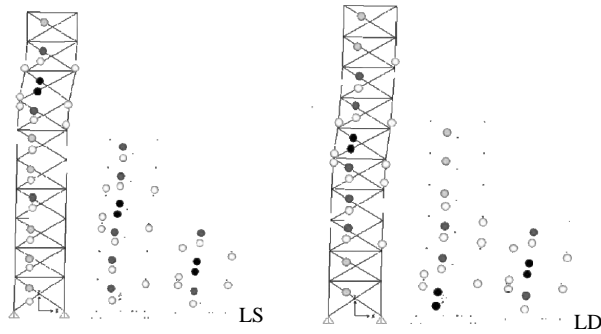


Figure 7. Failure modes for investigated CBF-X structures

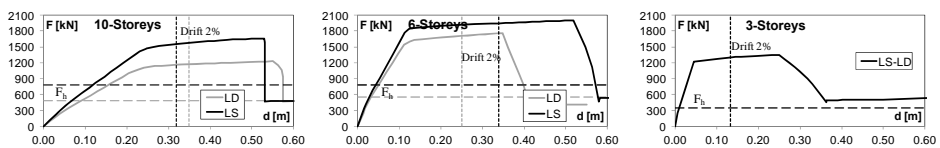


Figure 8. Pushover curves for investigated CBF-X structures.

Furthermore, acceptable values of ductility are ensured, q_u ranging from 2.1 to 2.9 when only some braces are yielded and from 3.0 to 4.0 when all braces are yielded. Table 5 shows the values of the behaviour factors q and $q_{2\%}$, as defined in Section 3.3. As far as the behaviour factor q is concerned, the obtained values are always greater than the standard one ($q = 4$). In particular, they range from 4.5 to 11.7 and show an increasing trend with the decreasing of the storeys number. The high values of the behaviour factor, for 3 and 6 storeys structures, are due to the oversizing of the structural members, as confirmed by the high Ω -values detected. These behaviour factors have a very high overstrength contribution (q_o), which attains values up to 3.88.

Table 5. Behaviour factors of investigated CBF-X structures.

Analysis Method	N. storeys	q			q _{2%}			% yielded bracing
		q _μ	q _Ω	q _μ ×q _Ω	q _μ	q _Ω	q _μ ×q _Ω	
LS	3	3.01	3.88	11.7	2.26	3.75	8.49	100
	6	3.98	2.91	11.6	2.91	2.83	8.24	100
	10	2.10	2.12	4.46	1.34	1.99	2.66	90
LD	3	3.01	3.88	11.7	2.26	3.75	8.49	100
	6	2.88	3.21	9.25	2.20	3.12	6.88	67
	10	2.15	2.52	5.42	1.32	2.42	3.19	60

On the other hand, the obtained values of the behaviour factor $q_{2\%}$ are quite lower than those of q factor with differences of about 70% for 10-storeys structures and 40% for the other structures. In the case of 10-storeys structures, $q_{2\%}$ ranges from 2.7 to 3.2 and is lower than the standard one, while for the other structures $q_{2\%}$ is greater, it ranging from 6.9 to 8.5. The difference between q and $q_{2\%}$ factor depends substantially by the lower ductility contribution in case where 2% drift attainment is assumed as ultimate condition ($q_{\mu}=1.3\div 2.9$), while very little differences are observed in terms of Ω -values.

This evidence demands a focus on the identification of the ultimate conditions to be referred to, aiming at the definition of the q factor, which should be also attributed according to the number of stories. Also the design objective at the ultimate limit state could be calibrated, considering that also partial collapse mechanism could correspond to suitable performances in terms of ductility and dissipation capabilities.

3.4.2 CBF-V

3.4.2.1 Performance evaluation by non-linear incremental static analysis (ISA)

The seismic performance of the study structures is evaluated in terms of failure modes and behaviour factors by means of non-linear static (pushover) analyses (Castaldo et al., 2014; Faggiano et al., 2017a). In Figure 9 pushover curves are represented both in the base shear (V_b) vs top displacement (δ) plane (Figs. 9a) and in the V_b/V_y vs δ/δ_y normalised plane, V_y and δ_y being respectively the shear related to the first plastic hinge and the corresponding displacement (Figs. 9b), where the V_b/V_y can be intended as an overstrength coefficient.

It can be noticed that generally the LS structures have V_b/V_y ratios greater than the LD structures.

CBF with HE braces always have increasing curves; if compared to CBFs with CHS braces, they exhibit greater stiffness and larger ultimate displacements (Fig. 9a). Moreover the CHS structures strength reserve after the first non-linear event is smaller, since they attain suddenly the ultimate resistance (Fig. 9b).

In Figure 10 the failure modes for the investigated CBF-V are depicted. In all cases, the collapse of structures occurs because of a beam mechanism located at the top storeys with the formation of plastic hinges in the beams. Generally, this condition leads towards a limited number of buckled braces for taller structures while the tension braces behave elastically leading to poor energy dissipation.

The generalized exhibited beam failure mechanisms are indicative of the low dissipative capacity of NTC08 CBF-V. This behaviour can be ascribed to the design criterion, which assumes $\gamma_{pb}=0.3$ for the calculation of the unbalanced vertical force applied to the beam (Table 1). In fact, according to the buckling curves b and c typical of the used bracing profiles (Fig. 11), the reduction factor χ for bracings with normalised slenderness close to the upper limit given in (Eq. 4) results to be equal to about 0.2. This value is smaller than the post-buckling residual strength ($\gamma_{pb}=0.3$) proposed by the code. In addition, for the investigated cases, the Georgescu model provides, at the maximum local ductility predicted by Tremblay,

a strength reduction of N_{pl} up to 6-7%. Therefore, the assumption $\gamma_{pb}=0.3$ is not conservative.

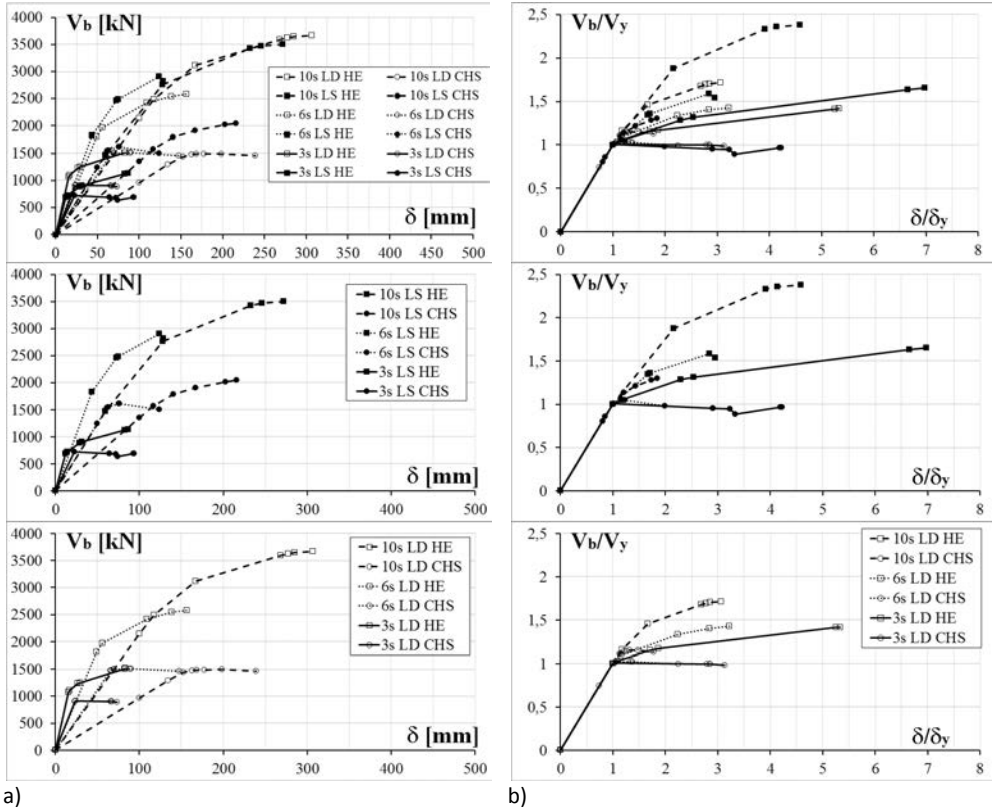


Figure 9. Pushover curves for study CBF-Vs.

Another key aspect responsible of the poor overall response of chevron CBFs has been recently evidenced in literature, it being related to the beam flexural stiffness (Shen et al., 2014; D’Aniello et al., 2015b).

For 3s frames, the behaviour factor for the CHS brace structures is greater than 2.5, for 6s and 10s frames, the behaviour factor is about 2.5. Nevertheless, in all investigated cases, structures with HE braces always have behaviour factor largely greater than 2.5 (Table 6 and Fig. 12).

Table 6. Behaviour factors for CBF-V.

N. storeys	CHS LD			CHS LS			HE LD			HE LS		
	q_{μ}	q_{Ω}	q	q_{μ}	q_{Ω}	q	q_{μ}	q_{Ω}	Q	q_{μ}	q_{Ω}	q
3	1.53	2.16	3.31	1.31	2.24	2.94	1.82	3.85	7.01	1.25	4.90	6.13
6	1.39	1.89	2.62	1.42	1.80	2.55	1.70	3.13	5.32	1.69	2.80	4.73
10	1.56	1.51	2.35	1.52	1.64	2.49	1.95	2.57	5.00	1.76	2.76	4.86

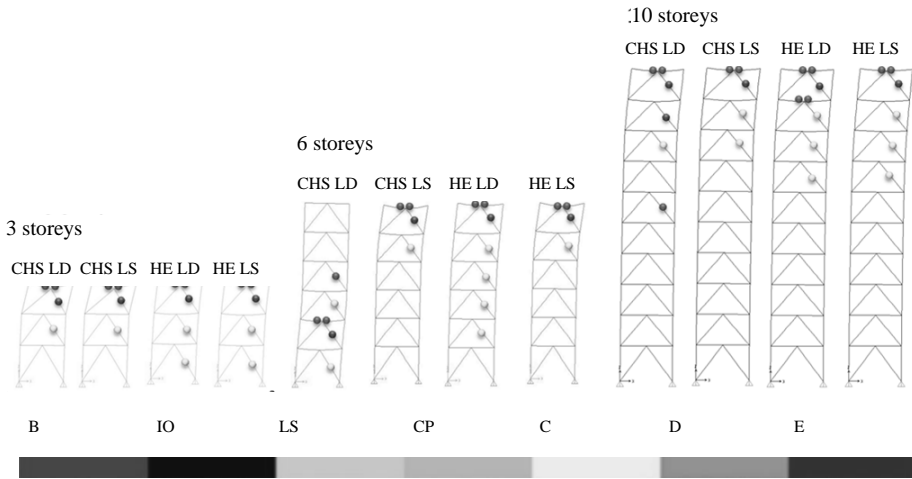


Figure 10. Failure modes for the investigated CBF-V.

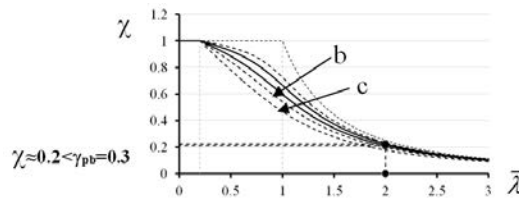


Figure 11. Limit value of the reduction factor χ for bracings with typical slenderness.

This result can be ascribed to the lower over-strength of structures with CHS braces. Moreover, in almost all cases, the collapse condition corresponds to the attainment of the local ductility limit of braces, whereas only in few cases, the value of the inter-storey drift reaches 2%.

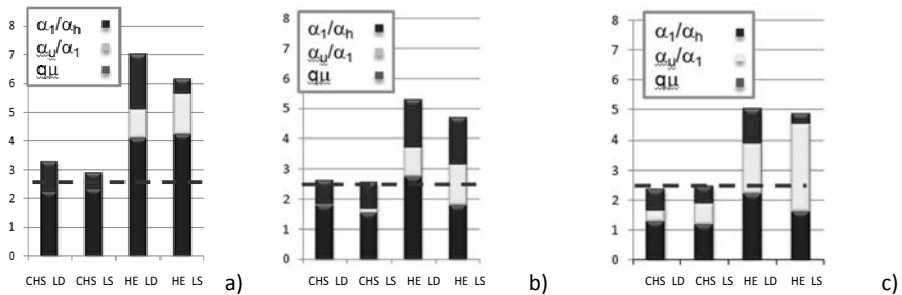


Figure 12. q-factor values for V-CBF structures with 3s (a), 6s (b) and 10s (c).

Based on the previous observations, it is apparent that the current design criteria lead to structures that behave all in all as expected and even better than previsions, in terms of ductility and dissipative capability, as testified by the comparison between the design and calculated behaviour factors, although the ideal collapse condition is not attained, it being

characterised by a local beam mechanism at the top story, in absence of brace plastic behaviour in tension. This issue underlines that the capability of the CB-V structural systems is not exploited, requiring a large improvements of the design criteria for enhancing the seismic structural behaviour. Among them, a more appropriate reduction factor γ_{pb} for the determination of the residual strength of buckling braces should be assumed.

3.4.2.2 Performance evaluation by non-linear incremental dynamic analysis (IDA)

Selection of the earthquake records

The random nature of earthquakes is one of the concerns in the determination of the seismic response of structures. Therefore, in order to take account of uncertainties in the frequency and spectral shapes of earthquakes a significant number of records is used for applying the Incremental Dynamic Analysis (IDA, Faggiano et al., 2017b). Seven acceleration records of remarkable earthquakes are selected, according to the Italian standards. They are listed in Table 7. Figure 13 shows the records defined by the Rexel Italian software (Iervolino and Cosenza, 2009), as well as the comparison between the natural signals and the design spectra.

Table 7. Earthquake records used for IDA.

Waveform ID	Earthquake ID	Station ID	Earthquake Name	Data	Mw
IT00014	4	TLM	Friuli Earthquake 1st shock	06/05/76	6.4
IT00136	35	PTT1	Patti Gulf Earthquake	15/04/78	6
IT00164	47	ALT	Irpinia Earthquake	23/11/80	6.9
IT00169	47	BSC	Irpinia Earthquake	23/11/80	6.9
IT00171	47	CTL	Irpinia Earthquake	23/11/80	6.9
IT00382	100	CSA	Umbria-Marche 2nd shock	26/09/97	6
IT00390	100	NCR	Umbria-Marche 2nd shock	26/09/97	6

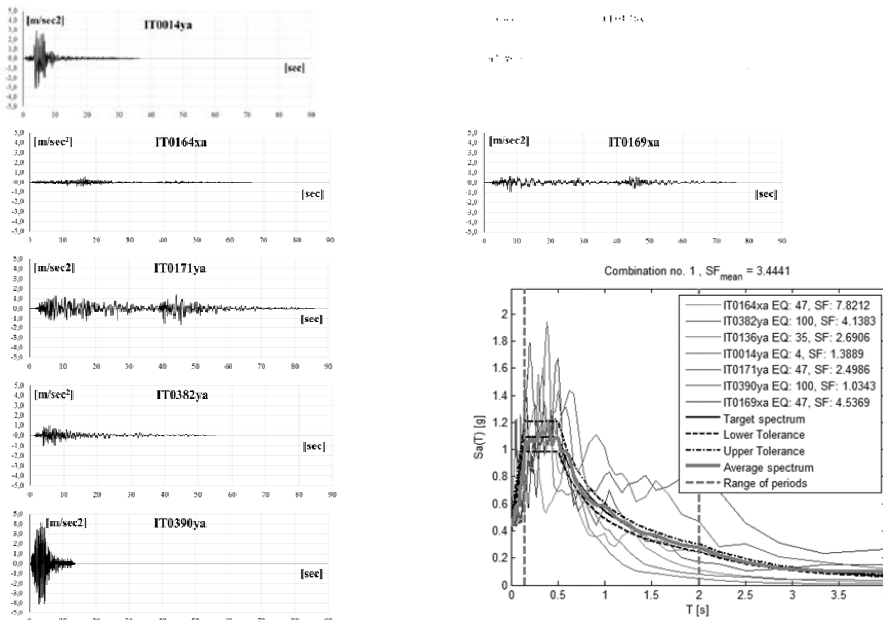


Figure 13. Selected earthquakes: Acceleration records and related spectra.

The records are scaled to take into consideration an adequate ranges of seismic intensities. In particular, the Intensity Measure (IM) is scaled from a very low value to a definite high value, in order to investigate the elastic response up to the collapse state. Hence, the response curve (IDA curve) is obtained by plotting, for each scaled record, intensity against damage measures (DM), the latter being the main deformation output. In this study, the spectral acceleration is the IM parameter and the maximum inter-story drift and beam rotation are the DM parameters. With regards to IM scaling, different amplification factor α_i are applied. At first, a very low level of seismic intensity is used to study the linear response of the structures. Then, the subsequent factors are selected to analyse the range of spectral accelerations, which give rise to damage. They are set as equal to 0.3, 0.5, 0.9, 1.0, 1.1, 3.0, 5.0, 7.5 and 10. Definitely, a total number of 840 cases are analysed. The IDA curves are then obtained as the average among the curves calculated for each record (MD 14/01/2008).

Structural performance parameters

Further to previously defined seismic performance parameters, the beam rotation θ at the mid-section, where the inverted V braces converge, and the stiffness ratio KF are also examined to study the global behaviour of structures. The beam rotation is the ratio between the mid-displacement of the beam and the beam half-length (Figure 14).

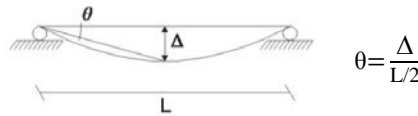


Figure 14. The beam rotation.

The parameter KF is the ratio between the flexural stiffness of the beam and the vertical stiffness of the braces, as shown in Eq. 14, being K_b and K_{br} the vertical stiffness of the beam at the brace intersection and the brace vertical stiffness, respectively:

$$K_F = \frac{K_b}{K_{br}} \qquad K_b = \xi \frac{EI_b}{L_b^3} \qquad K_{br} = 2 \frac{EA_{br}}{L_{br}} \sin^2 \alpha \qquad (14)$$

- where E is the steel elastic modulus,
- I_b is the second moment of area of the beam cross-section,
- L_b is the beam length,
- ξ is a factor depending on the beam boundary conditions ($\xi = 4$ for fixed ends and $\xi = 1$ for pinned ends).
- A_{br} is the brace cross-section area,
- α is the brace rotation angle,
- L_{br} is the brace length.

Seismic performance evaluation

Figures 15a and b show IDA amplification factor α versus inter-story drift curves, referred to the structures designed by Linear Static (LS) and Linear Dynamic (LD) analyses, respectively. The collapse conditions, corresponding to the attainment of the maximum inter-storey drifts as respect to the performance limit states, as indicated in Table 4, are evidenced in figure.

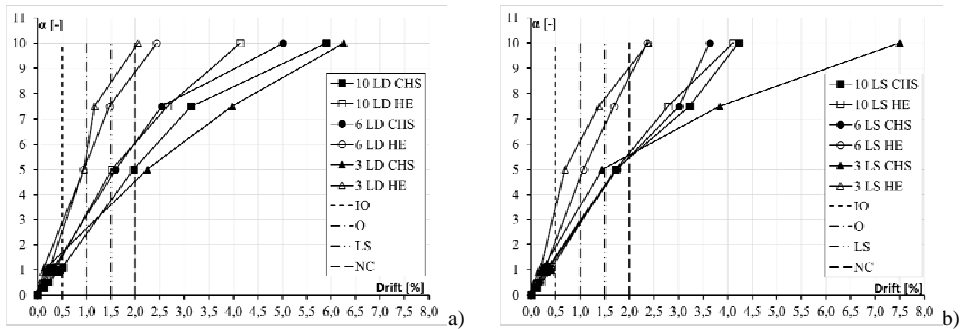


Figure 15. IDA curves: a) CBF-V LD structures; b) CBF-V LS structures.

It is apparent that HE braces structures are stiffer and reach higher strength than CHS braces structures.

In Table 8 the behaviour factors obtained for every case study at each limit state are reported.

Table 8. Behaviour factors for CBF-V structures.

Design Method	N. storeys	Ω_{min}		Limit states							
		CHS	HE	IO		O		LS		NC	
				CHS	HE	CHS	HE	CHS	HE	CHS	HE
LS	3	2.15	3.90	2.62	4.85	4.16	8.50	6.90	10.83	7.61	12.57
	6	2.11	4.04	1.63	2.69	3.20	5.90	4.77	8.52	6.10	10.93
	10	2.46	4.43	1.52	1.84	2.91	3.94	4.31	6.03	5.38	7.87
LD	3	2.32	4.21	1.62	3.73	2.51	7.29	3.42	11.01	4.44	12.83
	6	1.86	3.41	2.03	3.73	3.97	7.82	5.90	11.19	7.60	13.10
	10	2.34	3.70	1.15	1.91	2.54	4.04	3.93	6.18	5.32	7.56

It can be observed that the HE braces structures provide behaviour factors largely higher than CHS braces structures. Moreover in general for the 3sLS structures the behavior factors are higher than for 3sLD, the contrary occurs for 6s structures; whereas for 10s structures the behaviour factors are similar in both LS and LD cases. More evidently, in Figure 16 the trends of behaviour factors as respect to the number of storeys is indicated for the Near Collapse and Life Safety limit states; Optional and Immediate Occupancy limit states are not reported, because the structures show a predominantly elastic behaviour. Hence, for LS structures, behaviour factors decrease as far as the number of story increases; for LD structures, 6s structures have the largest behaviour factors.

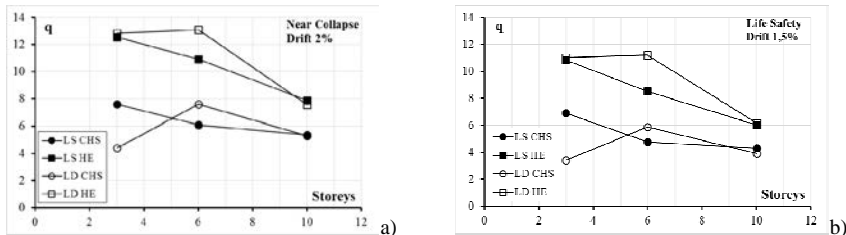


Figure 16. Trends of the behaviour factor vs number of storeys: a) Near Collapse; b) Life Safety limit states.

In order to make a comparison with the design q -factor value, indicated by the current codes for CBF-V, it being equal to 2.5, which depends only on ductility and plastic redistribution, the q_{Ω} factor related to the over-strength (Eq. 3) is deduced by the behaviour factor calculated through IDA. q_{Ω} is taken from Faggiano et al. (2017a), it being calculated through the static pushover non-linear analysis. The q_{μ} factor is then obtained (Table 9).

Table 9. Behaviour factors q_{μ} for CBF-V structures.

Design Method	N. storeys	Ω_{min}		Limit states							
				IO		O		LS		NC	
		CHS	HE	CHS	HE	CHS	HE	CHS	HE	CHS	HE
LS	3	2.15	3.90	2.00	3.88	3.18	6.80	5.27	8.67	5.81	10.06
	6	2.11	4.04	1.15	1.94	2.25	4.25	3.36	6.13	4.30	7.86
	10	2.46	4.43	1.20	1.57	2.31	3.37	3.42	5.15	4.27	6.73
LD	3	2.32	4.21	1.06	2.07	1.64	4.05	2.24	6.12	2.90	7.13
	6	1.86	3.41	1.20	2.19	2.35	4.60	3.49	6.58	4.50	7.70
	10	2.34	3.70	0.88	1.28	1.94	2.69	3.00	4.12	4.06	5.04

It can be noticed that at the Life Safety limit state in one case only (3s CHS LD) the behaviour factor is equal to $2.24 < 2.5$, the standard provisions on the q -factor being not conservative. It can be also noted that, q -factor is always greater for HE than CHS braces structures. At the design limit state, assumed as the Life Safety, such as at the inter-story drift equal to 1.5%, the damage distribution along the storeys height H of the structures, estimated in terms of the adimensional rotation of the beams, such as the ratio between the beam maximum rotation θ and the yielding rotation θ_y , is also assessed (Figures 17b, c and d). This is obtained for every beams in all the case studies through the procedure exemplified for the beam at the 9 story belonging to the structure 10s CHS LS in Figure 17a, where the IDA curve is built as respect to the Life Safety drift and compared to the IDA curve built as respect to the adimensional rotation.

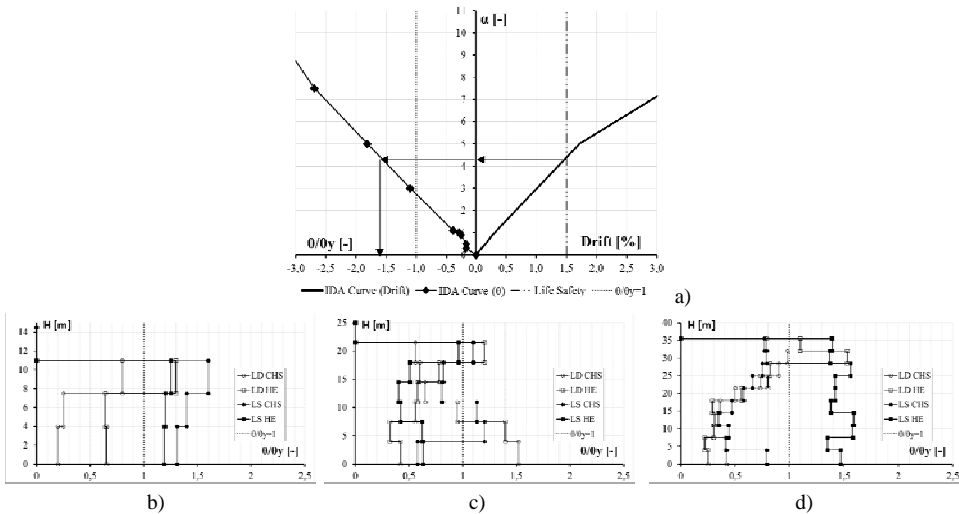


Figure 17. a) IDA curves expressed in terms of drift and adimensional rotation of the beam θ/θ_y ; θ/θ_y distributions along the height H of 3s (b), 6s (c) and 10s (d) structures.

As it can be noticed in Figure 17b, c and d, in 8 cases, such as 3s LS, 3s HE LD, 6s CHS, 6s HE LD, 10s HE structures, the Life Safety condition is reached with the beam plasticization at the connection with braces. In many cases, it is observed from the results of the analyses that this condition occurs with a limited number of buckled braces, mainly located at the upper floors, while the tension braces behave elastically, so to provide in all a poor energy dissipation capability of the overall structural system. This aspect is very important, since the design rules assume dissipative braces and non-dissipative beams, which must remain in the elastic range under seismic actions.

However, it is worth noticing from Figure 17 that in any case the beam rotation θ does not exceed the maximum value indicated by the NTC08 code (Section 4.2.3.1) for Class 1 cross-sections, corresponding to $\theta/\theta_y=3$. In fact, the maximum evaluated adimensional rotation values are in the range between 1.5 and 1.7.

The 10s HE LS structure is peculiar, as it can be noted in Figure 17c, because all the beams are in plastic range. This is due to the earthquake record “IT0164” (Fig. 13), in which the displacements assume very high values so to alter the average value.

Figures 18a, b and c show the inter-storey drift calculated by using the elastic spectrum referred to the Damage Limit State. It can be noted that the examined structures have an inter-storey drift largely smaller than 1%, which is the limit value used for the design at the DLS, evidencing that structures are strongly oversized. This is due to the high value of Ω_{min} .

Definitely, the role of the flexural stiffness of beams on the seismic behaviour of structures is investigated. Figure 19 shows the calculated values of the stiffness ratios K_F for each structure. In particular the value $K_F = 0.1$ is evidenced in figure, it being the limit proposed in literature (D’Aniello et al., 2015): higher values, corresponding to higher beam flexibility, increase the shortening of the compressed brace and, contemporary, reduce the extension of the tensile brace. In this way the ultimate configurations of the structure express lower ductility. Consequently, structures with stiff beam may enhance the dissipation capabilities, which q-factors higher than the design one can correspond to.

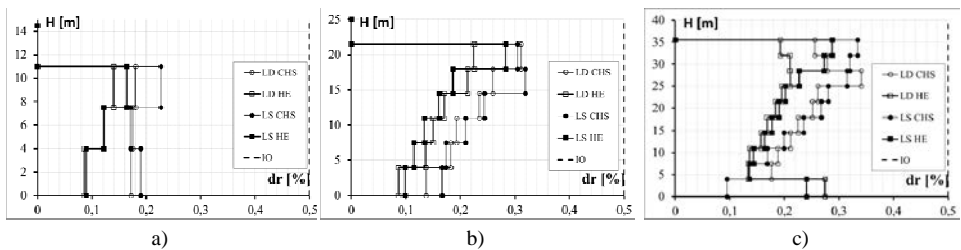


Figure 18. Drift distribution along the height H for CBF-V 3s (a), 6s (b), 10s (c) structures at the DLS.

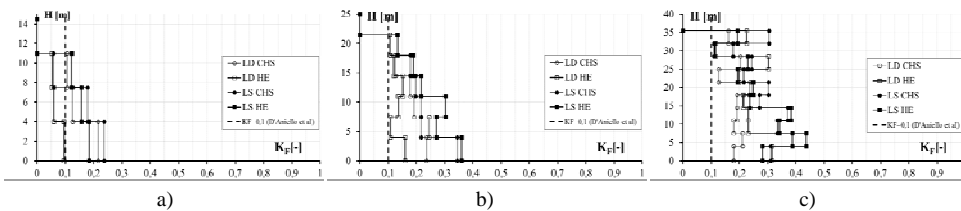


Figure 19. Stiffness ratios K_F for CBF-V 3s (a), 6s (b), 10s (c) structures.

From the examination of all the 76 beams of the study structures, it has been noticed that in 4 cases, such as the 4% of the examined cases, K_F is lower than 0.1, while in 57 cases, such as 75% of the examined cases, K_F ranges between [0.1 ÷ 0.3]. This also corroborates the fact that the number of braces reaching the maximum ductility in tension is low and, in general, the damage distribution is concentrated at the upper storeys.

3.5 Main remarks

From the previous investigations the following aspects are worth to be developed:

- Design procedure: specification of the procedure for the application of linear dynamic analysis coherently with the model of only tensile brace active for CBF-X; definition of different simplified relationships for the preliminary determination of the fundamental period of vibration, depending on the number of floors; definition of more pertinent rules for the top storey, in terms of slenderness of braces, in order to reduce the overstrength and then the Ω factor.
- Structural model: definition of the force-displacement behavioural model for bracing members in tension and compression, comprehensive of all the significant aspects of the actual behaviour.
- Behaviour factor: identification of the ultimate conditions for defining the q factor; attribution of the q factor according to the number of stories; calibration of the design objective at the ultimate limit state, considering that also partial collapse mechanism could correspond to suitable performances in terms of ductility and dissipation capabilities.

The case of V braces is peculiar for the beam design, due to the convergence of the diagonals at the beam, and in particular the relevant design rules should be better calibrated, they being actually poorly efficient in catching the actual structural capability of the CB-V systems.

The IDAs on CBF-V evidence some response and capability dissimilarities as respect to the ideal conditions at the basis of the design criteria by the current Italian Technical Standards (NTC08), based on the Eurocode 8. The results achieved allow to outline the following remarks:

- The use of CHS profiles for braces is more advantageous as respect to HE profiles. There is a larger availability of CHS different sizes, which implies a reduced structural overstrength. Therefore the overall structural sizes more strictly correspond to the design requirements. Moreover the structural performance more approximates the design expectations. q -factors are more suitable.
- In general the design through Linear Static analysis provides larger q -factor than Linear Dynamic analysis.
- The q -factors evaluated differ per number of floors and per ultimate condition assumed.
- The collapse modes do not correspond to the ideal design conditions: the beams undergo plastic deformations, although they do not reach the failure, few braces undergo plastic deformation in tension, several braces buckle. Most of the damage is concentrated at the upper floors.
- The stiffness ratio K_F appears to be an effective control parameter for ductile design of CBF-V.

It is important to note that the discussed results correspond to the average values of the parameters examined (according to the Technical Standard). Even though some general observations are reported, it would be relevant to correlate the seismic behavior of structures at every acceleration record considered.

Results acquired in the current study can be usefully adopted to plan an extensive campaign of experimental and numerical investigations, in order to confirm the above outlines and to both provide simplification to the design procedures and optimize the calculation models.

4 CBF-X: ANALYSIS OF MODELS AND DESIGN CRITERIA

4.1 Methodology of analysis

The SeismoStruct software is used for setting up the reliable numerical models. First of all, the model of a single brace subjected to both monotonic and cyclic loads has been calibrated as respect to the laboratory tests by Black et al. (1980). Based on this, the model of a one story CBF-X structural system has been set up and calibrated as respect to the test by Wakabayashi et al. (1970). Therefore a parametric analysis has been carried out in order to identify the ranges of braces slenderness that validate the calculation model of the tension only brace neglecting the brace in compression (Formisano et al., 2015).

4.2 Tests on single braces: set up of the numerical model

The reference experimental tests was carried out on single braces by Black et al. (1980). The analysed test specimens are listed in Table 10.

Table 10. Features of the brace specimens.

Test ID	Type of section	Size (mm)	f_{ym} (MPa)	L (mm)	L_{eff} (mm)	$\lambda=kL/r$
3	W	157x153x6,6x9,3	276,98	3070	2600	80
14	CHS	113,64x6,02	327,28	3070	2600	80
17	SHS	101,6x101,6x6,35	406,51	3050	2580	80

Frame elements with distributed inelasticity, formulated with a Force-Based approach, are adopted (section 3.2). The model of Menegotto and Pinto (1973) is used to simulate the material behaviour (Fig. 20b and Table 11).

Table 11. Calibrated parameters for the steel hysteretic model.

Steel model	$E_h(-)$	R_0 (-)	A_1 (-)	A_2 (-)	A_3 (-)	A_4 (-)
Menegotto-Pinto	0,015	20,00	19,00	0,15	0,00	1,00

where E_h is the kinematic hardening; R_0 is the curvature parameter characterizing the Bauschinger effect; A_1 and A_2 are the parameters affecting the shape of the hysteretic curve; A_3 and A_4 are the parameters quantifying the isotropic hardening.

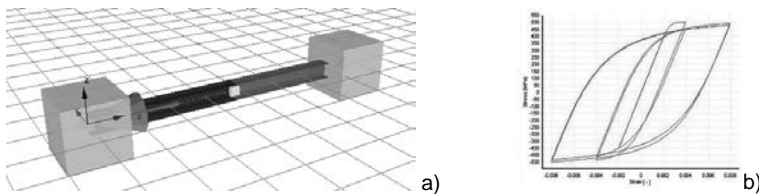


Figure 20. a) The numerical model implemented in SeismoStruct; b) the Menegotto-Pinto's law for steel.

Aiming at the model calibration, several parameters are investigated: the type of material, the shape and the amplitude of the initial camber (δ_0), the number of elements, the number of fibres, the number of Integration Points (IPs) used for each element. In particular, with regards to the initial camber the following formulations have been compared: ECCS (1978), Georgescu (1996), EN 1993: 1-1 (2005), Dicleli and Mehta (2007), Dicleli and Calik (2008). Monotonic and cyclic non-linear analysis are then performed in order to simulate the laboratory tests. The analysis of results are summarized in Figures 21.

The calibration has been achieved through the following features: the brace model is characterized by two elements (Fig. 20a), with 5 integration sections; the cross-section is meshed with 150 fibres, with two layers across the thickness of the plate components.

It can be observed that the initial camber value δ_0 calculated according to the Diciceli and Calik (2008) formulation, equal to $0.1\%L$ ($L/1000$), gives the better accuracy in the evaluation of the experimental critical loads (Figures 21a).

An optimal fit of the experimental results in the cyclic non-linear field of braces, especially in the post-buckling phases, is attained (Figures 21b).

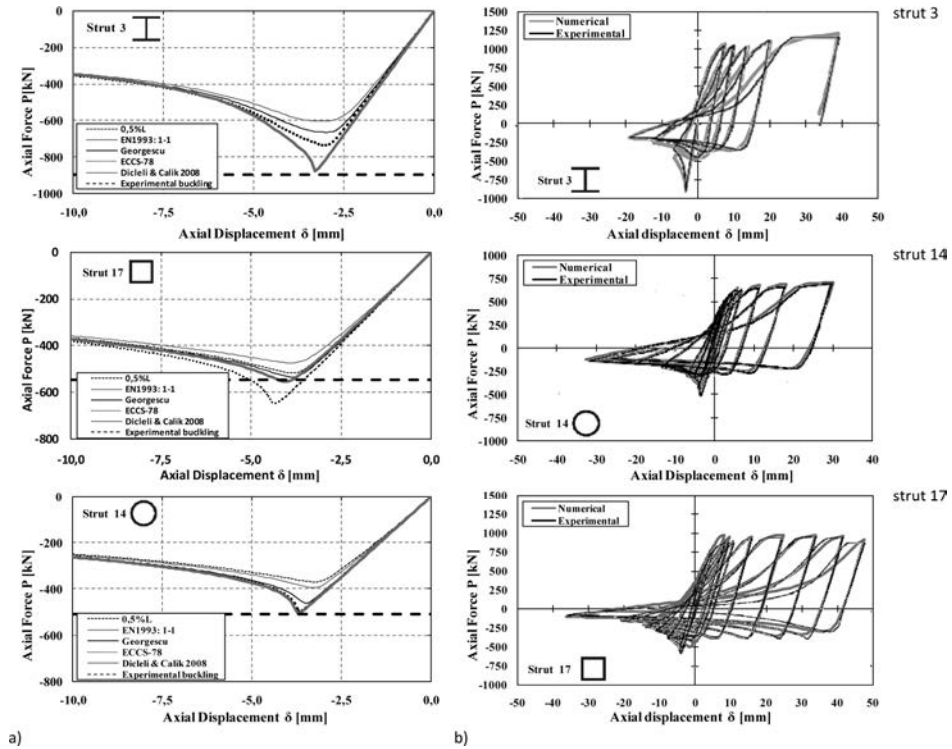


Figure 21. a) Calibration of the monotonic test; b) Numerical vs Experimental cyclic response.

4.3 Tests on one-storey CBF-X structural systems: set up of the numerical model

The reference experimental tests were carried out on a one-storey CBF-X structural system by Wakabayashi et al. (1970). Four one-storey X-braced frames were tested, with the same geometry (Fig. 22a), and different loading conditions. In particular, specimens BM0 and BM5 were tested under Monotonic loading conditions, with two different vertical loads applied to the columns, such as 0 and 700 kN, respectively; specimens BC0 and BC5 were tested under Cyclic loading conditions, with the same vertical loads as for the monotonic cases.

Figure 22b shows the model implemented in the software. Members model has the features above determined on the single brace (section 4.2). Moreover, full strength and full rigid beam-to-column joints are considered. Braces are modelled as perfectly pinned elements at the ends and the semi-lengths are divided into two FB distributed plasticity elements. Moreover, full-continuity at the intersection node is considered. A significant issue of the

modelling has been the analysis of the model sensitivity to the brace-to-brace interaction, since the buckling of the diagonal in compression is influenced by the diagonal in tension. The restraint effect of the diagonal in tension is taken into account in the calculation of the geometrical slenderness λ of the braces. This effect halves the in-plane buckling length of the brace. Hence, the geometrical in-plane slenderness is calculated considering the half brace length. The corresponding camber is calculated with the formulation proposed by Dicleli and Calik considering the half brace length (0.5L). Therefore the initial camber amplitude is applied in the centre nodes of each brace semi-length.

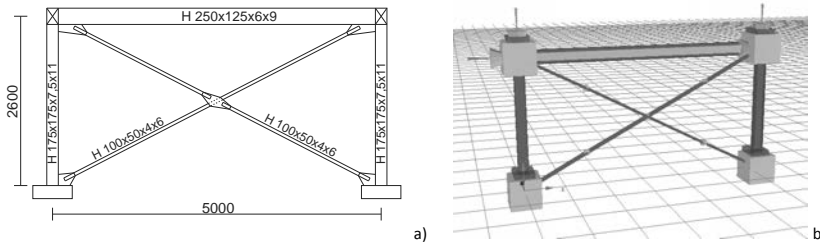


Figure 22. The CBF-X structural system: a) Geometry and b) Model implemented in SeismoStruct.

The steel yield stresses equal to 260MPa for columns, 290 MPa for beams and 320 MPa for braces, are derived from Wakabayashi experimental tests. In the monotonic and cyclic analyses, an incremental horizontal displacement history equal to the experimental loading protocol is applied to the CBF-X-specimen. As shown in Figures 23 and 24, both the monotonic and cyclic performances of the CBF-X systems are satisfactorily simulated.

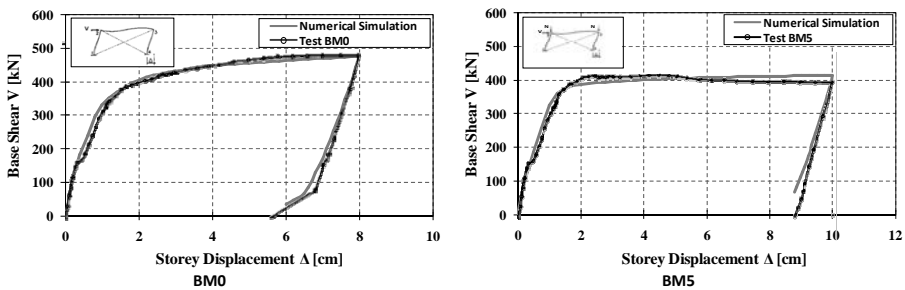


Figure 23. CBF-X structural systems: Numerical vs Experimental monotonic response.

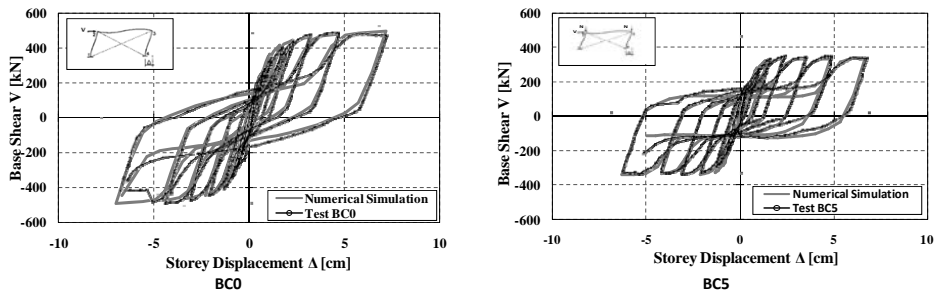


Figure 24. CBF-X structural systems: Numerical vs Experimental cyclic response.

4.4 Parametric analysis on the one story CBF-X structural system

A parametric analysis on one storey CBF-X structures, modelled by means of the SeismoStruct software, is performed by varying several geometrical parameters, as indicated hereafter:

- Width-to-height shape ratio (L/H) of frames: three values of the L/H shape ratio (1.0, 1.5 and 2.0), with the height H equal to 3.0m, are selected;
- Adimensional slenderness $\bar{\lambda}$: a large number of diagonal braces are designed for covering a wide range of $\bar{\lambda}$, this greatly influences the system overall behaviour; the extreme limits 1.3 and 2.0 imposed by the current codes are not considered, with the goal to investigate the real X-system mechanical behaviour; the assumed adimensional slenderness range is [0.8-2.3];
- Type of cross-sections: four types of cross-section (IPE, HEA, CHS, SHS), all belonging to class 1 are considered;
- In-plane and out-of-plane buckling cases: for systems with IPE and HEA cross-sections, both in-plane and out-of-plane buckling cases are analysed, while for systems with CHS and SHS cross-sections, only out-of-plane buckling cases are analysed, considering for the sake of simplicity that, even if these profiles have at least a double symmetry, the predominant buckling mode occurs out-of-plane.

In the numerical models, the steel material belongs to class S275 ($f_{yk}=275\text{MPa}$; $f_{ym}=318\text{MPa}$; $E=210000\text{ MPa}$). Figure 25 shows the geometrical configurations of the analysed CBF-X frames and the numerical models implemented in SeismoStruct software.

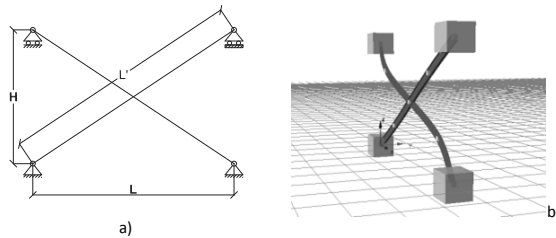


Figure 25. CBF-X structural system: a) Geometry; b) model implemented in SeismoStruct.

Seismic analyses in the static non-linear field (pushover analyses) are carried out with the purpose to identify the cases where the influence of the compression brace on the CBF-X behaviour is not negligible. In all case studies, the analyses are carried out until a target inter-story drift equal to 2%, according to a Collapse Prevention Limit State (FEMA 356). For the sake of example, in Figure 26 the pushover curves obtained for the X-bracing systems with IPE cross-section in the case of in-plane buckling are reported. It is apparent how the influence of the diagonal in compression on the global mechanical response of the systems decreases as far as the normalized slenderness of braces increases. Furthermore, it is worth noted that the pushover curves have only a strength increase as far as the L/H shape ratio increases, but the trend of the behavioural curves is the same, even varying the cross-section type of bracing members. Therefore, the behavioural trend of these systems is independent and invariant as respect to the L/H shape ratio.

Subsequently, the analysis results have been elaborated in terms of ρ - $\bar{\lambda}$ curves, relating the adimensional slenderness of braces $\bar{\lambda}$ with a so called overstrength factor ρ , which is the ratio between the story shear of the CBF-X system considering the contribution of the compressed diagonal and the story shear of the CBF-X systems with tensile diagonal only,

that is neglecting the mechanical contribution of the diagonal in compression.

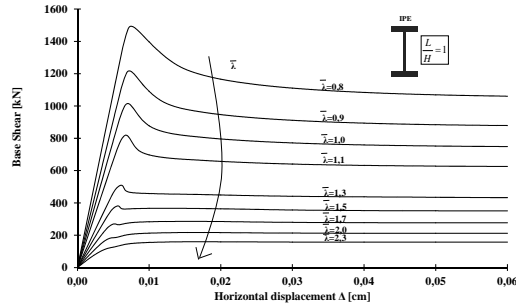


Figure 26. Pushover curves obtained for CBF-X with IPE cross-section (in-plane buckling).

Three different values of the ρ factor are calculated: the first corresponding to the peak strength of the global system; the second corresponding to a 1% interstory drift; and the third corresponding to a 2% interstory drift. For the sake of exemplification, Figure 27a shows the ρ - $\bar{\lambda}$ curves for the CBF-X systems with SHS brace cross-section, while Figure 27b shows the same curves for all the examined case studies.

In particular, from the latter figures, the following observations can be figure out:

- for $\bar{\lambda} < 0.8$, the design of CBF-X systems can be based on resistance;
- for $0.8 < \bar{\lambda} < 1.5$ both diagonals should be considered, taking account of buckling phenomena;
- for $\bar{\lambda} > 1.5$ the tension only brace model can be assumed.

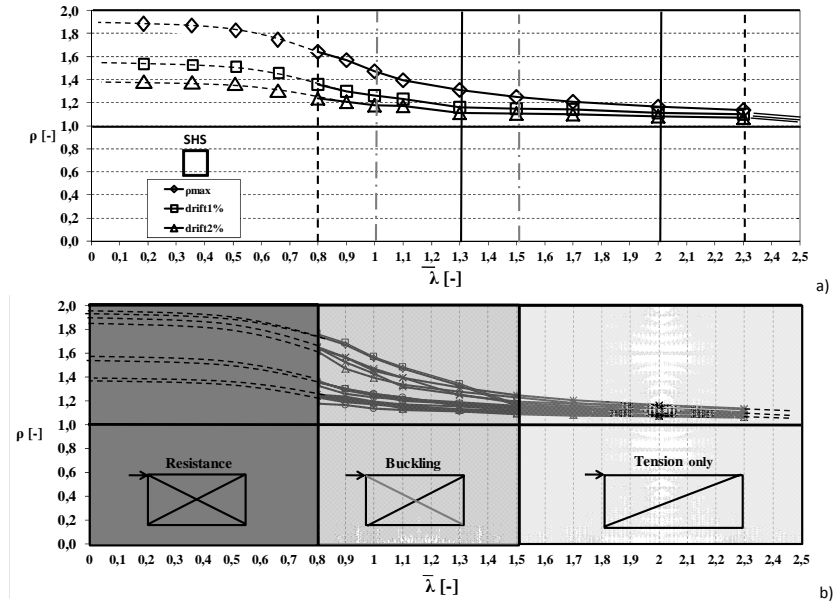


Figure 27. a) Curves ρ - $\bar{\lambda}$ for CBF-X systems with SHS cross-section; b) Design chart.

4.5 Main remarks

The design chart shown in Figure 27 can be a useful tool for selecting the design criteria for CBF-X structural systems at the ultimate limit states. In particular, three behavioural fields are identified:

1. Stocky diagonals $\bar{\lambda} < 0.8$
the CBF-X systems can be designed only for strength, both diagonals give contribution to the overall resistance;
2. Intermediate slenderness diagonals $0.8 < \bar{\lambda} < 1.5$
the influence of both diagonals should be taken into account, considering the possible buckling of the brace in compression;
3. Slender diagonals $\bar{\lambda} > 1.5$
the influence of the diagonal in compression can be neglected; the CBF-X system can be designed by considering only active the tensile brace.

Given the complex nature of the behaviour of CBF-X structures, the results presented, which are based on simplified assumptions, are just a first attempt for identifying the main physical aspects. They must be considered as the prelude to future developments, aiming at achieving a better knowledge on the global performances of X-bracing systems against earthquake. As a first important result, the parametric analysis has shown that the current codes have some shortcomings and does not interpret correctly the actual mechanical behaviour of CBF-X structural configurations. Therefore it is necessary to undertake a wide experimental and numerical tests campaign on single bracing members and on CBF-X systems, in order both to deepen the knowledge on their actual mechanical behaviour, and to better calibrate numerical models to be implemented in subsequent parametric analysis, also on multi-story systems, with the goal to further improve the seismic code provisions.

5 NUMERICAL STUDY ON STEEL BRACES UNDER REVERSED CYCLIC LOADS

5.1 Methodology of analysis

A focus on the single brace behaviour under cyclic loads is provided. To this aim a very refined FE numerical model has been generated by the ABAQUS software (Klarsson H. and Soresen, 2008). The model has been still calibrated upon the laboratory tests by Black et al. (1980) on three different types of struts (Table 10), so obtaining a very efficient tool for parametric analysis aimed at the achievement of a comprehensive knowledge on the cyclic behavior of braces (Faggiano et al., 2017c).

5.2 Numerical simulation of experimental tests

5.2.1 Setup and calibration of FE models

Braces are modeled through shell elements as an alternative to solid ones, because of both modeling simplicity and reduced computational time. Materials, boundary conditions and displacements histories of braces are assumed according to the experimental set up. Therefore, the calibration of the numerical model on the bases of the experimental results is made through the selection of the optimal both mesh size and initial imperfection value.

With regards to the mesh size, small elements imply more accurate results, with the counterbalance of an inevitable increase of the time analysis. A balance between the two conditions is beneficial. Therefore, the best mesh size is assumed as the value that does not cause significant changes to the analysis results. To this purpose, a sensitivity analysis is

performed. Figure 31 shows the numerical result for the strut 3, which is discretised with square elements having different side lengths (20, 30 and 60 mm). It is apparent that 20mm is a suitable fitting value. The result is analogous for struts 14 and 17.

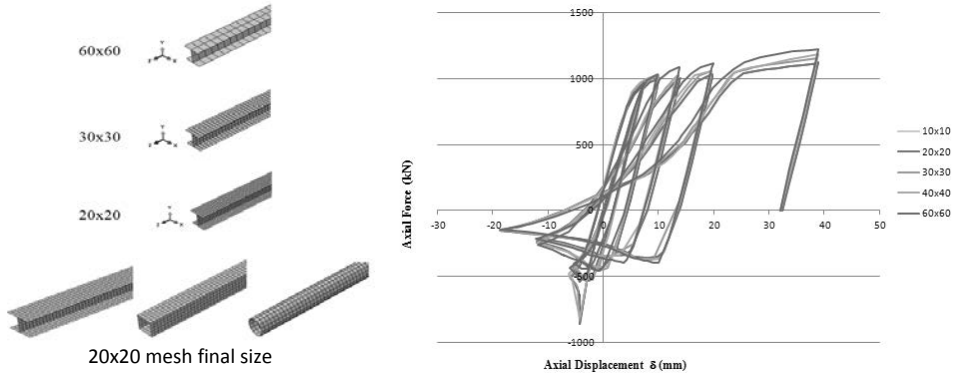


Figure 31. Mesh size calibration.

With regards to the geometrical imperfection, the initial camber (Δ_0) is referred to the initial non-straightness of the longitudinal axis of profiles. Besides, mechanical imperfections are difficult to be evaluated. Therefore, in the FE model, a value of the initial camber, which includes all types of imperfections, namely generalized imperfection, is assumed. The buckling resistance is very sensitive to the initial imperfection value, since, when the latter grows, a reduction of both tensile and compressive strengths of braces occurs.

Concerning the definition of the initial camber, Δ_0 , before performing a sensitivity analysis to assess the value that better reproduces the experimental results, some literature recommendations have been taken into account.

First, the value proposed by ECCS (1978) is considered. Based on the Ayrton-Perry's theory, the initial imperfection is formulated as it follows:

$$\Delta_0 = \frac{W}{A} \cdot \alpha \cdot \sqrt{\bar{\lambda}^2 - 0.04} \quad (13)$$

where W is the plastic section modulus in the instability plane of the profile,
 A is the cross-section area,
 $\bar{\lambda}$ is the normalised slenderness,
 α is the imperfection factor characterizing the instability curves adopted in ECCS [27].

Then, the Georgescu's formulation (1996) is taken into account:

$$\Delta_0 = \left(\frac{1}{\chi} - 1 \right) \cdot \left(1 - \frac{\chi f_y}{\sigma_E} \right) \cdot \frac{W}{A} \quad (14)$$

where σ_E is the Euler critical stress,
 W is the plastic section modulus in the instability plane of the profile,
 A is the cross-section area,
 χ is the reduction factor for instability according to Eurocode 3 (EN 1993:1-1).

Finally, Eurocode 3 provides the imperfection values in terms of Δ_0/L ratio, where L is the brace length. These values are listed in Table 12.

Table 12. Initial Imperfections Δ_0/L according to EN 1993: 1-1.

Buckling curve	Δ_0/L	
	Elastic analysis	Plastic analysis
a_0	1/350	1/300
a	1/300	1/250
b	1/250	1/200
c	1/200	1/150
d	1/150	1/100

In addition to the provisions of literature and standard references, a buckling analysis is carried out with the purpose to take the first global instability mode as initial shape of the imperfect brace. In this case, also according to the real evidence, an initial imperfection equal to $L/1000$ is applied. Therefore, for the sake of example, the sensitivity analysis, considering all the above imperfections, is performed on the strut 3. Figure 5 shows the results, evidencing that the best imperfection is represented by the value of $L/1000$ (3mm). Such imperfection is then assigned to a deformed out-of-plane configuration of the brace deriving from the buckling analysis. The same imperfection value is used also for the other examined braces.

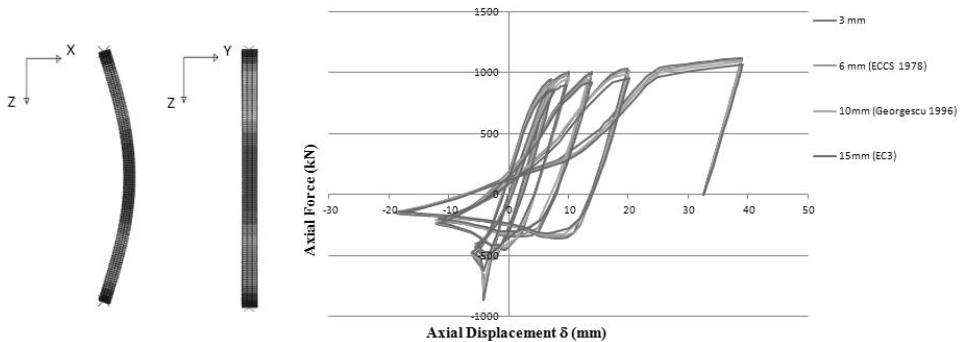


Figure 32. Sensitivity analysis for assessing the best initial camber for strut 3.

5.2.2 Results of numerical simulation

The three analyzed specimens have the same boundary conditions and slenderness ratio, but different cross-sectional shapes. Figure 33 shows the lateral displacement of specimens at the end of each cycle. Displacements are represented by a colors range from blue (zero displacement) to red (maximum displacement). Figure 34 shows the results of the quasi-static numerical analysis on the struts 3, 14 and 17, respectively, and the comparison with the experimental ones, in terms of axial force N versus axial displacement δ . In Figures 35, 36, 37 the areas of each single cycle, it representing the energy dissipated in every cycle, obtained through experimental tests and numerical analyses, are compared for struts 3, 14 and 17.

It is evident that the experimental-numerical comparison in terms of both force-displacement curves and dissipated energy is adequate. In particular, the experimental-numerical scatters in terms of dissipated energy detected for every single cycles range between -9.1% and 12.7% for strut 3, -7.6% and 12.4% for strut 14, -15.0% and 16.6%, for strut 17, whereas the numerical rate of the total energy dissipated by the brace overestimates the experimental one of only about 1%, 10%, 7% for struts 3, 14, 17 respectively.

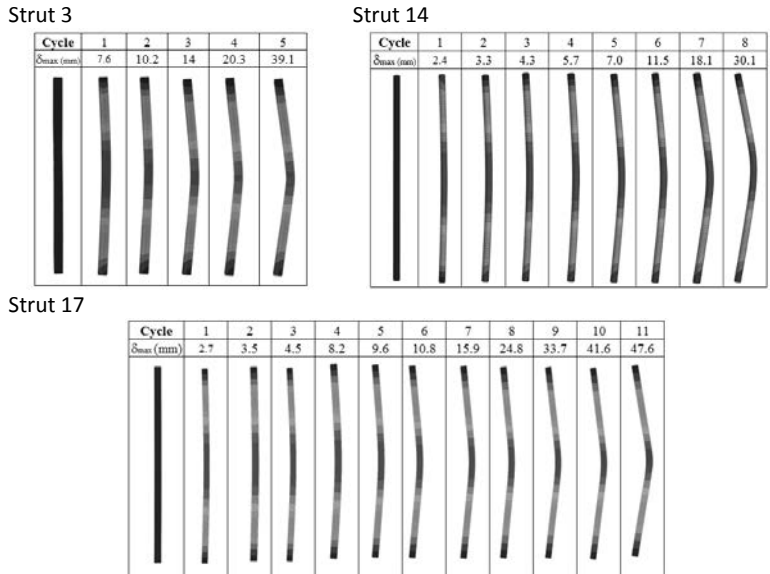


Figure 33. Deformed configuration and displacements of struts 3, 14 and 17 at the end of each cycle.

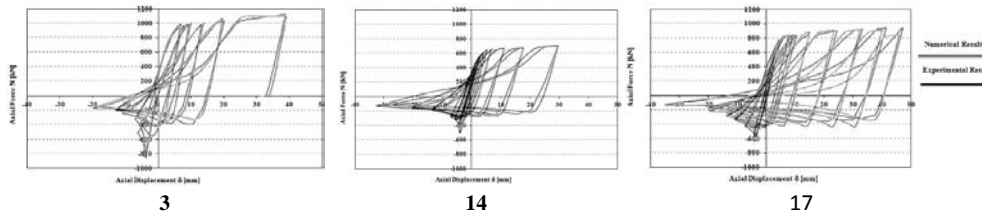


Figure 34. Numerical versus experimental results for strut 3, 14, 17.

For the sake of comparison and, therefore, for evaluating the best performance of study steel members in the plastic field, it is possible to introduce an energy efficiency factor ρ_E , that is the ratio between the dissipated energy and the elastic one as follows:

$$\rho_E = \frac{Ed}{E_{el}} \tag{15}$$

In particular, the elastic energy of the steel profile is formulated as it follows:

$$E_{el} = \frac{f_y \times A \times \delta_{max}}{2} \tag{16}$$

where f_y is the yielding stress,
 A is the cross-section area,
 δ_{max} is the maximum lateral displacement.

Accordingly, for every specimen, the ρ_E factor calculated is 0.09 for the double-T strut 3, 0.11 for the pipe strut 14 and 0.20 for the square hollow strut 17.

As a consequence, from the above results it is apparent that the square hollow section offers the best behaviour in the plastic field with a value of the energy efficiency factor about two times greater than those of the other tested profiles.

Cycle	Energy [kN×mm]		
	Experimental	Numerical	Scatter (%)
1	164.07	143.30	12.7%
2	187.24	167.59	10.5%
3	239.46	261.22	-9.1%
4	369.91	380.91	-3.0%
5	836.89	856.40	-2.3%
Total	1797.57	1809.42	-0.7%

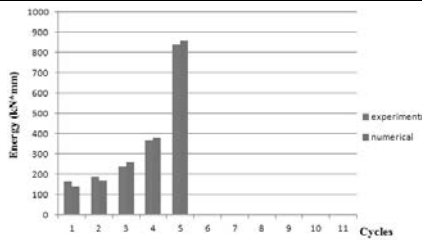


Figure 35. Numerical versus experimental results in terms of cycle areas for strut 3.

Cycle	Energy (kN×mm)		
	Experimental	Numerical	Scatter (%)
1	33.14	32.52	1.9%
2	36.28	39.05	-7.6%
3	63.03	55.64	11.7%
4	90.98	83.73	8.0%
5	139.89	122.55	12.4%
6	192.16	171.86	10.6%
7	290.54	260.35	10.4%
8	448.49	404.54	9.8%
Total	1294.51	1170.24	9.6%

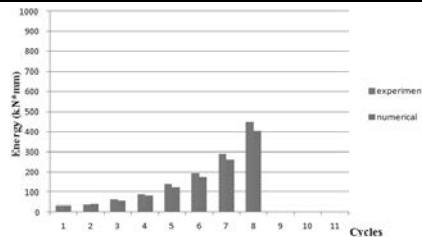


Figure 36. Numerical versus experimental results in terms of cycle areas for strut 14.

Cycle	Energy (kN×mm)		
	Experimental	Numerical	Scatter (%)
1	60.37	50.35	16.6%
2	124.89	111.98	10.3%
3	132.73	119.24	10.2%
4	236.09	262.93	-11.4%
5	267.58	278.55	-4.0%
6	282.55	306.47	-8.0%
7	414.10	401.96	3.0%
8	606.22	621.08	-2.0%
9	773.91	779.32	-0.7%
10	806.61	838.03	-4.0%
11	855.91	982.33	-15.0%
Total	4819.43	5170.93	-7.0%

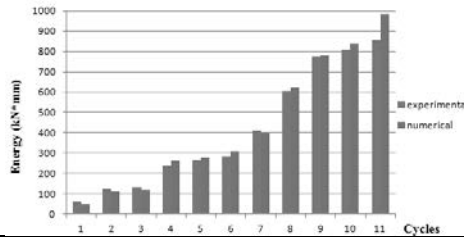


Figure 37. Numerical versus experimental results in terms of cycle areas for strut 17

5.3 Main remarks

The FE models, implemented through the software ABAQUS v. 6.13-1, is capable to simulate with satisfactory accuracy the experimental tests performed in 1980 by Black et al. on single braces loaded by axial cyclic force. Three specimens with various cross-sections, such as double-T section, circular hollow section and square hollow section, were selected.

The choice of the optimal mesh size and the initial imperfection is achieved through the calibration upon the experimental cycles. As a result, the best mesh has square 20x20mm elements, besides the best initial imperfection is equal to $L/1000$, being L the brace length. The experimental versus numerical comparison in terms of total dissipated energy provides satisfactory results, with scatters ranging between $[-10\% \div -1\%]$, confirming the reliability of the implemented FE models.

The FE models setup in the current study can be therefore effectively used to carry out a parametric analysis on different brace configurations, featuring several boundary conditions, cross-sections and slenderness ratios, aiming at simulating the behaviour under seismic actions with good approximation, as the basis for the improvement of design criteria.

6 CONCLUSIVE REMARKS AND FURTHER DEVELOPMENTS

The Italian technical code for constructions (NTC 2008), inspired by Eurocode 8, provides a number of design criteria for steel concentric bracing structures in seismic zone. Nevertheless, their application appears difficult and, sometimes, not effective in achieving the prefixed design objectives. Moreover the simplified computational models proposed by the code do

not allow to capture some key aspects of the behaviour of the investigated systems and, generally, to achieve the desired structural performance.

Based on the previous observations possible enhancements of the NTC2008-EC8 design criteria for CBF can be related on one side to the optimization of the design procedure and structural models. Hereafter a synthesis of the main aspects emerged f the study is reported.

Design procedure:

- The procedure for the application of linear dynamic analysis should be specified coherently with the model of only tensile brace active for CBF-X;
- Different simplified relationships should be defined for the preliminary determination of the fundamental period of vibration, depending on the number of floors, taking also into account the structural system type, it being differentiated in case of bracing systems and for type of bracings;
- More pertinent rules should be defined for the top storey, in terms of slenderness of braces, in order to reduce the overstrength and then the Ω factor.
- With regards to capacity design, it should be explicitly stated that the overstrength factor Ω should be in any case lower than the design behaviour factor q .
- The use of CHS profiles for braces is more advantageous as respect to HE profiles. There is a larger availability of CHS different sizes, which implies a reduced structural overstrength. Therefore the overall structural sizes more strictly correspond to the design requirements. Moreover the structural performance more approximates the design expectations. q -factors are more suitable.
- The use of HE profiles for structural members can become more convenient if a wider spectra of cross sections are produced, in order that profiles could best fit all the design requirements in terms of strength and stiffness, reducing the over strength that alters the effect of the design provisions as respect to the expectations. This could also either avoid the scatter in the geometrical variability of members composed by different parts, as it occurs for columns belonging to high rise buildings, or enhance the efficiency of the capacity design, or simplify the connection among members.
- The case of V braces is peculiar for the beam design, due to the convergence of the diagonals at the beam, and in particular the relevant design rules should be better calibrated, they being actually poorly efficient in catching the actual structural capability of the CB-V systems. The stiffness ratio KF appears to be an effective control parameter for ductile design of CBF-V.
- The brace design chart presented can be a useful tool for selecting the design criteria for CBF-X structural systems at the ultimate limit states, depending on the slenderness of braces. It should be strengthened by achieving a more comprehensive knowledge on the global performances of X-bracing systems against earthquake, through a wide experimental and numerical tests campaign on single bracing members and on CBF-X systems. To this purpose the FE model implemented through the software ABAQUS v. 6.13-1, opportunely calibrated to be capable to simulate with satisfactory accuracy the experimental tests performed in 1980 by Black et al.. on single braces loaded by axial cyclic force can be therefore effectively used to carry out a parametric analysis on different brace configurations, as the basis for the improvement of design criteria.

Structural model

The force-displacement behavioural model for bracing members in tension and compression should be improved to be comprehensive of all the significant aspects of the actual behaviour.

Behaviour factor

The ultimate conditions for defining the q factor should be identified. The design objective at the ultimate limit state should be calibrated considering that also partial collapse mechanism could correspond to suitable performances in terms of ductility and dissipation capabilities. The q factor should be attributed according to the number of stories.

It is important to note that the seismic structural performance evaluated through incremental dynamic analyses correspond to the average values of the parameters examined (according to the Technical Standard). Even though some general observations are reported, it would be relevant to correlate the seismic behavior of structures at every acceleration record considered.

More wide elaborations are required through further extensive campaign of both experimental and numerical investigations aiming at both optimizing the calculation models and providing simplification to the design methods.

7 ACKNOWLEDGEMENTS

The authors gratefully acknowledge the Department of Civil Protection for the research funding within the RELUIS-DPC 2010-2013 project. They also thank Engg. Giuseppe Marino, Luca Canicattì and Generoso Vaiano for the contribution to the development of numerical analysis carried out during their graduation theses.

8 REFERENCES

- Black, G.R., Wenger, B.A. and Popov, E.P., 1980. Inelastic Buckling of Steel Struts Under Cyclic Load Reversals, UCB/EERC-80/40, Earthquake Engineering Research Center, Berkeley, CA, USA.
- Bruneau M., Lee K. "Energy dissipation of compression members in concentrically-braced frames". *Journal of Structural Engineering*, DOI: 10.1061/(ASCE) 0733-9445(2005)/131:4 (552). 2005.
- Castaldo C., Macillo V., Formisano A., Fiorino L., Faggiano B., Mazzolani F. M., 2014. "Evaluation of the Italian seismic code for the design of concentrically V-braced steel structures". In 7th European Conference on Steel and Composite Structures (EUROSTEEL 2014), Napoli, Italia, 10-12 Settembre, Landolfo & Mazzolani (eds.), Published by ECCS European Convention for Constructional Steelwork. ISBN 978-92-9147-121-8, paper n.06-677.
- CEN, EN 1993-1: 2005. Eurocode 3: Design of steel structures Part 1-1: General rules and rules for buildings, European Committee for Standardization, EN 1993-1, Bruxelles, 2005.
- CEN, EN 1998-1: 2005. Eurocode 8: Design of structures for earthquake resistance – Part 1: General rules, seismic actions and rules for buildings, European Committee for Standardization, EN 1998-1, Bruxelles, 2005.
- CSI (2008). "Computer program SAP2000 version 14.0.0". Berkeley University, California, USA, June 2008.
- D'Aniello M., Costanzo S., Landolfo R. (2015). The influence of beam stiffness on seismic response of chevron concentric bracings. *Journal of Constructional Steel Research*. 112: 305-324. Doi: 10.1016/j.jcsr.2015.05.021.
- D'Aniello M., Portioli F., Landolfo R. (2010). "Modelling issues of steel braces under extreme cyclic actions". COST ACTION C26: Urban Habitat Constructions under Catastrophic Events - Proceedings of the Final Conference; pp. 335-341. Naples, 16-18 September 2010.
- D'Aniello M., La Manna Ambrosino G., Portoli F. and Landolfo R., (2012). "The effect of different modelling approach on seismic analysis of steel concentric braced frames", 15th World Conference on Earthquake Engineering 2012, Sociedade Portuguesa de Engenharia Sismica (SPES), 15WCEE.

- D'Aniello M., La Manna Ambrosino G., Portioli F., Landolfo R. (2013). "Modelling aspects of the seismic response of steel concentric braced frames". *Steel and Composite Structures, An International Journal*, Vol. 15, No. 5, pp 539-566.
- D'Aniello M., La Manna Ambrosino G., Portioli F., Landolfo R. (2015a). "The influence of out-of-straightness imperfection in Physical-Theory models of bracing members on seismic performance assessment of concentric braced structures". *The Structural Design of Tall and Special Buildings*, Vol. 24(3), 176-197, 2015, DOI: 10.1002/tal.1160.
- Dicleli M. and Calik E. E. (2008) "Physical Theory Hysteretic Model for Steel Braces", *Journal of Structural Engineering*, 134 (7), pp. 1215-1228.
- ECCS. "European recommendation for steel constructions". Brussels, 1978.
- Faggiano, B., Fiorino, L., Formisano, A., Macillo, V., Castaldo, C., Mazzolani, F.M., 2014 "Assessment of the design provisions for steel concentric X bracing frames with reference to Italian and European codes", *The Open Construction and Building Technology Journal* **8**, (Suppl 1: M3), 208-215, ISSN: 1874-8368.
- Faggiano B., Fiorino L., Formisano A., Castaldo C., Macillo V., Mazzolani F. M. (2015a). Appraisal of the design criteria for concentric braced steel structures according to Italian and European codes. In XXV Congresso C.T.A. Le giornate Italiane della costruzione in acciaio, 1-3 Ottobre 2015, Salerno, ISBN 9788894008944, pp.445-452.
- Faggiano B., Formisano A., Castaldo C., Fiorino L., Macillo V., Mazzolani F.M. (2015b) "Appraisal of seismic design criteria for concentric bracing steel structures according to Italian and European codes". In *Ingegneria sismica, international journal of earthquake engineering*, Patron editore, Anno XXXIII – Speciale CTA 2015 – Num. 3, pp. 42-51, ISSN: 0393-1420.
- Faggiano B., Formisano A., Castaldo C., Fiorino L., Macillo V., Mazzolani F.M.. (2015c). Non-linear seismic analysis and behaviour of CBF-V. In 8th International Conference on Behavior of Steel Structures in Seismic Areas STESSA 2015, Shanghai, China, July1-3, eds. F.M. Mazzolani, G.Q. Li, S. Chen, X. Qiang, China Architecture & Building Press, ISBN 978-7-112-18127-8, pp. 495-502.
- Faggiano B., Formisano A., Fiorino L., Castaldo C., Macillo V., Mazzolani F.M. (2017a). Assessment of the design criteria for concentric V-braced steel structures according to Italian and European codes. THE OPEN CIVIL ENGINEERING JOURNAL, ISSN: 1874-1495 — Volume 11, Betham Open, p. 464-474. DOI: 10.2174/1874149501711010464. SCOPUS eid= 2-s2.0-85027014295.
- Faggiano B., Formisano A., Castaldo C., Canicatti L., Landolfo R., Mazzolani F. M. (2017b). Seismic behaviour of steel Chevron bracing systems by non-linear dynamic analyses. In *ce/papers 1*, No. 2 & 3, pg. 3346-3355, Special Issue: Eurosteel 2017, Ernst & Sohn, a Wiley Brand, doi.org/10.1002/cepa.389.
- Faggiano B., Formisano A., Vaiano G., Landolfo R., Mazzolani F. M. (2017c). Numerical study on steel braces under reversed cyclic loads. In *ce/papers 1* (2017), No. 2 & 3, pg. 3119-3128, Special Issue: Eurosteel 2017, Ernst & Sohn, a Wiley Brand, doi.org/10.1002/cepa.364.
- Fell B.V., Kanvinde A.M., Deierlein G.G., Myers A.T. "Experimental investigation of inelastic cyclic buckling and fracture of steel braces". *Journal of Structural Engineering*, 10.1061/(ASCE)0733-9445(2009)135:1(19), 19–32, 2009.
- FEMA 356, 2000. "Prestandard and Commentary for the Seismic Rehabilitation of Buildings". American Society of Civil Engineers, Washington, DC.
- FEMA P695. "Quantification of building seismic performance factors". Rep. FEMA P695, Federal Emergency Management Agency, Washington, DC, 2009.
- Formisano, A., Faggiano, B., Landolfo, R., Mazzolani, F.M. (2006). "Ductile behavioural classes of steel members for seismic design", In: Mazzolani, F.M., Wada, A. *Behaviour of Steel Structures In Seismic Areas*, p. 225-232, London: Taylor & Francis Group/ Balkema, ISBN: 9780415408240, Yokohama, 14-17 August.
- Formisano A., Faggiano B., Marino G., Mazzolani F. M. (2015). Seismic behaviour of X bracings: analysis of models and design criteria. In 8th Intern. Conference on Behavior of Steel Structures in Seismic Areas STESSA 2015, Shanghai, China, July1-3, eds. F.M. Mazzolani, G.Q. Li, S. Chen, X. Qiang, China Architecture & Building Press, ISBN 978-7-112-18127-8, pp. 1261-1267.

- Georgescu D. (1996). "Earthquake-recent developments in theoretical and experimental results on steel structures. Seismic resistant braced frames". *Costruzioni metalliche*, 1, 39-52.
- Giugliano M. T., Longo A., Montuori R., Piluso V. (2010). "Plastic design of CB-frames with reduced section solution for bracing members". *Journal of Constructional steel research*, Vol. 66, Issue 5, pp. 611-621.
- Giugliano M. T., Longo A., Montuori R., Piluso V. (2011). "Seismic reliability of traditional and innovative concentrically braced frames". *Earthquake engineering and structural dynamics*, Vol. 40, Issue 13, pp. 1455-1474.
- Goggins J.M., Broderick B.M., Elghazouli A.Y., Lucas A.S., "Behaviour of tubular steel members under cyclic axial loading", *Journal of Constructional Steel Research*, 62, pp. 121-131, 2016
- Hines E.M., Appel M.E., Cheever P.J. "Collapse performance of low-ductility chevron braced steel frames in moderate seismic regions". *Engineering Journal*, (3), 149–180, 2009.
- Hsiao P.C., Lehman D.E., Roeder C.W. "A model to simulate special concentrically braced frames beyond fracture". *Earthquake Engineering and Structural Dynamic*, 42(2), 183–200, 2013.
- Huang Y., Mahin S. A. "Simulating the inelastic seismic behaviour of steel braced frames including the effects of low-cycle fatigue". Rep. No. PEER 2010/104, Pacific Earthquake Engineering Research Center, Univ. of California at Berkeley, CA, 2010.
- Iervolino I., Cosenza E., "Rexel: computer aided record selection for code-based seismic structural analysis". Bulletin No 8, Earthquake Engineering, Naples, 2009.
- Ikeda K., Mahin S.A. "Cyclic response of steel braces". *Journal of Structural Engineering*, 10.1061/(ASCE)0733-9445(1986)112:2(342), 342–361, 1986.
- Ikeda K., Mahin S.A., Dermizakis S.N. "Phenomenological modeling of steel braces under cyclic loading". Rep. No. UCB/EERC-84/09, Earthquake Engineering Research Center (EERC), Univ. of California, Berkeley, CA, 1984.
- Jain, A. K., Goel, S. C., Hanson, R. D. "Inelastic response of restrained steel tubes". *Journal of Structural Division*, 104 (6) , 897-910, 1978.
- Jin J., El-Tawil S. "Inelastic cyclic model for steel braces". *Journal of Engineering Mechanics*, 10.1061/(ASCE)0733-9399(2003)129:5(548), 548–557, 2003.
- Jinkoo K. e Choi H., "Response modification factors of chevron-braced frames", *Engineering Structure*, 27, pp. 285–300, 2005
- Jiun-Wei Lai and Mahin S. A., "Steel Concentrically Braced Frames using Tubular Structural Sections as Bracing Members: Design, Full-Scale Testing and Numerical Simulation", *International Journal of Steel Structures*, 14 (1), pp. 43-58, 2014
- Klarsson H., Sorensen. "ABAQUS Standard/explicit user's manual". Version 6.7, USA, 2008.
- Klarsson H., Sorensen. "ABAQUS Standard/explicit theory manual". Hibbit Klarsson and Sorensen, Version 6.7, USA, 2008.
- Krishnan S. "The modified elastofiber element for steel slender column and brace modeling". *Journal of Structural Engineering*, 10.1061/(ASCE)ST.1943-541X.0000238, 1350–1366, 2010.
- Kumar P.C. A., Dipti Ranjan Sahoo, Nitin Kumar, "Limiting values of slenderness ratio for circular braces of concentrically braced frames", *Journal of Constructional Steel Research*, 115: pp. 223-235, 2015
- Lignos D.G., Krawinkler, H. "Deterioration modeling of steel components in support of collapse prediction of steel moment frames under earthquake loading". *Journal of Structural Engineering*, 10.1061/(ASCE)ST.1943-541X.0000376, 1291–1302, 2011.
- Lignos D.G., Krawinkler, H. "Sidesway collapse of deteriorating structural systems under seismic excitations". Rep. No. TB 177, John A. Blume Earthquake Engineering Center, Stanford Univ., Stanford, CA, 2012.
- Lignos D.G., Krawinkler H. "Development and utilization of structural component databases for performance-based earthquake engineering". *Journal of Structural Engineering*, 10.1061/(ASCE)ST.1943-541X.0000646, 1382–1394, 2013.
- Longo, A., Montuori, R., Piluso, V. (2008a). "Failure mode control of X-braced frames under seismic actions", *Journal of Earthquake Engineering* 12 (5), 728-759.

- Longo, A., Montuori, R., Piluso, V., 2008b. "Plastic design of seismic resistant V-braced frames", *Journal of Earthquake Engineering* 12 (8), 1246-1266.
- Macillo V., Castaldo C., Fiorino L., Formisano A., Faggiano B., Mazzolani F. M. (2014a). Critical review of the NTC2008 design criteria for steel concentric bracing frames. In: (a cura di): D. Dubina, R. Landolfo, A. Stratan, C. Vulcu, *Application of High Strength Steel in Seismic Resistant Structures*. p. 233-242, Timisoara: Orizonturi Universitare Publishing House, ISBN: 9789736385520, Napoli, 28-29 Giugno 2013
- Macillo V., Castaldo C., Fiorino L., Formisano A., Faggiano B., Mazzolani F. M. (2014b). Evaluation of the Italian seismic code for the design of concentrically X-braced steel structures. In: (a cura di): R. Landolfo, F.M. Mazzolani, *Proceedings of Eurosteel 2014*. p. 05-693-1-05-693-6, NAPOLI: Doppia voce, ISBN: 9789291471218, Napoli, 10-12 Settembre 2014
- Marino, E. M., 2014. "A unified approach for the design of high ductility steel frames with concentric braces in the framework of Eurocode 8", *Earthquake Engineering and Structural Dynamics* 43, 97-118, DOI: 10.1002/eqe.2334, John Wiley & sons, Ltd.
- Mazzolani, F.M., Della Corte, G., 2008 "Steel structures in seismic zone – M.D. 2008" (in Italian), *Il Sole 24 Ore* (ed.).
- Mazzolani F.M., Piluso V., 1996. "Theory and Design of Seismic Resistant Steel Frames". Taylor and Francis CRC.
- Mazzolani, F., Landolfo, R., Della Corte, G., Faggiano, B., 2006 *Steel structures buildings in seismic zones* (in Italian), Pavia: Iuss Press, ISBN: 9788873580348.
- M.C. 02/02/2009, Ministerial Circular 02/02/2009 n. 617, 2009. *Instructions for application of the "New technical codes for constructions"* (in Italian).
- M.D.: (Decree of the Minister Council Presidency) 03/05/2005 n. 3431 (OPCM) (2005), Further modifications and integrations to the Decree of the Minister Council Presidency 20/03/2003 n. 3274 (in Italian)
- M. D. 14/01/2008, Ministerial Decree 14/01/2008. *New technical codes for constructions* (in Italian).
- Menegotto, M. and Pinto, P.E., 1973. "Method of analysis for cyclically loaded reinforced concrete plane frames including changes in geometry and non-elastic behavior of elements under combined normal force and bending", *Proceedings IABSE Symposium on Resistance and Ultimate Deformability of Structures Acted on by Well Defined Repeated Loads*, Lisbon, Portugal.
- Mussa Mahmoudi, Mahdi Zaree, "Evaluating response modification factors of concentrically braced steel frames", *Journal of Constructional Steel Research*, 66, pp. 1196-1204, 2010
- OPCM 3431: 2005, Decree of the Minister Council Presidency 03/05/2005 n. 3431, OPCM, 2005. *Further modifications and integrations to the Decree of the Minister Council Presidency 20/03/2003 n. 3274* (in Italian).
- Seismosoft "SeismoStruct v7.0 – A computer program for static and dynamic nonlinear analysis of framed structures", available from <http://www.seismosoft.com>, Pavia, Italy, 2014.
- Shen J., Wen R., Akbas B., Doran B., Uckan E., 2014. "Seismic demand on brace-intersected beams in two-story X-braced frames". *Engineering Structures*, vol.76, pp 295-312.
- Tang X., Goel S. C. "Brace fractures and analysis of phase I structures". *Journal of Structural Engineering*, 115(8), 1960-1976. 1989.
- Tremblay R. (2002). "Inelastic seismic response of steel bracing members", *Journal of Constructional Steel Research* 58(5-8), 665-701.
- Uang, C.M., 1991 "Establishing R (or R_w) and Cd Factors for Building Seismic Provisions". *Journal of structural Engineering*, 117, pp. 19-28.
- Wakabayashi, M., Matsui, C., Minami, K. and Mitani, I., 1970. *Inelastic Behaviour of Full Scale Steel Frames*, Kyoto University Research Information Repository, Disaster Prevention Research Institute annuals.

PROGRESSIVE COLLAPSE RISK ASSESSMENT OF SEISMIC DESIGNED STEEL MOMENT FRAMES

Massimiliano Ferraioli ^a, Alberto Mandara ^a, Angelo Lavino ^a

^a *University of Campania “Luigi Vanvitelli”, Aversa (CE), Italy,
massimiliano.ferraioli@unicampania.it, alberto.mandara@unicampania.it,
angelo.lavino@unicampania.it*

ABSTRACT

The paper deals with the progressive collapse risk assessment of seismic designed steel moment frames subject to column removal scenario. This study investigated three types of analysis methods linear static, nonlinear static and nonlinear dynamic. A design example of multi-story steel buildings is examined in the context of the European Standards and classification of steel sections. The influence of the fundamental parameters involved in progressive collapse analysis was highlighted. The effects of building properties and location of the removed column on the collapse mechanisms and catenary effects were studied. Finally, the paper investigated the dynamic increase factor to be applied in the simplified procedures to the bays that are affected by the removed column to compensate for the dynamic effects corresponding to the real load redistribution. The values obtained were finally compared with the GSA formulation based on the ductility factor.

KEYWORDS

Progressive collapse, Steel frame buildings, Dynamic increase factor.

1 INTRODUCTION

The progressive collapse design options explicitly defined in UFC (2009) are the alternate path direct design approach, the indirect design approach and the specific local resistance approach. Indirect design is used to develop resistance to progressive collapse by specifying a minimum level of strength, continuity, and ductility. The specific local resistance method requires all critical gravity load-bearing members to be designed and detailed to be resistant to an assumed abnormal loading. The suitability of the independent threat scenario of sudden column loss for robustness assessment of building structures under localized damage has made it an effective and simple structural integrity assessment in several design guidelines. The Alternate Path Method requires that the building structure has enough strength and ductility to resist the removal of a critical element, such as a column. This approach has been most widely used due to its connection to the response of a structure during an abnormal event. However, computationally expensive procedures are usually required to capture material and geometric nonlinearities that characterize the response of the system when the damage appears and the progressive collapse mechanism is developed. The benefits of the sudden column loss scenario have been implicitly recognised by recent USA design codes (UFC 2009, GSA 2003), where it has been incorporated as a scenario for progressive collapse

assessment and structural robustness design. As progressive collapse is a dynamic and nonlinear event, the applied load cases for the static procedures require the use of load increase factors or dynamic increase factors, which approximates inertial and nonlinear effects. However, for such a scenario the design codes permit the structural analysis to be performed using linear/nonlinear static or nonlinear dynamic analysis. In an attempt to capture the associated dynamic effects within a simplified design procedure based on equivalent static analysis, earlier guidance recommended the application of an amplification factor of 2 to the gravity loading. In particular, for both Linear Static and Nonlinear Static, the previous GSA Guidelines (2003) used a load multiplier of 2.0, applied directly to the progressive collapse load combination. However based on a study performed during the development of the UFC 4-023-03 (2009) modifications to the load increase factor were made for deformation-controlled actions. In fact, an amplification factor of 2 is correct only if the structural response following sudden column loss remains linear elastic, which implies a grossly conservative design. In order to deal with the effects of large deformations while retaining the simplification of equivalent static design, the use of nonlinear static analysis with amplified gravity loading is allowed. However, it has been recently established that the use of linear/nonlinear static analysis with a dynamic increase factor, can lead to a design that may be either too conservative or unsafe depending on the structural behaviour and configuration. On the other hand, detailed nonlinear dynamic time history analysis poses considerable computational demands and substantial care in terms of solution stability. In this context, the influence of ductility on the dynamic amplification factor, referred to in the USA codes as the dynamic increase factor (DIF) has been recognised recently. In fact, based on a study performed during the development of the UFC (2009) modifications to the dynamic increase factors for steel frames are used in GSA 2013 Guidelines, which are now a function of the allowable plastic rotation and element yield rotation. Finally, it should be observed that the Eurocodes do not include a specific separate standard for progressive collapse, but include the phenomenon in the accidental actions standards. Therein, only a generic definition of robustness is provided as “the ability of a structure to withstand events like fire, explosions, impacts or the consequence of human error, without being damaged to an extent disproportionate to the original cause.” This paper also aimed to investigate the applicability of the design procedures for progressive collapse in the context of the European Standards.

2 MODELS AND METHODS ANALYSIS

Three different analysis procedures (i.e., linear static, nonlinear static and nonlinear dynamic) are available for investigating the load redistribution behaviour of a building structure upon sudden removal of critical structural elements such as columns. The linear static analysis is the simplest option as it depend on a single factor to take into account the complicated geometric/material nonlinearity and dynamic effects. Thus, this analysis option is unable to accurately predict the actual nonlinear, dynamic structural behaviour following sudden element removal. In contrast, the nonlinear dynamic analysis is the most accurate yet the most expensive option because sophisticated finite element modelling is required to account for all possible types of nonlinearities. Moreover, computationally intensive time history calculation is needed to directly simulate the dynamic behaviour of the damaged structure. The nonlinear static analysis provides an appealing approach: although material and geometrical nonlinearities are still modelled, this option does not require the calculation of dynamic response time history. Instead, there are two ways to approximately account for the dynamic effects due to sudden column removal. One way is based on a balance between strain energy

and external work to find the controlling structural responses (Dusenberry et al. 2006, Izzuddin et al. 2008, Xu et al. 2011). The other way is to use a prescribed dynamic increase factor to amplify the gravity loads within the bays that are immediately affected by a suddenly removed element. This approach has been adopted in the current progressive collapse design guidelines (UFC 2009, GSA 2013). The value of the load increase factor depends on the structure type and the way that damage is controlled (i.e. deformation controlled or force controlled). The value of the dynamic increase factor specified in these Guidelines depends on the structure type and plastic rotation limit. Other factors, such as axial forces in beams (i.e. catenary effect) and structural configuration, which are known to have a significant effect on the nonlinear dynamic response, are not considered.

2.1 Linear static analysis

According to GSA 2013, the use of the linear static analysis is limited to structures that are: 1) 10-stories or less; 2) regular; 3) irregular but with Demand-Capacity Ratios (DCRs) less than or equal to 2.0. A structure is considered irregular if any one of the following conditions are satisfied. 1) Significant discontinuities exist in the gravity-load carrying and lateral force-resisting systems. 2) At any exterior column except at the corners, at each story in a framed structure, the ratios of bay stiffness and/or strength from one side of the column to the other are less than 50%. 3) For all external load-bearing walls, except at the corners, and for each story in a load-bearing wall structure, the ratios of wall stiffness and/or strength from one side of an intersecting wall to the other are less than 50%. 4) The horizontal lateral-load resisting elements are not parallel to the major orthogonal axes of the lateral force-resisting system.

The Demand-Capacity Ratios (DCRs) are calculated as shown below.

- 1) A linear model of the building with the removed column is used.
- 2) A deformation-controlled load case is applied, with gravity dead and live loads increased by a load increase factor Ω_{LD} .
- 3) The resulting actions (internal forces and moments) are calculated (Q_{UDLim}).
- 4) The DCRs for the deformation controlled actions are estimated as follows:

$$DCR = \frac{Q_{UDLim}}{Q_{CE}} \quad (1)$$

where Q_{CE} is the expected strength of the component or element.

Due to the different methods by which deformation-controlled and force-controlled actions are calculated, two load cases are applied and analyzed: one for the deformation-controlled actions, and one for the force-controlled actions. A synthesis of the definition of Force-Controlled and Deformation-Controlled Actions from ASCE 41 is shown in Table 1 and Figure 1. The model is analysed with two separate load cases: 1) to calculate the deformation-controlled actions Q_{UD} and 2) to calculate the force-controlled actions Q_{UF} . To calculate the deformation-controlled actions, it is necessary to simultaneously apply the following load conditions of gravity loads: 1) Increased Gravity Loads for floor areas above removed column; 2) Gravity Loads for floor areas away from removed column. The first load condition is defined as follows (Figure 2):

$$G_{LD} = \Omega_{LD}[1.2 D + (0.5 L \text{ or } 0.2 S)] \quad (2)$$

where: G_{LD} = Increased gravity loads for deformation-controlled actions for Linear Static analysis; D = Dead load; L = Live load including live load reduction; S = Snow load; Ω_{LD} = Load increase factor for calculating deformation-controlled actions for Linear Static analysis. The second load condition is given by:

$$G = 1.2 D + (0.5 L \text{ or } 0.2 S) \quad (3)$$

Table 1. Deformation-Controlled and Force-Controlled Actions (ASCE 41-06, 2007).

Component	Deformation Controlled Action	Force Controlled Action
Moment Frames <ul style="list-style-type: none"> • Beams • Columns • Joints 	Moment (M) M, Axial Load (P)	Shear (V) P, V V
Connections	M	V

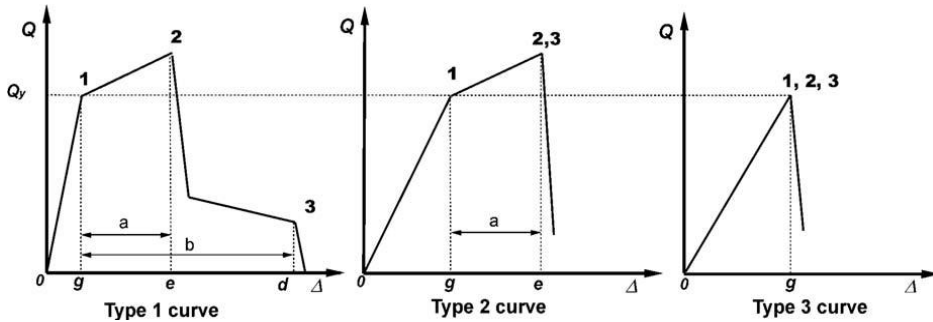


Figure 1. Definition of Force-Controlled and Deformation-Controlled Actions (ASCE 41-06, 2007).

To calculate the force-controlled actions, it is necessary to simultaneously apply the following load conditions of gravity loads: 1) Gravity Loads for Floor Areas Away From Removed Column: defined by Eq.3; 2) Increased Gravity Loads for Floor Areas Above Removed Column defined as follows:

$$G_{LF} = \Omega_{LF} [1.2 D + (0.5 L \text{ or } 0.2 S)] \quad (4)$$

where: G_{LF} = Increased gravity loads for force-controlled actions for Linear Static analysis; Ω_{LF} = Load increase factor. For deformation-controlled actions, the following check is required, both for primary and secondary members:

$$\Phi m Q_{CE} \geq Q_{UD} \quad (5)$$

where Q_{UD} = Deformation-controlled action, from Linear Static model; m = Component or element demand modifier (m -factor); Φ = Strength reduction factor from the appropriate material specific code; Q_{CE} = Expected strength of the component or element for deformation-controlled actions. For force-controlled actions in all primary and secondary components, it is necessary to check:

$$\Phi Q_{CL} \geq Q_{UF} \quad (6)$$

where Q_{UF} = Force-controlled action, from Linear Static model; Q_{CL} = Lower-bound strength of a component or element for force-controlled actions; Φ = Strength reduction factor from the appropriate material specific code. The component or element demand modifier (m -factor) in Eq.5 may be calculated using Table 5.5 from FEMA 356 (Tables 2-4). The load increase

factors to be used in Eq.2 and Eq.4 for deformation-controlled and force-controlled actions are provided in Table 5.

Table 2. Acceptance criteria for Linear Procedures from FEMA 356 (Beams).

Table 5-5 Acceptance Criteria for Linear Procedures—Structural Steel Components

Component/Action	<i>m</i> -factors for Linear Procedures ¹				
	IO	Primary		Secondary	
		LS	CP	LS	CP
Beams – flexure					
a. $\frac{b_f}{2t_f} \leq \frac{52}{\sqrt{F_{ye}}}$ and $\frac{h}{t_w} \leq \frac{418}{\sqrt{F_{ye}}}$	2	6	8	10	12
b. $\frac{b_f}{2t_f} \geq \frac{65}{\sqrt{F_{ye}}}$ or $\frac{h}{t_w} \geq \frac{640}{\sqrt{F_{ye}}}$	1.25	2	3	3	4

Table 3. Acceptance criteria for Linear Procedures from FEMA 356 (Columns).

Component/Action	<i>m</i> -factors for Linear Procedures ¹				
	IO	Primary		Secondary	
		LS	CP	LS	CP
For $0.2 < P/P_{CL} < 0.50$					
a. $\frac{b_f}{2t_f} \leq \frac{52}{\sqrt{F_{ye}}}$ and $\frac{h}{t_w} \leq \frac{260}{\sqrt{F_{ye}}}$	1.25	— ²	— ³	— ⁴	— ⁵
b. $\frac{b_f}{2t_f} \geq \frac{65}{\sqrt{F_{ye}}}$ or $\frac{h}{t_w} \geq \frac{400}{\sqrt{F_{ye}}}$	1.25	1.25	1.5	2	2

Table 4. Acceptance criteria for Linear Procedures from FEMA 356 (Connections).

Column Panel Zones – Shear	1.5	8	11	12	12
Fully Restrained Moment Connections¹⁵					
WUF ¹⁴	1.0	4.3-0.083d	3.9-0.043d	4.3-0.048d	5.5-0.064d
Bottom haunch in WUF with slab	1.6	2.7	3.4	3.8	4.7
Bottom haunch in WUF without slab	1.3	2.1	2.5	2.8	3.3
Welded cover plate in WUF ¹⁴	2.4-0.030d	4.3-0.067d	5.4-0.090d	5.4-0.090d	6.9-0.118d
Improved WUF-bolted web ¹⁴	1.4-0.008d	2.3-0.021d	3.1-0.032d	4.9-0.048d	6.2-0.065d
Improved WUF-welded web	2.0	4.2	5.3	5.3	6.7
Free flange ¹⁴	2.7-0.032d	6.3-0.098d	8.1-0.129d	8.4-0.129d	11.0-0.172d
Reduced beam section ¹⁴	2.2-0.008d	4.9-0.025d	6.2-0.032d	6.5-0.025d	8.4-0.032d
Welded flange plates					
a. Flange plate net section	1.7	3.3	4.1	5.7	7.3
b. Other limit states	force-controlled				
Welded bottom haunch	1.6	3.1	3.8	4.6	5.9
Welded top and bottom haunches	1.6	3.1	3.9	4.7	6.0
Welded cover-plated flanges	1.7	2.8	3.4	3.4	4.2

Table 5. Load Increase Factors for Linear Static Analysis (GSA 2013).

Material	Structure Type	Ω_{LD} , Deformation-controlled	Ω_{LF} , Force-controlled
Steel	Framed	0.9 m_{LIF} + 1.1	2.0
Reinforced Concrete	Framed ^A	1.2 m_{LIF} + 0.80	2.0
	Load-bearing Wall	2.0 m_{LIF}	2.0
Masonry	Load-bearing Wall	2.0 m_{LIF}	2.0
Wood	Load-bearing Wall	2.0 m_{LIF}	2.0
Cold-formed Steel	Load-bearing Wall	2.0 m_{LIF}	2.0

2.2 Nonlinear static analysis

The nonlinear static analysis have no DCR or geometric irregularity limitations on the use. To calculate the deformation-controlled and force-controlled actions, simultaneously apply the following combination of gravity loads: 1) Gravity Loads for Floor Areas Away From Removed Column: defined by Eq.3; 2) Increased Gravity Loads for Floor Areas Above Removed Column, defined as follows:

$$G_N = \Omega_N [1.2 D + (0.5 L \text{ or } 0.2 S)] \quad (7)$$

where: G_N = Increased gravity loads for force-controlled actions for nonlinear Static analysis; Ω_N = Load increase factor for calculating force-controlled actions for nonlinear static analysis. The nonlinear static dynamic increase factors (Ω_N) are provided in Table 6, where θ_{pra} is the plastic rotation angle and θ_y is the yield rotation. These parameters are given in the acceptance criteria tables from FEMA 356 (Tables 7-9). Both the modelling parameters and the acceptance criteria are defined from FEMA 356 (Figure 3).

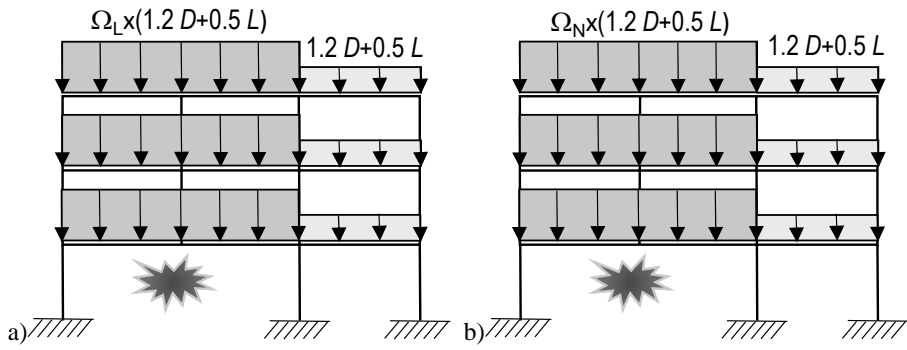


Figure 2. Gravity loads. a) Linear static analysis. b) Nonlinear static analysis.

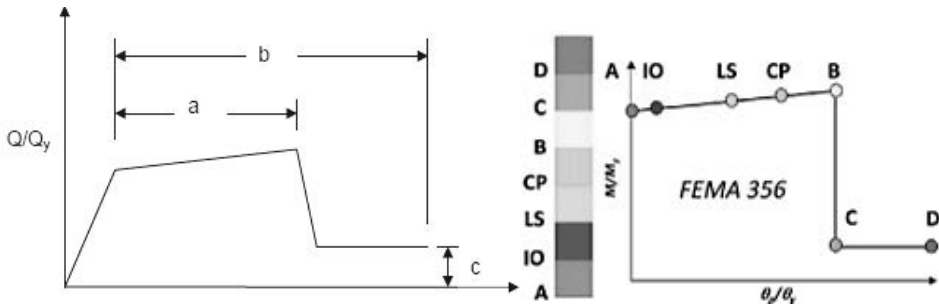


Figure 3. Modelling parameters and acceptance criteria (FEMA 356).

Table 6. Dynamic Increase Factors (Ω_N) for Nonlinear Static Analysis (GSA 2013).

Material	Structure Type	Ω_y
Steel	Framed	$1.08 + 0.76 / (\theta_{pra} / \theta_y + 0.83)$
Reinforced Concrete	Framed	$1.04 + 0.45 / (\theta_{pra} / \theta_y + 0.48)$
	Load-bearing Wall	2
Masonry	Load-bearing Wall	2
Wood	Load-bearing Wall	2
Cold-formed Steel	Load-bearing Wall	2

Table 7. Modelling parameters and acceptance criteria for Nonlinear Procedures (FEMA 356 - Columns).

Table 5-6 Modelling Parameters and Acceptance Criteria for Nonlinear Procedures—Structural Steel Components

Component/Action	Modeling Parameters			Acceptance Criteria				
	Plastic Rotation Angle, Radians		Residual Strength Ratio	Plastic Rotation Angle, Radians				
	a	b		IO	Primary		Secondary	
LS			CP		LS	CP		
Beams—flexure								
a. $\frac{b_f}{2t_f} \leq \frac{52}{\sqrt{F_{ye}}}$ and $\frac{h}{t_w} \leq \frac{418}{\sqrt{F_{ye}}}$	9 θ_y	11 θ_y	0.6	1 θ_y	6 θ_y	8 θ_y	9 θ_y	11 θ_y
b. $\frac{b_f}{2t_f} \geq \frac{65}{\sqrt{F_{ye}}}$ or $\frac{h}{t_w} \geq \frac{640}{\sqrt{F_{ye}}}$	4 θ_y	6 θ_y	0.2	0.25 θ_y	2 θ_y	3 θ_y	3 θ_y	4 θ_y
c. Other	Linear interpolation between the values on lines a and b for both flange slenderness (first term) and web slenderness (second term) shall be performed, and the lowest resulting value shall be used							
For $0.2 < P/P_{CL} < 0.50$								
a. $\frac{b_f}{2t_f} \leq \frac{52}{\sqrt{F_{ye}}}$ and $\frac{h}{t_w} \leq \frac{260}{\sqrt{F_{ye}}}$	— ³	— ⁴	0.2	0.25 θ_y	— ⁵	— ³	— ⁰	— ⁴
b. $\frac{b_f}{2t_f} \geq \frac{65}{\sqrt{F_{ye}}}$ or $\frac{h}{t_w} \geq \frac{400}{\sqrt{F_{ye}}}$	1 θ_y	1.5 θ_y	0.2	0.25 θ_y	0.5 θ_y	0.8 θ_y	1.2 θ_y	1.2 θ_y
c. Other	Linear interpolation between the values on lines a and b for both flange slenderness (first term) and web slenderness (second term) shall be performed, and the lowest resulting value shall be used							
Column Panel Zones	12 θ_y	12 θ_y	1.0	1 θ_y	8 θ_y	11 θ_y	12 θ_y	12 θ_y

Table 8. Acceptance criteria for Nonlinear Procedures (FEMA 356 - Beams).

Table 5-6 Modeling Parameters and Acceptance Criteria for Nonlinear Procedures—Structural Steel Components

Component/Action	Modeling Parameters			Acceptance Criteria				
	Plastic Rotation Angle, Radians		Residual Strength Ratio	Plastic Rotation Angle, Radians				
	a	b		Primary		Secondary		
			IO	LS	CP	LS	CP	
Beams—flexure								
a. $\frac{b_f}{2t_f} \leq \frac{52}{\sqrt{F_y E}}$ and $\frac{h}{t_w} \leq \frac{418}{\sqrt{F_y E}}$	9 θ_y	11 θ_y	0.6	1 θ_y	6 θ_y	8 θ_y	9 θ_y	11 θ_y
b. $\frac{b_f}{2t_f} \geq \frac{65}{\sqrt{F_y E}}$ or $\frac{h}{t_w} \geq \frac{640}{\sqrt{F_y E}}$	4 θ_y	6 θ_y	0.2	0.25 θ_y	2 θ_y	3 θ_y	3 θ_y	4 θ_y
c. Other	Linear interpolation between the values on lines a and b for both flange slenderness (first term) and web slenderness (second term) shall be performed, and the lowest resulting value shall be used							

Table 9. Acceptance criteria for Nonlinear Procedures (FEMA 356 - Connections).

Fully Restrained Moment Connections¹³

WUF ¹²	0.051-0.0013d	0.043-0.0008d	0.2	0.0128-0.0003d	0.0337-0.0009d	0.0284-0.0004d	0.0323-0.0005d	0.043-0.0008d
Bottom haunch in WUF with slab	0.026	0.036	0.2	0.0065	0.0172	0.0238	0.0270	0.036
Bottom haunch in WUF without slab	0.018	0.023	0.2	0.0045	0.0119	0.0152	0.0180	0.023
Welded cover plate in WUF ¹²	0.056-0.0011d	0.056-0.0011d	0.2	0.0140-0.0003d	0.0319-0.0008d	0.0426-0.0008d	0.0420-0.0008d	0.056-0.0011d
Improved WUF-bolted web ¹²	0.021-0.0003d	0.050-0.0006d	0.2	0.0053-0.0001d	0.0139-0.0002d	0.0210-0.0003d	0.0375-0.0005d	0.050-0.0008d
Improved WUF-welded web	0.041	0.054	0.2	0.0103	0.0312	0.0410	0.0410	0.054
Free flange ¹²	0.067-0.0012d	0.094-0.0016d	0.2	0.0168-0.0003d	0.0509-0.0009d	0.0670-0.0012d	0.0705-0.0012d	0.094-0.0016d
Reduced beam section ¹²	0.050-0.0003d	0.070-0.0003d	0.2	0.0125-0.0001d	0.0380-0.0002d	0.0500-0.0003d	0.0525-0.0002d	0.07-0.0003d
Welded flange plates								
a. Flange plate net section	0.03	0.06	0.2	0.0075	0.0228	0.0300	0.0450	0.06
b. Other limit states	force-controlled							
Welded bottom haunch	0.027	0.047	0.2	0.0068	0.0205	0.0270	0.0353	0.047
Welded top and bottom haunches	0.028	0.048	0.2	0.0070	0.0213	0.0280	0.0360	0.048
Welded cover-plated flanges	0.031	0.031	0.2	0.0078	0.0177	0.0236	0.0233	0.031

2.3 Nonlinear response-history analysis

There are no limitations regarding the Demand-Capacity Ratios (DCR) or geometric irregularity on the use of the nonlinear response-history analysis. Both the deformation-controlled and force-controlled actions are calculated applying the following gravity load for the entire structure (Figure 4):

$$G_{ND} = 1.2 D + (0.5 L \text{ or } 0.2 S) \quad (8)$$

where G_{ND} are the gravity loads for Nonlinear Dynamic Analysis.

The sudden removal of a column inevitably results in a dynamic transient response, with probably cyclic loading and plastic deformation demand. Although the dynamic analysis generally requires more effort to characterize the geometric and material nonlinearity, only this approach can give a complete understanding of the progressive collapse resistance. Thus, it is a more precise tool for the progressive collapse assessment of multi-storey buildings. The threat-independent approach using an 'initial conditions' methodology was applied. This involves finding the deformed shape of the undamaged structure under normal loading conditions and then applying those displacements as initial conditions for the dynamic analysis of the damaged model. The process that dynamically simulates the sudden loss of a column is based on the steps listed below.

- 1) The vertical loads are statically applied on the complete undamaged model (i.e. no removed column) under normal service loads. The end forces of the to-be-removed target column are determined (i.e. axial force N , shear force V and bending moment M).
- 2) The model with the removed column is analysed statically. The column is replaced by the corresponding reaction forces at the proper node in order to get the displacement configuration at the onset of the column removal. Practically, the dead and live loads ($DL+0.25LL$) and the calculated end forces in inverted directions (i.e. $-N$, $-V$, $-M$) are statically applied to the damaged frame (i.e. with removed column). This application takes 1s (during which loads are amplified linearly until they reach their full amounts) and then kept unchanged for 9s, so that the structure can reach a stable condition that replicates the state of the structure before the column loss. In other words, all the loads are applied to the structure in a sufficiently large time to be considered static.
- 3) The reaction forces are simultaneously and abruptly brought to zero. Practically, at 10s, once the damaged frame reaches a static equilibrium, the recorded end forces in original directions (i.e. N , V , M) are applied rapidly to the damaged frame to simulate the sudden removal of the column. The speed at which an element is removed during the dynamic analysis may have a noteworthy influence on the response of the structure. Because of this, the GSA Guidelines (2013) recommend that the column is removed over a time period not higher than 1/10 of the period associated with the structural response mode for the vertical element removal.

The nonlinear direct-integration time-history analysis including P-delta effects and large displacements is performed. The sudden removal of column origins the residual damaged structure to vibrate vertically. Its behaviour is analysed to control if enough residual capacity or alternate load paths occur to prevent the further propagation of failure.

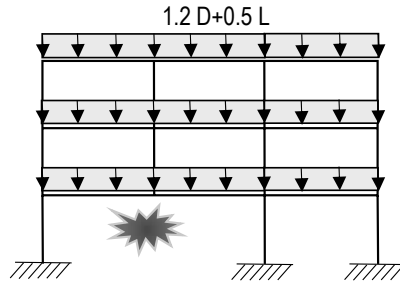


Figure 4. Imposed gravity loads for dynamic analysis.

3 EXAMPLE OF PROGRESSIVE COLLAPSE DESIGN

The design example is based on the baseline preliminary design utilized in Appendix E of UFC for a typical four-story steel frame facility located in a non-seismic region. In this paper, the design was based on the European Standards, and the European steel sections were used as structural members. Thus, the potential for progressive collapse with Alternate Path Method was carried out in the context of the European Guidelines. The structure is a four-story steel structure with perimeter moment frames. The baseline design, shown in Figures 5-7 was sized to meet the requirements of the Eurocodes 1 and 3. In addition, the lateral drift of the frame was evaluated for the performance limit under a 50-year wind. The baseline design included perimeter moment frames with moment connections at all beam elements, with the exception of those that connect to the column weak-axis.

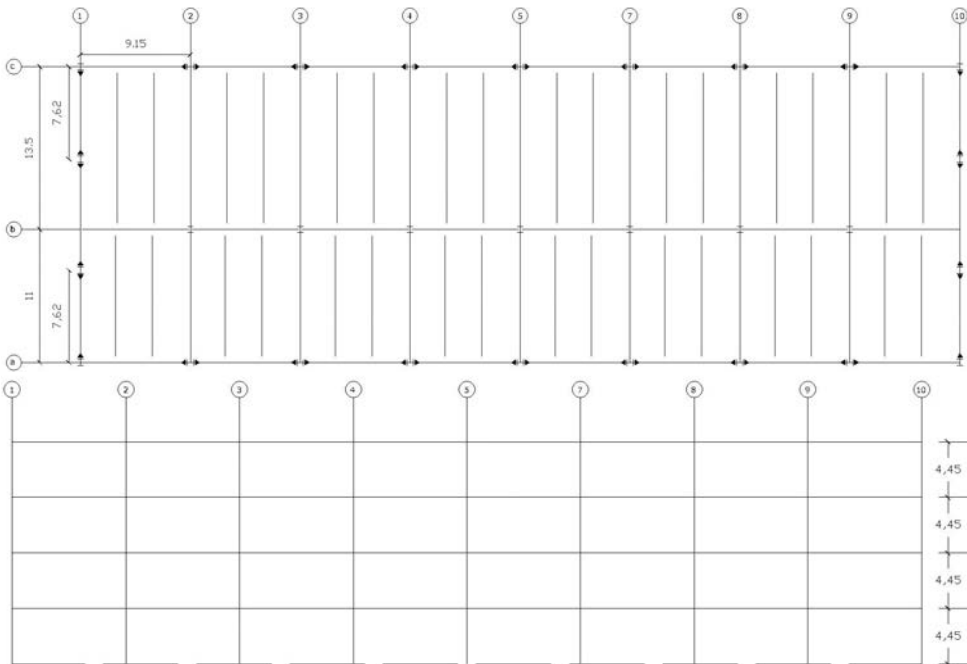


Figure 5. Plan and elevation of a typical four-story steel frame facility in a non-seismic region.

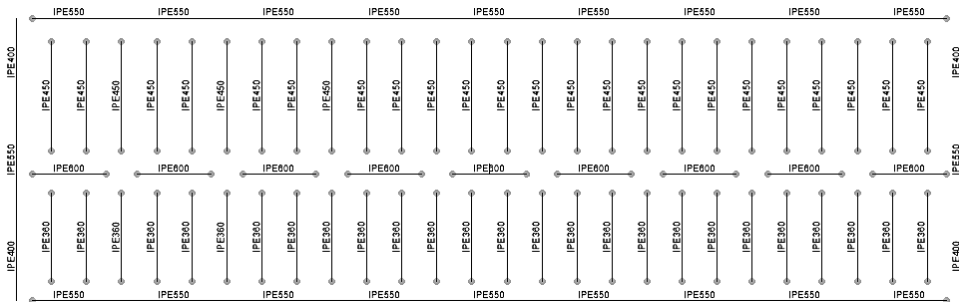


Figure 6. Floor Plan (Levels 2,3,4).

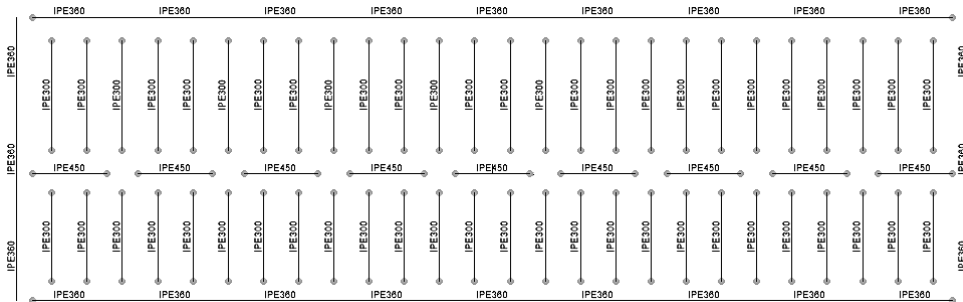


Figure 7. Roof Floor Plan.

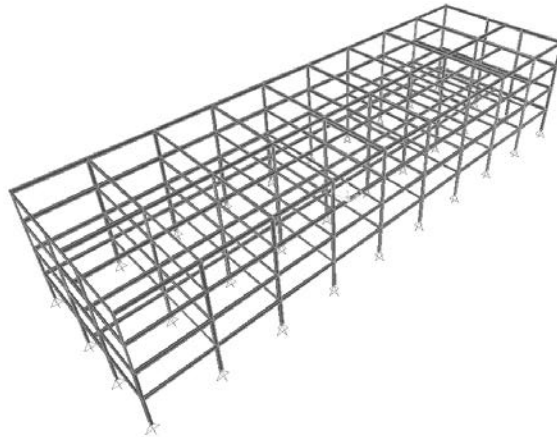


Figure 8. Three-dimensional model.

For the purposes of the Alternate Path analysis, the columns were assumed to be continuous over the height of the structure and to have a pinned connection at the foundation. The roof is bare metal deck with no concrete fill (corrugated sheet type HI-BOND, type A55/P600, total thickness of 55 mm). Floor systems are composite metal deck with a 55 mm concrete topping for a total slab thickness of 120 mm. Both the floor and roof system were modelled as rigid diaphragms and were assumed to be non-composite with the steel framing. IPE and HE profiles (according to the Eurocode rules), C20/25 concrete and high strength structural steel

EN 10025-2 S355 ($E=2.10E5$ MPa, $f_y=355$ MPa, $\nu=0.3$ and $\rho=7850$ kg) were considered in the analysis. The program code SAP2000 (2014) was used to create a three-dimensional analytical model (Figure 8). Baseline preliminary member sizes resulting from design are shown in Figure 9-11.

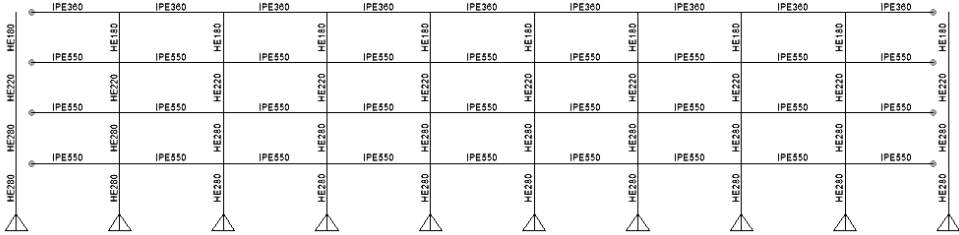


Figure 9. Original Design along Gridlines a) and c).

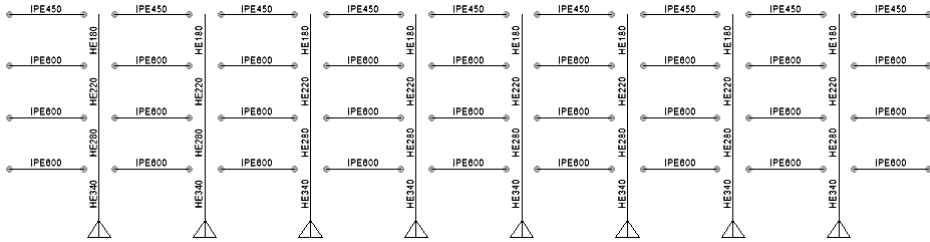


Figure 10. Original Design along Gridline b).

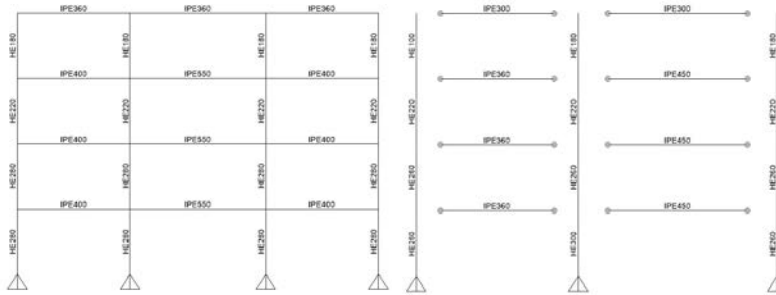


Figure 11. Original Design along Gridlines 1) and 10), and along Gridlines from 2) to 9).

3.1 Linear Static Procedure

The baseline design does not trigger the irregularity limitations as: 1) it does not have any vertical discontinuities; 2) bay stiffness/strength does not vary in either direction at corner columns; 3) all lateral-load resisting elements are parallel to the major orthogonal axes of the building. Therefore, the Linear Static Procedure can be used. Three representative column removal locations were considered in this analysis example, as shown in Figure 12: C1) Corner column condition; C2) Long side column condition. C3) Short side column condition. Prior to developing the building model, elements need to be classified as either primary or secondary. Primary elements and their rotational stiffness/resistance were explicitly included in the model. The stiffness and resistance of those elements classified as secondary were not. For the purposes of this example, only the perimeter moment frames were classified as

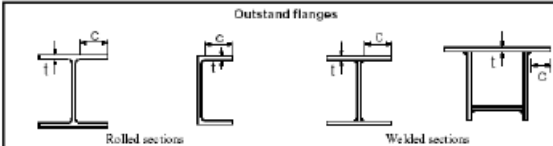
primary. All gravity framing is classified as secondary. While beams at column gridlines are included in the model to distribute gravity loads to columns, their contribution to the stiffness and resistance of the structure is neglected and their end connections are modelled as pin-pin. The classification of structural steel sections was based on the contemporary definition of the membership class of web and flange (Table 10). In order to develop the appropriate load combinations and acceptance criteria for the analysis all elements need to be classified as either deformation or force-controlled. Classification of deformation and force-controlled actions was based on GSA 2013 and guidance provided in ASCE 41. A summary of the classification of deformation and force-controlled actions for each element is provided in Table 1. Evaluation of whether columns are deformation or force controlled is a function of the axial load under the column removal scenario. Thus, a check is required after completing the analysis. The bending moments for the different column removal scenarios are plotted in Figures 13-15. Each component within the structure is assigned an *m*-factor, or demand modifier. The demand-modifier can be considered as the allowable Demand-Capacity-Ratio and is evaluated as the force or deformation-controlled action divided by the design strength.

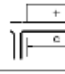


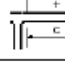
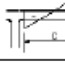
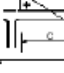
Table 10. Cross section classification (Table 5.2 of EC3-1-1).

Internal compression parts			
Class	Part subject to bending	Part subject to compression	Part subject to bending and compression
Stress distribution in parts (compression positive)			
1	$c/t \leq 72\epsilon$	$c/t \leq 33\epsilon$	when $\alpha > 0,5$: $c/t \leq \frac{396\epsilon}{13\alpha - 1}$ when $\alpha \leq 0,5$: $c/t \leq \frac{36\epsilon}{\alpha}$
2	$c/t \leq 83\epsilon$	$c/t \leq 38\epsilon$	when $\alpha > 0,5$: $c/t \leq \frac{456\epsilon}{13\alpha - 1}$ when $\alpha \leq 0,5$: $c/t \leq \frac{41,5\epsilon}{\alpha}$
3	$c/t \leq 124\epsilon$	$c/t \leq 42\epsilon$	when $\psi > -1$: $c/t \leq \frac{42\epsilon}{0,67 + 0,33\psi}$ when $\psi \leq -1^*)$: $c/t \leq 62\epsilon(1 - \psi)\sqrt{(-\psi)}$
$\epsilon = \sqrt{235/\bar{f}_y}$	\bar{f}_y	235	275
	ϵ	1,00	0,92
			355
			420
			0,81
			0,75
			460
			0,71

*) $\psi \leq -1$ applies where either the compression stress $\sigma < f_y$ or the tensile strain $\epsilon_y > f_y/E$

Outstand flanges



Class	Part subject to compression	Part subject to bending and compression	
		Tip in compression	Tip in tension
Stress distribution in parts (compression positive)			
1	$c/t \leq 9\epsilon$	$c/t \leq \frac{9c}{\alpha}$	$c/t \leq \frac{9c}{\alpha\sqrt{\epsilon}}$
2	$c/t \leq 10\epsilon$	$c/t \leq \frac{10\epsilon}{\alpha}$	$c/t \leq \frac{10c}{\alpha\sqrt{\epsilon}}$
Stress distribution in parts (compression positive)			
3	$c/t \leq 14\epsilon$	$c/t \leq 21\epsilon\sqrt{k_s}$	
For k_s , see EN 1993-1-5			
$\epsilon = \sqrt{235/f_y}$	f_y	235	275
	s	1,00	0,92
			355
			420
			460
			0,75
			0,71

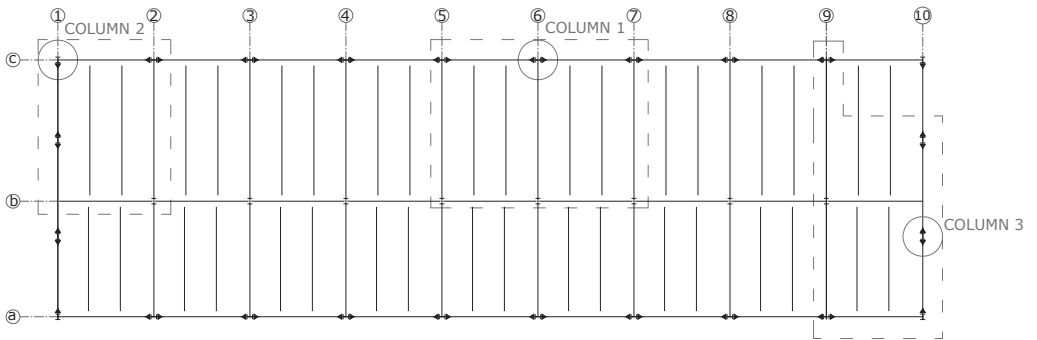


Figure 12. Column removal scenarios.

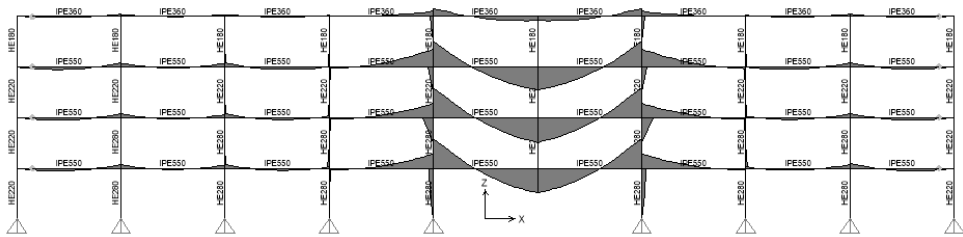


Figure 13. Column removal 1. Bending Moments. Gridline c).

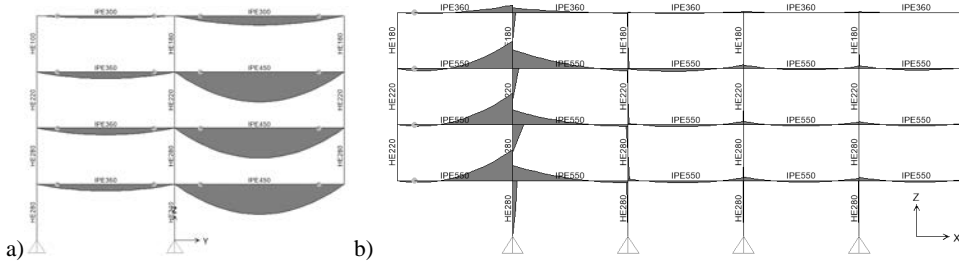


Figure 14. Bending Moments. a) Column removal 1. Gridline 6). b) Column removal 2. Gridline c).

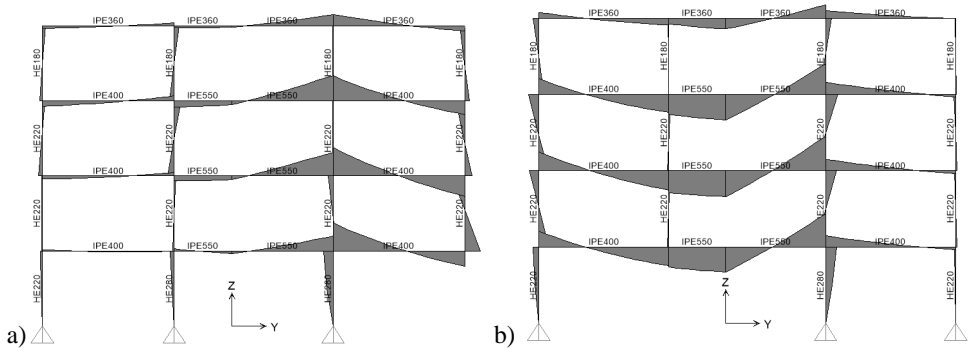


Figure 15. Bending Moments. a) Column removal 2. Gridline 1). b) Column removal 3. Gridline 10).

The governing m -factor for each component is based on the smallest of the element or its connection. The m -factors for all the baseline design beams and columns (primary components) used in this example are listed in Table 11 and Table 12. The load increase factors for this example are shown in Table 13 for each column removal. For steel frame structures, the load increase factor for forced-controlled actions is 2.0. For deformation-controlled actions, the load increase factor is a function of the smallest m -factor of any primary beam, girder or column that is directly above the removal location. After each analysis case converges, the demand-capacity-ratio (DCR) of each component is evaluated ($Q_{UD}/\Phi Q_{CE}$ or $Q_{UF}/\Phi Q_{CL}$) and compared to the defined acceptance criteria. For deformation-controlled elements, the DCR is compared to the governing m -factor for the element and its connections. For force-controlled elements, the DCR must be less than 1.0. To verify the assumption of deformation-controlled actions for columns, the deformation-controlled model is reviewed to determine the axial load ratio (P/P_{CL}) for each removal scenario. In accordance with ASCE 41-06 (2007), any column with an axial load ratio greater than or equal to 0.5 must be reclassified as force-controlled, and reevaluated under the force-controlled modelling assumptions. Analysis results for the performance of the baseline design under each column removal are shown in Figures 16 through Figure 19. Resulting DCR's of each element are shown directly below the section size. Values in red indicate that the acceptance criterion is not met for that particular section and upgrade is required. Values in blue indicate that the acceptance criterion is met by the current member size. Many elements require redesign to meet the acceptance criteria. As the members are redesigned, the m -factors must be adjusted accordingly for the redesigned members. The adjusted m -factors for the redesigned members

are shown in Table 14 and Table 15. The analysis results for the redesigned members are shown in Figures 20-21.

Table 11. Beam m -factors. Original Design. Deformation Controlled Actions of Primary Components.

Column Removal	Beam Location (Level)	Beam Size	Component m -factors	Connection m -factors
1	2, 3, 4	IPE550	8.00	2.41
	Roof	IPE360	8.00	2.65
	2, 3,4	IPE600*	8.00	2.34
	Roof	IPE450*	8.00	2.53
	2,3,4	IPE360*	8.00	2.65
	Roof	IPE300*	8.00	2.72
2	2, 3, 4	IPE550	8.00	2.41
	Roof	IPE360	8.00	2.65
	2,3,4	IPE400	8.00	2.59
	Roof	IPE360	8.00	2.65
	2, 3,4	IPE600*	8.00	2.34
	Roof	IPE450*	8.00	2.53
3	2, 3, 4	IPE550	8.00	2.41
	Roof	IPE360	8.00	2.65
	2,3,4	IPE400	8.00	2.59
	Roof	IPE360	8.00	2.65
	2, 3,4	IPE600*	8.00	2.34
	Roof	IPE450*	8.00	2.53
	2,3,4	IPE450*	8.00	2.53
	2,3,4	IPE360*	8.00	2.65
	Roof	IPE300*	8.00	2.72

* Secondary components

Table 12. Column m-factors. Original Design. Deformation Controlled Actions of Primary Components.

Column Removal	Column Location (Level)	Column Size	P / P_{CL}	Governing m -factors
1	1-2	HE 280	>0.5	Force-Controlled
	2-3	HE 280	>0.5	Force-Controlled
	3-4	HE 220	>0.5	Force-Controlled
	4- Roof	HE 180	>0.5	Force-Controlled
	1-2	HE 340	>0.5	Force-Controlled
	2-3	HE 280	>0.5	Force-Controlled
	3-4	HE 220	>0.5	Force-Controlled
	4- Roof	HE 180	0.33	5.4
2	1-2	HE 280	>0.5	Force-Controlled
	2-3	HE 280	>0.5	Force-Controlled
	3-4	HE 220	>0.5	Force-Controlled
	4- Roof	HE 180	>0.5	Force-Controlled
	1-2	HE 280	>0.5	Force-Controlled
	2-3	HE 280	>0.5	Force-Controlled
	3-4	HE 220	>0.5	Force-Controlled
	4- Roof	HE 180	0.46	2.8
	1-2	HE 340	>0.5	Force-Controlled
	2-3	HE 280	>0.5	Force-Controlled
	3-4	HE 220	>0.5	Force-Controlled
	4- Roof	HE 180	0.36	4.8
3	1-2	HE 280	>0.5	Force-Controlled
	2-3	HE 280	>0.5	Force-Controlled
	3-4	HE 220	>0.5	Force-Controlled
	4- Roof	HE 180	>0.5	Force-Controlled
	1-2	HE 280	>0.5	Force-Controlled
	2-3	HE 280	>0.5	Force-Controlled
	3-4	HE 220	>0.5	Force-Controlled
	4- Roof	HE 180	>0.5	Force-Controlled
	1-2	HE 340	>0.5	Force-Controlled
	2-3	HE 280	>0.5	Force-Controlled
	3-4	HE 220	>0.5	Force-Controlled
	4- Roof	HE 180	>0.5	Force-Controlled
	1-2	HE 280	>0.5	Force-Controlled
	2-3	HE 280	>0.5	Force-Controlled
	3-4	HE 220	>0.5	Force-Controlled
	4- Roof	HE 180	>0.5	Force-Controlled

Table 13. Load Increase Factors (Ω). Original Design.

Column Removal	Deformation-Controlled		Force-Controlled
	m_{LIF} (smallest m -factor)	$\Omega_{LD} = 0.9 m_{LIF} + 1.1$	Ω_{LF}
1	2.34	3.206	2
2	2.34	3.206	2
3	2.34	3.206	2

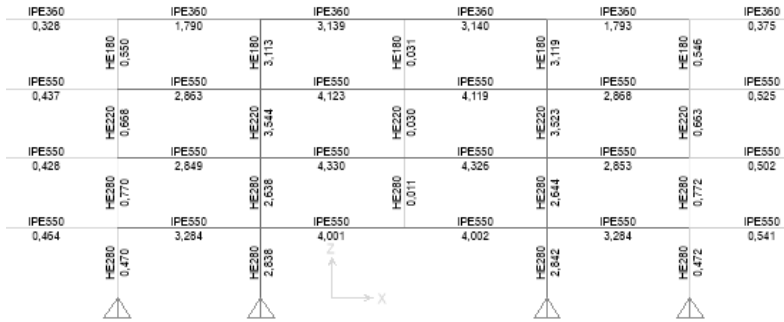


Figure 16. Column removal 1. Original Design along Gridline c) (Deformation-controlled).

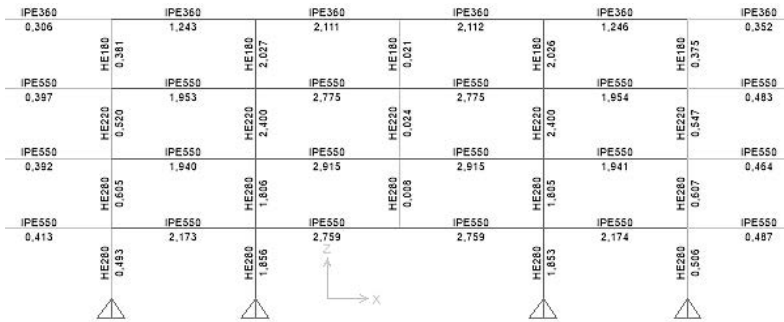


Figure 17. Column removal 1. Original Design along Gridline c) (Force-controlled).

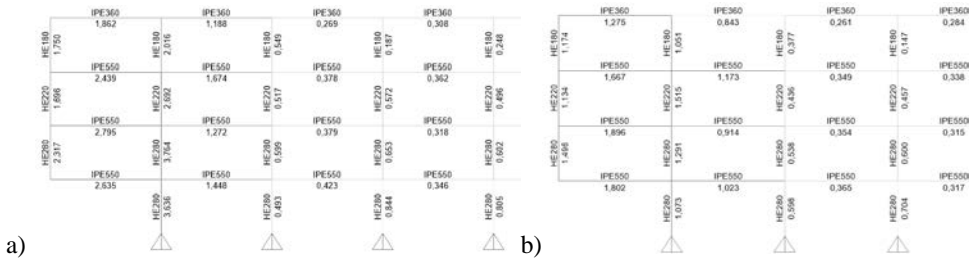


Figure 18. Column removal 2. Original Design along Gridline c).
a) Deformation-controlled- b) Force-controlled .

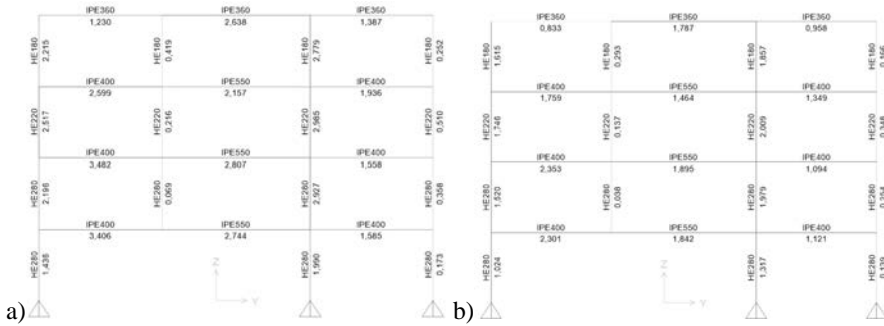


Figure 19. a) Column removal 3. Original Design along Gridline 10) (Deformation-controlled)
 b) Column removal 3. Original Design along Gridline 10) (Force-controlled).

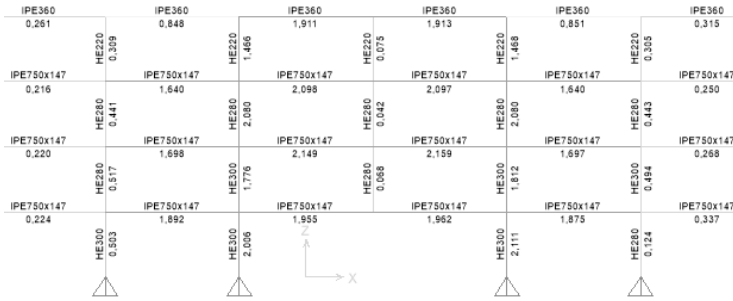


Figure 20. Column removal 1. Upgraded Design along Gridline C).

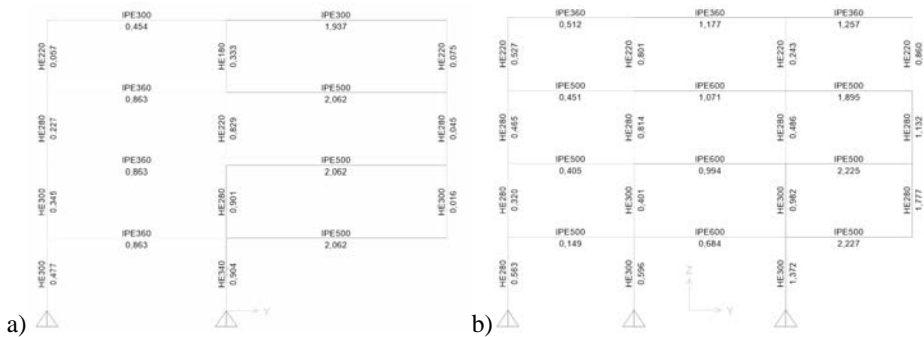
Table 14. Re-Designed Beam *m*-factors. Deformation Controlled Actions of Primary Components.

Column Removal	Beam Location (Level)	Beam Size	Component <i>m</i> -factors	Connection <i>m</i> -factors
1	2,3,4	IPE750	8.00	2.34
	Roof	IPE360	8.00	2.65
	2,3,4	IPE600*	8.00	2.34
	Roof	IPE450*	8.00	2.53
	2,3,4	IPE450*	8.00	2.53
2	Roof	IPE360*	8.00	2.65
	2,3,4	IPE300*	8.00	2.72
	Roof	IPE750	8.00	2.34
	2,3,4	IPE360	8.00	2.65
	Roof	IPE500	8.00	2.44
3	2,3,4	IPE360	8.00	2.65
	Roof	IPE600*	8.00	2.34
	2,3,4	IPE450*	8.00	2.53
	Roof	IPE600	8.00	2.34
	2,3,4	IPE360	8.00	2.65
	Roof	IPE500	8.00	2.44
	2,3,4	IPE300	8.00	2.72
	Roof	IPE600*	8.00	2.34
	2,3,4	IPE450*	8.00	2.53
	2,3,4	IPE450*	8.00	2.53
	Roof	IPE360*	8.00	2.65

* Secondary components

Table 15. Re-Designed Column m -factors. Deformation Controlled Actions of Primary Components.

Column Removal	Column Location (Level)	Column Size	P / P_{CL}	Governing m -factors
1	1-2	HE 300	2.05	Force-Controlled
	2-3	HE 300	2.16	Force-Controlled
	3-4	HE 280	2.31	Force-Controlled
	4- Roof	HE 220	1.41	Force-Controlled
	1-2	HE 340	0.90	Force-Controlled
	2-3	HE 280	0.90	Force-Controlled
	3-4	HE 220	0.80	Force-Controlled
	4- Roof	HE 180	0.33	5.4
2	1-2	HE 300	1.37	Force-Controlled
	2-3	HE 300	1.43	Force-Controlled
	3-4	HE 280	1.46	Force-Controlled
	4- Roof	HE 220	0.97	Force-Controlled
	1-2	HE 300	1.37	Force-Controlled
	2-3	HE 300	0.98	Force-Controlled
	3-4	HE 280	0.51	Force-Controlled
	4- Roof	HE 220	0.24	7.2
	1-2	-	>0.5	Force-Controlled
	2-3	HE 280	1.77	Force-Controlled
	3-4	HE 280	1.13	Force-Controlled
	4- Roof	HE 220	0.86	Force-Controlled
	1-2	HE 300	1.32	Force-Controlled
	2-3	HE 300	2.05	Force-Controlled
	3-4	HE 280	2.09	Force-Controlled
	4- Roof	HE 220	1.87	Force-Controlled
3	1-2	HE 280	1.60	Force-Controlled
	2-3	HE 280	2.03	Force-Controlled
	3-4	HE 280	1.79	Force-Controlled
	4- Roof	HE 220	1.37	Force-Controlled
	1-2	HE 340	0.86	Force-Controlled
	2-3	HE 280	0.9	Force-Controlled
	3-4	HE 220	0.83	Force-Controlled
	4- Roof	HE 180	0.51	Force-Controlled
	1-2	HE 300	-	Force-Controlled
	2-3	HE 300	0.32	5.8
	3-4	HE 280	0.11	9.8
	4- Roof	HE 220	0.61	Force-Controlled



**Figure 21. a) Column removal 1. Upgraded Design along Gridline 6.
b) Column removal 2. Upgraded Design along Gridline 1.**

3.2 Nonlinear Static Procedure

This analysis has no DCR or geometric irregularity limitations on the use. The plastic hinge rotation (θ_{pra}), yield rotation (θ_y) and factor of ductility supply for beams and connections are plotted in Tables 16-18. The minimum factor of ductility is 1.32, and the corresponding load increase factor is $\Omega_N=1.43$. The structural model incorporates material and geometric nonlinearities. Both P-delta and large displacements were considered in the analysis. The small displacement analysis was often used in literature for simplification purposes. However, it may be questionable whether neglecting catenary effects is undoubtedly conservative. Certainly, the tensile loads transmitted to the beam-column connections and to the rest of the structure would not be detected by a small displacement analysis. This is the reason because large displacements were considered in the analysis. Theoretically, concentrated plastic hinges can occur anywhere along the beam. However, the hinges were allowed to occur at the ends of each member. This simplifies the model by placing flexural plastic hinges in the most probable locations. The plastic hinges were represented by nonlinear moment-curvature and P-M interaction relationships for beams and beam-columns. The parameters of the plastic hinges were defined based on FEMA-356 (Chapter 5). The sudden strength degradation was neglected since the acceptable plastic rotation angle of the steel members, as defined in FEMA-356 (2000), is always within the first post-yield linear branch of the moment-rotation curve (preceding the strength degradation). The nonlinear buckling response was evaluated using the nonlinear static analysis. This procedure takes an iterative approach while implementing P-Delta and large-displacement effects. The total load was applied incrementally. Stiffness was evaluated at each increment. Between each displacement step, stiffness may change due to P-Delta effect, Large-Displacement effect and nonlinear material behaviour. The P-Delta effect was integrated along the length of the frame element, taking into account the deflection within the element. The transverse deflected shape was assumed to be cubic for bending. The assumed cubic shape is usually a good approximation to the true deflected shape. However, the accuracy of the results depends on the discretization of the frame objects. Thus, the structural members, both columns and beams, were subdivided into at least 20 frame elements with lengths small enough to capture the geometric nonlinearity. As this discretization is refined, the solution was expected to be accurate. The applied loading was incrementally increased until a small change in load level causes a large change in displacement. This condition indicates that the structure has become unstable. Together with this condition of instability, the structural performance from all structural components was checked at every stage of the analysis. The acceptance criteria suggested by FEMA-356 (2000) were considered in the analysis. The FEMA acceptance criteria of columns includes deformation-controlled and force-controlled actions. The controlling actions to be considered to check failure of the columns depend on the level of axial load. Columns with low axial load ($P/P_{CL} \leq 0.5$, where P_{CL} is the lower-bound axial load capacity) are classified as deformation-controlled for flexural behaviour and force controlled for compressive behaviour. The interaction between bending moment capacity and axial load capacity of the column was determined using Eq.(5-10)-(5-11) in FEMA 356. Columns under high axial load ($P/P_{CL} > 0.5$) were classified as force-controlled for both axial loads and flexure and were evaluated using Eq.(5-12) of FEMA 356. In this case, the column was assumed as failed if the P-M interaction equation exceeds unity. A comparison of plastic hinging zones under the Column Removal Scenario 1 is shown in Figure 22.

Table 16. Plastic hinge rotation (θ_{pra}), yield rotation (θ_y) and factor of ductility supply for beams.

Beam	θ_{pra}		θ_y	θ_{pra}/θ_y
	a	b	$\frac{Z F_{ye} l_b}{6 E I_b}$	
IPE 600	9 θ_y	11 θ_y	0.00970	9.0
IPE 550	9 θ_y	11 θ_y	0.01177	9.0
IPE 450	9 θ_y	11 θ_y	0.00143	9.0
IPE 400	9 θ_y	11 θ_y	0.01352	9.0
IPE 360	9 θ_y	11 θ_y	0.00333	9.0
IPE 300	9 θ_y	11 θ_y	0.00511	9.0

Table 17. Plastic hinge rotation (θ_{pra}), yield rotation (θ_y), factor of ductility. Fully restrained connections.

Beam	D [m]	θ_{pra}		θ_y	θ_{pra}/θ_y
		a [rad]	b [rad]	Beam [rad]	
		(0.021-0.0003D)	(0.05-0.0006D)	$\frac{Z F_{ye} l_b}{6 E I_b}$	a
IPE 550	0.55	0.0143	0.0365	0.0110	1.32
IPE 400	0.40	0.0161	0.0402	0.0117	1.37
IPE 360	0.36	0.0166	0.0412	0.0033	4.98

Table 18. Plastic hinge rotation, yield rotation, factor of ductility. Partially restrained connections.

Beam	d_{bg} [in]	θ_{pra}		θ_y	θ_{pra}/θ_y
		a [rad]	b [rad]	Beam [rad]	
		(0.0502-0.0015D)	(0.072-0.0022D)	$\frac{Z F_{ye} l_b}{6 E I_b}$	
IPE 600	0.60	0.01348	0.018144	0.0097	1.39
IPE 450	0.45	0.02266	0.031608	0.0014	15.84
IPE 300	0.30	0.03184	0.045072	0.0051	6.23

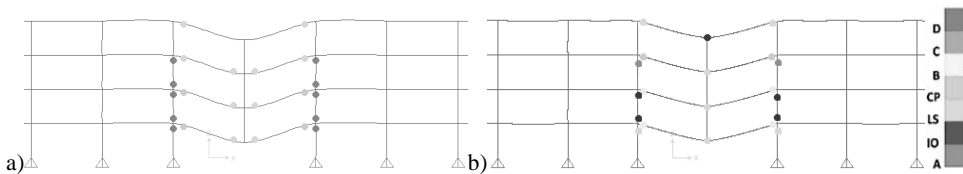


Figure 22. Plastic hinges. Column Removal 1. Gridline c).

a) Model not including large displacement effects. b) Model including large displacement effects

In the model of Figure 22a) the beams were subdivided into at least 20 frame elements to capture the geometric nonlinearity. In the model of Figure 22b) the beams were not subdivided. The pushdown curves obtained with the two models are plotted in Figure 23. In the same way, the plastic hinging zones under the Column Removal Scenario 2 and 3 are shown in Figures 24-26. The corresponding pushdown curves are plotted in Figures 27-28. The results shows that the collapse mechanism and thus, the shape of the pushdown curve are

strongly dependent on the model used. In particular, only in the model where the beams were subdivided into at least 20 frame elements, the hardening associated with the catenary stage may be developed. As shown in the pushdown figures, in many cases the collapse is reached under a load factor lower than 1. This means that some structural members should be redesigned. The re-designed members are shown in Figure 29 through Figure 31. The analysis results of re-designed frames for the model with beams subdivided into at least 20 frame elements are plotted in Figures 32-34.

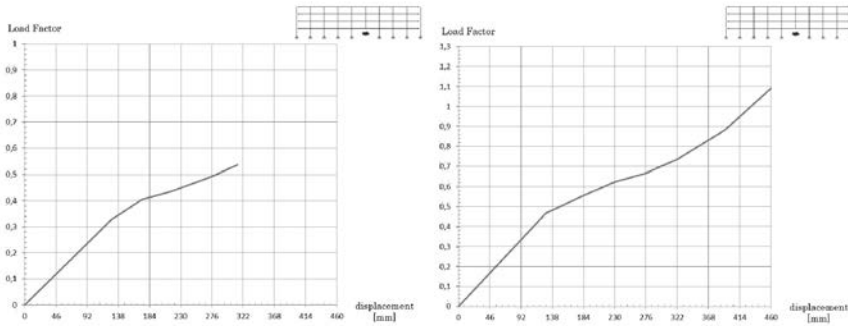


Figure 23. Pushdown curve. Column Removal 1. a) Model not including large displacement effects. b) Model including large displacement effects.

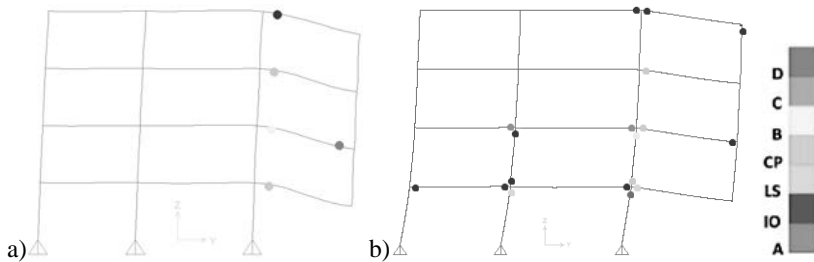


Figure 24. Plastic hinges. Column Removal 2. Gridline 1). a) Model not including large displacement effects. b) Model including large displacement effects.

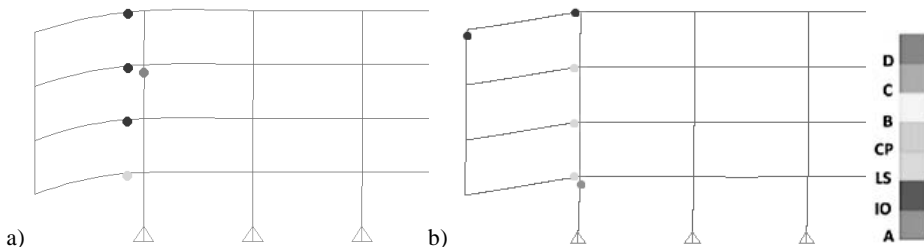


Figure 25. Plastic hinges. Column Removal 2. Gridline c). a) Model not including large displacement effects. b) Model including large displacement effects.

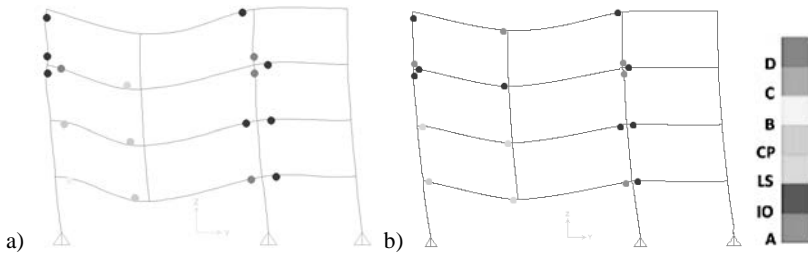


Figure 26. Plastic hinges. Column Removal 3. Gridline 10).

a) Model not including large displacement effects. b) Model including large displacement effects.

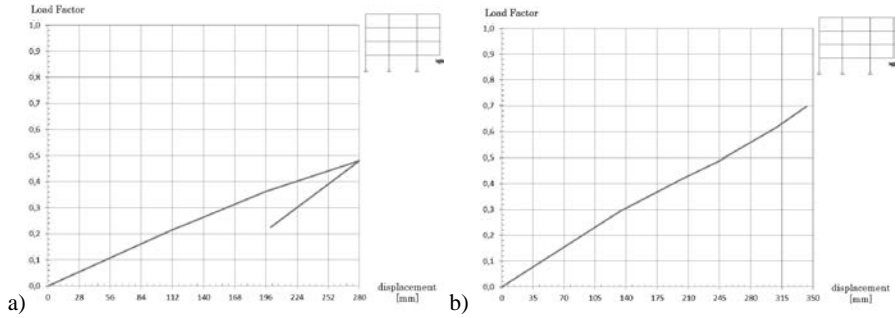


Figure 27. Pushdown curve. Column Removal 2.

a) Model not including large displacement effects. b) Model including large displacement effects.

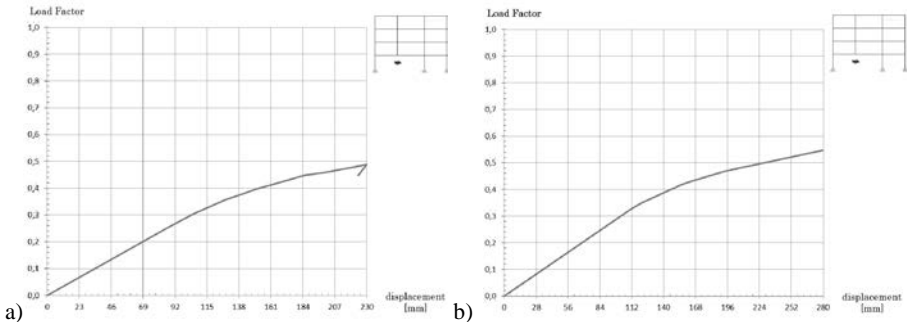


Figure 28. Pushdown curve. Column Removal 3.

a) Model including large displacement effects. b) Model including large displacement effects.

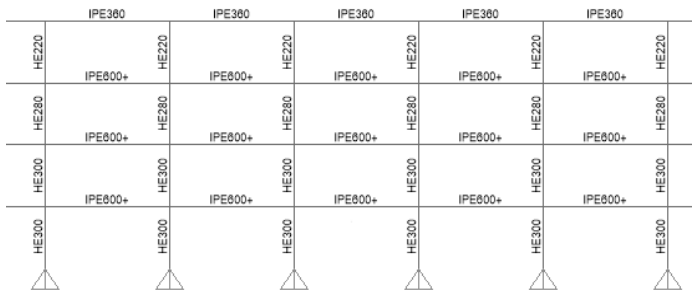


Figure 29. Upgraded Design along Gridlines a) and c).

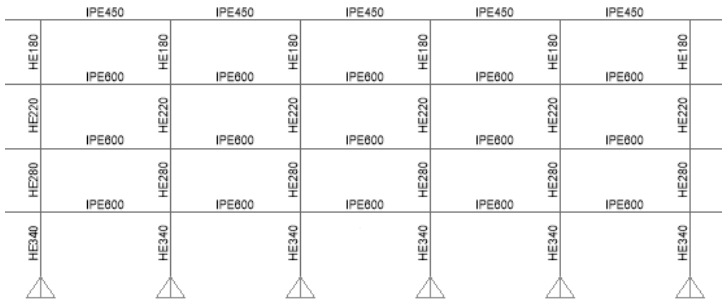


Figure 30. Upgraded Design along Gridline b).

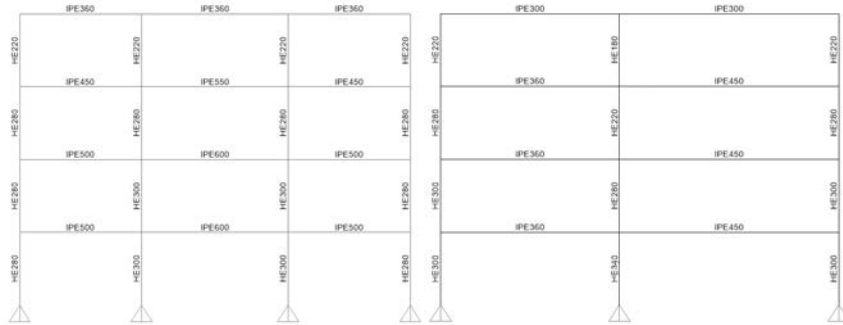


Figure 31. Upgraded Design. a) Gridlines 1) and 10); b) Gridlines 2) and 9).

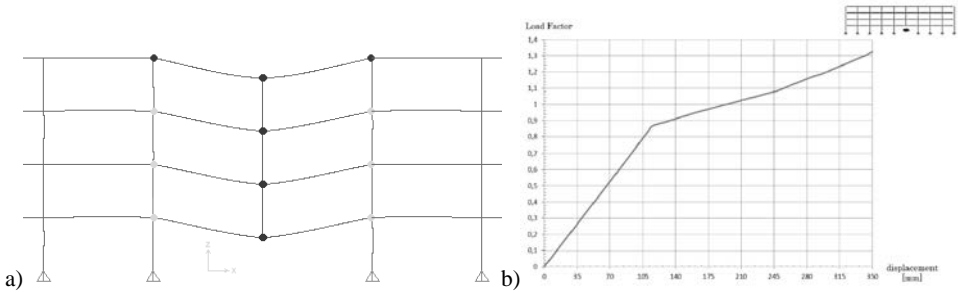


Figure 32. Re-designed structure. Column Removal 1. a) Plastic hinges. Gridline c). b) Pushdown curve.

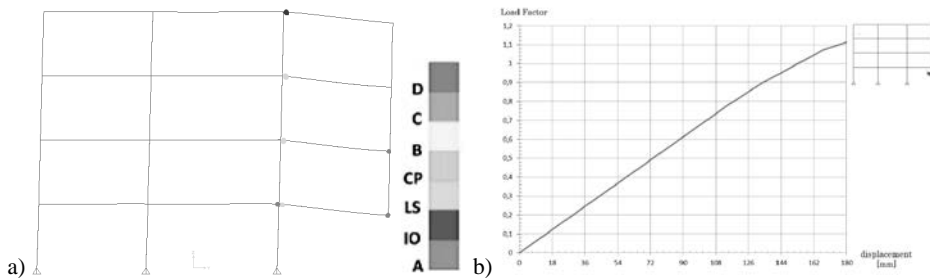


Figure 33. Re-designed structure. Column Removal 2. a) Plastic hinges. Gridline 1). b) Pushdown curve.

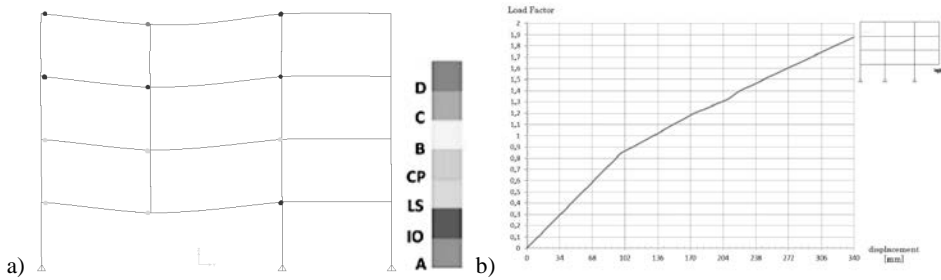


Figure 34. Re-designed structure. Column Removal 3. a) Plastic hinges. Gridline 10). b) Pushdown curve.

3.3 Nonlinear Dynamic Procedure

The process that dynamically simulates the sudden loss of a column is based on the steps listed in par.2.3. The simulations used the Rayleigh damping model that considers a mass-proportional and a stiffness-proportional damping coefficient to achieve the real critical damping ratio of 2% for both the first and second mode shapes. The sudden removal of a column causes the residual damaged structure to vibrate vertically. Its behaviour was analysed to control if enough residual capacity or alternate load paths occur to prevent the further propagation of failure. In the case study examined herein, for all the Column Removal Scenarios the gravity loads of Eq.8 lead to collapse of the structure. The plastic hinges at collapse during Nonlinear Dynamic Analysis are shown in Figures 35-36. This means that some structural members should be re-designed. The re-designed members are shown in Figure 37-38. The analysis results of re-designed frames are plotted in Figures 39-40. In Figure 41 the vertical displacement time-history at the joint where the column is removed is plotted. The starting time of the time-history plot begins at the time when the column is removed. The C3 scenario shows displacements with values lower than the other scenarios.

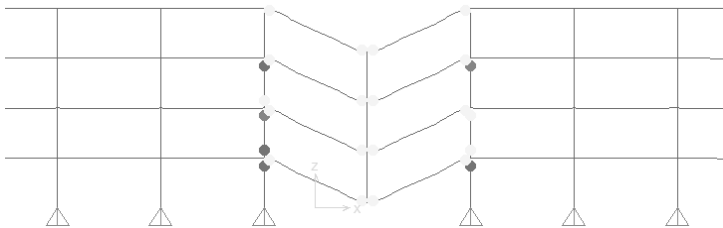


Figure 35. Plastic hinges at collapse during Nonlinear Dynamic Analysis. Column Removal 1. Gridline c).

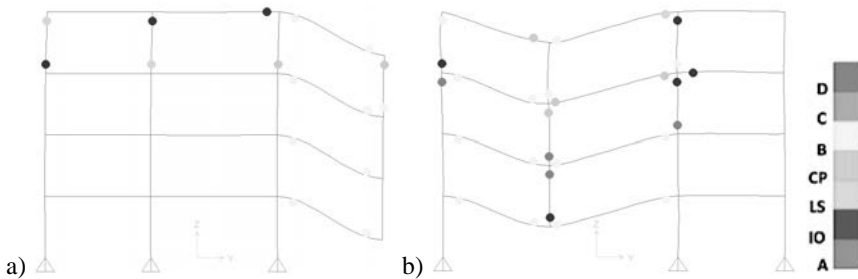


Figure 36. Plastic hinges at collapse during Nonlinear Dynamic Analysis. a) Column Removal 2 - Gridline 1). b) Column Removal 3. Gridline 10).

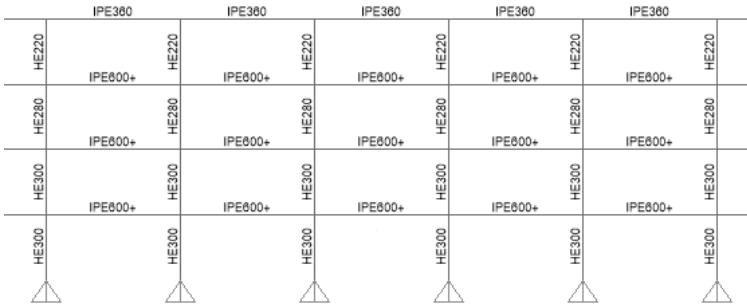


Figure 37. Upgraded Design along Gridlines a) and c).

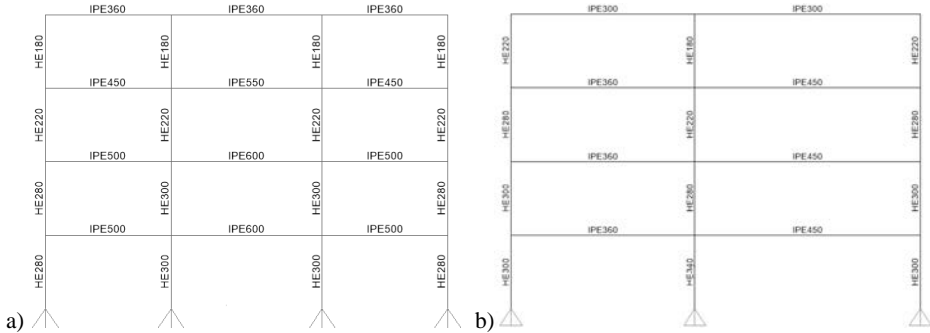


Figure 38. Upgraded Design. a) Gridlines 1) and 10). b) Gridlines 2) and 9).

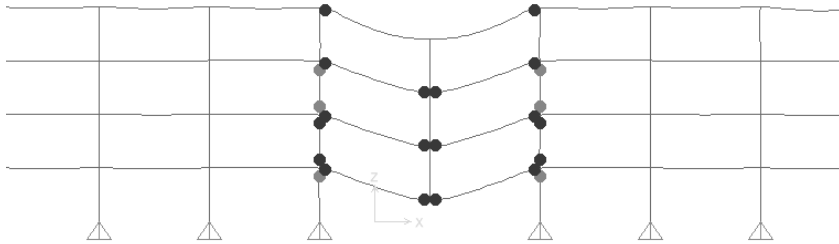


Figure 39. Re-designed structure. Plastic hinges. Column Removal 1. Gridline c).

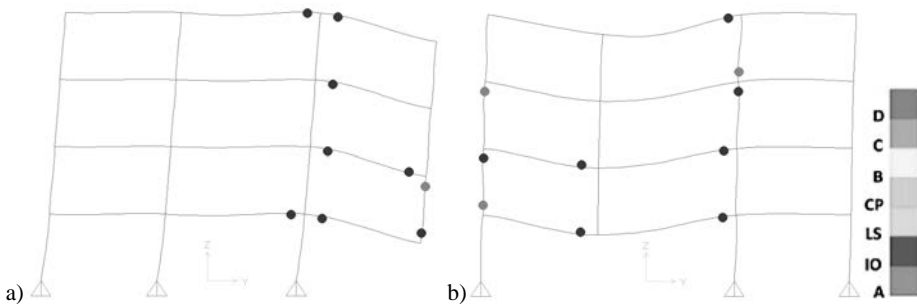


Figure 40. Re-designed structure. Plastic hinges.
a) Column Removal 2. Gridline 1). b) Column Removal 3. Gridline 10).

Tables 19-20 shows that linear and nonlinear static analyses both tend to overestimate the column size in the upper stories. The linear analysis strongly overestimates the beam size, while nonlinear static analysis tends to give the same results of nonlinear dynamic analysis.

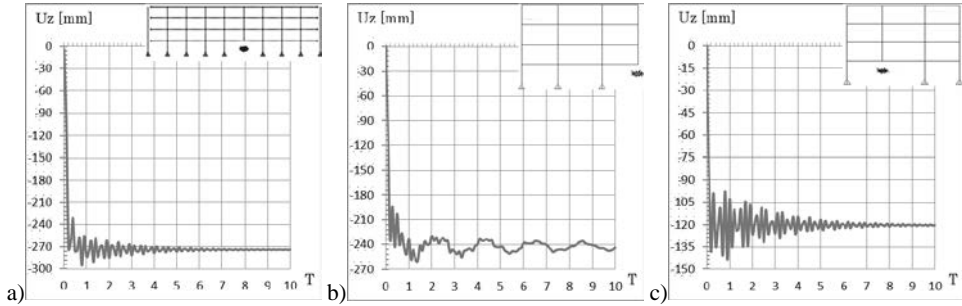


Figure 41. Re-designed structure. Displacement time-history.
 a) Column Removal 1. b) Column Removal 2. c) Column Removal 3.

Table 19. Comparison of beam size.

Position	Level	Original Beam Size	Re-Design Linear Analysis	Re-Design Nonlinear Static Analysis	Re-Design Nonlinear Dynamic Analysis
Long Side of plan	2	IPE 550	IPE 750	IPE 600+	IPE 600+
Long Side of plan	3	IPE 550	IPE 750	IPE 600+	IPE 600+
Long Side of plan	4	IPE 550	IPE 750	IPE 600+	IPE 600+
Long Side of plan	Roof	IPE 360	IPE 360	IPE 360	IPE 360
External Short Side	2	IPE 400	IPE 550	IPE 500	IPE 500
External Short Side	3	IPE 400	IPE 550	IPE 500	IPE 500
External Short Side	4	IPE 400	IPE 550	IPE 450	IPE 450
External Short Side	Roof	IPE 360	IPE 360	IPE 360	IPE 360
External Short Side	2	IPE 550	IPE 600	IPE 600	IPE 600
External Short Side	3	IPE 550	IPE 600	IPE 600	IPE 600
External Short Side	4	IPE 550	IPE 600	IPE 550	IPE 550
External Short Side	Roof	IPE 360	IPE 360	IPE 360	IPE 360

Table 20. Comparison of column size.

Position	Level	Original Column Size	Re-Design Linear Analysis	Re-Design Nonlinear Static Analysis	Re-Design Nonlinear Dynamic Analysis
Internal Long Side	1-2	HE 280	HE 300	HE 300	HE 300
Internal Long Side	2-3	HE 280	HE 300	HE 300	HE 300
Internal Long Side	3-4	HE 220	H3 280	HE 280	HE 280
Internal Long Side	4 - Roof	HE 180	HE 220	HE 220	HE 220
Internal Long Side	1-2	HE 280	HE 300	HE 300	HE 300
Internal Long Side	2-3	HE 280	HE 300	HE 300	HE 300
Internal Long Side	3-4	HE 220	HE 280	HE 280	HE 220
Internal Long Side	4 - Roof	HE 180	HE 220	HE 220	HE 180
Corner	1-2	HE 280	HE 280	HE 280	HE 280
Corner	2-3	HE 280	HE 280	HE 280	HE 280
Corner	3-4	HE 220	HE 280	HE 280	HE 220
Corner	4 - Roof	HE 180	HE 220	HE 220	HE 180

4 LOAD INCREASE FACTOR FOR NONLINEAR STATIC ANALYSIS

The formula presently adopted in both UFC 2009 and GSA 2013 is written as:

$$\text{DIF} = 1.08 + \frac{0.76}{\theta_{\text{pra}}/\theta_y + 0.83} \quad (9)$$

This formula reveals that DIF is equal to 2.0 if $\theta_{\text{pra}}/\theta_y=0$. This means that when a structure behaves in a perfectly linear elastic manner ($\theta_{\text{pra}}/\theta_y=0$) the maximum dynamic deflection is twice the static deflection (DIF=2). It can be noticed that the value of the DIF defined in both guidelines is governed only by the structure type, the classification of the structural actions and the plastic rotation limit, while other parameters playing an important role, such as structural configuration and axial forces in beams (i.e. catenary effect), are not considered. Furthermore, even though this formulation for DIF is an upgrading over the standard load factor approach in which a constant DIF is assumed, the monotonic decreasing of DIF with ductility is not generally correct and is currently under discussion. For evaluating the accuracy of the DIF formulations, six regular steel moment frames with different number of stories and bays are constructed (Figure 42): 3S3B (3-storey, 3-bay); 5S3B (5-storey, 3-bay); 7S5B (7-storey, 5-bay); 7S3B (7-storey, 3-bay); 9S3B (9-storey, 3-bay); 9S5B (9-storey, 5-bay). The frames were designed according to the Italian Code (NTC 2008). The interstorey height is 3.5m for the first floor and 3.0m for the other floors. The bay length is 5.00 m in both orthogonal directions. The steel material used for all beams and columns is S275, with a lower-bound yield and tensile strength values equal to 275 MPa and 430 MPa, respectively. The steel frames were designed for soil class A, damping ratio 5% and behaviour factor $q=6.5$. Three values of the design Peak Ground Acceleration (PGA) for Life-Safety Limit State were considered in the analysis: 1) PGA=0.15g; 2) PGA=0.25g; 3) PGA=0.35g. The comparison between the results from static and dynamic analysis was used to adjust the Dynamic Increase Factor (DIF) in order to produce static responses that can best match the peak dynamic responses. At every step of the pushdown analysis, the amount of equivalent load corresponding to each displacement level was expressed by means of the ‘‘Load Factor’’ LF that is the ratio of the vertical load to the full gravity load. This gives the load-displacement pushdown curve. In the same way, the load factor of each response-history analysis and the corresponding peak displacement response gives the load-displacement envelopes for comparison with the pushdown curve.

In Figure 43, both the pushdown curves and the IDA envelopes are plotted for a DIF varied in the range [1.0÷2.0]. Two different column-removal scenarios were considered: internal or external column removal. The hardening associated with the catenary stage is fully developed in low-rise frames. On the contrary, in the case of middle and high-rise frames the ductility limit may be very low because conditioned by the restrictive acceptance criteria for columns. Thus, the ultimate limit state may be reached when the overall capacity of the structure is still increasing, and the hardening of the catenary stage is not developed. In Figure 44-45 the DIF is plotted as a function of the deflection at the location of the removed column divided by the bay length (d/L). The DIF generating the best match of the dynamic response are compared with the values obtained from Eq.9 for the Life Safety (LS) and Collapse Prevention (CP) Limit States. In cases where the hardening of the catenary stage is not activated, a monotonic reduction of DIF with vertical deflection is observed and the GSA formulation is conservative. On the contrary, in the cases when hardening and catenary action are fully developed, the curve of DIF first decreases and then increases with the vertical deflection and the GSA formulation becomes inaccurate.

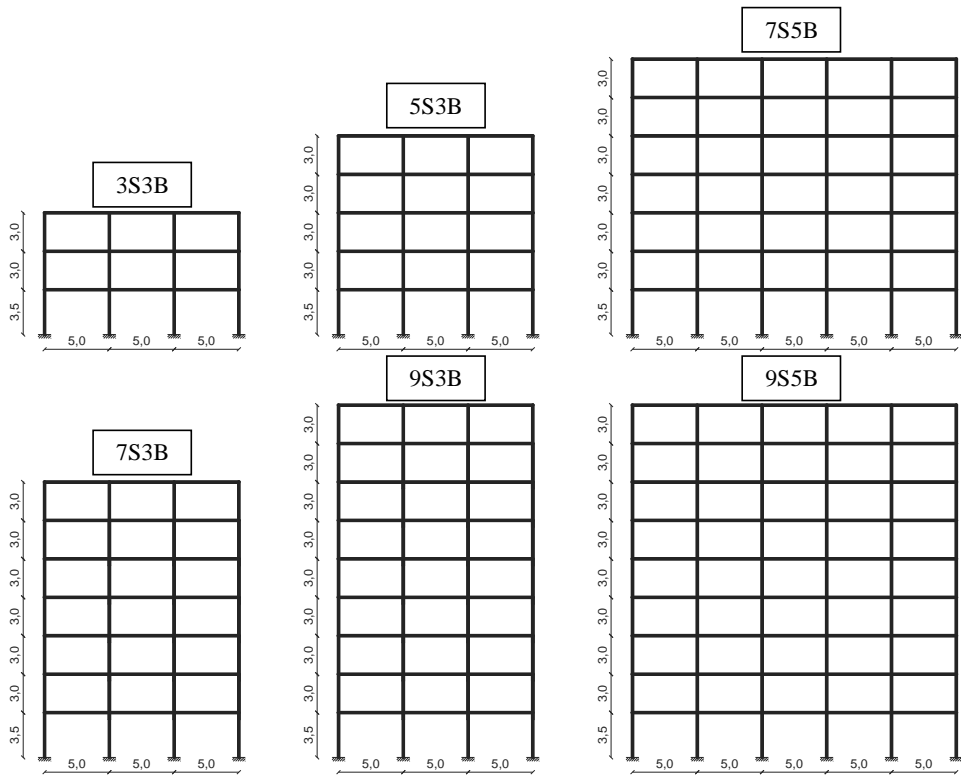


Figure 42. Steel moment resisting frames considered in the analysis.

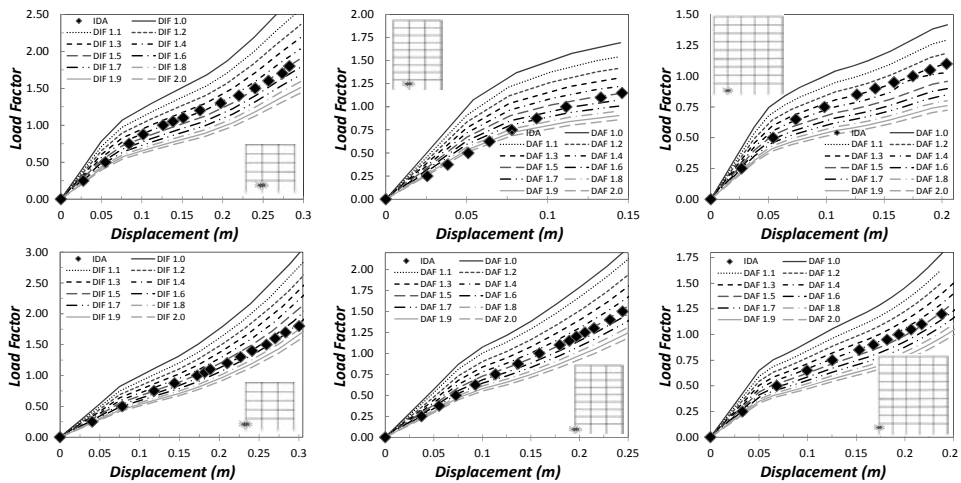


Figure 43. Pushdown curves and load-displacement envelopes from IDA (Design level: $PGA=0.25g$).

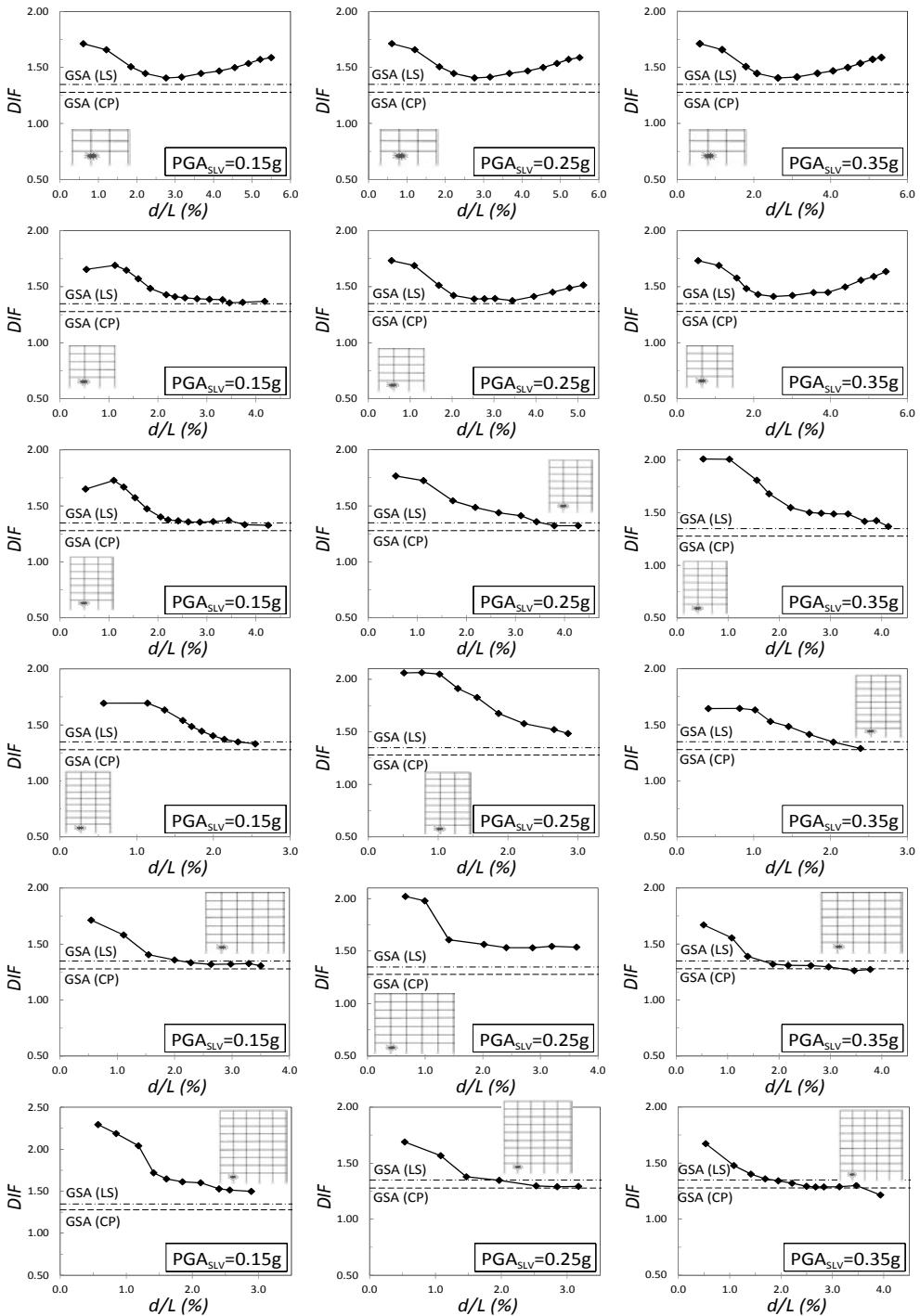


Figure 44. Variation of DIF with vertical displacement and design level (Internal column removal).

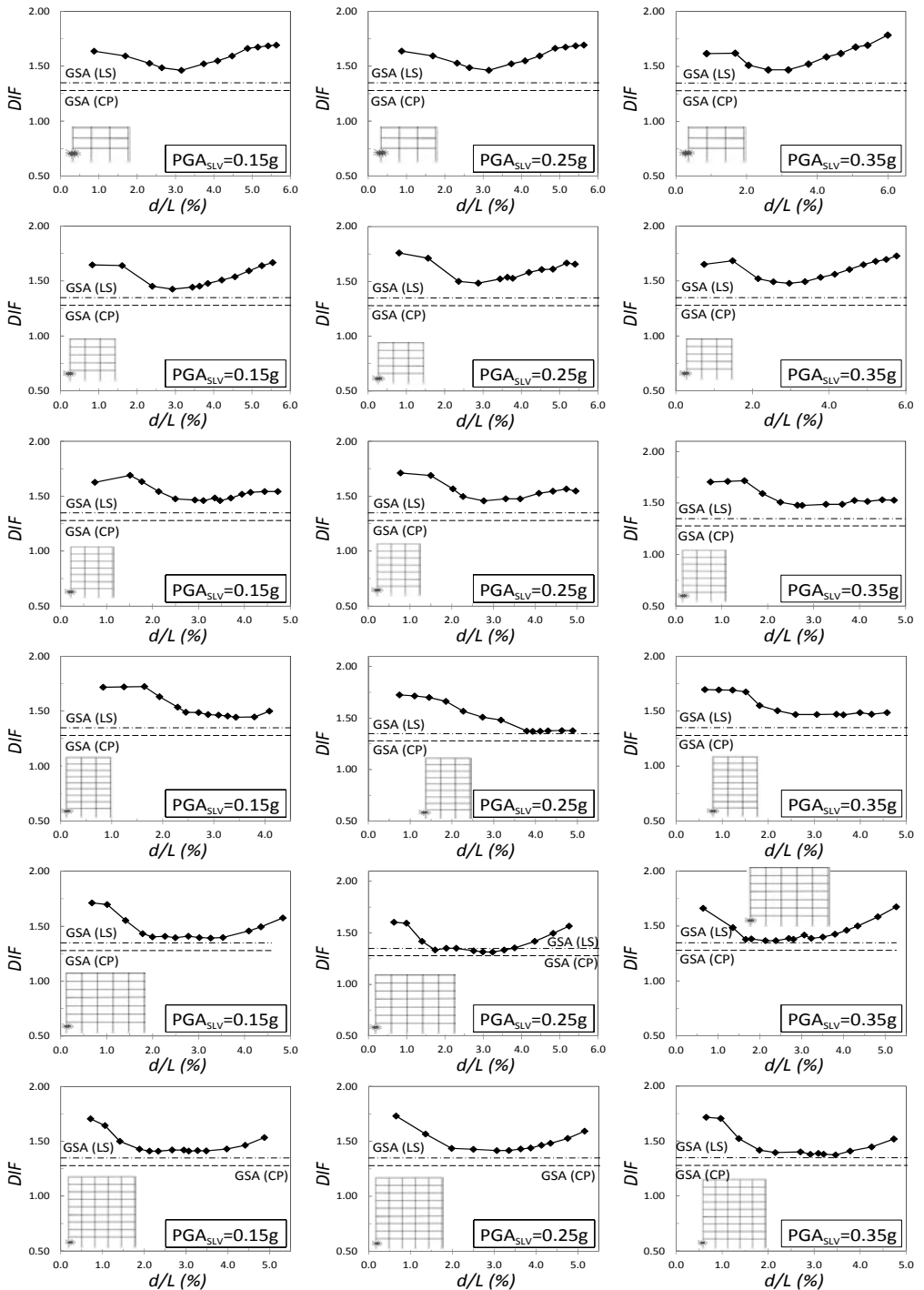


Figure 45. Variation of DIF with vertical displacement and design level (External column removal).

5 CONCLUSIONS

The paper investigated the models and methods for the assessment of the risk of progressive collapse of steel moment-resisting frame. To this aim, three types of design procedures were applied: Linear Static Procedure, Nonlinear Static Procedure and Nonlinear Dynamic Procedure. The design for progressive collapse was carried out in the context of the European Standards using the classification of European steel sections based on the contemporary definition of the membership class of web and flange. The results of the analyses were usefully employed to highlight the different aspects of the phenomenon (collapse mechanisms, large displacements and catenary effects, dynamic amplification). The conventional small displacement analysis proved to give considerably smaller load factors if compared to the large displacement analysis where the hardening behaviour of the catenary stage may be fully developed. The results obtained from Linear Static and Nonlinear Static Procedures are conservative when compared to Nonlinear Dynamic Procedure. In particular, the linear static procedure seems too conservative. In fact, the real dynamic effect of the gravity loads on the progressive collapse response may be much less than what is predicted by the linear static analysis. This results from using overconservative load increase factors to amplify the gravity loads. The amplification factor of 2.0 is correct only if the structural response following the sudden column loss remains linear elastic. Conversely, during extreme loading events such as losing a critical element, the structure usually respond in the nonlinear range. Thus, the load increase factor that permits the nonlinear static solution to approximate a nonlinear dynamic solution is usually less than 2.0. This implicates an excessively conservative estimation of progressive collapse resistance for a column-removed building. Thus, the load increase factor may decrease in the range 1.15-1.50 for the displacement corresponding to the ultimate load.

6 REFERENCES

- ASCE 41-06 (2007). "Seismic Rehabilitation of Existing Buildings", *American Society of Civil Engineers*, 1801 Alexander Bell Drive, Reston, VA 20191-4400.
- Dusenberry, D.O. and Hamburger, R.O. (2006). "Practical means for energy-based analyses of disproportionate collapse potential", *Journal of Performance of Constructed Facilities*, ASCE, 20(4), pp.336-48.
- FEMA-356 (2000). "Prestandard and Commentary for the Seismic Rehabilitation of Buildings", *American Society of Civil Engineers for the Federal Emergency Management Agency*. Washington.
- Ferraioli, M. and Avossa, A.M. (2012). "Progressive collapse of seismic resistant multistory frame buildings", *Proc. of 3rd International Symposium on Life-Cycle Civil Engineering*, IALCCE.
- Ferraioli, M., Avossa, A.M. and Mandara, A. (2014a). "Assessment of Progressive Collapse Capacity of Earthquake-Resistant Steel Moment Frames Using Pushdown Analysis", *The Open Construction and Building Technology Journal*, 8, pp.324-336.
- Ferraioli, M., Lavino, A. and Mandara, A. (2014b). "Behaviour factor of code-designed steel moment-resisting frames", *International Journal of Steel Structures*, 14(2), pp.1-12.
- Ferraioli, M., Avossa, A.M., Lavino, A. and Mandara, A. (2014c). "Accuracy of Advanced Methods for Nonlinear Static Analysis of Steel Moment-Resisting Frames", *The Open Construction and Building Technology Journal*, 8, pp.310-323.
- Ferraioli, M. (2016). "Dynamic increase factor for pushdown analysis of seismically designed steel moment-resisting frames", *International Journal of Steel Structures*, 16, Issue 3, pp. 857-875.
- Ferraioli, M., Lavino, A. and Mandara, A. (2017). "Assessment of dynamic increase factors for progressive collapse analysis of steel frames subjected to column failure", *Proc. XXVI Congresso C.T.A.*, pp. 1113-1122.

- Ferraioli, M., Lavino, A. and Mandara, A. (2015). "An adaptive capacity spectrum method for estimating seismic response of steel moment-resisting frames", *Ingegneria Sismica*, 33, pp. 47-60.
- Gerasimidis, S. and Baniotopoulos, C.C. (2011). "Steel moment frames column loss analysis: the influence of time step size", *Journal of Construction Steel Research*, Elsevier, 67, pp.557-564.
- Grierson, D. E., Xu, L., and Liu, Y. (2005). "Progressive-Failure Analysis of Buildings Subjected to Abnormal Loading", *Computer-Aided Civil and Infrastructure Engineering*, 20(3), pp.155-171.
- GSA(2003). "Progressive Collapse Analysis and Design Guidelines for New Federal Office Buildings and Major Modernization Projects", *General Services Administration*, Washington, DC, USA.
- GSA(2013). "Alternate Path Analysis and Design Guidelines for Progressive Collapse Resistance", *General Services Administration*, Washington, DC, USA.
- Italian Code - NTC08 (2008). "Norme tecniche per le costruzioni in zone sismiche", *Ministerial Decree D.M. 14.01.08, G.U. No.9 – 04.02.08* (in Italian).
- Izzuddin, B.A., Vlassis A.G, Elghazouli A.Y. and Nethercot D.A. (2008). "Progressive collapse of multi-storey buildings due to sudden column loss – Part I: Simplified assessment framework", *Engineering Structures*, 30(5), pp.1308-18.
- Izzuddin, B. A, Nethercot, D. A. (2009). "Design-Oriented Approaches for Progressive Collapse Assessment: Load-Factor vs Ductility-Centred Methods", *Proc. of Structures Congress'09*, Austin, Texas.
- Kim, T., Kim J. and Park, J. (2009a). "Investigation of progressive collapse-resisting capability of steel moment frames using push-down analysis", *Journal of Performance of Construction Facilities*, ASCE, 23(5), pp.327-335.
- Kim, J. and Kim, T. (2009b). "Assessment of progressive collapse-resisting capacity of steel moment frames", *Journal of Constructional Steel Research*, Elsevier, 65(1), pp.169-179.
- Kim, J., Park J.H. and Lee, T.H. (2011). "Sensitivity analysis of steel buildings subjected to column loss", *Engineering Structures*, Elsevier, 33, pp.421-432.
- Kwasniewski, L. (2010) "Nonlinear dynamic simulations of progressive collapse for a multistory building", *Engineering Structures*, Elsevier, 32, pp.1223-1235.
- Liu, M. (2013). "A new dynamic increase factor for nonlinear static alternate path analysis of building frames against progressive collapse", *Engineering Structures*, 48, pp.666-673.
- Málaga-Chuquitaype, C., Elghazouli, A. and Enache. R. (2016), "Contribution of secondary frames to the mitigation of collapse in steel buildings subjected to extreme loads", *Structure and Infrastructure Engineering*, 12, pp.45-60.
- Mazzolani, F.M. and Piluso, V. (1997). "Plastic design of seismic resistant steel frames", *Earthquake Engineering and Structural Dynamics*, 26(2), pp.167-191.
- McKay, A., Marchand, K. and Diaz, M. (2012) "Alternate path method in progressive collapse analysis: variation of dynamic and nonlinear load increase factors", *Practice Periodical on Structural Design and Construction*, ASCE, 17(4), pp.152-60.
- Mohamed, O. A. (2015). "Calculation of load increase factors for assessment of progressive collapse potential in framed steel structures", *Case Studies in Structural Engineering*, 3, pp.11-18.
- Ruth, P., Marchand, K.A. and Williamson, E.B. (2006). "Static equivalency in progressive collapse alternative path analysis reducing conservatism while retaining structural integrity", *Journal of Performance of Construction Facilities*, ASCE, 20(4), pp. 349-364.
- SAP2000, (2014). "Linear and nonlinear static and dynamic analysis of three-dimensional structures", *Advanced Version 17.0, Analysis Ref. Manual, Computer and Structures*, Berkeley, CA.
- Stoddart E.P., Byfield, M.P. Davison, J.B. Tyas, A. (2013). "Strain rate dependent component based connection modelling for use in non-linear dynamic progressive collapse analysis", *Engineering Structures*, 55, pp. 35-43.
- UFC (2009). "Design of Buildings to Resist Progressive Collapse, Department of Defence", *Unified Facilities Criteria*, UFC 4-023-03, Washington, DC, USA.
- Xu, G. and Ellingwood B.R. (2011). "An energy-based partial pushdown analysis procedure for assessment of disproportionate collapse potential", *Journal of Constructional Steel Research*, 67, pp.547-55.

THE GUIDELINES FOR THE DESIGN OF STEEL-CONCRETE COMPOSITE MOMENT RESISTING FRAMES IN SEISMIC AREAS

Claudio Amadio ^a, Marco Fasan ^b, Maria Rosaria Pecce ^c, Giuseppe Logorano ^d

^a *University of Trieste, Trieste, Italy, amadio@units.it*

^b *University of Trieste, Trieste, Italy, mfasan@units.it*

^c *University of Sannio, Benevento, Italy, pecce@unisannio.it*

^d *University of Sannio, Benevento, Italy, logorano@unisannio.it*

ABSTRACT

In this paper the design guidelines for steel-concrete frames are applied to various numerical examples. A multilevel building was defined and various structural solutions were developed. Firstly a plane frame was extracted from the building and designed as Moment Resisting Frame (MRF) in 3 different seismic zone characterized by various intensity of the seismic action pointing out the procedure for dimensioning the elements and the differences due to the effect of earthquake. In one case the alternative system of Concentric Braced Frame (CBF) with steel columns and composite beams was implemented detailing the beam-column joint. Finally the entire building was designed with MRFs considering 3 constructive systems: steel, RC and steel-concrete composite; the results are examined evidencing the peculiarities of the composite solution.

KEYWORDS

Composite frames, composite brace, steel-composite beams, seismic design.

1 INTRODUCTION

In Moment Resisting Frame (MRF) solutions, an optimal seismic performance of the structure can be attained when a global mechanism is achieved at the ultimate limit state; this result is effective in RC structures when the dissipative mechanism involves all ends of the beams and the column bases (global mechanism), conversely for steel and steel-concrete composite constructions the dissipation of the beams can be substituted also by the joint panels, as clearly provided by Eurocode 8 [Eurocode 8,2004] and confirmed in various studies [as example Aribert et al, 2006; Braconi et al, 2008; Braconi et al. 2008; Thermou et al. 2004; Bursi and Gramola, 2000].

However, for the steel-concrete composite frames, the Italian code [NTC 2008] allows only the plasticization of the beam ends; therefore the capacity design method is suggested to obtain a weak beam-strong column behavior in the MRF global mechanism. This result is exploited if a suitable hierarchy is realized between the beams and the joints/columns, which ensures a ductile and stable response of the dissipative elements [D'Aniello et, 2012].

In this paper the main aspects of reliable seismic modeling and design of steel-concrete composite structures are dealt with considering the MRF and Concentric Braced Frames

(CBF). The codes applied for the design are the Italian NTC2008, Eurocode 4 (EN 1994-1-1:2004 for the general rules) and Eurocode 8 (EN 1998-1:2004 for the seismic rules). Furthermore the results of two numerical examples of frames are presented, one MRF and one CBF realized with composite elements. Finally MRFs buildings are compared considering the 3 solutions of composite, steel and RC structures.

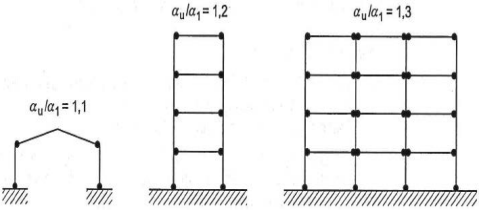
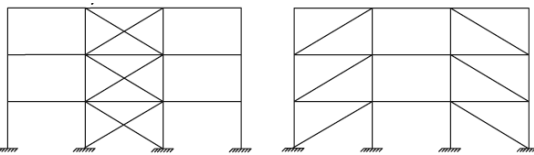
2 THE DESIGN OF COMPOSITE FRAMES

2.1 The behaviour factor

For dissipative steel and composite structures EC8 and NTC2008 rules allow the achievement of ductile global mechanisms giving a great energy dissipation in the post-elastic field. In this case the capacity of the structure depends on the performance in the plastic field and it is arisen by detailed design rules. However the structure capacity can be taken into account also applying a linear elastic analysis if a suitable behavior factor q is introduced according to codes provisions to define the design inelastic spectrum that reduces the elastic spectrum of accelerations damped by plasticity diffusion.

The value of q is given by the codes for different types of structures and depends also on the overstrength factor α_u / α_1 , defined as the ratio between ultimate load (load at the collapse of the structure) and the load at the first plasticization. In this study the design approach is examined for MRF and CBF, that are reported in Table 1.

Table 1. Types of structures and upper limit of the behaviour factor.

Type of structure	q	
	DC" B "	DC" A "
<p>MRF: the seismic capacity of the structure is due to the bending behaviour of the elements</p> 	4	$5 \alpha_u / \alpha_1$
<p>CBF: the seismic capacity of the structure is due to the axial behaviour of the braces</p> 	4	4

2.2 The resistance hierarchy

According to the resistance hierarchy the MRFs have to be designed to form the plastic hinges in the beams; therefore the principle of strong column/weak beam has to be applied through the following relation [NTC2008 7.6.6.4]:

$$\Sigma M_{Rc} \geq \gamma_{Rd} \Sigma M_{Rb} \quad (1)$$

being ΣM_{Rc} e ΣM_{Rb} the sum of the resistant moments of the columns and beams of the same joint respectively, γ_{Rd} a factor equal to 1.3 in CD “A” and 1.1 in CD “B”.

In order to have ductile hinges at the ends of the beams it is necessary to verify that the plastic resistant moment and the rotation capacity are not reduced by compression or shear, therefore the conditions of [§EC8 1-1 7.7.1, §NTC 7.5.4.1] have to be respected for steel and composite frames.

The columns need to be verified for compression-bending considering the more unfavorable combination of axial load and bending moment, evaluating the design stresses $M_{Ed,c}$, $N_{Ed,c}$ and $V_{Ed,c}$ as follows:

$$N_{Ed,c} = N_{Ed,G} + 1.1 \cdot \gamma_{Rd} \cdot \Omega \cdot N_{Ed,E} \quad (2)$$

$$M_{Ed,c} = M_{Ed,G} + 1.1 \cdot \gamma_{Rd} \cdot \Omega \cdot M_{Ed,E} \quad (3)$$

$$V_{Ed,c} = V_{Ed,G} + 1.1 \cdot \gamma_{Rd} \cdot \Omega \cdot V_{Ed,E} \quad (4)$$

where the index “ Ed,G ” is for the stresses due to the conventional vertical loads assumed in the seismic combination while “ Ed,E ” indicates the stresses due to the seismic actions.

The symbol Ω defines the minimum overstrength $\Omega_i = M_{pl,Rd,i} / M_{Ed,i}$ of the beams where the plastic hinges formed, γ_{Rd} represents the overstrength factor, furthermore it have to be verified that $V_{Ed} / V_{pl,Rd} \leq 0.5$, in the web panel $V_{Wp,Ed} / V_{Wp,Rd} \leq 1$ and in composite columns $N_{Ed} / N_{pl,Rd} \leq 0.3$.

The equations 2, 3 and 4 have to assure that the columns are dimensioned for the actions at the formation of the plastic hinges in the beams. EC8 assumes that this amplification has to be evaluated both for the static loads, $M_{Ed,G}$, and the seismic loads $M_{Ed,E}$. Really this overstrength of the beams Ω_i doesn't take correctly account of the influence of the vertical loads on the global behavior of the structure (Elghazouli A., 2007); in fact the $M_{Ed,G}$ remain constant and only $M_{Ed,E}$ increase with the earthquake intensity.

This aspect becomes relevant in frames with design governed by gravity loads (for example with very long spans) where the overstrength of the beams could be underestimated. A more accurate evaluation of the overstrength that considers this circumstance is the following one (Elghazouli A., 2008):

$$\Omega_{mod,i} = (M_{pl,Rd,i} - M_{Ed,G,i}) / M_{Ed,E,i} \quad (5)$$

According to the resistance hierarchy the joints have to be overstrength respect to the resistant shear and plastic moment of the beams as follows:

$$M_{pl,Rd,j} \geq 1.1 \cdot \gamma_{Rd} \cdot M_{b,pl,Rd} \quad (6)$$

$$V_{pl,Rd,j} \geq V_{Ed,G} + 1.1 \cdot \gamma_{Rd} \cdot V_{Ed,E} \quad (7)$$

2.3 The linear modelling

The definition of the linear model of the composite structure requires to establish the following aspects:

- The section to be assumed for calculating the stiffness of the beam taking in account the variation of the effective width along the beam according to the moment sign and the effect of cracking under hogging moment;
- The section to be assumed for evaluating the beam resistance under hogging and sagging moment in the critical zone;
- The steel-concrete connectors for obtaining the full strength.

The codes give different formulations for the effective width under vertical or seismic loads, but the seismic combination is comprehensive of vertical loads, therefore both the seismic combination and the vertical ultimate state are analyzed assuming the stiffness of the seismic code provisions.

The codes don't give the length to which the effective width have to be attributed in the seismic analysis; however this choice is not simple because the seismic actions make the length under sagging or hogging moment very long from joint (usually a bi-triangular trend occurs), therefore it is not adequate to apply the provisions up to the zero point of bending (Pecce and Rossi, 2011). Furthermore the cyclic action could require the continuous variation of the effective width with a step by step procedure. In conclusion, in case of moderate seismic actions respect to gravity loads (Figure 1) or not dissipative structures, it is not clear what is the value to be applied in the sagging moment zone. In (Pecce and Rossi, 2011) a parametric analysis is reported that considers various effective width for SLD and it results a variation of the global deformability of the frames lower than 15%.



Figure 1. Bending moment diagram due to low seismic action when vertical loads are predominant.

In order to have a simple solution [§EC8 7.7.2 (3); §NTC 7.6.6.1] allow to introduce an equivalent inertia of the beams in the analysis of frames; this equivalent inertia is evaluated by the following formulation:

$$I_{eq} = 0.6 \cdot I_1 + 0.4 \cdot I_2 \quad (8)$$

being I_1 the moment of inertia of the uncracked section evaluated using b_{ei} of the sagging moment according to code provisions [§EC8 prospetto 7.5.I; §NTC Tab. 7.6.III], I_2 is the moment of inertia of the cracked section, assuming b_{ei} of the hogging moment indicated in the same table. The same expression, with the same role of the two moments of inertia, is provided by the code AISC2010 for the analysis of frames under vertical loads; for the evaluation of the drift under the seismic actions the same code suggests to use a factor 0.5 for both the moments of inertia. This solution is adopted in the examples of this paper.

In conclusion the various formulations for the effective width don't give significant differences in the structural analysis of frames.

In order to evaluate the plastic strength of the section the effective width can be calculated according to codes [§EC8 prospetto 7.5.I; §NTC Tab. 7.6.IV].

The structural analysis can be developed as follows [§NTC08 4.3.2.4]:

- first order analysis, adopting the initial configuration of the structure for the equilibrium;
- second order analysis, adopting the deformed configuration of the structure for the equilibrium.

Under seismic actions, the geometrical non linearities are considered through the parameter θ , that is defined as:

$$\theta = (P \cdot d_r) / (V \cdot h) \quad (9)$$

where:

P is the total vertical load due to the floor examined and floor above it, d_r is mean relative horizontal displacement at SLV, calculated like the difference between the displacement of the floor examined and the below one, V is the horizontal total force at the floor evaluated by a linear analysis with behavior factor, h is the interstorey height.

The effect of geometrical non linearity can give the following effects:

- can be neglected when θ is lower than 0.1 (lower than 10%);
- can be considered increasing the effects of the seismic horizontal action by a factor $\alpha = 1/(1 - \theta)$, when θ is in the range 0.1 - 0.2;
- have to be evaluated by a non linear analysis when θ is in the range 0.2 - 0.3. The factor θ cannot be higher than 0.3.

3 THE CASE STUDIES

3.1 The case study building

The case study is a six story building for offices; it has a regular shape in plane and is assumed regular along the height. The interstorey height is 4m at the ground floor and 3.5m at the other floors, for a total height of 21.50m. The building is considered in two cases: MRFs in one direction and CBFs in the other direction or CBFs along both directions (Figure 2).

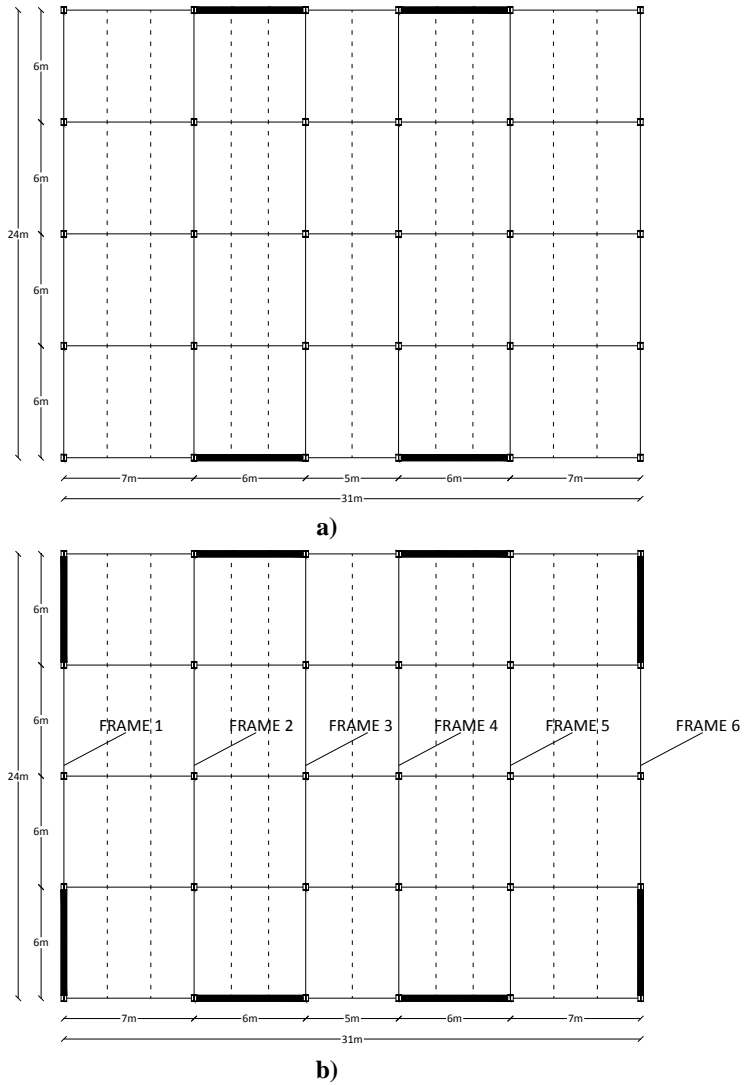


Figure 2. Plan of the building. a) case of MRFs in one direction; b) case of CBFs in both directions.

The loads applied to the structures are reported in Table 2.

Table 2. Load analysis of the floors.

Intermediate floor					
		H [m]	Weight for unit volume [kN/m³]	Load kN/m²	Total [kN/m²]
G1	Slab (concrete thickness above profiled steel sheeting)	0.065	25	1.63	2.41
	Slab (concrete in the ribs of the profiled steel sheeting)	0.055	25	0.69	
	Profile steel sheeting (type Hi-Bond A55/P600)	-	-	0.10	
G2	Screed (cement mortar)	0.04	18	0.72	2.22
	Pavement	-	-	0.40	
	Ceiling	-	-	0.10	
	Partitions	-	-	1.00	
	Infill walls	-	-	1.00	
		-	-	-	
Q	Live load (office)	-	-	3.00	3.00
Roof floor					
		H [m]	Weight for unit volume [kN/m³]	Load [kN/m²]	Total [kN/m²]
G1	Slab (concrete thickness above profiled steel sheeting)	0.065	25	1.63	2.41
	Slab (concrete in the ribs of the profiled steel sheeting)	0.055	25	0.69	
	Profile steel sheeting (type Hi-Bond A55/P600)	-	-	0.10	
G2	Screed (cement mortar)	0.04	18	0.72	1.22
	Pavement	-	-	0.30	
	Ceiling	-	-	0.10	
	Thermal insulation	-	-	0.10	
		-	-	-	
Q	Live load (office)	-	-	3.00	3.00
Qn	Snow	-	-	0.48	0.48

The loads on the beams were calculated considering the effect of half distance of the secondary beams on one side (1.17m) and the effect of a cantilever of 0.50m on the external side, that is necessary for the anchorage of the slab reinforcement.

In Table 3 the loads for unit length of the beams are reported. In the weight of the roof floor also a RC parapet 1.5m high is added; furthermore the load of the main beams is applied to the columns as axial loads reported in Table 4.

Table 3. Loads on the beams.

intermediate floor				roof floor				
G_{1,CAL}	G_{2,CAL}	G_{2,tam,CAL}	Q_{CAL}	G_{1,COP}	G_{2,COP}	G_{2,tam,CAL}	Q_{COP}	Q_{NEV}
[kN/m]	[kN/m]	[kN/m]	[kN/m]	[kN/m]	[kN/m]	[kN/m]	[kN/m]	[kN/m]
4.02	3.70	3.50	5.00	4.02	2.03	1.50	5.00	0.80

Table 4. Axial loads applied to the columns.

intermediate floor									
external columns					internal columns				
$F_{G1,CAL}$	$F_{G2,CAL}$	$F_{G2,tam,CAL}$	F_{QCAL}		$F_{G1,CAL}$	$F_{G2,CAL}$	F_{QCAL}		
[kN]	[kN]	[kN]	[kN]		[kN]	[kN]	[kN]		
16.89	15.54	12.25	21.00		33.78	31.08	42.00		
roof floor									
external columns					internal columns				
$F_{G1,COP}$	$F_{G2,COP}$	$F_{G2,tam,COP}$	$F_{Q,COP}$	$F_{Qn,COP}$	$F_{G1,COP}$	$F_{G2,COP}$	$F_{Q,COP}$	$F_{Qn,COP}$	
[kN]	[kN]	[kN]	[kN]	[kN]	[kN]	[kN]	[kN]	[kN]	
16.89	8.54	5.25	21.00	3.36	33.78	17.08	42.00	6.72	

The fundamental combinations at SLU are:

- Intermediate floor: $Q_{(SLU)} = 1.3 \cdot G1 + 1.5 \cdot G2 + 1.5 \cdot Q$
- Roof floor: $Q_{(SLU)} = 1.3 \cdot G1 + 1.5 \cdot G2 + 1.5 \cdot Q + 1.5 \cdot 0.5 \cdot Qn$

while for the seismic combination SLV are:

- Intermediate floor: $Q_{(SLV)} = G1 + G2 + 0.3 \cdot Q$
- Roof floor : $Q_{(SLV)} = G1 + G2 + 0.3 \cdot Q$

The seismic action has been evaluated for 3 different locations of the building: Benevento (zone 1, $a_g > 0.25$); Caserta (zone 2, $0.15 < a_g \leq 0.25$); Roma (zone 3, $0.05 < a_g \leq 0.15$).

For the evaluation of the seismic actions the design characteristics are: $V_R = 50$ years; class II, soil C, topographic situation T1. The following parameters were defined:

Table 5. Parameters of the pericolosity of the seismic zones.

Benevento (zone 1)				
limit state	T_r	a_g	F_0	T_c^*
	[years]	[g]	[-]	[s]
SLO	30	0.062	2.384	0.279
SLD	50	0.083	2.351	0.294
SLV	475	0.257	2.304	0.369
SLC	975	0.349	2.335	0.390
Caserta (zone 2)				
limit state	T_r	a_g	F_0	T_c^*
	[years]	[g]	[-]	[s]
SLO	30	0.053	2.353	0.283
SLD	50	0.068	2.345	0.311
SLV	475	0.179	2.414	0.377
SLC	975	0.231	2.443	0.405

Roma (zone 3)				
limit state	T_r	a_g	F_0	T_c^*
	[years]	[g]	[-]	[s]
SLO	30	0.042	2.534	0.255
SLD	50	0.052	2.511	0.270
SLV	475	0.110	2.628	0.306
SLC	975	0.136	2.646	0.316

The vibration period T of the structure is calculated using the simple formulation for the static linear analysis according to NTC2008:

$$T = c_1 \cdot H^{3/4} = 0.85s \quad (10)$$

The ductility class B and the behaviour factor $q=4$ were assumed.

Considering the distribution of the forces along the height for the linear static analysis, the forces are reported in Table 6.

Table 6. Seismic forces.

floor	Benevento		Caserta		Roma	
	$F_{i,SLV}$	$F_{i,SLD}$	$F_{i,SLV}$	$F_{i,SLD}$	$F_{i,SLV}$	$F_{i,SLD}$
	[kN]	[kN]	[kN]	[kN]	[kN]	[kN]
6	150.8	196.5	125.3	166.8	71.6	121.8
5	133.1	173.5	110.6	147.2	63.3	107.5
4	107.2	139.8	89.1	118.6	51.0	86.6
3	82.2	107.2	68.3	91.0	38.9	66.1
2	56.4	73.5	46.8	62.3	26.6	45.3
1	30.4	39.7	25.3	33.7	14.4	24.5

3.1.1 Design of the composite MRF

The frame in Figure 3 is realized with columns partially encased and composite beams with slab. The floor is a steel-concrete composite one 120 thick with profiled steel sheeting type Hi-Bond A55/P600 with a thickness of 0.8mm and a concrete slab 65mm thick above the sheet obtaining a total slab of 120mm. This floor is connected to the steel profile of the beam by studs.

The materials are concrete C20/25, steel for reinforcement B450C and construction steel S235 for beams and columns.

The frame was pre-dimensioned considering only the vertical loads and then also the seismic action was introduced. The seismic verification of the displacement at SLD has been the most significant one. The design was carried out by an iterative procedure to reach a good solution. At the end of the design procedure the dimensions of the elements resulted adequate also for SLV considering the hierarchy of strength; the dimensions of the elements are reported in Figure 4 and the columns are all oriented along the strong axis.

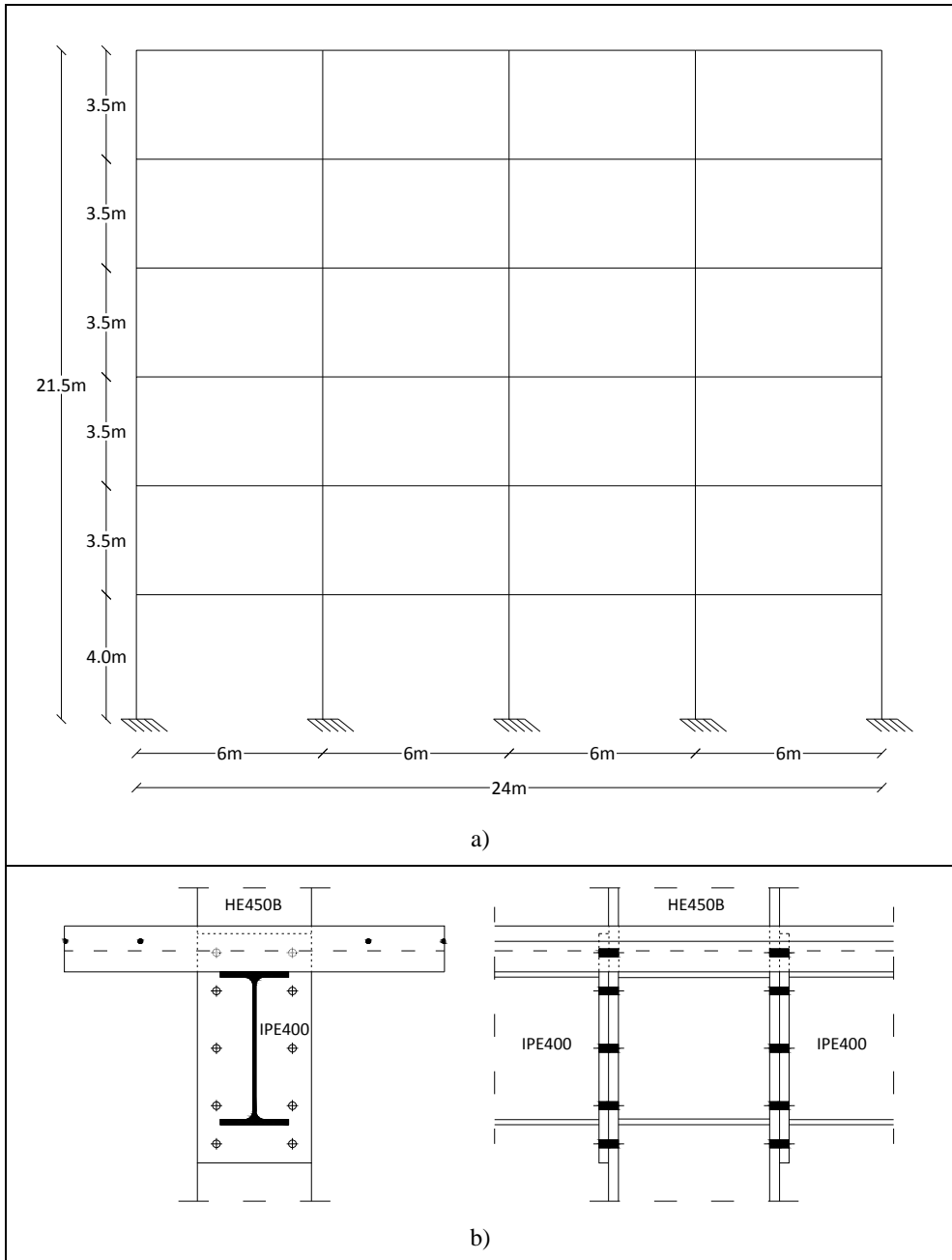


Figure 3. a) Geometry of the frame; b) type of beam-column joint.

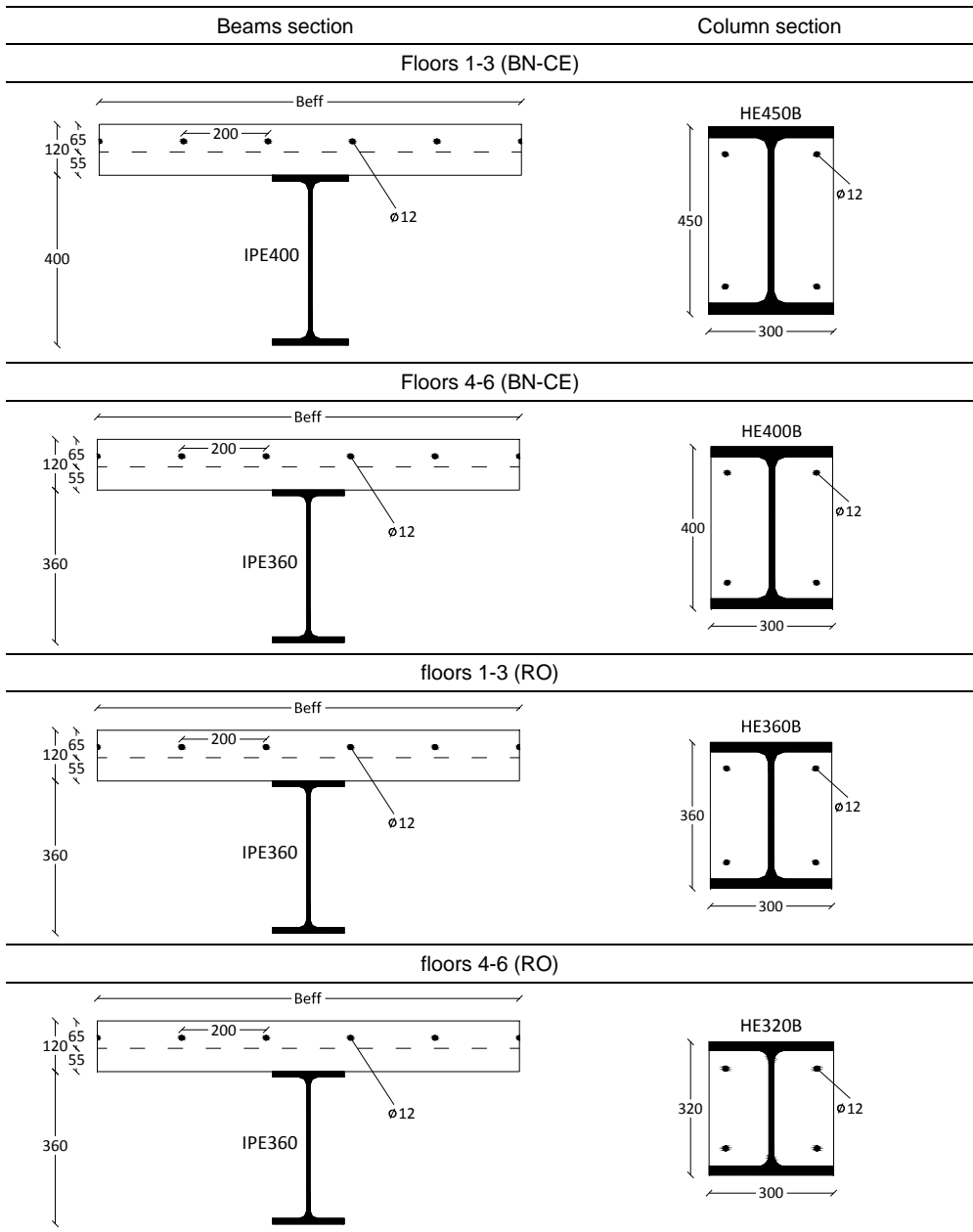


Figure 4. Cross sections of composite beams and columns of the frame considered for the 3 seismic zones.

The model of the frame was implemented assuming the moment of inertia of the beams according to the provisions of chapter 7 of NTC2008, neglecting the indications of chapter 4 in order to use the same model both for the seismic combination and the combination only

due to vertical loads. In particular chapter 4 suggests to calculate the moment of inertia of the beams assuming the following effective width, b_{eff} , for the slab:

$$b_{eff} = b_0 + 2 \cdot b_{ei} \quad (11)$$

being $b_{ei} = L_e/8$ and L_e variable from the zone of hogging moment to the one of sagging moment.

Conversely chapter 7 suggests to assume the following stiffness for beams and columns, respectively:

$$EI_{eq} = 0.6EI_1 + 0.4EI_2 \quad (12)$$

$$(EI)_C = 0.9(EI_a + rE_{cm}I_c + EI_c) \quad (13)$$

where:

- I_1 is the moment of inertia of the uncracked section;
- I_2 is the moment of inertia of the cracked section;
- E e E_{cm} are the elastic modulus of concrete and steel;
- I_a , I_c e I_s are the moment of inertia of steel, concrete and steel reinforcement, respectively;
- The reduction factor r depends on the type of section, but usually is assumed equal to 0.5.

This simple approach allows to make the calculation less onerous without a significant effect because the different effective width in static and seismic conditions gives bending moments different of about 5%.

In the case of seismic analysis, b_{eff} for evaluating I_1 e I_2 is defined according to NTC08 at par. 7.6.5.1.1.:

$$b_{eff,1} = 2 \cdot b_{ei} = 2 \cdot 225 = 450mm$$

$$b_{eff,2} = 2 \cdot b_{ei} = 2 \cdot 300 = 600mm$$

Being $b_{ei} = 0.05L$ e $0.0375L$ respectively for the zone under hogging moment and the zone under sagging moment; in presence of seismic action L is the length of the beam.

3.1.2 Design of the composite CBF

The external frames have concentric X bracing with diagonal in tension. The steel-concrete floor is realized with profiled steel sheeting type Hi-Bond A55/P600 0.8mm thick with a concrete thickness of 65mm above the sheet obtaining a total slab of 120mm. The slab is connected to the steel profile by Nelson studs. The columns are realized with steel profiles.

The materials used for the design of the structures are concrete C20/25, reinforcement steel B450C, constructional steel S235 for the beams, the columns of the frames without braces and the braces, while steel S355 is used for the columns where the braces are connected.

The beams and columns were pre-dimensioned considering only the vertical loads and the seismic action was totally assigned to the braces.

The analysis reported herein regards the braced frame (frame 1 of Figure 2) and the two internal frames (frame 2, 3 of Figure 2) due to the symmetry of the structure.

The beams of frames 2, 3 are the same of frame 1 (Figure 5); The columns of frames 2, 3 are the same of the central ones of frame 1 except the external columns where the braces are connected, that are equal to the external ones of frame 1 (Figure 5).

The diagonal elements of the braces are realized with the profiles listed in Table 7.

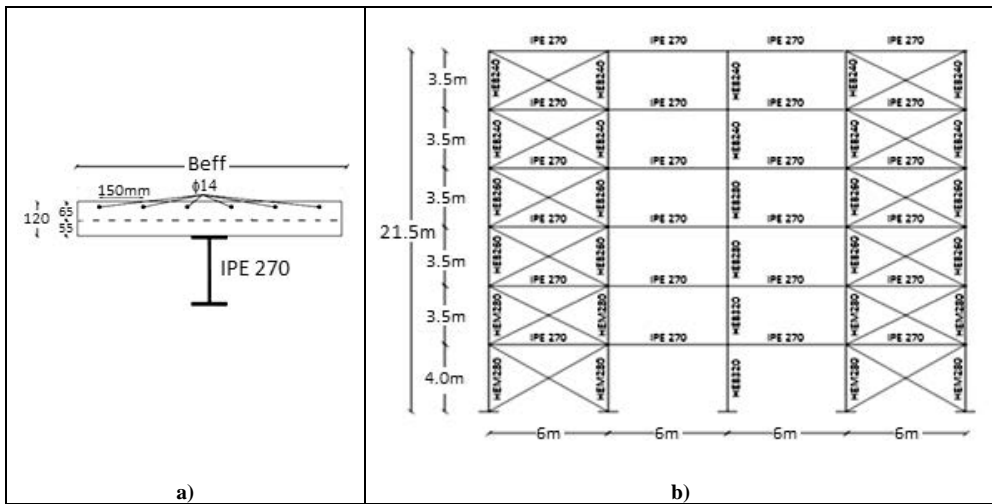


Figure 5. a) Example of beam section. b) Front view of frame 1.

Table 7. Profiles of the braces diagonal.

Piano	Hollow profiles UNI EN 10210
1	rectangular 180x80x16
2	rectangular 150x100x16
3	rectangular 150x100x14.2
4	rectangular 150x100x12.5
5	rectangular 140x80x8.8
6	circular 114.3x5

Firstly the concrete slab is considered completely separated from the column at the joint, with a gap of 3cm.

Therefore the strut and tie mechanism (as discussed in the Design Guidelines [1]) cannot develop. Secondly the slab is considered completely adherent to the column without gap; the longitudinal rebars at the joint are continuous so that the beam works as continuous beam under the vertical loads.

The beam-column joint is realized with a bolted plate (Figure 7) as reported in [2].

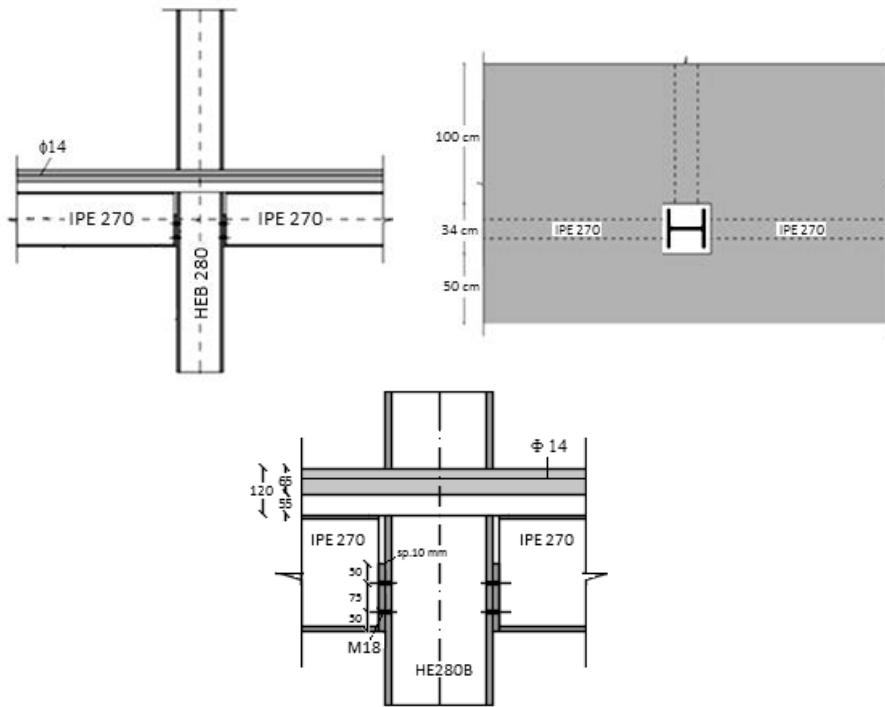


Figure 7. Details of the composite joint of the braced frame.

The effective widths, b_{eff} , of the RC slab for evaluating the moment of inertia I_J , I_2 and bending resistances were calculated according the provisions of par. 4.3.2.3 of NTC08:

$$b_{eff} = b_0 + b_{e1} + b_{e2} \quad (14)$$

being:

$b_{ei} = \min(L_e/8, b_i)$ and $L_e=3\text{m}$ for the zones under hogging moment and $L_e=4.2\text{m}$ for the zones under sagging moment.

For the beams of external frames:

$$b_{eff,1} = 1025\text{mm}$$

$$b_{eff,2} = 750\text{mm}$$

For the beams of the internal frames:

$$b_{eff,1} = 1050\text{mm}$$

$$b_{eff,2} = 750\text{mm}$$

3.1.3 Verification of the composite MRF

The effective widths, b_{eff} , under seismic conditions were calculated according par. 7.6.5.1.1. of NTC08, as follows:

$$b_{eff,1} = 2 \cdot b_{ei} = 2 \cdot 450 = 900\text{mm}$$

$$b_{eff,2} = 2 \cdot b_{ei} = 2 \cdot 600 = 1200\text{mm}$$

where $b_{ei}=0.1L$ and $0.75L$ respectively for the evaluation of hogging and sagging resistant moment, being L the beam length.

In Table 8 the overstrength factors $\Omega_{min} = M_{pl,Rd} / M_{Ed}$ are listed for the 3 seismic zones. The shear verification was carried out evaluating the design shear applying the hierarchy shear-bending. The verification is respected if $V_{Ed} \leq 0.5V_{Rd}$; in Table 9 the safety factors $SF=0.5V_{Rd}/V_{Ed}$ are reported.

In Figure 8 $M_{U,Rd}=1.1 \cdot \gamma_{Rd} M_{Rd}$.



Figure 8. Load pattern for the shear design at SLV.

Table 8. Ω_{min} for the 3 seismic zones.

Zone 1	Zone 2	Zone 3
Ω_{min}	Ω_{min}	Ω_{min}
[-]	[-]	[-]
1.36	1.59	1.76

Table 9. Safety factors for the shear verification of the beams.

Zone 1	Zone 2	Zone 3
SF	SF	SF
[-]	[-]	[-]
1.32	1.32	1.32

The verification is respected because $SF > 1$. The composite columns were verified considering the most unfavorable combination of axial and bending stresses.

The design stresses of the composite columns were evaluated as in case of steel columns under seismic actions considering the resistance hierarchy

$$N_{Ed,c} = N_{Ed,G} + 1.1 \cdot \gamma_{Rd} \cdot \Omega \cdot N_{Ed,E} \tag{15}$$

$$M_{Ed,c} = M_{Ed,G} + 1.1 \cdot \gamma_{Rd} \cdot \Omega \cdot M_{Ed,E} \tag{16}$$

$$V_{Ed,c} = V_{Ed,G} + 1.1 \cdot \gamma_{Rd} \cdot \Omega \cdot V_{Ed,E} \tag{17}$$

$\Omega = \min(M_{pl,Rd} / M_{Ed})$ of all beams, the steel is S235 and $\gamma_{Rd}=1.2$.

In order to verify the columns, the resistant domain for axial and bending loads were carried out for the various sections of the columns.

In Figure 10 the domain on the profile HE450B is drawn.

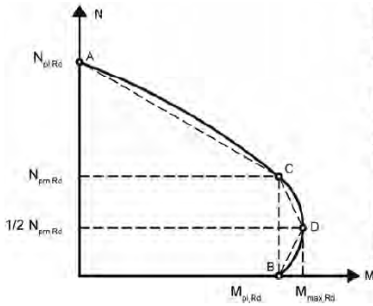


Figure 9. Identification of the main points of the domain.

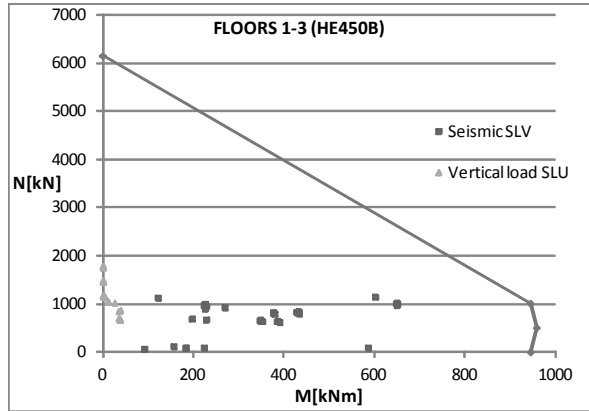


Figure 10. Resistant domain of HE450B.

The verification is respected for all 3 seismic zones because the point of the design stresses are inside the domain. The shear verification is respected if $V_{Ed} \leq 0.5V_{Rd}$ with V_{Ed} evaluate by Eq. (17), the safety factors $SF = 0.5V_{Rd} / V_{Ed}$ are listed in Table 10.

Table 10. Safety factors for the shear verification of the columns.

Zone 1	Zone 2	Zone 3
SF	SF	SF
[-]	[-]	[-]
2.21	2.28	2.38

According to the code provisions the design shear in the columns has to be evacuate assuming the formation of plastic hinges when the plastic resistant moment is attained at the ends without amplification (7.5.3(3) of Eurocode 8-Part 1) $M_{U,Rd} = M_{pl,Rd}$.

The verification was carried out at the ground floor of the building where the plastic hinges can really forms: the verifications $V_{Ed} \leq V_{Rd}$ are synthesized in Table 11.

Table 11. Safety factors for the shear verification of the columns considering the shear-bending hierarchy.

Zone 1	Zone 2	Zone 3
SF	SF	SF
[-]	[-]	[-]
2.05	2.05	2.33

The design of the frame case study is governed by SLD in all 3 seismic zones. The maximum stresses on the beams result from the seismic combination also for the example 3 (low seismic intensity), because in the frame there are the secondary beams that are subject to low vertical loads.

In example 3 the safety factors of the beams in bending vary between 1.36 and 1.76, but the reduction of the sections would make the verification at SLD not respected and the columns

section had to be enlarged. It is worth noticing that the variation of the seismic action, a_g , from SLD to SLV is different between zone 1 and 3.

In Table 12 the percentage variations of acceleration in the 3 zones are indicated.

Table 12. Percentage variation of acceleration in the 3 zones.

	Zone			Variation of acceleration		
	1	2	3	1-2	2-3	1-3
	a_g	a_g	a_g	$(a_{g1}-a_{g2})/a_{g1}$	$(a_{g2}-a_{g3})/a_{g2}$	$(a_{g1}-a_{g3})/a_{g3}$
	[g]	[g]	[g]	[%]	[%]	[%]
SLD	0.083	0.068	0.052	18.1	23.3	37.2
SLV	0.257	0.179	0.110	30.4	38.3	57.1

It is clear that the variation of acceleration, i.e. the equivalent static forces, from SLD and SLV is 30% in zone 1 and 18% in zone 2.

It is clear that a variation of 18% gives the same dimensions of elements for the two seismic zones (Benevento and Caserta), also because standard steel profiles can be employed; in fact the profiles are the same for both the seismic zones because for zone 1 allow to respect the limit drift 0.005 but are also necessary for zone 3 albeit over-dimensioned. In conclusion the design depends mainly on the presence of a seismic action not much bit on its intensity.

3.1.4 Verification of the CBF

The design procedure is provided in par. 7.5.5 of NTC08.

Table 13. Profiles of braces diagonals.

Floor	$N_{Ed, contr}$ [KN]	Steel	A_{min} [mm ²]	Hollow sections UNI EN 10210	Area [mm ²]
1	1517	S235	6776	rectangular 180x80x16	7020
2	1379	S235	6164	rectangular 150x100x16	6700
3	1228	S235	5489	rectangular 150x100x14.2	6080
4	1007	S235	4501	rectangular 150x100x12.5	5460
5	717	S235	3203	rectangular 140x80x8.8	3480
6	357	S235	1594	circular 114.3x5	1720

The design of the braces diagonals was carried out assuming an effective length $L_0=0.7L_{diag}$ in the plane and $L=L_{diag}$ out of plane, being L_{diag} the length of the diagonal. The bracing elements with rectangular section are mounted with the maximum moment of inertia in the plane.

In the following the slenderness and overstrength required by the code for the design of braces with active diagonal in tension are verified.

In particular, the non dimensional slenderness of diagonals has to respect the following condition:

$$1.3 < \lambda / \lambda_y < 2 \quad (18)$$

Furthermore, in order to attain a homogeneous dissipative behavior of the diagonals of the structure, the factors of overstrength $\Omega_i = N_{pl,Rd,i} / N_{Ed,i}$ evaluated for all the braces, have to respect a variation between the minimum and maximum value not greater than 25%.

Table 14. In plane buckling.

Profil	h/t < 18	d/t < 36	λ/λ_y	1.3 < λ/λ_y < 2	N_{plRd}	Ω_i	$\Omega_{max}/\Omega_{min} < 1.25$
180x80x16	11	-	1.87	VERIFIED	1571.14	1.04	1.17
150x100x16	9	-	1.44	VERIFIED	1499.52	1.09	
150x100x14.2	11	-	1.42	VERIFIED	1360.76	1.11	
150x100x12.5	12	-	1.39	VERIFIED	1222.00	1.21	
140x80x8.8	16	-	1.67	VERIFIED	778.86	1.09	
114.3x5	-	23	1.34	VERIFIED	384.95	1.08	

Table 15. Out of plane buckling.

Profile	h/t < 18	d/t < 36	λ/λ_y	1.3 < λ/λ_y < 2	N_{plRd}	Ω_i	$\Omega_{max}/\Omega_{min} < 1.25$
180x80x16	11	-	1.33	VERIFIED	1571.14	1.04	1.17
150x100x16	9	-	1.47	VERIFIED	1499.52	1.09	
150x100x14.2	11	-	1.44	VERIFIED	1360.76	1.11	
150x100x12.5	12	-	1.42	VERIFIED	1222.00	1.21	
140x80x8.8	16	-	1.51	VERIFIED	778.86	1.09	
114.3x5	-	23	1.91	VERIFIED	384.95	1.08	

Verification of the columns overstrength

This verification has to be developed in agreement with par. 7.5.5. of NTC2008.

$$N_{Ed} / N_{pl,Rd}(M_{Ed}) \leq 1 \quad (19)$$

being N_{Ed} evaluated with Eq. (15) in which $\Omega = \min(N_{pl,Rd} / N_{Ed})$ of all braces considering steel S235 and $\gamma_{Rd}=1.2$.

Table 16. Values of Ω .

Floor	Column profile	$N_{Ed,G}$ [KN]	$N_{Ed,E}$ [KN]	N_{Ed} [KN]	$N_{b,Rd}$ [KN]	$N_{b,Rd}/N_{Ed}$
1	HE280M	797	3204	5221	5847	1.120
2	HE280M	660	2362	3924	6286	1.602
3	HE260B	523	1667	2897	2910	1.004
4	HE260B	386	1048	1940	2910	1.500
5	HE240B	249	540	1100	2478	2.252
6	HE240B	112	180	425	2478	5.830

Verification at SLD

In Table 17 the values of the drift at SLD are reported; the results are lower than the limit one $d_r/h=0.005$.

Table 17. Verification SLD.

Floor	d_r [mm]	h [mm]	d_r/h
1	4.36	4000	0.00109
2	5.14	3500	0.00147
3	6.5	3500	0.00186
4	7.6	3500	0.00217
5	8.9	3500	0.00254
6	9.5	3500	0.00271

Design and verification of the composite joint

The design of the joint of the frame is carried out by the procedure described in the design guideline for composite joint [1] and report for the design of the composite joints with isolated slab [2].

Firstly the basic components of the joint under hogging moment are defined according the “simply model 1” of the the slab isolated from the column in order to evaluate the hogging resistant moment to verify the moment due to gravity loads.

When the slab is isolated from the column the beam is continuous in bending under the vertical loads due to the longitudinal reinforcement continuous at the internal joint. The external joint is considered as only in steel (i.e. hinge).

For the frames and sections considered herein six types of internal joints can be defined (Figure 12):

- TYPE A: Columns HE320B – beams IPE270;
- TYPE B: Columns HE280B – beams IPE270;
- TYPE C: Columns HE240B – beams IPE270;
- TYPE D: Columns HE280M – beams IPE270;
- TYPE E: Columns HE260B – beams IPE270;
- TYPE F: Columns HE240B – beams IPE270;

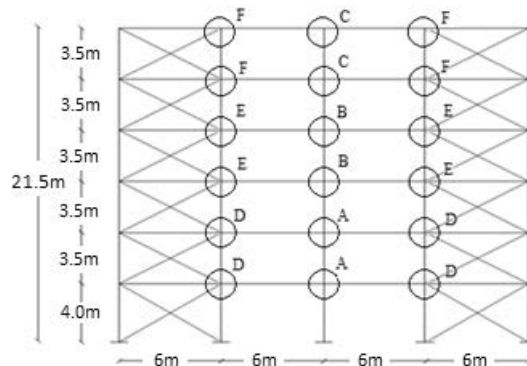


Figure 12. Types of internal joints.

Table 18. Weight of materials for MRF.

MRF						
Profiles	n°	L _{tot}	Weight	TOT steel	Concrete	Weight of reinforcement
	[-]	[m]	[kg/m]	[kg]	[m ³]	[kg]
IPE400	72	432	66.3	28642	-	-
IPE360	72	432	57.1	24667	-	-
HE 450 B	90	330	171.1	56463	37.6	2041
HE 400 B	90	315	155.3	48920	31.8	1948
Total				158691	69	3990

Table 19. Weight of materials for CBF.

CBF				
Profiles	n°	L _{tot}	Weight of steel per unit length	TOT Steel
	[-]	[m]	[kg/m]	[kg]
IPE270	144	864	36.1	31190
HE 280 M	32	120	188.5	22623
HE 260 B	32	112	93.0	10414
HE 240 B	60	210	83.2	17472
HE 320 B	28	105	126.7	13299
HE 280 B	28	98	103.1	10106
Brace 180x80x16	16	115.4	65.4	7545
Brace 150x100x16	16	111.1	62.9	6988
Brace 150x100x14.2	16	111.1	58.0	6450
Brace 150x100x12.5	16	111.1	49.1	5460
Brace 140x80x8.8	16	111.1	30.4	3382
Brace 114.3x5	16	111.1	13.48	1498
Total				136428

The braced structure has a weight of steel lower respect to the framed structure, furthermore this last one has also the weight of RC of the columns; the result is due to the high deformability of MRF structures that requires greater sections to satisfy the verification at SLD. Therefore, the composite structure used (partially encased columns) is not convenient respect to the aim, because the CBF solution requires an amount of steel and cost lower than about 15%.

4 COMPARISON BETWEEN DIFFERENT TYPES OF FRAMED BUILDINGS

The same building was also designed adopting the resistant system of frames but using 3 solutions: composite frames, steel frames and RC frames.

The live loads and the seismic actions are the same for all the 3 cases; the live load at the intermediate floors refers to the use destination of offices (3kN/m^2), on the roof floor the snow is considered (0.48kN/m^2). The seismic action is evaluated assuming the location in Benevento, already introduced for the study of the plane frame.

4.1 The composite building

The design of the framed building was carried out using composite frames in both directions and attaining the hierarchy of resistances at the beam-column joint also along the weak direction of the column profile introducing additional reinforcement in the composite column. The choice of using all composite MRFs in the building make the hierarchy of beam-column joint the most important verification with the lower safety factor ($SF=1.06$).

The plan of the building is the same already presented in Figure 3, but in this case the strong axes of the columns are oriented in different way (Figure 14); also along the height the geometry is the same of the 2D frame introduced in par.3.1 (Figure 3).

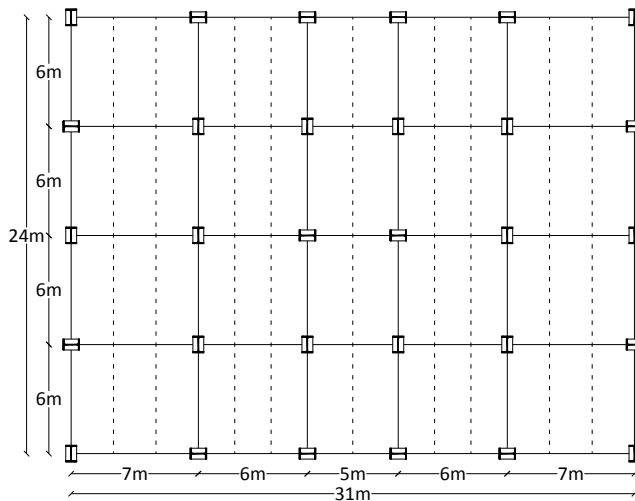


Figure 14. The plan of the building.

The columns are partially encased and the beams have a collaborating slab. The floor is a steel-concrete composite one 120 thick with profiled steel sheeting type Hi-Bond A55/P600 with a thickness of 0.8mm and a concrete slab 65mm thick above the sheet obtaining a total slab of 120mm. This floor is connected to the steel profile of the beam by studs.

The materials are: concrete C25/30, steel for reinforcement B450C and construction steel S235 for beams and S355 for columns.

The structure was pre-dimensioned considering only the vertical loads and then reviewed by iterative procedure introducing the verifications for the seismic actions.

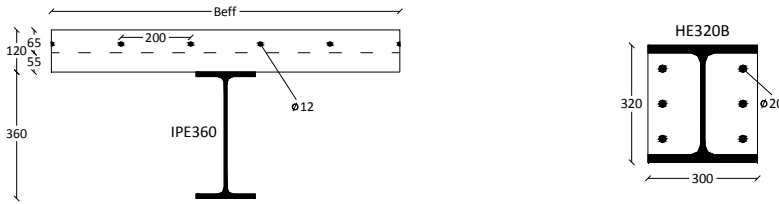


Figure 15. Sections of the composite beams and columns.

The 3D model was implemented assuming the same hypothesis already introduced in par.3.1. In this case study the beams spans are different thus the effective width varies with the length of the beams:

- L=7m:

$$b_{eff,1} = 2 \cdot b_{ei} = 2 \cdot 262.5 = 525mm$$

$$b_{eff,2} = 2 \cdot b_{ei} = 2 \cdot 350 = 700mm$$
- L=6m:

$$b_{eff,1} = 2 \cdot b_{ei} = 2 \cdot 225 = 450mm$$

$$b_{eff,2} = 2 \cdot b_{ei} = 2 \cdot 300 = 600mm$$
- L=5m:

$$b_{eff,1} = 2 \cdot b_{ei} = 2 \cdot 187.5 = 375mm$$

$$b_{eff,2} = 2 \cdot b_{ei} = 2 \cdot 250 = 500mm$$

being L the beam length, $b_{ei} = 0.05L$ and $0.0375L$ the length under hogging and sagging moments respectively. The loads and loads combinations are the same of par. 3.1, but only the case of location in Benevento (zone 1) was considered; class B of ductility and behavior factor $q=4$ were adopted. The dynamic analysis was applied in the linear field using the elastic spectrum at SLD and the design spectrum at SLV (reduced by q). In Table 20 the values of the displacements are reported and compared to the limit $d_r/h=0.005$ of the Italian code.

The verification of $\theta = (P \cdot d_r) / (V \cdot h)$ was performed evaluating the actual displacements, $d_{a,eff}$, of the structure under the design seismic action at SLV multiplying the results of the linear dynamic analysis, d_a , by the factor μ_d :

$$d_{a,eff} = \pm \mu_d \cdot d_a \quad (21)$$

where

$$\mu_d = q \text{ se } T_1 \geq T_c \quad (22)$$

$$\mu_d = 1 + (q-1) \cdot T_c / T_1 \text{ se } T_1 < T_c \quad (23)$$

being $T_1 = 1.58s$ and $T_c = 0.54s$, it results $\mu_d = q$.

The values of θ , listed in Table 21, are always less than 0.1 therefore it isn't necessary to amplify stresses to take into account the second order effects.

Table 20. Verification at SLD.

Direction x				
Floor	h_i	d_a	d_r	d_r/h
	[m]	[m]	[m]	[-]
1	4	0.0158	0.0158	0.0040
2	3.5	0.0319	0.0160	0.0046
3	3.5	0.0456	0.0137	0.0039
4	3.5	0.0565	0.0109	0.0031
5	3.5	0.0643	0.0077	0.0022
6	3.5	0.0684	0.0042	0.0012
Direction y				
Floor	h_i	d_a	d_r	d_r/h
	[m]	[m]	[m]	[-]
1	4	0.0154	0.0154	0.0039
2	3.5	0.0313	0.0159	0.0045
3	3.5	0.0450	0.0137	0.0039
4	3.5	0.0559	0.0109	0.0031
5	3.5	0.0636	0.0078	0.0022
6	3.5	0.0679	0.0042	0.0012

Table 21. Verification of the second order effect.

Direction X										
Floor	h_i	P	V	$\mu=q$	d_a	$d_{a,eff}$	d_r	ϑ	ϑ_{max}	α
	[m]	[kN]	[kN]	[-]	[m]	[m]	[m]	[-]	[-]	[-]
1	4	-26030.3	3635.8	4.00	0.012	0.050	0.050	0.089	0.093	1.00
2	3.5	-21531.0	3356.2		0.025	0.101	0.051	0.093		
3	3.5	-17031.7	2939.4		0.036	0.144	0.044	0.072		
4	3.5	-12532.3	2462.8		0.045	0.179	0.035	0.050		
5	3.5	-8033.3	1868.8		0.051	0.203	0.025	0.030		
6	3.5	-3534.7	1028.9		0.054	0.216	0.013	0.013		
Direction Y										
Floor	h_i	P	V	$\mu=q$	d_a	$d_{a,eff}$	d_r	ϑ	ϑ_{max}	α
	[m]	[kN]	[kN]	[-]	[m]	[m]	[m]	[-]	[-]	[-]
1	4	-26030.3	3662.6	4.00	0.012	0.048	0.048	0.086	0.091	1.00
2	3.5	-21531.0	3384.0		0.025	0.099	0.050	0.091		
3	3.5	-17031.7	2965.4		0.036	0.142	0.043	0.071		
4	3.5	-12532.3	2484.2		0.044	0.177	0.035	0.050		
5	3.5	-8033.3	1885.3		0.050	0.201	0.024	0.030		
6	3.5	-3534.7	1037.7		0.054	0.214	0.013	0.013		

The resistance verifications were carried out defining the effective width l_{eff} according to par. 7.6.5.1.1 of NTC08: .

- $L=7m$:
 $b_{eff,1} = 2 \cdot b_{ei} = 2 \cdot 525 = 1050mm$
 $b_{eff,2} = 2 \cdot b_{ei} = 2 \cdot 700 = 1400mm$
- $L=6m$:
 $b_{eff,1} = 2 \cdot b_{ei} = 2 \cdot 450 = 900mm$
 $b_{eff,2} = 2 \cdot b_{ei} = 2 \cdot 600 = 1200mm$
- $L=5m$:
 $b_{eff,1} = 2 \cdot b_{ei} = 2 \cdot 375 = 750mm$
 $b_{eff,2} = 2 \cdot b_{ei} = 2 \cdot 500 = 1000mm$

being L the length of the beam and $b_{ei} = 0.1L$ and $0.075L$ respectively for evaluating the hogging and sagging resistant moment. The shear verifications were conducted respecting the shear-bending hierarchy.

Table 22. Bending verification of beams.

Floors	L [m]	Type of section	Profile	M_{Ed}^+ [kNm]	$M_{pl,Rd}^+$ [kNm]	Ω^+	M_{Ed}^- [kNm]	$M_{pl,Rd}^-$ [kNm]	Ω^-	Ω^{MIN}
1-3	7	S1	IPE 360	160	423	2.63	-247	-329	1.33	1.33
	6	S2	IPE 360	95	409	4.30	-207	-320	1.54	
	5	S3	IPE 360	94	394	4.20	-213	-310	1.46	
4-6	7	S1	IPE 360	161	423	2.63	-207	-329	1.59	
	6	S2	IPE 360	96	409	4.26	-171	-320	1.87	
	5	S3	IPE 360	62	394	6.40	-160	-310	1.93	

Table 23. Shear verification of the beams.

Floors	L [m]	Type of section	Profile	$M_{pl,Rd}^+$ [kNm]	$M_{pl,Rd}^-$ [kNm]	$q_{sisma,grav}$ [kN/m]	V_{Rd} [-]	$V_{ed,sisma}$ [kN]	V_{Rd} [kN]	$V_{Ed} < 0.5V_{Rd}$
1-3	7	S1	IPE 360	423	-329	33.2	1.15	258.5	531.3	TRUE
	6	S2	IPE 360	409	-320			261.3	531.3	TRUE
	5	S3	IPE 360	394	-310			261.6	531.3	TRUE
4-6	7	S1	IPE 360	423	-329			258.5	531.3	TRUE
	6	S2	IPE 360	409	-320			261.3	531.3	TRUE
	5	S3	IPE 360	394	-310			261.6	531.3	TRUE

The composite columns have to be verified under axial and bending stresses amplifying the values from the analysis by a factor $\gamma_{Rd}=1.15$ for steel S275 and Ω already introduced:

$$\Omega = M_{pl,Rd(IPE360)}^- / M_{Ed(IPE360)}^- = 329/247 = 1.33$$

The verifications of compression-bending and shear are respected with various safety factors variable in the range of 2.4 and 10. Finally the verification of the beam-column hierarchy was checked (Table 24); this is the most restrictive condition when the column is oriented along the weak axis, in fact 6 rebars with 20mm diameter are necessary (Figure 15).

Table 24. Verification of the beam-column hierarchy.

		Strong axis of columns	Weak axis of columns
$M_{B,pl,Rd}^+$	kNm	423	423
$M_{B,pl,Rd}^-$	kNm	-320	-320
$M_{C,pl,Rd}^{inf}$	kNm	807	431
$M_{C,pl,Rd}^{sup}$	kNm	807	431
γ_{Rd}	-	1.1	1.1
$\gamma_{Rd}\Sigma M_{B,pl,Rd}$	kNm	816.4	816.4
$\Sigma M_{C,pl,Rd}$	kNm	1613	862
SF	-	1.98	1.06

4.2 The steel building

The same building previously analyzed was designed adopting MRF with steel columns and beams, not realizing the collaboration of the RC slab. In this case the design was carried out using the software Edilus of ACCA Software. The floor is the same type used for the composite building, i.e. realized with profiled steel sheeting.

In Figure 16 and 17 the typical plan and the 3D structural model, with rigid joints, are depicted; the design procedure give the sections summarized in Table 25.

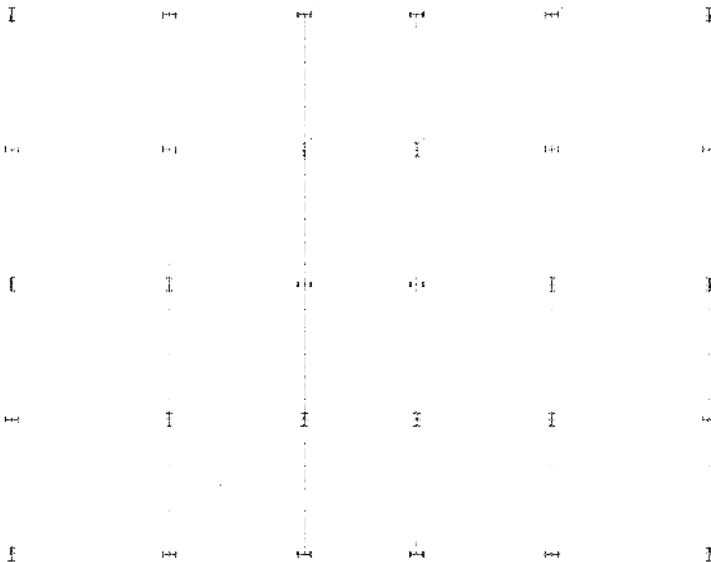


Figure 16. Typical plan of the steel building.

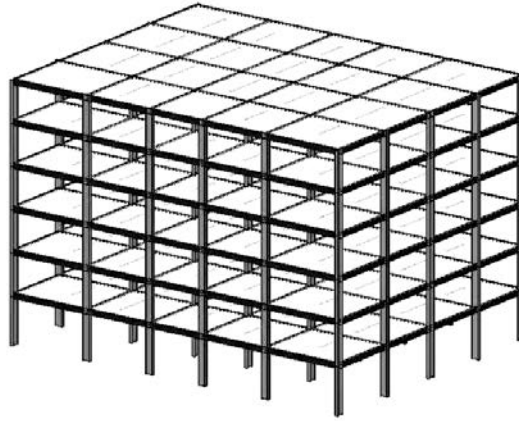


Figure 17. 3D model of the steel building.

This solution is unusual for steel structures that usually are braced or the frames are realized with hollow (circular or square) or crossed double T (Austrian cross) profiles in order to respect the hierarchy and the SLD verification.

An alternative choice is to consider as seismic resistant only the frames with the profiles oriented along the strong axis and the others are considered as cantilevers with hinged beams active only for bearing the vertical loads. In this last case the beam-column joint for bending is realized only with the connection of the steel beam to the flanges of the columns, according the type previously introduced that can assure the respect of the hierarchy.

Table 25. Sections of the steel elements.

	Beams	Columns
Sections	IPE450	HE600M

4.3 The RC building

The RC building (Figure 18) was designed using the software Edilus of ACCA Software. The columns were oriented in order to have about the same stiffness and strength along the two principal directions; the floor is a typical lightened RC floor (25cm thick) that assures a rigid in plane behavior in order to distribute the seismic action to the resistant elements according their stiffness. In Table 26 the load analysis is reported; in Figure 20 the 3D model is depicted.

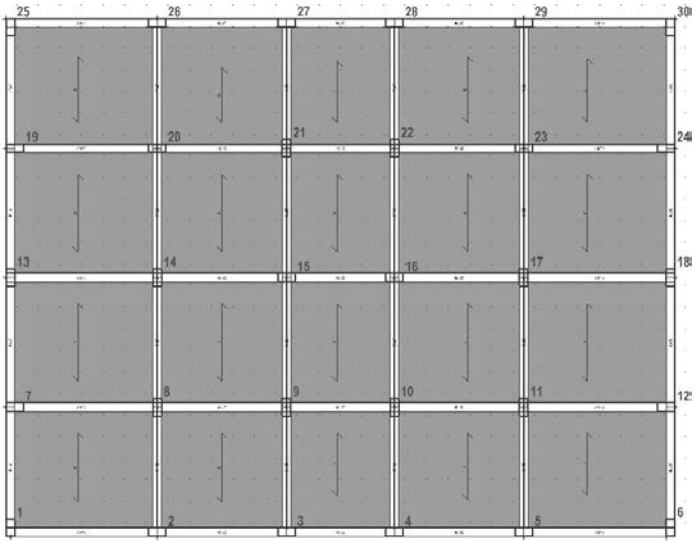


Figure 18. Plano f the RC building.

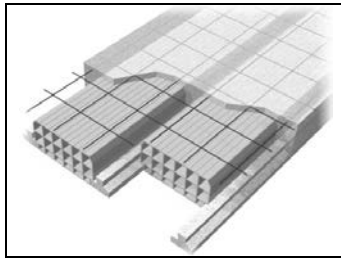


Figure 19. Type of RC floor.

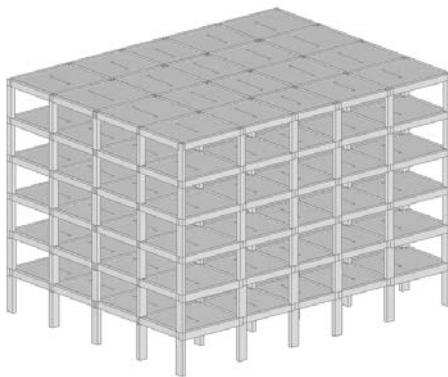


Figure 20. 3D Model.

Table 26. Load analysis of the floor.

Intermediate floor						
dead structural loads G_{1k}						
	Length	N° elements	H	Width 2	γ material [kN/m]	G_{1k} [kN/m ²]
Joist	0.1	2	0.2	1	25	1
Slab	1	-	0.05	1	25	1.25
Brick	0.4	2	0.2	1	8	1.28
3.53						
dead non structural loads G_{2k}						
	Width		H		γ material [kN/m]	G_{2k} [kN/m ²]
Screed	1		0.05		18	0.9
Pavement	1		0.02		27	0.54
Plaster	1		0.02		18	0.36
Partitions						0.8
2.6						
live load	Q_k [kN/m²]=3					
Roof floor						
Dead structural loads G_{1k}						
	Length 1	N° elements	H	Width 2	γ material [kN/m]	G_{1k} [kN/m ²]
Joist	0.1	2	0.2	1	25	1
Slab	1		0.05	1	25	1.25
Brick	0.4	2	0.2	1	8	1.28
3.53						
Dead non structural loads G_{2k}						
	Length 1		H	Width 2	γ material [kN/m]	G_{2k} [kN/m ²]
Plaster	1		0.02	1	18	0.36
Screed	1		0.1	1	18	1.8
			N° a m ²			
Thermal insulation			0.02	2	0.1	0.004
2.16						

The design of steel reinforcement was carried out according to the provisions of NTC2008; the dimensions of the elements vary along the height for optimizing the result.

In particular, the columns sections were dimensioned with a percentage of reinforcement of approximately 2% (the code indicate a range of 1%-4%), that is a little greater at the lower floors. The dimensions of the elements are listed in the following:

COLUMNS:

Floors 1 and 2: 40x80cm;

Floors 3 and 4: 40x70cm;

Floors 5 and 6: 40x60cm.

BEAMS:

Floors 1 and 2: 40x70cm for the beams 7m long and 40x60cm for the others;

Floors 3, 4, 5 and 6: 40x60cm.

In Table 27 the reinforcement percentages are summarized:

Table 27. Reinforcement percentages.

Floor	Column	b [mm]	H [mm]	A _c [mm ²]	φ [mm]	A _s [mm ²]	n°	%A _s
P1	14-17	400	800	320000	12	113	0	2.14
					16	201	34	
P2	14-17	400	800	320000	12	113	0	2.14
					16	201	34	
P3	14-17	400	700	280000	12	113	0	1.87
					16	201	26	
P4	14-17	400	700	280000	12	113	0	1.87
					16	201	26	
P5	8-11-14-17	400	600	240000	12	113	0	1.67
					16	201	20	
P6	8-11-14-17	400	600	240000	12	113	0	1.67
					16	201	20	

4.4 Discussion of the 3 buildings

The comparison between the 3 solutions for the same building (composite, steel and RC) can be focalized on the discussion of the safety factors (SF) of the columns, the verification at SLD and the structural weights, but also an economic analysis is interesting.

The safety factor $SF=R/S>1$ is the ratio of the strength, R, to the stress, S, thus the structure can be considered safe when it is greater than 1. The values of SF indicate the efficiency of the design procedure and the measure of the overstrength; if SF is much greater than 1 the element was clearly over dimensioned. However, it is not easy to evaluate the efficiency of the design because there are global capacity and demand but, thus only some observations are highlighted. In Table 28 the SF of the columns of one typical frame for each type of building are summarized.

The values of SF are particularly high only for the composite building; this is due to the application of the beam-column hierarchy conditioned by the great strength of the composite beam under sagging moment (great effect of the RC slab).

In Table 29 the displacements of an external column (number 1) at the SLD (δ_{rel}) are reported and compared with the code limit, $\delta_{rel,max}$.

Table 28. Values of SF for one frame of each type of building.

Column	Floor					
	P1	P2	P3	P4	P5	P6
RC building						
1	1.05	1.47	1.21	1.38	1.49	1.77
2	1.03	1.17	1.09	1.21	1.39	2.2
3	1.05	1.37	1.12	1.02	1.21	2.16
4	1.05	1.37	1.12	1.02	1.21	2.16
5	1.03	1.17	1.09	1.21	1.39	2.2
6	1.05	1.47	1.21	1.38	1.49	1.77
Steel building						
19	1.94	1.01	1.32	1.39	1.89	2.03
20	2.04	1.04	1.34	1.45	2.03	2.18
21	1.84	1.07	1.33	1.44	2.02	2.09
22	1.84	1.07	1.33	1.44	2.02	2.09
23	2.04	1.04	1.34	1.45	2.03	2.18
24	1.94	1.01	1.32	1.39	1.55	1.67
Steel-concrete composite building						
1	1.91	2.80	3.35	6.17	8.16	8.57
2	1.81	2.91	3.50	2.52	3.47	6.86
3	1.82	2.80	3.35	2.43	3.29	6.58
4	1.83	2.80	3.35	2.43	3.29	6.58
5	1.82	2.91	3.50	2.52	3.47	6.86
6	1.91	2.80	3.35	6.17	8.16	8.57

Table 29. Displacements at SLD.

Floor	δ_{rel} (cm)			$\delta_{rel,max}$ (cm) limit
	RC	Steel	Composite	
1	0.54	1.00	1.58	2
2	0.57	1.51	1.60	1.75
3	0.57	1.52	1.37	1.75
4	0.46	1.32	1.09	1.75
5	0.35	1.07	0.77	1.75
6	0.21	0.87	0.42	1.75

The relative displacement occurs in the composite building, not much higher than the ones in the steel building, therefore the SLD verification governs the design of composite building but not the design of steel and RC buildings. In Table 30 the structural masses are summarized.

Table 30.

RC building			
		Density	Mass
RC floor s=25cm	4190 m ²	353 kg/m ²	1479070 kg
RC reinforcement type B450C	-	-	132406 kg
concrete C25/30	799 m ³	2300 kg/m ³	1836826 kg
		M_{tot}	3448302 kg
			3448 t
Steel building			
		density	Mass
Composite floor	4190 m ²	240 kg/m ²	1005600 kg
Steel profiles for beams and columns	-	-	370489 kg
Nelson Studs	800	0.14 kg/m ³	112 kg
		M_{tot}	1376201kg
			1376 t
Composite building			
		density	Mass
Composite floor	4190 m ²	240 kg/m ²	1005600 kg
Steel profiles for beams and columns	-	-	258118 kg
Nelson studs	10584	0.14 kg/m ³	1482 kg
concrete C25/30	68.86 m ³	2300 kg/m ³	158378 kg
RC reinforcement type B450C	-	-	3289 kg
		M_{tot}	1426867 kg
			1426.9 t

The RC building has a mass more than double of the composite and steel buildings that have a similar mass, the composite one is a little bit higher than the steel one.

The constructions costs (only the materials were considered without excavations, forms, etc. of the 3 structures were estimated using the list of costs for year 2015 indicated by the region where are located the buildings.

In Table 31 the quantities and costs of the 3 buildings are compared.

The analysis of materials costs indicates the RC building as the most convenient, but the composite one is less expensive of the steel one; assuming the composite building as the reference one, the cost of materials is 37% lower for the RC building and 64% higher for the steel building.

It is clear that further costs would be considered that are necessary for the construction (transportation, forms, foundations, ecc...) therefore the actual differences are smaller; anyway the steel MRFs building is clearly not convenient conversely the composite MRFs building could result competitive with the RC one especially introducing the reduction of the construction time and considering the smaller dimensions of the structural elements.

Table 31. Costs of the structure for the 3 buildings.

RC building				
	U.M.	quantity	price [€/U.M.]	Cost [€]
Concrete ... - Class C 25/30	m ³	798.62	130.56	104267.83
RC steel B450C ...	Kg	132406.12	1.43	189340.75
RC floor lighthened by hollow bricks, ... total thickness 25 cm	m ²	3985.62	56.91	226821.63
TOTAL				520430
Steel building				
	U.M.	quantity	price [€/U.M.]	Cost [€]
Steel profiles for beams and columns series IPE, HEA, HEB, HEM, ...	Kg	370489	3.04	1126286.6
Composite floors comprehensive of hangs, welds, cut, ... steel sheeting 8/10 mm thick	m ²	4190	53.53	224290.7
Steel stud connector zinc coated, diameter 19mm and height 80mm with head, ...	One	650	2.06	1339
TOTAL				1351916
Composite building				
	U.M.	quantity	price [€/U.M.]	Cost [€]
Composite floors comprehensive of hangs, welds, cut, ... steel sheeting 8/10 mm thick	m ²	4190.00	53.53	224290.70
Steel stud connector zinc coated, diameter 19mm and height 80mm with head, ...	cad.	13800	2.06	28428
Steel profiles for beams and columns series IPE, HEA, HEB, HEM, ...	kg	184116	3.04	559712.34
Concrete ... - Class C 25/30	m ³	68.86	130.56	8989.84
RC steel B450C ...	kg	3289	1.43	4703
TOTAL				826124

5 CONCLUSIONS

The numerical examples developed for the plane frames allowed to define in detail the procedure for designing steel-composite MRFs buildings according to Italian and European code that require the application of shear-bending and beam-column-joint hierarchy. Furthermore, the details of beam-column bolted joints were defined both for composite MRF system and CBF system realized by steel columns and composite beams; in this last case the joint doesn't transmit the slab stresses to the column allowing to use the composite beam only for vertical loads.

The results of the design of plane frames and entire buildings underlined many interesting aspects:

- the effective width defined by the codes is different under vertical and seismic loads, but when the combinations of the loads have to be considered the provisions referring to the seismic load can be applied;
- the design of steel-concrete MRFs is strongly influenced by the rules of seismic design according Italian and European codes especially for the beam-column hierarchy,

therefore the comparison of the 3 frames designed for different earthquake intensities (design seismic zone) showed few differences;

- the comparison of MRF and CBF systems evidences the convenience of the braced solution with steel columns and composite beams especially if the partially encased column is used for the composite frame;
- the comparison of the steel, RC and composite buildings realized with MRFs points out the less expensive in terms of materials is the RC one, but the steel-concrete composite one appears competitive especially considering the possible reduction of the construction time and the smaller dimensions of the elements; conversely the MRFs solution is surely more onerous for steel structures.

In conclusion the design procedure for steel-concrete composite buildings realized with MRFs has completely explained and applied, but also details for using the composite beam in CBFs has been proposed.

6 ACKNOWLEDGEMENTS

DPC-RELUIS 2014-2016 is gratefully acknowledged for funding the research activity.

7 REFERENCES

- Amadio C., Pecce M., Fasan M., Logorano G. (2016). "Linee guida per la progettazione sismica di strutture intelaiate composte acciaio - calcestruzzo e l'analisi non lineare", *ReLUIs*, Napoli.
- Aribert J-M, Ciutina AL, Dubina D. (2006). "Seismic response of composite structures including actual behaviour of beam-to-column joints", *Composite construction in steel and concrete V. ASCE*.
- Braconi A, Bursi OS, Fabbrocino G, Salvatore W, Tremblay R. (2008). "Seismic performance of a 3D full-scale high-ductility steel-concrete composite moment-resisting structure. Part I: Design and testing procedure", *Earthq Eng Struct Dyn*, 37:1609-34.
- Braconi A, Bursi OS, Fabbrocino G, Salvatore W, Taucer F, Tremblay R. (2008). "Seismic performance of a 3D full-scale high-ductility steel-concrete composite moment-resisting structure. Part II: Test results and analytical validation", *Earthq Eng Struct Dyn*, 37:1635-55.
- Bursi OS, Gramola G. (2000). "Behaviour of composite substructures with full and partial shear connection under quasi-static cyclic and pseudo-dynamic displacements", *Mater Struct/Mater Construct*, 33:154-63.
- CEN, European Committee for Standardization. (2005a). "Eurocode 3: Design of steel structures - Part 1-8: Design of joints", EN 1993-1-8.
- CEN, European Committee for Standardization. (2005b). "Eurocode 4: Design of composite steel and concrete structures - Part 1-1: General rules and rules for buildings, EN 1994-1-1.
- CEN, European Committee for Standardization. (2013). "Eurocode 8: Design of structures for earthquake resistance - Part 1: General rules, seismic actions and rules for buildings", EN 1998-1.
- Circolare 2 febbraio 2009 n. 617 del Ministero delle Infrastrutture e dei Trasporti (G.U. 26 febbraio 2009 n. 27 - Suppl. Ord.) "Istruzioni per l'applicazione delle 'Norme Tecniche delle Costruzioni' di cui al D.M. 14 gennaio 2008".
- D. M. Infrastrutture Trasporti 14 gennaio 2008 (G.U. 4 febbraio 2008 n. 29 - Suppl. Ord.) "Norme tecniche per le Costruzioni".
- D'Aniello, M., Landolfo, R., Piluso, V., Rizzano, G. (2012) "Ultimate behavior of steel beams under non-uniform bending", *Journal of Constructional Steel Research*, 78, pp. 144-158.
- Thermou GE, Elnashai AS, Plumier A, Doneux C. (2004). "Seismic design and performance of composite frames", *J Constr Steel Res*, 60:31-57.

SECTION 4

CONVENTIONAL ONE-STOREY BUILDINGS

SEISMIC VULNERABILITY ANALYSIS OF SINGLE-STOREY INDUSTRIAL BUILDINGS

Francesco Morelli ^a, Raffaele Laguardia ^b, Andrea Piscini ^a, Marco Faggella ^b,
Rosario Gigliotti ^b, Walter Salvatore ^a

^a *Department of Civil and Industrial Engineering, University of Pisa, Pisa, Italy,
francesco.morelli@dic.unipi.it, andrea.piscini@ing.unipi.it, walter@ing.unipi.it*

^b *Sapienza University of Rome, Via Eudossiana 18,
raffaele.laguardia@uniroma1.it, marco.faggella@uniroma1.it, rosario.gigliotti@uniroma1.it*

ABSTRACT

Evaluation of seismic vulnerability of industrial constructions is a more and more relevant issue considering the damage occurred as consequence of recent earthquakes all over the world. Each industrial construction, on the other hand, has its own peculiarities depending on, for example, age of constructions and aging, hosted industrial activities, structural and morphological during its lifetime, and so on. In the present work the seismic assessment of an existing industrial steel structure, characterized by a large mass placed at relevant altitude, is executed through several Incremental Dynamic Analyses. To this purpose, a refined nonlinear model of the structure was developed, taking into account the most relevant aspects such as II order effects, global buckling of the elements, mechanical nonlinearities, etc. Finally, the influence of the ground motions scaling methods on the global seismic assessment is evaluated analyzing and comparing the results obtained through several possible methods.

KEYWORDS

steel industrial building, seismic assessment, ground motions selection, scaling criteria.

1 INTRODUCTION

Industrial facilities often store a large amount of hazardous material and the probability that accidental scenarios such as fire, explosion, toxic or radioactive dispersion may occur in the case of seismic event is very high. The ensuing disaster is sure to harm the people working in the installation and it may endanger the population living in the neighbourhood or in the urban area where the industrial installation is located.

For this class of structures it is very common that the overall geometry and the elements configuration are usually more influenced by operability issues than structural performances optimization. Consequently, depending on the industrial plant overall organization, a variety of geometrical configurations, structural resisting systems, element shapes and sizes can be often found. These aspects make the seismic evaluation and risk assessment of industrial buildings a quite complex task, which needs a different approach compared with risk assessment of residential and commercial buildings.

Several national and international standards and guidelines regulate the seismic design of industrial structures, such as ASCE/SEI 7-05 (2013), ASCE/SEI 43-05 (2005) (Nuclear facilities), FERC (2015) (Liquified Natural Gas facilities), API 620 (2009) and API 650 (2007) (Storage Tanks), EN 1998-4 (2007) (Silos, tanks and pipelines), EN 1998-6 (2007) (Towers, piles and chimneys). Such international codes define rules for performance assessment at the component level, for checking/comparing member demand with capacity through a classical Performance Based Earthquake Engineering (PBEE) approach. These codes also prescribe methods of nonlinear analysis, both static and dynamic, and rules for Response History Analysis (RHA) and Ground Motions (GMs) selection. A comprehensive review of NonLinear Response History Analysis (NL RHA) code procedures for different types of structures is carried out in the NIST document (NIST 2011). In general, the different seismic design codes foresee a reference spectrum, indicate the number of GMs needed to execute NL RHA and rules to perform spectrum matching of GMs and reference spectrum. The general requirement is to use 7 different GMs and to process results in terms of best estimates, or to use 3 different GMs and the maximum response values. Reference spectra are commonly derived from Uniform Hazard Spectra (UHS) obtained through a Probabilistic Seismic Hazard Analysis (PSHA) at the facility site. In recent years, traditional PBEE approaches oriented to component check/design are being complemented with novel analysis methods with a broader focus on risk/loss assessment (Hamburger, 2003; Moehle and Deierlein, 2004). To this purpose the Pacific Earthquake Engineering Research center (PEER) developed a new methodology, tested on several building structures and culminated in the release of the FEMA P-58 guidelines. Although initially intended to and benchmarked on building structures, the FEMA P-58 can be considered as a general and comprehensive reference framework to perform seismic risk/loss assessment. In FEMA P-58 the seismic hazard is defined in terms of Uniform Hazard Spectrum or, alternatively, in terms of Conditional Mean Spectrum (CMS) (Baker, 2011) and Conditional Spectrum (CS) (Lin *et al.*, 2013). The use of CMS and CS stems from the consideration that the coherence of GMs with UHS can be over-conservative and not realistic, with important implications both for design/assessment and risk analysis, since it is very unlikely that in a single event the spectral ordinates of the UHS are observed at all periods, especially for rare events.

A further important issue linked to a more robust representation of the seismic action when performing NL RHA is the selection of an Intensity Measure (IM) in conjunction with choice of a proper scaling criterion of the input ground motions, as observed by Faggella *et al.*, 2013 and Luco *et al.*, 2005. In the PEER PBEE and FEMA P-58 methodologies, the spectral ordinate $S_a(T_1)$ of the ground acceleration component in the direction of the fundamental mode with period T_1 on the uniform hazard spectrum is suggested as a commonly accepted optimal Intensity Measure for a suite of records. This scaling criterion has also been extended for use in the analysis of 3D structures, with the same scaling applied to all three seismic input components. The studies of Faggella *et al.*, 2013 and Luco *et al.* 2005 raised concern regarding the adequacy of such an assumption for 3-D analysis of structures, and this can be particularly significant for structures characterized by different resisting systems in the two directions. Thus, even though there has been significant research on ground motion selection and scaling (Baker and Cornell, 2006; Hancock *et al.* 2008; Faggella *et al.* 2016; Kohrangi *et al.* 2016a, b, c), the application of PBEE to complex 3-D structural models and analyses for multi-component ground motion excitations, such as the one analyzed described in this paper, deserves further attention.

The main objective of this work is to highlight aspects of seismic vulnerability assessment of a complex 3D industrial steel structure characterized by very different behaviors in the two horizontal directions. Two main aspects are analyzed: the ground motion recordings scaling

criteria and the assessment of the main vulnerability sources. The complete results of such work are detailed analyzed in Morelli *et al.*, 2017 and Morelli *et al.*, 2017b, where are described also a possible retrofit intervention adopting self-centering hysteretic devices and the results obtained adopting a Conditional Mean Spectrum coherent set of ground motions.

To this ends, first, the seismic vulnerability assessment is carried out adopting a UHS based ground motions set, highlighting the main results of the vulnerability assessment.

Then the results of NL RHA with several GM sets obtained with different scaling criteria and different reference spectra are presented and compared with focus on the efficiency and sufficiency of the IMs adopted for scaling. The Efficiency and sufficiency are intended as proposed by Luco and Cornell, 2007, in other words, an efficient IM is one that, once its value is fixed, results in low variability of significant Engineering Demand Parameters (EDPs) such as maximum displacements, maximum storey drift ratio and maximum base shear. A sufficient IM is one that renders the EDP conditionally statistically independent of other IMs (different than the one assumed for scaling). The results obtained, even if related to a specific case study, highlight important aspects of seismic vulnerability of industrial structures and the GM scaling methods effectiveness when dealing with the NL RHA of 3D buildings characterized by a significantly different behavior in the two horizontal directions.

2 CASE STUDY DESCRIPTION

The building analyzed within this work is characterized by a large mass placed at high altitude and different typologies of horizontal forces resisting systems (see Figure 1). It has the function of filtering the gasses coming from the steelwork and can be schematized as made up of a supporting structure, the silos containing the filtered material and the roof.

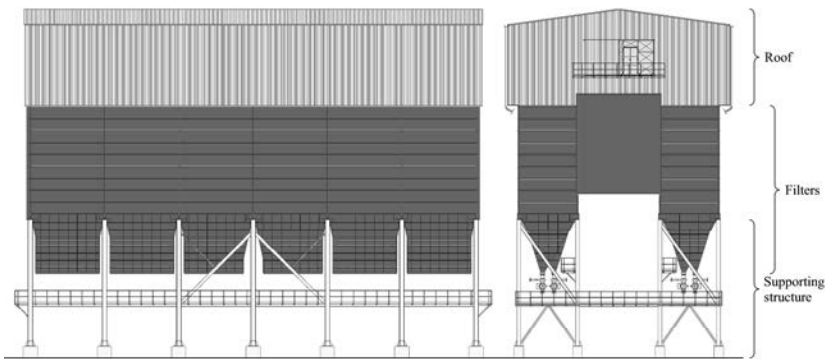


Figure 1. Front (left) and lateral (right) view of the case study.

The building has a regular plan, with overall dimensions 37.80 m x 16.94 m and total height 29.64m. The supporting structure, with a total height of about 10.80 m, has six bays in the longitudinal direction and three in the transversal one. As is typical of industrial buildings, where the functionality issues often prevaricate the rules for an optimized structural design, different horizontal resisting systems (Figure 2) can be individuated such as moment resisting frames (X direction - ground floor), inverted V bracings (Y direction - ground floor) and diagonal bracings (X and Y directions - first floors).

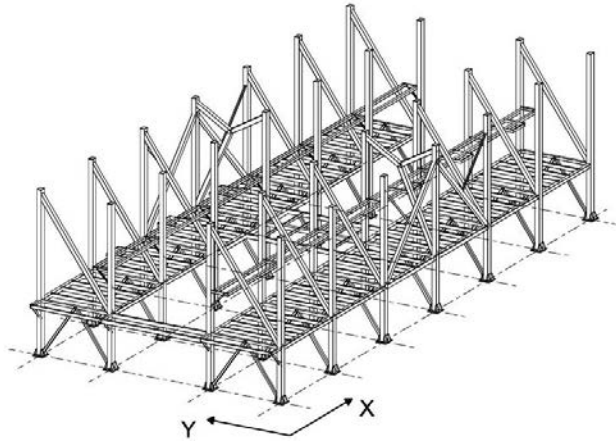


Figure 2. 3D view of the supporting system.

The silos are realized with thin (4 mm) walls stiffened with a close series of horizontal UPN and vertical HEA profiles. The total mass of the silo (23700 kN), considering the structural elements and the infill material, represents the 86% of the total mass (27650 kN).

The roof is connected directly to the filter walls and its contribution is considered only in terms of vertical load and mass.

2.1 Linear and non linear modelling

A preliminary comparison between a full-comprehensive linear model (Figure 3a) and a geometrically-simplified (Figure 4) model was carried out given the need to simplify the structural scheme to obtain a reliable and time-saving nonlinear model. The infill material was modelled as five different lumped masses connected to the silo wall by elastic springs (figure 4b), whose stiffness was evaluated on the base of the edometric modulus of the infill material.

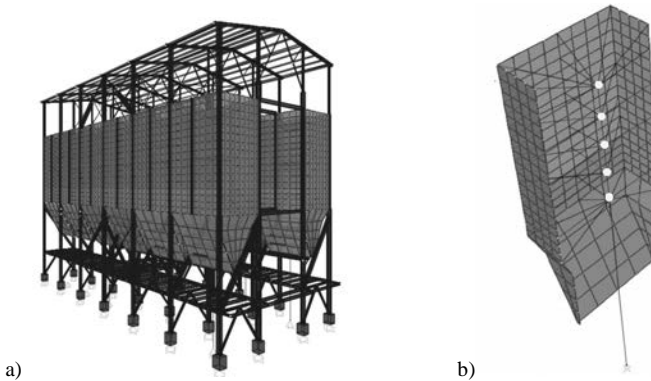


Figure 3. "Complete" linear model: a) global view; b) modelling of the infill-silo interaction.

The "complete" linear model highlighted a structural behavior similar to that of a single degree of freedom, where the great part of the displacement demand is located in the supporting structure. The silos and the roof acted as a rigid body and the resultant stresses were far below the yielding or buckling threshold. It was therefore assumed that the structural

behavior could be represented by the simplified model shown in figure 5, where the roof was considered simply as dead load and mass, while the silos were substituted by an elastic trusses system, whose characteristics were evaluated to obtain the same first period and modal shape of the "complete" model.

In the simplified model, used to perform nonlinear analyses, each frame was modelled, in OpenSEES (Mazzoni *et al.*, 2007) using fiber elements and the material was assumed to be elasto-plastic, see figures 6b and 6c. The global second-order effects were explicitly taken into account. The bracings were modelled introducing an initial local bow imperfection, e_0 , equal to $L/300$, where L is the length of the bracing, following the indications of Eurocode 3 in order to consider their post-critic behavior when subjected to compression forces, see Figure 5. The viscous damping is taken into account introducing a damping ratio associated to the first and second vibrating modes equal to 2%.

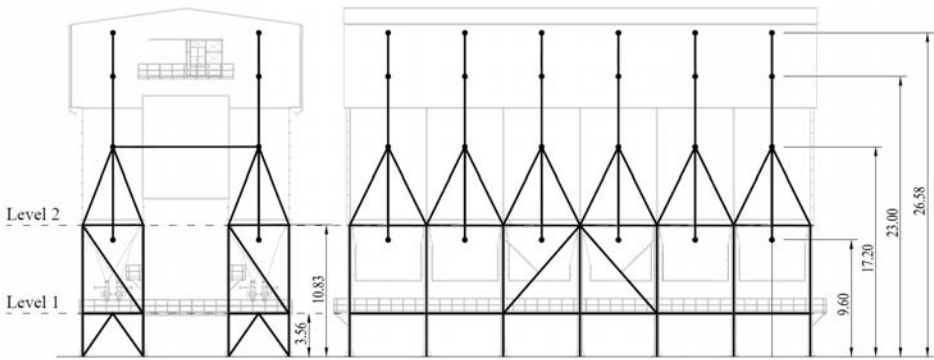


Figure 4. Case study simplified model geometry

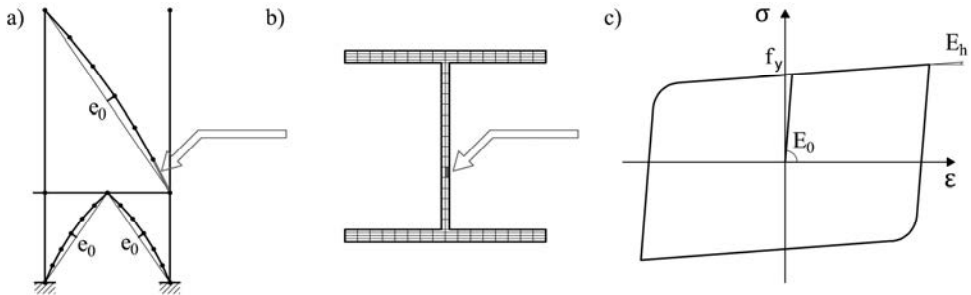


Figure 5. Scheme of a braced frame modelling: a) bracings initial bow imperfection; b) subdivision of section into fibers; c) elasto-plastic stress-strain relationship (OpenSEES Steel02 material) associated to each fiber.

The building performances in its current, un-retrofitted, state were evaluated using both nonlinear static and Incremental Dynamic Analyses. For the latter, three different Engineering Demand Parameters, EDPs, were evaluated:

1. maximum displacements evaluated at levels 1 and 2 (Figure 4);
2. residual deformations evaluated at levels 1 and 2 (Figure 4);
3. seismic energy components.

In particular, four type of seismic energy components were analyzed: *i*) input energy, defined as the energy transmitted by the ground movement to the structure; *ii*) kinetic energy, related to the building velocity; *iii*) adsorbed (elastic strain + dissipated) energy, related to the damaging of the structure; *iv*) viscous energy.

3 SELECTION OF GROUND MOTIONS FOR THE NL RHA

The case study was analyzed carrying out several non linear analyses adopting:

- 9 scaling factors for the vulnerability assessment. This set of analysis will be in the following referred as IDA.
- 2 scaling factors for the assessment of the scaling method influence. This set of analysis will be in the following referred as NL RHA.

All the non linear analyses of the case study structure were performed using a set of 11 GMs selected for an Italian high seismicity zone, the site of Reggio Calabria. The set is coherent with the spectral shape of UHS. The set is composed by 11 records, instead of 7 records strictly required for design purposes, in order to obtain a larger sample to perform statistical analyses. The reference spectrum is matched with the GeoMean spectrum of the two orthogonal GM components, ensuring that the mean spectral ordinates of each set are never less than 90% of reference spectrum in the period range between 0 sec and 2 sec, consistent with the spectrum-matching requirements of Eurocode 8 (§3.2.3.1).

The reference spectrum chosen was the Italian code NTC08 Design Spectrum computed for Reggio Calabria (Lat 38.111, Long 15.647), with Soil C, reference period $VR=100$ years and a Probability of Exceedance (PoE) 10%, which corresponds to a return period of 949 years. Such spectrum represents the uniform hazard condition desired, even if it is expressed through a conventional shape. GMs were selected in accordance with Magnitude-distance (M-R) hazard deaggregation in the range of $6 < Mw < 8$ and $0 < R[km] < 40$. The selected GMs are listed in Table 1, the GeoMean, longitudinal and transversal components spectra are shown in Figure 6 and the scale factor used for the execution of the seismic vulnerability assessment through the IDA are listed in Table 2.

Table 1. UHS coherent set. GMs characteristics.

Tag	Earthquake Name	Mw	Fault Mechanism	R(kM)	Site Class	Date
UHS1	South Iceland	6.40	strike slip	5	A	2000
UHS2	Montenegro	6.90	thrust	25	B	1979
UHS3	Erzincan	6.60	strike slip	13	B	1992
UHS4	Gazli	6.70	thrust	11	D	1976
UHS5	Izmit	7.60	strike slip	20	C	1999
UHS6	South Iceland	6.50	strike slip	5.25	A	2000
UHS7	Duzce	7.10	strike-slip	5.27	C	1999
UHS8	Darfield	7.10	strike-slip	17.82	C*	2010
UHS9	Imperial Valley	6.50	strike-slip	27.03	C	1979
UHS10	Loma Prieta	6.90	oblique	7.1	B	1989
UHS11	Northridge	6.70	reverse	20.25	C	1994

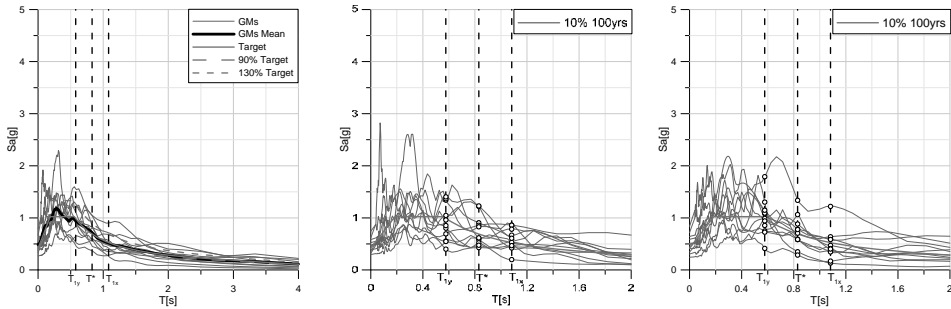


Figure 6. Set UHS coherent. Unscaled GeoMean (left), Longitudinal (center) and Transversal (right) components

Table 2. Scaling factors used for the execution of the seismic vulnerability assessment through the IDA.

Reggio Calabria					
V_r	P_{vr}	T_r	a_g	S.F.	
years	%	years	g		
1	100	4%	2450	0,5120	1,430
2	100	5%	1950	0,4687	1,307
3	100	10%	949	0,3586	1,000
4	100	22%	402	0,2502	0,698
5	100	30%	280	0,2122	0,592
6	100	39%	202	0,1829	0,510
7	100	50%	144	0,1552	0,433
8	100	63%	101	0,1292	0,360
9	100	81%	60	0,0987	0,275

3.1 Scaling techniques

In order to reduce the dispersion of the EDPs obtained through NL RHA, it could be necessary to scale the ground motions in order to reduce the dispersion of the IM that influences the most the structural response. This operation can be performed in several ways and, to date, there is no unique and recognized method in international codes and literature. The selection of the scaling technique should be made on the basis of the structure characteristics, in particular through the selection of IMs that most influence the EDPs, and must be consistent with the GMs selection criteria and seismic action definition.

For the case study analyzed herein, the structural configuration shows that the building resisting system is strongly different in the two orthogonal directions and, given the overall geometrical organization, it is expected that the structural mass is excited mainly by the first two modal shapes, one for each direction.

The choice of the scaling technique should, on one hand, accurately reflect the three-dimensional behavior of the building, so to obtain a realistic 3D global response. On the other hand, it should be considered that the behavior of the building in one direction can strongly affect the global response.

For these reasons, different scaling techniques, adapted and calibrated for the two different GM selections methods, were studied, in particular:

- "Unscaled". The GMs set were applied as they are with no further scaling (see Figure 6).
- Scaled on the spectral acceleration, $S_a(T_{1x})$, associated to the first modal shape in the X direction.
- Scaled on the spectral acceleration, $S_a(T_{1y})$, associated to the first modal shape in the Y direction.
- Scaled on the spectral ordinate of the average X-Y period $S_a(T^*)$, see eq. (1).

The longitudinal component of each GM spectrum was scaled to the chosen IM. The associated spectra, for both directions, are shown in Figure 7, Figure 8 and Figure 9. When the GM set was scaled to $S_a(T_{1x})$, $S_a(T_{1y})$ and $S_a(T^*)$, the orthogonal component was scaled applying the same scale factor. This method has as the advantage that the chosen IM represents exactly the desired spectral accelerations for the desired hazard level and the dispersion of set around these IMs is strongly reduced. On the other hand, the dispersion of spectral accelerations in the other direction is quite high for all the spectral ordinates and the coherence with the reference spectrum is not controlled (Figure 7-9 (right)).

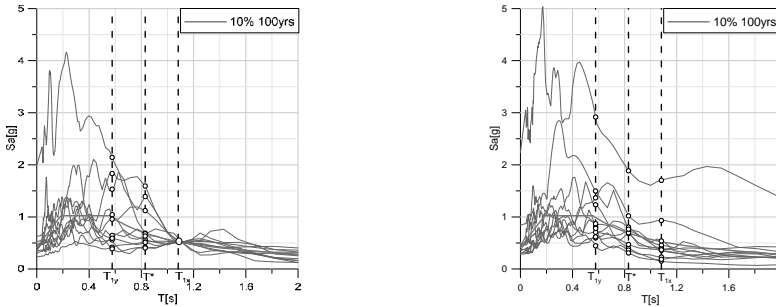


Figure 7. Set UHS scaled to $S_a(T_{1x})$. Longitudinal (left) and Transversal (right) components.

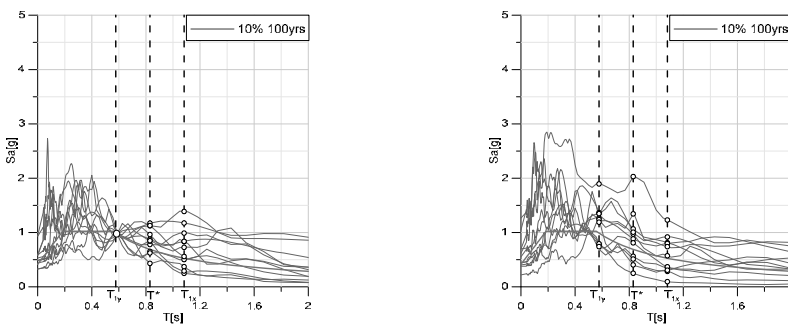


Figure 8. Set UHS scaled to $S_a(T_{1y})$. Longitudinal (left) and Transversal (right) components.

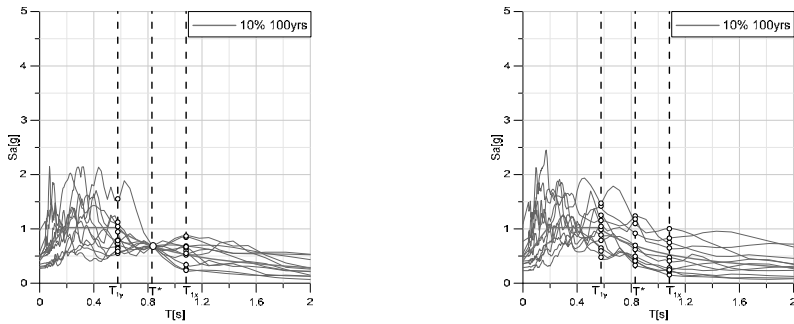


Figure 9. Set UHS scaled to $Sa(T^*)$. Longitudinal (left) and Transversal (right) components.

4 SEISMIC VULNERABILITY OF THE CASE STUDY IN THE CURRENT STATE

The seismic vulnerability of the case study is studied through the non linear static (pushover) and incremental dynamic analyses (IDAs). For the latter the unscaled GM of Figure 6 and the scale factors of Table 2 were used.

4.1 Static nonlinear analyses results

The capacity curves reported in Figure 10 clearly point out the different behavior of the structure in the two horizontal directions. A uniform acceleration force distribution is adopted and the control point is assumed to be the center of level 2.

In the X direction the structure is more flexible than in the Y direction and post-yielding behavior is governed mainly by the flexural deformations of the moment resisting frames at ground and first floor. At this level, indeed, the few concentric braces are not capable to influence the overall behavior. The capacity curve shows a ductile behavior with a smooth transition between the elastic and the plastic ranges and a softening post-yielding behavior. This is mainly due to second order effects. In the Y direction, the behavior is completely different and the ductility is limited due to the buckling of the inverted V diagonal bracings, causing a drastic drop of the global force after reaching the maximum strength. The collapse mechanism is thus characterized by the formation of a soft-storey at the ground level, while the first floor remains substantially elastic.

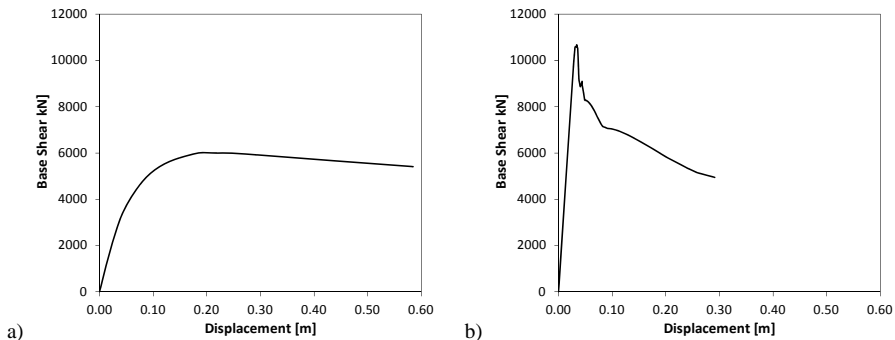


Figure 10. Pushover curves associated to the uniform acceleration distribution in the a) X direction and b) Y directions.

The structural performances associated to the Damage limitation Limit State (DLS) and to the Life-Safety Limit State (LLS) were evaluated plotting the capacity curves in the Acceleration-Displacement form together with the corresponding Acceleration-Displacement Response Spectra (ADRS). The performance points are evaluated through the bi-linearization method of the pushover curve proposed by Eurocode 8, represented in Figure 11. In the X direction, the structure experiences some limited plastic deformation for the seismic action associated to the DLS (PoE=50%), while it develops a complete plastic mechanism for the LLS (PoE=10%). For the DLS limit state the expected displacement, evaluated at level 2, is 8.3 cm while for the LLS it is 20.2 cm, corresponding respectively to drifts of 0.77% and 1.87%. In the Y direction, for the seismic action associated to the DLS, the structure reaches and passes the maximum strength and shows a displacement of about 3.7 cm (drift of 0.35%), highlighting that also for this limit states the bracings at ground floor start to buckle. For the LLS the estimated performance displacement is 6.2 cm (drift of 0.57%) and the associated force is the 75% of the maximum resistance, demonstrating that a significant number of bracings have buckled.

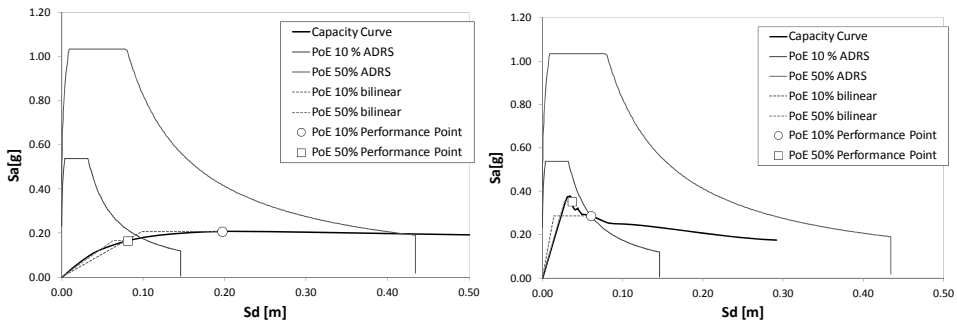


Figure 11. ADRS Pushover analysis and determination of performance points for PoE 10% and 50%.

4.2 IDAs results

Tha IDA results are expressed in terms of IDA curves (Figure 12 and Figure 13) where the Intensity Measure, IM, is quantified through the scale factors defined in Table 2, while the EDPs are registered at the two different level of the supporting structure.

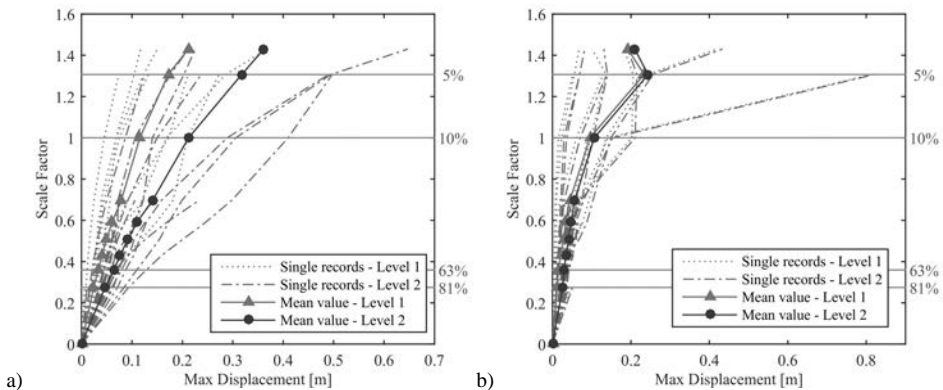


Figure 12. Maximum displacements (mean values) at different level in the a) X and b) Y directions.

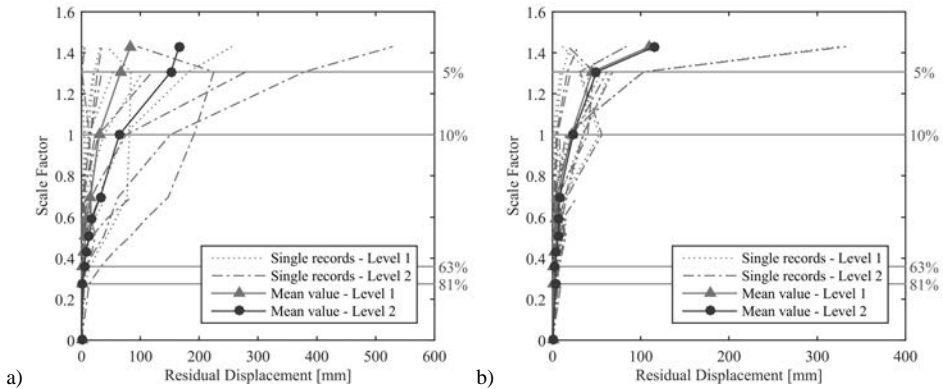


Figure 13. Residual displacements (mean values) at different level in the a) X and b) Y directions.

The analysis of IDA curves leads to conclusions similar to the one highlighted by the pushover analyses: in the X direction the displacement demand is equally distributed between the ground floor, where there are no bracings, and first one, where a low number of bracings are present. Equally, important residual displacements, evaluated as mean value of the displacements registered at the end of each time-history analysis, are evident at both levels.

In the Y direction, the displacement demand, both in terms of maximum and residual term, is concentrated at the ground floor, confirming the early plasticization of the inverted V bracings and the formation of a weak storey mechanism.

The presence of such residual displacements lowers considerably the resilience of the building, given the great difficulties in repairing a deformed and unstable structure.

Interesting information on the building behavior, especially in view of the retrofiting study and optimization, are supplied by the analysis of the input seismic energy transmitted by the earthquake to the structure and the stored and/or dissipated one. In Figure 14 an example of the energy time-histories recorded for the ground motion IN113A (the final "A" letter means that the main horizontal component is applied in the X direction) is reported considering two different scale factors. It can be observed that, for the low scale factor, the energy dissipation is due mainly to viscous damping phenomena, while, increasing the seismic action, the energy adsorbed by the structure, strictly related to the structural damage and to the residual displacements, represents the main component of the input energy.

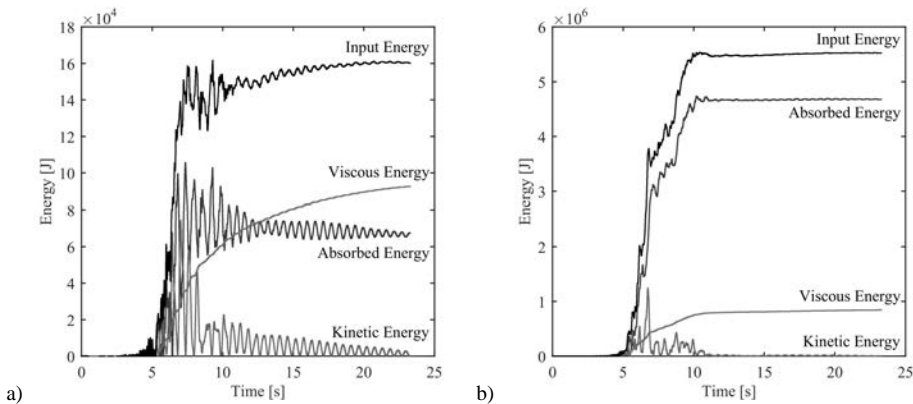


Figure 14. Energy time-histories for the IN113A GM recording: a) SF = 0.275; b) SF= 1.430.

Interesting results can be also obtained comparing the ratio between the adsorbed or the viscous energy and the input one for all the ground motions and scale factors considered, as shown in Figure 15. It can be noticed that, for all the ground motions, the ratio of the input energy dissipated by viscous phenomena tends to reduce as the scale factor increases, while the one dissipated by hysteresis increases. Both of them, for high levels of the seismic action, show asymptotic values, meaning that, after the complete collapse mechanism is developed, the ratio of the energy dissipated by the two phenomena tends to remain constant.

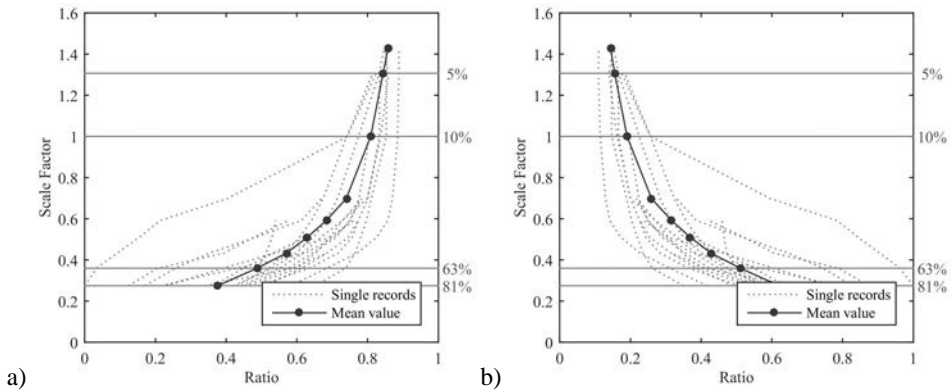


Figure 15. Ratios between: a) adsorbed and input energy; b) viscous and input energy.

5 INFLUENCE OF THE GROUND MOTION RECORDINGS SELECTION AND SCALING CRITERIA

The NL RHAs are performed applying the three acceleration components, two horizontals and one vertical, of each GM.

Table 3 summarizes the analyses performed for the evaluation of the seismic response under an earthquake with a PoE of 10% in 100 years (thus associated to the LLS). The same number and typology of analyses were performed for the evaluation of the building behavior associated to the Damage Limitation Limit State, DLS, (PoE 50%). To do so, all the GMs sets considered were scaled by a factor of 0.433, consistent with the hazard curve of the site.

Table 3. NL RHA performed for Hazard Level with PoE 10%.

GM selection	Scaling technique	Direction in which the likelihood of EDP is expected to be enhanced	Total number of analyses	Directional Concurrent Components
UHS	Unscaled	None	22	11 analyses GM long. comp. - building X dir. GM trans. comp. - building Y dir.
	Scaled on $S_a(T)$	Both directions	22	11 analyses GM long. comp. - building Y dir. GM trans. comp. - building X dir.
	Scaled on $S_a(T_{1x})$	X direction	11	11 analyses GM long. comp. - building X dir. GM trans. comp. - building Y dir.
	Scaled on $S_a(T_{1y})$	Y direction	11	11 analyses GM long. comp. - building Y dir. GM trans. comp. - building X dir.

The results of the NL RHA are represented in a base shear vs. maximum drift plot and are compared to the capacity curve obtained through the static nonlinear analyses. The maximum

drift is obtained dividing the maximum displacement recorded at level 2 by the height of the level (10.80 m).

It is worth noting that, for multi degree of freedom system, the maximum base shear, V_{max} , is not necessarily attained at the same instant of time at which the maximum drift d_{max} is reached, see Figure 16. This circumstance is particularly significant when the system is characterized by a marked softening behavior.

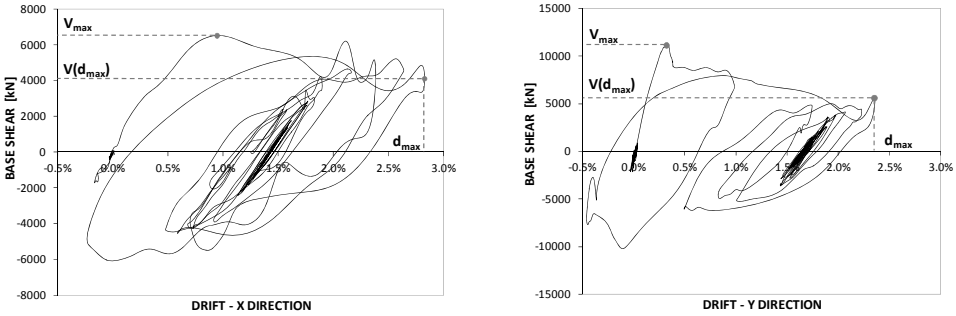


Figure 16. NL RHA results: comparison between the representation methods for the X (left) and Y directions (right).

The comparison of NL RHA with the pushover curve can therefore be represented mainly by two different approaches:

- displaying, for each NL RHA, a point representing the maximum values of the control point drift, d_{max} , and of the base shear, V_{max} , recorded during the analysis;
- displaying, for each NL RHA, a point representing the maximum value of the control point drift, d_{max} , and the associated base shear value, $V(d_{max})$.

The choice of one of the two methods of representation can be done on a case-by-case basis. For the sake of clarity, Figure 17 reports the pushover curves in the X and Y directions and the results of the NL RHAs represented with both the aforementioned methods. The representation of the maximum force is in good agreement with the pushover curve in the case of moderate softening, see Figure 17 (left). An even closer matching is expected in the case of hardening behavior. On the contrary, the representation of the base shear corresponding to the maximum displacement provides better agreement in the case of significant softening behavior, see Figure 17 (right).

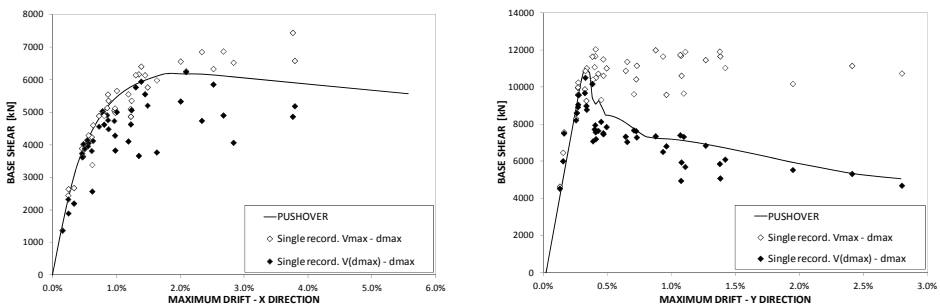


Figure 17. NLRHA results: comparison between the representation methods for the X (left) and Y directions (right).

It is worth reminding that the aforementioned methods are representation methods and that, in any case, the displacements reported are equal for both cases.

In the following, the results of the NL RHA in the X direction will be represented in terms of $V_{max} - d_{max}$ while the results in the Y direction in terms of $V(d_{max}) - d_{max}$.

5.1 NL RHA in the X direction

Figure 18 shows, for each scaling technique adopted, the pushover curve and the results of the NL RHA in terms of $V_{max} - d_{max}$ in the X direction. Each plot reports also the performance points evaluated through the N2 method (see also Figure 11) and the points representing the average values of the maximum base shear and maximum displacement obtained through the NL RHA.

For all the GMs sets investigated, the global EDPs Displacement, Drift and Base Shear obtained through dynamic NL analysis are reported in terms of mean, dispersion and Coefficient of Variation (CoV) for the X-direction in Table 4 and Table 5 for PoE=50% and PoE=10%, respectively, and compared with static NL analysis results.

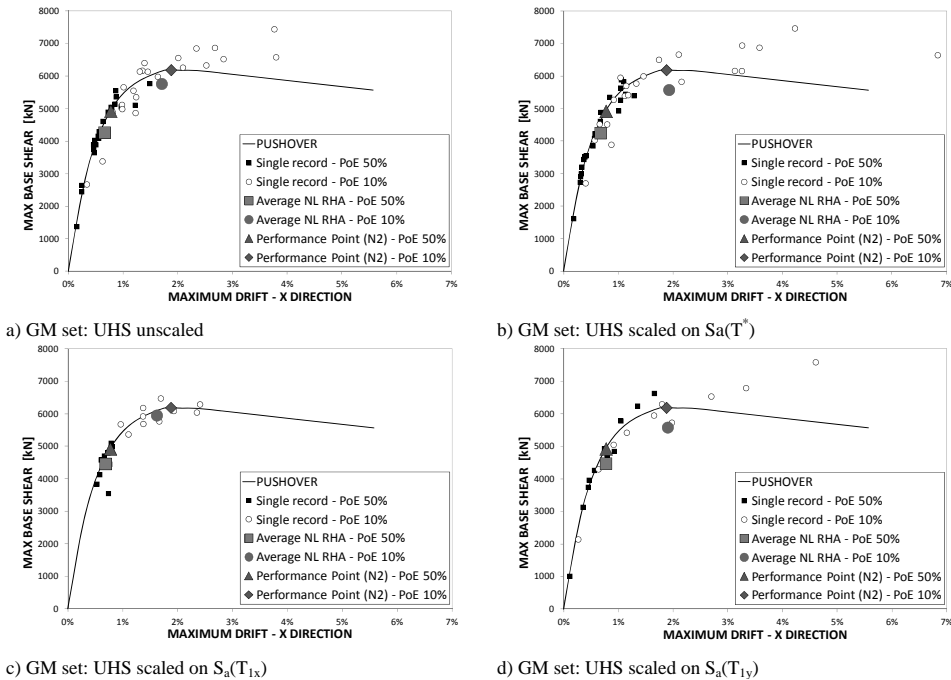


Figure 18. Pushover curve and NL RHA results, in terms of maximum base shear - maximum displacement, in the X direction.

In almost all the cases, the values of EDPs estimated by dynamic analyses are lower than those obtained through the nonlinear static analysis. Considering first the “Unscaled set”, it should be noted that for PoE=50% the results obtained adopting CMS and UHS sets are very similar. On the contrary, for PoE=10% the CMS gives values of EDPs lower by about 12% in terms of displacements and drift, due to the elongation of the period and to the lower spectral accelerations associated to the CMS set for $T > T_{1x}$ compared to the UHS set. The CoVs are very similar between the two Unscaled sets and there is only a slight increase of this

parameter for PoE=10%, as expected. Comparing “Scaled” and “Unscaled” sets, we observe that when $S_a(T_{1x})$ is adopted as reference IM, the results are less scattered for both the PoE considered herein and, as expected, especially when scaling is performed only on one of the components (i.e. for UHS set $S_a(T_{1x})$ CoV=12% for PoE=50% and CoV=29% for PoE=10%), compared to when the scaling is carried out on the GeoMean component (i.e. CMS set $S_a(T_{1x})$ CoV=29% for PoE=50% and CoV=42% for PoE=10%). On the contrary, the sets scaled to $S_a(T_{1y})$ and $S_a(T^*)$ do not provide any advantage in terms of dispersion and, furthermore, it should be observed that the mean values of EDPs are significantly higher (up to 17% for UHS scaled to $S_a(T_{1y})$ set with PoE=50%) if compared with Unscaled sets.

Table 4. NL RHA demand and PO Performance points associated to the PoE 50%.

		N2	UHS unscaled	UHS T^*	UHS T_{1x}	UHS T_{1y}
Displ [mm]	Average	83	71	72	74	83
	σ	-	33	35	9	48
	CoV	-	46%	49%	12%	58%
Drift [%]	Average	0.70	0.60	0.61	0.63	0.70
	σ	-	0.28	0.30	0.08	0.40
	CoV	-	46%	49%	12%	58%
Force [kN]	Average	4924	4268	4254	4460	4473
	σ	-	1048	1140	449	1547
	CoV	-	25%	27%	10%	35%

Table 5 NL RHA demand and PO Performance points associated to the PoE 10%.

		N2	UHS unscaled	UHS T^*	UHS T_{1x}	UHS T_{1y}
Displ [mm]	Average	202	184	208	175	205
	σ	-	100	165	50	139
	CoV	-	54%	79%	29%	68%
Drift [%]	Average	1.71	1.56	1.76	1.48	1.73
	σ	-	0.85	1.39	0.42	1.17
	CoV	-	54%	79%	29%	68%
Force [kN]	Average	6187	5762	5578	5951	5581
	σ	-	1099	1150	314	1510
	CoV	-	19%	21%	5%	27%

5.2 NL RHA in the Y direction

Figure 19, Table 6 and Table 7 report the results in the Y direction.

The results of static and dynamic nonlinear analysis in terms of mean, dispersion and CoV for the Y-direction are shown in Table 6 and Table 7, for PoE=50% and PoE=10%, respectively. For PoE=50% the results of static and dynamic analysis are comparable in terms of mean values, the set “Scaled on $S_a(T_{1y})$ ” gives the lowest dispersion, as expected, while the other GM sets have similar values of dispersion. The analysis of results for PoE=10% shows how the static analysis underestimate significantly drift and displacements, and, more importantly, the dispersion of results is very high for all the investigated cases. Furthermore, scaling on $S_a(T_{1y})$ does not give the expected advantages in terms of CoV and mean values, on the contrary, these values are considerably higher compared to the other case, also due to a few analyses with a very high final displacements which affect the final estimate.

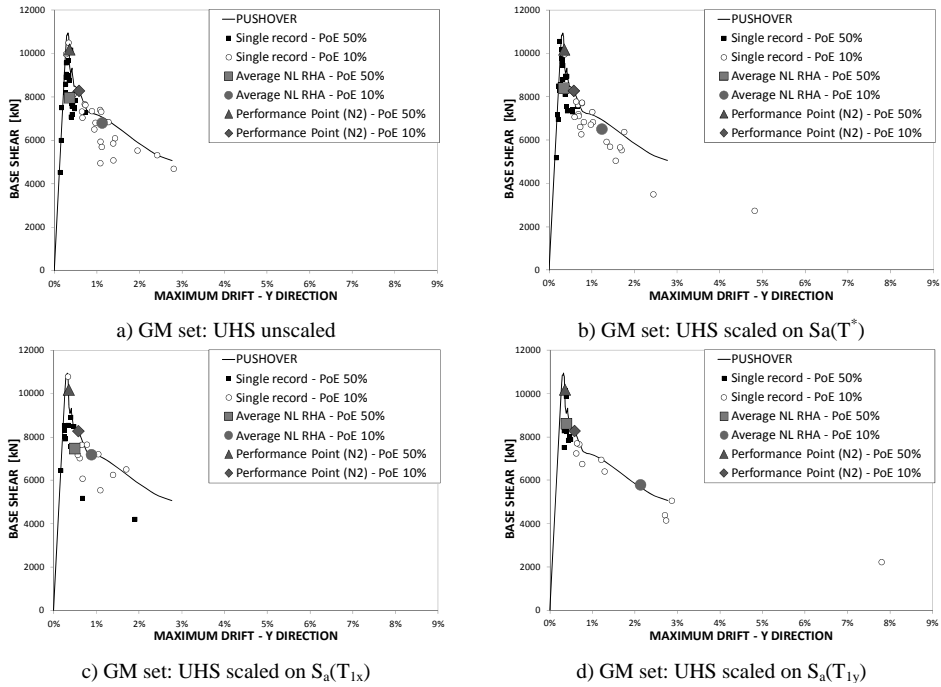


Figure 19. Pushover curve and NL RHA results, in terms of base shear associated to the maximum displacement - maximum displacement, in the Y direction.

Table 6 NL RHA demand and PO Performance points associated to the PoE 50%.

		N2	UHS unscaled	UHS T^*	UHS T_{1x}	UHS T_{1y}
Displ [mm]	Average	37	38	36	53	41
	σ	-	14	13	50	6
Drift [%]	Average	0.31	0.32	0.30	0.45	0.35
	σ	-	0.12	0.11	0.42	0.05
Force [kN]	Average	10193	7969	8411	7477	8617
	σ	-	1226	1240	1464	877
			CoV	15%	15%	20%
					20%	10%

Table 7 NL RHA demand and PO Performance points associated to the PoE 10%.

		N2	UHS unscaled	UHS T^*	UHS T_{1x}	UHS T_{1y}
Displ [mm]	Average	62	121	133	95	230
	σ	-	66	100	43	225
Drift [%]	Average	0.52	1.02	1.12	0.80	1.94
	σ	-	0.56	0.85	0.36	1.90
Force [kN]	Average	8283	6806	6519	7196	5800
	σ	-	1451	1476	1366	1808
			CoV	21%	23%	19%
					19%	31%

5.3 Consideration on the selected GMs set effectiveness

In summary, analysis of the results shows very different behaviors for the two analyzed directions. In the X direction the structural response is fairly predictable and similar to a building structure. In these cases, then, it is clear how UHS provides conservative results compared to CMS, in particular when the structure exhibits inelastic behaviour and elongation of the period occurs. The results through different scaling techniques have also shown that the most effective technique to reduce the dispersion of EDPs in the desired direction is scaling on $S_a(T_1)$. On the other hand, this method greatly amplifies the dispersions in the other direction (e.g. EDPs for X- direction for Scaled on $S_a(T_{1y})$ GMs sets) and therefore requires the execution of a higher number of analyses to obtain reliable values of EDPs in all directions and situations. Finally, the sets scaled on the GeoMean component show that this scaling technique scarcely influences the results since, although it reduces to some extent the dispersion, it does not eliminate scattering of spectral accelerations in each direction and the advantages with respect to Unscaled sets are not very significant. In the Y-direction the behavior is quite complex and not comparable to a typical building structure, in particular for PoE=10% when inelastic phenomena occur. Due to the absence of an IM which clearly governs the response, unscaled sets should be preferred for NL RHA. Alternative enhanced reference spectra as CMS can be used as long as it is possible to justify the choice of the conditioning period.

5.4 Sufficiency of the selected GM sets

The scaling techniques studied in this work assume that the key EDPs are strongly correlated to the IM adopted as a reference for scaling (i.e. $S_a(T_1)$, $S_a(T^*)$, etc.) and that other IM have a weak correlation with EDPs. If this condition is verified, the selected IM is sufficient for the 3-D nonlinear response history analysis and the scaling operation is justified, otherwise, the IM is not sufficient and then not suitable for scaling. In order to verify satisfaction of this criterion, the statistical correlation between the storey drifts at level 1 and 2 obtained through NL RHA and spectral accelerations at a range of periods between 0s and 4s is investigated. In particular the following statistical correlations are studied for both the UHS and CMS coherent sets:

- Drift in the X direction and UHS coherent sets (Figure 20)
- Drift in the Y direction and UHS coherent sets (Figure 21)

The results of the statistical correlation are represented through the 'correlation spectra', in which the values of the statistical correlation coefficient (CF) between the computed EDPs set and the corresponding input spectral accelerations S_a at the period T of a relevant IM, are plotted as a continuous function of the period T. The correlation spectrum is thus intended to provide insight into which frequency content and range of IMs most influence and introduce dispersion into a related EDP.

Figure 20 shows the correlation spectra of the storey drift at each hazard level for the X direction for the spectral acceleration associated to the period T and evaluated for the GM component applied in the X direction. When unscaled GMs are used (Figure 20a) the CF is maximum, or almost maximum, in correspondence of the first mode period, as expected, and assumes high values ($CF > 0.7$) for spectral ordinates with lower frequencies (i.e. $T > T_{1x}$). On the contrary, the correlation is low, or negative, for higher frequencies (i.e. $T < T_{1x}$). The correlation is higher for the seismic action with PoE=10% where the structure exhibits a marked inelastic behaviour with a ductile flexural mechanism and elongation of the period. When scaled GMs sets are used (Figure 20b-c and **Errore. L'origine riferimento non è stata trovata.**b-c), as expected, the correlation in correspondence of the IM adopted as reference

for scaling is null for the UHS set or almost null for the CMS set, where the GeoMean component $S_{agm}(T_{1x})$ is adopted for scaling. However, the correlation with lower frequencies remains very high in all the cases and in particular for PoE=10%, suggesting that none of the IM and the scaling criteria analyzed is sufficient to render the investigated EDP conditionally statistically independent of other ground motion characteristics given this IM.

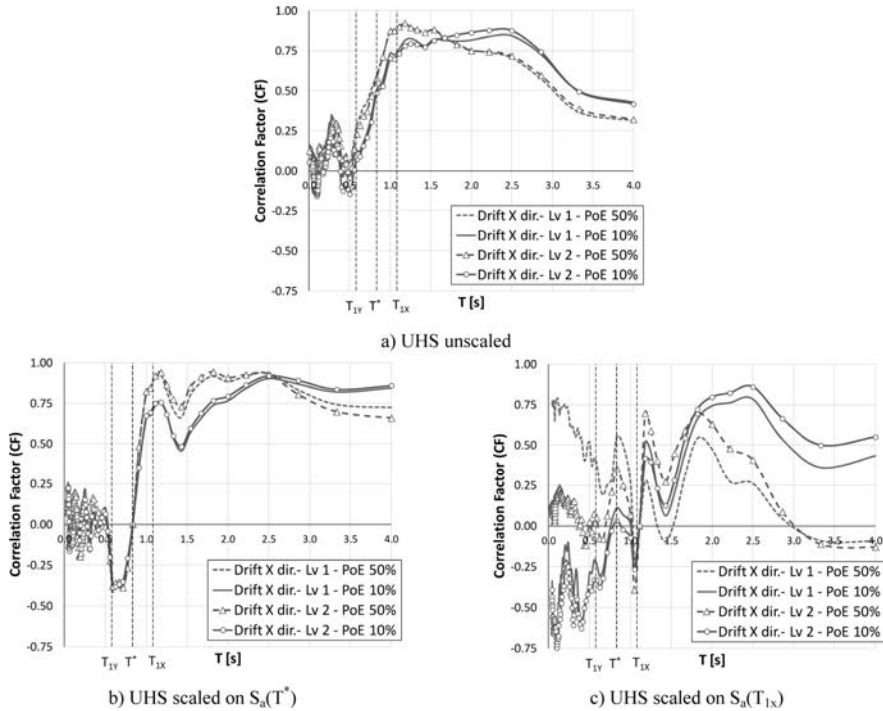


Figure 20. Correlation of IM-EDP pairs in the X direction for UHS coherent sets.

The CFs between the spectral accelerations $S_a(T)$ and the storey drift of each floor for the Y direction are shown in Figure 21. When unscaled GMs are used (Figure 21a) the CF is maximum in correspondence of the first mode period, but the correlation is good only for the seismic action with PoE=50%. For the seismic action with PoE=10% the structural behavior is modified by the buckling of some braces at the first floor. This leads to an elongation of the period, as demonstrated by the achievement of the maximum correlation factors for structural periods slightly higher than the elastic one. As occurred for the X-direction, scaling GMs does not influence significantly the statistical correlation, as it can be observed in Figure 21b-c. The scaling on $S_a(T_{1y})$ of both UHS and CMS coherent set provides the best sufficiency attribute, compared to the other cases, for the seismic action with PoE=50%. On the other hand, the drift response obtained for seismic action with PoE=10% is strongly correlated, especially for the UHS coherent set, to almost all the spectral acceleration with $T > T_{1y}$. In summary, the correlation factors analysis shows that the first mode spectral acceleration $S_a(T_1)$ is not sufficient to control the structural response in the case of relevant inelastic behaviour and the elongation of the period. Furthermore, the significant difference between the structural behaviour in the two horizontal directions does not allow to find an IM as a good predictor of response for both directions in 3-D analyses. Comparing the correlation

factors obtained with “Unscaled” and “Scaled” GMs it should be observed that scaling techniques do not influence the sufficiency conditions in a sensitive manner. It can be than concluded that for 3-D analysis on complex structures, as the one analyzed herein, the adoption of specific scaling criteria does not necessarily lead to an improvement of results that justify the efforts and drawbacks of the scaling operation. Thus the adoption of “Unscaled” GMs is the most reliable method for the execution of NL RHA, due to the impossibility of finding IM that are sufficient to describe the structural response.

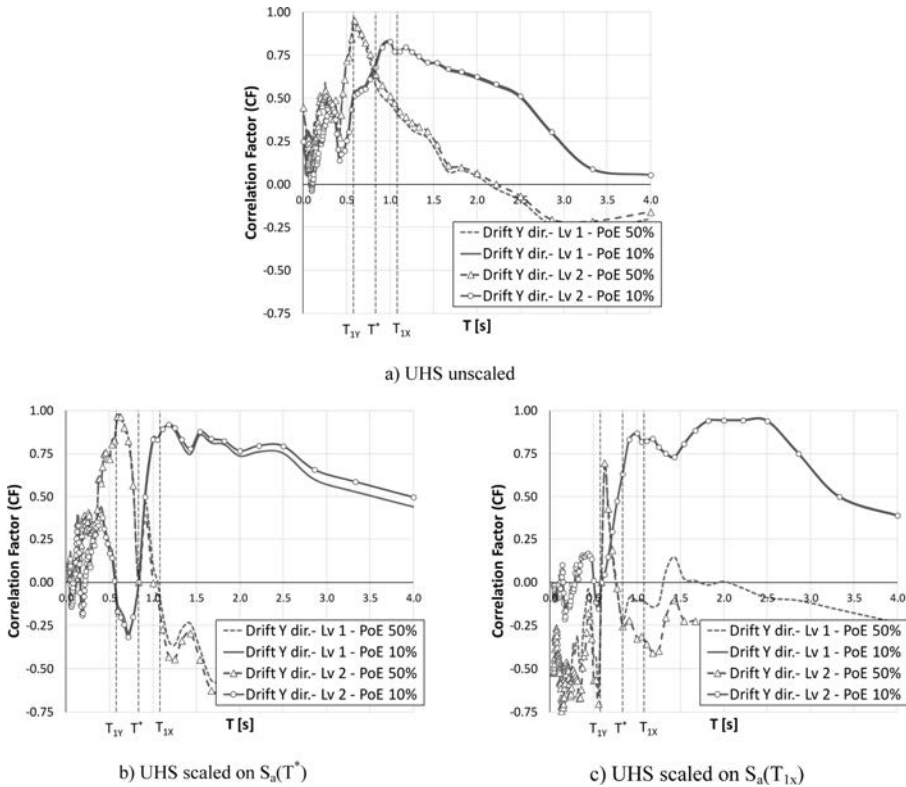


Figure 21. Correlation of IM-EDP pairs in the Y direction for UHS coherent sets.

Further, UHS should be preferred for the spectrum-matching instead of CMS, because the latter is conditioned on a specific IM (in this case $S_a(T^*)$) and, given the not sufficiency of such IM, further analyses on different GMs sets coherent with CMS conditioned on other spectral ordinates (e.g. $S_a(1.5 \div 2T^*)$) would thus be needed and the maximum structural response should be evaluated as the envelope of these sets, as it is observed in Baker, 2011.

6 CONCLUSIONS

The scope of this work was to investigate the main aspects of seismic vulnerability assessment of a complex 3D industrial steel structure characterized by very different behaviors in the two horizontal directions. Two main aspects were analyzed: the assessment of the main vulnerability sources and the ground motion recordings scaling criteria.

The nonlinear static and incremental dynamic analyses proved the following main structural problems of the analyzed structure:

- X direction: the building is characterized by a low horizontal stiffness both at the ground and first floor. The elastic and inelastic displacements associated to the seismic action tend to be distributed between the two floors leading to a global and ductile collapse mechanisms.
- Y direction: the high horizontal initial stiffness avoids excessive elastic displacements, whereas the inelastic deformations tend to accumulate on the ground floor due to the buckling of the inverted V bracings. The collapse mechanism is characterized by the formation of a soft-storey mechanism at the ground level, while the first floor remains substantially elastic.
- the structure shows the tendency to accumulate residual displacements in both directions. In particular, in the X direction they are present at both levels, while in the Y direction only at the first level.

Regarding the GMs, the selected set, coherent with an Uniform Hazard Spectrum (UHS), was scaled on different IMs, selected as the possible best predictors of the investigated EDPs.

The EDPs obtained, were compared in terms of mean, dispersion and coefficient of variations, to assess the predictive efficiency of the different methods. A correlation study was then elaborated to investigate the predictive sufficiency of different IMs and scaling methods.

The analyses showed that the use of Unscaled GMs consistent with UHS seems the most suitable technique to obtain reliable results through a limited number of analyses, in case of complex structures characterized by different behaviors in horizontal directions, as in the case study analyzed herein.

This method, although not optimal from an efficiency point of view, has the advantage of being independent from the structural response and allowing to not tamper the natural records. It can be thus adopted without any need of record modification when different buildings belonging to the same site are analyzed or when it is necessary to compare the structural response of a structure in as-it-is state and in the retrofitted state.

7 ACKNOWLEDGEMENTS

The authors acknowledge the support of the European Union's Research Fund for Coal and Steel (RFCS) research programme through the project PROINDUSTRY, "Seismic PROtection of INDUSTRial plants by enhanced steel based sYstems", grant agreement n° [RFSR-CT-2013-00019] and from the Italian Department of Civil Protection within the Italian Research Project RELUIS-DPC 2014-2018. The content of this paper reflects the opinions of the authors and do not necessarily represent the opinions of the funding agencies.

8 REFERENCES

- API. (2007). API 650: Welded Steel Tanks for Oil Storage, 11th Edition. American Petroleum Institute. Washington D.C.
- API. (2009). API 620: Design and Construction of Large, Welded, Low Pressure Storage Tanks. 11th Edition. American Petroleum Institute. Washington D.C.
- ARIA. (2013). When Natural and Technological Hazards Collide - Overview of the Industrial Accidents caused by the Great Tohoku Earthquake and Tsunami. French Ministry of Ecology, Sustainable Development and Energy.

- ASCE/SEI 43-05. (2005). Seismic Design Criteria for Structures, Systems, and Components in Nuclear Facilities. American Society of Civil Engineers.
- ASCE/SEI 7-05. (2013). Minimum Design Loads for Buildings and Other Structures, 3rd Printing. ASCE standard. American Society of Civil Engineers. <http://doi.org/10.1061/9780784412916>
- Baker, J. W. (2011). "Conditional Mean Spectrum: Tool for Ground-Motion Selection". *Journal of Structural Engineering*, 137(3), pp. 322–331. [http://doi.org/10.1061/\(ASCE\)ST.1943-541X.0000215](http://doi.org/10.1061/(ASCE)ST.1943-541X.0000215).
- Baker, J. W., & Cornell, C. A. (2006). "Which spectral acceleration are you using?" *Earthquake Spectra*, 22(2), pp. 293–312. <http://doi.org/10.1193/1.2191540>
- Baker, J. W., & Cornell, C. A. (2008). "Vector-valued Intensity Measures Incorporating Spectral Shape For Prediction of Structural Response". *Journal of Earthquake Engineering*, 12(4), pp. 534–554. <http://doi.org/10.1080/13632460701673076>
- Baldassino, N., & Bernuzzi, C. (2000). "Analysis and behaviour of steel storage pallet racks". *Thin-Walled Structures*, 37, pp. 277–304.
- Belleri, A., Brunesi, E., Nascimbene, R., Pagani, M., & Riva, P. (2015). "Seismic Performance of Precast Industrial Facilities Following Major Earthquakes in the Italian Territory". *Journal of Performance of Constructed Facilities*, 29(5), pp. 1–10. [http://doi.org/10.1061/\(ASCE\)CF.1943-5509.0000617](http://doi.org/10.1061/(ASCE)CF.1943-5509.0000617).
- EN 1993-1-1. (2005). Eurocode 3: Design of steel structures - Part 1-1: General rules and rules for buildings. European Committee for Standardization, Brussels, 2005.
- EN 1998-1. (2004). Eurocode 8: Design of structures for earthquake resistance - Part 1: General rules, seismic actions and rules for buildings. European Committee for Standardization, Brussels, 2004.
- EN 1998-4. (2007). Eurocode 8 - Design of structures for earthquake resistance - Part 4: Silos, tanks and pipelines. European Committee for Standardization, Brussels, 2007.
- EN 1998-6. (2007). Eurocode 8 Design of structures for earthquake resistance Part 6: Towers, masts and chimneys. European Committee for Standardization, Brussels, 2007.
- Faggella, M., Barbosa, R., Conte, J. P., & Spacone, E. (2013). "Probabilistic seismic response analysis of a 3-D reinforced concrete building". *Structural Safety*, 44, pp. 11–27. <http://doi.org/10.1016/j.strusafe.2013.04.002>
- FEMA. (2012). Next-Generation Methodology for Seismic Performance Assessment of Buildings, prepared by the Applied Technology Council for the Federal Emergency Management Agency, Report No. FEMA P-58. Fema P-58-1 (Vol. 1).
- FERC. (2015). Assessment of Demand Response & Advanced Metering, Staff Report, Federal Energy Regulatory Commission. The effects of brief mindfulness intervention on acute pain experience: An examination of individual difference (Vol. December). <http://doi.org/10.1017/CBO9781107415324.004>
- Hamburger, R. (2003). "A vision for performance based earthquake engineering," Unpublished white paper for the ATC- 58 project, Applied Technology Council, Redwood City, CA, 2003.
- Kohrangi, M., Bazzurro, P., & Vamvatsikos, D. (2016a). "Vector and scalar IMs in structural response estimation, Part II: Demand Assessment". *Earthquake Spectra*, 32(3), pp. 1525–1543. <http://doi.org/10.1193/053115EQS080M>
- Kohrangi, M., Bazzurro, P., & Vamvatsikos, D. (2016b). "Vector and Scalar IMs in Structural Response Estimation: Part I - Hazard Analysis". *Earthquake Spectra*, 32(3), pp. 1525–1543. <http://doi.org/10.1193/053115EQS081M>
- Kohrangi, M., Vamvatsikos, D., & Bazzurro, P. (2016). "Implications of intensity measure selection for seismic loss assessment of 3-D buildings. *Earthquake Spectra*", 32(4), pp. 2167–2189. <http://doi.org/10.1193/112215EQS177M>
- Lin, T., Harmsen, S. C., Baker, J. W., & Luco, N. (2013). "Conditional Spectrum Computation Incorporating Multiple Causal Earthquakes and Ground-Motion Prediction Models". *Bulletin of the Seismological Society of America*, 103(2A), pp. 1103–1116.
- Luco, N., Manuel, L., Baldava, S., & Bazzurro, P. (2005). "Correlation of damage of steel moment-resisting frames to a vector-valued set of ground motion parameter". In G. Augusti, G. I. Schuëller, & M. Ciampoli (Eds.), *Proceedings of the 9th International Conference on Structural Safety and Reliability*, ICOSSAR'05, Rome, Italy, June 19–23, 2005 (pp. 2719–2726). Rome.

- Moehle, J., & Deierlein, G. G. (2004). "A Framework Methodology for Performance-Based Earthquake Engineering". *13th World Conference on Earthquake Engineering*, Vancouver, B.C., Canada, August 1-6, 2004., (679).
- Morelli, F., Piscini, A., & Salvatore, W. (2017). " Seismic behavior of an industrial steel structure retrofitted with self-centering hysteretic dampers", *Journal of Constructional Steel Research*, 139, pp. 157-175. <https://doi.org/10.1016/j.jcsr.2017.09.025>.
- Morelli, F., Laguardia, R., Faggella, M., Piscini, A., Gigliotti R., Salvatore, W. (2017a)."Ground motions and scaling techniques for 3D performance based seismic assessment of an industrial steel structure". *Bulletin of Earthquake Engineering*. DOI 10.1007/s10518-017-0244-1
- NIST. (2011). *Selecting and Scaling Earthquake Ground Motions for Performing Response-History Analyses*, GCR 11-917-15.
- NTC. (2008). *Norme Tecniche per le Costruzioni*, D.Min. Inf. 14 gennaio 2008, *Gazzetta Ufficiale* n. 29 of february 4th 2008 - Suppl. Ordinario n. 30. In Italian.

SINGLE-STOREY STEEL INDUSTRIAL BUILDINGS: DESIGN STRATEGIES EVALUATION BASED ON ECONOMIC AND ENVIRONMENTAL ANALYSES

Chiara Calderini ^a, Riccardo Berardi ^b, Sara Rossi ^c

^a DICCA, University of Genoa, Italy, chiara.calderini@unige.it

^b DICCA, University of Genoa, Italy, riccardo.berardi@unige.it

^c DICCA, University of Genoa, Italy, sara.rossi@unige.it

ABSTRACT

The research aims to define efficient criteria to design single storey steel industrial buildings in seismic-prone areas, in terms of environmental and economic costs. The analysis of the Italian code for these type of buildings highlights the need of improve certain aspects that are not clear and may be barely understood from structural designers (e.g. structural scheme in the transversal direction and related behaviour factor). By considering both structural and foundation issues, a set of parametric analyses shows the most efficient choices as a function of the chosen structural behaviour (low dissipative or dissipative), base constraints, ground type, seismicity site.

KEYWORDS

Industrial buildings, Single-storey buildings, Foundation systems, Economic evaluation, Environmental evaluation.

1 INTRODUCTION

The research aims to define efficient criteria for improve the structural design of single storey steel industrial buildings in seismic-prone areas, trying to reduce their environmental and economic costs.

These type of buildings are commonly light and slender. Specific design aspects arise from these features:

- seismic action is not always predominant
- ultimate limit states are not always predominant
- ductile seismic design is not always convenient

In particular, this latter aspect is controversial. For functional reasons, the structure of industrial buildings is made of moment resisting frames or girder trusses in the transversal direction and concentric or eccentric braced frames in the longitudinal direction. Transversal frames may be classified, from the structural point of view as:

- a) *MRF (Moment Resisting Frames)*, in which the horizontal forces are mainly resisted by members acting in an essentially flexural manner and dissipative zones are mainly located in plastic hinges in the beams or the beam-column joints so that energy is dissipated by means of cyclic bending.
- b) *Inverted pendulum structures*, in which dissipative zones are located at the bases of columns.

In the Italian Code (NTC, 2008), by assuming a ductility class “B”, the behaviour factor is $q_0=4$ for a) and $q_0=2$ for b). However, in section 7.5.4. (NTC, 2008), it is specified that, for MRF, the requirement of locating dissipative zones in the beams or the beam-columns joints may be disregarded for single-storey buildings. Actually, for MRF, ductile design is admitted with $q_0=4$ without fulfilling beam-column hierarchy criterion (only a column-foundation hierarchy criterion should be fulfilled).

Also EC8 (2007), section 6.6.1., outlines that MRF shall be designed so that plastic hinges form in the beams or in the connections of the beams to the columns, but not in the columns. Also in this case, exception is made for single storey buildings. However, section 6.3.1 specifies those cases in which dissipative zones could be located at the top and bottom of columns in MRF. Among others, there is the case of single-storey buildings in which N_{Ed} in columns conform to the inequality $N_{Ed}/N_{pl,Rd} < 0.3$. In the same section, it clarifies that *inverted pendulum structures* may be considered as moment resisting frames provided that the earthquake resistant structures possess more than one column in each resisting plane and that the following inequality of the limitation of axial force: $N_{Ed} < 0.3 N_{pl,Rd}$ is satisfied in each column.

In summary, EC8 (2007) (Figure 1) states that single-storey steel buildings satisfying the inequality $N_{Ed} < 0.3 N_{pl,Rd}$ in each column could be considered as MRF (at least in the transversal direction) in which dissipative zone are located at the top and the bottom of columns and in which is $q_0=4$. It is worth noting that this criterion is the same adopted in the Italian code for r.c. single-storey buildings, but not for steel ones.

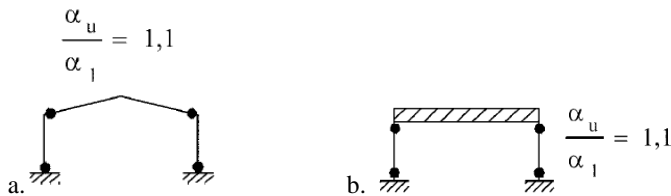


Figure 1. Schemes of MRF (a) and inverted pendulum (b) single-storey buildings by EC8.

Furthermore, it should be observed that in both MRF and inverted pendulum schemes, it is assumed that columns are fixed at their base. However, in many industrial buildings columns are not fixed but hinged at their base. In this case, it is not possible to assume the inverted pendulum model at all: a MRF scheme, where dissipation is located at the top of the columns or on the beams, should be considered.

In this framework, there is a clear need to define design criteria for industrial single-storey steel buildings. In particular, the objective of this research is to provide first answers to the following questions:

- Is it more convenient to design the structure with a low dissipative (elastic) ($q_0=1$) or a dissipative structural behaviour ($q_0>1$)?
- Is it more convenient to design the structure with columns hinged or fixed at their base?

There are not simple answers to these questions; they depend on many factors, such as building use (likely to cause adverse effects on human or animal health or the environment), site (determining the magnitude of hazard), class and type of foundation soil. In order to define the convenience of one choice over the other and find the best solution, quantitative parameters should be defined and compared. To this end, the following parameter were selected:

- economic cost, commonly expressed, for these type of buildings, as cost for cubic meter ($\text{€}/\text{m}^3$);
- environmental impact, expressed in term of Primary Energy Demand (PED), expressed in MJ/m^3 and Global Warming Potential (GWP), expressed in $\text{CO}_2\text{-Equiv.}/\text{kg}$.

The comparison of the different solutions should take into account the whole structural system, including both elevation and foundation structures. In this research work, the entire structural system was considered.

2 DESIGN OF A REFERENCE BUILDING

2.1 Case study and reference parameters

A very simple single-storey steel industrial building, clad with light prefabricated panels (weight $0,1 \text{ kN}/\text{m}^2$), was defined (Figure 2). The following parameters were varied in the analyses:

- length L (30 m or 48 m);
- width B (12 m or 24 m);
- base constraints in the transversal direction (fixed or hinged columns);
- ground type (C or D);
- soil type (fine and coarse grained soils – namely clayey and sandy soils);
- position of lateral bracings;
- building site (low or high seismicity);
- type of seismic behaviour (low dissipative or dissipative).

Concerning the building sites, two sites comparable in terms of snow and wind actions, but quite different in terms of seismic hazard, were selected: Reggio Emilia (RE – low seismicity) and Gemona sul Friuli (GE – high seismicity).

In Table 1 the different structural design choices considered are collected. It can be observed that, following the unclear definition of the Italian code, a behaviour factor $q_0=2$ was considered for MRF schemes also. In Table 2 the different cases considered are summarized.

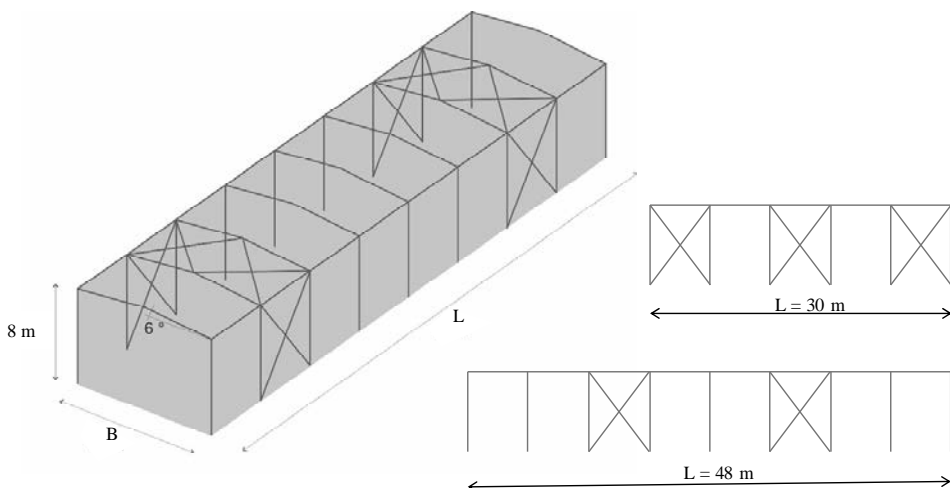


Figure 2. Reference building considered in the analyses.

Table 1. Structural parameters considered.

Direction	Str. behaviour	Str. type	Base con.	q_0	Dissipative zones	
Transversal	Low Dissipative	-	Hinged	1	-	
			Fixed	1		
	Dissipative		MRF	Hinged	2	Beam/column joint
			Inverted pendulum	Fixed	2	Column base
Longitudinal	Low Dissipative	-	Hinged	1	-	
	Dissipative	Concentric bracings	Hinged	4	Bracings	
Vertical	Low Dissipative	-	-	1	-	
	Dissipative	-	-	1.5	-	

Table 2. Set of analyses carried out in the research.

N°	Name	L [m]				B [m]		Site		Base con.		Ground type		Soil type	
		30	48	12	24	RE	GE	Hing.	Fix.	C	D	Sand	Clay		
1	B12 L30 FIX RE C SD	x		x		x		x		x		x		x	
2	B12 L30 FIX RE C CL	x		x		x		x		x		x			x
3	B12 L30 FIX RE D SD	x		x		x		x				x		x	
4	B12 L30 FIX RE D CL	x		x		x		x				x			x
5	B12 L30 HIN RE C SD	x		x		x				x		x		x	
6	B12 L30 HIN RE C CL	x		x		x				x		x			x
7	B12 L30 HIN RE D SD	x		x		x				x			x		x
8	B12 L30 HIN RE D CL	x		x		x				x		x			x
9	B12 L30 FIX GE C SD	x		x				x		x		x			x
10	B12 L30 FIX GE C CL	x		x				x		x		x			x
11	B12 L30 FIX GE D SD	x		x				x		x			x		x
12	B12 L30 FIX GE D CL	x		x				x		x		x			x
13	B12 L30 HIN GE C SD	x		x				x		x		x			x
14	B12 L30 HIN GE C CL	x		x				x		x		x			x
15	B12 L30 HIN GE D SD	x		x				x		x			x		x
16	B12 L30 HIN GE D CL	x		x				x		x		x			x
17	B12 L48 FIX RE C SD		x		x			x		x		x			x
18	B12 L48 FIX RE C CL		x		x			x		x		x			x
19	B12 L48 FIX RE D SD		x		x			x				x		x	
20	B12 L48 FIX RE D CL		x		x			x				x			x
21	B12 L48 HIN RE C SD		x		x					x		x			x
22	B12 L48 HIN RE C CL		x		x					x		x			x
23	B12 L48 HIN RE D SD		x		x					x			x		x
24	B12 L48 HIN RE D CL		x		x					x		x			x
25	B12 L48 FIX GE C SD		x		x					x		x			x
26	B12 L48 FIX GE C CL		x		x					x		x			x
27	B12 L48 FIX GE D SD		x		x					x			x		x
28	B12 L48 FIX GE D CL		x		x					x			x		x
29	B12 L48 HIN GE C SD		x		x					x		x			x
30	B12 L48 HIN GE C CL		x		x					x		x			x
31	B12 L48 HIN GE D SD		x		x					x			x		x
32	B12 L48 HIN GE D CL		x		x					x			x		x
33	B24 L30 FIX RE C SD	x			x					x		x			x
34	B24 L30 FIX RE C CL	x			x					x		x			x
35	B24 L30 FIX RE D SD	x			x							x		x	
36	B24 L30 FIX RE D CL	x			x							x			x
37	B24 L30 FIX GE C SD	x			x					x		x			x
38	B24 L30 FIX GE C CL	x			x					x		x			x
39	B24 L30 FIX GE D SD	x			x					x			x		x
40	B24 L30 FIX GE D CL	x			x					x			x		x

2.2 Actions

The structures were analysed by considering both standard and seismic actions. In particular, besides permanent loadings, the following standard actions were considered: roof live load ($0,5 \text{ kN/m}^2$); snow ($q_{sk}=1.50 \text{ kN/m}^2$); wind ($v_{b,0}=25 \text{ m/s}$; CNR, 2006).

The seismic action was evaluated by assuming a nominal life $V_N = 50$ year and an importance class II (it is assumed that environmentally dangerous activities are not carried out in the building). The effects of the seismic actions were determined by means of a modal response spectrum analysis, with reference to the following limit states:

- Ultimate Limit State: Life Safety (SLV) - $P_{Vr} = 10\%$ - $T_R=475$ years;
- Serviceability Limit State: Damage (SLD) - $P_{Vr} = 63\%$ - $T_R=50$ years.

In Table 3, the seismic parameters of the two considered building sites are summarized.

Table 4 shows the spectral parameters adopted for the two ground types considered; in both cases a topographic class T1 (no amplification) were considered. The related spectra ($q_0=1$) are plotted in Figure 3.

Table 3. Seismic parameters adopted.

Site	SLV			SLD		
	a_g/g	F_0	$T_c^* [s]$	a_g/g	F_0	$T_c^* [s]$
Reggio Emilia (RE)	0.1571	2.37	0.29	0.0599	2.5	0.26
Gemona del Friuli (GE)	0.2590	2.41	0.33	0.0917	2.45	0.26

Table 4. Spectral parameters.

Site	Limit State	$T_c^* [s]$	Ground type "C"					Ground type "D"				
			S_S	C_C	$T_B [s]$	$T_C [s]$	$T_D [s]$	S_S	C_C	$T_B [s]$	$T_C [s]$	$T_D [s]$
RE	SLV	0.29	1.48	1.58	0.15	0.46	2.23	1.80	2.32	0.22	0.67	2.23
	SLD	0.26	1.50	1.64	0.14	0.43	1.84	1.80	2.45	0.21	0.64	1.84
GE	SLV	0.33	1.33	1.51	0.17	0.50	2.64	1.46	2.18	0.24	0.72	2.64
	SLD	0.26	1.50	1.64	0.14	0.43	1.97	1.80	2.45	0.21	0.64	1.97

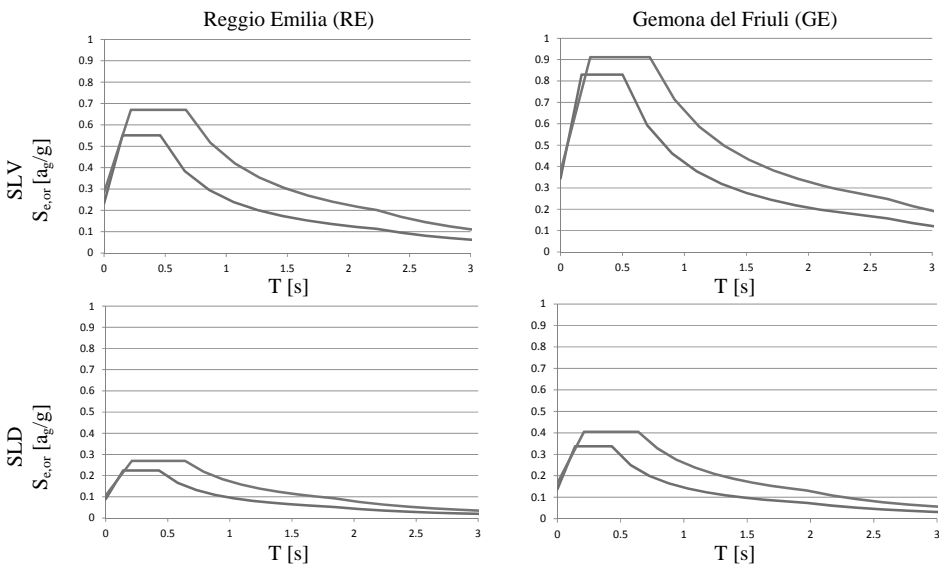


Figure 3. Horizontal elastic response spectra ($q_0=1$) as a function of site, limit state considered and ground type (ground type "C" in red and ground type "D" in blue).

The vertical seismic component was considered in every analyses. For vertical elastic response spectra, the following parameters were considered: $S_S=1,0$; $T_B = 0.05$ s; $T_C = 0.15$ s; $T_D = 1.00$ s.

2.3 Structural design

The buildings were analysed by means of 3D finite elements models (SAP), Figure 4. The analyses and the sizing of structural elements were carried out under the Italian code NTC 2008 and its subsequent implementation decrees (NTC, 2008).

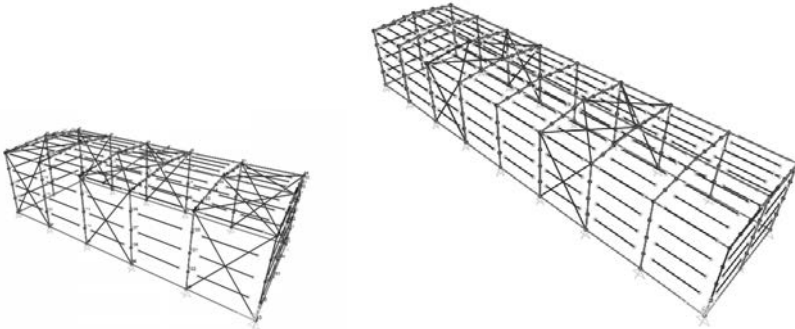


Figure 4. Finite element models of the considered buildings.

The structural profiles obtained for columns and beams for the set of cases with $B=12$ m and $L=30$ m (see Table 2) are summarized in Table 5. Principal structural elements of the building with $B=12$ m and $L=30$ m.; for each case, the sizing load combination is highlighted. In all the cases, bracings are tubular elements D219.1X10. From Table 5, it can be observed that:

- Load combinations related to serviceability limit states are the dimensioning ones; for this reason, the choice of designing the structure with a low dissipative or a dissipative structural behaviour is irrelevant in this case.
- Structures tend to have large horizontal displacements in the transverse direction (due to wind and seismic loadings); for this reason, sections are much smaller when columns are fixed at their base.
- HEB 340 profiles were obtained in all cases when columns were considered fixed at their base. In these cases, the displacements produced by the load combination CSLE_R 4.3 (serviceability LS standard combination with wind as prevalent action along the transversal direction X) were very similar to those produced by the load combination CSX(SLD) (serviceability LS seismic combination along the transversal direction X).

In Table 6 the profiles obtained for $B=12$ m and $L=48$ m (see Table 2) are summarized. The following remarks can be made:

- For buildings hinged at the base, serviceability limit states are still decisive.
- For buildings fixed at their base, ultimate limit states become decisive; the load combination CSX is dimensioning if $q_0=1$, whereas CSLU 2.0 is dimensioning if $q_0>1$. For this reason, the site is determining only if $q_0=1$.
- The differences from the previous case ($B=12$ m and $L=30$ m) may be attributed to the increased torsional effects.

Table 5. Size of principal structural elements of the building with B=12 m and L=30 m.

Configuration	$q_0=1$			$q_0>1$		
	Load comb.	Columns	Beams	Load comb.	Columns	Beams
B12_L30_FIX_RE_C_SD	CSLE_R 4.3	HEB 340	HEB 340	CSLE_R 4.3	HEB 340	HEB 340
B12_L30_FIX_RE_C_CL	CSLE_R 4.3	HEB 340	HEB 340	CSLE_R 4.3	HEB 340	HEB 340
B12_L30_FIX_RE_D_SD	CSX (SLD)	HEB 340	HEB 340	CSX (SLD)	HEB 340	HEB 340
B12_L30_FIX_RE_D_CL	CSX (SLD)	HEB 340	HEB 340	CSX (SLD)	HEB 340	HEB 340
B12_L30_HIN_RE_C_SD	CSX (SLD)	HEB 550	HEB 550	CSX (SLD)	HEB 550	HEB 550
B12_L30_HIN_RE_C_CL	CSX (SLD)	HEB 550	HEB 550	CSX (SLD)	HEB 550	HEB 550
B12_L30_HIN_RE_D_SD	CSX (SLD)	HEB 600	HEB 550	CSX (SLD)	HEB 600	HEB 550
B12_L30_HIN_RE_D_CL	CSX (SLD)	HEB 600	HEB 550	CSX (SLD)	HEB 600	HEB 550
B12_L30_FIX_GE_C_SD	CSX (SLD)	HEB 340	HEB 340	CSX (SLD)	HEB 340	HEB 340
B12_L30_FIX_GE_C_CL	CSX (SLD)	HEB 340	HEB 340	CSX (SLD)	HEB 340	HEB 340
B12_L30_FIX_GE_D_SD	CSX (SLD)	HEB 340	HEB 340	CSX (SLD)	HEB 340	HEB 340
B12_L30_FIX_GE_D_CL	CSX (SLD)	HEB 340	HEB 340	CSX (SLD)	HEB 340	HEB 340
B12_L30_HIN_GE_C_SD	CSX (SLD)	HEB 800	HEB 550	CSX (SLD)	HEB 800	HEB 550
B12_L30_HIN_GE_C_CL	CSX (SLD)	HEB 800	HEB 550	CSX (SLD)	HEB 800	HEB 550
B12_L30_HIN_GE_D_SD	CSX (SLD)	HEB 1000	HEB 550	CSX (SLD)	HEB 1000	HEB 550
B12_L30_HIN_GE_D_CL	CSX (SLD)	HEB 1000	HEB 550	CSX (SLD)	HEB 1000	HEB 550

Table 6. Size of principal structural elements of the building with B=12 m and L=48 m.

Configuration	$q_0=1$			$q_0>1$		
	Load comb.	Columns	Beams	Load comb.	Columns	Beams
B12_L48_FIX_RE_C_SD	CSX (SLU)	HEB 340	HEB 340	CSLU 2.0	HEB 340	HEB 340
B12_L48_FIX_RE_C_CL	CSX (SLU)	HEB 340	HEB 340	CSLU 2.0	HEB 340	HEB 340
B12_L48_FIX_RE_D_SD	CSX (SLU)	HEB 340	HEB 340	CSLU 2.0	HEB 340	HEB 340
B12_L48_FIX_RE_D_CL	CSX (SLU)	HEB 340	HEB 340	CSLU 2.0	HEB 340	HEB 340
B12_L48_HIN_RE_C_SD	CSLE_R 4.4	HEB 550	HEB 550	CSLE_R 4.4	HEB 550	HEB 550
B12_L48_HIN_RE_C_CL	CSLE_R 4.4	HEB 550	HEB 550	CSLE_R 4.4	HEB 550	HEB 550
B12_L48_HIN_RE_D_SD	CSX (SLD)	HEB 600	HEB 550	CSX (SLD)	HEB 600	HEB 550
B12_L48_HIN_RE_D_CL	CSX (SLD)	HEB 600	HEB 550	CSX (SLD)	HEB 600	HEB 550
B12_L48_FIX_GE_C_SD	CSX (SLU)	HEB400	HEB 400	CSLU 2.0	HEB 340	HEB 340
B12_L48_FIX_GE_C_CL	CSX (SLU)	HEB400	HEB 400	CSLU 2.0	HEB 340	HEB 340
B12_L48_FIX_GE_D_SD	CSX (SLU)	HEB400	HEB 400	CSLU 2.0	HEB 340	HEB 340
B12_L48_FIX_GE_D_CL	CSX (SLU)	HEB400	HEB 400	CSLU 2.0	HEB 340	HEB 340
B12_L48_HIN_GE_C_SD	CSX (SLD)	HEB 700	HEB 550	CSX (SLD)	HEB 700	HEB 550
B12_L48_HIN_GE_C_CL	CSX (SLD)	HEB 700	HEB 550	CSX (SLD)	HEB 700	HEB 550
B12_L48_HIN_GE_D_SD	CSX (SLD)	HEB 900	HEB 550	CSX (SLD)	HEB 900	HEB 550
B12_L48_HIN_GE_D_CL	CSX (SLD)	HEB 900	HEB 550	CSX (SLD)	HEB 900	HEB 550

Finally, the profiles obtained for the larger building ($B=24$ m and $L=30$ m) are reported in Table 7. It can be observed that only fixed solutions were considered, since too large displacements would have been obtained otherwise. In this case, bending on beams is decisive and results in large H profiles determined by the static load combination CSLU 2.0 (ultimate LS standard combination with snow as prevalent action).

Table 7. Size of principal structural elements of the building with $B=24$ m and $L=30$ m.

Configuration	$q_0=1$			$q_0>1$		
	Load comb.	Columns	Beams	Load comb.	Columns	Beams
B24_L30_FIX_RE_C_SD	CSLU 2.0	H400x509	H 400x509	CSLU 2.0	H400x509	H 400x509
B24_L30_FIX_RE_C_CL	CSLU 2.0	H400x509	H 400x509	CSLU 2.0	H400x509	H 400x509
B24_L30_FIX_RE_D_SD	CSLU 2.0	H400x509	H 400x509	CSLU 2.0	H400x509	H 400x509
B24_L30_FIX_RE_D_CL	CSLU 2.0	H400x509	H 400x509	CSLU 2.0	H400x509	H 400x509
B24_L30_FIX_GE_C_SD	CSLU 2.0	H400x509	H 400x509	CSLU 2.0	H400x509	H 400x509
B24_L30_FIX_GE_C_CL	CSLU 2.0	H400x509	H 400x509	CSLU 2.0	H400x509	H 400x509
B24_L30_FIX_GE_D_SD	CSLU 2.0	H400x509	H 400x509	CSLU 2.0	H400x509	H 400x509
B24_L30_FIX_GE_D_CL	CSLU 2.0	H400x509	H 400x509	CSLU 2.0	H400x509	H 400x509

2.4 Design of foundation systems

Ultimate limit states only, inherent to the development of failure mechanisms due to the mobilization of soil strength and the achievement of the bearing capacity of the foundation elements, have been taken into account for the design of foundations. Both short-term (undrained) and long-term (drained) conditions were considered.

The verifications were carried out according to the "Approach 2" of NTC (2008). Two sets of soil parameters (relating only on soil strength) were assumed (Table 8 and Table 9).

Table 8. Characteristic soil parameters (sand) assumed in the analyses.

Soil type	Ground type	N_{SPT} [blows/30cm]	γ [kN/m^3]	c'_k [kPa]	ϕ'_k
Sand	C	20	19	0	34°
	D	12	19	0	30°

Table 9. Characteristic soil parameters (clay) assumed in the analyses.

Soil type	Ground type	γ [kN/m^3]	c_{uk} [kPa]
Clay	C	19	50
	D	19	30

As far as structures designed with $q_0=1$ are concerned, the actions transmitted to the foundation system have been calculated based on the reactions of the elevation to which static and seismic actions are applied.

For structures having $q_0>1$, the foundation design and the safety assessment of the soil-foundation system are based on the minimum action among the following: the resistances of the structural elements of the elevation; the actions transferred from the structural elements of

the elevation, amplified by $\gamma_{Rd}=1.1$; the actions resulting from an elastic analysis of the elevation, performed with $q_0=1$.

Since the elevation is made up of a combination of beams and pillars and the vertical actions are relatively low, it was chosen in the preliminary analyses to adopt spread footings embedded 0.80 m. For the purpose of this study, in addition to the structural verifications on the footings, the following geotechnical verifications have been performed: bearing capacity in seismic conditions using the Brinch-Hansen (1970) formulation, modified according to EC8 (2007); sliding along foundation plane. Settlement assessment has been carried out as well, even if for the study aim (ultimate limit state) the obtained results are not significant. According to the current regulations, the foundation system in seismic zones must have high extensible stiffness in the horizontal plane and spread footings have to be appropriately connected in order to minimize the effects of the spatial variability of the seismic motion. Thus, in the performed analyses, two different connection systems were hypothesized:

- Strap footings, adopting connecting beams having 0.50 m x 1.00 m section, reinforced, to withstand tensile stress caused by relative displacements, with 10 longitudinal bars (diameter $\phi 16$ mm) and vertical stirrups $\phi 8/300$ mm.
- Thin reinforced slabs (current thickness 0.30 m - thickness 0.60 m in correspondence of the pillars). The slab is cast in place and reinforced with two electro welded nets $\phi 12/200 \times 200$ mm. This solution is frequently used because of its easier and quicker execution.

Only in a second phase, when the solution with isolated footings resulted unsuitable, two alternative solutions were considered, according to the following mechanisms and schemes:

- for problems of foundation sliding: a soil improvement intervention;
- for problems related to excessive eccentricity and bearing capacity: foundation on piles.

As a ground improvement intervention it was assumed to replace the surficial layer of soil (almost 1 m) with 0.30 m of compacted well-graded gravel (right under the footings) and the remaining 0.70 m (around and above the footings) using the previously excavated material (Figure 5).

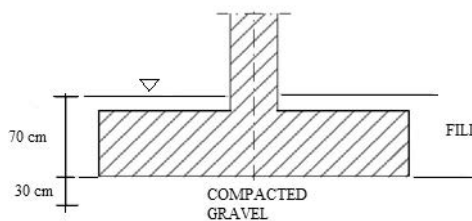


Figure 5. Scheme of the soil improvement intervention.

As far as the deep foundation solution is concerned, micropiles have been preferred for their easier and faster execution, for their applicability in different soil conditions and for their relatively low cost. When considering a steel frame structure, a square footing ($B=L=3.00$ m) is placed at the base of each pillar, connecting the heads of the micropiles and distributing the load transmitted by the pillar itself. Four 200 mm diameter micropiles are placed at the vertices of the footing in order to avoid eccentricity (Figure 6).

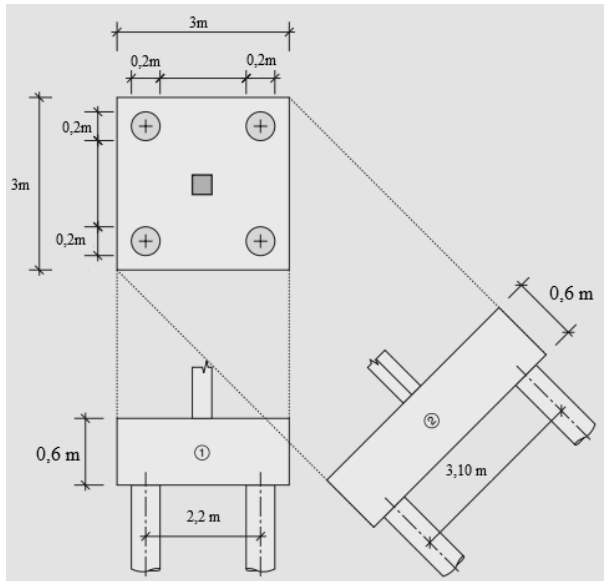


Figure 6. Scheme of foundation on micropiles.

For single-storey industrial buildings having $B = 12$ m and $L = 30$ m, reports the types of foundations defined in accordance with the various cases here analysed. It is therefore possible to remark:

- In relation to foundation verifications, the use of a factor $q_0 > 1$ greatly reduces the base reactions and thus the actions on the foundations, allowing, in some configurations hinged at their base, to have spread footings, possibly with ground improvement intervention.
- For the buildings fixed at their base, the reactions at foundation level are very high. In particular, the bending moment in the plane of the transverse frames results in considerable eccentricities that generates reduced footing areas that force to a piled foundation solution.

Table 11 reports the types of foundations obtained in the various cases, for long buildings having $B = 12$ m and $L = 48$ m. In these cases, a factor $q_0 > 1$ allowed, in the configuration referred to a medium-low seismic zone, with portal hinged at the base, to adopt spread footings with ground improvement especially in sandy soils. When considering a medium-high seismic zone, the horizontal actions caused by the earthquake continue to remain too high and consequently pile foundations have to be adopted.

The reactions for the large buildings cases ($B=24$ m) were almost of an order of magnitude greater than those calculated in the other two cases; consequently, it was thought to adopt directly a foundation on piles, without even attempting a shallow foundation solution. However, in this case the adopted micropiles have not sufficient resistance to withstand the great efforts transmitted by the superstructure. Designing a foundation on large diameter piles, on the other hand, could be a convenient solution for a prestressed concrete superstructure, but is quite expensive for lightweight steel structures. For this reason, it was chosen to not investigate this particular solution.

Table 10. Foundation type – Building B=12 m and L=30 m.
 (Note: ecc./red. base: eccentricity/reduced base - high hor. act.:high horizontal actions)

Configuration	Comb.	q ₀ =1		q ₀ >1	
		Problem	Foundation	Problem	Foundation
B12_L30_FIX_RE_C_SD	CSX (SLU)	ecc./red. base	micropiles	ecc./red. base	micropiles
B12_L30_FIX_RE_C_CL	CSX (SLU)	ecc./red. base	micropiles	ecc./red. base	micropiles
B12_L30_FIX_RE_D_SD	CSX (SLU)	ecc./red. base	micropiles	ecc./red. base	micropiles
B12_L30_FIX_RE_D_CL	CSX (SLU)	ecc./red. base	micropiles	ecc./red. base	micropiles
B12_L30_HIN_RE_C_SD	CSX (SLU)	high hor. act.	micropiles	-	spread footings
B12_L30_HIN_RE_C_CL	CSX (SLU)	high hor. act.	micropiles	-	spread footings
B12_L30_HIN_RE_D_SD	CSX (SLU)	high hor. act.	micropiles	high hor. act.	spread footings + ground improv.
B12_L30_HIN_RE_D_CL	CSX (SLU)	high hor. act.	micropiles	-	spread footings
B12_L30_FIX_GE_C_SD	CSX (SLU)	ecc./red. base	micropiles	ecc./red. base	micropiles
B12_L30_FIX_GE_C_CL	CSX (SLU)	ecc./red. base	micropiles	ecc./red. base	micropiles
B12_L30_FIX_GE_D_SD	CSX (SLU)	ecc./red. base	micropiles	ecc./red. base	micropiles
B12_L30_FIX_GE_D_CL	CSX (SLU)	ecc./red. base	micropiles	ecc./red. base	micropiles
B12_L30_HIN_GE_C_SD	CSX (SLU)	high hor. act.	micropiles	high hor. act.	spread footings + ground improv..
B12_L30_HIN_GE_C_CL	CSX (SLU)	high hor. act.	micropiles	-	spread footings
B12_L30_HIN_GE_D_SD	CSX (SLU)	high hor. act.	micropiles	high hor. act.	spread footings + ground improv..
B12_L30_HIN_GE_D_CL	CSX (SLU)	high hor. act.	micropiles	-	spread footings

Table 11. Foundation type – Building B=12 m and L=48 m.
 (Note: ecc./red. base: eccentricity/reduced base - high hor. act.:high horizontal actions)

Configuration	Comb.	q ₀ =1		q ₀ >1	
		Problem	Foundation	Problem	Foundation
B12_L48_FIX_RE_C_SD	CSX (SLU)	ecc./red. base	micropiles	ecc./red. base	micropiles
B12_L48_FIX_RE_C_CL	CSX (SLU)	ecc./red. base	micropiles	ecc./red. base	micropiles
B12_L48_FIX_RE_D_SD	CSX (SLU)	ecc./red. base	micropiles	ecc./red. base	micropiles
B12_L48_FIX_RE_D_CL	CSX (SLU)	ecc./red. base	micropiles	ecc./red. base	micropiles
B12_L48_HIN_RE_C_SD	CSX (SLU)	high hor. act.	micropiles	high hor. act.	spread footings + ground improv.
B12_L48_HIN_RE_C_CL	CSX (SLU)	high hor. act.	micropiles	-	spread footings
B12_L48_HIN_RE_D_SD	CSX (SLU)	high hor. act.	micropiles	high hor. act.	spread footings + ground improv.
B12_L48_HIN_RE_D_CL	CSX (SLU)	high hor. act.	micropiles	-	spread footings
B12_L48_FIX_GE_C_SD	CSX (SLU)	ecc./red. base	micropiles	ecc./red. base	micropiles
B12_L48_FIX_GE_C_CL	CSX (SLU)	ecc./red. base	micropiles	ecc./red. base	micropiles
B12_L48_FIX_GE_D_SD	CSX (SLU)	ecc./red. base	micropiles	ecc./red. base	micropiles
B12_L48_FIX_GE_D_CL	CSX (SLU)	ecc./red. base	micropiles	ecc./red. base	micropiles
B12_L48_HIN_GE_C_SD	CSX (SLU)	high hor. act.	micropiles	high hor. act.	micropiles
B12_L48_HIN_GE_C_CL	CSX (SLU)	high hor. act.	micropiles	high hor. act.	micropiles
B12_L48_HIN_GE_D_SD	CSX (SLU)	high hor. act.	micropiles	high hor. act.	spread footings + ground improv.
B12_L48_HIN_GE_D_CL	CSX (SLU)	high hor. act.	micropiles	-	spread footings

Table 12 reports the structural characteristics of the spread footings obtained for those cases where it was sufficient to consider this type of shallow foundation with or without soil improvement intervention. Note that although the CSX (SLU) (ultimate LS seismic combination along the transversal direction) is the decisive combination from the geotechnical point of view, the designing combination for these structural elements is CSLU 4.4 (ultimate LS standard combination with wind as prevalent action along the transversal direction). Table 13 reports the friction angles of the compacted gravel layer, requested in order to satisfy the sliding verification.

Table 12. Structural characteristics of the spread footings (measures in mm).

Configuration	Comb.	Lon. bars	Stirrups	Bolts (6.8)	Steel plate
B12_L30_HIN_RE_C_SD ($q_0 > 1$)	CSLU 4.4	10 ϕ 20 + 2 ϕ 20 p.	ϕ 12/300	2 ϕ 16	830x830
B12_L30_HIN_RE_C_CL ($q_0 > 1$)	CSLU 4.4	10 ϕ 20 + 2 ϕ 20 p.	ϕ 12/300	2 ϕ 16	830x830
B12_L30_HIN_RE_D_CL ($q_0 > 1$)	CSLU 4.4	10 ϕ 20 + 2 ϕ 20 p.	ϕ 12/300	2 ϕ 16	900x900
B12_L30_HIN_GE_C_CL ($q_0 > 1$)	CSLU 4.4	10 ϕ 20 + 2 ϕ 20 p.	ϕ 12/300	2 ϕ 16	1200x1200
B12_L30_HIN_GE_D_CL ($q_0 > 1$)	CSLU 4.4	10 ϕ 20 + 2 ϕ 20 p.	ϕ 12/300	2 ϕ 16	1500x1500
B12_L48_HIN_RE_C_CL ($q_0 > 1$)	CSLU 4.4	10 ϕ 20 + 2 ϕ 20 p.	ϕ 12/300	2 ϕ 16	830x830
B12_L48_HIN_RE_D_CL ($q_0 > 1$)	CSLU 4.4	10 ϕ 20 + 2 ϕ 20 p.	ϕ 12/300	2 ϕ 16	900x900
B12_L30_HIN_RE_D_SD ($q_0 > 1$)	CSLU 4.4	10 ϕ 20 + 2 ϕ 20 p.	ϕ 12/300	2 ϕ 16	900x900
B12_L30_HIN_GE_C_SD ($q_0 > 1$)	CSLU 4.4	10 ϕ 20 + 2 ϕ 20 p.	ϕ 12/300	2 ϕ 16	1200x1200
B12_L30_HIN_GE_D_SD ($q_0 > 1$)	CSLU 4.4	10 ϕ 20 + 2 ϕ 20 p.	ϕ 12/300	2 ϕ 16	1500x1500
B12_L48_HIN_RE_C_SD ($q_0 > 1$)	CSLU 4.4	10 ϕ 20 + 2 ϕ 20 p.	ϕ 12/300	2 ϕ 16	830x830
B12_L48_HIN_RE_D_SD ($q_0 > 1$)	CSLU 4.4	10 ϕ 20 + 2 ϕ 20 p.	ϕ 12/300	2 ϕ 16	900x900

Table 13. Minimum friction angles for compacted gravel layers

Configuration	Req. friction angle
B12_L30_HIN_RE_D_SD ($q_0 > 1$)	42°
B12_L30_HIN_GE_C_SD ($q_0 > 1$)	42°
B12_L30_HIN_GE_D_SD ($q_0 > 1$)	41°
B12_L48_HIN_RE_C_SD ($q_0 > 1$)	38°
B12_L48_HIN_RE_D_SD ($q_0 > 1$)	40°

In Table 14-Table 17 the micropiles sizes obtained in those cases where it was necessary to adopt this solution, are indicated. It can be noted that:

- In the shorter building, the pile lengths are reduced by introducing a factor $q_0 > 1$, as in most cases the designing combination becomes CSLU 4.3 and no longer CSX (SLU).
- The long building is affected mostly by the forces generated by the CSLU 4.3 combination, except in the portals fixed at the base and in the D ground type, where the required length increases, remaining in any case below those required in the shorter building.
- In the long building, with $q_0 > 1$, the designing combination is always CSLU 4.3 and the earthquake is no longer decisive. As a result, small differences in length are related to the ground type (C, D).

Table 14. Micropiles lengths – Configuration B=12 m - L=30 m – $q_0=1$. (Long. Bars 10 ϕ 20 + 2 ϕ 20 p.).

Configuration	Comb	Problem	Length (m)	Comb.	Stirrups	Bolts (6.8)	Plate (mm)
B12_L30_FIX_RE_C_SD	CSLU 4.3	min. length	6	CSX (SLU)	ϕ 12/200	4 ϕ 20	680x680
B12_L30_FIX_RE_C_CL	CSLU 4.3	min. length	6	CSX (SLU)	ϕ 12/200	4 ϕ 20	680x680
B12_L30_FIX_RE_D_SD	CSX (SLU)	min. length	6	CSX (SLU)	ϕ 12/200	4 ϕ 20	680x680
B12_L30_FIX_RE_D_CL	CSX (SLU)	bear. cap.	8	CSX (SLU)	ϕ 12/200	4 ϕ 20	680x680
B12_L30_HIN_RE_C_SD	CSLU 4.3	min. length	6	CSLU 4.4	ϕ 12/300	2 ϕ 16	830x830
B12_L30_HIN_RE_C_CL	CSLU 4.3	min. length	6	CSLU 4.4	ϕ 12/300	2 ϕ 16	830x830
B12_L30_HIN_RE_D_SD	CSLU 4.3	min. length	6	CSX (SLU)	ϕ 12/200	2 ϕ 20	900X900
B12_L30_HIN_RE_D_CL	CSLU 4.3	bear. cap.	6	CSX (SLU)	ϕ 12/200	2 ϕ 20	900X900
B12_L30_FIX_GE_C_SD	CSX (SLU)	min. length	6	CSX (SLU)	ϕ 12/150	4 ϕ 24	680X680
B12_L30_FIX_GE_C_CL	CSX (SLU)	min. length	6	CSX (SLU)	ϕ 12/150	4 ϕ 24	680X680
B12_L30_FIX_GE_D_SD	CSX (SLU)	min. length	6	CSX (SLU)	ϕ 12/150	4 ϕ 24	680X680
B12_L30_FIX_GE_D_CL	CSX (SLU)	bear. cap.	9	CSX (SLU)	ϕ 12/150	4 ϕ 24	680X680
B12_L30_HIN_GE_C_SD	CSLU 4.3	min. length	6	CSX (SLU)	ϕ 12/300	2 ϕ 20	1200X1200
B12_L30_HIN_GE_C_CL	CSLU 4.3	min. length	6	CSX (SLU)	ϕ 12/300	2 ϕ 20	1200X1200
B12_L30_HIN_GE_D_SD	CSLU 4.3	min. length	6	CSX (SLU)	ϕ 12/300	2 ϕ 20	1500X1500
B12_L30_HIN_GE_D_CL	CSLU 4.3	bear. cap.	6	CSX (SLU)	ϕ 12/300	2 ϕ 20	1500X1500

Table 15. Micropiles lengths – Configuration B=12 m - L=30 m – $q_0>1$ (Long. Bars 10 ϕ 20 + 2 ϕ 20 p.).

Configuration	Comb.	Problem	Length (m)	Comb.	Stirrups	Bolts (6.8)	Plate (mm)
B12_L30_FIX_RE_C_SD	CSLU 4.3	min. length	6	CSLU 4.4	ϕ 12/250	4 ϕ 16	1500x1500
B12_L30_FIX_RE_C_CL	CSLU 4.3	min. length	6	CSLU 4.4	ϕ 12/250	4 ϕ 16	680x680
B12_L30_FIX_RE_D_SD	CSLU 4.3	min. length	6	CSLU 4.4	ϕ 12/250	4 ϕ 16	680x680
B12_L30_FIX_RE_D_CL	CSLU 4.3	bear. cap.	6	CSLU 4.4	ϕ 12/250	4 ϕ 16	680x680
B12_L30_FIX_GE_C_SD	CSLU 4.3	min. length	6	CSLU 4.4	ϕ 12/250	4 ϕ 16	680x680
B12_L30_FIX_GE_C_CL	CSLU 4.3	min. length	6	CSLU 4.4	ϕ 12/250	4 ϕ 16	680x680
B12_L30_FIX_GE_D_SD	CSX (SLU)	min. length	6	CSLU 4.4	ϕ 12/250	4 ϕ 16	680x680
B12_L30_FIX_GE_D_CL	CSX (SLU)	bear. cap.	9	CSLU 4.4	ϕ 12/250	4 ϕ 16	680x680

Table 16. Micropiles lengths – Configuration B=12 m - L=48 m – $q_0=1$ (Long. Bars 10 ϕ 20 + 2 ϕ 20 p.).

Configuration	Comb.	Problem	Length (m)	Comb.	Stirrups	Bolt (6.8)	Plate (mm)
B12_L48_FIX_RE_C_SD	CSLU 4.3	min. length	6	CSLU 4.4	ϕ 12/250	4 ϕ 16	680x680
B12_L48_FIX_RE_C_CL	CSLU 4.3	min. length	6	CSLU 4.4	ϕ 12/250	4 ϕ 16	680x680
B12_L48_FIX_RE_D_SD	CSX (SLU)	min. length	6	CSX (SLU)	ϕ 12/250	4 ϕ 20	680x680
B12_L48_FIX_RE_D_CL	CSX (SLU)	bear. cap.	7	CSX (SLU)	ϕ 12/250	4 ϕ 20	680x680
B12_L48_HIN_RE_C_SD	CSLU 4.3	min. length	6	CSLU 4.4	ϕ 12/300	2 ϕ 16	830x830
B12_L48_HIN_RE_C_CL	CSLU 4.3	min. length	6	CSLU 4.4	ϕ 12/300	2 ϕ 16	830x830
B12_L48_HIN_RE_D_SD	CSLU 4.3	min. length	6	CSLU 4.4	ϕ 12/300	2 ϕ 16	900X900
B12_L48_HIN_RE_D_CL	CSLU 4.3	bear. cap.	6	CSLU 4.4	ϕ 12/300	2 ϕ 16	900X900
B12_L48_FIX_GE_C_SD	CSLU 4.3	min. length	6	CSX (SLU)	ϕ 12/200	4 ϕ 24	800X800
B12_L48_FIX_GE_C_CL	CSLU 4.3	min. length	6	CSX (SLU)	ϕ 12/200	4 ϕ 24	800X800
B12_L48_FIX_GE_D_SD	CSX (SLU)	min. length	6	CSX (SLU)	ϕ 12/150	4 ϕ 24	800X800
B12_L48_FIX_GE_D_CL	CSX (SLU)	bear. cap.	8	CSX (SLU)	ϕ 12/150	4 ϕ 24	800X800
B12_L48_HIN_GE_C_SD	CSLU 4.3	min. length	6	CSLU 4.4	ϕ 12/300	2 ϕ 16	1050X1050
B12_L48_HIN_GE_C_CL	CSLU 4.3	min. length	6	CSLU 4.4	ϕ 12/300	2 ϕ 16	1050X1050
B12_L48_HIN_GE_D_SD	CSLU 4.3	min. length	6	CSX (SLU)	ϕ 12/300	2 ϕ 20	1350X1350
B12_L48_HIN_GE_D_CL	CSLU 4.3	bear. cap.	6	CSX (SLU)	ϕ 12/300	2 ϕ 20	1350X1350

Table 17. Micropiles lengths – Configuration B=12 m - L=48 m – $q_0>1$ (Long. Bars 10 ϕ 20 + 2 ϕ 20 p.).

Configuration	Comb.	Problem	Length (m)	Comb.	Stirrups	Bolts (6.8)	Plate (mm)
B12_L48_FIX_RE_C_SD	CSLU 4.3	min. length	6 m	CSLU 4.4	ϕ 12/250	4 ϕ 16	680x680
B12_L48_FIX_RE_C_CL	CSLU 4.3	min. length	6 m	CSLU 4.4	ϕ 12/250	4 ϕ 16	680x680
B12_L48_FIX_RE_D_SD	CSLU 4.3	min. length	6 m	CSLU 4.4	ϕ 12/250	4 ϕ 16	680x680
B12_L48_FIX_RE_D_CL	CSLU 4.3	bear. cap.	7 m	CSLU 4.4	ϕ 12/250	4 ϕ 16	680x680
B12_L48_FIX_GE_C_SD	CSLU 4.3	min. length	6 m	CSLU 4.4	ϕ 12/250	4 ϕ 16	680X680
B12_L48_FIX_GE_C_CL	CSLU 4.3	min. length	6 m	CSLU 4.4	ϕ 12/250	4 ϕ 16	680X680
B12_L48_FIX_GE_D_SD	CSLU 4.3	min. length	6 m	CSLU 4.4	ϕ 12/250	4 ϕ 16	680X680
B12_L48_FIX_GE_D_CL	CSLU 4.3	bear. cap.	7 m	CSLU 4.4	ϕ 12/250	4 ϕ 16	680X680
B12_L48_HIN_GE_C_SD	CSLU 4.3	min. length	6 m	CSLU 4.4	ϕ 12/300	2 ϕ 16	1050X1050
B12_L48_HIN_GE_C_CL	CSLU 4.3	min. length	6 m	CSLU 4.4	ϕ 12/300	2 ϕ 16	1050X1050
B12_L48_HIN_GE_D_SD	CSLU 4.3	min. length	6 m	CSLU 4.4	ϕ 12/300	2 ϕ 16	1350X1350
B12_L48_HIN_GE_D_CL	CSLU 4.3	bear. cap.	6 m	CSLU 4.4	ϕ 12/300	2 ϕ 16	1350X1350

In conclusion, the following remarks can be made:

- for all buildings, foundations on micropiles should be used when a non-dissipative behaviour ($q_0=1$) is assumed;
- for shorter buildings ($L = 30$ m), assuming dissipative behaviour ($q_0>1$), in case of fixed end base, it is necessary to use micropiles (although shorter than the case with $q = 1$), whereas in case of hinged base, spread footings can be adopted, although often with soil improvement;
- for long buildings ($L=48$ m) with dissipative behaviour ($q_0>1$) and fixed end base, micropiles are still required (although shorter than in case $q=1$), while in the case of hinged base, spread footings with soil improvement can be adopted only in case of medium to low seismic sites.

3 ECONOMIC EVALUATION

In this research, the Emilia Romagna regional rates (Elenco Regionale dei prezzi e delle opere pubbliche della regione Emilia-Romagna, 2015), integrated with the annual report on materials and building works published by the Chamber of Commerce of Reggio Emilia (Prezzi informativi materiali da costruzione ed opere edili, Camera di Commercio di Reggio Emilia, 2015), was used. It has been assessed that the prices collected are in line with those of other Italian regions, including Friuli-Venezia Giulia (Gemona site). However, it has also been assessed that market prices are in general lower for some special operations such as installation of micropiles and geotechnical investigations.

The prices used refer to completed works carried out in conformity with the Law and regulations (UNI and CEI). In accordance with art. 32 of D.P.R. n. 207/2010 of the Italian Law, prices include costs related to general expenses and profits (26,50%). Thus, prices include materials, labour, freight and transport costs, whereas do not include building site costs and security charges.

Prices were obtained by calculating the amount of works in terms of size (length/volume) or weight. In particular, the following assumptions were employed:

- Two types of excavation were considered: the first one consists in the removal of the top soil over the entire area, while in the second case only the soil directly in the footing area have been removed. Soil replacement under the footing, with compacted gravel as ground improvement, has been accounted as well. The excavated soil volumes have been precisely evaluated in both cases and in the cost assessment also the effect of the different lifting equipments has been taken into account. The amount of concrete employed in foundation structures was computed based on their actual volume (comprehensive of the volume of reinforcing bars), while the amount of steel was computed on percentage.
- R.C. formworks were computed based on actual surfaces; their prices include propping works up to 4 m; additional costs were considered for higher formworks.
- Since floors were subjected to high loads, they should be plane and thick (up to 0.1 m). In case of foundations connected with beams, it was assumed that such concrete layer was built on a 0.2 m thick layer of gravel or sand mixed with medium sized gravel with separating polyethylene films. In case of foundations connected with a 0.60 m thick slab, the floor was supposed to be built directly on this structural element.
- As far as soil investigation is concerned, the cost for soundings, recovering of at least five undisturbed clay samples, execution of at least five SPT's, have been considered.

- For micropiles foundations, prices were computed considering the number of micropiles and the weight (i.e. diameter and thickness) of reinforcing steel tubes.
- For soil interventions (soil removal and replacement), the cost of gravel and the cost of compaction and backfilling were computed, considering a layer 0.3m thick under the foundation of columns.

The overall costs of each building was evaluated under these assumptions. For each case, two different types of foundation linking have been designed, either by beams or by slabs.

4 ENVIRONMENTAL EVALUATION

Buildings were compared in terms of environmental impacts too. In particular, the following impacts were evaluated for each case: Primary Energy Demand (PED) and Global Warming Potential (GWP).

A simplified approach was adopted instead of the traditional Life Cycle Assessment (LCA). Developed by the University of Liege (Rossi, 2010), it provides an acceptably reliable estimation of PED and GWP along the life cycle.

Concerning the production phase, the weights of structural elements were multiplied for the unitary Energy Demand expressed in MJ/kg (PED) and for the content of equivalent CO₂ expressed in kg CO₂ eq./kg (GWP). Two different inventories of energy and carbon were used for structural steel (Steel inventory, 2010) or steel bars for reinforced concrete elements (Concrete inventory, 2001). Although these inventories are not specifically referred to Italian products, their use is deemed to be acceptable for these evaluation. The following hypotheses were done: 0.85 kg of scrap content for 1 kg of steel profiles; 0.69 kg of scrap content for 1 kg of steel bars.

As regards the transport from the place of production to the building site, it was assumed that steel profiles and steel bars required a road transport 100 km long, while concrete required a road transport 50 km long. These distances were multiplied by the amount of MJ/(kg x km) and CO₂ eq./kg (kg x km) obtained from a specific inventory for transport impacts (Ecoinvent database, 2010).

Finally, to evaluate the environmental impacts at end-of-life (demolition and landfill) it was assumed that 99% of steel profiles, 67% of steel bars and 90% of concrete were recycled. Then, the amount of material for disposal was multiplied for the unitary energy and the equivalent CO₂ of construction and demolition waste disposal (Ecoinvent database, 2010). The amount of recycle material was instead considered as an environmental credit. Finally, the impacts related to the transport from the building to the landfill was evaluated as those related to the transport from the production site to the building site, considering a distance of 50 km.

5 CRITICAL COMPARISONS

The critical comparisons are provided in terms of economic costs and PED only (as GWP resulted to be linearly dependent on PED). The shorter building costs in mean 382 €/m³ and requires 4120.5 MJ/m³, while the longer one costs 348 €/m³ (with a moderate standard deviation of 58 €/m³) and 3741.75 MJ/m³ (standard deviation 758 MJ/m³). It is worth noting that, in mean, foundations result in approximately 80% of the total costs of the building and 92% of PED in all cases.

From Figure 7, it can be observed that costs and PED of buildings in high seismicity sites (GE-Gemona) is only slightly higher than those in a low seismicity sites (RE – Reggio Emilia). This depends on the influence of some design criteria of the Italian code (NTC, 2008), which are independent from the level of the seismic action, but may be sometimes more stringent than structural requirements (minimum length of micropiles, percentage of reinforcing bars, etc...).

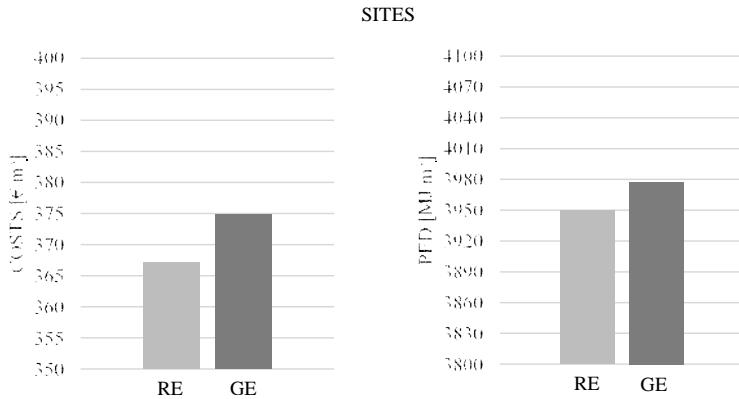


Figure 7. Economic costs and PED as a function of the site seismicity.

The most relevant parameters are the behaviour factor and the base constraints. From Figure 8, it can be observed that, in general, the costs of a low dissipative structures are higher. This is mainly own to the foundation costs: high horizontal actions require extensive and expensive use of micropiles. Figure 9 indicates that hinged columns are more expensive than fixed ones, due to the higher costs of the upper steel structure.

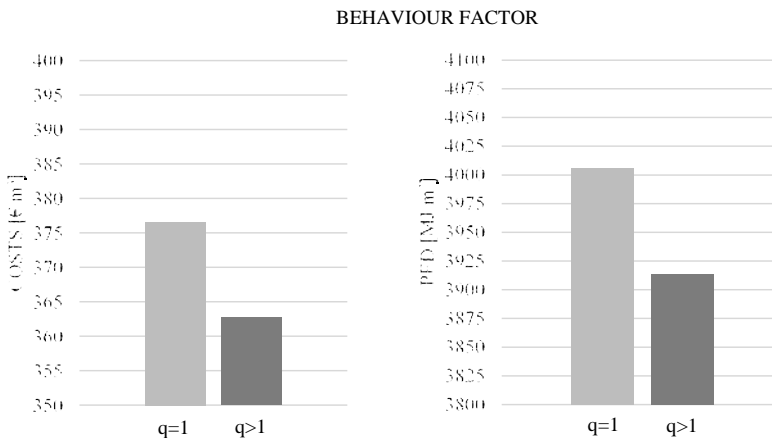


Figure 8. Economic costs and PED as a function of the behaviour factor.

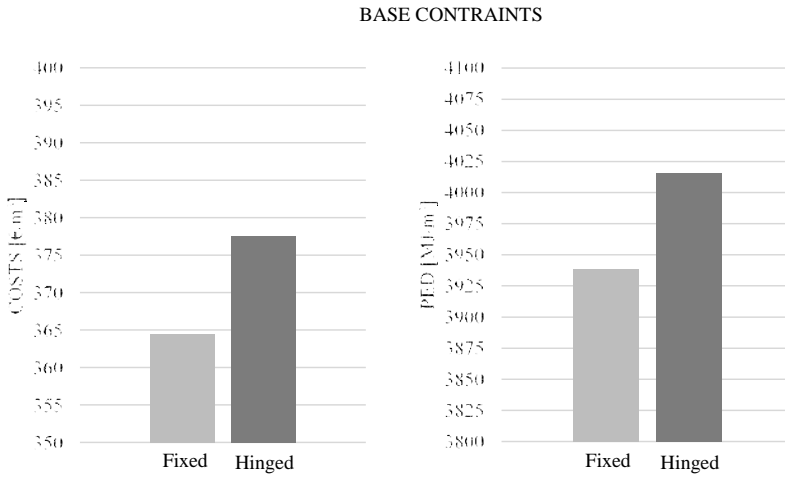


Figure 9. Economic costs and PED as a function of the base constraints.

The crossing of the costs of the behaviour factor and base constraints (Figure 10) highlights that the behaviour factor is much more relevant in base hinged structures. Also in this case, foundation design plays a decisive role. In most of the cases, in fact, serviceability limit states are decisive in the design of the upper steel structures. In fixed buildings, the adoption of a dissipative structural behaviour results only in a small reduction of foundation costs: in both cases expensive pile foundation should be used (even with little size differences). In hinged buildings, instead, shallow foundations (in some case with ground improvement) could be used when $q_0 > 1$.

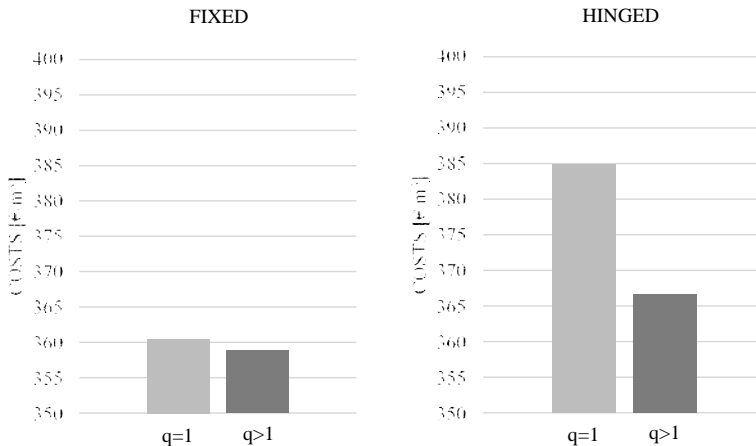


Figure 10. Economic costs and PED as a function of the base constraints.

The role of ground type (Figure 11) and (Figure 12) influences the seismic action and results in larger steel profiles when a class D is considered and the building is fixed at its base. When the building is fixed at its base, higher costs are mainly related to the foundation design, since

in this case longer piles are required. The role of soil type was also investigated, but no significant differences were found between clay and sand. Although in clay soil longer piles are usually required from the geotechnical point of view, the minimum length imposed by the code (NTC, 2008) (6 m) reduces differences. Moreover, the slight increasing of cost due to ground improvement interventions needed for dissipative buildings on clay soil, was not decisive.

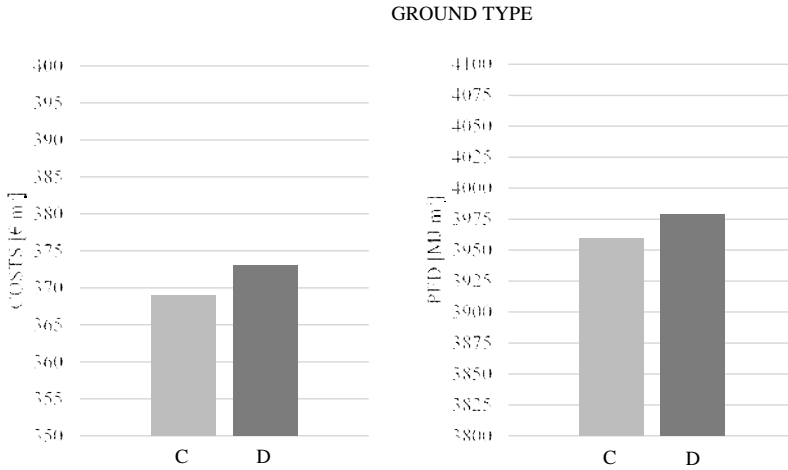


Figure 11. Economic costs and PED as a function of the ground type.

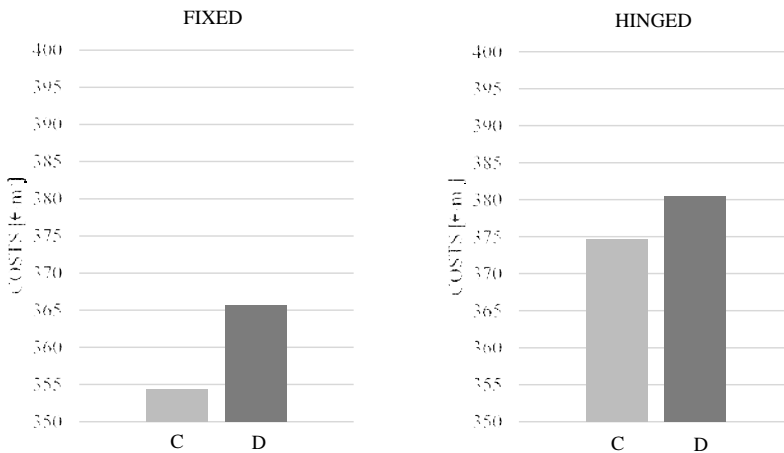


Figure 12. Economic costs and PED as a function of the ground type and base constraints.

6 CONCLUSIONS

This work is a first attempt to address the design of single-storey industrial steel buildings under seismic actions. Fully aware that these buildings do not have major structural problems, this paper aims at improving their design in terms of economic costs and environmental

impact. The number of cases considered in the analyses is still limited; nevertheless, some critical remarks could be done:

- The analysis of the Italian code for single-storey steel buildings highlighted the possible improvement of certain aspects that are not clear and may be barely understood from structural designers. In particular, reference is made to the choice of the structural scheme in the transversal direction (MRF or inverted pendulum) and related behaviour factor.
- In most of the cases, serviceability limit states are decisive in the structural design of these buildings. For this reason, the behaviour factor does not affect the element size to a significant extent. Nevertheless, the behaviour factor plays a significant role in foundation design, leading to different foundation types and influencing building costs and PED.
- The choice of the base constraints may be relevant. Steel structures, when hinged at their base, requires larger columns than fixed ones to satisfy serviceability limit states. Nevertheless, the choice of hinging the columns at their base considerably reduce foundation costs to satisfy ultimate limit states (in particular if a dissipative behaviour is assumed), making the two choices actually comparable.
- The adoption of a dissipative behaviour is slightly more convenient, mainly for the reduction of seismic actions on the foundation system.
- The design is strongly influenced by conventional/practical rules of the code.

7 REFERENCES

- Norme tecniche per le costruzioni* (NTC 2008), D.M. 14 Gennaio 2008 and Circolare n. 617, D.M. 2 Febbraio 2009.
- UNI EN 1998-1:2005, Eurocodice 8 – Progettazione delle strutture per la resistenza sismica, versione italiana Gennaio 2007.
- Consiglio nazionale delle ricerche (CNR), CNR-DT 207/2008, Istruzioni per la valutazione delle azioni e degli effetti del vento sulle costruzioni.
- SAP2000, Computer and Structures Inc., Berkeley California, USA.
- Brinch-Hansen J., (1970), *A revised and extended formula for bearing capacity*, «The Danish Geotechnical Institute», Copenhagen, Bull. N. 28, pp. 5-11.
- Elenco Regionale dei prezzi e delle opere pubbliche della regione Emilia-Romagna, Deliberazione di Giunta n.683/2015, Giugno 2015.
- Prezzi informativi materiali da costruzione ed opere edili, Camera di Commercio di Reggio Emilia, Luglio 2015.
- Rossi, B. (2010). Sustainable steel constructions – Life-cycle inventory, methods and applications, *Proc. sustainability workshop*, University of Liège, Brussels (2010)
- Steel inventory (2010), World Steel Association.
- Ecoinvent database (2010).

SECTION 5

NON-CONVENTIONAL BUILDINGS: STICK BUILT SYSTEMS

NON-CONVENTIONAL BUILDING: STICK-BUILT SYSTEMS – METHODOLOGIES FOR PREDICTION OF SHEAR WALL RESPONSE

Raffaele Landolfo ^a, Maria Teresa Terracciano ^b, Bianca Bucciero ^c,
Tatiana Pali ^d, Vincenzo Macillo ^e, Ornella Iuorio ^f, Luigi Fiorino ^g

^a *University of Naples Federico II, Naples, Italy, landolfo@unina.it*

^b *University of Naples Federico II, Naples, Italy, mariateresa.terracciano@unina.it*

^c *University of Naples Federico II, Naples, Italy, bianca.bucciero@hotmail.it*

^d *University of Naples Federico II, Naples, Italy, tatiana.pali@unina.it*

^e *University of Naples Federico II, Naples, Italy, vincenzo.macillo@unina.it*

^f *University of Leeds, Leeds, UK, O.Iuorio@leeds.ac.uk*

^g *University of Naples Federico II, Naples, Italy, lfiorino@unina.it*

ABSTRACT

In the last years, the applications of cold-formed steel structures in domain of low-rise buildings are increasing. The seismic behaviour of these structures is influenced by the lateral response of shear walls, which are usually sheathed with panels. Different approaches are available to evaluate the lateral response of sheathed cold-formed steel (SCFS) walls: tabulated, numerical and analytical methodologies. In literature, a large number of methods developed for the analysis of sheathed wood shear walls is available and their application is also reasonable in the case of steel-framed shear walls. This paper aims to show the methodologies for prediction of SCFS shear wall response. The application of presented methodologies is illustrated using a calculation example by showing the results in terms of resistance and stiffness for SCFS shear wall.

KEYWORDS

Stick-built walls, sheathing-braced, tabular, numerical and analytical methods, capacity design.

1 INTRODUCTION

The demand for low-cost high-performance constructions is propagating the adoption of cold-formed steel (CFS) systems as a competitive and eco-friendly solution. CFS systems provide the benefits associated with dry constructions (short execution time, quality of products and reduced disruption and noise on site as well as minimum site waste), typical distinctive features of CFS systems (e.g. lightness, high structural performance and good behaviour under seismic actions) and economic value, due to the simplicity of assembling and erection, short execution time, and few man-hours. In addition, the use of recyclable materials, the flexibility of systems and the possible reuse of elements assure a low environmental impact. The CFS systems can be categorized into three large families on the basis of the prefabrication level: modular, panelised and stick-built systems. In particular, modular constructions use pre-engineered modular units, made by assembling completed frames made of any finishing elements (e.g. doors, windows and any finishing material) in the workshop and by the vertical and horizontal addition of the units on site. Panelised constructions are

made of two-dimensional elements (wall and floor sub-frames and roof trusses), which are prefabricated in the workshop. Thermal insulation and some of the lining and finishing materials may also be applied to the steel sub-frame to form boards and to reduce execution times. This system is particularly suited to build houses characterized by repetitive elements. Stick-built constructions are obtained by assembling on site, a modest number of members (e.g. studs, joists and rafters) and sheathing boards, which are fastened together by screws, nails or bolts. This chapter focuses on stick-built systems that represent the most widespread typology, due to the simplicity of realization.

The main structural subsystems of a CFS stick-built construction can be identified in the foundation, walls and floors. The lightness of CFS systems allow the erection of low-rise buildings on minimal foundations, and therefore, the construction can be easily set on poured concrete walls or slab-on-ground foundations. The walls can be subdivided into load bearing and non-bearing walls. The load bearing walls are comprised of studs, i.e. vertical load bearing members spaced (s) at 300 - 600 mm, in line with floor joists. The studs are fastened at each end to wall tracks, which have the function of supporting the studs laterally and to distribute loads among the studs. At mid-wall height, straps may be installed and connected to both flanges of the studs, and some lipped channel profiles (blocking) can be introduced at the ends, with an aim of reducing the stud in-plane unbraced length. In a seismic area, the ability to resist horizontal in-plane actions can be achieved by different systems in CFS constructions:

- X-bracing;
- Mixed solutions obtained by the introduction of both sheathing boards and X-bracing;
- Fastening structural sheathing boards on one or both wall sides.

Moreover, in order to prevent the wall from up-lift due to horizontal in-plane actions, hold-down anchors have to be introduced at the end of each resisting wall. The result is a sandwich construction, where each board can bear perpendicular pressure on its surface as well as in-plane loads. The internal wall cavity is ideal for inserting cables, pipes and insulation. An unlimited range of materials can be used as finishing of both the inner and the outer surface: paint, wallpaper, coating, fabric, etc..

Floors are realized with horizontal load bearing members (joists) and a cladding made of gypsum or woodbased boards. Joists are usually C or Z shaped members, located in line with the wall studs, fastened at each end to a floor track. Floor spans can range from about 4 up to 8 meters depending on the depth and type of the joist. A lightweight steel building can feature pitched or mono-pitched, flat or curved roofs. In any case, the main structural components of roof framing are:

- Rafters, which are structural framing members (usually sloped C section profiles) that support roof loads;
- Ceiling joists, i.e. horizontal, structural CFS profiles that support the ceiling and attic loads (typically C section profiles);
- Ridge members, i.e. horizontal members placed at the intersection between the top edges of two sloping roof surfaces.

2 SEISMIC DESIGN FOR COLD-FORMED STRUCTURE

2.1 General

In the seismic areas, the ability to resist horizontal in-plane actions is achieved by CFS stick-built walls generally braced with either sheathing panels, solution named as “*sheathing-braced*”, or steel diagonals, solution named as “*all-steel*”.

The structural design of CFS thin gauge members and sheathing in Europe can be carried out according to rules given in EN1993-1-3. However, the EN1993-1-3 does not give any specify rules to evaluate the lateral resistance of wall when it is sheathed with panels. In fact, the North American Specification for design of cold-formed steel structural members (AISI S400) is one of the most advanced standards on CFS bracing systems. In particular, the AISI S400 gives the design rules for these systems, by referring to both solution as *sheathing-braced* and *all-steel*, e.g. behaviour factor, limits on aspect ratio of the walls and rules of *capacity design*. Furthermore, for *sheathing-braced* solutions, the code provides a relationship to evaluate their lateral displacement and tables with the design resistance for typical configurations of walls.

In order to provide the designer with valid design tools on *sheathing-braced* walls, this Section is divided into three parts. In particular, first part shows an overview of the main calculation methods available in literature, second part presents an analytical procedure based on principles of mechanics, and, finally, in the third part an example of calculation is illustrated.

2.2 Main calculation methods available in literature

Different methods are available to study the lateral in-plane response of sheathed lightweight steel shear walls. In particular, the methods available in literature can be classified as tabular methods, numerical methods and analytical methods. Generally, the tabular method is the most used method and is based on experimental values obtained by tests on full-scale prototype walls. AISI S400 provides in tables the resistance values for walls with different types of sheathing and screw spacing based on experimental test results. The provided resistance values can be used only for wall consistent with fixed limitation such as maximum aspect ratio, stud thickness, steel grade and screw size. In order to overcome the limitations of tabular approach, finite element methods can be used to evaluated wall resistance based on available test results. In literature there are different methods available to predict the lateral resistance and stiffness for sheathing braced timber walls. Since the lateral response of the two systems is very similar, the analytical methods valid for timber walls can also be used for CFS walls. The main analytical methods to evaluate the lateral response of the walls are the following: McCutcheon and Tuomi (1978), McCutcheon (1985), Easley et al. (1982), Kallsner and Lam (1995), Finnish timber Code RIL 120-2001 (Hieta and Kesti 2002), Fiorino et al. (2003). These methods have common assumptions, which can be summarized as follows:

- local failure of sheathing-to-wall framing connections governs the global collapse mode;
- studs (vertical elements) and tracks (horizontal elements) are rigid and hinged to each other;
- panels are rigid or shear strain of panels only is considered;
- relative displacements between the sheathing and framing are small compared with the panel size;
- the edges of the panel are free to rotate without interference from adjacent sheathings and the foundation or other stories;
- the wall is fully anchored to the foundation or lower storey.

Moreover, each method formulates additional hypotheses concerning assumptions especially on the wall deformation, force distribution and connection load-deflection relationship. In the following sections, a summary of the main methods available in literature will be presented.

McCutcheon and Tuomi (1978) and McCutcheon (1985)

McCutcheon and Tuomi (1978) developed an analytical procedure for calculating the racking strength of sheathing panels, removing the limitation where a set of tests are required for new combinations of sheathing, framing and fasteners. The assumed geometry and distortion of a panel are as shown in Figure 1. This procedure is based on the following assumptions and limitations:

- the lateral load versus deflection curve is linear for a single nail;
- the frame becomes a parallelogram while the shape of the sheathing panel remains unchanged. The edges of the panel are free to rotate without interference from adjacent sheets and the foundation/lower storey;
- the panel is parallel to the frame and is of the same height;
- nails are spaced evenly and symmetrically;
- the loading speed is slow enough to eliminate dynamic or impact effects;
- distortions and deflections are small;
- the four corner nails distort along the lines of the sheathing diagonals;
- all the external work is completely dissipated by the distortion of the nails.

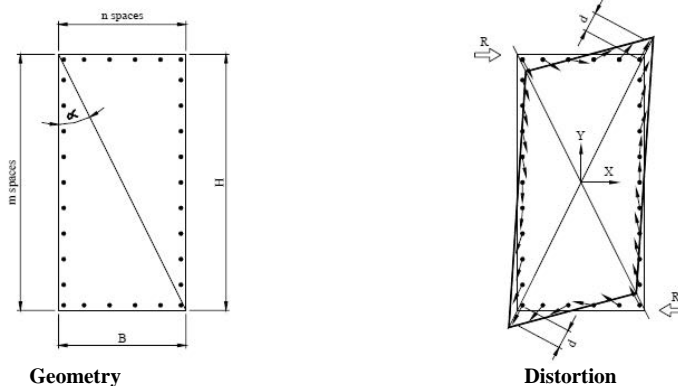


Figure 1. Geometry and Distortion of a Panel (Tuomi & McCutcheon, 1978).

The racking force of a panel with perimeter nailing was derived as:

$$R = r[(K_n + K_m)_p + (a^2 K_{na} + b^2 K_{nb} + a^2 K_{ma} + b^2 K_{mb})_f] \quad (1)$$

where:

$$K_n = K_{na} + K_{nb} ; K_m = K_{ma} + K_{mb} ;$$

$$K_{na} = n \cdot \sin^3 \alpha ; K_{nb} = \frac{n^2+2}{3n} \sin \alpha \cdot \cos^3 \alpha ;$$

$$K_{ma} = \frac{m^2+2}{3m} \sin^3 \alpha ; K_{mb} = m \cdot \cos^2 \alpha \cdot \sin \alpha ;$$

r is the lateral strength of single nail;

α is the angle between vertical and diagonal lines (Figure 1);

m is the number of fastener spaces along vertical side;

n is the number of fastener spaces along horizontal side;

f is the subscript denoting nails in the interior (field) of the panel;

p is the subscript denoting nails around the perimeter of the panel;

a is the ratio of "field height" to "perimeter height", H_f/H_p , (Figure 2);

b is the ratio of "field width" to "perimeter width", B_f/B_p , (Figure 2).

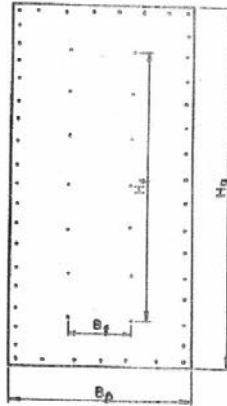


Figure 2. Walls with field nails within the panel (Tuomi & McCutcheon, 1978).

The Eq. (1) takes into account essentially the geometry of the sheathing panels, the strength, the number and the spacing of nails and the lateral resistance of a single nail. The frame contribution is not considered.

Tuomi e McCutcheon performed 63 tests, 34 full-scale tests and 29 small-scale tests, to verify their analytical model. These tests adopted seven different sheathing materials with different grades, four different geometries and three different nail patterns. Theoretical and actual loads agreed with each other very well in the low load range (less than 7000 lb or 31.15 kN). Due to the linear assumption, this method cannot be used for the high load range.

McCutcheon (1985) presented a general approach for calculating racking deformations of wood framed shear walls, using the same energy approach employed by Tuomi and McCutcheon (1978) in the racking strength prediction, but removing the limitation that the behaviour of the nails is linear. The shear deformation of sheathing is also included when determining the total racking displacement.

In this method, the load (p) – slip (x) curve of sheathing fasteners can be expressed as power curve:

$$p = A \cdot x^B \tag{2}$$

in which A is the amplitude; and the exponent B is between 0 (which corresponds to a perfectly plastic response) and 1 (in which case the nail load-slip relationship is linear).

The author evaluated the racking displacement, Δ_t , as sum of nail deformation, Δ_n , and sheathing shear deformation:

$$\Delta_t = \Delta_n + \Delta_s \tag{3}$$

where

$\Delta_s = \left(\frac{RH}{NGtL}\right)^{1/B}$ is the horizontal displacement caused by shear in the sheathing;

$\Delta_n = \left(\frac{R}{N \cdot \bar{A}}\right)^{1/B}$ is the horizontal displacement caused by nail distortions;

R is the horizontal resistance of the wall.

$$\bar{A} = A \frac{(\sin\alpha)^{B+1}}{2^B} \cdot S \tag{4}$$

$$S = \sum_{i=1}^{n_x} \left[\sin^2 \alpha + \left(2 \frac{i}{n_x} - 1 \right)^2 \cdot \cos^2 \alpha \right]^{(B+1)/2} + \sum_{j=1}^{n_y} \left[\left(2 \frac{j}{n_y} - 1 \right)^2 \cdot \sin^2 \alpha + \cos^2 \alpha \right]^{(B+1)/2} \tag{5}$$

In the previous relationships only perimeter nailing was considered, whereas the reduced width $r_x L$ and the reduced height $r_y H$ should be considered when the connections are collocated also within the panels, as shown in Figure 3.

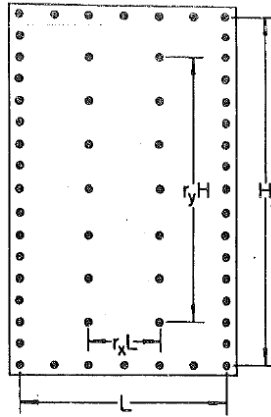


Figure 3. Fastener within panel between sheathing panels and frame (McCutcheon, 1985).

In this case, the Eq. (4) and (5) can be expressed in a general way, as follows:

$$\bar{A} = A \frac{(\sin \alpha)^{B+1}}{2^B} \cdot \sum_{rect} S \tag{6}$$

$$S = \sum_{i=1}^{n_x} \left[r_y^2 \sin^2 \alpha + r_x^2 \left(2 \frac{i}{n_x} - 1 \right)^2 \cdot \cos^2 \alpha \right]^{(B+1)/2} + \sum_{j=1}^{n_y} \left[r_y^2 \left(2 \frac{j}{n_y} - 1 \right)^2 \cdot \sin^2 \alpha + r_x^2 \cos^2 \alpha \right]^{(B+1)/2} \tag{7}$$

where

- N is the number of vertical sheathing panels;
- H is the distance between the upper and bottom connections;
- t is the thickness of sheathing panel;
- L is the distance between the lateral connections;
- G shear modulus of sheathing panel.

Easley et al.

Easley et al. (1982) developed closed-form formulas for shear wall displacement and strength based on the deformation patterns of specimens observed in load tests. In particular, on the base of the experimental observations, Easley et al. assumed the following hypothesis with respect to fastener forces and wall behaviour (Figure 4):

- fastener forces in the panel ends have both x- and y- components. The x-components along the end of the panel, F_{ex} , are uniform. The y-components, F_{eyi} , are proportional to the distances from the panel centreline, X_{ei} ;
- fastener forces, F_{si} in the interior studs, and F_s in the panel sides, act only along the studs and are proportional to the distances from the panel centreline, X_{si} ;
- when the wall is loaded, no separations occur in the framing member joints between the studs and the header or sill;
- shear wall panels can be satisfactorily represented as isotropic materials.

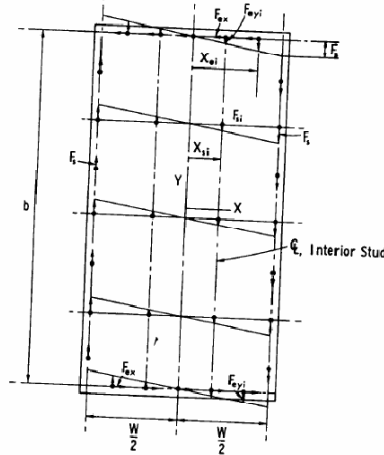


Figure 4. Nail Force Distribution of a Shear Wall Panel (Easley et al., 1982).

A closed-form equation was derived based on force and moment equilibrium for a particular panel. In particular, for side fasteners is valid the following relationship:

$$F_s = \frac{Nb}{\beta} \tag{8}$$

Whereas, for fasteners located along the tracks is valid the following:

$$F_{ei} = [F_{ex}^2 + F_{eyi}^2]^{1/2} = N \left[\left(\frac{W}{n_e} \right)^2 + \left(2X_{ei} \frac{b}{W\beta} \right)^2 \right]^{1/2} \tag{9}$$

where

$$F_{ex} = Nw/n_e; F_{eyi} = 2x_{ei}/w \cdot F_s; F_{si} = 2x_{si}/wF_s;$$

$$\beta = n_s + \frac{4I_e + 2n_{si}I_s}{w^2};$$

$$I_e = \sum_{i=1}^{n_e} X_{ei}^2; I_s = \sum_{i=1}^m X_{si}^2;$$

N is the shear force per unit length acting on the shear wall;

n_s is the number of side fasteners;

n_e is the number of end fasteners;

n_{si} is the number of fasteners in each interior stud;

m is the number of interior studs;

w is the distance between two side fastener centrelines;

b is the distance between two end fastener centrelines.

The largest nail force in the sheathing will occur either at the panel side fasteners or in two fasteners on each end located at the greatest distance from the panel centre line. Furthermore, the wall resistance can be evaluated from equation (8), as follows:

$$N = \frac{F_s \beta}{b} \quad (10)$$

in which F_s is the fasteners resistance.

The shear strain, γ , is assumed to be the sum of γ_1 and γ_2 .

$$\gamma = \gamma_1 + \gamma_2 = N/G' \quad (11)$$

where

$\gamma_1 = \frac{2\Delta_s}{w}$ is the shear strain due to the localized deformations at the fasteners;

$\gamma_2 = \frac{N}{Gt}$ is the shear strain in the individual panels;

$G' = \frac{1}{\left[\frac{2b}{Kw\beta} + \frac{1}{Gt} \right]}$ is the linear stiffness of a shear wall;

$\Delta_s = F_s/k$, is the total localized deformation at each side fastener;

G is the shear modulus of elasticity of the sheathing material;

t is the thickness of the sheathing panels;

k is derived from load-slip curves for connection tests which are typically nonlinear depending on the size and type of the fastener and the thickness and type of the sheathing material.

From the comparison between the results obtained by means the equations and those obtained by means experimental tests and finite element analyses Easley et al. concluded that, in order to evaluate the strength and initial stiffness, the accuracy of the prediction with these formulas is acceptable in engineering practice.

Kallsner and Lam

Kallsner and Lam (1995) described three models to predict shear wood wall performance. All three models, one of which is elastic and two are plastics, can be used to predict the stiffness (only elastic model) and strength (all three models).

In the elastic model, the following assumptions were made:

- the load-displacement curve of sheathing-to-frame connections is linear and elastic until failure;
- relative displacements between the sheathing panels and the frame are null in the centre point;
- the fastener force distribution is shown in Figure 5.

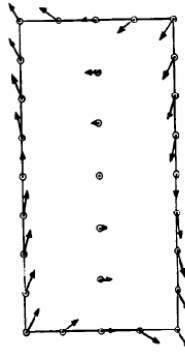


Figure 5. Force distribution in the “Elastic method” (Kallsner e Lam, 1995).

The authors determined the deformation and shear resistance on the base of the minimum potential energy principal. In particular, the shear resistance H_d can be evaluated as follows:

$$H_d = \frac{F_d}{h \cdot \sqrt{\left(\frac{x_{max}}{\sum_{i=1}^N x_i^2}\right)^2 + \left(\frac{y_{max}}{\sum_{i=1}^N y_i^2}\right)^2}} \tag{12}$$

Whereas the horizontal displacement at the wall top can be evaluated as:

$$u_{frame} = (\gamma + \gamma_s)h = \frac{1}{K} Hh^2 \left(\frac{1}{\sum_{i=1}^N x_i^2} + \frac{1}{\sum_{i=1}^N y_i^2} \right) + \gamma_s h \tag{13}$$

In these two equations:

- x_i, y_i are coordinates referring to the centre of gravity of the fasteners;
- N is the number of all fasteners;
- K is the slip modulus for the fastener;
- H is the applied lateral load;
- F_d is the design capacity per fastener;
- $\gamma_s = \frac{H}{Gbt}$ is the shear deformation in the sheathing.

In the “*lower bound method*” it is assumed that the load-displacement relationships of the fasteners are completely plastic. The force distribution is shown in Figure 6. The shear resistance is expressed by the following relationship:

$$H_d = n \cdot F_d \tag{14}$$

where

n is the number of fastener spaces along the top end of the panel.

The “*upper bound method*” is relatively complex if compared with the “*elastic method*” and the “*lower bound methods*”. This method is based on the following assumptions:

- each frame member is regarded as a rigid body rotating around its own centre of rotation on the panel. The frame with one interior stud on the centre is composed of five members per panel (Figure 7), three vertical (AC, EF, BD) and two horizontal (AB, CD). Stud AC rotates about O1, similarly, BD about O2, CD about O3, AB about O4 and EF about O;
- the frame members are hinged to each other. This requires that the rotation centres for frame members satisfy the condition shown in Figure 7. The straight lines between rotation centres must pass through the hinges. For example, the line linking O2 and O4 must pass through point B;
- all fasteners can simultaneously reach their plastic capacity.

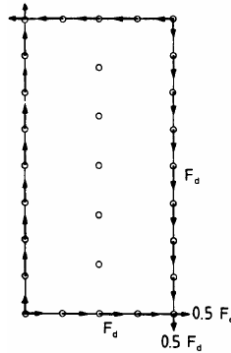


Figure 6. Force distribution in the “Lower Bound Method” (Kallsner & Lam, 1995).

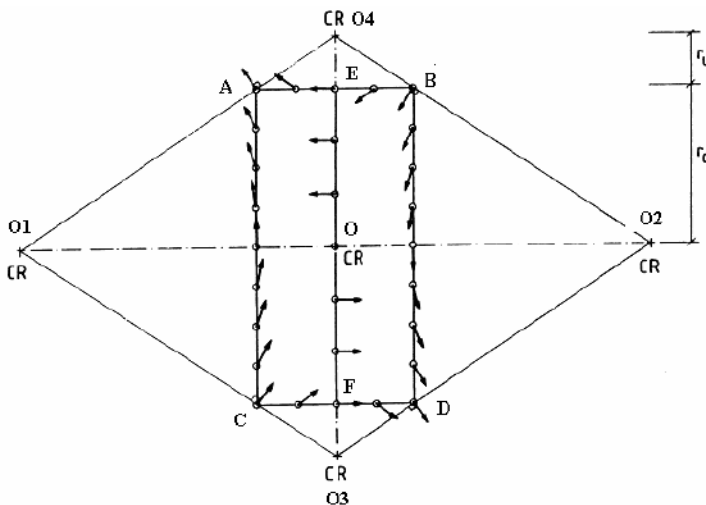


Figure 7. Force distribution in the “upper bound method” (Kallsner & Lam, 1995).

The horizontal resistance is evaluated as:

$$H_d = \frac{\sum_{hor} F_d \cdot r_i + \sum_{ver} F_d \cdot r_i \cdot \frac{r_u}{r_c}}{h \left(\frac{r_u}{r_c} + 1 \right)} \quad (15)$$

where

$$\frac{r_u}{r_c} = \frac{\gamma}{\varphi} - 1;$$

$$\gamma = \frac{1}{k} Hh \left(\frac{1}{\sum_{i=1}^N x_i^2} + \frac{1}{\sum_{i=1}^N y_i^2} \right) \text{ is the frame rotation;}$$

$$\varphi = \frac{1}{k} Hh \frac{1}{\sum_{i=1}^N x_i^2} \text{ is the sheathing panels rotation;}$$

r_i is the rotation radius of each fastener, which can be calculated after the rotation centres of frame members were decided.

Kallsner and Lam concluded that the elastic model underestimated the capacity, and the upper bound plastic method overestimated the capacity of shear walls based on a comparison with full-scale tests. However, the difference in capacity obtained from these three methods is small, and the difference in the force distributions is moderate. Finally, Kallsner and Lam recommended as a general rule that the elastic model be used; however, the lower bound plastic method gives reasonable results and is very simple to incorporate into design.

Finnish timber Code

According to the calculation method proposed by Hieta and Kesti (2002) and given in *Finnish timber code*, the design horizontal resistance V_d is evaluated as:

$$V_d = \frac{1}{\gamma_M} \cdot \frac{F_{vk} \cdot B}{\gamma \cdot c} \quad (16)$$

where:

F_{vk} is the experimentally determined maximum characteristic fastening strength;

B is the panel or diaphragm width;

γ_M is the material safety factor, $\gamma_M = 1.3$ with gypsum plasterboards;

$$\gamma = \sqrt{\frac{4}{\left(2 + \frac{H}{B}\right)^2} + \frac{9}{\left(\frac{B}{H} + 3\right)^2}}, \quad \text{is valid when the uplift of the wall corner is prevented;}$$

c is the fastener spacing on the perimeter of sheathing panels.

Furthermore, a relationship to evaluate the wall deformability is give:

$$\frac{\delta}{F} = \sum_{i=1}^2 \left(\beta \cdot \frac{c_i}{k_i} \cdot \frac{H^2}{B^3} + \frac{H}{B \cdot G_i \cdot t_i} \right) \quad (17)$$

where:

$$\beta = \frac{4}{2 \cdot \left(\frac{H}{B}\right)^2 + \left(\frac{H}{B}\right)^3} + \frac{6}{1 + 3 \cdot \left(\frac{H}{B}\right)}, \text{ is valid when the uplift of the wall corner is prevented;}$$

H and B are the panel height and width, respectively;

k_i is the stiffness of a single fastening;

φ_f and φ_p are the rotations of the frame and panel, respectively;
 u_{p0} is the translation of the panel along X direction;
 h and b are the height and width of the wall, respectively;
 x_i and y_i are the coordinates along X and Y directions, respectively.

The authors, from equilibrium considerations obtained the following formulas:

$$\sum_{i=1}^N (-F_{x,i}y_i + F_{y,i}x_i) = 0 \quad (20)$$

$$\sum_{i=1}^N F_{x,i} = 0 \quad (21)$$

$$Vb - F_{x,e}n_e - \frac{1}{h} \sum_{i=1}^m F_{x,i}y_i = 0 \quad (22)$$

where

$F_{x,i}$ and $F_{y,i}$ are the force components of sheathing-to-frame connections along X and Y directions, respectively;

$F_{x,e}$ is the force component of sheathing-to-top track connections along the X direction, which is constant according to the considered hypotheses;

V is the horizontal external force per unit of length;

n is the total number of sheathing-to-frame connections;

m is the number of fasteners connecting the sheathing to studs;

n_e is the number of fasteners connecting the sheathing to the top track.

The force components of sheathing-to-frame connections can be expressed as functions of relative displacements between the steel framing members and panel by:

$$F_{x,i} = k_{x,i}u_i \quad (23)$$

$$F_{y,i} = k_{y,i}v_i \quad (24)$$

where

$k_{x,i}$ and $k_{y,i}$ are the stiffnesses of sheathing-to-frame connections for displacement along X and Y directions, respectively.

By replacing the Equations (18) and (19) in (23) and (24), the parameters describing the deformation of the wall (φ_f , φ_p , u_{p0}) can be expressed as function of the wall geometry, stiffnesses of sheathing-to-frame connections ($k_{x,i}$, $k_{y,i}$) and horizontal external force per unit of length (V):

$$\varphi_f = \frac{2bh \left[K_x I_x - (S_x)^2 - \frac{bK_x S_y}{2} + K_x I_y \right] V}{(S_{x,m} S_x - I_{x,m} K_x + S_e S_x - I_e K_x) (2I_y - bS_y)} \quad (25)$$

$$\varphi_p = \frac{-2bh[K_x I_x - (S_x)^2]V}{[(I_{x,m} + I_e)K_x - (S_{x,m} + S_e)S_x](2I_y - bS_y)} \quad (26)$$

$$u_{p,0} = \frac{bhS_x V}{[I_{x,m} + I_e]K_x - [S_{x,m} + S_e]S_x} \quad (27)$$

in which:

$$\begin{aligned} K_x &= \sum_{i=1}^n k_{x,i} ; & S_x &= \sum_{i=1}^n k_{x,i} y_i ; & I_x &= \sum_{i=1}^n k_{x,i} (y_i)^2 ; \\ S_y &= \sum_{i=1}^n k_{y,i} x_i ; & I_y &= \sum_{i=1}^n k_{y,i} (x_i)^2 ; & S_{x,m} &= \sum_{i=1}^m k_{x,i} y_i ; & I_{x,m} &= \sum_{i=1}^m k_{x,i} (y_i)^2 ; \\ K_e &= k_{x_e} n_e ; & S_e &= k_{x_e} n_e h ; & I_e &= k_{x_e} n_e h . \end{aligned}$$

When for sheathing-to-frame connections a linear load-displacement response is assumed ($k_{x,i}$ e $k_{y,i}$ are constant values), Equation (25) gives a closed-form solution and the top wall displacement (d) can be evaluated as follows:

$$d = d_1 = \varphi_f h \quad (28)$$

where

$d_1 = \varphi_f h$ is the displacement obtained by assuming that the panel has rigid body rotation;
 φ_f is the frame rotation and it is calculated from Equation (25).

2.3 Design method

General

As for the structural design of traditional buildings, also in the case of CFS structures, there are two main performance requirements: to transfer the vertical loads and the horizontal forces acting on the structure to the ground. The design under vertical loads does not represent a very complex issue. In fact, considering that the construction systems consist of dry assemblies, in which boards and profiles are connected by pinned joints, the structural analysis for vertical loads is the resolution of a statically determined pendulum scheme, where the internal forces for each element can be easily obtained by the acting loads. An interesting feature is the possibility to carry out the structural checks according to two different approaches: *all-steel design* and *sheathing-braced design*. The first approach does not consider the presence of sheathing boards, and the generic profile is assumed as isolated, by neglecting the interaction between the profile itself and the panel, whereas the latter approach calculates the load bearing capacity of a member taking into account the presence of the sheathing. In fact, when the sheathing has sufficient strength and stiffness and it is effectively connected to steel profiles, the bending resistance (for beams) and the axial resistance (for studs) are increased because of the interaction with the sheathing boards. The design under horizontal loads, mainly wind and seismic loads, represents a more delicate issue. In fact, when the building is subjected to a horizontal load, floors and roofs have to be able to act as a diaphragm and transfer the loads to the walls, which, in turn, have to resist these loads and transfer them to the foundations.

Therefore, also for design under horizontal loads, it is possible to distinguish between the *all-steel design* and *sheathing-braced design* approaches. In the following paragraphs, *sheathing-braced design* approach is explained.

When the design is carried out according to the *sheathing-braced* methodology, floor decks and walls act as a diaphragm. In particular, floors can be considered as simple supported horizontal diaphragms subjected to a uniform load, while walls are cantilever vertical diaphragms subjected to a uniform horizontal force acting on the top edge. The structural behaviour of diaphragms can be assumed as that of a composite I-beam, in which sheathing boards are the web and the chord profiles are the flanges. In particular, sheathing boards absorb the shear actions, while the compression and tension axial load due to bending are resisted by chord profiles.

Obviously, it is clear that the global structural response of the diaphragm (wall or floor) basically depends on the local structural response of its components. It is possible to individually specify the main structural components such as steel frame, sheathing boards, sheathing-to-frame connections and connections between steel frame and external structures.

Design rules given by AISI S400

A valid code for seismic design of CFS shear walls is the American code AISI S400. This code gives the design rules for these structural systems and it introduces the possibility to consider the bracing contribution offered by sheathing panels.

According to this code, the design of shear walls that resist the seismic loads shall be classified as either *Type I shear walls* or *Type II shear walls*. *Type I shear walls* are sheathed to full height and are provided with *hold-downs* and anchorage at each end of wall segment to resist the lateral actions, as shown in Figure 9.

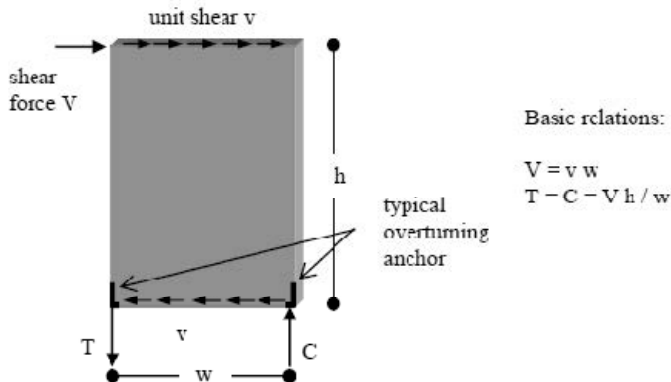


Figure 9. Model of a simple Type I shear wall.

Type I shear walls are permitted to have openings where details are provided to account for force transfer around openings. The properties of *Type I shear walls* should be evaluated by neglecting the openings and by considering only the resisting “segments” of walls between two consecutive openings, as shown Figure 10.a. On the other hand, *Type II shear walls* are permitted to have openings without specific details to account for force transfer around openings. *Hold-downs* and anchorage at each end of the *Type II shear walls* shall be required. Therefore, the properties of *Type II shear walls* should be evaluated by considering a unique element including the openings, as shown in Figure 10.b.

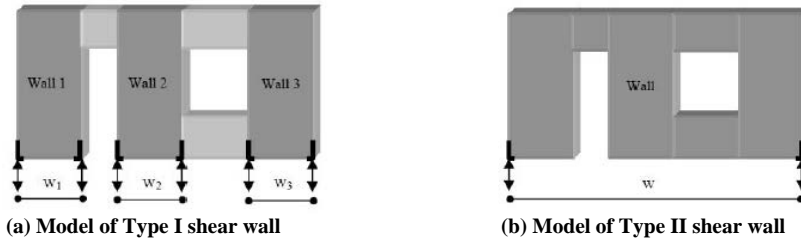


Figure 10. Comparison between the models given by AISI S400.

The *Type I shear wall* shall be designed according to the following rules:

- the height-to-length aspect ratio of *Type I shear walls* shall be limited to a maximum of 2:1;
- for a *Type I shear wall* with the same sheathing materials and fastener spacing on opposite faces of the wall, the resistance should be multiplied by two. On the contrary, for walls having more than one type of sheathing material or different fastener spacing on the same face of the wall, the resistance of the complete wall shall not be calculated by adding the resistance from the different individual walls. Particularly in this case, the resistance shall be taken either assuming that the weaker (lower resistance) material or fastener configuration exists for the entire length of the wall, or the stronger (higher resistance) material or fastener configuration exists for its own length, whichever is greater. Finally, in the case of more than one type of sheathing material or fastener configuration on opposite faces of the wall, the nominal resistance shall be taken equal to the greater value obtained either assuming the weaker material or fastener configuration exists for both faces of the wall, or the stronger material or fastener configuration exists for its own face alone.

Design under horizontal loads: evaluation of lateral stiffness

The evaluation of lateral displacement at the top of the wall, d , under horizontal loads, H , can be obtained by adding in series the deformation contribution of each structural component (Figure 11) as follows:

$$d = d_s + d_a + d_p + d_f \quad (29)$$

in which:

d_s , d_a , d_p and d_f are the deformation contributions of steel frame, frame-to-foundation anchors, sheathing panels and sheathing-to-frame connections, respectively.

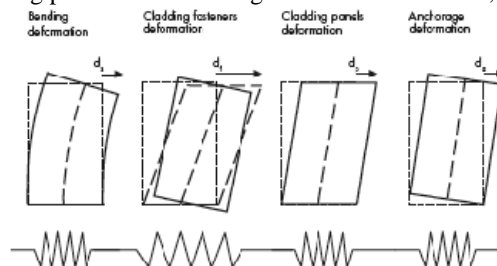


Figure 11. Deformation contributions of a wall with sheathing panels under lateral loads.

Therefore, the lateral stiffness of wall can be evaluated by considering a system of elastic spring, corresponding to the different structural components, by means of the following relationship:

$$K = \frac{1}{\frac{1}{K_s} + \frac{1}{K_a} + \frac{1}{K_p} + \frac{1}{K_f}} \quad (30)$$

Generally, the local behaviour of panels-to-frame connections governs the global lateral response of walls, the relevant deformation produces wall lateral displacement greater than those produced by other components:

$$d_s \ll d_f ; \quad d_a \ll d_f ; \quad d_p \ll d_f$$

In addition, d_s , d_p and d_a can be assumed as linear functions of the horizontal external force (H), while the non-linear lateral response of the wall is the result of the inelastic behaviour of the sheathing fasteners (d_f is a non-linear function of H).

In particular, lateral displacement due to the steel frame deformation, d_s , may be evaluated by considering the wall as a cantilever having a cross-section made of the only end studs:

$$d_s = \frac{2h^3}{3EA_cL^2}H \quad (31)$$

where

h is the height of the wall;

L is the length of the wall;

A_c is the gross cross-sectional area of an end stud (generally a coupled back-to-back C-section);

E is the Young's modulus of steel.

The lateral displacement due to frame-to-foundation anchors (d_a) is calculated from the following equation:

$$d_a = \frac{h^2}{k_a \cdot L^2}H \quad (32)$$

where

k_a is the axial stiffness of the hold-down device.

The lateral displacement due to the shear deformation of the sheathing panels (d_p) is obtained by adopting the equation for shear deformation of a thin, edge-loaded, plate:

$$d_p = \frac{h}{Gbt_p}H \quad (33)$$

where

b is the width of the sheathing panel;

t_p is the panel thickness;

G is the shear modulus of elasticity of the panel material.

Finally, the wall displacement contribution of sheathing-to-frame connections can be evaluated by different formulations, as shown in *Section 2* (McCutcheon et al., Easley et al., Kallsner and Lam, Finnish timber Code, Fiorino et al.). Particularly interesting is the relationship given by *Finnish timber Code*, showed in *Section 2*, which gives d_f as follows:

$$d_f = \frac{\beta c h^2}{b^3 k_f} H \quad (34)$$

where

k_f is the shear stiffness of a single connection;

c is the fastener spacing on the perimeter of sheathing panels;

$\beta = \frac{4}{2 \cdot \left(\frac{H}{B}\right)^2 + \left(\frac{H}{B}\right)^3} + \frac{6}{1 + 3 \cdot \left(\frac{H}{B}\right)}$, is valid when the uplift of the wall corner is prevented.

Design under horizontal loads: evaluation of lateral resistance

The wall lateral resistance (H_{Rd}) can be obtained by the wall lateral strength associated to the failure of steel frame ($H_{Rd,s}$), frame-to-foundation anchors ($H_{Rd,a}$), sheathing panels ($H_{Rd,p}$) and sheathing-to-frame connections ($H_{Rd,f}$) as follows:

$$H_{Rd} = \min(H_{Rd,s}; H_{Rd,a}; H_{Rd,p}; H_{Rd,f}) \quad (35)$$

The steel frame failure under lateral load is usually governed by the buckling failure of the end stud in compression and the corresponding wall resistance ($H_{Rd,s}$) is given by:

$$H_{Rd,s} = \frac{N_{s,Rd}}{h} L \quad (36)$$

where

$N_{s,Rd}$ is the design buckling resistance of the end stud;

L is the length of the wall;

h is the height of the wall.

The resistance associated to the failure of frame-to-foundation anchors ($H_{Rd,a}$) is the lateral load which corresponds to the minimum of the shear resistance or the axial resistance of this anchorage:

$$H_{Rd,a} = \min\left(n_a V_{a,Rd}; \frac{N_{a,Rd}}{h} L\right) \quad (37)$$

where

$n_a V_{a,Rd}$ is the design resistance to the sliding;

n_a is the number of the anchorage;

$V_{a,Rd}$ is the shear design resistance of the anchorage;

$\frac{N_{a,Rd}}{h} L$ is the design resistance to the overturning;

$N_{a,Rd}$ is the axial design resistance of the anchorage.

The failure of sheathing panel is generally due to shear and the corresponding wall resistance ($H_{c,p}$) is the lateral load which induces ultimate shear stress in the sheathing panel. In case of wood based panel, the resistance is given by:

$$H_{Rd,p} = k_{mod} \frac{f_{p,v,k}}{\gamma_{p,m}} t_p L \quad (38)$$

where

$f_{p,v,k}$ is the characteristic shear strength of panel material;

$\gamma_{p,m}$ is the partial safety factor of panel material, which ranges from 1.4 and 1.5 according to *NTC – D.M. 14/01/08*;

k_{mod} is the modification factor due to duration of load and moisture content, ranges from 0.8 and 1.0 according to Italian code

The resistance associated to the sheathing-to-frame connections ($H_{Rd,f}$) can be evaluated by different methods, as shown in *Section 2* (McCutcheon et al., Easley et al., Kallsner and Lam, Finnish timber Code, Fiorino et al.). Therefore, the resistance $H_{Rd,f}$ can be evaluated according to the Hieta & Kesti for timber shear walls approach, in which the lateral resistance of wall due to connection ($H_{c,f}$) is based on maximum connection force in the panel corner, as follows:

$$H_{Rd,f} = \frac{b}{\gamma \cdot c} \frac{F_{k,f}}{\gamma_{f,m}} \quad (39)$$

where

$F_{k,f}$ is the characteristic strength of single connection between sheathing panel and steel frame;

$\gamma = \sqrt{\frac{4}{(2+\frac{H}{B})^2} + \frac{9}{(\frac{B}{H}+3)^2}}$ is valid when the uplift of the wall corner is prevented;

$\gamma_{f,m}$ is the partial safety factor of material assumed equal to 1.25;

c is the fastener spacing.

Example of calculation

In this section, an interesting example of calculation is shown by referring to an experimental study on the seismic behaviour of CFS walls sheathed by oriented strand board (OSB) and gypsum wallboard (GWB) panels, carried out by the Department of Structures for Engineering and Architecture of the University of Naples “Federico II”. The experimental program was based on two nominally identical prototypes, shown in Figure 12. One prototype was tested under monotonic loading and the other was instead subjected to a purposely developed cyclic loading history.

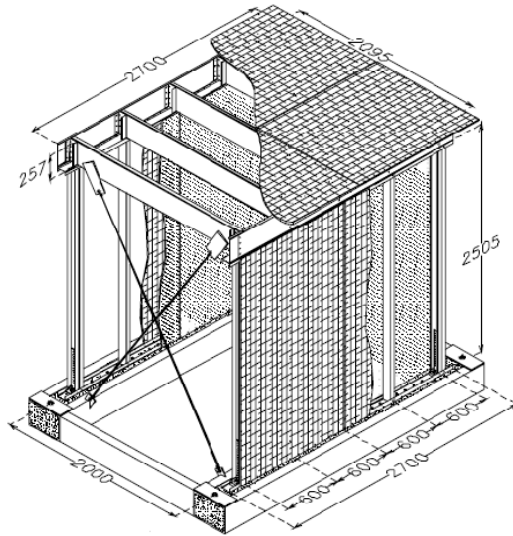


Figure 12. Global 3D view of prototype tested by University of Naples.

The prototypes were designed starting from a case study consisting in a one-family one-story dwelling. The structure is stick-built construction in which both horizontal (roof and floors) and vertical (walls) diaphragms are cold-formed frames sheathed with structural panels.

The generic wall framing, which was 2400 mm long and 2500 mm high, consisted of single top and bottom tracks, single intermediate studs, and double back-to-back end studs, spaced at 600 mm on centre. The floor framing consisted of joists spaced 600 mm on centre, with a single span of 2000 mm. The foundation was constituted by two 280×380 mm (depth \times width) rectangular concrete beams.

The walls were connected to the foundation by intermediate shear anchors and purposely designed steel hold-down connectors placed corresponding to the end studs, as shown in Figure 13. The test set-up is shown in Figure 14.

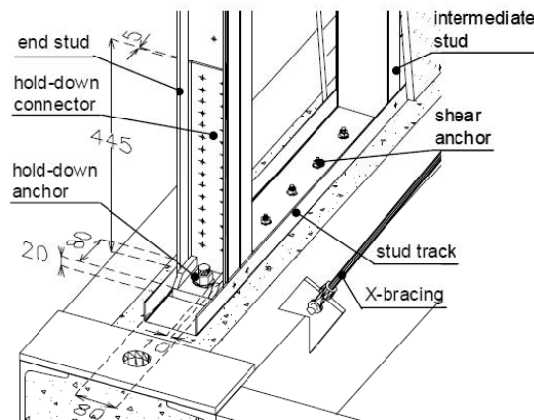


Figure 13. Drawing of detail of foundation anchorages.

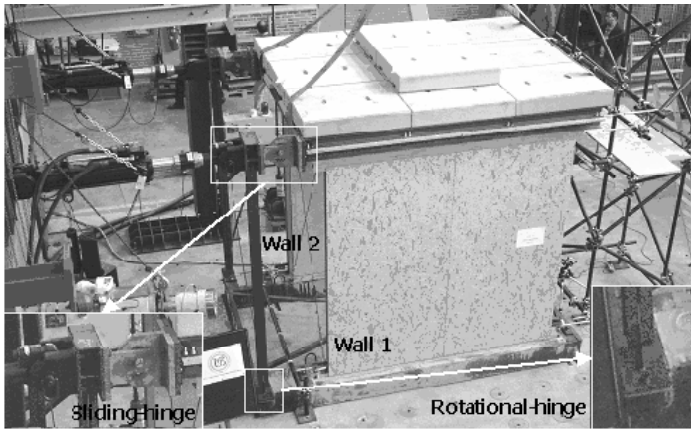


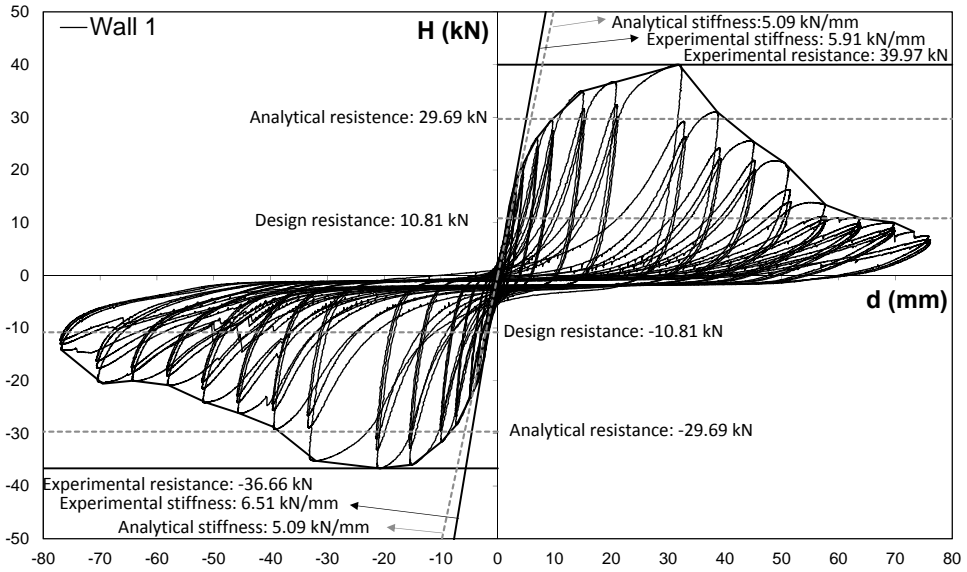
Figure 14. Test set-up.

All frame members were cold-formed, fabricated from FeE350G (S350GD+Z/ZF) hot dipped galvanized (zinc coated) grade steel (nominal yield strength $f_y = 350$ MPa and nominal tensile strength $f_t = 420$ MPa). In particular, the walls constructive details are listed in the following:

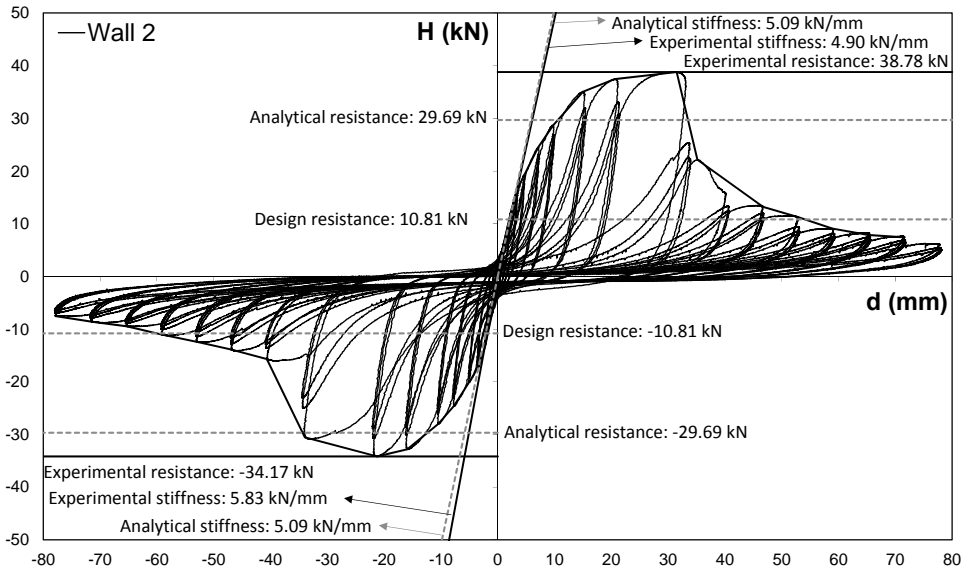
- Studs: C100×50×10×1.00 mm lipped channel sections (outside-to-outside web depth × outside-to-outside flange size × outside-to-outside lip size × thickness) spaced at 600 mm on centre;
- Tracks: U100×40×1.00 mm unlipped channel sections (inside-to-inside web depth × outside-to-outside flange size × thickness);
- External sheathing: Type 3 oriented strand board (OSB/3) panels, vertically oriented, of dimensions 1250×2500×9.0 mm (length × height × thickness);
- Internal sheathing: gypsum wallboard (GWB), vertically oriented, of dimensions 1200×2500×12.5 mm (length × height × thickness);
- Framing fasteners: No. 8 (4.2×13 mm: diameter × length) modified truss-head self-drilling screws;
- External sheathing fasteners: No. 8 (4.2×25 mm) flat-head self-drilling screws spaced at 150 mm at the perimeter and 300 mm in the field;
- Internal sheathing wall fasteners: No. 6 (3.5×25 mm) bugle head self-drilling screws spaced at 150 mm at the perimeter and 300 mm in the field;
- Shear anchors: HST M8 mechanical anchors (by HILTI Italia) spaced at 100 mm;
- Hold-down connectors: purposely designed welded steel hold-down;
- Hold-downs-to-studs fasteners: 6 mm diameter bolts;
- Hold-down anchors: HIT-RE 500 with HIS-N (8.8) M20 adhesive-bonded anchors (by HILTI Italia).

The lateral resistance and stiffness for single wall were evaluated on the basis of the cyclic test. The cyclic response in terms of load vs lateral displacement curve is shown in

Figure 15. The envelope curves for the positive and negative branch were obtained. Furthermore, the resistance, H_p , assumed equal to the maximum applied load, the conventional elastic resistance, F_e , assumed equal to $0.4H_p$ and the corresponding displacement d_e were obtained. Finally, the conventional elastic stiffness was evaluated as the ratio between the conventional elastic resistance, F_e , and the corresponding displacement, d_e . The experimental results are shown in Table 1.



(a) Wall 1



(b) Wall 2

Figure 15. Load vs displacement curve.

Table 1. Cyclic tests results.

	Resistance			Conventional elastic stiffness		
	Positive envelope	Negative envelope	Average	Positive envelope	Negative envelope	Average
	H_p^+ [kN]	H_p^- [kN]	H_p [kN]	K_e^+ [kN/mm]	K_e^- [kN/mm]	K_e [kN/mm]
Wall 1	39.97	-36.66	38.31	5.91	6.51	6.21
Wall 2	38.78	-34.17	36.48	4.90	5.83	5.37
Average			37.40			5.79

In order to compare the experimental results with analytical values and to check the reliability of the analytical values, the resistance and stiffness were evaluated by means of procedure illustrated previously. Relationships given previously were applied by assuming the average values for the properties of materials. In particular, the conventional elastic stiffness, K , was obtained by considering the deformation contribution of each structural component, using the following relationship:

$$K = \left(\frac{1}{K_s} + \frac{1}{K_a} + \frac{1}{K_p} + \frac{1}{K_f} \right)^{-1} = \left(\frac{2h^3}{3EA_cL^2} + \frac{h^2}{k_aL^2} + \frac{1}{K_p} + \frac{1}{K_f} \right)^{-1} \quad (40)$$

where

$$\begin{aligned} h &= 2500 \text{ mm}; \\ L &= 2400 \text{ mm}; \\ A_c &= 440 \text{ mm}^2; \\ E &= 210 \square 000 \text{ Nmm}^{-2}; \\ k_a &= 60 \square 000 \text{ Nmm}^{-1}. \end{aligned}$$

The evaluation of the stiffness contribution of panels should consider the different typologies of sheathing panels present on the two faces of wall. The two systems work in parallel and the stiffness K_p can be evaluate by means of following relationship:

$$\begin{aligned} K_p &= K_{p,OSB} + K_{p,GWB} = \frac{G_{OSB}bt_{p,OSB}}{h} + \frac{G_{GWB}bt_{p,GWB}}{h} \\ &= \frac{b(G_{OSB}t_{p,OSB} + G_{GWB}t_{p,GWB})}{h} \end{aligned} \quad (41)$$

where

$$\begin{aligned} b &= 1200 \text{ mm}; \\ G_{OSB} &= 1500 \text{ Nmm}^{-2}; \\ t_{p,OSB} &= 9 \text{ mm}; \\ G_{GWB} &= 800 \text{ Nmm}^{-2}; \\ t_{p,GWB} &= 12.5 \text{ mm}. \end{aligned}$$

Also for the sheathing-to-frame connections, the stiffness contribution should consider the different typologies of sheathing panel present on the two faces of wall. Therefore, the stiffness K_f can be evaluated as follows:

$$K_f = K_{f,OSB} + K_{f,GWB} = \frac{b^3 k_{f,OSB}}{\beta c h^2} + \frac{b^3 k_{f,GWB}}{\beta c h^2} = \frac{b^3}{\beta c h^2} (k_{f,OSB} + k_{f,GWB}) \quad (42)$$

where

$$\begin{aligned} \beta &= 1.05; \\ c &= 150 \text{ mm}; \\ k_{f,OSB} &= 1000 \text{ Nmm}^{-1}; \\ k_{f,GWB} &= 1500 \text{ Nmm}^{-1}. \end{aligned}$$

The obtained results in terms of lateral stiffness for each structural component are shown in Table 2.

Table 2. Stiffness obtained by means of the proposed procedure.

Structural component	Stiffness	
Steel frame	K_s [kN/mm]	51.09
Frame-to-foundation anchors	K_a [kN/mm]	55.30
Sheathing panels	K_p [kN/mm]	22.56
Sheathing-to-frame connections	K_f [kN/mm]	8.75
Wall stiffness K [kN/mm]		5.09

The obtained values confirm that the wall lateral response is governed by the deformability of the sheathing-to-frame connections.

The comparison between the analytical and experimental results, shown in Figure 15, highlights an acceptable prevision. In fact, the analytical procedure gives an average underestimation of stiffness by 14% ($K_e / K = 5.79 / 5.09 = 1.14$).

In order to check the reliability of the analytical method and to verify that the obtained safety factors adequate, the comparison in terms of resistance was carried out.

In order to evaluate the safety factor using the proposed methodology, the lateral resistance was evaluated by means of characteristic or nominal properties of the materials and considering appropriate partial safety factors for materials. In particular, the wall lateral design resistance, H_{Rd} , was calculated using the following formulation:

$$H_{Rd} = \min \left\{ \frac{N_{s,Rd}}{h} L; \min \left(n_a V_{a,Rd}; \frac{N_{a,Rd}}{h} L \right); H_{Rd,p}; H_{Rd,f} \right\} \quad (43)$$

where

$$\begin{aligned} N_{s,Rd} &= 68.00 \text{ kN}; \\ n_a &= 24; \\ V_{a,Rd} &= 11.20 \text{ kN}; \\ N_{a,Rd} &= 184.05 \text{ kN}. \end{aligned}$$

The resistance contributions associated to the different typology of sheathing panels, $H_{Rd,p}$, and sheathing-to-frame connections ($H_{Rd,f}$) on the two faces of the wall were evaluated according to AISI S400. In particular, in a first step the resistance contributions of the two wall faces are separately evaluated:

- Design resistances associated to the panels failure:

$$H_{Rd,p,OSB} = k_{mod,OSB} \frac{f_{p,v,k,OSB}}{\gamma_{p,m,OSB}} t_{p,OSB} L \quad (44)$$

$$H_{Rd,p,GWB} = k_{mod,GWB} \frac{f_{p,v,k,GWB}}{\gamma_{p,m,GWB}} t_{p,GWB} L \quad (45)$$

where

$k_{mod,OSB} = 0.9$, modification factor for instantaneous loading;

$f_{p,v,k,OSB} = 6.8 \text{ N/mm}^2$;

$\gamma_{p,m,OSB} = 1.4$;

$k_{mod,GWB} = 0.9$, the same value considered for OSB panels was assumed;

$f_{p,v,k,GWB} = 6.8 \text{ N/mm}^2$;

$\gamma_{p,m,GWB} = 1.4$, also in this case the same value considered for OSB panels was assumed.

- Design resistances associated to the failure of connections:

$$H_{Rd,f,OSB} = \frac{b}{\gamma \cdot c} \frac{V_{f,k,OSB}}{\gamma_{f,m}} \quad (46)$$

$$H_{Rd,f,GWB} = \frac{b}{\gamma \cdot c} \frac{V_{f,k,GWB}}{\gamma_{f,m}} \quad (47)$$

where

$\gamma = 0.99$;

$V_{f,k,OSB} = 0.84 \text{ kN}$;

$V_{f,k,GWB} = 0.31 \text{ kN}$;

$\gamma_{f,m} = 1.25$.

Subsequently, for each mechanism a resistance equal to the greater between the value of the stronger face and two times the value of the weaker face was assumed:

- Design resistance associate to the failure of sheathing panels:

$$H_{Rd,p} = \max\{\max(H_{Rd,p,OSB}; H_{Rd,p,GWB}); 2 \min(H_{Rd,p,OSB}; H_{Rd,p,GWB})\} \quad (48)$$

- Design resistance associate to the failure of connections:

$$H_{Rd,f} = \max\{\max(H_{Rd,f,OSB}; H_{Rd,f,GWB}); 2 \min(H_{Rd,f,OSB}; H_{Rd,f,GWB})\} \quad (49)$$

The obtained results in terms of lateral resistance for each mechanism are shown in Table 3.

Table 3. Design resistance obtained by means of the proposed procedure.

Structural component		Lateral resistance			
Steel frame				$H_{Rd,s}$ [kN]	65.28
Frame-to-foundation anchors				$H_{Rd,a}$ [kN]	176.69
Sheathing panels	OSB	$H_{Rd,p,OSB}$ [kN]	94.42	$H_{Rd,p}$ [kN]	94.42
	GWB	$H_{Rd,p,GWB}$ [kN]	28.93		
Sheathing-to-frame connections	OSB	$H_{Rd,f,OSB}$ [kN]	10.81	$H_{Rd,f}$ [kN]	10.81
	GWB	$H_{Rd,f,GWB}$ [kN]	4.03		
				H_{Rd} [kN]	10.81

From the comparison between the design resistance obtained by applying the proposed method and the test results, shown in

Figure 15, it can be noticed that the minimum safety factor (evaluated for the weaker wall in the test) was obtained equal to the ratio between the experimental and the design resistance, $H_p / H_{Rd} = 36.48 / 10.81 = 3.37$.

In order to check the reliability of the methodology in terms of lateral resistance, the relationships given in this section were applied also by considering the average values of the mechanical properties of the materials and the unitary values for the partial safety factor. Therefore, the relationships given Eq. (50) estimate the average resistance of the wall, H_m . Since the resistances associated to the other mechanisms are sufficiently stronger, the resistance H_m was evaluated by considering only the resistance associated to the failure of the connections, $H_{m,f}$, as:

$$H_m = H_{m,f} \quad (50)$$

- Average resistances associated to the failure of connections:

$$H_{m,f,OSB} = \frac{b}{\gamma \cdot c} \frac{V_{f,m,OSB}}{\gamma_{f,m}} \quad (51)$$

$$H_{m,f,GWB} = \frac{b}{\gamma \cdot c} \frac{V_{f,m,GWB}}{\gamma_{f,m}} \quad (52)$$

where

$$\gamma = 0.99;$$

$$V_{f,m,OSB} = 1.34 \text{ kN};$$

$$V_{f,m,GWB} = 0.5 \text{ kN};$$

$$\gamma_{f,m} = 1.0.$$

The average lateral resistance of the wall can be evaluated by considering that the two faces of the wall work in parallel, simply by adding the contribution of all connections on the two faces:

$$H_{m,f} = H_{m,f,OSB} + H_{m,f,GWB} \quad (53)$$

The obtained results are shown in Table 4.

Table 4. Average resistance obtained by the proposed methodology.

Structural component	Lateral resistance				
	Sheathing-to-frame connections	OSB	$H_{m,f,OSB}$ [kN]	21.62	$H_{m,f}$ [kN]
GWB		$H_{m,f,GWB}$ [kN]	8.07		
				H_m [kN]	29.69

It can be concluded that, by comparing the analytical value and the experimental value, an acceptable prevision was obtained. In fact, the resistance evaluated with the proposed methodology underestimates, about 26% of the resistance of the wall ($H_p / H_m = 37.40 / 29.69 = 1.26$).

3 CONCLUSIONS

Different methods are available to study the lateral in-plane response of sheathed lightweight steel shear walls. The methods available in literature can be classified as tabular methods, numerical methods and analytical methods. In particular, there are different methods available in literature to predict the lateral resistance and stiffness for sheathing braced timber walls. Since the lateral response of the two systems is very similar, the analytical methods valid for timber walls can also be used for CFS walls. Furthermore, this Section presents an analytical procedure based on principles of mechanics. The evaluation of lateral displacement at the top of the wall, d , under horizontal loads, H , can be obtained by adding in series the deformation contribution of each structural component, whereas the wall lateral resistance (H_{Rd}) can be obtained by the wall lateral strength associated to the failure of steel frame ($H_{Rd,s}$), frame-to-foundation anchors ($H_{Rd,a}$), sheathing panels ($H_{Rd,p}$) and sheathing-to-frame connections ($H_{Rd,f}$). Generally, the local behaviour of panels-to-frame connections governs the global lateral response of walls, the relevant deformation produces wall lateral displacement greater than those produced by other components. Finally, an interesting example of calculation is shown. In particular, on the basis of the cyclic test results, the lateral resistance and stiffness for single wall of a prototype were evaluated with the proposed design method, in order to compare the experimental results with analytical values and to check the reliability of the analytical values. The obtained values confirm that the wall lateral response is governed by the deformability of the sheathing-to-frame connections.

The comparison between the analytical and experimental results highlights an acceptable prevision. In fact, the analytical procedure gives an average underestimation of stiffness by 14% ($K_e / K = 5.79 / 5.09 = 1.14$), whereas the resistance evaluated with the proposed methodology underestimates, about 26% of the resistance of the wall ($H_p / H_m = 37.40 / 29.69 = 1.26$).

4 ACKNOWLEDGEMENTS

The Authors thank the financial support of the RELUIS project “Linea di Ricerca Acciaio e Composte Acciaio-Calcestruzzo” 2014-2015, 2015-2016 and 2016-2017.

5 REFERENCES

AISI S400 (2015). “North American Standard for Seismic Design of Cold-Formed Steel Structural Systems,” *AISI (American Iron and Steel Institute)*, December 2015, Washington DC, USA.

- Circolare n. 617, (2009), "Istruzioni per l'applicazione delle Nuove Norme Tecniche per le Costruzioni", *Ministro delle infrastrutture*, February 2009, Rome, Italy.
- D.M. 14/01/2008, "Norme Tecniche per le Costruzioni", *Ministero delle infrastrutture*.
- Easley, J. T, Foomani, M., Dodds, R. H. (1982). "Formulas for Wood Shear Walls", *Journal of Structural Division, ASCE*, 108(ST11), pp. 2460-2478.
- EN 1993-1-3 (2006). "Eurocode 3: Design of steel structures - Part 1-3: General rules – Supplementary rules for cold-formed members and sheeting", *European Committee for Standardization*.
- ENV 1995-1-1:1993, "Eurocode 5 – Design of Timber Structures – Part 1-1: General Rules and Rules for Buildings".
- Finnish timber code (2001). RIL 120-2001. Puurakenteiden suunnitteluohjeet.
- Fiorino, L., Della Corte, G., Landolfo, R. (2006). "Lateral Response of Sheathed Cold-Formed Shear Walls: An Analytical Approach". *18th International Specialty Conference on Cold-Formed Steel Structures*, pp. 603-619, October 26 & 27, 2006, Orlando, Florida, U.S.A.
- Hieta, J. and Kesti, J. (2002). "Design recommendations for shearwalls braced with sheathings", Teräsrakenteiden tutkimus- ja kehityspäivät 13.-14.6.2002, Mikkeeli, Finnish Constructional Steelwork association.
- Kaellsner, B. and Lam F. (1995). "Diaphragms and Shear Walls". *STEP Lectures: Holzbauwerke nach Eurocode 5-Grundlagen, Entwicklungen, Ergaenzungen, Fachverlag Holz*, Duesseldorf, Germany, pp. 15/1-15/19.
- Landolfo, R., Fiorino, L., Della Corte, G. (2006). "Seismic Behavior of Sheathed Cold-Formed Structures: Physical Tests", *Journal of Structural Engineering, ASCE*, April 2006, 570-581.
- McCutcheon, W. J., (1985). "Racking deformation in Wood Shear Walls", *Journal of Structural Engineering*, Vol.111, No.2, February 1985, P257-269.
- Tuomi, R. L. and McCutcheon, W. J. (1978). "Racking Strength of Light-Frame Nailed Walls", *Journal of the Structural Division, ASCE*, Vol. 104, No. ST7, July 1978, pp.1131-1140.

NON-CONVENTIONAL BUILDING: STICK-BUILT SYSTEMS – DESIGN BY TESTING

Nadia Baldassino ^a, Martina Bernardi ^b, Riccardo Zandonini ^c

^a *University of Trento, Trento, Italy, nadia.baldassino@unitn.it*

^b *University of Trento, Trento, Italy, martina.bernardi@unitn.it*

^c *University of Trento, Trento, Italy, riccardo.zandonini@unitn.it*

ABSTRACT

The use of cold-formed steel profiles for the load-bearing structure of residential buildings is progressively spreading in the Italian building market. The behaviour of this kind of structures is complex and, nowadays, not in deep investigated. This is reflected in the European and Italian standards, which do not take into account explicitly the design of these structures. Therefore, to characterize the behaviour of buildings made of cold-formed steel profiles, the so-called ‘design by testing’ should be adopted.

The activities of the University of Trento in the framework of the ReLUIS-DPC 2014-2016 project, focused on the experimental characterisation of the key elements of these structures in view of seismic design. This led to the definition of guidelines for their design assisted by testing. In this chapter, besides the key elements to be tested and analysed in view of the seismic structural design, the main contents of the guidelines are reported.

KEYWORDS

Cold-formed profiles, lightweight constructions, seismic design, design by testing, guidelines.

1 INTRODUCTION

The use of cold-formed thin-walled profiles to make the bearing frames for residential housing has been gaining in popularity also in the Italian building context.

These construction systems, that envisage the use of thin cold-formed steel profiles for the creation of load-bearing structural frames, allow to achieve ‘complete’, technologically advanced and environment-friendly industrialised construction systems. The versatility in the sections’ geometry and lightness, associated with ease of transport and simple assembly and flexibility of the construction system, are all aspects that favour the spreading of this building technique.

From the construction viewpoint, the buildings made with thin-walled profiles can be made using various construction techniques, by assembling the basic construction components, i.e the cold-formed profiles. The latter can be assembled on site to form the necessary vertical and horizontal structures. In this case, the individual elements are delivered ready to be assembled and interconnected. As an alternative, to shorten on-site assembly time, the profiles can be assembled at the plant to create wall and floor panels, thus allowing for less work on site. Finally, a more prefab-oriented construction technique is to create building modules at

the plant, complete with interior finishing and utility systems, to be assembled on site to create the building.



Figure 1. Example of residential building made using cold-formed steel profiles (photo by Cogi s.r.l.).

In order to design these building systems, it is necessary to define the behaviour of the structural system and therefore to know the performance of profiles, fasteners, wall and floor systems. This requires the definition of the individual sections and structural subsystems, also taking into account the functions and performance of the joints, so as to define the performance of the system as a whole.

1.1 Walls resistant to vertical and horizontal forces

In the cold-formed based buildings, the walls are realized assembling vertical profiles (the studs) at a regular spacing, usually corresponding to the spacing of the main elements of the floor systems. The vertical studs are connected at their ends using horizontal profiles (the chords). To reduce the slenderness of the vertical elements, some transversal elements could be placed at an intermediate height (Figure 2 b and Figure 2 c). In general, the walls perform the tasks to lead to the ground both the vertical forces transferred by the floor systems and the horizontal forces due, for example, to the seismic actions. The ability to bear the horizontal forces is usually given by bracing systems, which could be made, for example, of trussed systems (Figure 2 b) or of diagonal straps connecting the opposite corners of the walls (Figure 2 c).

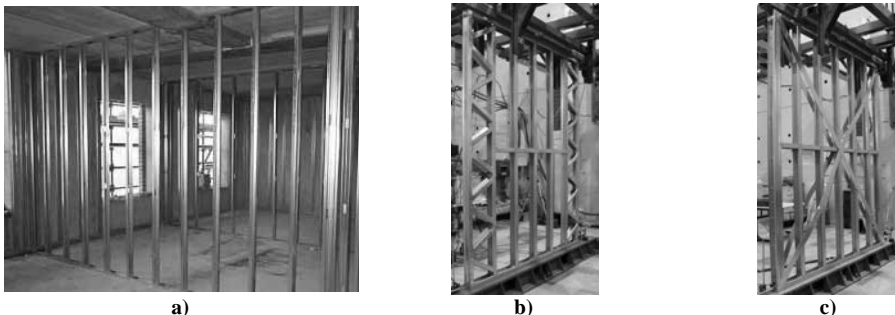


Figure 2. Examples of walls: a) without any bracing system; b) with truss bracings at each end; c) with diagonal straps.

The walls are usually completed by a thermal insulation and a cladding constituted by gypsum-fibre or wood panels, which could also contribute to the load-bearing resistance of the walls. Hold-downs are usually adopted as ground anchoring systems. They are located at the end of each wall panel, and are connected to the foundation by shear connectors and chemical or mechanical fasteners. The connections between the sub-systems (walls, bracing systems and beams) are generally realized using self-drilling screws or rivets.

1.2 Floor systems subjected to shear forces

In buildings made with cold-formed members, in general, floor systems are obtained using a system of horizontal bearing elements that form the frame of the slab, completed by a decking. The beams typically consist of cold-formed C- or Z-profiles, mounted individually or in pairs, set at regular intervals, or of cold-formed truss beams, equi-distanced and possibly braced with diagonal or horizontal elements that allow to increase the spans (Figure 3). Stiffeners can be introduced at the ends of each profile to prevent the elements from buckling phenomena.



Figure 3. Examples of frames for floor systems made with cold-formed profiles.

The decking, that allows to distribute the loads to the structure, can be made in various ways, using OSB (Oriented Strand Board) wood panels, plywood or chipboard panels, or fibre-cement panels assembled onto the beams using screws. As an alternative, concrete slabs can be used, made by casting the concrete in place on corrugated sheets that also function as formworks, and with or without shear connection elements. If the corrugated sheet is not completed with concrete casting, it can be covered with suitably connected wooden or plasterboard panels or with other similar material.

In general, the floor systems transmit the vertical loads acting on them to the vertical elements below. The sheathing plays a fundamental role in the floor's behaviour. Because it consists of panels (or metal sheets) adequately interconnected one with the other and suitably connected with the secondary beams (using screws, for example), the sheathing also represents a shear-resistant system, a so-called "horizontal diaphragm", exploited to withstand the in-plane forces generated by the horizontal forces acting on the structure. The diaphragm's ability to withstand the in-plane forces is a function of its ultimate shear strength. The overall performance of the floor system is affected by various factors such as the deck's type and geometry, the system of beams, the connection with the vertical elements, the type and characteristics of the connections between the floor elements.

2 CRITERIA FOR THE SEISMIC DESIGN, ASSISTED BY TESTING, OF COLD-FORMED STEEL STRUCTURES

2.1 General

The work of the Trento unit within the context of the ReLUIIS-DPC 2014-2016 project was focused on defining the guidelines for the seismic design, assisted by testing, of structures made using thin cold-formed steel profiles.

To date, only a limited number of studies regarding the behaviour of structures built using thin profiles and subjected to seismic forces are available, as pointed out, for example, in Accorti et al. (2016) and ReLUIIS-DPC *Prodotto 2* (2015). Moreover, international and especially national standards and regulations regarding the design of these construction systems are rather few. When designing these structures, therefore, one must refer to the design-by-testing principle, as indicated in UNI EN 1990:2006. To this end, the Trento unit has carried out a series of shear tests on full-scale floor and wall systems, as well as on the structural sub-components and fasteners, in order to investigate their behaviour. Based on the experimental experience gained, and with reference to the contents of the regulatory documents available, the guidelines were then defined for the design of walls and floor systems subjected to shear forces under monotonic and cyclic testing, as detailed in ReLUIIS-DPC *Prodotto 1* (2015) and ReLUIIS-DPC *Prodotto 2* (2016).

2.2 The State of the art

Studies on the response of walls made using unsheathed cold-formed steel elements are rather few. In general, the performance of sheathed walls has been analysed, while unsheathed walls have been considered only in comparison with the former. These studies have highlighted the significant contribution of wall 'sheathing' to their overall stiffness and resistance. The literature (Accorti et al. (2016)) shows how the influence of parameters such as the relationship between the wall's geometrical dimensions, the type of connection of the diagonals, the layout of the bracings, the type of studs used and the possible diagonals' pretensioning was analysed. The studies also proved the importance of the correct evaluation of the performance of the connections and of the walls' steel framing. Some aspects regarding the wall systems made using cold-formed profiles have not been investigated in depth, such as the response of panels with truss bracings.

The response to vertical forces of individual cold-formed profiles and of structural components obtained via assembly of such profiles has been widely analysed, including in recent years. Conversely, the shear force response of floor systems is still a scarcely studied subject. In particular, although the literature regarding the response of floor and roof systems made with corrugated sheeting completed or not with concrete is quite abundant, studies regarding the floors of buildings made with thin-walled cold-formed profiles are still few in number, for more details see ReLUIIS-DPC *Prodotto 2* (2015).

Therefore, a review of the literature concerning floor systems and wall systems shows the need for proceeding further with the study of the response of both construction systems when subjected to shear stresses. It should also be noted that, as regards regulations and standards, to date no national or international provisions dedicated specifically to the design of floor and roof systems made using cold-formed profiles are available, as pointed out in as detailed in ReLUIIS-DPC *Prodotto 1* (2015) and ReLUIIS-DPC *Prodotto 2* (2016). This means that the only sufficiently reliable tool currently available for accurately characterising the response of floor and roof systems is the experimental approach. Hence the unit of Trento has experimentally analysed, within the framework of the ReLUIIS-DPC 2014-2016 Project, the

response to shear forces of these two construction systems and of the subcomponents, and has developed guidelines for their design assisted by testing.

2.3 Tests conducted on walls

2.3.1 Wall testing

The tests conducted in the course of the project included a series of tests on full-scale wall specimens to study the response of the wall system as a whole (ReLUIIS-DPC *Prodotto 2* (2014)).

2.3.1.1 Test procedure

The specimens studied consist of wall systems made using thin-walled cold-formed (C-profile) profiles assembled using rivets. The walls consist of studs and chords placed at the top and bottom ends of the wall. To limit the buckling length of the studs, moreover, a cross-member is also foreseen at half height. The studs at the ends are equipped with an anchorage to ground consisting of so-called hold-downs. The metal framing configurations tested are shown in Figure 4 below.

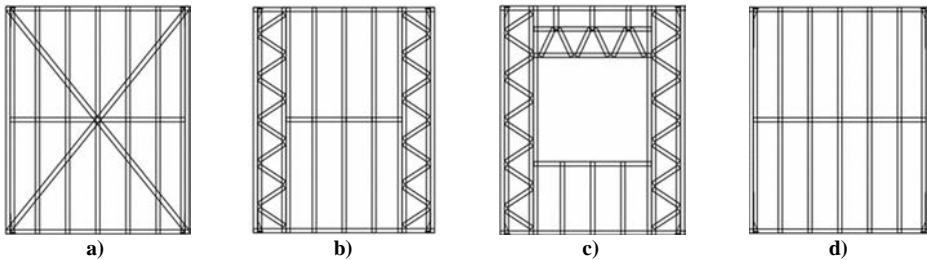


Figure 4. Configuration of the metal framings analysed: a) studs and diagonal flat bracings; b) studs and truss bracings at each end; c) truss framing and opening for window; d) studs only, without bracings.

The testing equipment used, such as to allow the application of both vertical and horizontal monotonic and cyclic loads, is illustrated in Figure 5.

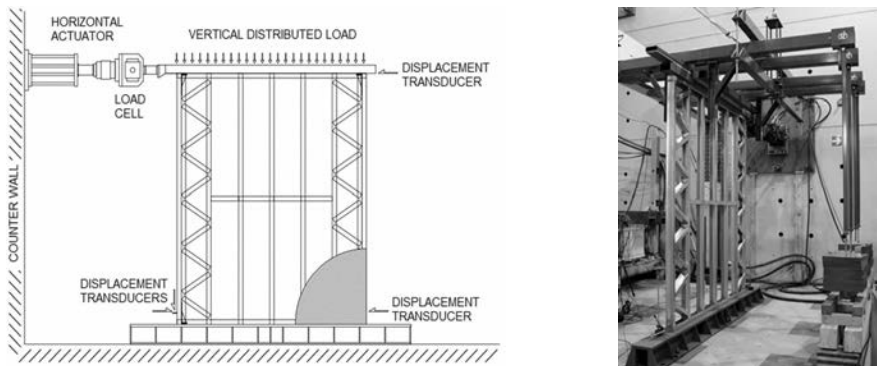


Figure 5. Test set-up used for full-scale specimens.

The specimens were tested with a distributed vertical load to represent the factored load acting on the lower wall of a two-storey building, applied using a distribution beam placed on

the upper edge of the wall. The horizontal load was applied via an actuator and out of plane displacements were prevented. During the test, the displacements occurring at the base and at the top of the walls as well as the lateral load applied were measured.

The specimens tested were divided into two different categories:

- Walls without sheathing panels;
- Walls with sheathing panels (of various kinds).

Just one test was performed for each wall type and for each testing protocol (monotonic test or cyclic test), for a total of 10 tests.

2.3.1.2 Testing protocol

The specimens were subjected to monotonic and cyclic tests. The cyclic tests were defined on the basis of the results of the previous monotonic tests, as envisaged in ECCS n. 45 (1986). The test procedure used can therefore be divided into two distinct phases:

- (1) execution of a monotonic test and calculation of the force (F_{y_conv}) and of the displacement (e_{y_conv}) associated with the conventional wall's yield, identified as the intersection point between the tangent to the origin (with slope E_t) and the tangent to the curve having a slope of $E_t/10$ (Figure 6);
- (2) execution of a cyclic test, defined as a sequence of symmetric cycles with amplitude defined as a function of the displacement e_{y_conv} resulting from the monotonic test (Figure 7).

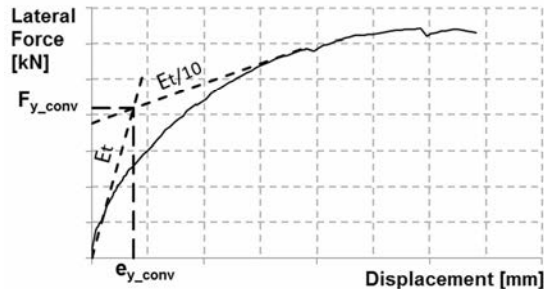


Figure 6. Definition of force and displacement associated with the conventional yield according to the ECCS n.45 (1986) procedure.

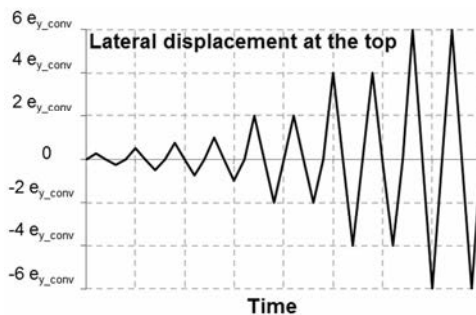


Figure 7. Loading history for cyclic tests.

2.3.1.3 Resistance parameter calculation procedure

In order to understand and compare the test response of the specimens, it is useful to calculate a resistance parameter. Having defined an elastic-perfectly plastic law to represent the response of the wall systems, and once defined the load associated with the elastic limit and its related displacement, the calculation of the stiffness of the elastic portion is immediate. Since only one test was performed for each wall type and for each test protocol (monotonic test and cyclic test), no statistical analysis was possible.

For the monotonic tests, having considered the load-top lateral displacement envelope curve, the following quantities were defined:

- The maximum load achieved during the test F_{\max} (Figure 8);
- The load associated with the conventional elastic limit $F_{y_{\text{conv}}}$ equivalent to 85% of F_{\max} (Figure 8);
- The displacement at the conventional elastic limit $e_{y_{\text{conv}}}$ calculated via the energy balance set by equalising areas 1 and 2 (two different grey areas) indicated in Figure 8;
- The secant stiffness associated with the conventional elastic limit k_{conv} , defined as the $F_{y_{\text{conv}}}/e_{y_{\text{conv}}}$ ratio.

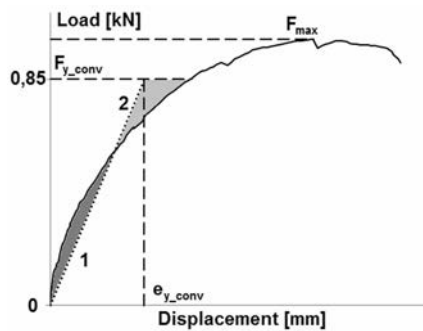


Figure 8. Calculation of the conventional elastic limit from the monotonic curve.

For the cyclic tests, instead, the procedure was as follows:

- calculation of the envelope curve for positive loads and for negative loads;
- calculation of the average envelope curve of the envelope curves for positive loads and for negative loads considered as absolute values;
- calculation of the load associated with the conventional elastic limit $F_{y_{\text{conv}}}$ equivalent to 85% of F_{\max} (Figure 8, where the curve is intended as the average envelope curve);
- calculation of the displacement $e_{y_{\text{conv}}}$ via the energy balance set by equalising areas 1 and 2 indicated in Figure 8, where the curve is intended as the average envelope curve;
- calculation of the displacement $e_{y_{\text{conv}}}$ via the energy balance set by equalising areas 1 and 2 indicated in Figure 8, where the curve is intended as the average envelope curve;
- calculation of the secant stiffness k_{conv} defined as the $F_{y_{\text{conv}}}/e_{y_{\text{conv}}}$ ratio.

2.3.1.4 Test results

A detailed illustration of the results achieved is given in document ReLUIS-DPC *Prodotto 2* (2014). Table 1 shows, for all wall systems tested, the maximum horizontal loads achieved and the secant stiffness calculated as specified in § 2.3.1.3 above. Figure 9 and Figure 10 show the collapse modes observed for unsheathed and sheathed walls, respectively.

Analysis of the test results revealed the substantial contribution of the sheathing to the overall behaviour of the wall systems subjected to shear forces. Comparison between the results for the unsheathed and sheathed walls shows that the presence of sheathing significantly changes the wall's response in terms of stiffness, resistance and collapse mode. The sheathing, and the sheathing-metal frame connection redistribute the forces among the steel elements and prevent or delay buckling phenomena in the studs and chords. This shear force transmission mechanism appears to be more efficient when compared to bare metal framing. The forces that engage the anchorage elements at the bottom, however, are significantly higher and therefore the connections between the hold-downs and the end studs are more stressed and could become the critical elements of the system.

These observations underline the need for adequate evaluation of the sheathing's behaviour when subjected to shear forces as well as of the characterisation of the connection between sheathing and steel structure and of the anchoring systems.

Table 1. Tests on full-scale wall specimens.

Specimen	Test protocol	Maximum horizontal load from envelope (F_{max})	k_{conv}
		[kN]	[kN/m]
G5 100 400 BB-1	Monotonic	64,20	5,23
G5 100 400 BB-2	Cyclic	61,93	4,77
G7 100 400 AB-1	Monotonic	40,40	1,90
G8 100 400 BB-1	Monotonic	66,48	5,15
G8 100 400 EF-1	Monotonic	70,04	3,77
G8 100 400 EF-2	Cyclic	68,63	4,47
G9 100 400 GH-1	Monotonic	76,92	3,95
G9 100 400 GH-2	Cyclic	68,65	3,25
G9 100 400 XX-1	Monotonic	35,92	2,02
G9 100 400 XX-2	Cyclic	36,71	2,08

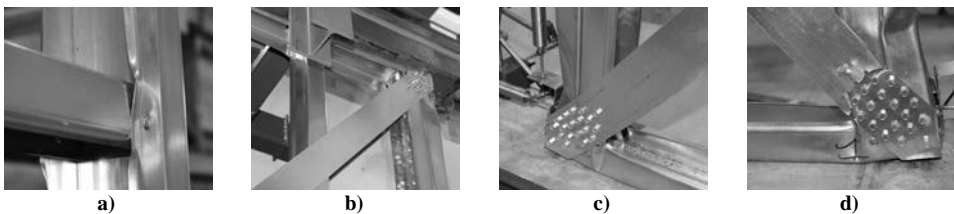


Figure 9. Details of the collapse mode observed for an unsheathed wall: a) post deformation at the intersection with the beam; b) top deformation of end studs where bracing is connected; c) bottom deformation of end studs where bracing is connected; d) failure of bracing.

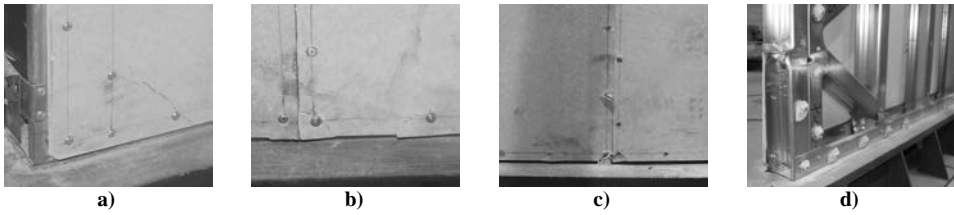


Figure 10. Details of the collapse mode observed for a sheathed wall: a) crack at the edges of the slabs; b) failure of the corners due to rotation of the two panels; c) cracks along the internal perimeter of the slabs due to screw slack; d) buckling of the external compressed stud at hold-down level.

2.3.2 Tests on sheathing specimens

The tests conducted on the wall systems (§ 2.3.1.4) have underlined the fundamental role played by the sheathing in the wall's overall behaviour, both in terms of stiffness and of resistance. This calls for a more in-depth analysis of the shear response of the sheathing alone.

2.3.2.1 Test procedure

To define the shear resistance and shear modulus of sheathing panels, experimental shear tests were conducted as per the test procedure indicated in ASTM D1037 (2006). The specimens, obtained from panels of the same material used for the sheathings selected for the investigation, were subjected to a displacement-controlled monotonic compression test (Figure 11). More than one test was conducted for each specimen type, for a total of 29 shear tests.

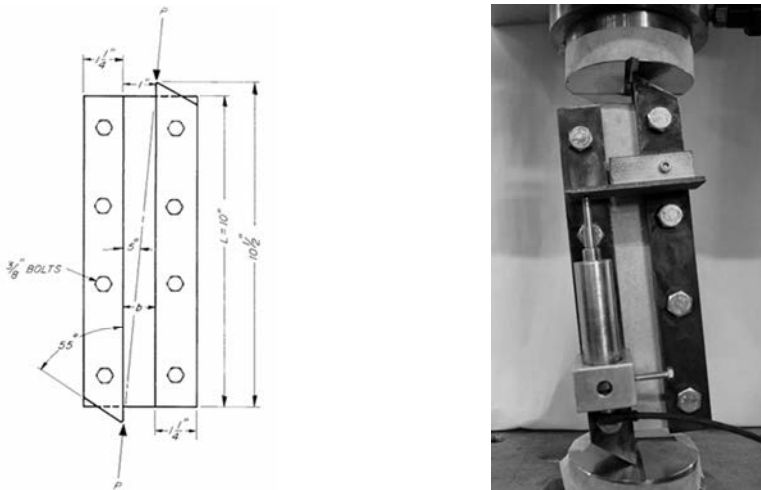


Figure 11. Test on a sheathing specimen, according to ASTM D1037 (2006) prescriptions.

2.3.2.2 Resistance parameter calculation procedure

The processing of the results was conducted according to the following procedure:

1. calculation of maximum resistance T_{\max} for each test;
2. calculation of average resistance T_m and of variation coefficient V_x ;
3. calculation of the characteristic value of resistance evaluated as:

$$T_{y_conv} = T_m \{1 - k_n V_x\} \quad (1)$$

where k_n is defined in relation to the number of tests performed;

4. for each test, calculation of displacement Δ_{y_conv} associated with T_{y_conv} ;
5. calculation of the conventional shear stress τ_{y_conv}

$$\tau_{y_conv} = \frac{T_{y_conv}}{d * L} \quad (2)$$

where $d*L$ is the shear area;

6. calculation of the drift value evaluated as

$$\gamma_{y_conv} = \frac{\Delta_{y_conv}}{d_b} \quad (3)$$

where d_b distance between the rails (in this specific case, $d_b=58\text{mm}$);

7. calculation of the average value of the drifts found in point 6;
8. calculation of the conventional shear modulus G_{y_conv} as ratio between τ_{y_conv} and γ_{y_conv} .

2.3.2.3 Test results

Test results are shown in extended form in the ReLUI document ReLUI-DPC *Prodotto 2* (2014). Figure 12 shows a typical example of collapse of a sheathing specimen, while Table 2 lists the results obtained for the six types of sheathing tested, in terms of conventional shear stress and conventional shear modulus.



Figure 12. Example of collapse mode observed in a sheathing specimen.

Table 2. Results of the shear tests on the sheathing specimens.

Sheathing type	τ_{y_conv} [MPa]	G_{y_conv} [MPa]
A	1,71	3141,78
B	3,42	1345,79
E	6,59	1584,10
F	5,59	1395,23
G	2,73	791,70
H	3,88	1234,70

2.3.3 Tests on the connection between sheathing and steel framing

Analysis of the behaviour of the full scale wall system specimens has shown how the progressive loss in resistance and stiffness of the walls with increasing loads is mainly due to damage to the connections and to the sheathing itself, rather than to damages to the internal frame. It is therefore important to characterise the performance of the connections.

2.3.3.1 Test procedure

To characterise the response of the connections between the sheathing and the structural system, experimental shear tests were carried out in accordance with the test procedure indicated by Serrette et al. (1997), who in turn modified the procedure indicated in ASTM D1761 (2000), defined for the calculation of the mechanical properties of metal fasteners in wood. The specimens were subjected to a displacement-controlled tensile test that determines a shear stress on the connections. Different sheathing specimens underwent a total of 39 tests. Each specimen consisted of three portions of steel sections: two coupled at the base and a third at the top edge. The sections were connected to two sheathing panels using the same type of screw used for the wall tests (Figure 13).

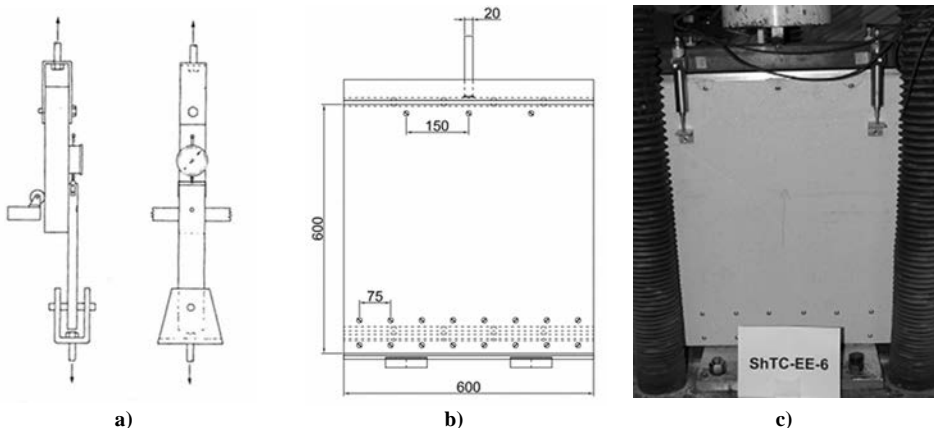


Figure 13. a) Lateral and frontal view of the specimen, according to ASTM D1761 (2000) prescriptions, regarding the tests for mechanical fasteners in wood; b) test set-up according to the test procedure indicated by Serrette et al. (1997) (measures in mm); c) specimen during the test.

2.3.3.2 Resistance parameter calculation procedure

To characterise the behaviour of the connection between the sheathing and the structural system, there are two significant parameters to be calculated: the shear strength and stiffness of the connection.

For each sheathing type the following procedure was applied:

1. calculation of maximum resistance T_{\max} for each test;
2. calculation of average resistance T_m and of variation coefficient V_x ;
3. calculation of the characteristic value of resistance evaluated as:

$$T_{y_conv} = T_m \{1 - k_n V_x\} \quad (4)$$

where k_n is defined in relation to the number of tests performed;

4. for each test, calculation of displacement Δ_{y_conv} associated with T_{y_conv} ;
5. calculation of stiffness k_{conv} relative to each specimen and of average stiffness.

2.3.3.3 Test results

Figure 14 shows an example of collapse mode observed, while Table 3 lists the results obtained for the 6 types of sheathing tested in terms of conventional shear strength and average conventional stiffness. Further details about test results are found in ReLUIIS-DPC Prodotto 2 (2014).

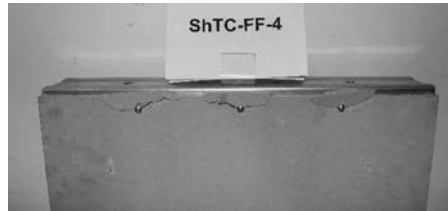


Figure 14. Collapse mode observed after shear test on the sheathing-metal frame connection for type F sheathing.

Table 3. Results of shear tests on connections between sheathing and metal frame.

Sheathing type	τ_{y_conv} [kN]	$k_{conv-media}$ [kN/mm]
AA	0,62	0,46
BB	1,19	0,58
EE	1,10	0,40
FF	0,95	0,34
GG	0,46	0,35
HH	0,77	0,43

2.3.4 Tests on ground anchoring systems

Ground anchoring obtained using hold-downs allows for better load transmission to ground, making sure the wall shows better stiffness and reaches higher resistance against lateral forces.

2.3.4.1 Test procedure

The test performed on the hold-downs was carried out in accordance with AISI S913 (2008). The hold-down/connection to ground/metal structure system was analysed via a displacement-controlled monotonic test.

2.3.4.2 Resistance parameter calculation procedure

Having the results of only one test available, resistance parameters were calculated using the procedure illustrated below. Considering the load-vertical displacement curve in Figure 15, the following quantities were determined:

- the maximum load achieved during the test P_{max} (Figure 15);
- the load associated to the conventional elastic limit P_{y_conv} equivalent to 85% to P_{max} (Figure 15);
- the displacement at the conventional elastic limit Δ_{y_conv} calculated via the energy balance set by equalising areas 1 and 2 indicated in Figure 15;
- the secant stiffness associated to the conventional elastic limit k_{conv} defined as the $P_{y_conv} / \Delta_{y_conv}$ ratio.

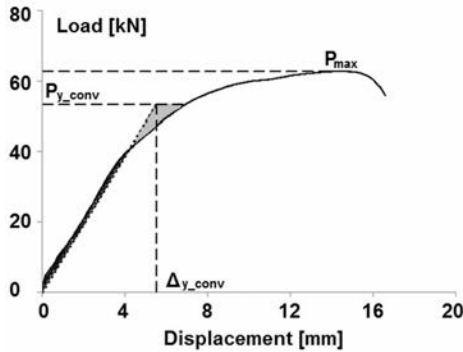


Figure 14. Load-displacement curve for the anchorage-to-ground system and resistance parameters calculation procedure.

2.3.4.3 Test results

Table 4 gives load P_{y_conv} and secant stiffness k_{conv} obtained with the test, associated to the conventional elastic limit. For further details, refer to document ReLUIIS-DPC *Prodotto 2* (2014).

Table 4. Main results of the testing of the ground anchorage device.

P_{y_conv} [kN]	k_{conv} [kN/mm]
53,30	9,66

2.4 Guidelines for the design assisted by testing of walls

The proposed operational procedure for the shear characterisation of wall systems made with cold-formed profiles is based on the experience gained in a campaign of experimental tests conducted on these systems at the universities of Trento and Naples, as well as on the currently available standards to which in general it is possible to refer for the characterisation of wall systems and of their components. The guidelines for the design assisted by testing of wall systems and wall system components developed and summarised in this chapter are described in detail in ReLUIIS document ReLUIIS-DPC *Prodotto 1* (2015).

2.4.1 The standards available for testing

As already mentioned above (§ 2.2), considering the limited knowledge of the response of wall systems made using cold-formed profiles and the lack of specific standards and regulations, the most reliable way of achieving a precise characterisation is based on design assisted by testing principles (UNI EN 1990:2006). It is also important to refer to the documentation currently available regarding the various test procedures used for the characterisation under monotonic and cyclic testing of structural elements. Following is a list of the publications/standards used as reference:

- ECCS, n. 45 (1986) “Seismic Design, Recommended Testing Procedure for Assessing the Behaviour of Structural Steel Elements under Cyclic Loads”, defining a testing procedure for characterising steel structures and components under cyclic loads;

- ASTM E564 (2012) “Standard Practice for Static Load Test for Shear Resistance of Framed Walls for Buildings”, providing the experimental procedure for characterising the shear resistance and stiffness of wall systems under monotonic loads;
- ASTM E2126 (2011) “Standard Test Method for Cyclic (Reversed) Load Test for Shear Resistance of Vertical Elements of the Lateral Force Resisting Systems for Buildings”, providing the procedure for the characterisation of the stiffness, resistance and ductility of wooden or metal wall systems under lateral cyclic loads;
- Standard UNI EN 15512:2009, “Steel static storage systems – Adjustable pallet racking systems – Principles for structural design”, relating to the procedure for the calculation of the design moment at the base joints in pallet racking systems, considered here because it introduces several aspects relating to the analysis method proposed.

In view of the importance of the sheathing, of the sheathing-frame structure connections and of the anchorage-to-ground system (hold-downs) in terms of wall system performance, the following standards have also been taken into consideration:

- ASTM D1037 (2006) “Standard Test Methods for Evaluating Properties of Wood-Base Fiber and Particle Panel Material”, describing the test methods for evaluating the main properties of sheathing panels made of wood-based fibre and particle materials;
- ASTM D1761 (2000) “Standard Test Methods for Mechanical Fasteners in Wood”, describing the test methods for calculating the mechanical properties of mechanical fasteners in wood or wood-based materials;
- AISI S913 (2008) “Test Standard for Hold-downs Attached to Cold-Formed Steel Structural Framing”, describing the methods for calculating the resistance and deformability properties of anchorage-to-ground systems used in buildings made with thin-walled steel profiles.

2.4.2 Wall system test protocols

Following is a summary of the test procedures proposed for the execution of monotonic or cyclic tests on wall systems and how to interpret the experimental data and calculate the relating parameters (further details are reported in ReLUIS-DPC *Prodotto 1* (2015)). The suggested operational approach consists in two phases: characterisation of the wall under monotonic testing first and then under cyclic testing. The two operational procedures proposed for cyclic testing are taken one from the ECCS, n.45 (1986) document and the other from the ASTM E2126 (2011) standard. The details of the procedures proposed are given in the document ReLUIS-DPC *Prodotto 1* (2015). The calculation of the design value of the lateral resistance R_d , as envisaged in UNI EN 1990:2006, must be done by reducing the value to the conventional elastic limit F_{y_conv} by a specific coefficient γ_M . The test set-up proposed is the one shown in Figure 5.

2.4.2.1 Procedure performed as per ECCS, n. 45 (1986)

Monotonic test

The monotonic test:

- identifies the conventional elastic limit of the wall needed to define the cyclic test;
- identifies the design value of the lateral resistance for symmetrical walls not subjected to cyclic lateral forces.

Test data analysis can be performed based on two methods according to the purpose of the test, as shown in Table 5.

Table 5. Diagram for the monotonic test according to the procedure as per ECCS, n. 45 (1986).

AIM	Definition of cyclic test procedure	Calculation of design resistance
No. of tests	1	3

TESTING PROTOCOL		
	DATA ANALYSIS	<div style="display: flex; justify-content: space-around;"> <div style="width: 45%;"> <ol style="list-style-type: none"> 1. Conventional elastic limit $F_{y_conv} = 0,85 F_{max}$ 2. e_{y_conv} calculated via the energy approach </div> <div style="width: 45%;"> <ol style="list-style-type: none"> 1. Conventional elastic limit F_{y_conv} as per UNI EN 1990: 2006 2. e_{y_conv} calculated via the energy approach </div> </div>

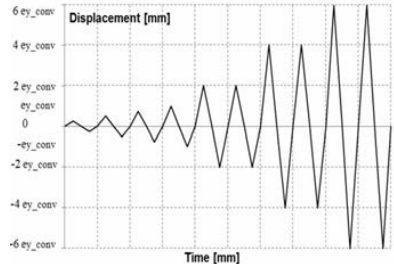
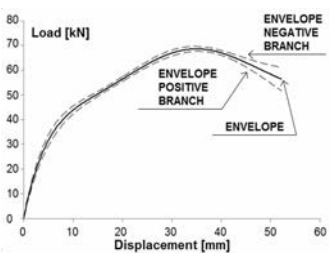
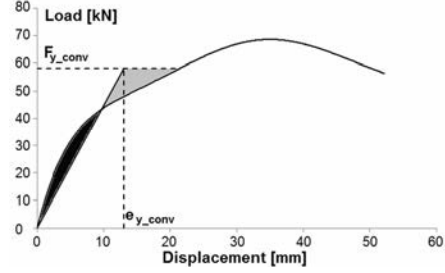
Cyclic test

The cyclic test:

- identifies the design value of the lateral resistance for symmetrical walls subjected to cyclic lateral forces;
- allows to define the kinematic and cyclic ductility parameters for characterising the wall's post-elastic strength reserves;
- allows to evaluate the wall's dissipation capacity.

The test and the data processing were conducted as indicated in Table 6.

Table 6. Cyclic test diagram according to the procedure as per ECCS, n. 45 (1986).

AIM	Calculation of design resistance
No. of tests	3
<p>TESTING PROTOCOL (based on the monotonic function as a function of e_{y_conv})</p>	
<p>DATA ANALYSIS</p>	<ol style="list-style-type: none"> <li data-bbox="327 591 1113 646">Average envelope curve between the positive and negative branches of the cyclic test, the latter as absolute value  <ol style="list-style-type: none"> <li data-bbox="327 900 1113 937">Conventional elastic limit F_{y_conv} as per UNI EN 1990: 2006 <li data-bbox="327 937 1113 973">e_{y_conv} calculated via the energy approach  <ol style="list-style-type: none"> <li data-bbox="327 1246 1113 1283">Definition of kinematic and cyclic ductility parameters <li data-bbox="327 1283 1113 1304">Evaluation of dissipation capacity

2.4.2.2 Procedure as per ASTM E2126 (2011)

Monotonic test

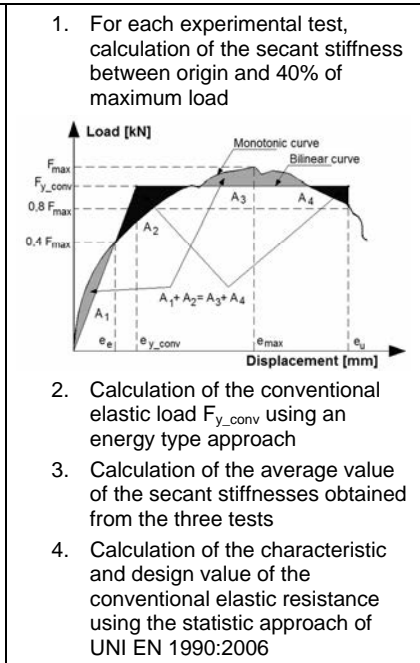
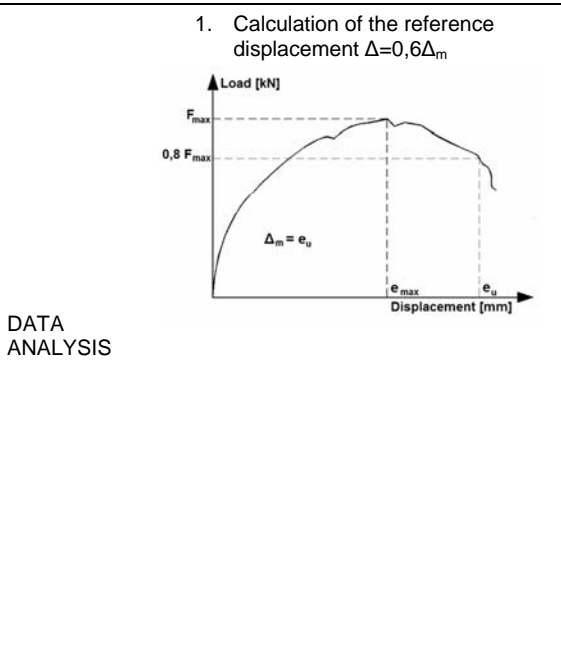
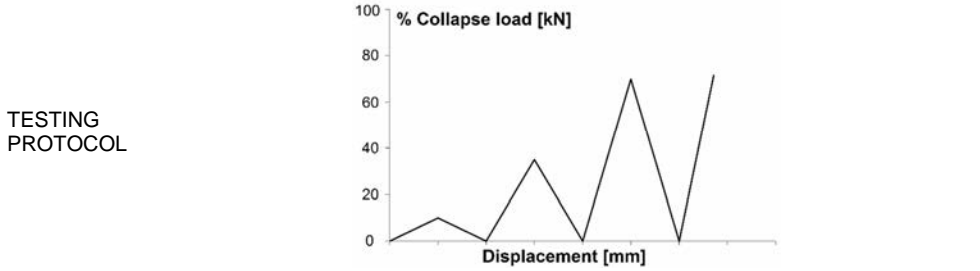
The monotonic test:

- identifies the reference displacement of the wall needed to define the cyclic test;
- identifies the design value of the lateral resistance for symmetrical walls not subjected to cyclic lateral forces.

Test data analysis can be performed based on two methods according to the purpose of the test, as shown in Table 7.

Table 7. Diagram for the monotonic test according to the procedure as per ASTM E2126 (2011).

AIM	Definition of cyclic test procedure	Calculation of design resistance
No. of tests	1	3



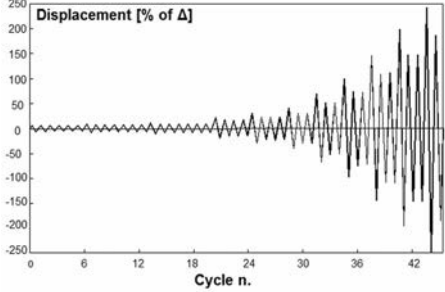
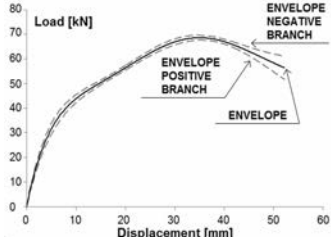
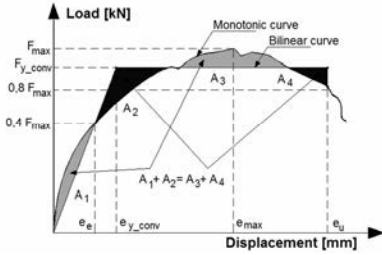
Cyclic test

The cyclic test:

- identifies the design value of the lateral resistance for symmetrical walls subjected to cyclic lateral forces;
- allows to define the ductility parameters for characterising the wall’s post-elastic strength reserves;
- allows to evaluate the wall’s dissipation capacity.

The test and the data processing are conducted as indicated in Table 8.

Table 8. Cyclic test diagram according to the procedure as per ASTM E2126 (2011).

AIM	Calculation of design resistance
No. of tests	3
<p>TESTING PROTOCOL (based on the monotonic function as a function of the reference displacement Δ)</p>	
	<p>1. Average envelope curve between the positive and negative branches of the cyclic test, the latter as absolute value</p> 
<p>DATA ANALYSIS</p>	<p>2. Calculation of secant stiffness traced between the origin and 40% of maximum load</p> <p>3. Calculation of conventional elastic load calculated via the energy approach</p>  <p>4. Definition of suitable ductility parameters</p> <p>5. Evaluation of dissipation capacity</p>

2.4.3 Test methods on individual components

To characterise the structural subcomponents, it is possible to briefly summarise the testing procedures suggested in the ReLUI document ReLUI-DPC *Prodotto 1* (2015), as follows:

- for the calculation of the sheathing resistance, it is recommended to perform the testing procedure indicated in standard ASTM D1037 (2006);
- for the calculation of the mechanical properties of the connections between sheathing and wall metal framing, the use of a procedure is envisaged that constitutes a variant

of the test procedure indicated in ASTM D1761 (2000), similar to that described by Serrette et al. (1997) and modified by Fiorino et al. (2007);

- for the characterisation of the anchoring system (hold-down), the approach suggested in AISI S913 (2008) is recommended.

The procedures for calculation of the mechanical properties proposed for each case are taken from the calculation procedure also proposed for wall systems, briefly mentioned in § 2.3.1.3 and reported in full in ReLUIIS-DPC *Prodotto 1* (2015).

2.5 Tests conducted on floor systems

2.5.1 Tests on profiles and beams for floor systems

With a view to performing the experimental characterisation of floor systems, a set of tests was carried out on the profiles and beams used for the manufacture of the floor systems tested later. The types of floor considered envisage the use of two kinds of beams: truss beams obtained by using thin-walled steel C-profiles 100 mm height (B100), and beams obtained by coupling two C-profiles 200 mm height (B200), both with a thickness of 1,2 mm. Four point bending tests were carried out in order to characterise the individual profiles used to make the truss beams (B100 profiles), the beams obtained by coupling the B200 profiles and the truss beams. As regards the truss beams, the aim of the study conducted was to also analyse the contribution of the decking to the response of the beam system (corrugated sheet, corrugated sheet finished with a gypsum-fibre panel and corrugated sheet finished with an OSB wood panel). The results of the tests on the components allowed for the preliminary evaluation of the floors' performance under bending stresses and were then used to design the floors to be subsequently subjected to shear tests.

2.5.1.1 Material characterisation

A series of tensile tests was conducted to define the main mechanical properties of the steel types used in the specimens subjected later to the bending tests (§ 2.5.1.2 and 2.5.1.3). The tests were performed as per standard UNI EN ISO 6892-1:2009. Further details and the results of the tensile tests are found in ReLUIIS-DPC *Prodotto 3* (2015).

2.5.1.2 Tests on individual profiles and on beams

Four point bending tests were conducted to evaluate the load-bearing capacity of B100 and B200 type profiles in presence of bending loads, considering the two main bending planes. In order to obtain the complete characterisation of profiles featuring only one axis of symmetry, it is necessary to conduct three bending tests as per the three configurations shown in Figure 16. The B200 profiles were tested using the method shown in Figure 16 a, while the B100 profiles were tested using all three methods indicated in Figure 16. The coupling of the profiles (mode a) was achieved using self-tapping screws.

The tests were conducted as per the indications given in UNI EN 1993-1-3:2007. To obtain a more precise estimate of the length of the specimens, and especially of the constant moment zone, to be applied to detect any local/distortional buckling phenomena, a buckling analysis was conducted on the members under investigation using the CUFSM finite strips methods program (Li et al. (2010)). The details and results of the analysis are given in the document ReLUIIS-DPC *Prodotto 3* (2015).

Each test was performed via a complete loading-unloading cycle (with peak load equivalent to 10% of the expected failure load) and the load acting on the specimen was then increased until it collapsed. For the evaluation of the specimens' bending behaviour, six inductive transducers and one load cell were used.

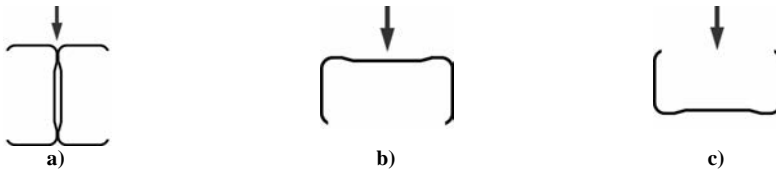


Figure 16. Configurations used for bending tests.

The results obtained are listed in detail in the in the document ReLUIIS-DPC *Prodotto 3* (2015). For each type of profile and for each length of the constant moment zone considered, ultimate load and ultimate moment were obtained and the relating standard deviation and the associated variation coefficient were calculated. The collapse modes observed can be ascribed to localised buckling phenomena.

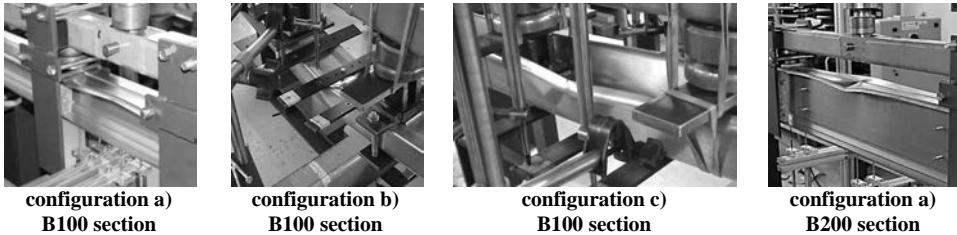


Figure 17. Specimens after testing.

2.5.1.3 Tests on truss beams

To study the behaviour of the truss beams obtained using B100 (beam type 1) profiles, four point bending tests were carried out.

Each one of the specimens analysed consists of three truss beams and of a deck. At the bearing points, the beams are connected by a C-section profile to prevent their lateral buckling, while at the bottom the chords are constrained by Omega-shaped profiles that simulate the constraint offered by the counter ceiling support.

Three types of decks were considered:

1. corrugated sheet, fastened to the top chords with self-tapping screws;
2. corrugated sheet and gypsum-fibre panel connected to the corrugated sheet and to the top chord of the beams with self-tapping screws;
3. OSB3 panel fastened with self-tapping screws.

In all specimens, collapse was observed associated to connection rivet failure between the diagonal bracings and the chords (Figure 18).



Figure 18. Collapse due to combined shear-tensile failure of rivets.

Table 9 lists the peak load values and associated mean displacement for each specimen. Notice how the type of decking does not contribute significantly to the bending response of the floor system.

Table 9. Results of the four point bending tests.

Specimen	Top finish	Q_{max} [kN]	δ_{max-medio} [mm]
RE_GL_01	Steel deck	45,52	45,75
RE_G_01 (double rivet)	Steel deck	41,44	43,10
RE_O_01	Steel deck and gypsum fibre board	44,16	45,95
RE_GR_01	OSB3	43,33	44,34

2.5.2 Tests on floor systems

In order to characterize the response to shear loads of the floor systems made using thin-walled cold-formed profiles, a test campaign was planned for four floor types as defined below.

Two distinct types of floor were identified, based on the beam systems used. One case envisages the use of truss beams (beam type 1) obtained using thin-walled steel C-profiles 100 mm height (B100 profiles), while the second case envisages the use of beams obtained by coupling two thin-walled steel C-profiles 200 mm height (B200 profiles) (beam type 2). In both cases, the centre-to-centre distance between beams is equal to 400 mm. Also as regards the decking, two solutions have been found: deck made using corrugated sheet completed with panels of gypsum-fibre or similar material ('dry' floor – deck type A), and deck made using corrugated sheet and a light concrete slab ('wet' floor – deck type B).

By combining the two beam types and the two deck types, it was possible to identify 4 floor types: floor 1A (obtained by coupling beam type 1 with deck type A) (Figure 19), floor 1B (obtained by coupling beam type 1 with deck type B) (Figure 20), floor 2A (obtained by coupling beam type 2 with deck type A) (Figure 21) and floor 2B (obtained by coupling beam type 2 with deck type B) (Figure 22).

The corrugated sheeting used for cases 1A and 2A is of the dovetailed kind with optimised 'S-shaped' geometry. This ensures high stiffness values and, in the case of wet finishing, a good degree of bonding with the concrete. The gypsum-fibre panel used for solutions 1A and 2A is a slab made of fibrous gypsum plaster, cellulose fibers and mineral additives. The concrete used for solutions 1B and 2B is a premixed light structural concrete for stiffening the floors. The connections between the various floor elements have been ensured using self-tapping screws of variable diameter in function of the elements to be connected: larger diameter screws were used for the connection between beams and corrugated sheet and smaller diameter screws were used for connecting the corrugated sheets with the gypsum-fibre panels ReLUIIS-DPC *Prodotto 1* (2016).

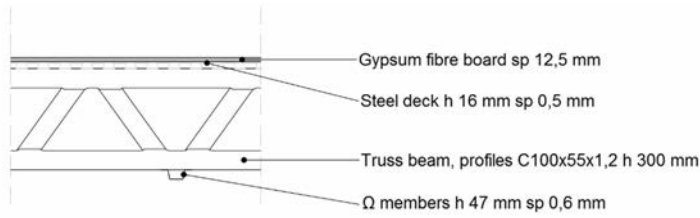


Figure 19. Specimen type 1A, truss beams with dry deck.

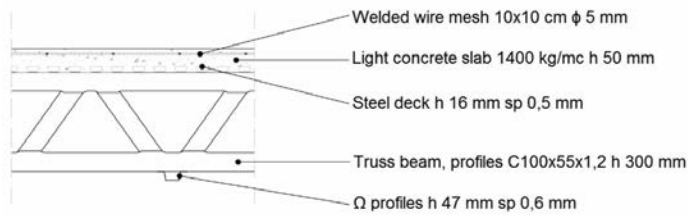


Figure 20. Specimen type 1B, truss beams with wet deck.

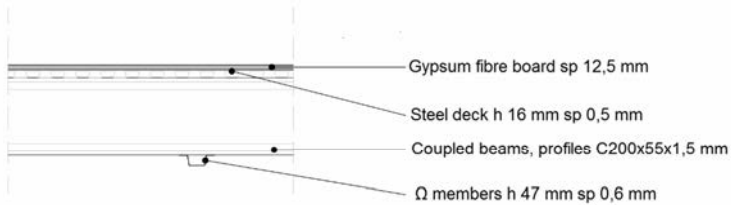


Figure 21. Specimen type 2A, coupled beams with dry deck.

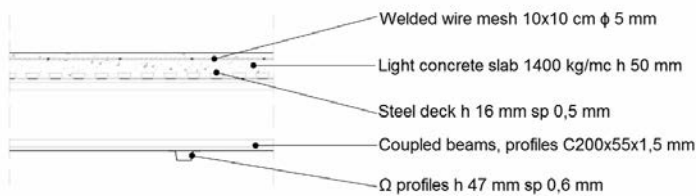


Figure 22. Specimen type 2B, coupled beams with wet deck.

2.5.2.1 Tests on truss beams

To perform the shear tests, a set-up was designed on purpose so as to allow to apply the shear force to the floors made using thin-walled members (design details are reported in ReLUIS-DPC *Prodotto 1* (2016)). Figure 23 and Figure 24 show the views of the test frame and of the floor mounted onto and connected with the test frame. A hydraulic actuator was used to apply the force.

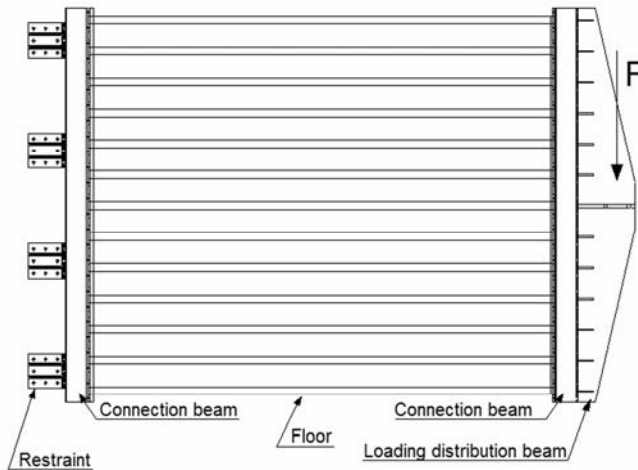


Figure 23. View of test frame and test system.

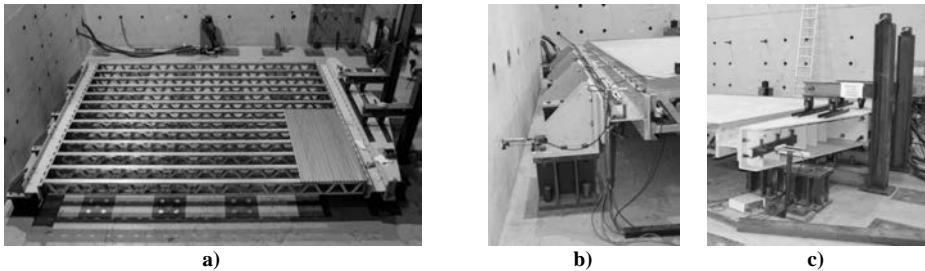


Figure 24. a) View of test frame and test system; b) fixed constraint; c) load application system.

In order to characterise the response of the floors correctly, the following parameters were measured: applied load, relative displacement components between testing system and floor, relative drift between deck and framing, and absolute displacement components (such as rotation and angular deformation of the floor). To this end, a set of instruments common to all of the tests was used, to which, where necessary, instruments specific for the peculiarities of each type of floor were added.

2.5.2.2 The testing protocol

The floor specimens were subjected to displacement-controlled monotonic tests with loading and unloading cycles and without load inversion (Figure 25).

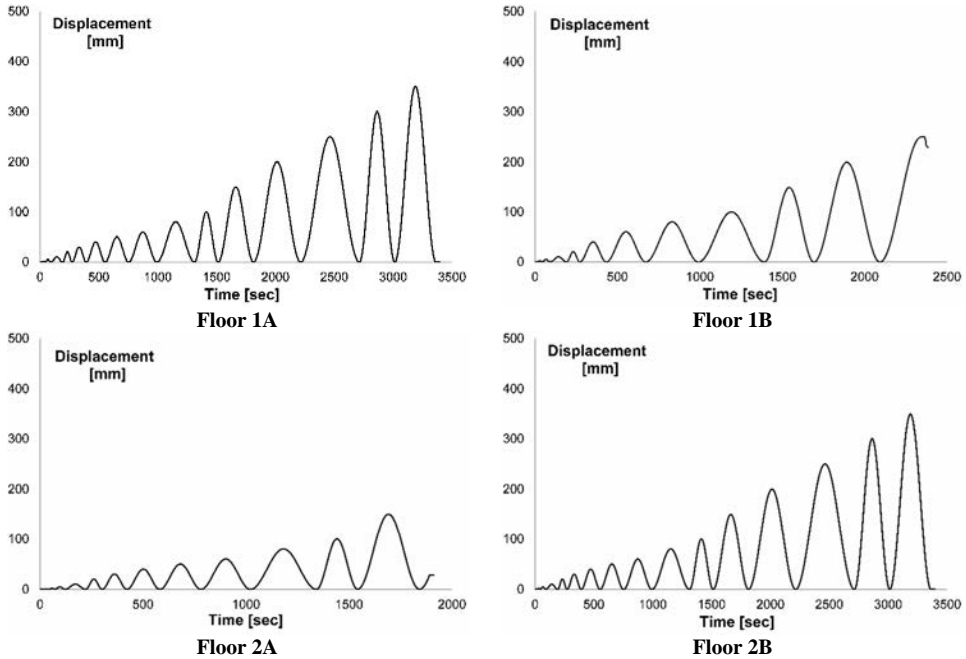


Figure 25. Load cycles.

2.5.2.3 Stiffness parameters calculation procedure

To calculate the shear stiffness of the floor, the procedure given in AISI S907 (2013) was followed:

$$G' = \left(\frac{P_d \cdot a}{\Delta_d \cdot b} \right) \quad (5)$$

where

$$P_d = 0,4 \cdot P_{\max}$$

with

- P_{\max} peak load measured during test;
- Δ_d floor displacement associated to P_{\max} ;
- a floor span;
- b floor width (in the direction of load application).

2.5.2.4 Test results

Test data analysis has generated information regarding the maximum force withstood by the specimen and its displacement, the angular deformation of the specimen, the rotation of the beam where the load was applied, the relative drift of the decking system with respect to the fixed supports of the test framing and the relative drift of the decking system with respect to the underlying beams. Moreover, in the case of the specimens using dry deck, it was possible to measure the relative drift of the gypsum-fibre panels in the direction parallel to the load application direction. The results are listed in full in the document ReLUIS-DPC *Prodotto 1* (2016).

Table 10 lists the stiffness values calculated using formula (5) for the four floors tested under monotonic loading.

Table 10. Floors shear stiffness values.

Specimen	Type	G' [kN/mm]
1A	Truss beams + steel deck and gypsum fibre boards	1,93
1B	Truss beams + steel deck and concrete slab	4,06
2A	Coupled beams + steel deck and gypsum fibre boards	3,20
2B	Coupled beams + steel deck and concrete slab	6,05

Figure 26 - Figure 29 show several details of the collapse observed in the four floors tested.



Figure 26. Collapse mode of floor 1A.



Figure 27. Collapse mode of floor 1B.

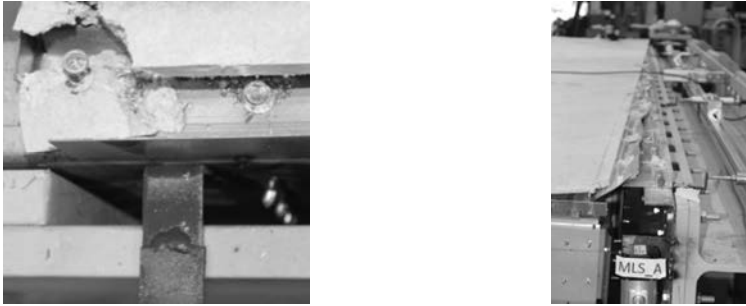


Figure 28. Collapse mode of floor 1B.

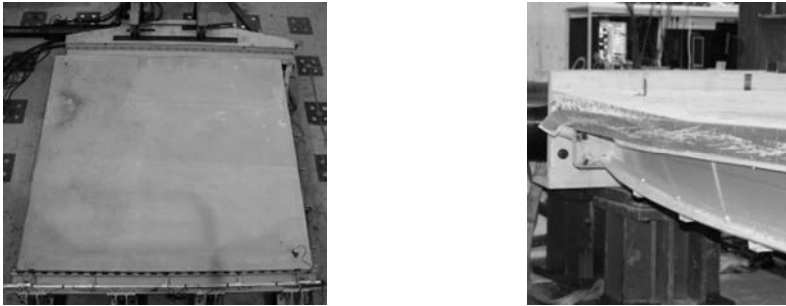


Figure 29. Collapse mode of floor 1B.

Collapse of the specimens with dry deck (floors 1A and 2A) has involved the interior connections of the decking, and especially the connections between the gypsum-fibre and the corrugated sheet panels and those between the corrugated sheet and the beams underneath it. The specimens with concrete slab (floors 1B and 2B) showed very high stiffness and a concentration of the stresses on the more external lateral beams. In both specimens, the collapse therefore involved these beams. In one case, the failure of the connection joint between beam and test frame was observed, while in the other case a plastic hinge formed in the beams, located at approximately one third of their length. Comparison of the test results show that the floors with dry deck (floors 1A and 2A) have less shear stiffness compared to the floors made with light concrete slabs. The minor stiffness allowed for a more ‘even’ distribution of the stresses, which led to an increase in the specimens’ deformation capacity, but to a lower resistance. This has highlighted the central role played by the decking system and by the connections in the stress diffusion and transfer mechanism.

2.6 Guidelines for the design assisted by testing of floor systems

As with the wall systems, guidelines for the design assisted by testing of floor systems made using thin-walled profiles were developed. The proposal is based on the experience gained by the University of Trento in the testing of these structural systems and on the regulations and standards available. The procedures proposed and briefly summarised in this chapter are reported and analysed in detail in the document ReLUIS-DPC *Prodotto 2* (2016).

2.6.1 *The standards available for testing*

As already mentioned above (§ 2.2), considering the limited knowledge of the response of floor systems made using cold-formed profiles subjected to shear forces and the lack of specific standards and regulations, the most reliable way of achieving their precise characterisation is experimentation based on design assisted by testing principles UNI EN 1990:2006. It is also important to refer to the documentation currently available regarding the various test procedures used for the characterisation of structural elements under monotonic and cyclic testing. Following is a list of the documents used as reference:

- ECCS, n. 45 (1986) “Seismic Design, Recommended Testing Procedure for Assessing the Behaviour of Structural Steel Elements under Cyclic Loads”, defining a testing procedure for characterising steel structures and structural components under cyclic loads;
- CUREE Publication No. W-02 (2001), “Development of a Testing Protocol for Woodframe Structures”, providing a testing protocol regarding tests on woodframe structure buildings subjected to cyclic loads;
- ECCS, n.88 (1995), “Practical Improvement of Design Procedures, European Recommendations for the Application of Metal Sheeting acting as a Diaphragm”, introducing a testing procedure regarding the shear characterisation of metal sheeting diaphragms towards the application of design methods that consider the diaphragm’s action both as roof and as floor;
- AISI S907 (2013), “Test standard for Cantilever Test Method for Cold-Formed Steel Diaphragms”, defining the requisites for the monotonic and cyclic testing of deckings, roofing and walls acting as diaphragms and made using cold-formed steel panels;
- ReLUIIS-DPC Prodotto 1 (2015), relating to the testing protocol proposed for the shear characterisation of wall systems under monotonic and cyclic testing (§ 2.4).

2.6.2 *Floor system test protocols*

The test set-up shall be such as to guarantee the application of a shear force to the floor system. During the test, shear forces, specimen and test system displacements shall be measured continuously until the ultimate specimen conditions are reached. The displacements parallel to the sides of the floor system shall be measured (layout of the type 2 measurement apparatus as per document AISI S907 (2013)) and, in addition or as an alternative, the lengthening of the diagonals of the floor system (layout of the type 1 measurement apparatus as per document AISI S907 (2013)). It is also useful to measure the displacements that characterise the local response of the system and, moreover, to monitor any test system deformations, so as to identify any system displacement components caused by the load application method.

The calculation of the design value of the lateral resistance R_d , as envisaged in UNI EN 1990:2006, must be done by reducing by a specific coefficient γ_M the value to the conventional elastic limit F_{y_conv} , defined as specified further below.

2.6.2.1 *Monotonic test*

In function of the type of cyclic test to be performed next, the monotonic test:

- identifies the conventional elastic limit of the floor system needed to define the cyclic test based on ECCS, n.45 (1986);
- identifies the displacement of reference of the floor system needed to define the cyclic test based on the CUREE Publication No. W-02 (2001).

Moreover, the monotonic test allows to determine the design value of the floor system’s lateral resistance.

Experimental data analysis can be performed based on two methods according to the purpose of the test, as shown in Table 11.

Table 11. Diagram for the monotonic test.

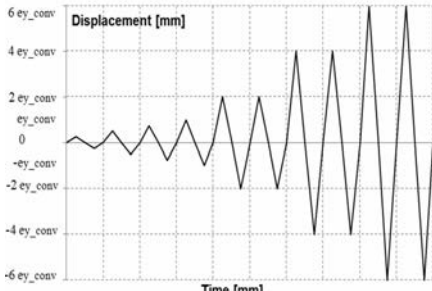
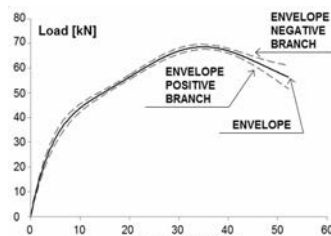
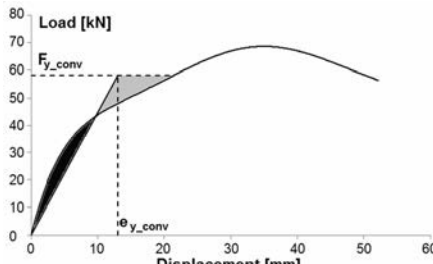
AIM	Definition of cyclic test procedure	Calculation of design resistance
No. of tests	1	3
TESTING PROTOCOL		
DATA ANALYSIS FOR NEXT CYCLIC TEST AS PER ReLUIS-DPC <i>Prodotto 1</i> (2015)	<ol style="list-style-type: none"> 1. Calculation of conventional elastic limit $F_{y_conv} = 0,85 F_{max}$ 2. e_{y_conv} calculated via energy approach 	<ol style="list-style-type: none"> 1. Calculation of conventional elastic limit F_{y_conv} as per UNI EN 1990:2006 2. e_{y_conv} calculated via energetic approach
DATA ANALYSIS FOR NEXT CYCLIC TEST AS PER CUREE Publication No. W-02 (2001)	<ol style="list-style-type: none"> 1. Calculation of the displacement of reference $\Delta = 0,6 \Delta_m$. Δ_m is the displacement at the load applied reaches, for the first time, a value of 80% of the load in the descending part of the load vs displacement curve 	<ol style="list-style-type: none"> 1. Calculation of the displacement of reference $\Delta = 0,6 \Delta_m$. Δ_m is the displacement at the load applied reaches, for the first time, a value of 80% of the load in the descending part of the load vs displacement curve 2. Average of the displacement value of reference Δ obtained for each

2.6.2.2 Cyclic test as per ECCS n. 45 (1986) and ReLUIS-DPC *Prodotto 1* (2015)
The cyclic test:

- identifies the design value of the resistance and shear stiffness for floor systems subjected to oscillatory lateral forces;
- allows to define the kinematic and cyclic ductility parameters for characterising the floor system’s post-elastic strength reserves;
- allows to evaluate the floor system’s dissipation capacity.

The test procedure and the data processing are conducted as indicated in Table 12.

Table 12. Diagram for the cyclic test according to the procedure as per ECCS n.45 (1986).

AIM	Calculation of design resistance
No. of tests	3
<p>TESTING PROTOCOL (based on monotonic test, defined in function of e_{y_conv})</p>	
	<p>1. Average envelope curve between the positive and negative branches of the cyclic test, the latter as absolute value</p> 
	<p>2. Conventional elastic limit F_{y_conv} as per UNI EN 1990:2006</p>
	<p>3. e_{y_conv} calculated via energy approach</p>
<p>DATA ANALYSIS</p>	
	<p>4. Definition of secant stiffness</p>
	<p>5. Average value of the three testing stiffnesses</p>
	<p>6. Definition of kinematic and cyclic ductility parameters</p>
	<p>7. Evaluation of dissipation capacity</p>

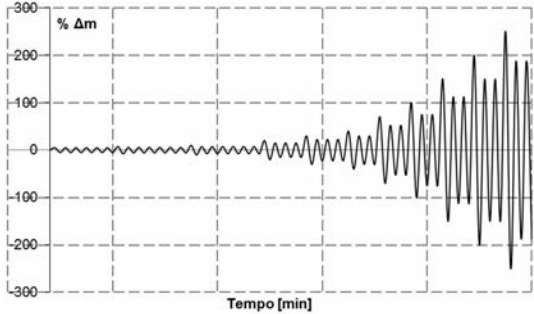
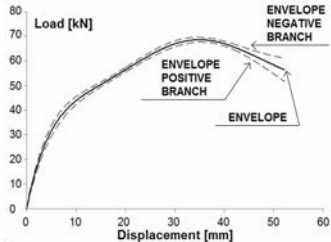
2.6.2.3 Cyclic test as per CUREE Publication No. W-02 (2001)

The cyclic test:

- identifies the design value of the lateral resistance for floor systems subjected to cyclic lateral forces;

- allows to define the ductility parameters for characterising the floor system's post-elastic strength reserves;
 - allows to evaluate the floor system's dissipation capacity;
- and is defined based on the displacement of reference Δ identified under monotonic testing. The test and the data processing are conducted as indicated in Table 13.

Table 13. Diagram for the cyclic test based on the procedure as per CUREE Publication No. W-02 (2001).

AIM	Calculation of design resistance
No. of tests	3
TESTING PROTOCOL (based on monotonic test, in function of displacement reference Δ_m)	
DATA ANALYSIS	<ol style="list-style-type: none"> 1. Average envelope curve between the positive and negative branches of the cyclic test, the latter as absolute value  <ol style="list-style-type: none"> 2. Calculation of shear stiffness and of resistance of the diaphragm as per ReLUIS-DPC <i>Prodotto 1</i> (2015) 3. Definition of suitable ductility parameters 4. Evaluation of dissipation capacity

3 CONCLUSIONS

At present, a limited number of studies regarding the seismic response of light steel residential buildings built-up with thin-walled profiles are available. Consequently, there is a lack of recommendations in National and International design codes.

The first part of this chapter is devoted to a brief overview of the main characteristics of these structural systems. The attention is focused mainly on the response of walls resisting to vertical and horizontal forces and of the floor systems subjected to in-plane shear forces.

The complexity of such structural systems leads to the use of the so-called 'design by testing' in order to suitably characterize their behaviour. The practitioner does not have any standard reference to apply this methodology.

In the framework of the ReLUIIS-DPC 2014-2016 activities, at the University of Trento, a series of experimental tests on the key components of the load-bearing system were designed and performed. Four different types of walls and four different types of floor systems were investigated. Additional tests on the main sub-components were also carried out in order to have the complete set of data needed for design. In particular, these sub-components were the studs and the beam profiles, the sheathing, the connections between sheathing and steel framing, the anchoring systems to the foundation.

The analysis of the state of the art, the experimental results and the ‘know-how’ acquired during the study led to the definition of guidelines for the seismic design assisted by testing of both walls and floor systems.

In the present chapter, the tests on the different components and sub-components are summarised. Furthermore, the main contents of the design guidelines are presented.

4 ACKNOWLEDGEMENTS

The study was funded by the Project ReLUIIS-DPC 2014-2016 of the Italian Civil Protection Department. The contribution of the company Cogi s.r.l., which provided the specimens, is also appreciated. The Authors gratefully acknowledge the work by the Laboratory staff of the University of Trento: Stefano Girardi and Marco Graziadei.

5 REFERENCES

- Accorti M., Baldassino N., Rogers C., Scavazza F., Zandonini R. (2016). “Studio sperimentale sulla risposta a taglio di pannelli di parete con struttura in elementi piegati a freddo”, *Reference to Costruzioni Metalliche*, anno LXVIII, numero 6, nov/dic 2016, 24-37.
- AISI S907 (2013). “Test standard for Cantilever Test Method for Cold-Formed Steel Diaphragms”, and AISI S907-13-C (2013). “Commentary on Test Standard for Cantilever Test Method for Cold-Formed Steel Diaphragms”, *AISI (American Iron and Steel Institute)*, Washington, USA.
- AISI S913 (2008). “Test Standard for Hold-downs Attached to Cold-Formed Steel Structural Framing”, *AISI (American Iron and Steel Institute)*, Washington, USA.
- ASTM D1037 (2006). “Standard Test Methods for Evaluating Properties of Wood-Base Fiber and Particle Panel Material”, *American Society for Testing and Materials International*, West Conshohocken, PA, USA.
- ASTM D1761 (2000). “Standard Test Methods for Mechanical Fasteners in Wood”, *American Society for Testing and Materials International*, West Conshohocken, PA, USA, 1988, reaffirmed 2000.
- ASTM E564 (2012). “Standard Practice for Static Load Test for Shear Resistance of Framed Walls for Buildings”, *American Society for Testing and Materials International*, West Conshohocken, PA, USA, 2006, reaffirmed 2012.
- ASTM E2126 (2011). “Standard Test Method for Cyclic (Reversed) Load Test for Shear Resistance of Vertical Elements of the Lateral Force Resisting Systems for Buildings”, *American Society for Testing and Materials International*, West Conshohocken, PA, USA.
- ECCS n. 45 (1986). “Recommended Testing Procedure for Assessing the Behaviour of Structural Steel Elements under Cyclic Loads”, *ECCS – Technical Committee 1 – Structural Safety and Loadings – Technical Working Group 1.3 – Seismic Design*.
- ECCS n. 88 (1995). “European Recommendations for the Application of Metal Sheeting acting as a Diaphragm – Stressed Skin Design”, *ECCS – Technical Committee 7 – Thin-walled, cold-formed sheet steel in Building – Technical Working Group 7.5 – Practical Improvement of Design Procedures*.

- Fiorino L., Della Corte G., Landolfo R. (2007). "Experimental tests on typical screw connections for cold-formed steel housing", *Engineering Structures*, n. 29: 1761-1773.
- Krawinkler H., Parisi F., Ibarra L., Ayoub A., Medina R. (2001). "Development of a Testing Protocol for Woodframe Structures", *CUREE Publication No. W-02*, Richmond, CA, USA.
- Li Z., Schafer B.W. (2010). "Buckling analysis of cold-formed steel members with general boundary conditions using CUFSM: conventional and constrained finite strip methods", *Proceedings of the 20th Int. Specialty Conference on Cold-Formed Steel Structures, St. Louis: Missouri, 3-4 November 2010*.
- ReLUIS-DPC *Prodotto 2* (2014). "Prodotto 2: Documento di sintesi della campagna sperimentale effettuata per il progetto ReLUIS III-2014", *Progetto ReLUIS-DPC 2014-2016 – Unità di ricerca: Università degli Studi di Trento, Area Tematica: Temi generali; Linea: Strutture di acciaio e composte acciaio calcestruzzo; Tipologie strutturali non convenzionali*.
- ReLUIS-DPC *Prodotto 1* (2015). "Prodotto 1: Linee guida per la progettazione assistita da sperimentazione di pannelli di acciaio realizzati con profili formati a freddo utilizzati in edifici residenziali per resistere ad azioni taglianti", *Progetto ReLUIS-DPC 2014-2016 – Unità di ricerca: Università degli Studi di Trento e Università degli Studi di Napoli, Area Tematica: Temi generali; Linea: Strutture di acciaio e composte acciaio calcestruzzo; Tipologie strutturali non convenzionali*.
- ReLUIS-DPC *Prodotto 2* (2015). "Prodotto 2: Analisi bibliografica relativa ai sistemi di piano per edifici residenziali in elementi leggeri di acciaio", *Progetto ReLUIS-DPC 2014-2016 – Unità di ricerca: Università degli Studi di Trento, Area Tematica: Temi generali; Linea: Strutture di acciaio e composte acciaio calcestruzzo; Tipologie strutturali non convenzionali*.
- ReLUIS-DPC *Prodotto 3* (2015). "Prodotto 3: Report sulla sperimentazione condotta nel primo semestre", *Progetto ReLUIS-DPC 2014-2016 – Unità di ricerca: Università degli Studi di Trento, Area Tematica: Temi generali; Linea: Strutture di acciaio e composte acciaio calcestruzzo; Tipologie strutturali non convenzionali*.
- ReLUIS-DPC *Prodotto 4* (2015). "Prodotto 4: Report sulla sperimentazione condotta nel secondo semestre", *Progetto ReLUIS-DPC 2014-2016 – Unità di ricerca: Università degli Studi di Trento, Area Tematica: Temi generali; Linea: Strutture di acciaio e composte acciaio calcestruzzo; Tipologie strutturali non convenzionali*.
- ReLUIS-DPC *Prodotto 1* (2016). "Prodotto 1: Sperimentazione su sistemi di piano realizzati con profili di acciaio piegati a freddo", *Progetto ReLUIS-DPC 2014-2016 – Unità di ricerca: Università degli Studi di Trento, Area Tematica: Temi generali; Linea: Strutture di acciaio e composte acciaio calcestruzzo; Tipologie strutturali non convenzionali*.
- ReLUIS-DPC *Prodotto 2* (2016). "Prodotto 2: Linee guida per la progettazione assistita da sperimentazione di sistemi di piano realizzati con profili formati a freddo utilizzati in edifici residenziali per resistere ad azioni taglianti", *Progetto ReLUIS-DPC 2014-2016 – Unità di ricerca: Università degli Studi di Trento e Università degli Studi di Napoli, Area Tematica: Temi generali; Linea: Strutture di acciaio e composte acciaio calcestruzzo; Tipologie strutturali non convenzionali*.
- Serrette R.L., Encalada J., Juadines M., Nguyen H. (1997). "Static cracking behavior of plywood, OSB, gypsum, fiberbond walls with metal framing", *Journal of Structural Engineering*, n. 123(8): 1079-1086.
- UNI EN 1990:2006 (2006). "Eurocode 0 – Basis of structural design", *UNI – Ente Nazionale Italiano di Unificazione*, Milano, Italy.
- UNI EN 1993-1-3:2007 (2007). "Design of steel structures – Part 1-3: General rules – Supplementary rules for cold-formed members and sheeting", *UNI – Ente Nazionale Italiano di Unificazione*, Milano, Italy.
- UNI EN 15512:2009 (2009). "Steel static storage systems – Adjustable pallet racking systems – Principles for structural design", *UNI – Ente Nazionale Italiano di Unificazione*, Milano, Italy.
- UNI EN ISO 6892-1:2009 (2009). "Tensile testing – Part 1: Method of test at room temperature", *UNI – Ente Nazionale Italiano di Unificazione*, Milano, Italy.

SECTION 6

NON-CONVENTIONAL BUILDINGS: SHEAR PANEL SYSTEMS

SHEAR PANEL SYSTEMS

Gianfranco De Matteis ^a, Giuseppe Brando ^b

^a *Department of Architecture and Industrial Design, University of Campania “L. Vanvitelli”, Aversa, Italy, gianfranco.dematteis@unicampania.it*

^b *Department of Engineering and Geology, University “G. d’Annunzio” of Chieti-Pescara, Pescara, Italy, giuseppe.brando@unich.it*

ABSTRACT

This Chapter deals with the use of metal shear panels for seismic protection of steel buildings and gathers all the activities carried out by the University of Campania and the University of Chieti-Pescara within the ReLuis Project within the period 2014-2016.

Firstly, a synthesis of the previous research activities related to metal shear panels and developed by the authors before this reference period is provided. Then the experimental and numerical results obtained for perforated metal shear panels are presented. This research activity was devoted to identify design formulations to be used for this panel typology, whose dissipative capacity is maximized by properly perforating the base plate in order to divert the internal stresses and to avoid detrimental effects due to buckling phenomena. Finally, the structural performance of steel frames equipped with metal panels characterized by hysteretic cycles affected by different pinching effects is presented. Also, the force reduction q-factor of the considered structures is evaluated, as a useful design parameter to be used in conventional linear analyses.

KEYWORDS

Metal Shear Panels, Perforated Plates, Incremental Dynamic Analyses, Design Criteria, q-factor.

1 INTRODUCTION

In order to satisfy the performance levels commonly required by codes and provisions, a large amount of research was conducted, over the second half of the last century until today, for developing innovative earthquake-resistant systems aiming at improving the seismic performance of structures while keeping either construction or retrofitting costs reasonable. Therefore, the “response control” methodology was developed as alternative to the “traditional” one. The former is based on controlling and limiting the dynamic effects on the structural elements by means of added special devices (Brando et al., 2015). Contrarily, the “traditional” design methodology exploits the ductility resources of sections and connections, leading to the seismic input dissipation by means of plastic hinges developing.

For the response control methodology, different approaches can be distinguished, namely Active Control, Semi-Active Control and Passive Control (Soong and Dargush, 2007). As for the Passive Control approach, it consists in designing buildings in order to dissipate energy by supplemental damping mechanisms and/or in limiting the transmission of seismic energy to

the main structure by decoupling the structure movements the ground shaking (seismic isolation).

Supplemental damping systems are based on the use of special devices, also known as dampers. They are arranged in the structure and are designed in order to start to dissipate energy by hysteretic (De Matteis et al., 2008), friction (Montuori et al., 2014) or viscous mechanisms as soon as the structure is shaken, hence reducing its overall dynamic response. The advantages in using dampers may be synthetically listed as follows (Christopoulos and Filiatrault, 2007; De Matteis et al., 2007):

- (i) They may be designed and arranged in the construction in order to conveniently change both the damping and the dynamic features of the structure, also reducing possible non regularities;
- (ii) They may be conceived to dissipate energy under low movements of the structure so that their protective function is activated when the other elements are still in the elastic fields;
- (iii) After a strong ground motion event, they can be inspected and, when damaged, conveniently replaced.

Among the existing dampers, in recent decades, dissipative metal shear panels have collected an increasingly wide consensus (De Matteis et al. 2003).

A shear metal panel is generally made of a metal plate working in shear connected to a surrounding steel frame by means of bolted and/or welded connections. The frame has the task of delivering the forces from the primary members of the protected structure to the plate. This type of function can be carried out throughout a direct connection of the panels to the structure (Full-Bay or Partial-Bay configurations; Figure 1a and Figure 1b) - this leading to the concept of Metal Plate Shear Walls- or by way of steel braces (Bracing Type configuration; Figure 1c).

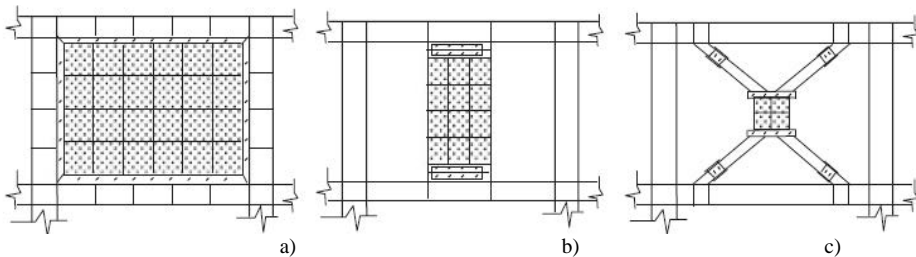


Figure 1. Metal Shear Panels arrangements in a frame: (a) Full-Bay configuration; (b) Partial-Bay configuration and (c) Bracing Type configuration.

Apart from the high in-plane stiffness, that allows to solve easily some critical issues related to the lateral deformability of buildings, in particular when they are made of steel moment resisting frames (De Matteis, 2005), one of the main prerogatives of shear panels is the easiness in controlling the shear resistance. In fact, unlike the more traditional braced frames, the use of extremely thin elements is made possible by a stable post-buckling behaviour due to the onset of "tension field" type resisting mechanisms (Shishkin et al., 2009). Furthermore, even in presence of reduced thicknesses, the possibility of combining the base plate with other elements – for example, transversal stiffeners - allows the control of the level of demand leading to buckling phenomena as well as to mitigate possible pinching effects producing detriment on the hysteretic cycles.

All the prerogatives described above led to significant research efforts, which have been addressed to the definition of innovative metal shear panels conceived in order to provide convenient solutions able to comply with the several demands posed for their employment in seismic prone zone.

In this framing of research, this Chapter deals with the use of metal shear panels for the seismic protection of steel buildings and gathers all the activities carried out by the University of Campania and the University of Chieti-Pescara within the ReLuis Project during the triennium 2014-2016.

The Chapter is organized as follows:

1. Overview on the previous research activities on metal shear panels carried out by the authors;
2. Presentation of an experimental and numerical study carried out on a metal shear panels, whose dissipative capacity is maximized by properly perforating the base plate so to divert the internal stresses and to avoid detrimental effects due to buckling phenomena. The activity was devoted to identify design formulation to be used for this panel typology.
3. Analysis of the structural performance of steel frames equipped with metal panels characterized by hysteretic cycles that are differently affected by pinching effects, in order to give information about their structural performance.
4. Evaluation of the force reduction q -factor of the considered structures, as a useful design parameter to be used in conventional linear analyses.

2 PAST RESEARCH ON DISSIPATIVE METAL SHEAR PANELS

2.1 General

This Section discusses metal dissipative shear panels investigated by the Authors in the recent past. In particular, two panels typologies are presented: (i) Pure Aluminium Stiffened Shear Panels and (ii) Buckling Inhibited Shear Panels.

For the first typology, panels in several configurations have been investigated, but for brevity purposes, only tests and numerical analyses carried out on the “Bracing-Type” configurations are dealt with.

For the same reason, although Buckling Inhibited Shear Panels made of either steel or aluminium have been studied, only the last typology, which however presented the best dissipative performance, is here discussed.

2.2 Bracing Type Pure Aluminium Shear Panels (BTPASPs)

For this type of shear panels the EN-AW 1050A H24 alloy has been used as base material. It has been properly subjected to a heat treatment that led to a very low conventional yield strength (about 20 MPa) and a high ductility (40%), which are profitable features for manufacturing dampers.

In a first stage, four full-scale specimens were tested under shear cyclic forces. These specimens are shown in Figure 2, together with the nomenclature that was used for their identification.

The coupons were characterized by global dimensions of 500 mm by 500 mm and thickness of 5 mm. As a consequence they presented slenderness ratio values b/t (where b is the spacing

of the transversal stiffeners and t is the thickness of both the base plate and the stiffeners) of 100 (panel “type 1”), 25 (“type 2”), 33 (“type 3”) and 25 (“type 4”), respectively.

Tested shear panels were positioned into a square articulated steel frame made of four rigid built up members obtained by coupling two channel shape profiles. Each aluminium plate was connected to the steel profiles by means of 8.8 grade bolts having a diameter of 14 mm and a spacing of 50 mm.

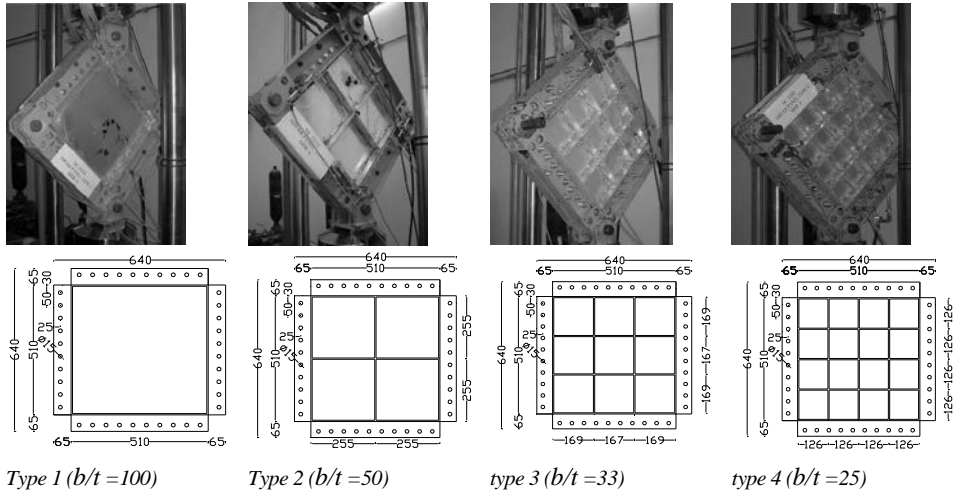


Figure 2. The four tested Multi-Stiffened Pure Aluminium Shear Panels.

The steel frame was scarfed to a MTS810 universal machine, able to reproduce a maximum displacement of ± 75.0 mm and a maximum compression/tensile force of ± 500 kN. A diagonal cyclic force was imposed according to the loading protocol shown in Figure 3, which was established following the ECCS-CECM provisions (1985).

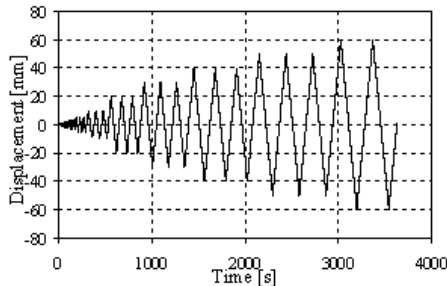


Figure 3. The loading protocol used for tests.

In Figure 4, the obtained hysteretic cycles for the tested specimens are shown. These results clearly emphasize that the proposed panel configurations provided a good hysteretic performance, with large hysteretic cycles also for high deformation levels.

Obviously, the obtained results were influenced by different collapse modes depending on the different slenderness associated to the four stiffeners configurations. In particular, it was observed that, for shear panels “type 1” and “type 2” failure was concentrated on the base plate and was strongly influenced by buckling phenomena, whereas, for panels “type 3” and

“type 4” the collapse of the perimeter connecting system was revealed. In fact, in case of lower slenderness ratio, the rib system acted as a sort of internal frame axially stressed, providing an additional resisting contribution to the panels, therefore transferring larger forces to the connecting system, which represented the weakest component of the studied devices.

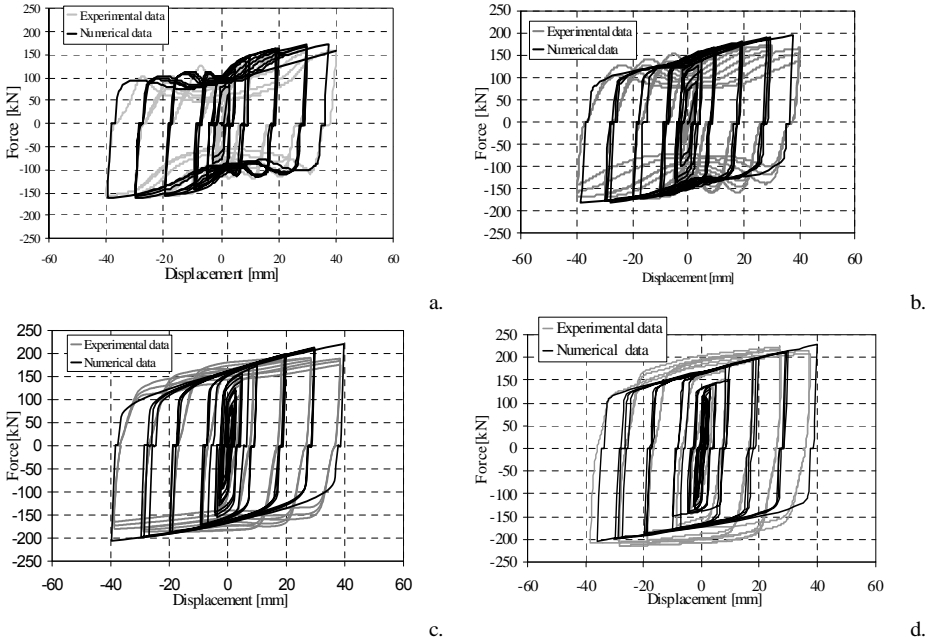


Figure 4. Comparison between numerical and experimental results in terms of hysteretic cycles: shear panel “type1” (a), “type2” (b), “type3” (c) and “type4” (d).

It is worth noticing that the higher values of the equivalent viscous damping factor (about 50%) was achieved for large shear strains (about 6%) which however are compatible with the possible demanded shear strain during a severe earthquake. More details on the above tests are given in (De Matteis et al. 2011).

Also, in Figure 4, the results of some FEM numerical models, calibrated on the basis of the criteria described in (Brando and De Matteis, 2011), are depicted in terms of hysteresis cycles. A good agreement between numerical and experimental results is recognizable.

The above numerical models were used in order to implement parametrical numerical analyses by taking into account, for each stiffened configuration, different slenderness values obtained by varying the panel thickness. Moreover, the role of stiffeners inertia on the potential coupled instabilities was investigated (Brando and De Matteis, 2014).

2.3 Buckling Inhibited Pure Aluminium Shear Panels

When low yield strength shear panels are used, one of the main critical issues is that very thin plate are often necessary, even in presence of a base material characterized by a low yield stress point. This could entail economical and technological counter-indications, as well as technological problems related to an excessive use of welded transversal ribs. As a convenient alternative to the use of stiffened shear panels, recently, the authors proposed a new type of shear panel, based on the concept of buckling phenomena inhibition (Brando et al., 2013).

In particular, two different technological solutions for restraining the out-of-plane deformations of the system have been proposed. They are based on the use of not connected steel elements, able to restrain the first and more important critical modes of the panel. These elements react only in the direction perpendicular to the base plate, leaving the base plate work according to a pure shear resistant mechanism.

In the following, the main results of an experimental campaign carried out on two selected configurations are shown. The first is a partially buckling inhibited solution, for which the out-of-plane displacement that could develop along the two diagonal of the panel are restrained. The latter is a totally buckling inhibited shear panels, for which the out-of-plane displacements are restrained for the whole plate. Both the investigated solutions are conceived to work in a bracing-type configuration and are made of the same pure aluminium used for the stiffened plate dealt with previously.

Moreover, in order to prove the effectiveness of the proposed solution, the performances of the tested panels are compared with the ones obtained downstream the previous presented experimental activity carried out on bracing type pure aluminium shear panels.

In Figure 5 the two proposed buckling inhibited shear panels are shown. They were obtained by inserting a 5 mm thick pure aluminium shear plate in the same square articulated steel frame used for the experimental tests carried out on the multistiffened panel typology dealt with in the previous Paragraph.

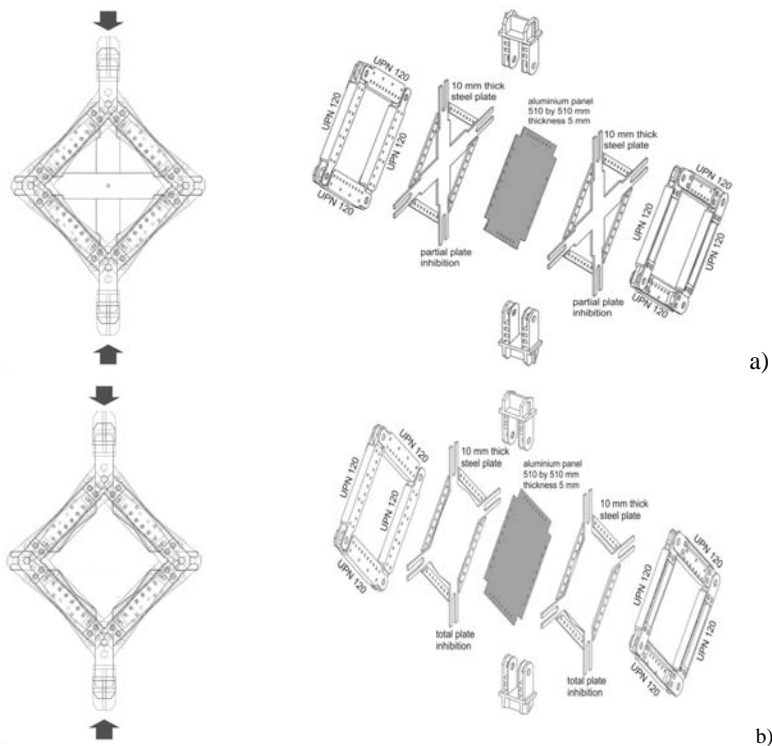


Figure 5. The studied (a) Partially Buckling Inhibited Panel (p-BIP) and (b) Totally Buckling Inhibited Panel (t-BIP).

For the first solution (p-BISP, acronym of “partially Buckling Inhibited Shear Panels”), two cross shape 10mm thick/140 mm wide steel elements were used for inhibiting the first four critical modes of the base plate. These were arranged on both side of the base plate along the two diagonal.

In the second technological solution (“t-BISP”, acronym of “totally Buckling Inhibited Shear Panels”), two octagonal steel plates were mounted for restraining the out-of-plane displacements of the whole plate in shear.

In both cases, lexan sheeting were employed in order to reduce the friction between the parts. The hysteretic behaviour of the two panels are shown in Figure 6.

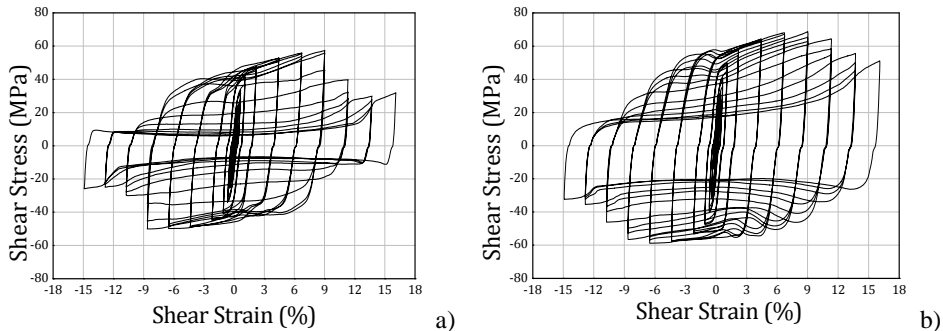


Figure 6. The obtained hysteretic cycle: a) “p-BIP” and b) “t-BIP”.

The obtained large hysteretic cycles prove the high dissipative capacity of the devices, guaranteed, also for high shear demands, by a substantial absence of significant pinching effects. However, it is to be underlined that the t-BIPSP configuration behaved in a more performing way, as it was not influenced by the secondary buckling phenomena that, contrarily, developed for the p-BIP solution. Furthermore, larger cycles given from the t-BIP configuration were due to the confinement effects produced by the more extended contact of the restraining plates.

2.4 Performance of the studied Shear Panels

Based on the definition given in Figure 7f, global response parameters obtained by the experimental results are shown for both the panel typologies described in the Sections 2.3 and 2.4.

In particular, in order to compare the dissipative capacities, an “energy efficiency factor” η has been introduced (Figure 7a). This parameter represents the ratio between the area of the actual hysteretic cycle and the area of an ideal cycle obtained, for the same demand, by reversing an ideal bilinear elasto-plastic curve. The adopted bilinear relationship, which is considered as the potential optimal response for the proposed devices, has the first elastic branch characterized by the slope of the unloading branch of the cycle of the real hysteretic response and is characterized by a post-elastic stiffness k_2 (Figure 7b) read as the slope of the tangent of the envelope curve of each experimental cycle.

It is possible to observe that the tested panels with buckling restrained systems (both types “p-BIP” and “t-BIP”), have an energy dissipation performance better than the multistiffened shear panels. In particular “t-BIP” shear panel gives η factor higher than 0.9 for shear strains ranging between 1.5% and 6.5%, therefore behaving as a fully dissipative damper. On the other hand, the “p-BIP” type with partial buckling inhibition device reaches a value $\eta=90\%$

only for a 2.2% shear strain demand; for larger strain demands, the dissipative capacity is about 85% of the one corresponding to the ideal bilinear behaviour.

A similar behaviour can be noticed for multi-stiffened shear panel BTPASP “type 3”, which, indeed, provides η factor slightly lower than 85%. On the contrary, the unstiffened shear plate “BTPASP type 1”, as underwent relevant detrimental effects due to buckling for shear strain larger than 1,0%, evidences a significant decrease of the η factor.

In addition, the analysis of the equivalent viscous damping factor ξ_{eq} given in Figure 7c, which retrieves a measure the fractional part of the strain energy (E_s) dissipated during each deformation cycle, evidences that:

- i) both buckling inhibited and multi-stiffened shear panels allow increasing of about 1.3 times the dissipative capacity of the simple plate in shear;
- ii) the specific energy dissipated by “BTPASP type 3” shear panel is larger than the one offered by the buckling inhibited plates for very large shear strain demands, namely greater than 4% and 6.5% for p-BIP and t-BIP, respectively;

With reference to the last comment, it is to be pointed out that although shear panel “t-BIP” presents always larger hysteretic cycles with respect to other panels, the lower ξ_{eq} factor registered for very large shear deformation is due to the fact that the strain energy is higher as well. This is justifiable because of the higher strength caused by the confinement adjustment effects which has been previously discussed. For a better comprehension of this phenomenon, in Figure 7d the variation of hardening ratio h , defined as the ratio between the maximum attained shear strength for each shear demand and the conventional yielding one, is shown. From the same figure it is also evident that the “t-BIP” solution and the “BTPASP type 3” shear panel provide a similar strength for medium and high shear strain levels, whereas the stiffened plate is clearly weaker for smaller strain levels.

Finally, in Figure 7e the response of the four tested aluminium panels are compared in terms of effective secant stiffness.

Also according to this parameter, the buckling inhibited shear panels were more performing than the conventional ones (shear plate with welded stiffeners). In fact, a larger initial stiffness is retrievable for low shear demands, while in the large strain field the obtained responses are quite comparable to each other. This result is evidently due to the absence of residual stresses and other imperfections which have to be ascribed to welding processes of multi-stiffened shear panels.

3 THE RESEARCH ON STEEL PERFORATED SHEAR PLATE

3.1 General

An alternative fruitful way for obtaining dissipative shear panels may consist in weakening the base plate by removing some of its parts. This type of operation, if well implemented, allows to obtain a variation of the internal stress pattern and potentially to mitigate the negative effects generated by possible buckling phenomena. On the other hand it leads to a reduction of the shear strength, also in presence of thick plates and of materials that are more conventional with respect to the one used for the panels typologies described in Section 2, so to accomplish more easily capacity design criteria.

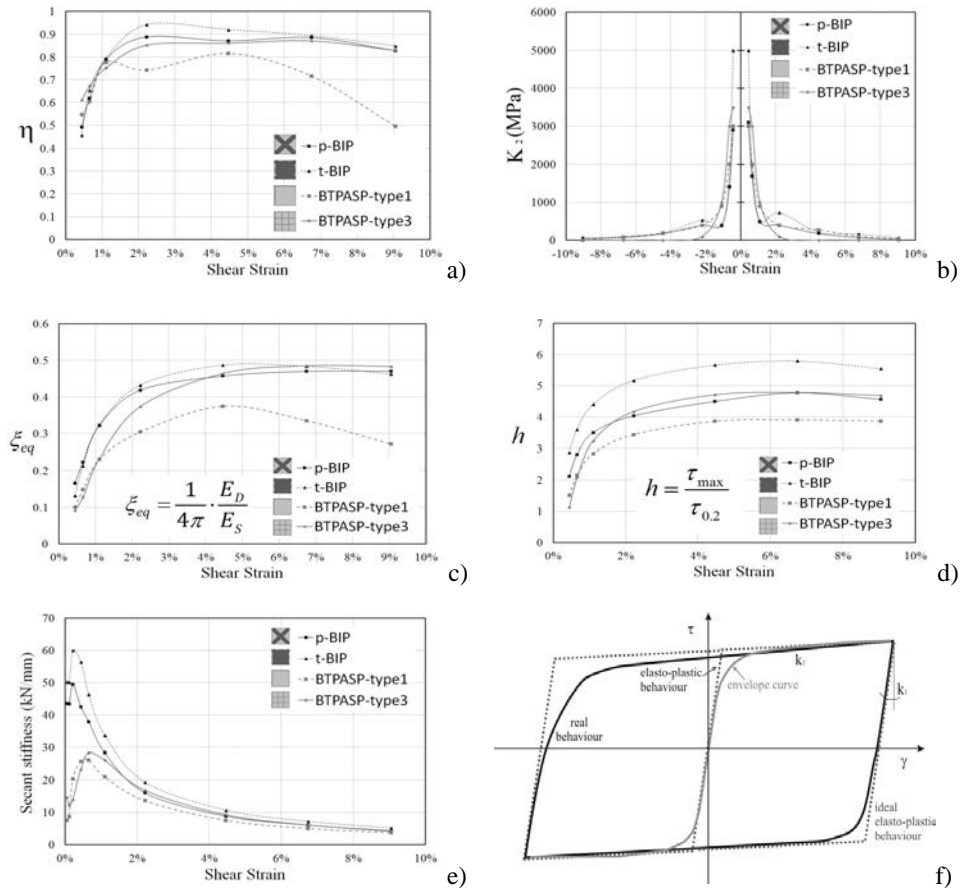


Figure 7. Global response parameters obtained by the experimental tests and comparison with PASPs “type 1” and “type 3”: (a) Energy efficiency factor; (b) Post elastic stiffness; (c) Equivalent viscous damping; (d) Hardening ratio;; (e) Secant stiffness; (f) definition of the main behavioural parameters.

A significant literature concerning the use of weakened shear panels has been proposed in the last decade. For example, panels weakened by means of vertical slits were extensively investigated by Hitaka and Matsui (2003) and Pohlenz (2010); for this panel typology, the shear force acting on the whole system is commuted in a bending mechanism for the plate portions confined by a couple of slits, which undergo large flexural deformations producing a significant dissipative capacity.

Vian, Bruneau and Purba (2009) carried out experimental tests on shear panels weakened by holes arranged in a staggered configuration, providing design formulations of the shear strength accounting for the holes diameters and spacing, also considering the influence of the surrounding frame stiffness.

Valizadeh et al. (2012) quantified the influence of the holes diameter on the loss of dissipated energy due to the pinching effects on the hysteretic cycles. Furthermore, they highlighted some brittle failures around the perforations when very thin plates are adopted, due to the strong concentration of stresses.

Alavi and Nateghi (2013) proved, by experimental tests on 1:2 scaled single-story SPSWs, that perforated diagonally stiffened shear panels allow to obtain the same stiffness of un-ribbed solid panels, with an increase of ductility of more than 14%. In addition, an extension of the design formulation of the shear strength given previously by other Authors was provided, accounting for the diagonal stiffeners contribution.

In this framing of research, in the following, the main results obtained downstream experimental and numerical studies on steel perforated shear panels, are shown. Primarily, the response of the studied devices determined by cyclic tests is analyzed. It is evidenced that the hysteretic performance of steel perforated shear panels might be detrimentally influenced by pinching effects and softening due to cumulated damage produced by lateral-torsion buckling that may arise when the plate portions delimited by contiguous perforations are excessively slender. Based on tests results, a suitable analytical formulation for the prediction of the strength at several shear demands, accounting for the influence of the above detrimental effects, is provided. Also, a parametric study based on a FEM numerical model calibrated on the basis of the experimental tests is developed.

Two main goals are achieved: *i*) to establish the influence of the main geometric parameters on the panel hysteretic response, with particular regard to the pinching effects provoked by buckling phenomena; *ii*) to determine analytical formulations able to give back the ratio between the “pinching” strength and the maximum strength, the former being the force corresponding to a null shear strain in a cycle. Therefore a useful predictive tool for defining the optimal perforation geometry to be adopted as a function of the expected shear demand is provided.

3.2 The experimental tests

Two Perforated Shear Panels were tested. These, that will be henceforth referred as PSP1 and PSP2, were made of 2.5 mm thick plates.

Their geometric features are described in Figure 8, where the sizes are expressed in mm. Each specimen was obtained by applying nine perforations according to a rectangular pattern. This type of choice ensures a better performance with respect to a staggered configuration. Hole diameters of 127.5 mm and 107.4 mm were imposed for PSP1 and PSP2, respectively.

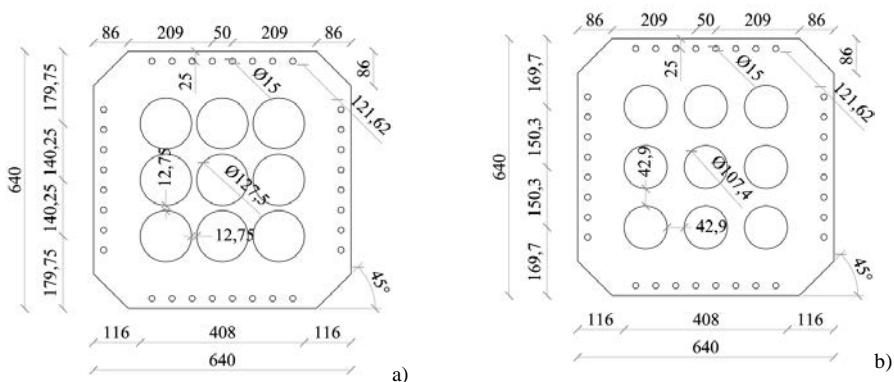


Figure 8. Plate geometry for tested shear panels: (a) PSP1 and (b) PSP2 (sizes in mm).

At the same manner of the panels dealt with previously, each plate was connected to a perimeter articulated frame made of four built up members obtained by coupling two UPN

120 channel section profiles. The plate-to-perimeter frame connections were realized by 8.8 grade M14 steel friction bolts spaced by a pitch of 50 mm. In addition, in order to increase the contact area between the plate and the built up members, double sided internal 10 mm thick plates (two for each edge of the articulated frame) were applied, as it can be seen in Figure 9.a where the panel is shown during the assemblage process.

The experimental set-up was completed by two hinged steel jigs connecting two opposite vertices of the panel to the MTS machine used for carrying out pseudo-static cyclic tests (see Figure 9b).

The material mechanical features of the plates were preliminarily investigated by means of uniaxial tensile tests. They were carried out on dog-bone specimens extracted from the same metal sheeting from which both the two plates were obtained. In particular, four coupons (namely H1, H2, H3 and H4) about the lamination direction and five coupons (namely V1, V2, V3, V4 and V5) about the perpendicular one were taken out.

The obtained results, which are reported in Figure 10 together with the curves fitting the average values and the true strain-true stress, showed that the yield stress measured in the lamination direction (about 300 MPa) differs from the one considered perpendicularly (about 270 Mpa), whereas any significant difference was not revealed in terms of tangential stiffness and ductility.

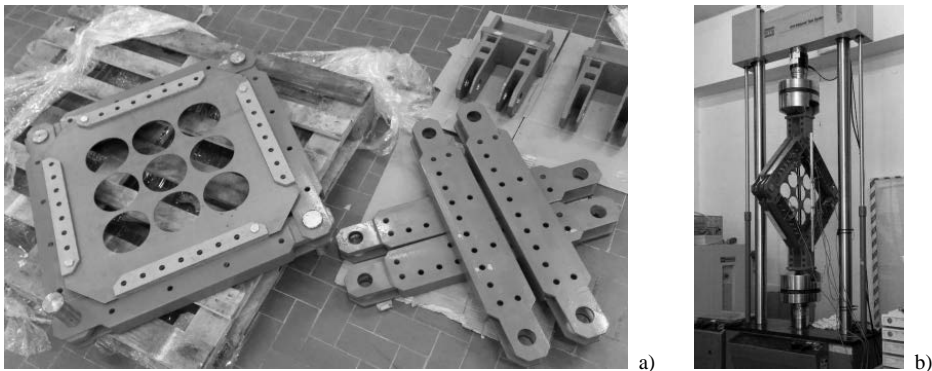


Figure 9. The experimental set-up: specimen (a) during the assemblage and (b) during the test.

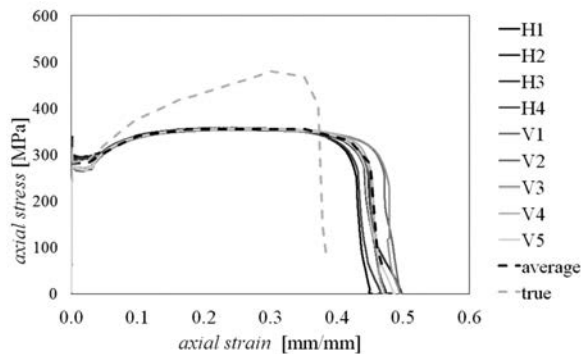


Figure 10. Mechanical stress-strain curves of the tested plate base material (engineering and true values).

The two tested perforated shear panels were subjected to pseudo-static cyclic tests according to the loading protocol already shown in Figure 3.

As already shown in Figure 9b, the diagonal displacements of the tested panels were measured by a mechanical transducer, whereas the corresponding diagonal force was appraised by the loading cell installed in the testing machine. Also, four mechanical LVDT transducers were placed on the perimeter of the panels, to measure the possible relative movements between the plate edges and the frame elements.

The obtained responses are described in Figure 11.a and Figure 11.b for panel PSP1 and PSP2, respectively. Indeed, some slipping phenomena were registered, but they never exceeded 1.5 mm, resulting not significantly influencing for the shear panel response.

The testing apparatus was completed by two uniaxial strain gauges glued on the central plate portions detected by the perforations, in order to monitor the developed material strain.

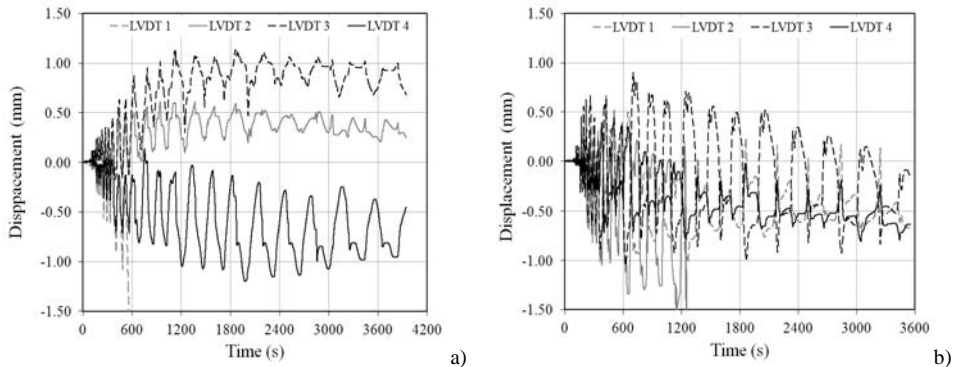


Figure 11. Lateral LVDT transducer responses for panel PSP1 (a) and PSP2 (b).

3.3 The experimental evidences

Following an initial phase where the shear panels behaved as a system under pure shear, the former “global” buckling waves arose in the plate cores centred around the two diagonals. They were triggered at diagonal displacements of $\pm 5\text{mm}$ (shear strain of $\pm 1.1\%$; Figure 12.a) and $\pm 2\text{mm}$ (shear strain of $\pm 0.4\%$; Figure 12,b) for PSP1 and PSP 2, respectively.



Figure 12. The first buckling phenomena revealed for (a) the specimen PSP1 at a displacement of $\pm 5.00\text{ mm}$ (shear strain of $\pm 1.1\%$) and (b) specimen PSP2 at a displacement of $\pm 2.00\text{ mm}$ (shear strain of $\pm 0.4\%$).

For the latter panel, instability phenomena were anticipated due to the lower influence of the perforations. In fact, in this phase, the specimen PSP2 behaved more similarly to a not-perforated shear panel than the specimen PSP1, thus resulting more influenced by buckling phenomena.

Indeed, as it is shown in the figure, the amplitude of the diagonal buckling waves described above remained fundamentally unchanged for larger shear demands, for both PSP1 and PSP2 specimens, proving the effectiveness of the perforation pattern in diverting the internal stresses and, therefore, in mitigating those instability effects which commonly develop for solid shear plates.

Nevertheless, when larger diagonal displacements were attained, the activation of higher critical modes was noticed. These modes consisted in lateral-torsional buckling of the panel portions included within the perforations and were due to a rotation of the principal stresses. These phenomena were clearly visible for a diagonal displacement of 10mm (shear strain of 2.2%) for both PSP1 and PSP2 specimens, as it is shown in Figure 13.

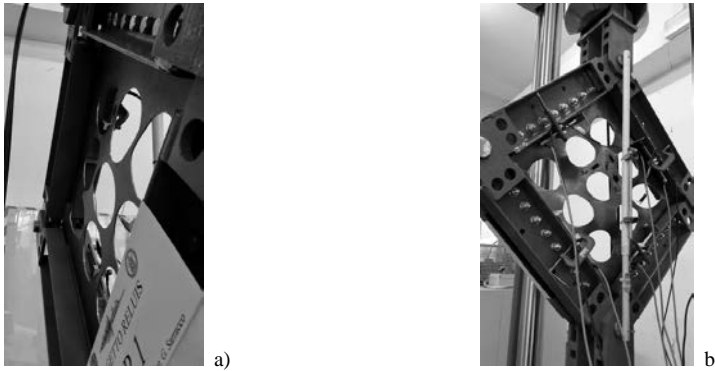


Figure 13. Lateral-torsion buckling of the panel portions included within the perforations activated for a displacement of ± 10.00 mm (shear strain of $\pm 2.2\%$): (a) specimen PSP1 and (b) specimen PSP2.

The main effects consisted in twisting of the buckled plates portions, with a significant damage cumulated with increasing number of cycles. When a diagonal displacement of 20 mm (shear strain of 4.4%) was attained the torsion became permanently visible, as shown in Figure 14.

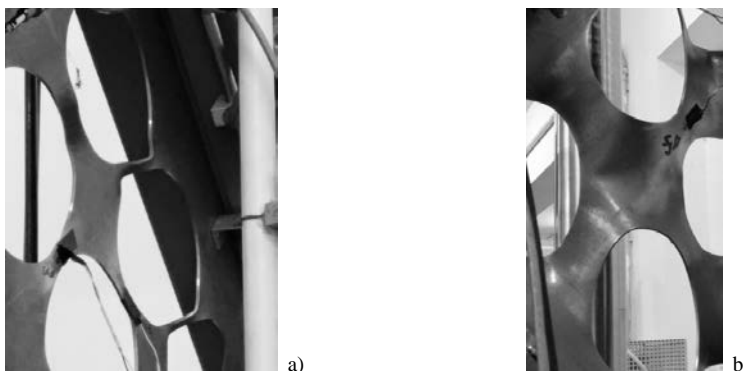


Figure 14. Experimental evidences registered for the specimens PSP1 (a) and PSP2 (b) at a diagonal displacement of 20 mm (shear strain of $\pm 4.4\%$).

For higher shear strains, failures due to low cycle fatigue were triggered around the perforations. They influenced the panel performance when diagonal displacements of 30 mm (shear strain of 6.7%) and 40 mm (shear strain of 9.6%) were attained. In Figure 15, the plate configurations as they appear at this deformation stage are shown.

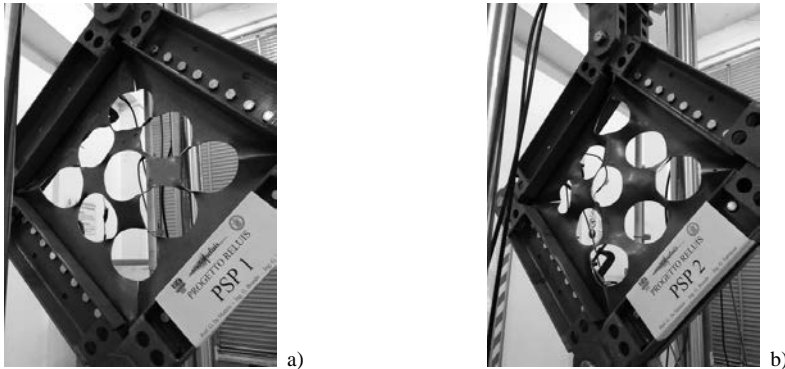


Figure 15. Collapse modes of PSP1 (a) and PSP2 (b) specimens.

3.4 The obtained test hysteretic cycles

The cyclic response of tested shear panels is plotted in Figure 16 in terms of diagonal displacements vs. diagonal forces. As it can be observed, conspicuous pinching effects were revealed in both cases. These were due to several detrimental phenomena caused by cumulated plastic deformations induced by local buckling, which led to a cyclic decay of the maximum strength for each shear demand.

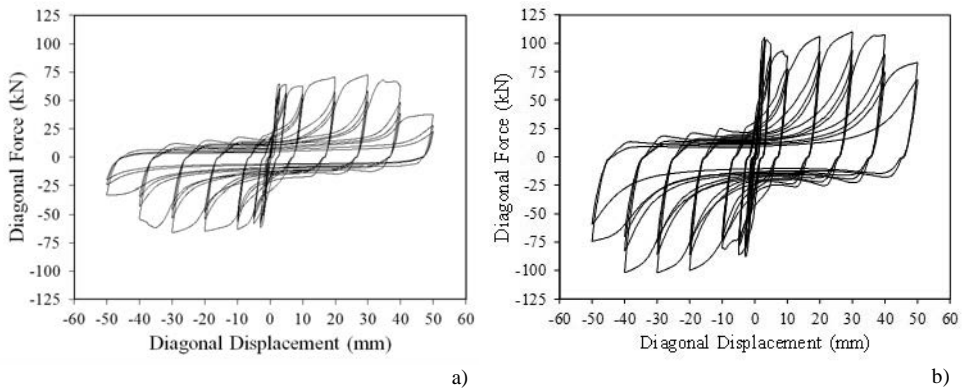


Figure 16. The obtained hysteretic cycles for specimen PSP1 (a) and PSP2 (b).

The registered cyclic decay is highlighted in Figure 17, where the maximum diagonal forces are plotted. Moreover, in the same figure, the difference at each cycle between the maximum and the minimum strength (normalised to the maximum one) is provided.

The analysis of the obtained results puts into evidence some significant outcomes; firstly, it has been noticed that in order to recover the strength reduction developed after three cycles at

a certain level of strain demand, it is necessary to impose an increase of diagonal displacement of more than 5 mm.

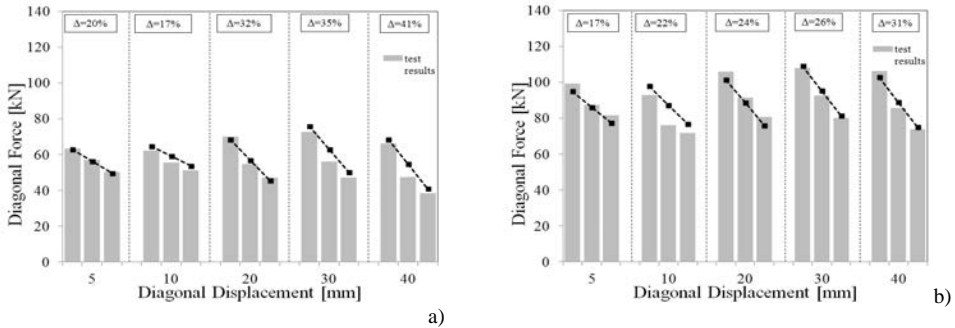


Figure 17. Experimental vs. analytical (eq.1) strength for specimen PSP1 (a) and PSP2 (b).

Also, it must be observed that the panel characterized by larger perforations (PSP1) provided lower ductility, the latter intended as the inelastic deformation capacity for which a strength decay is observed (6% shear strain for PSP1 and 9% shear strain for PSP2).

Furthermore, it has been found that the strength levels developed at each deformation, when the number of cycles increases, are basically aligned on a straight line. This allowed to determine the closed form analytical formulation given in eq. (1), which is able to reproduce with acceptable approximation the measured experimental values of diagonal force shown in Figure 17.

$$F_{diag} = -0.0024 \cdot d^3 + 0.14 \cdot d^2 - 1.55 \cdot d + F_{y,diag} - a \cdot n \tag{1}$$

In the above equation, F_{diag} is the diagonal force corresponding to the diagonal displacement d , $F_{y,diag}$ is the diagonal force corresponding to yielding, n is the number of performed cycles, a is a coefficient measuring the strength decay due to low cycle fatigue. The coefficient a must be investigated for each panel geometry, as it relies on the slenderness of the plate portions between by perforations, according to the shear demand that is expected on the system. As for the tested specimens, PSP1 returned values of a equal to 6.52, 5.42, 11.37, 12.81 and 13.79 for diagonal displacements of 5 mm, 10 mm, 20 mm, 30 mm and 40 mm. Instead, for specimen PSP2, a was found to be 8.75, 10.45, 12.69, 13.87, 18.87 for diagonal displacements of 5 mm, 10 mm, 20 mm, 30 mm and 40 mm, respectively. The above equation is valid under the hypothesis, not investigated during the tests, that after three cycles, the strength decay is negligible.

Finally, in order to measure the loss of dissipative capacity due to pinching effects, the ratio F_{pinc}/F_{max} (averaged on the three cycles performed for each shear strain demands) of the diagonal force corresponding to a zero displacement (F_{pinc}) by the maximum diagonal force (F_{max}) measured on each cycle is given in Table 1.

Table 1. The average value of the F_{max}/F_{pinc} ratios for several diagonal displacement demands.

Tested Specimen	F_{pinc}/F_{max} (-)				
	for each hysteretic cycle at displacement (mm)=				
	5	10	20	30	40
PSP 1	0.28	0.31	0.25	0.20	0.16
PSP 2	0.27	0.32	0.21	0.17	0.15

This parameter gives a measure of the potential dissipative capacity that is (ideally) maximum when a unitary value of such a value is attained. As it can be observed, for the tested shear panels the loss of dissipative capacity is significant.

3.5 The numerical study

Tested shear panels were modelled by using the Abaqus finite element software. For the base plate in shear, the 6-node triangular thin shell (STRI65 in Abaqus), with five degrees of freedom per node, was used around the perforations, whereas the general purpose shell S8R elements with 8-node and reduced integration were adopted at the edges. The NLGEOM parameter has been imposed in order to allow large rotations and the stiffness matrix updating process.

The meshing algorithm was based on the assumption that at least two elements should be present transversally to the plate portions between perforations, whereas a less refined mesh (average size of 25 mm) was considered at the panel edges.

A preliminary evaluation was done for the hourglass control stiffness factor ($r_\theta G$), which is assumed according to eq. (2), considering not only the effect of the material shear elastic modulus (G), but also the influence of the plate thickness (t):

$$(r_\theta G) = 0.00375 \frac{12 \int_{-t/2}^{t/2} G t^2 dt}{t^3} \quad (2)$$

In the case being, assuming $t=2.5$ mm and $G=79230$ MPa, the above factor is equal to 279.

The members of the testing perimeter articulated steel frame panels were modelled by using three-dimensional beam element B31. All the members were connected by means of the three-dimensional two-nodes hinge connector elements CONN3D2, while the whole external frame and the plate zones included into the steel arms were restrained towards the out-of plane deformations by means of effective boundary conditions. The bottom point of the surrounding frame was fixed to the ground. The frame-to-panel connection was imposed by using the TIE constraint of the Abaqus program library, which was applied between the panel edges and the corresponding frame members. As observed by the analysis of the experimental results, this type of assumption is justified by the fact that the lateral movements between the plate and the frame members are negligible.

In Figure 18, the model used for panel PSP1 is represented, together with an enlarged swatch that allows to appreciate the type of meshing algorithm adopted.

The mechanical features of the base material has been modelled accounting for its actual non linear behaviour. According to the outcomes of the performed uniaxial tensile tests described in Figure 10, an average stress-strain relationship has been determined, which, then, has been transformed in terms of true characteristics in order to take into account correctly the effects of finite deformations.

The experimental tests evidenced several buckling modes, affecting the panel deformation at both global and local level, which needed to be correctly stimulated by adequate initial imperfections in order to capture the correct inelastic behaviour. In particular, it was observed that, apart from the buckling waves along the panel diagonals, the lateral torsion buckling of the plate portions between perforations significantly influenced the hysteretic response of the system.

On the other hand, a preliminary study for better understanding the importance of initial imperfections was carried out on the model shown in Figure 19a.

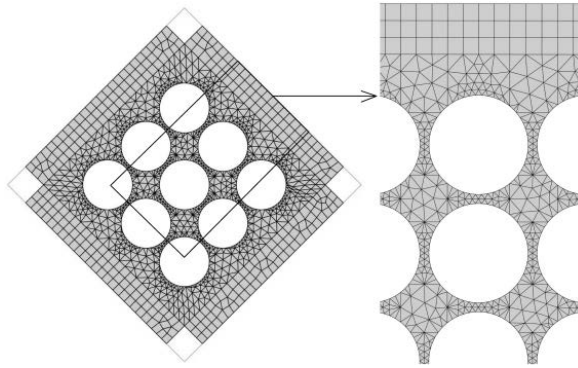


Figure 18. Adopted finite element model (PSP1 specimen).

It represents a simplification of the plate portions involved in the above described instability modes. On the bottom edge, the model was fixed to the ground, whereas the top was subjected to pseudo-static analysis, according to the lateral displacements cyclic load history depicted in Figure 19b, and restrained with respect to the other degrees of freedom. The analysis has been carried out firstly on the model without out-of-plane deformations and then by imposing an initial deformation given by the twisted shape corresponding to the first critical mode shown in Figure 19c. In order to emphasize the influence of the above imperfection a maximum amplitude of 10 mm, which is higher than the out of plane displacements registered on the base plate of the studied panels, was considered as a limit condition. The results given in Figure 19d, in terms of shear force vs. shear strain, showed that the above imperfections could provoke significant detrimental effects, with a reduction of strength and with cycles that are not stable due to the cumulated plastic deformation. For this reason, the critical mode shapes shown in Figure 20 were superimposed in order to get the initial deformation of the plates. They lead to have both out-of-plane deformations along the two diagonals of the panel and simultaneously a twisted shape for the plate portions included between two perforations.

An amplitude of 2.5 mm, namely the plate thickness, was imposed for the maximum out-of-plane displacement of the plate, as it was judged reasonable.

It must be underlined that the reliability of the proposed models was also corroborated by sensitivity analyses conducted with respect to all the other modelling assumptions described previously (i.e. finite element typology, mesh size, etc), that allowed to consider the obtained numerical results stable.

A standard pseudo-static cyclic analysis was carried out for reproducing the experimental tests. To this purpose, the same diagonal displacements history used during the experimental analysis, depicted in figure 4, was imposed to the top node of the model.

The comparison between the obtained results, shown in Figure 21 in terms of diagonal displacement vs. diagonal force, proved that the adopted approach is reliable enough for using the considered FEM model with the aim of carrying out parametric analyses. In fact all the main behavioural features of the tested plates, namely strength, stiffness, ductility, dissipative capacity and strength decay, were perfectly reproduced for each shear demand.

Furthermore, the analysis of the internal stresses at several shear demands allowed to better interpret some of the observed experimental evidences.

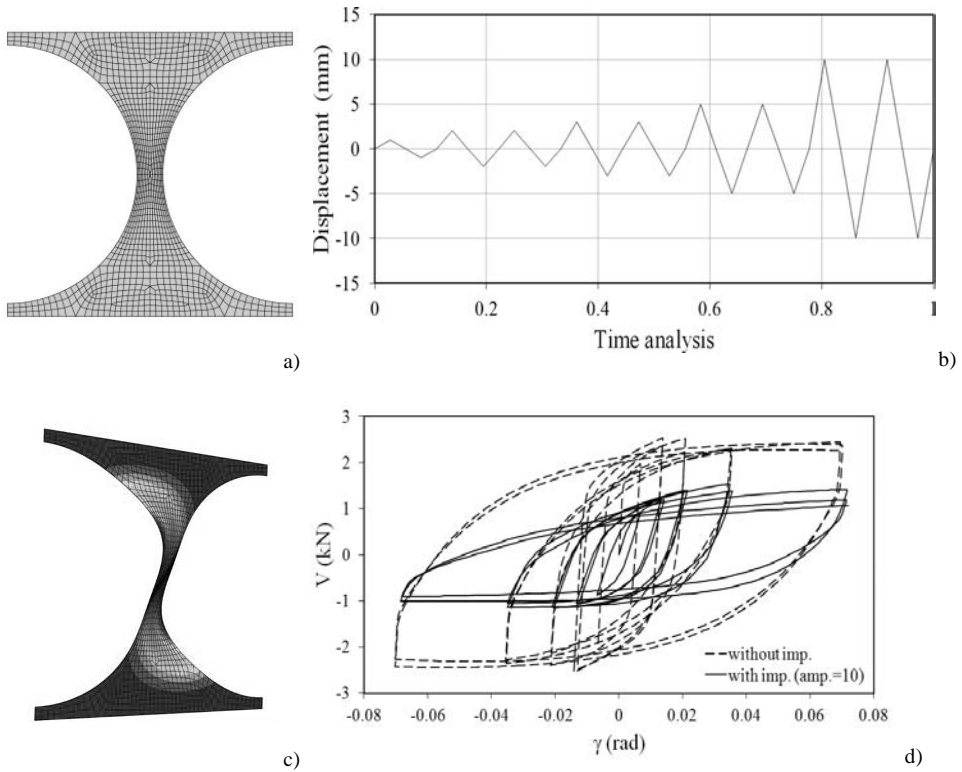


Figure 19. Imperfection sensitivity analysis on a plate portion included between perforations: a) model meshing; b) imposed lateral displacement history; c) imposed initial imperfections (maximum amplitude of 10 mm); d) obtained results.

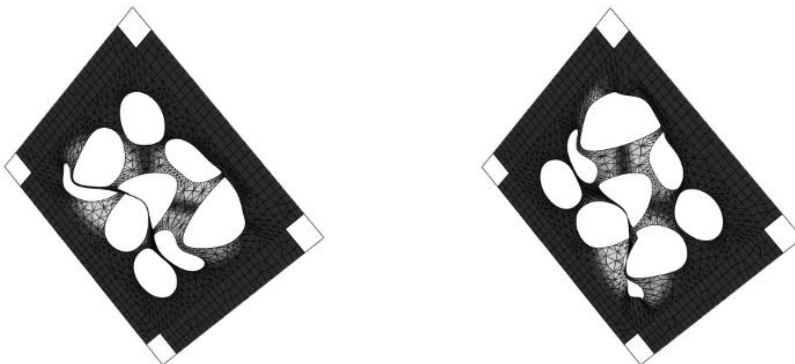


Figure 20. The two deformed shapes superimposed for modelling the initial imperfection of the plate.

For example, the stress pattern shown for specimen PSP2 in Figure 22, corresponding to a diagonal displacement demand of 10 mm, allowed to understand that the rotation of the principal stress at the bottleneck of the panel portions included within two consecutive

perforations originated bending moment that lead to the lateral-torsion buckling phenomena discussed previously.

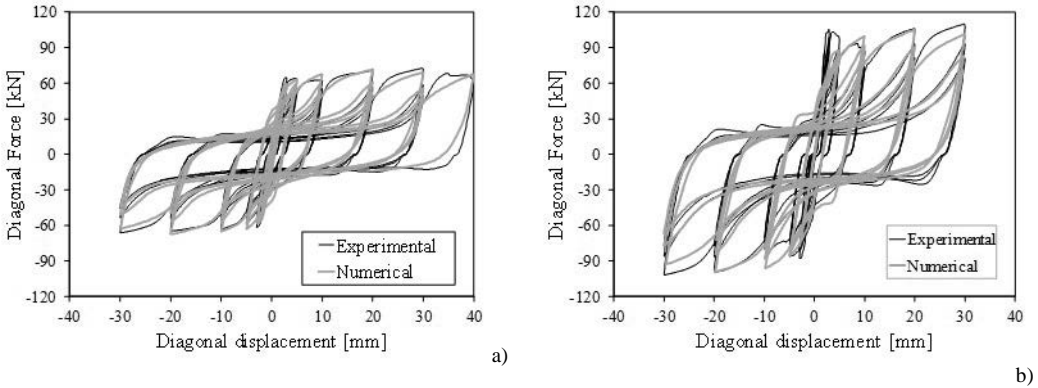


Figure 21. Numerical vs. Experimental results for shear panels PSP-1 (a) and PSP-2 (b).

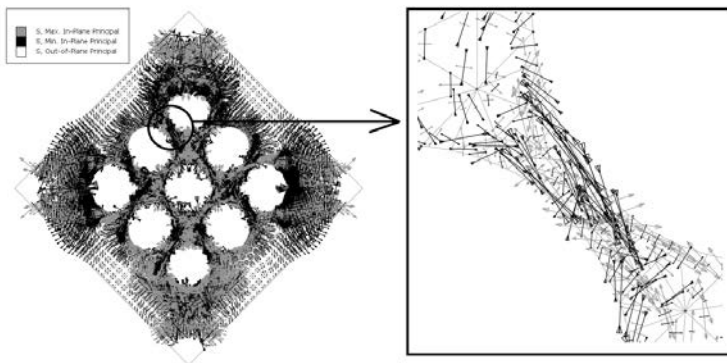


Figure 22. Internal principal stresses for specimen PSP-2 (diagonal displacement demand of 10 mm - shear strain of 2.2%).

3.6 Design Formulations

A parametric analysis has been carried out varying the number of perforations, with the main purpose to provide an analytical tool able to predict the panel response depending on the main geometrical parameters influencing the performance of the device. The following parameters have been considered: perforation diameter (D), minimum spacing between holes (s) and depth e of the not perforated area, namely the distance between the outer holes and the plate area bolted to the perimeter frame (named as constrained area). While the dissipative performance of the panel is to be ascribed to the perforated central core shown in Figure 22a, the not perforated area serves to avoid negative overlapping of stresses that could lead to brittle failure mechanism. On the other hand, it allows a strength resource for the overall resistance of the perforated plate.

The three parameters e , s and D relate to each other through the following expression (eq. 3):

$$e = \frac{1}{2} [L_p - (n_h \cdot D) - s \cdot (n_h - 1)] \quad (3)$$

where L_p is the width of the free area of the panel and n_h is the number of perforations. Moreover e and L_p give the parameter ξ , reported in eq. (4), that is strongly related to the influence of perforations on the dissipative capacity of the shear panel.

$$\xi = 1 - \frac{2 \cdot e}{L_p} \quad (4)$$

When ξ is 0, the panel performance coincides with the one of a solid plate, while $\xi=1$ means that the not perforated area does not exist.

Another influencing parameter for the plate performance is the ratio between its shear net area $A_{p,net}$ and the transversal area of the corresponding A_p solid plate (see eq. 5), which is strictly related to the actual shear strength of the plate.

$$\frac{A_{p,net}}{A_p} = \frac{L_p - n_h \cdot D}{L_p} \quad (5)$$

The parametric analysis has been carried out considering twenty-two geometries described in Tab 2, which have been obtained by varying the above parameters.

Among the studied cases also the solid panel ($\xi=0$) has been considered, as for this specimens an experimental test was preliminarily carried out. The comparison between the cyclic response retrieved during this test and the numerical results (Figure 22b) proves the reliability of the proposed model in capturing the real system response also in absence of perforations.

In Figure 24 the obtained maximum shear strength, F_{max} conventionally normalised to the yielding shear strength computed for the solid panel, is given as a function of the ratio $A_{p,net}/A_p$.

It is possible to observe that the obtained results, for each shear strain, are well fitted by simple analytical curves.

Such analytical curves are given in eqs. (6), (7), (8), (9) and (10) for shear strains of 0.66% (diagonal displacements $d=3$ mm), 1.1% ($d=5$ mm), 2.2% ($d=10$ mm), 4.4% ($d=20$ mm) and 6.6 ($d=30$ mm), respectively.

$$\frac{F_{\max,0.7\%}}{F_y} = 7 \cdot 10^{-5} \cdot \left(\frac{A_{p,net}}{A_p} \right)^2 \cdot 0.0176 \cdot \frac{A_{p,net}}{A_p} \quad (6)$$

$$\frac{F_{\max,1.1\%}}{F_y} = 5 \cdot 10^{-5} \cdot \left(\frac{A_{p,net}}{A_p} \right)^2 \cdot 0.0153 \cdot \frac{A_{p,net}}{A_p} \quad (7)$$

$$\frac{F_{\max,2.2\%}}{F_y} = 4 \cdot 10^{-5} \cdot \left(\frac{A_{p,net}}{A_p} \right)^2 \cdot 0.0157 \cdot \frac{A_{p,net}}{A_p} \quad (8)$$

$$\frac{F_{\max,4.4\%}}{F_y} = 4 \cdot 10^{-5} \cdot \left(\frac{A_{p,net}}{A_p} \right)^2 \cdot 0.0160 \cdot \frac{A_{p,net}}{A_p} \quad (9)$$

$$\frac{F_{\max,6.6\%}}{F_y} = 4 \cdot 10^{-5} \cdot \left(\frac{A_{p,net}}{A_p} \right)^2 \cdot 0.0153 \cdot \frac{A_{p,net}}{A_p} \quad (10)$$

Table 2. Geometrical features of the perforated shear panels considered for parametric analysis.

Specimen	n_h (-)	D (mm)	s (mm)	e (mm)	$A_{p,net}/A_p$ (%)	D/s (-)	ξ (-)
Not-perforated	0	0.00	0.00	255.00	100.0	0.00	0.00
PSP 1	3	127.50	12.75	51.00	25.0	10.00	0.80
PSP 2	3	107.40	42.90	51.00	36.8	2.50	0.80
M 2x2-D87	2	87.00	50.00	143.00	65.9	1.74	0.44
M 3x3-D32	3	31.88	63.79	143.40	81.3	0.50	0.44
M 3x3-D51	3	51.27	51.00	127.50	69.8	1.01	0.50
M 3x3-D100	3	100.00	10.00	95.00	41.2	10.00	0.63
M 3x3-D109	3	109.29	12.14	78.93	35.7	9.00	0.69
M 3x3-D128	3	127.63	10.00	53.55	24.9	12.76	0.79
M 3x3-D131	3	130.98	5.00	53.55	23.0	26.20	0.79
M 4x4-D72	4	71.94	21.48	78.90	43.6	3.35	0.69
M 4x4-D99	4	98.84	2.28	53.90	22.5	43.35	0.79
M 5x5-D48	5	48.29	27.54	79.20	52.7	1.75	0.69
M 5x5-D74	5	74.00	8.26	53.48	27.5	8.96	0.79
M 5x5-D81	5	81.00	3.00	46.50	20.6	27.00	0.82
M 5x5-D85	5	85.00	15.00	12.50	16.7	5.67	0.95
M 5x5-D90	5	90.00	10.00	10.00	11.8	9.00	0.96
M 5x5-D95	5	95.00	5.00	7.50	6.9	19.00	0.97
M 9x9-D27	9	26.62	20.34	53.90	53.0	1.31	0.79
M 9x9-D43	9	42.50	7.50	33.75	25.0	5.67	0.87
M 9x9-D45	9	45.00	5.00	32.50	20.6	9.00	0.87
M 9x9-D48	9	47.50	2.50	31.25	16.2	19.00	0.88

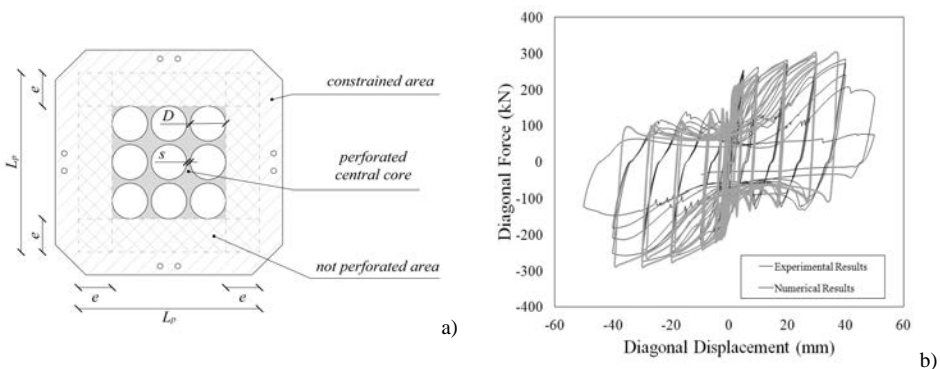


Figure 23. a) Geometrical parameters influencing the perforated panel response. b) comparison between the experimental and numerical results for solid panel.

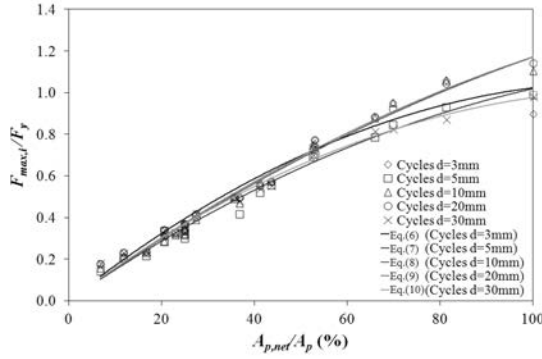


Figure 24. The parametric analysis results in terms $F_{max,i}/F_y$ compared with the analytical values given by eqs (6-10).

Similarly, it has been observed that linear equations (11), (12), (13) and (14) allow to predict, respectively for shear strains of 1.1% ($d=5$ mm), ($d=10$ mm), ($d=20$ mm) and ($d=30$ mm), the ratio F_{pinc}/F_{max} , as a function of both the ratio D/s and the parameter ξ , as it is shown in Figure 25.

$$\frac{F_{pinc,1.1\%}}{F_{max,5}} = 0.001 \cdot \left(\frac{D}{s}\right) + 0.02 \cdot \xi + 0.45 \quad (11)$$

$$\frac{F_{pinc,2.2\%}}{F_{max,10}} = 0.004 \cdot \left(\frac{D}{s}\right) + 0.04 \cdot \xi + 0.32 \quad (12)$$

$$\frac{F_{pinc,4.4\%}}{F_{max,20}} = 0.008 \cdot \left(\frac{D}{s}\right) + 0.05 \cdot \xi + 0.21 \quad (13)$$

$$\frac{F_{pinc,6.6\%}}{F_{max,30}} = 0.008 \cdot \left(\frac{D}{s}\right) + 0.05 \cdot \xi + 0.186 \quad (14)$$

4 STEEL FRAMES WITH METAL SHEAR PANELS CHARACTERIZED BY DIFFERENT PINCHING

4.1 General

The analysis reported above on different types of metal dissipative shear panels evidenced that their hysteric behavior could be affected by detrimental phenomena (in particular, buckling) which results in pinching on the cycles. The entity of this pinching could be different according to the adopted technological details: in general, more expensive details entail a better hysteric behavior.

Based on this premise, this Section analyzes the structural performance of steel frames equipped with metal dampers characterized by hysteric cycles which are differently affected by pinching. Three plane steel frame are considered and their behavior is investigated under several historical records that are suitably scaled in order to carry out Incremental Dynamic Analysis (IDA).

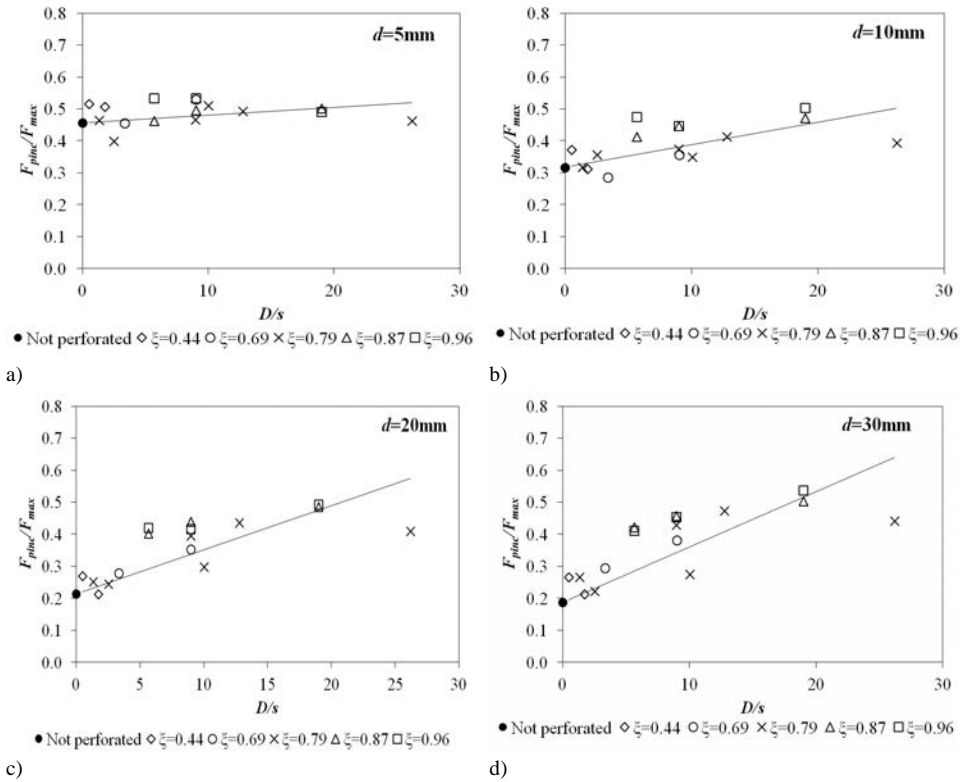


Figure 25. a) Results of parametric analysis in terms F_{max}/F_{pinc} and comparison with analytical values given by eqs (9-12).

4.2 The modelling approach for the shear panels

In order to carry out the aforementioned analyses, shear panels have been modelled by adopting two sub-assembly of NN-Links (**Errore. L'origine riferimento non è stata trovata.**a). Each sub-assembly is given by a single Bouc-Wen NN-Link (Bouc-Wen 1), working in parallel to two further links in series. The first is characterized again by a Bouc-Wen relationship (Bouc-Wen 2), whereas the other is a GAP NN-link. The last is characterized by the fact that for axial displacements lower than a predetermined value it does not oppose resisting forces, while for higher displacements it is rigid.

Once that the features of the shear panels without degrading phenomena, therefore with hysteretic cycles not affected by pinching, have been selected, the mechanical features of the above Bouc-Wen NN-links have been chosen in order to reproduce the required stiffness, strength and ductility. Then the characteristic limit displacement of the GAP NN-link has been varied so to have three shear panels characterized by pinched hysteretic cycles with dissipated energy equal to 25%, 50% and 75% of the energy dissipated by the not degraded system. The obtained cycles are represented in Figure 26b, where the η factor, namely the “energy efficiency factor” introduced by Brando et al. (2013), represents the above imposed percentage of energy dissipation capacity.

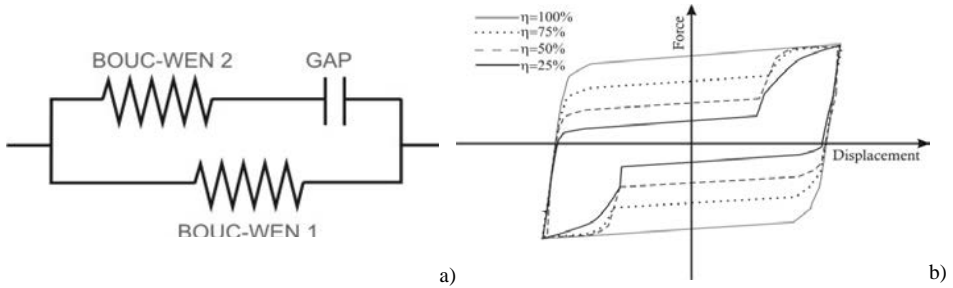


Figure 26. a) Non Linear Link sub-assembly for the applied degraded dampers.

4.3 The studied frames

The analyzed steel frames, characterized by both a bay-length and a storey height of 3.5 m, are shown in Figure 27. Beams and columns have been sized so that, under selected design earthquakes, a maximum transient lateral drift of 2.5% is not exceeded by the bare frame, according to the limit proposed by the FEMA 356 (ASCE, 2000) for the life safety performance level that has to be assured for rehabilitated MRFs. In detail, the Reykjavik–Island (2000) earthquake with a maximum PGA (Peak Ground Acceleration) of 0.5g has been considered for the 3 bays–4 storeys frame, while the Hachinohe–Japan (1979) record, with the same PGA, has been applied on both the 3 bays–8 storeys and the 3 bays–12 storeys frame. In addition, structural elements have been chosen in order to get a first modal participation mass ratio larger than 85%, so that their first vibration mode, characterized by an almost linear shape, prevails on the higher ones.

The above frames have been therefore equipped with shear panels characterized by not-degraded hysteretic cycles, according to the design criteria explained in Brando et al. (2015). In detail, the added elements have been selected in order that the whole structure is able to satisfy, under the same design earthquakes used for the bare MRFs, the requirements provided by FEMA 356 for braced frames, namely a maximum transient lateral drift of 1.5%. The arrangement of the proposed devices is shown in Figure 28.

Then, the same panels have been degraded following the procedure described in the previous Paragraph.

4.4 The implemented analyses

The non linear dynamic behaviour of the described frames has been analysed by implementing time history analyses, following the imposition of the permanent vertical loads, according to the direct integration procedure. P-Delta effects have been also accounted for. The Newmark method has been used for the numerical solution. Iterative analyses by the Newton-Raphson method have been carried out in each time step in the process of obtaining the displacement increment until that the unbalance between the members and the external forces is minimized.

Two different “families” of natural records have been selected. The former consists in the seven time histories, normalized to the relative peak ground acceleration, depicted from Figure 29a to Figure 29g. They have been applied on the 3 bays–4 storeys frames. The second set of records is also made of seven time histories, which are shown from Figure 29f to Figure 29n.

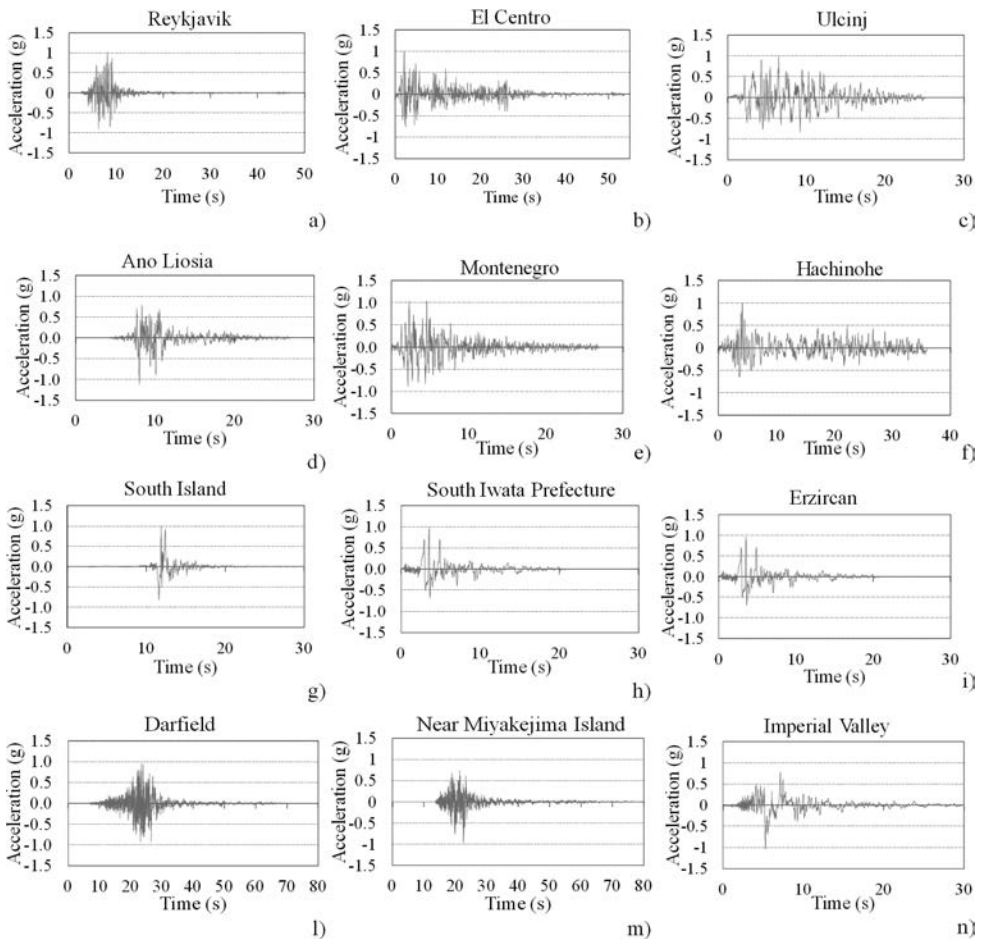


Figure 29. The normalized natural records applied to the 3 bays-4 storeys frames (from a to g) and to the 3 bays-8 storeys and 5 bays-12 storeys steel frames (from f to n).

They have been applied on the higher frames (3 bays-8 storeys and 5 bays-12 storeys), due to the fact that they present higher spectral accelerations for lower frequencies with respect to the records belonging to the first group.

4.5 The obtained results

The obtained damage, interstorey drifts, residual drifts and accelerations on the roof have been evaluated for all the studied structures. For brevity purpose, these data will be presented in the following for the 3 bays - 4 storeys steel frame.

As far as the damage distribution concerns (Figure 30), in the most cases of frames equipped with devices characterized by degraded hysteretic cycles, the activation of the first inelastic hinges has been registered for accelerations 0.1 g lower than the ones given for frames with shear panels with $\eta = 100\%$. The same type of consideration can be done for the accelerations associated to the collapse: accelerations given by the panels with degraded cycles are generally 0.1g - 0.2g lower than the ones given by frames with shear panels without

detrimental effects on the hysteretic cycles. Moreover, they are associated to a larger number of plastic hinges.

The application on the frames of panels with lower dissipative capacity gave higher interstorey drifts, which increased almost proportionally with the reduction of the “efficiency energy factor” of the panels (Figure 31, Figure 32, Figure 33, Figure 34).

As for the observed residual drifts (Figure 35) the degraded shear panels led to values that, in some specific cases, resulted even doubled with respect to the values observed for dampers with $\eta = 100\%$. Nevertheless, in general, the application of dampers with a larger hysteretic cycles do not lead to improvements of behaviour.

The variation of the dissipative capacity of the applied dampers have not caused a substantial variation of the maximum accelerations registered (Figure 36) on the roof of the building, considering that degraded and not degraded cycles returned the same frequencies. On the contrary, a general improvement can be observed in terms of maximum roof displacements (Figure 37).

4.6 *q-factor evaluation*

The application of seismic protection systems determines a deep variation of the structural inelastic response. Linear analysis should contemplate such an effect by a proper seismic reduction factor, namely the q behavior factor, which, on the other hand, has to account for the different energies that the structure is able to dissipate according to the level of pinching affecting the hysteretic cycles of the applied panels.

The evaluation of the q -factor can be performed by means of several methods, as for example the “Setti Method”. This procedure (Setti 1985) is useful for frames able to develop global collapse mechanisms, which have a dominant first vibration mode.

In detail, on the basis of the outcomes obtained by the incremental dynamic analysis for each earthquake, the maximum value of the roof displacements (d), normalized to the displacement able to produce the first yielding on the structure (d_y), is put in relation to the relative peak ground accelerations (a), normalized to the acceleration (a_y) retrieving d_y . In this way, the so-called pushover dynamic curve can be obtained.

The q -factor given by each record is expressed as the minimum a/a_y ratio among those giving back one of the following situations: *i*) attainment of a limit in-terstorey drift (established, in the case being, as 1.5%) or *ii*) loss of global stability for the whole frame.

In particular, the a/a_y ratio corresponding to the last situation has been detected by the intersection of the dynamic pushover curve plotted in the $(d/d_y, a/a_y)$ datum plane and the bisector of the datum plane itself, it representing the ideal elastic behavior of the system. In fact the point $(d/d_y, a/a_y)$ belonging to the region upon this bisector represents unstable structural responses (Figure 38).

In Figure 39, Figure 40 and Figure 41 the values of q -factors calculated for the studied frames, in both cases of the unprotected structure and of the frame with different “energy efficiency factor” panels, for all the time histories, are depicted, whereas both the minimum and maximum measured values obtained by the analyses are listed in table 3.

In the case of devices with $\eta=25\%$, applied on the 3 bays - 4 storeys frame, the increment of the q -factor, with respect to the bare frame, varies between a minimum of 11% and a maximum of 65%, while for the frame of 3 bays – 8 storeys this range goes from 33% to 114%. A comparable behaviour has been registered for the 5 bays – 12 storeys frame, with increments going from 26% to 100%.

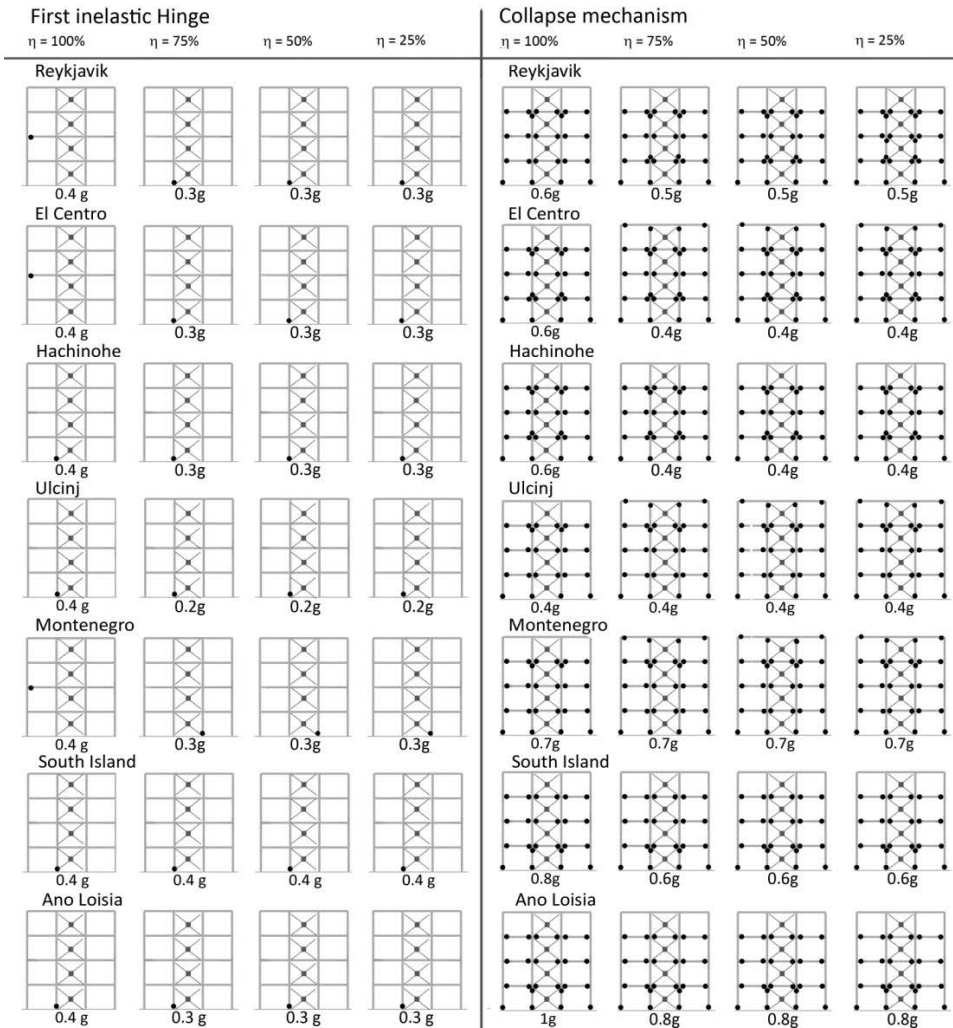


Figure 30. Damage distribution on the 3bays-4 storeys steel frame: a) first inelastic hinge formation, b) development of the collapse mechanism.

For an “efficiency energy factor” equal to 50 % the q-factor value got an increment ranging from the 39 % up to a maximum of 186 %. While, in the case of the 3 bays -4 storeys and 5 bays – 12 storeys frames the minimum increasing has been respectively of 23 % and 40 %, whereas the maximum of 110% and 129%.

A comparable behaviour has been noted for the structures protected by the devices with $\eta=75\%$ % and $\eta=100\%$: the value of q-factor got increment of of 257% and 293% in the case of 3 bays – 4 storeys frame. Instead, lower results have been registered in the others two typologies frames.

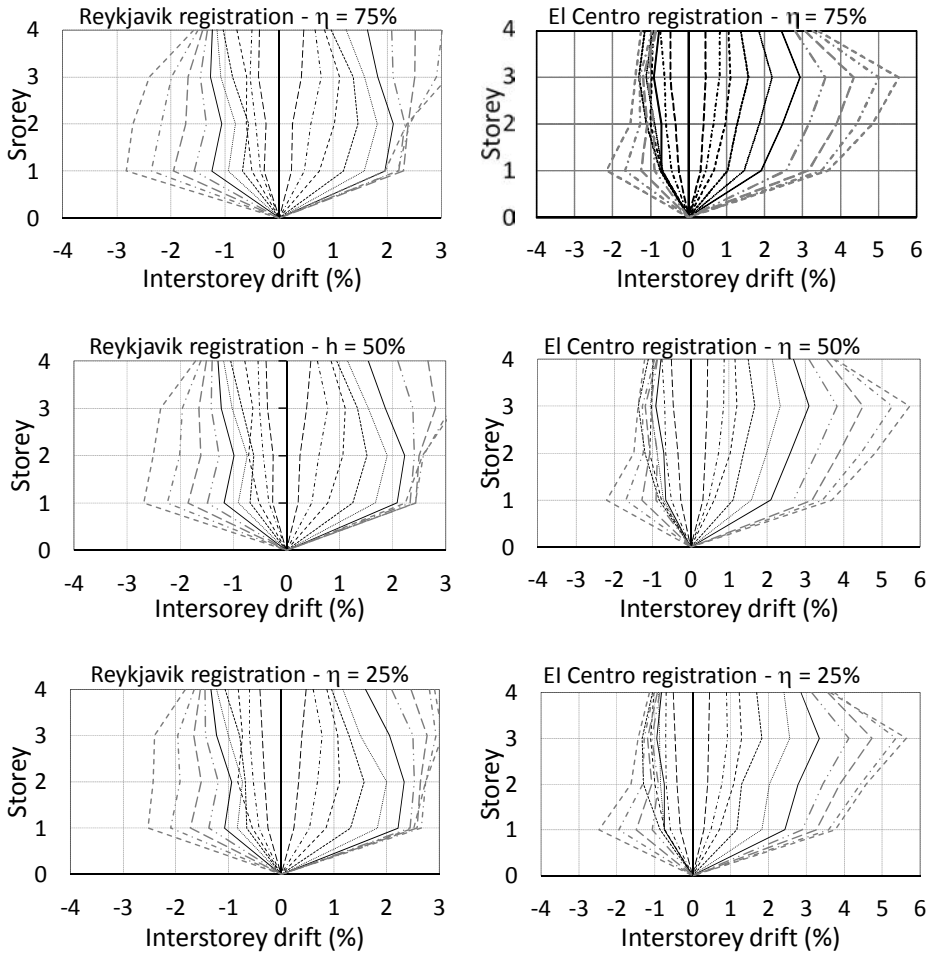


Figure 31. Interstorey drifts registered on the 3 bays – 4 storeys frames equipped with different “energy efficiency factor” for the accelerogram of the events: Reykjavik–Island (2000), El Centro–USA (1940).

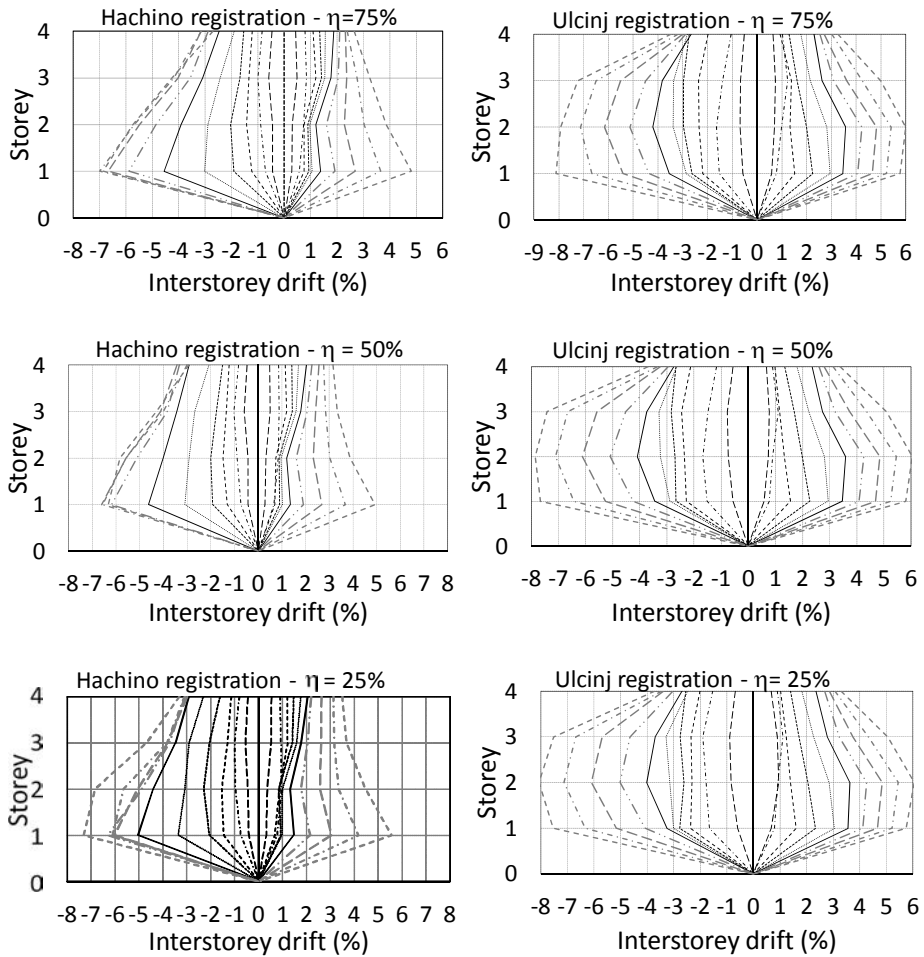


Figure 32. Interstorey drifts registered on the 3 bays – 4 storeys frames equipped with different “energy efficiency factor” for the accelerogram of the events: Hachinohe–Japan (1979) e Ulcinj–Montenegro (1979).

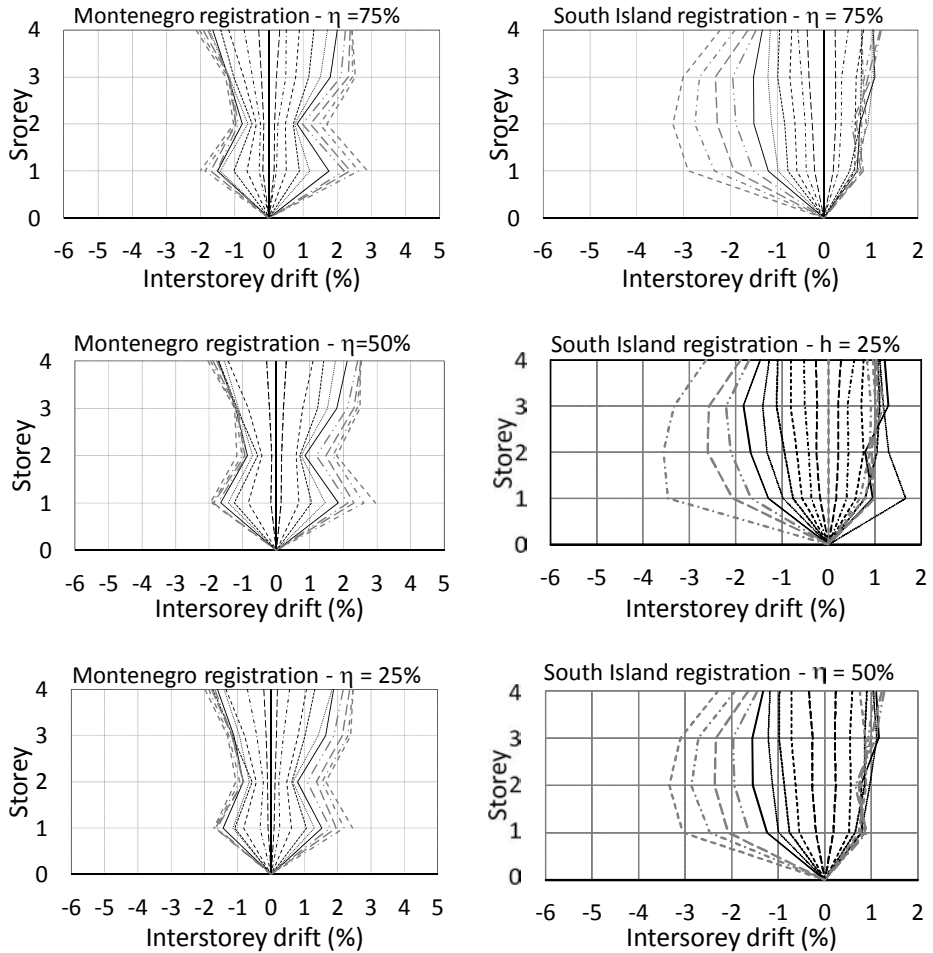


Figure 33. Interstorey drifts registered on the 3 bays – 4 storeys frames equipped with different “energy efficiency factor” for the accelerogram of the events: South Island (2000) and Ano Loisia-Grecia (1999).

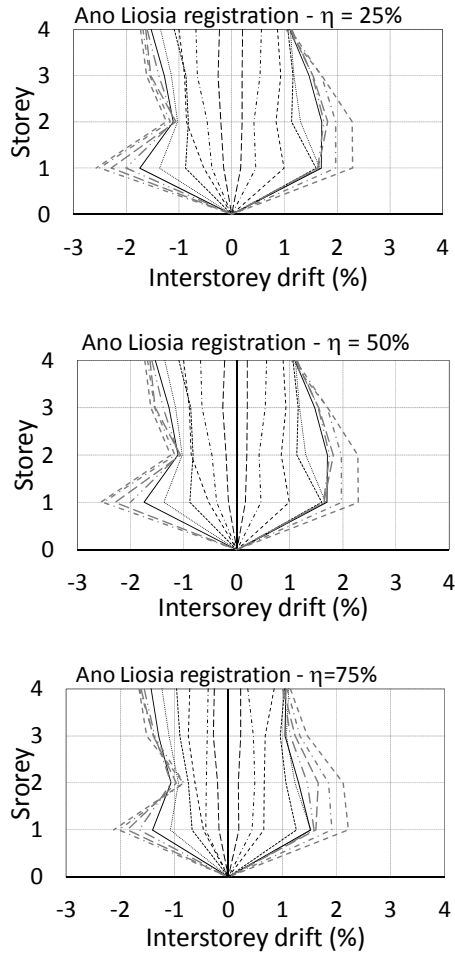


Figure 34. Interstorey drifts registered on the 3 bays – 4 storeys frames equipped with different “energy efficiency factor” for the accelerogram of the events Montenegro (1999).

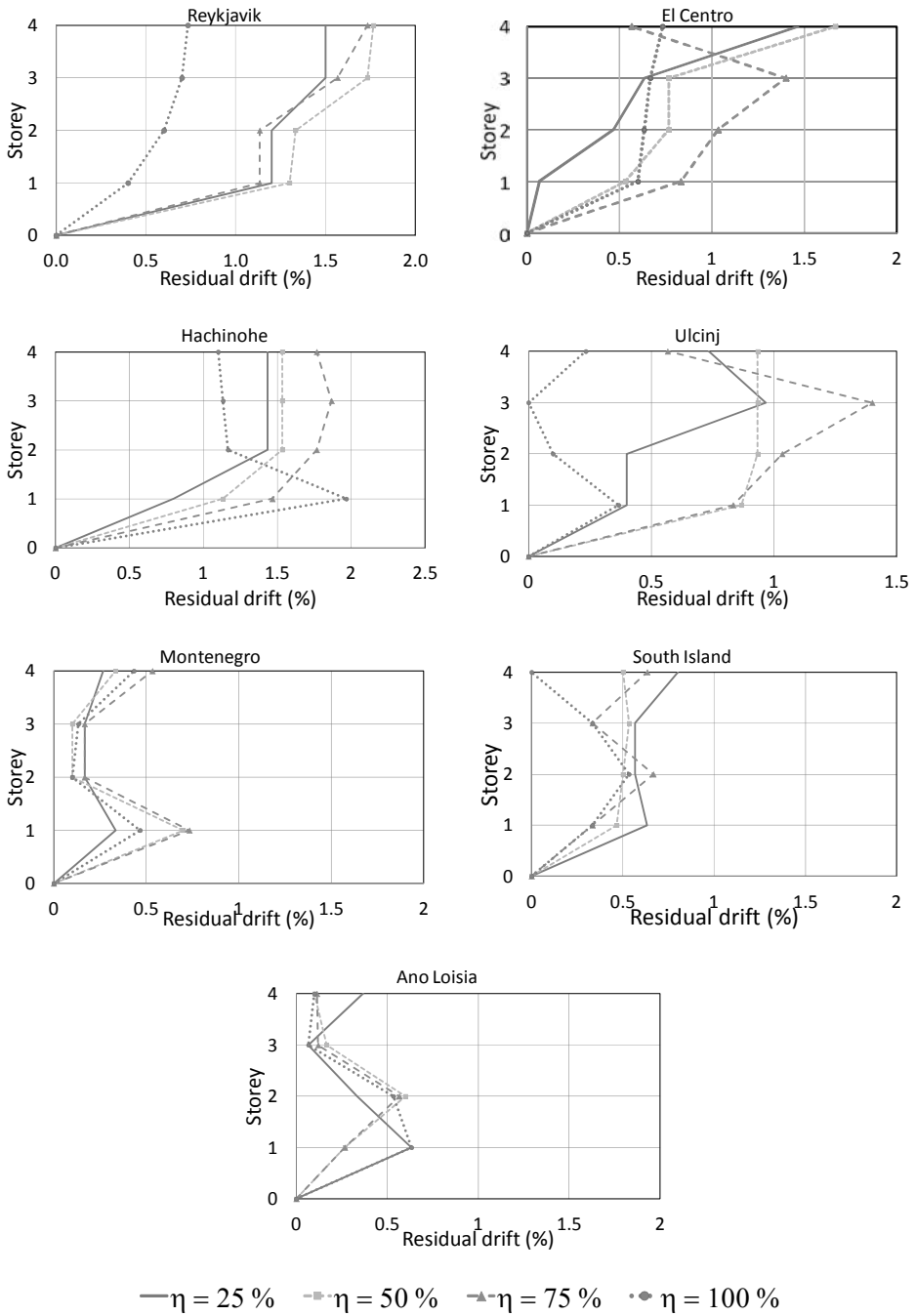


Figure 35. Residual displacements registered for each accelerogram for a PGA of 0.9g on the 3bays – 4 storeys.

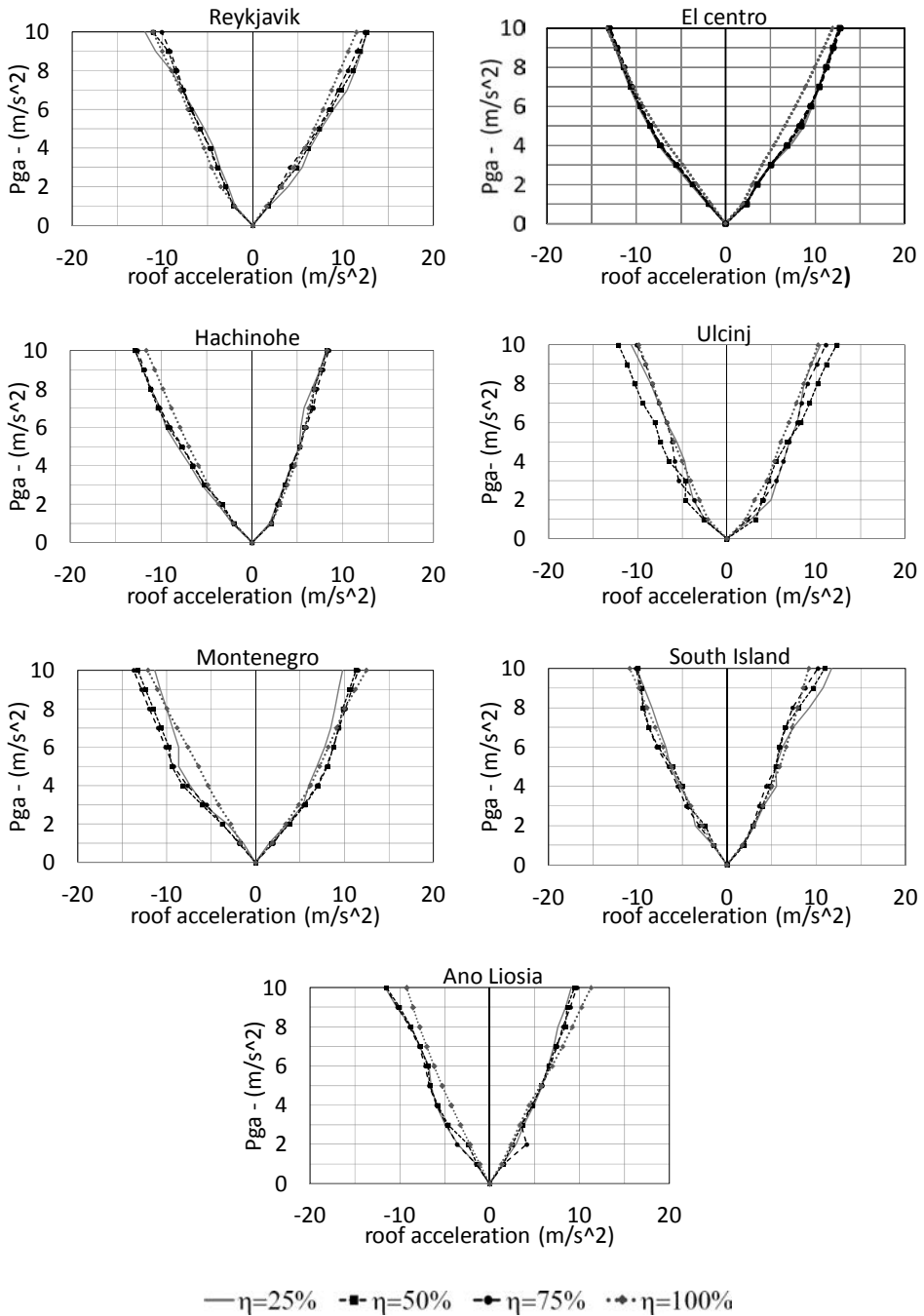


Figure 36. Roof accelerations registered for each accelerogram at different scaled PGA on the 3bays – 4 storeys.

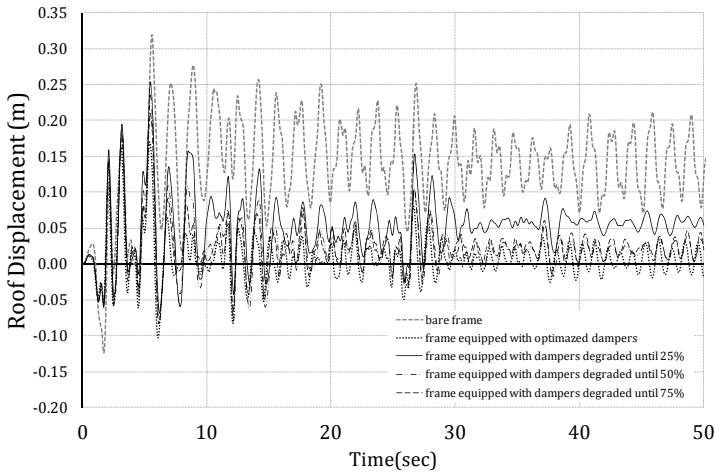


Figure 37. El Centro Earthquake Results in terms of roof displacement registered on the roofs of the 3 bays – 4 storeys frames.

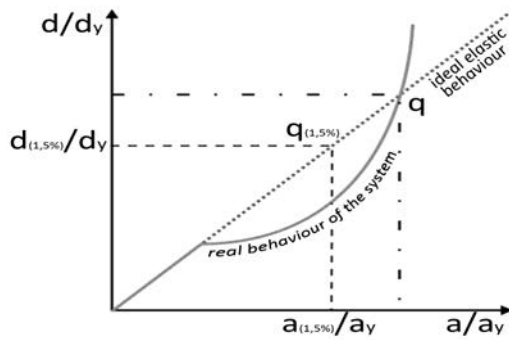


Figure 38. Figure 10. Behavior factor according to the Setti Method.

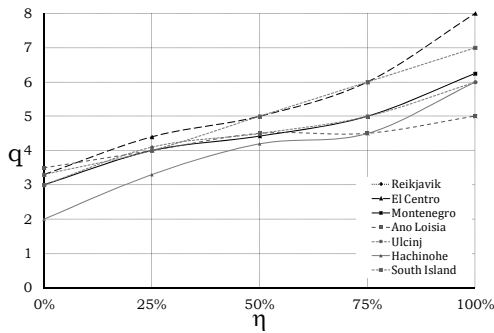


Figure 39. q-factor calculated for the 3 bays – 4 storeys frame.

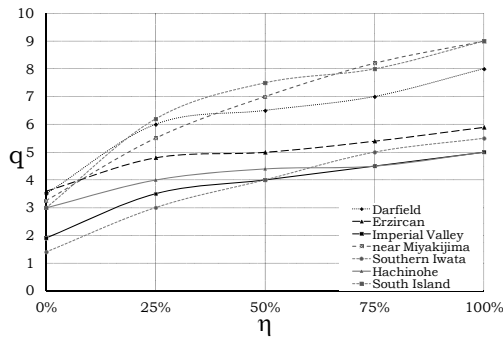


Figure 40. q-factor calculated for the 3 bays – 8 storeys frame.

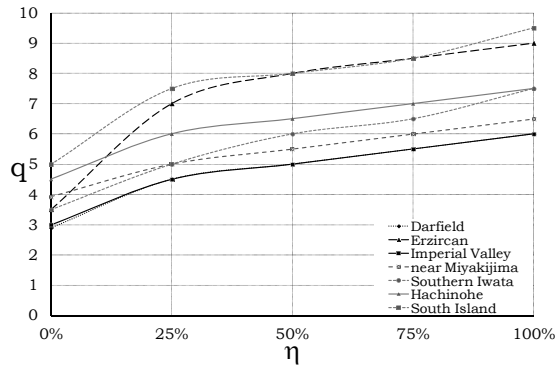


Figure 41. q-factor calculated for the 5 bays – 12 storeys frame

Table 3. q factors corresponding to different “efficiency energy factor” and steel frame

“efficiency Energy factor”	q factor	Frame typology		
		3 bays - 4 storeys	3 bays - 8 storeys	5 bays - 12 storeys
η 0%	q	2 ÷ 3.6	1.4 ÷ 3.6	2.5 ÷ 5
η 25%	q	3.3 ÷ 4.4	3 ÷ 6	4.5 ÷ 7
η 50%	q	4.2 ÷ 5	4 ÷ 7	5 ÷ 8
η 75%	q	4.5 ÷ 6	4.5 ÷ 8.2	5.5 ÷ 8.5
η 100%	q	5.5 ÷ 8	5 ÷ 9	6 ÷ 9.5

5 CONCLUSIONS

In this chapter, the Research activity focused on shear panels carried out by the University of Campania and of Chieti-Pescara in the triennium 2014-2016 within the Research Project DPC-ReLuis has been described.

In particular, the described investigation has dealt with the use of a new type of dissipative shear panels based on the use of perforated plates, as well as on the seismic performance of steel frames protected with shear panels characterized by different dissipative capacity.

The obtained results encourage to application of metal shear panels as a convenient solution for designing steel buildings in seismic-prone zones.

6 REFERENCES

- Alavi, E., Nateghi, F. (2013). "Experimental study on diagonally stiffened steel plate shear walls with central perforation". *Journal of Constructional Steel Research*, n.89, pp. 9–20.
- Brando, G., De Matteis, G. (2011). "Experimental and numerical analysis of a multi-stiffened pure aluminium shear panel" *Thin-Walled Structures*, 49 (10), pp. 1277-1287.
- Brando, G., D'Agostino, F., De Matteis, G. (2013). "Experimental tests of a new hysteretic damper made of buckling inhibited shear panels". *Materials and Structures/Materiaux et Constructions* 46 (12) PP. 2121 – 2133. doi: 10.1617/s11527-013-0040-6.
- Brando, G., De Matteis, G. (2014). "Design of low strength-high hardening metal multi-stiffened shear plates". *Engineering Structures*, 60, pp. 2-10.
- Brando, G., D'Agostino, F., De Matteis, G. (2015). "Seismic performance of MR frames protected by viscous or hysteretic dampers". *Structural Design of Tall and Special Buildings*, 24 (9), pp. 653-671.
- Christopoulos, C., Filiatrault, A. (2007). "Principles of Passive Supplemental Damping and Seismic Isolation". *IUSS Press, Pavia*. ISBN 88-7358-037-8.
- De Matteis, G., Landolfo, R., Mazzolani, F. M. (2003). Seismic Response of MR Steel Frames with low-yield Steel Shear Panel. *Engineering Structures*, Vol. 25 (2): 155-168.
- De Matteis, G. (2005). Effect of lightweight cladding panels on the seismic performance of moment resisting steel frames. *Engineering Structures*, Vol. 27/11: 1662-1676.
- De Matteis, G., Mazzolani F.M., Panico, S. (2007). Pure aluminium shear panels as dissipative devices in moment-resisting steel frames. *Earthquake Engineering and Structural Dynamics*, vol. 36: 841-859.
- De Matteis, G., Panico, S., Mazzolani, F.M. (2008). Experimental tests on pure aluminium shear panels with welded stiffeners. *Engineering Structures*, Vol. 30 (6): 1734-1744.
- De Matteis, G., Brando, G., Mazzolani, F.M. (2011). Hysteretic behaviour of bracing-type pure aluminium shear panels by experimental tests. *Earthquake Engineering and Structural Dynamics*, 40 (10):1143-1162.
- ECCS-CECM. Recommended testing procedure for assessing the behaviour of structural steel elements under cyclic loads
- Hitaka, T., Matsui, C. (2003). "Experimental study on steel shear wall with slits" *Journal of Structural Engineering*, 129 (5), pp. 586-595.
- Montuori, R., Natri, E., Piluso, V. (2014b). "Theory of plastic mechanism control for the seismic design of braced frames equipped with friction dampers" *Mechanics Research Communications* 58, pp. 112-123
- Pohlentz, A. J., (2010). "Development of Steel Slit Wall Dampers with Embedded Condition Assessment Capabilities", *Ph.D. thesis*, University of Kyoto, Japan.
- Shishkin, J.J., Driver, R.G., Grondin, G.Y. (2009). "Analysis of steel plate shear walls using the modified strip model" *Journal of Structural Engineering*, 135 (11), pp. 1357-1366
- Soong, T. T, Dargush, G. F. (2007). "Passive Energy Dissipation Systems in Structural Engineering". *John Wiley & Sons, Inc, New York*. ISBN-13: 9780471968214.
- Valizadeh, H., Sheidaii, M., and Showkati, H. (2012). "Experimental investigation on cyclic behaviour of perforated steel plate shear walls." *Journal of Constructional Steel Research*. 70 308-316.
- Vian, D., Bruneau, M., Purba, R. (2009). "Special perforated steel plate shear walls with reduced beam section anchor beams. II: Analysis and design recommendations" *Journal of Structural Engineering*, 135 (3), pp. 221-228.

SECTION 7

NON-CONVENTIONAL BUILDINGS: HYBRID SYSTEMS

DESIGN PROCEDURE FOR FAILURE MODE CONTROL OF HYBRID MRF-EBF SYSTEMS

Rosario Montuori ^a, Elide Nastri ^a, Vincenzo Piluso ^a

^a *University of Salerno, Fisciano, Italy, r.montuori@unisa.it, enastri@unisa.it, v.piluso@unisa.it*

ABSTRACT

In this work, a design procedure for hybrid MRF-EBF systems (MRF-EBF dual systems) based on the Theory of Plastic Mechanism Control (TPMC) is reported. As it is known, Eurocode 8 does not provide any specific design criterion regarding such structural typology, so that practitioners commonly carry out the design process by combining the design rules suggested for simple MRFs and EBFs. Therefore, the aim of this work is to provide a complete and exhaustive design procedure for MRF-EBF dual systems, considering all the brace configurations commonly adopted and with the goal of assuring the development of a collapse mechanism of global type. The design procedure to assure this ambitious design goal is based on TPMC whose aim is to derive the column sections required to assure the desired collapse mechanism starting from the knowledge of the dissipative zones. In order to point out the accuracy of the proposed design approach a number of MRF-EBF dual systems have been designed and their performances have been evaluated by means of both push-over and IDA analyses.

KEYWORDS

Dual-systems, EBFs, hybrid systems, TPMC, seismic design.

1 INTRODUCTION

Within the unconventional structural typologies, Moment Resisting Frames-Eccentrically Braced Frames (MRF-EBF) systems are of great importance because, although poorly coded, they are often used to combine the advantages offered by individual structural systems. In particular, dual systems allow, on one hand, to exploit the lateral stiffness of Eccentrically Braced Frames in order to fulfil serviceability requirements and, from the other hand, to exploit the ductility of the Moment Resisting Frame part. Nowadays, international seismic codes do not provide sufficient guidelines for the proper design of such structural systems. In fact, they only provide the value of the behaviour factor and, in some cases, indicate the percentage of seismic design forces to entrust to the braced part of the dual system.

In the framework of dual systems, MRF-EBFs constitute a suitable compromise between seismic resistant MR-frames and concentrically braced frames. In fact, they exhibit both adequate lateral stiffness, due to the high contribution coming from the axial stiffness of diagonal braces, and ductile behaviour, due to the ability of the links, constituting the dissipative zones of this structural typology, in developing wide and stable hysteresis loops. Therefore, the dual system resulting from the coupling of MRFs and EBFs is able to provide significantly improved seismic performances, because it is characterised by a primary seismic

force resisting system constituted by the eccentrically braced bays, and a secondary fail-safe system, constituted by moment resisting bays. This secondary fail-safe system can be considered as an additional dissipative system where plastic hinges are concentrated at the beam ends. Conversely, the main dissipative system is constituted by the link members, located in the braced bays, which can be either horizontal (K-braced, D-braced and V-braced) or vertical (inverted Y-braced) (Figure 1).

Particular attentions has to be devoted to connections of the brace members at their bottom ends. The design practice is divided between those who privilege hinge connections and those who privilege fixed connections at the lower brace end. This second solution is undoubtedly stiffer, but the corresponding structural details are more expensive. In addition, being the braces able to transmit not only the axial force but also the bending moment, at their lower end, the development of plastic hinges at the bottom brace ends has to be considered in the design process (Mastrandrea *et al.*, 2003; Mastrandrea and Piluso, 2009; Chao and Goel, 2006). Herein, it is assumed that bottom brace ends are unable to transmit the bending moment and, therefore, they are modelled with actual hinges.

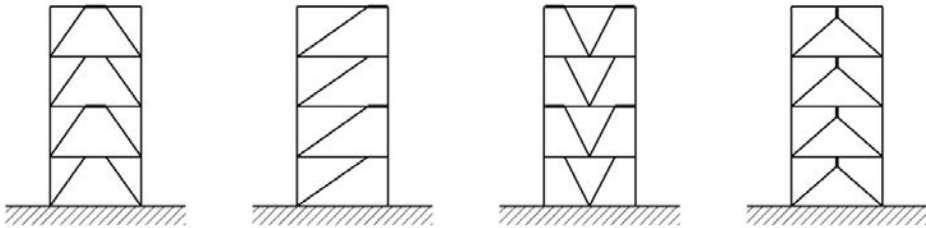


Figure 1. Geometrical configurations of braced bays.

In order to provide a unified design procedure for hybrid MRF-EBF dual systems collapsing with a global mechanism it is needed to start at storey level by applying a local hierarchy criterion needed to assure that yielding occurs in the link elements only while beams, columns and diagonal braces remain in elastic range. In the following, at global level, the Theory of Plastic Mechanism Control (TPMC) has to be applied to prevent undesired partial or storey mechanisms.

TPMC allows the theoretical solution of the problem of designing a structure failing in global mode, i.e. assuring that the yielding involves the dissipative zones only while all the columns, which are the unknown of the design problem, remain in elastic range with the only exception of base sections of first storey columns. Conversely, dissipative members, i.e. link, beam and diagonal sections in case of MRF-EBF dual systems, are assumed as known quantities.

Regarding Eurocode 8, it does not provide specific hierarchy criteria for MRF-EBF dual systems, so that the common design procedure consists in the simple application of the hierarchy criteria suggested for MRFs and for EBFs. In particular, the application rule to design the columns is based on the use of an amplifying factor whose aim is the prevention of yielding or buckling of non-dissipative elements, when the most stressed dissipative zone is yielded and strain-hardened up to its ultimate condition. The design rules suggested by Eurocode 8 are generally able to avoid soft storey mechanisms, but are not able to lead to structures exhibiting a collapse mechanism of global type.

There are a number of reasons why the beam-column hierarchy criterion cannot achieve the above mentioned design goal and these have been widely discussed both with reference to reinforced concrete frames (Panelis and Kappos, 1997) and to steel frames (Mazzolani and

Piluso, 1997). The main reason is that the second principle of capacity design (Engelhardt and Popov, 1989) cannot be easily applied in case of multiple resisting mechanisms not located in series. In fact, according to the second principle of capacity design, non-dissipative zones need to be designed considering the maximum internal actions that the dissipative zones are able to transmit at their ultimate conditions. The beam-column hierarchy criterion is based on the possibility to accurately evaluate, at any beam-to-column joint, the sum of the bending moments which the beams are able to transmit when ultimate conditions occur, but, conversely, because of the shifting of the contraflexure point in columns during the seismic excitation, it is practically impossible to predict how the above sum is shared between the end sections of the top and bottom column converging in the joint (Park, 1986; Mazzolani and Piluso, 1996; Bruneau et al., 2011; Akiyama, 1985; Rosenblueth, 1980; Dowrich, 1977; Paulay and Priestley, 1995; Wakabayashi, 1986; Bertero and Popov, 1977; Lee, 1996). For this reason, it is well known that the beam-column hierarchy criterion, being based on simple joint equilibrium, is only able to prevent “soft storey” mechanisms, but it does not allow the development of a collapse mechanism of global type.

For these reasons, a rigorous design procedure, based on the kinematic theorem of plastic collapse, has been originally presented in 1997 by Mazzolani and Piluso, for MRFs aiming to assure a collapse mechanism of global type where plastic hinges develop at the beam ends only, while all the columns remain in elastic range. Obviously, exception is made for base section of first storey columns, leading to a kinematic mechanism. Starting from this first work, the “Theory of Plastic Mechanism Control” (TPMC) has been outlined as a powerful tool for a unified approach to the seismic design of steel structures (Piluso *et al.*, 2015). It consists on the extension of the kinematic theorem of plastic collapse to the concept of mechanism equilibrium curve. In fact, for any given structural typology, the design conditions to be applied in order to prevent undesired collapse mechanisms can be derived by imposing that the mechanism equilibrium curve corresponding to the global mechanism has to be located below those corresponding to all the other undesired mechanisms up to a top sway displacement level compatible with the local ductility supply of dissipative zones. This design approach was successively extended to MRFs with semi-rigid connections (Montuori and Piluso, 2000), MRFs with RBS connections (Montuori and Piluso, 1999), EB-Frames with horizontal links (i.e. split-K scheme and D-scheme) (Mastrandrea *et al.*, 2003) or with inverted Y scheme (Montuori *et al.*, 2014a; 2014b), knee-braced frames (Conti *et al.*, 2009), dissipative truss-moment frames DTMFs (Longo *et al.*, 2012a; 2012b), MRF-CBF dual systems (Longo *et al.*, 2014), reinforced concrete MR-Frames, structure equipped with friction devices (Montuori *et al.*, 2014c; Piluso *et al.*, 2014) and with HSS (Longo *et al.*, 2014b). Therefore, the application of TPMC to MRF-EBF dual systems, herein presented, completes the whole framework of traditional seismic resistant typologies for steel structures. A number of MRF-EBFs dual systems has been designed by TPMC with the aim to point out, on one hand, the accuracy of the proposed design procedure (TPMC) which assures a global mechanism. In particular, the validation of the proposed design procedure and the comparison in terms of seismic performance have been carried out by means of both push-over analyses and incremental dynamic analyses.

2 PLASTIC MECHANISM TYPOLOGIES

The number of possible collapse mechanisms of eccentrically braced frames is very high, because at each storey yielding can develop in links, beams, columns and diagonal braces depending on the relative flexural strength of members. For this reason, the attention needs to

be preliminarily focused on one-storey structures to derive the design conditions to be satisfied in order to assure that yielding occurs according to the desired collapse mechanism, namely A-type, (Figure 2) while all the other undesired mechanisms namely B-type, C-type and D-type, are avoided. These design conditions can be derived by combining the plastic domain, the normal flow rule, the kinematic compatibility requirements and the kinematic theorem of plastic collapse (Montuori *et al.*, 2014a). The derived hierarchy criteria, are summarized in Table 1 where:

$$M^{(A)} = \frac{M_f + M_w \sqrt{1 - 4 \frac{M_f^2 - M_w^2}{V_p^2 e^2}}}{1 + 4 \frac{M_w^2}{V_p^2 e^2}} \quad \text{and} \quad V^{(A)} = 2 \frac{M_f + M_w \sqrt{1 - 4 \frac{M_f^2 - M_w^2}{V_p^2 e^2}}}{e \left(1 + 4 \frac{M_w^2}{V_p^2 e^2}\right)} \quad (1)$$

$$M_p = f_y W_{pl} \quad \text{and} \quad V_p = f_y t_w (h - t_f) / \sqrt{3} \quad (2)$$

while $V^{(B)}$ is given by:

$$V^{(B)} = \frac{1}{e} \left(\frac{M_f \left(1 - \frac{M_b + M_d}{M_f} \frac{M_w^2}{V_p^2 e^2}\right) + M_w \sqrt{1 - \frac{(M_f + M_b + M_d)^2}{V_p^2 e^2} + \frac{M_w^2}{V_p^2 e^2}}}{1 + \frac{M_w^2}{V_p^2 e^2}} + M_b + M_d \right) \quad (3)$$

for D-scheme,

$$V^{(B)} = \frac{1}{e} \left(\frac{M_f \left(1 - \frac{M_b + M_d}{M_f} \frac{M_w^2}{V_p^2 e^2}\right) + M_w \sqrt{1 - \frac{(M_f + M_b + M_d)^2}{V_p^2 e^2} + \frac{M_w^2}{V_p^2 e^2}}}{1 + \frac{M_w^2}{V_p^2 e^2}} + M_b + M_d \right) \quad (4)$$

for V-scheme and:

$$V^{(B)} = \frac{1}{e} \left(\frac{M_f \left(1 - 2 \frac{M_b}{M_f} \frac{M_w^2}{V_p^2 e^2}\right) + M_w \sqrt{1 - \frac{(M_f + 2M_b)^2}{V_p^2 e^2} + \frac{M_w^2}{V_p^2 e^2}}}{1 + \frac{M_w^2}{V_p^2 e^2}} + 2M_b \right) \quad (5)$$

for Inverted Y-scheme. Finally, $V^{(C)}$ is needed for Inverted Y-scheme only and it is given by:

$$V^{(C)} = \frac{1}{e} \left(\frac{M_f \left(1 - 2 \frac{M_d}{M_f} \frac{M_w^2}{V_p^2 e^2}\right) + M_w \sqrt{1 - \frac{(M_f + 2M_d)^2}{V_p^2 e^2} + \frac{M_w^2}{V_p^2 e^2}}}{1 + \frac{M_w^2}{V_p^2 e^2}} + 2M_d \right) \quad (6)$$

where W_{pl} , M_f and M_w are the plastic modulus, the plastic moment provided by the flanges and the plastic moment provided by the web of a double T profile, respectively. Conversely, M_b and M_d are the plastic moment of the beam and of the diagonal, respectively.

In addition, according to the second principle of capacity design, the hierarchy criteria derived in Table 1, have to be applied by making reference to the ultimate domain rather than to the plastic domain of the link. To this scope, a non-homothetic expansion of the plastic domain (Figure 3) is obtained by considering an ultimate value of the bending moment resulting from an overstrength factor equal to 1.20 and an ultimate shear obtained by means of an overstrength factor equal to 1.50 (Montuori *et al.*, 2014a).

Table 1. Design conditions to avoid undesired mechanisms.

EBFs configuration	Short link $e \leq 1.6 \frac{M_p}{V_p}$	Intermediate link $1.6 \frac{M_p}{V_p} \leq e \leq 3 \frac{M_p}{V_p}$	Long link $e \geq 3 \frac{M_p}{V_p}$
	$\frac{V_p e}{2} \leq M_b + M_d$	$M^{(A)} \leq M_b + M_d$	$M_p \leq M_b + M_d$
	No condition	$V^{(A)} \leq V^{(B)}$	$M_p \leq M_b + M_d$
	No condition	$2V^{(A)} \leq V^{(B)}$	$M_p \leq M_b + M_d$
	$\frac{V_p e}{2} \leq M_b + M_d$	$V^{(A)} \leq V^{(B)}$ $V^{(A)} \leq V^{(C)}$ $M^{(A)} \leq M_b + M_d$	$M_p \leq 2M_b$ $M_p \leq 2M_d$ $M_p \leq M_b + M_d$

	DESIRED MECHANISM	UNDESIRED MECHANISMS		
	A-Type	B-Type	C-Type	D-Type
K-Scheme		NOT DEVELOPS	NOT DEVELOPS	
D-Scheme			NOT DEVELOPS	NOT DEVELOPS
V-Scheme			NOT DEVELOPS	NOT DEVELOPS
Inverted Y-Scheme				

Figure 1. Mechanism typologies for one-storey EB-Frames considering the interaction between moment and shear.

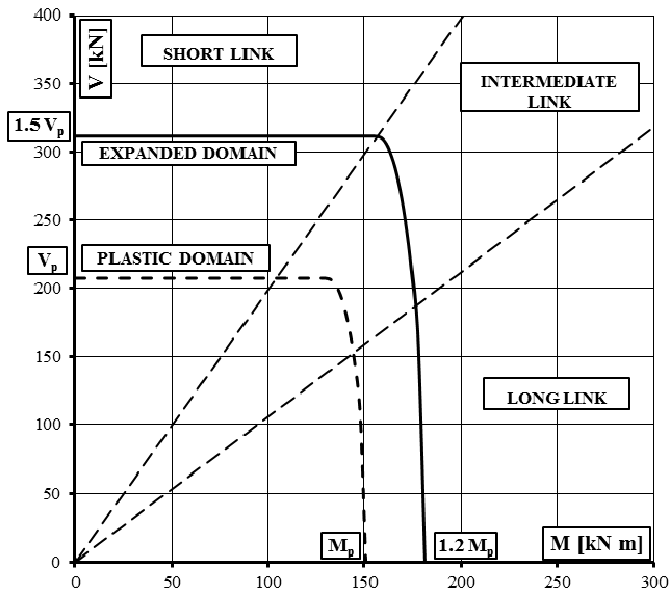


Figure 2. M-V interaction domain (reference is made, as an example to a HEB 200 section with steel grade S235).

In case of multi-storey MRF-EBF dual systems, dealing with the overall behaviour of the structure and provided that the A-type mechanism at storey level is assured by imposing the design requirement given in Table 1, collapse mechanisms can be considered as belonging to three main typologies depicted in Figure 4. Type-1, type-2 and type-3 mechanisms have to be considered undesired, because they do not involve all the dissipative zones.

The global mechanism, which represents the design goal, is always a particular case of type-2 mechanism involving all the storeys. However, in the case of MRF-EBF dual systems with horizontal links also type-1 mechanism becomes coincident with the global mechanism when the mechanism index i_m is equal to the number of storey n_s . This peculiarity, is of paramount importance for the development of TPMC in closed form solution.

Another difference between the case of horizontal links and the case of vertical links is that, in the first case, both type-1 and type-3 mechanisms do not exhibit plastic hinges at the top end of the i_m -th storey, as it occurs in the case of vertical links, but at the column base of $i_m + 1$ storey. Finally, it is important to observe that, diagonal members, are hinged at their bases so that they remain in elastic range when A-type mechanism at storey level is assured.

Given the above, from the overall point of view, TPMC needs to be applied to assure the development of a global type mechanism. The design problem consists in the evaluation of the column sections required at each storey to assure the desired collapse mechanism, whereas beam, diagonal and link sections are assumed as known properties.

The operative steps for the application of TPMC are herein given for structures with either horizontal or vertical links.

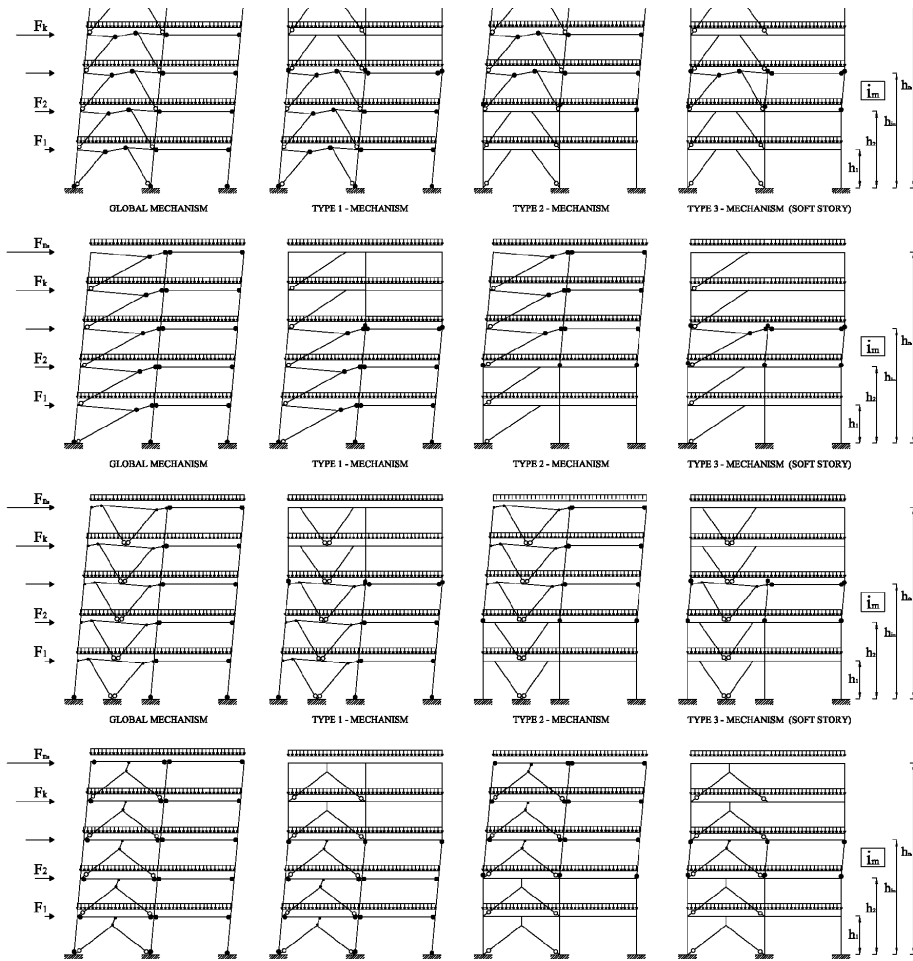


Figure 3. Collapse mechanism typologies for MRF-EBF dual systems when A-type is assured.

3 DESIGN OF LINKS

According to the first principle of capacity design, links are preliminarily designed to withstand the internal actions due to the design seismic shear acting at the storey level. Regarding the rate of seismic action the braced part has to bear, ASCE 7-10 requires for a dual system that the moment frames shall be capable of resisting at least 25 percent of the design seismic forces while the remaining part is entrusted to the EBF.

In the case of EBFs with vertical links, the design shear action in the links is immediately derived as the rate of the seismic shear that the designer intends to entrust to the braced bay. Conversely, in the case of EBFs with horizontal links, the design internal action can be computed by means of the approximate equilibrium equation around point A of Figure 5 applied at each storey.

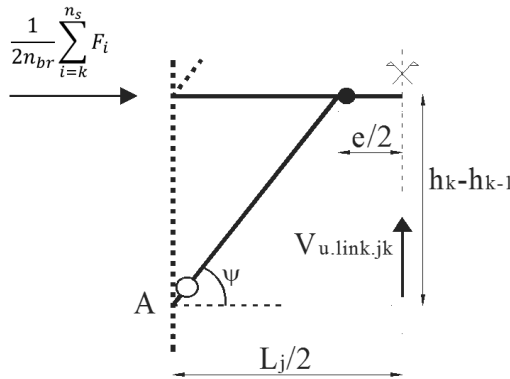


Figure 4. Estimation of link design shear.

This equilibrium is carried out on the basis of the following assumptions (Kasai and Han, 1997a): the link member is subjected to a bi-triangular diagram of bending moment with zero value at midspan; the bending moment at the column bottom end is negligible. Therefore, the following design formulas are obtained for horizontal and vertical link, respectively:

$$V_{link.Sd} = \frac{1}{n_{br}} \frac{\sum_{i=k}^{n_s} F_i}{L_j} (h_k - h_{k-1}) \leq V_{link.Rd} \quad (7)$$

$$V_{link.Sd} = \frac{1}{n_{br}} \sum_{i=k}^{n_s} F_i \leq V_{link.Rd} \quad (8)$$

where F_i is the rate of the storey seismic horizontal force entrusted to the braced bays, L_j is the length of the j -th bay, $V_{link.Rd}$ is the link shear resistance at k -th storey, and n_{br} is the number of braced bays.

4 DESIGN OF BEAMS AND DIAGONALS

According to the second principle of capacity design, non-dissipative zones need to be designed considering the maximum internal actions which the dissipative zones are able to transmit in their fully yielded and strain-hardened state. For this reason, in order to account for the significant strain-hardening occurring in link elements (Engelhardt and Popov, 1989; Hera Publication, 2013) reference is made to an overstrength equal to 50% in case of shear links and to an overstrength equal to 20% in case of long links, according to the following equations:

$$V_u = 1.5 f_y t_w (h - t_f) / \sqrt{3} \quad (9)$$

$$M_u = 1.2 f_y W_{pl} \quad (10)$$

$$M_{fu} = 1.2 f_y b_f t_f (h - t_f) \quad (11)$$

$$M_{wu} = M_u - M_{fu} \quad (12)$$

where W_{pl} is the plastic modulus of the link section, h is the height, b_f and t_f are the flange width and thickness, respectively, t_w is the web thickness and f_y is the yield strength of steel.

In order to account for the influence of the link length on their plastic behaviour, the concept of equivalent plastic bending moment is used. It allows the development of rigid-plastic analyses accounting for moment-shear interaction, so that short, intermediate and long links can be properly modelled. The equivalent moment (Montuori *et al.*, 2014a; 2014b) accounts for the mechanical behaviour of the link as short, intermediate or long, according to the classification reported in Eurocode 8 (CEN, 2004). It allows the modelling of the link as an element with plastic hinge in simple bending, with the scope to write the internal work simply as the product between the equivalent plastic moment and the equivalent plastic rotation, even in the case of moment-shear interaction. By means of this approach, the virtual internal work can be written as:

$$W_i^{link} = 2M_{eq} \frac{\theta L_j}{e} \quad (13)$$

$$W_i^{link} = 2M_{eq} \frac{\theta H_i}{e} \quad (14)$$

for EBFs with horizontal and vertical link, respectively; where H_i and θ are the interstorey height and the plastic rotation at beam ends, respectively, and M_{eq} is the equivalent plastic moment of the link for the desired mechanism, accounting for the influence of the link length, given by (Montuori *et al.*, 2014a; 2014b):

$$M_{eq}^{(short)} = \frac{V_u e}{2} \quad (15)$$

$$M_{eq}^{(intermediate)} = \frac{M_{fu} + M_{wu} \sqrt{1 - 4 \frac{M_{fu}^2 - M_{wu}^2}{V_u^2 e^2}}}{1 + 4 \frac{M_{wu}^2}{V_u^2 e^2}} \quad (16)$$

$$M_{eq}^{(long)} = M_u \quad (17)$$

where V_u and M_u denote the ultimate shear resistance and the ultimate moment resistance, respectively, and e denotes the link length.

The beam and the brace sections are preliminarily designed to assure that, at each storey, yielding occurs in the link only, i.e. by imposing the design requirements given in Table 1. In this way, only A-type mechanism can develop. In addition, it is required that beam sections have to resist also vertical loads according to the load combinations provided by the seismic code. Finally, beam-to-column connections in the structural modelling are assumed as rigid full-strength connections.

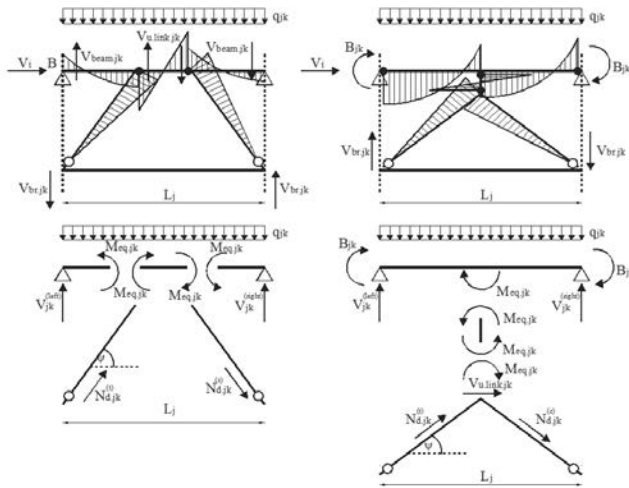


Figure 5. Bending moment diagram in beam, link and diagonal braces in ultimate conditions and corresponding free body internal actions.

Regarding the axial forces occurring in the diagonal braces in the ultimate conditions, according to the second principle of capacity design, they can be derived from the knowledge of the maximum shear force, $V_{u.link,jk}$, which the link is able to transmit (Figure 5).

In the case of horizontal link, the axial load acting in the diagonals when the global mechanism is completely developed can be obtained by means of the equilibrium equation around point B, as suggested by Kasai and Han (1997a), (Kasai and Popov, 1986; Kasai and Han, 1997b). Therefore, with reference to the j -th bay and the k -th storey, the axial force in the tensile $N_{d,jk}^{(t)}$ and compressed $N_{d,jk}^{(c)}$ diagonal are given by:

$$N_{d,jk}^{(t)} = N_{d,jk}^{(c)} = \frac{V_{u.link,jk} L_j}{2(h_k - h_{k1}) \cos \psi} \quad (18)$$

In the case of vertical links the axial force in the tensile $N_{d,jk}^{(t)}$ and compressed $N_{d,jk}^{(c)}$ diagonal are given by:

$$N_{d,jk}^{(t)} = N_{d,jk}^{(c)} = \frac{V_{u.link,jk}}{2 \cos \psi} \quad (19)$$

As a consequence, the section of diagonal braces has to be selected in order to comply with in-plane stability check under the action of the bending moment $M_{d,jk}$ derived from Table 1, needed to avoid local undesired mechanisms at the storey level and an axial load given by Eq. (18) or Eq. (19). Moreover, resistance against out-plane buckling under the axial force given by Eq. (18) or Eq. (19) needs also to be checked.

5 COLUMN AXIAL FORCES AT COLLAPSE

The design of the column sections requires the knowledge of the flexural resistance needed to avoid the undesired collapse mechanisms. This flexural resistance is obtained by means of TPMC. However, such flexural resistance is the required plastic moment reduced due to the

contemporary action of the axial load. Therefore, in order to design the column sections also the axial loads acting in the columns at collapse, i.e. when the global mechanism is completely developed, are required. In the following, the relation for the computation of axial loads acting at the collapse state are reported for EBFs with horizontal link or vertical link.

- EBFs with horizontal links

The value of the axial load acting in the columns when the global mechanism is completely developed can be obtained by means of simplified equilibrium equations, as suggested by Kasai and Han (1997a; 1997b). In Figure 6 the corresponding simplified schemes are reported. According to capacity design the internal actions are calculated on the basis of the maximum shear force (i.e. the ultimate shear $V_{u.link.jk}$) that the link in the fully yielded and strain-hardened condition, is able to transmit. In particular, with reference to Figure 6, by assuming that the bending moment at the beam ends and at the bottom end of braces is negligible, the vertical equilibrium equation provides:

$$V_{jk}^{(left)} = N_{d.jk} \sin\psi - V_{u.link.jk} + \frac{q_{jk}L_j}{2} \tag{20}$$

$$V_{jk}^{(right)} = -N_{d.jk} \sin\psi + V_{u.link.jk} + \frac{q_{jk}L_j}{2} \tag{21}$$

So that, the vertical equilibrium provides the following relationship (Figure 6):

$$N_{c.ik} = \sum_{m=k}^{n_s} (V_{i-1,m}^{(right)} + V_{i,m}^{(left)}) + \sum_{m=k+1}^{n_s} (N_{d.i-1,m} \sin\psi_{i-1,m} - N_{d.i,m} \sin\psi_{i,m}) \tag{22}$$

Eq. (22) provides the axial load at the collapse state, $N_{c.ik}$, for each column.

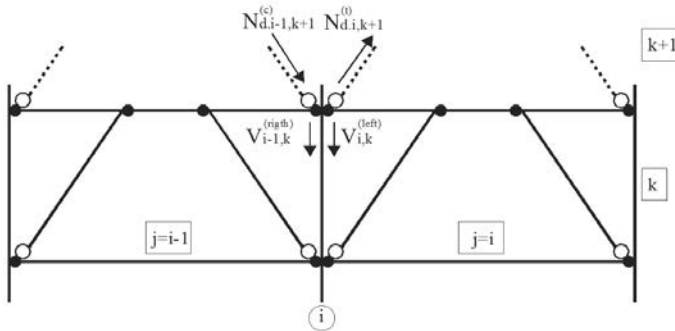


Figure 6. Evaluation of column axial forces at collapse for EBFs with horizontal links

- EBFs with vertical links

The value of the axial load acting in the columns when the global mechanism is completely developed can be obtained as the sum of the shear forces transmitted by the adjacent beams at and above the considered storey and of the vertical components of the axial forces in the diagonal braces above the considered storey.

With reference to the j -th beam of the k -th storey, the shear force transmitted by the beam to the columns at collapse can be easily derived as (Figure 7):

$$V_{jk} = V_{q,jk} \pm V_{M,jk} = \frac{q_{jk}l_j}{2} \pm \frac{B_{i,k} + M_{eq,jk}/2}{L_j/2} \tag{23}$$

where the sign plus is valid for $V_{jk}^{(right)}$ and the sign minus is valid for $V_{jk}^{(left)}$; $B_{j,k}$ is the beam plastic moment; $M_{eq,jk}$ is the link equivalent plastic moment accounting for moment-shear interaction when needed and L_j is the bay span. The vertical component of the axial force in the diagonal braces is given by:

$$V_{br,jk} = \frac{V_{u,link,jk}}{2} tg\psi \tag{24}$$

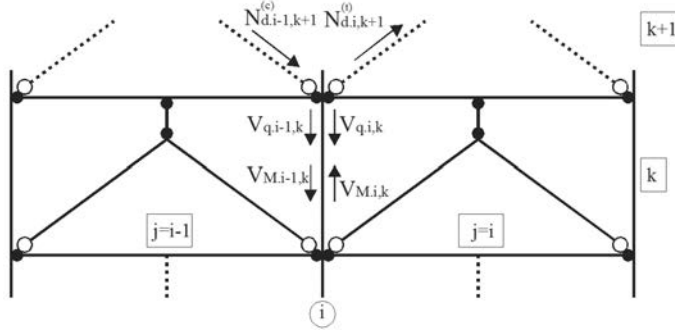


Figure 7. Evaluation of column axial forces at collapse for EBFs with vertical links.

Therefore, the axial load acting at collapse state in the i -th column of the k -th storey, being $j = i - 1$ and $j = i$ the adjacent bays, can be computed as (Figure 7):

$$N_{c,ik} = \sum_{m=k}^{n_s} (V_{q,i-1,m} + V_{q,i,m}) + \sum_{m=k}^{n_s} (V_{M,i-1,m} - V_{M,i,m}) + \sum_{m=k+1}^{n_s} (V_{br,i-1,m} - V_{br,i,m}) \tag{25}$$

being the first sum representative of the contribution due to the uniform loads acting on the beams, namely $N_{q,ik}$, the second sum the contribution due to the bending moment transmitted by the link to the beam and to the bending moments at the beam ends, namely $N_{M,ik}$ and the third sum the contribution due to the actions transmitted by the diagonal braces, namely $N_{br,ik}$. Obviously, the design of the column sections has to be carried out considering, for each column, the most severe axial load deriving from both positive and negative direction of seismic horizontal forces.

6 EQUILIBRIUM CURVES OF THE ANALYSED PLASTIC MECHANISMS

The Theory of Plastic Mechanism Control (TPMC) (Mazzolani and Piluso, 1997; Piluso *et al.*, 2015), which has the primary aim to assure the development of a collapse mechanism of global type, is based on the kinematic theorem of plastic collapse and on second order rigid-plastic analysis. The design problem is constituted by the definition of the column sections required at each storey to assure the desired collapse mechanism, whereas beam, brace and link sections are assumed as known properties designed by means of the relationships reported in the previous paragraphs.

TPMC is based on the extension of the kinematic theorem of plastic collapse to the concept of mechanism equilibrium curve. Therefore, it accounts also for the influence of second order effects in plastic range that cannot be neglected in the seismic design of steel structures.

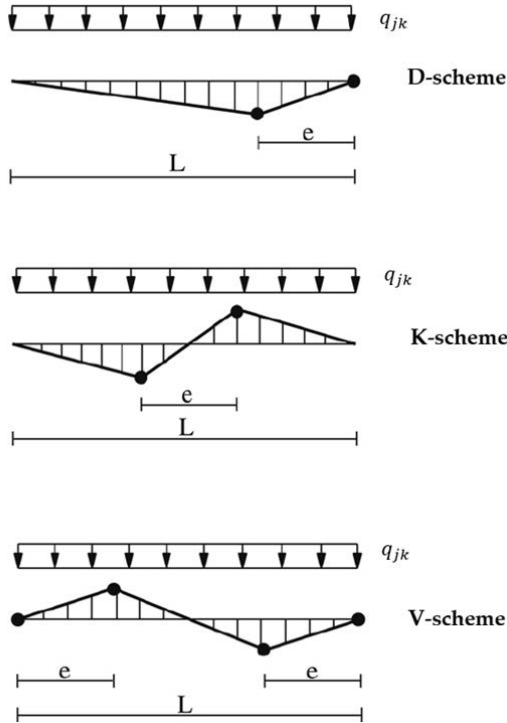


Figure 8. Vertical displacement diagram of horizontal members.

In particular, the plastic section modulus of each column has to be defined by imposing that the mechanism equilibrium curve corresponding to the global mechanism, i.e. the desired mechanism, has to be located below those corresponding to all the undesired mechanisms within a displacement range compatible with the local ductility supply of members. It means that, according to the upper bound theorem, the true collapse mechanism is the global mechanism. Collapse mechanism equilibrium curves can be obtained by applying the virtual work principle, i.e. by equating the virtual internal work and virtual external work including second order effects.

With reference to the global mechanism, the external work due to a virtual rotation $d\theta$ of column plastic hinges is given by:

$$W_e = \alpha \sum_{k=1}^{n_s} F_k h_k d\theta + \frac{\delta}{h_{n_s}} \sum_{k=1}^{n_s} V_k h_k d\theta + \sum_{k=1}^{n_s} \sum_{j=1}^{n_b} W_{q,jk} d\theta \tag{26}$$

where α is the multiplier of horizontal forces, F_k and h_k are, respectively, the seismic force applied at k -th storey and the k -th storey height with respect to the foundation level, h_{n_s} is the value of h_k for the top storey, δ is the top sway displacement and V_k is the total vertical load

acting at k-th storey. The first term of Eq. (26) represents the external work due to seismic horizontal forces, the second term is the second order work due to vertical loads (Mazzolani and Piluso, 1997) while the third term is the virtual external work due to the uniform loads acting on the beams. Therefore, $W_{q,jk}$ represents the external work due to the uniform loads acting on the beam of j-th bay of k-th storey, for $d\theta = 1$. In particular, regarding unbraced bays, it is assumed that $q_{jk} \leq 4M_{b,jk}/L_j^2$ which assures that plastic hinges develops at beam ends only (Mazzolani and Piluso, 1997). Conversely, this work is delivered in Table 2 for the different bay configurations and it is different to zero only for the D-scheme (Figure 9). As regards the quantities reported In Table 2, $M_{b,jk}$ is the beam plastic moment of j-th bay of the k-th storey, L_j is the bay span, e_{jk} is the link length at j-th bay of k-th storey and $M_{eq,jk}$ is the corresponding equivalent bending moment accounting for moment-shear interaction. The internal work due to a virtual rotation $d\theta$ of column plastic hinges can be written as:

$$W_i = \left(\sum_{k=1}^{n_c} M_{c.i1} + \sum_{k=1}^{n_s} \sum_{j=1}^{n_b} W_{d,jk} \right) d\theta \tag{27}$$

where $M_{c.ik}$ is the plastic moment of i-th column of k-th storey (k=1 in this case) reduced due to the contemporary action of the axial force; $W_{d,jk}$ is the internal work due to the dissipative zones located in the j-th bay of k-th storey, to be evaluated depending on the bay configuration as delivered in Table 2; n_c , n_b and n_s are the number of columns, bays and storeys, respectively.

Table 2. Internal and external work evaluation for different bay configurations.

Structural typology	$W_{d,jk}$	$W_{q,jk}$
Unbraced	$2M_{b,jk}$	0
K-scheme braced	$2 M_{eq,jk} L_j/e_{jk}$	0
D-scheme braced	$2 M_{eq,jk} L_j/e_{jk}$	$q_{jk}L_j(L_j - e_{jk})/2$
V-scheme braced	$4 M_{eq,jk} L_j/e_{jk}$	0
Inverted Y-scheme braced	$2 M_{eq,jk} (h_k - h_{k-1})/e_{jk}$	0

*in case of unbraced bays of V-scheme $W_{d,jk} = 0$ and $W_{q,jk} = 0$ for $k=i_m$ and $t=1$ or $t=3$

By equating the internal work to the external one, the mechanism equilibrium curve can be always expressed as:

$$\alpha = \alpha_0 - \gamma\delta \tag{28}$$

where α_0 is the kinematically admissible multiplier of horizontal forces according to first order rigid-plastic analysis and γ is the slope of the mechanism equilibrium curve.

In the case of global mechanism, the kinematically admissible multiplier α_0 of horizontal forces is given by:

$$\alpha_0 = \alpha_0^{(g)} = \frac{\sum_{i=1}^{n_c} M_{c.i1} + \sum_{k=1}^{n_s} \sum_{j=1}^{n_b} (W_{d,jk} - W_{q,jk})}{\sum_{k=1}^{n_s} F_k h_k} \tag{29}$$

while the slope of the mechanism equilibrium curve γ is the same given by (Mazzolani and Piluso, 1997):

$$\gamma = \gamma^{(g)} = \frac{1}{h_{ns}} \frac{\sum_{k=1}^{n_s} V_k h_k}{\sum_{k=1}^{n_s} F_k h_k} \quad (30)$$

It is important to point out that the above equations (29) and (30) are valid for MRFs and for either EBFs or MRF-EBF dual systems independently of the brace configuration.

6.1 First order kinematically admissible multipliers

As already underlined, the mechanism equilibrium curves are given by Eq. (30) where α_0 is the kinematically admissible multiplier of horizontal forces derived according to the classical first order rigid-plastic analysis. Such multiplier is provided in this Section for type-1, type-2 and type-3 mechanisms considering both the case of vertical links and the case of horizontal links. With reference to i_m -th mechanism of type-1, in the case of vertical links (i.e. inverted Y-scheme), the following relationship is obtained

$$\alpha_{0.i_m}^{(1)} = \frac{\sum_{i=1}^{n_c} M_{c.i1} + \sum_{i=1}^{n_c} M_{c.ii_m} + \sum_{k=1}^{i_m} \sum_{j=1}^{n_b} W_{d.jk}}{\sum_{k=1}^{i_m} F_k h_k + h_{i_m} \sum_{k=i_m+1}^{n_s} F_k} \quad (31)$$

which is valid for $i_m = 1, 2, \dots, n_s$. It is useful to note that for $k = i_m$ the work of the dissipative zones $W_{d.jk}$ is due to the link only being $W_{d.ji_m} = 0$ for the unbraced bays.

In the case of schemes with horizontal links, the i_m -th kinematically admissible multipliers is given by:

$$\alpha_{0.i_m}^{(1)} = \frac{\sum_{i=1}^{n_c} M_{c.i1} + \sum_{i=1}^{n_c} M_{c.ii_m+1} + \sum_{k=1}^{i_m} \sum_{j=1}^{n_b} W_{d.jk} - \sum_{k=1}^{i_m} \sum_{j=1}^{n_b} W_{q.jk}}{\sum_{k=1}^{i_m} F_k h_k + h_{i_m} \sum_{k=i_m+1}^{n_s} F_k} \quad (32)$$

which is valid for $i_m = 1, 2, \dots, n_s - 1$. This difference is due to the fact that, in the case of vertical links, the columns involved in the collapse mechanism are those of the first storey and those of i_m th storey while, in case of horizontal links, the involved columns are those of the first and $(i_m + 1)$ th storey.

With reference to the i_m -th mechanism of type-2, the kinematically admissible multiplier is given by:

$$\alpha_{0.i_m}^{(2)} = \frac{\sum_{i=1}^{n_c} M_{c.ii_m} + \sum_{k=i_m}^{n_s} \sum_{j=1}^{n_b} (W_{d.jk} - W_{q.jk})}{\sum_{k=i_m}^{n_s} F_k (h_k - h_{i_m-1})} \quad (33)$$

This equation is valid for $i_m = 1, 2, \dots, n_s$. In addition, it is valid for any link location, i.e. both in the case of vertical links and in the case of horizontal links. However, it has to be remembered that in case of vertical links $W_{q.jk} = 0$ is obtained.

Finally, with reference to the i_m -th mechanism of type-3, the following relationship is obtained in the case of vertical links:

$$\alpha_{0.i_m}^{(3)} = \frac{2 \sum_{i=1}^{n_c} M_{c.ii_m} + \sum_{j=1}^{n_b} W_{d.ji_m}}{(h_{i_m} - h_{i_m-1}) \sum_{k=i_m}^{n_s} F_k} \quad (34)$$

which is valid for $i_m = 1, 2, \dots, n_s$ while, in the case of horizontal links, it results:

$$\alpha_{0,i_m}^{(3)} = \frac{\sum_{i=1}^{n_c} M_{c,i i_m} + \sum_{i=1}^{n_c} M_{c,i i_m+1} + \sum_{j=1}^{n_b} (W_{d,j i_m} - W_{q,j i_m})}{(h_{i_m} - h_{i_m-1}) \sum_{k=i_m}^{n_s} F_k} \quad (35)$$

which is valid for $i_m = 1, 2, \dots, n_s - 1$ while, for the specific case of $i_m = n_s$

$$\alpha_{0,n_s}^{(3)} = \frac{\sum_{i=1}^{n_c} M_{c,i n_s} + \sum_{j=1}^{n_b} W_{d,j n_s} - \sum_{j=1}^{n_b} W_{q,j n_s}}{F_{n_s} (h_{n_s} - h_{n_s-1})} \quad (36)$$

is obtained.

It is useful to underline that, in the case of type-3 mechanism, while in the case of vertical links the columns involved in the collapse mechanisms are those of i_m th storey only, conversely both i_m th and $(i_m + 1)$ th storey columns are involved in the case of horizontal links.

6.2 Slope of mechanism equilibrium curves

The slope of the linearized mechanism equilibrium curves is related to the ratio between the second-order external work due to the gravity loads acting on the structure and the external work due to the seismic horizontal forces. These works are not affected by the structural scheme. Therefore, they are independent of the structural typology while are affected by the magnitude of the gravity loads and by the collapse mechanism typology. For any structural scheme the following relationships are derived:

$$\gamma_{i_m}^{(1)} = \frac{1}{h_{i_m}} \frac{\sum_{k=1}^{i_m} V_k h_k + h_{i_m} \sum_{k=i_m+1}^{n_s} V_k}{\sum_{k=1}^{i_m} F_k h_k + h_{i_m} \sum_{k=i_m+1}^{n_s} F_k} \quad (37)$$

$$\gamma_{i_m}^{(2)} = \frac{1}{h_{n_s} - h_{i_m-1}} \frac{\sum_{k=i_m}^{n_s} V_k (h_k - h_{i_m-1})}{\sum_{k=i_m}^{n_s} F_k (h_k - h_{i_m-1})} \quad (38)$$

$$\gamma_{i_m}^{(3)} = \frac{1}{h_{i_m} - h_{i_m-1}} \frac{\sum_{k=i_m}^{n_s} V_k}{\sum_{k=i_m}^{n_s} F_k} \quad (39)$$

for type-1, type-2 and type-3 mechanism, respectively.

For any given geometry of the structural system, the slope of mechanism equilibrium curve attains its minimum value when the global type mechanism is developed. This issue assumes a paramount importance in TPMC allowing to exploit the extension of the kinematic theorem of plastic collapse to the concept of mechanism equilibrium curve.

6.3 Column design requirements to prevent undesired collapse mechanisms

The design conditions that column sections have to satisfy in order to prevent the undesired failure modes are derived by imposing that the mechanism equilibrium curve corresponding to the global mechanism has to be located below those corresponding to all the undesired mechanisms within a top sway displacement range, δ_u , compatible with the ductility supply of dissipative zones, i.e. the plastic rotation of members which govern the design procedure; therefore:

$$\alpha_0^{(g)} - \gamma^{(g)} \delta_u \leq \alpha_{i_m}^{(t)} - \gamma_{i_m}^{(t)} \delta_u \quad \text{for } i_m = 1, 2, 3, \dots, n_s \quad t = 1, 2, 3 \quad (40)$$

Such equation constitutes the statement of the Theory of Plastic Mechanism Control (Piluso et al., 2015) and it is valid independently of the structural typology. It is based on the kinematic theorem of plastic collapse, extended to the concept of mechanism equilibrium curve.

Regarding the ultimate displacement, it has to be observed that dissipative zones in MRF-EBF dual systems are both the beam ends and the link members, so that the ultimate design displacement has to be selected as the minimum among those corresponding to the attainment of either beam or link rotation capacity. With reference to the life safety limit state, the ultimate plastic rotation of links, γ_u , is assumed equal to 0.08 rad for short links and 0.02 rad for long links while an interpolation between these two values is applied for intermediate links. The plastic rotation capacity of beams is assumed equal to 0.04 rad. However, because of the influence of the structural geometry the link capacity always governs the ultimate design displacement which can be obtained by means of the following relations:

$$\delta_u = \min \left\{ \gamma_u \frac{e_{jk}}{L_j} h_{n_s} \right\} \quad j = 1, 2, \dots, n_b \quad k = 1, 2, \dots, n_s \quad (41)$$

in the case of horizontal links and K-scheme or D-scheme,

$$\delta_u = \min \left\{ \gamma_u \frac{2e_{jk}}{L_j} h_{n_s} \right\} \quad j = 1, 2, \dots, n_b \quad k = 1, 2, \dots, n_s \quad (42)$$

in the case of horizontal links and V-scheme and

$$\delta_u = \min \left\{ \gamma_u \frac{e_{jk}}{h_k - h_{k-1}} h_{n_s} \right\} \quad j = 1, 2, \dots, n_b \quad k = 1, 2, \dots, n_s \quad (43)$$

in the case of inverted Y-scheme with vertical links.

6.4 Design procedure for plastic mechanism control

The application of the Theory of Plastic Mechanism Control (TPMC) consists in the solution of the design requirements expressed by Eq. (40). This solution was originally carried out by means of an iterative procedure (Mazzolani and Piluso, 1997) requiring the development of specific computer programs. However, with reference to moment resisting frames (Piluso et al., 2015), it has been successively pointed out that a closed form solution can be provided. Such advances in the theory of plastic mechanism control are herein exploited to identify the most appropriate design procedure for the plastic mechanism control of MRF-EBF dual systems.

According to the first principle of capacity design, it is assumed that dissipative zones are preliminarily designed to withstand the internal actions resulting from the design seismic forces and the gravity loads occurring in the seismic load combination ($F_d = G_k + \psi_2 Q_k + E$ according to Eurocode 8). Such design can be carried out by distributing the resistance of dissipative zones among the different storeys according to the storey seismic shear distribution, as suggested in (Piluso et al., 2015), and by establishing the sharing of the seismic shear between the moment resisting part and the eccentrically braced part of the structural scheme.

Successively, the columns are designed to be non dissipative zones according to the second principle of capacity design. To this scope, TPMC is applied by means of the following steps:

- a) Selection of a design top sway displacement δ_u compatible with the ductility supply of structural members (Equations (41)41-43)).

- b) Computation of the slopes of mechanism equilibrium curves $\gamma_{i_m}^{(t)}$ by means of Eqs. (37), (38) and (39). The slope of the global mechanism equilibrium curve, $\gamma^{(g)}$, is provided by Eq. (30) and it is the minimum among the $\gamma_{i_m}^{(t)}$ values computed before.
- c) Computation of the axial load acting in the columns at collapse state, i.e. when a collapse mechanism of global type is completely developed (Eq. (18-19) Eq. (22)) depending on the structural scheme).
- d) Computation of the required sum of plastic moment of first storey columns, reduced due to the contemporary action of the axial load ($N_{c.i1}$). This computation is carried out by observing that, for $i_m = 1$, mechanism type-2 is coincident with the global mechanism and, in addition, type-1 and type-3 mechanisms are coincident (soft-storey mechanism at first storey). Therefore, for $i_m = 1$, Eq. (40) provides only one design condition to be satisfied.

In the case of vertical links (i.e. inverted Y-scheme) only the first storey columns are involved, so that the following design requirement is obtained:

$$\sum_{i=1}^{n_c} M_{c.i1} \geq \frac{\sum_{k=1}^{n_s} \sum_{j=1}^{n_b} W_{d.jk} + (\gamma_1^{(3)} - \gamma^{(g)}) \delta_u \sum_{k=1}^{n_s} F_k h_k - \frac{\sum_{k=1}^{n_s} F_k h_k}{h_1 \sum_{k=1}^{n_s} F_k} \sum_{j=1}^{n_b} W_{d.j1}}{2 \frac{\sum_{k=1}^{n_s} F_k h_k}{h_1 \sum_{k=1}^{n_s} F_k} - 1} \quad (44)$$

where $W_{q.jk}=0$ has been taken into account.

Conversely in the case of structures with horizontal links (K-scheme, D-scheme and V-scheme), it is easy to recognize that, for $i_m = 1$, the only one design requirement resulting from Eq. (40) involves both the first storey columns and the second storey columns. Therefore, by introducing the parameter:

$$\psi = \frac{\sum_{i=1}^{n_c} M_{c.i2}}{\sum_{i=1}^{n_c} M_{c.i1}} \quad (45)$$

i.e. the ratio between the overall flexural resistance of second order storey columns and the overall flexural resistance of first storey columns, the following design requirement is obtained:

$$\sum_{i=1}^{n_c} M_{c.i1} \geq \frac{\sum_{k=1}^{n_s} \sum_{j=1}^{n_b} (W_{d.jk} - W_{q.jk}) + (\gamma_1^{(3)} - \gamma^{(g)}) \delta_u \sum_{k=1}^{n_s} F_k h_k - \frac{\sum_{k=1}^{n_s} F_k h_k}{h_1 \sum_{k=1}^{n_s} F_k} \sum_{j=1}^{n_b} (W_{d.j1} - W_{q.j1})}{(1 + \psi) \frac{\sum_{k=1}^{n_s} F_k h_k}{h_1 \sum_{k=1}^{n_s} F_k} - 1} \quad (46)$$

As the second storey columns cannot be greater than those of first storey, the parameter ψ can be initially selected according to the limitation $\psi \leq 1$. Eq. (46) shows that the minimum first storey column sections are obtained for $\psi = 1$. Therefore, in case of horizontal links a preliminary design of first storey columns is carried out by means of Eq. (46) with $\psi = 1$.

- e) The sum of the required plastic moments of columns at first storey is distributed among the columns so that, the design internal actions ($M_{c.i1}, N_{c.i1}$ for $i = 1, 2, \dots, n_c$) are derived and the column sections at first storey can be designed. As column sections are selected from standard shapes, the value obtained of $\sum_{i=1}^{n_c} M_{c.i1}$, namely $\sum_{i=1}^{n_c} M_{c.i1}^*$ is generally greater than the required minimum value provided by Eq. (44) or Eq. (46). Therefore, the mechanism equilibrium curve $\alpha = \alpha_0^{(g)} - \gamma^{(g)} \delta$ has to be evaluated accordingly, i.e. by

means of Eq. (28) by replacing the term $\sum_{i=1}^{n_c} M_{c,i,1}$, with the value $\sum_{i=1}^{n_c} M_{c,i,1}^*$ resulting from standard shapes. In addition, the multiplier of seismic horizontal forces corresponding to the ultimate design displacement can be computed as $\alpha^{(g)} = \alpha_0^{(g)} - \gamma^{(g)} \delta_u$.

- f) As soon as the first storey columns have been designed according to the previous steps, so that $\sum_{i=1}^{n_c} M_{c,i,1} = \sum_{i=1}^{n_c} M_{c,i,1}^*$ is a known quantity, the columns of the upper storeys can be designed by applying Eq. (40). In particular, the column sections required to prevent partial mechanisms belonging to type-1 are derived, in the case of vertical links (i.e. inverted Y-scheme), according to the following relationship obtained from Eq. (40) with $t=1$:

$$\sum_{i=1}^{n_c} M_{c,i,i_m}^{(1)} \geq \left(\alpha^{(g)} + \gamma_{i_m}^{(1)} \delta_u \right) \left(\sum_{k=1}^{i_m} F_k h_k + h_{i_m} \sum_{k=i_m+1}^{n_s} F_k \right) - \sum_{i=1}^{n_c} M_{c,i,1}^* - \sum_{k=1}^{i_m} \sum_{j=1}^{n_b} W_{d,jk} \quad (47)$$

Where it is useful to remember that, for $k = i_m$, the links of braced bays are actively involved in the collapse mechanism while the beams of unbraced bays are not involved (see endnote of Table 2). Eq. (47) has to be applied for $i_m = 1, 2, \dots, n_s$.

Similarly, in the case of structures with horizontal links, Eq. (40) with $t=1$ provides:

$$\begin{aligned} \sum_{i=1}^{n_c} M_{c,i,i_m+1}^{(1)} \geq & \left(\alpha^{(g)} + \gamma_{i_m}^{(1)} \delta_u \right) \left(\sum_{k=1}^{i_m} F_k h_k + h_{i_m} \sum_{k=i_m+1}^{n_s} F_k \right) - \sum_{i=1}^{n_c} M_{c,i,1}^* - \sum_{k=1}^{i_m} \sum_{j=1}^{n_b} W_{d,jk} \\ & + \sum_{k=1}^{i_m} \sum_{j=1}^{n_b} W_{q,jk} \end{aligned} \quad (48)$$

This relationship has to be applied for $i_m = 1, 2, \dots, n_s - 1$.

The column sections required to prevent partial mechanisms belonging to type-2 are derived by means of Eq. (40) with $t=2$, thus obtaining:

$$\sum_{i=1}^{n_c} M_{c,i,i_m}^{(2)} \geq \left(\alpha^{(g)} + \gamma_{i_m}^{(2)} \delta_u \right) \sum_{k=i_m}^{n_s} F_k (h_k - h_{i_m-1}) - \sum_{k=i_m}^{n_s} \sum_{j=1}^{n_b} W_{d,jk} + \sum_{k=i_m}^{n_s} \sum_{j=1}^{n_b} W_{q,j} \quad (49)$$

Such relationship has to be applied for $i_m = 2, \dots, n_s$ and is valid both for structural schemes with vertical links and structural schemes with horizontal links. The only difference is that, in case of vertical links, $W_{q,jk} = 0$.

Finally, the column sections required at each storey to prevent soft storey mechanisms, i.e. type-3 mechanisms, are obtained by Eq. (40) with $t=3$. In particular, in case of vertical links, the following relationship is obtained:

$$\sum_{i=1}^{n_c} M_{c,i,i_m}^{(3)} \geq \frac{1}{2} \left[\left(\alpha^{(g)} + \gamma_{i_m}^{(3)} \delta_u \right) (h_{i_m} - h_{i_m-1}) \sum_{k=i_m}^{n_s} F_k - \sum_{j=1}^{n_b} W_{d,j,i_m} \right] \quad (50)$$

which has to be applied for $i_m = 2, \dots, n_s$.

In case of horizontal links, the development of a soft storey mechanism at i_m th storey is characterized by the involvement of columns both at i_m th and $(i_m + 1)$ th storey. For this reason, the column section needed to prevent soft storey mechanisms have to be derived starting from the top storey, thus obtaining:

$$\sum_{i=1}^{n_c} M_{c.in_s}^{(3)} \geq (\alpha^{(g)} + \gamma_{n_s}^{(3)} \delta_u) F_{n_s} (h_{n_s} - h_{n_s-1}) - \sum_{j=1}^{n_b} W_{d.jn_s} + \sum_{j=1}^{n_b} W_{q.jn_s} \quad (51)$$

This relationship is obtained from Eq. (40) with $t=3$ and $i_m = n_s$. In addition, it is coincident with the one obtained from Eq. (49) for $i_m = n_s$, because for $i_m = n_s$ type-2 and type-3 mechanism are coincident.

Starting from the top storey, the column sections required to prevent soft-storey mechanisms are derived according to the following relationship:

$$\sum_{i=1}^{n_c} M_{c.ii_m}^{(3)} \geq (\alpha^{(g)} + \gamma_{i_m}^{(3)} \delta_u) (h_{i_m} - h_{i_m-1}) \sum_{k=i_m}^{n_s} F_k - \sum_{i=1}^{n_c} M_{c.ii_m+1}^{(3)} - \sum_{j=1}^{n_b} W_{d.ji_m} + \sum_{j=1}^{n_b} W_{q.ji_m} \quad (52)$$

This relationship, derived from Eq. (40) with $t=3$, has to be applied for $i_m = n_s - 1, n_s - 2, \dots, 1$. In addition, it is useful to underline that, in this case, $W_{d.ji_m} = 0$ for unbraced bays (see endnote in Table 2).

- g) Computation of the required sum of the reduced plastic moments of columns for each storey as the maximum value among those coming from the above design conditions:

$$\sum_{i=1}^{n_c} M_{c.ii_m} = \max \left\{ \sum_{i=1}^{n_c} M_{c.ii_m}^{(1)}, \sum_{i=1}^{n_c} M_{c.ii_m}^{(2)}, \sum_{i=1}^{n_c} M_{c.ii_m}^{(3)} \right\} \quad (53)$$

- h) The sum of the required plastic moment of columns at each storey, reduced due to the contemporary action of the axial force, is distributed among all the columns. The knowledge of these plastic moments $M_{c.ii_m}$, coupled with the axial force $N_{c.ii_m}$ at the collapse state, allows the design of column sections from standard shapes.

The steps of the design procedure described above constitute in case of vertical links, a closed form solution from a theoretical point of view. However, because of the selection of column sections from the standard shapes some iteration could be required, because the sum of plastic moment of columns at first storey actually obtained, $\sum_{i=1}^{n_c} M_{c.i1}^*$, is generally greater than the value strictly needed provided by Eq. (44), thus affecting the design values at the upper storeys resulting from Eq. (47), (49) and (50) where the value of $\alpha^{(g)}$ has to be updated with the appropriate value of $\sum_{i=1}^{n_c} M_{c.i1}^*$. Therefore, the procedure has to restart from step d).

Conversely, in the case of structural schemes with horizontal links, some iteration is always required because of the need to update the value (44) of the ψ parameter in Eq. (46).

7 STUDY CASES

In this Section, different study cases are presented and designed by TPMC (Nastri, 2015). In particular, in this work 12 structures are reported. The validation of the procedure has been carried out both comparing the theoretical curve, i.e. the collapse mechanism equilibrium curve, with the push-over curve. In addition, the plastic hinge distribution obtained by the push-over analyses has been compared with the expected collapse mechanism, i.e. the global mechanism.

It is also important to observe that only short links have been considered for the design of structures because they present many advantages with respect to long and intermediate links. In fact, the main parameter governing the seismic response of such structural typology, both in elastic and post-elastic range, is the length e of the links, constituting the dissipative zones.

This parameter influences the lateral stiffness of the structure, the ability to dissipate the seismic input energy and the link plastic rotation capacity. In particular, the lateral stiffness of the bracing system increases as far as the link length decreases (Chao and Goel, 2006; Mastrandrea and Piluso, 2009). Due to their performance in terms of both stiffness and ductility, short links are in several cases the most suitable choice for seismic-resistant EBFs. In fact, the cyclic behaviour of short links is characterized by wide and stable cycles allowing the development of high energy dissipation capacity, provided that adequate web stiffeners are adopted along the element length to prevent web local buckling. Finally, intermediate links are characterized by a behavior in-between those of short and long links.

From the design point of view, on one hand, it has to be considered that short links provide the highest plastic rotation supply, but also, on the other hand, that they are subjected to the highest plastic rotation demand for a given lateral displacement; the opposite case occurs when long links are adopted, while intermediate links provide an intermediate behaviour. For this reason, care has to be taken in the selection of the link length, which governs the overall ultimate behaviour, the local ductility (both demand and supply) and the stiffness of the structure. Consequently, the main goal of the design process of an eccentrically braced frame is the identification of the best compromise between the need, on one hand, to develop high lateral stiffness and plastic rotation supply which increase as far as the link length decreases and, on the other hand, the need to reduce the plastic rotation demands which, conversely, decrease as far as the link length increases.

The study cases herein investigated are referred to a building whose plan configuration is depicted in Figure 9. The seismic resistant structural system is a perimeter system constituted by MRF-EBF dual systems while the inner bays are pinned and designed only for gravity loads. The building constituting the study cases are of 4-storey, 6-storeys and 8-storeys. The seismic resistant scheme is a MRF-EBF dual system whose EBF part is configured with K-scheme, D-scheme, V-scheme and inverted Y-scheme. Therefore, a total of 12 study cases have been analysed. For sake of shortness, the seismic response of the buildings is herein analyzed with reference to seismic actions in the longitudinal direction only. The corresponding seismic resistant schemes are depicted in Figure 10, for the K-scheme, D-scheme, V-scheme and inverted Y-scheme and only for the 6-storey and 8-storey structures. In addition in such figures also the leaning column adopted in structural modelling to account for second order effects due to the internal gravity load resisting system is reported. In fact, gravity loads acting on the leaning part of the structure significantly contribute to the structural seismic masses and to second order effects.

The link length governs the ultimate design displacement. It is equal to 1.20 m for the K-scheme and D-scheme, 0.60 m for V-scheme buildings and 0.70 m for the inverted Y-scheme, at each storey.

The characteristic values of the vertical loads are equal to 4.0 kN/m² and 2.0 kN/m² for permanent (G_k) and live (Q_k) loads, respectively. As a consequence, with reference to the seismic load combination provided by Eurocode 8 (CEN, 2004), $G_k + \psi_2 Q_k + E_d$ (where ψ_2 is the coefficient for the quasi-permanent value of the variable actions, equal to 0.3 for residential buildings), the vertical loads acting on the floor are equal to 4.6 kN/m². The structural material adopted for all the members is S355 steel grade ($f_{yk} = 355 \text{ MPa}$). The beams of the MRF part have been designed to withstand vertical loads accounting also for serviceability requirements. They are IPE 330 for the external bays and IPE 270 for the intermediate bays. As regards the braced bay, they are made of the same section adopted for links in case of EBFs with horizontal links, while, they are IPE 300 for EBFs with inverted-Y scheme. The design horizontal forces have been determined according to Eurocode 8, assuming a peak ground acceleration equal to 0.35g, a seismic response factor equal to 2.5, a

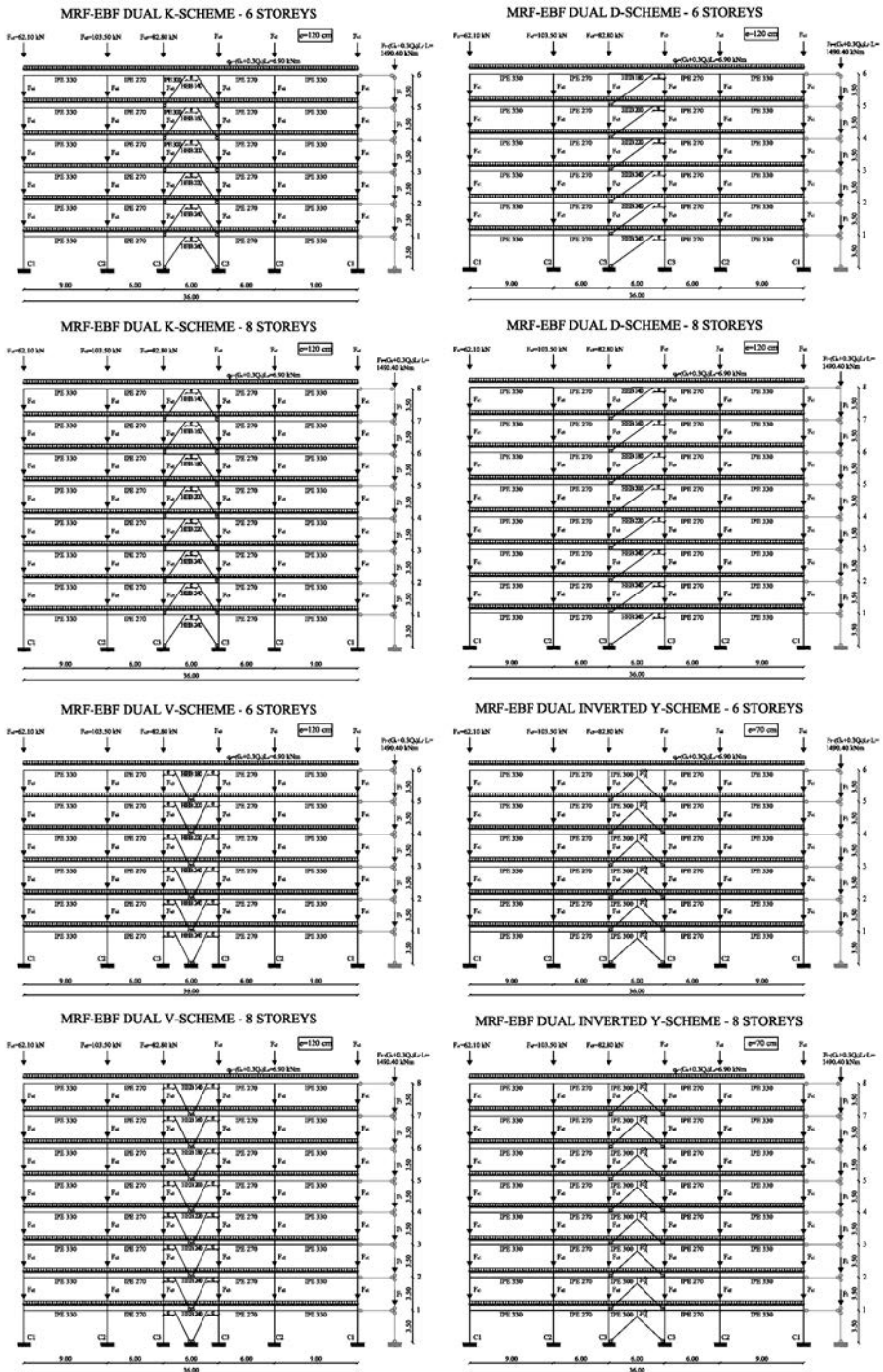


Figure 10. Structural schemes of the longitudinal seismic resistant system for 6-storey buildings.

Table 3. Design seismic forces, link and diagonal sections for the designed buildings.

	STOREY	F	K-Scheme		D-Scheme		V-Scheme		INVERTED Y-Scheme	
			i_m	[kN]	LINKS	DIAGONAL SECTIONS	LINKS	DIAGONAL SECTIONS	LINKS	DIAGONAL SECTIONS
4-STOREY	1	96.097	HEB 240	CHS 323.9x20	HEB 240	CHS 323.9x20	HEB 160	CHS 323.9x20	HEB 300	CHS 244.5x20
	2	192.195	HEB 200	CHS 323.9x20	HEB 200	CHS 323.9x20	HEB 140	CHS 323.9x20	HEB 300	CHS 244.5x20
	3	288.293	HEB 180	CHS 323.9x20	HEB 180	CHS 323.9x20	HEB 140	CHS 323.9x20	HEB 240	CHS 244.5x20
	4	384.391	HEB 140	CHS 323.9x20	HEB 140	CHS 323.9x20	HEB 140	CHS 323.9x20	HEB 180	CHS 244.5x20
6-STOREY BUILDING	1	50.643	HEB 240	CHS 355.6x16	HEB 240	CHS 355.6x16	HEB 180	CHS 355.6x16	HEB 200	CHS 244.5x20
	2	101.285	HEB 240	CHS 355.6x16	HEB 240	CHS 355.6x16	HEB 180	CHS 355.6x16	HEB 200	CHS 244.5x20
	3	151.928	HEB 220	CHS 355.6x16	HEB 220	CHS 355.6x16	HEB 180	CHS 355.6x16	HEB 200	CHS 244.5x20
	4	202.571	HEB 200	CHS 355.6x16	HEB 200	CHS 355.6x16	HEB 160	CHS 355.6x16	HEB 180	CHS 244.5x20
	5	253.214	HEB 160	CHS 355.6x16	HEB 160	CHS 355.6x16	HEB 140	CHS 355.6x16	HEB 160	CHS 244.5x20
	6	303.856	HEB140	CHS 355.6x16	HEB140	CHS 355.6x16	HEB 140	CHS 355.6x16	HEB 160	CHS 244.5x20
8-STOREY BUILDING	1	31.745	HEB 240	CHS 406.4x32	HEB 240	CHS 406.4x32	HEB 220	CHS 406.4x12.5	HEB 340	CHS 406.4x32
	2	63.489	HEB 240	CHS 406.4x32	HEB 240	CHS 406.4x32	HEB 220	CHS 406.4x12.5	HEB 340	CHS 406.4x32
	3	95.234	HEB 240	CHS 406.4x32	HEB 240	CHS 406.4x32	HEB 220	CHS 406.4x12.5	HEB 320	CHS 406.4x32
	4	126.978	HEB 220	CHS 406.4x32	HEB 220	CHS 406.4x32	HEB 200	CHS 406.4x12.5	HEB 300	CHS 406.4x32
	5	158.723	HEB 200	CHS 406.4x32	HEB 200	CHS 406.4x32	HEB 180	CHS 406.4x12.5	HEB 280	CHS 406.4x32
	6	190.467	HEB 180	CHS 406.4x32	HEB 180	CHS 406.4x32	HEB 180	CHS 406.4x12.5	HEB 240	CHS 406.4x32
	7	222.212	HEB 160	CHS 406.4x32	HEB 160	CHS 406.4x32	HEB 140	CHS 406.4x12.5	HEB 200	CHS 406.4x32
	8	253.956	HEB 140	CHS 406.4x32	HEB 140	CHS 406.4x32	HEB 140	CHS 406.4x12.5	HEB 140	CHS 406.4x32

Table 4. Column sections.

	Storey	K-scheme			V-scheme			D-scheme			Inverted Y-scheme		
		C1	C2	C3	C1	C2	C3	C1	C2	C3	C1	C2	C3
4-STOREY BUILDING	1	HEB 280	HEB 280	HEB 260	HEB 260	HEB 260	HEB 360	HEB 260	HEB 260	R=HEB 400 L=HEB 340	HEB 260	HEB 280	HEB 400
	2	HEB 280	HEB 280	HEB 260	HEB 260	HEB 260	HEB 360	HEB 260	HEB 260	R=HEB 400 L=HEB 340	HEB 260	HEB 260	HEB 360
	3	HEB 280	HEB 280	HEB 260	HEB 260	HEB 260	HEB 360	HEB 260	HEB 260	R=HEB 340 L=HEB 280	HEB 260	HEB 260	HEB 340
	4	HEB 280	HEB 280	HEB 260	HEB 260	HEB 260	HEB 360	HEB 260	HEB 260	R=HEB 340 L=HEB 240	HEB 240	HEB 260	HEB 260
6-STOREY BUILDING	1	HEB 300	HEB 300	HEB 280	HEB 300	HEB 300	HEB 450	HEB 280	HEB 280	R=HEB 550 L=HEB 500	HEB 300	HEB 300	HEB 500
	2	HEB 300	HEB 300	HEB 280	HEB 300	HEB 300	HEB 450	HEB 280	HEB 280	R=HEB 500 L=HEB 450	HEB 300	HEB 300	HEB 450
	3	HEB 300	HEB 300	HEB 280	HEB 300	HEB 300	HEB 450	HEB 280	HEB 280	R=HEB 450 L=HEB 400	HEB 300	HEB 300	HEB 450
	4	HEB 300	HEB 300	HEB 280	HEB 300	HEB 300	HEB 450	HEB 280	HEB 280	R=HEB 450 L=HEB 400	HEB 300	HEB 300	HEB 450
	5	HEB 300	HEB 300	HEB 280	HEB 300	HEB 300	HEB 450	HEB 280	HEB 280	R=HEB 450 L=HEB 340	HEB 300	HEB 300	HEB 360
	6	HEB 240	HEB 260	HEB 280	HEB 280	HEB 280	HEB 400	HEB 280	HEB 280	R=HEB 400 L=HEB 260	HEB 240	HEB 260	HEB 260
8-STOREY BUILDING	1	HEB 320	HEB 340	HEB 300	HEB 320	HEB 320	HEB 650	HEB 300	HEB 320	HEB 700	HEB 320	HEB 340	HEB 650
	2	HEB 320	HEB 340	HEB 300	HEB 320	HEB 320	HEB 600	HEB 300	HEB 320	HEB 650	HEB 320	HEB 340	HEB 600
	3	HEB 320	HEB 340	HEB 300	HEB 320	HEB 320	HEB 600	HEB 300	HEB 320	HEB 600	HEB 320	HEB 340	HEB 600
	4	HEB 320	HEB 340	HEB 550	HEB 320	HEB 320	HEB 600	HEB 300	HEB 320	R=HEB 600 L=HEB 550	HEB 320	HEB 340	HEB 550
	5	HEB 320	HEB 340	HEB 500	HEB 320	HEB 320	HEB 550	HEB 300	HEB 320	HEB 550	HEB 320	HEB 340	HEB 500
	6	HEB 320	HEB 320	HEB 450	HEB 320	HEB 320	HEB 550	HEB 300	HEB 320	R=HEB 550 L=HEB 500	HEB 320	HEB 320	HEB 450
	7	HEB 300	HEB 300	HEB 360	HEB 300	HEB 300	HEB 450	HEB 300	HEB 320	R=HEB 500 L=HEB 400	HEB 300	HEB 300	HEB 360
	8	HEB260	HEB260	HEB260	HEB 280	HEB 280	HEB 400	HEB 300	HEB 300	R=HEB 400 L=HEB 280	HEB260	HEB260	HEB260

Table 5. Collapse mechanism multiplier and slope of mechanism equilibrium curve of TPMC designed structures.

	K-scheme		D-scheme		V-scheme		Inv. Y-scheme	
	α_0	γ	α_0	γ	α_0	γ	α_0	γ
4-storey	2.2263	0.005539	2.1652	0.005539	1.7719	0.005539	2.341	0.005539
6-storey	2.1428	0.004851	2.1009	0.004851	1.7375	0.004851	2.1994	0.004851
8-storey	2.0803	0.004439	2.0415	0.004439	1.9104	0.004439	2.1279	0.004439

8 RESULTS OF PUSH-OVER ANALYSES

With reference to the longitudinal seismic resistant system of the designed buildings, push-over analyses have been carried out by means of SAP2000 computer program. The aim of these analyses is to check the collapse mechanism actually developed to provide a first quick comparison between the performances in plastic range of the structures designed.

Member yielding has been taken in account by modelling the dissipative zones by means of plastic hinge elements, i.e. with a lumped plasticity model. Column, beam, diagonal and link members have been modelled with an elastic beam-column frame element with two rigid-plastic hinge elements located at the member ends. With reference to beams, plastic hinge properties are defined in pure bending (M3 hinge) while in case of columns and diagonals plastic hinge properties are defined to account for the interaction between bending and axial force (P-M3 hinges). Regarding link members, as short links yielding in shear are of concern, their behavior is governed by shear. However, as preliminarily reported it is more useful to exploit the concept of equivalent moment (Eq. (15)). For this reason, plastic hinges in pure bending (M3) have been considered with a tri-linear behavioral curve relating the bending moment to the plastic rotation. The trilinear curve corresponds to a rigid-hardening-perfectly plastic behavior. In particular, an overstrength of 1.5 has been considered for a link plastic rotation of 0.08 rad. The use of a rigid-hardening behaviour for the plastic shear hinges of link elements is justified because of the significant overstrength that link elements are able to exhibit (Bruneau *et al.*, 2011; Hera Publication, 2103; Hjelmsstad and Popov E.P., 1983). Even though many doubts have been raised concerning the amount of overstrength arising in short links due to strain-hardening (Rai, 1998; Dusicka, 2004; Dusicka *et al.*, 2004; Okazaki *et al.*, 2004; Okazaki *et al.*, 2009; Neal, 1961; Malley and Popov, 1983; Roeder, 1978); the overstrength factor has been assumed equal to 1.50 as suggested in code provisions for short link.

The push-over analyses have been led under displacement control taking into account both geometrical and mechanical non-linearities. In addition, out-of-plane stability checks of compressed members have been performed at each step of the non-linear analysis for both the examined structures.

The results provided by the pushover analyses are reported in

Figure 11, Figure 12 and Figure 13 where both the push-over curves and the mechanism equilibrium curves corresponding to the global mechanism are depicted. In particular, the results provided by the analyses show that the softening branch of the push-over curve corresponding to the structure designed by means of TPMC tends towards the mechanism equilibrium curve obtained by means of second order rigid-plastic analysis. It is also useful to underline that, in the examined cases, push-over curves exhibit a softening behavior, because the occurrence of strain-hardening in shear links does not counterbalance the softening due to second order effects.

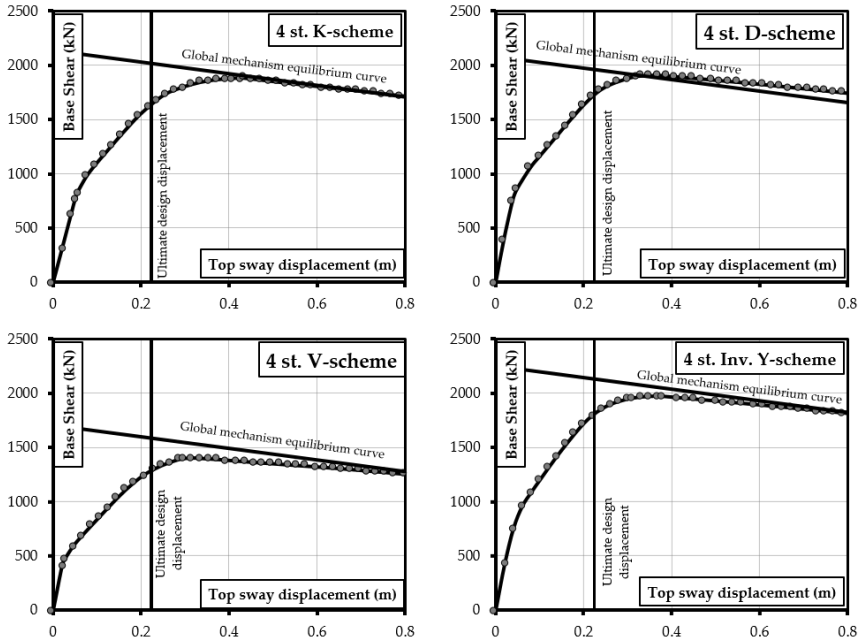


Figure 11. Push-over curves for 4-storey structures.

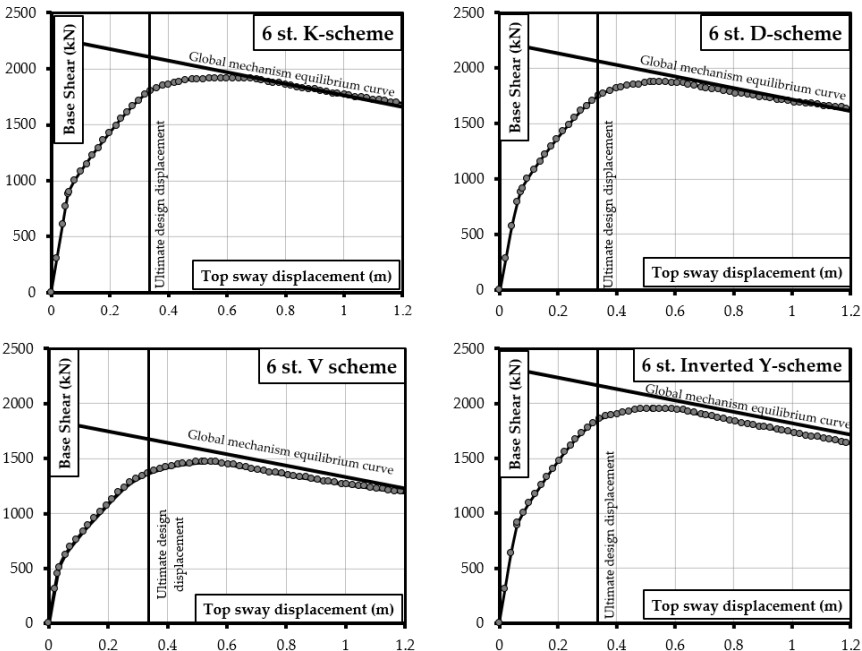


Figure 12. Push-over curves for 6-storey structures.

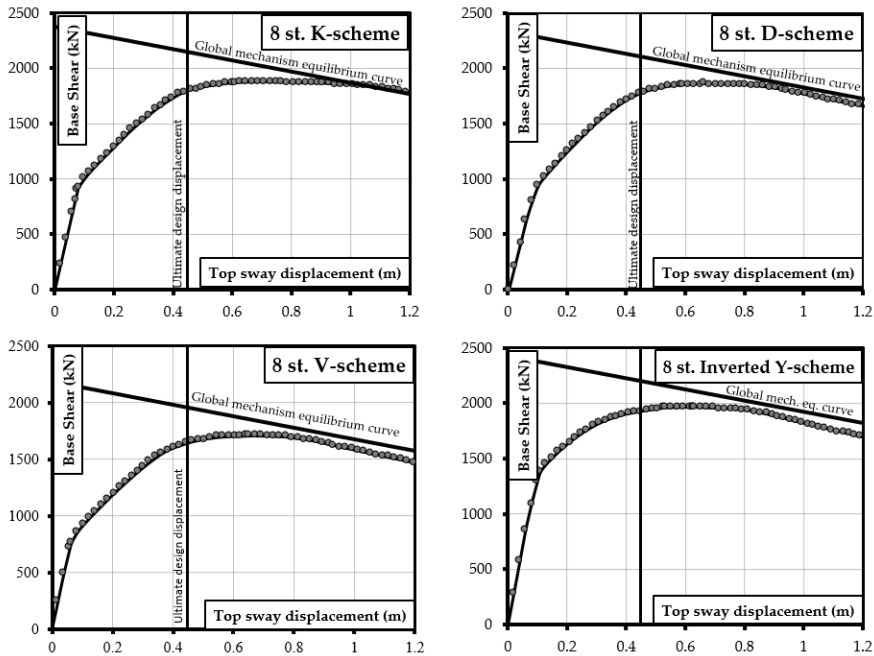


Figure 13. Push-over curves for 8-storey structures.

9 IDA ANALYSES

The aim of IDA analyses is the evaluation of the actual seismic performances of the structures in order to investigate the influence of the four bracing schemes proposed by seismic codes (CEN, 2004). With reference to the analyzed seismic resistant systems, IDA analyses have been carried out by means of SAP2000 computer program by using the same modeling proposed for push-over analyses. In addition, 5% damping according to Rayleigh has been assumed with the proportional factors computed with reference to the first and third mode of vibration reported in Table 6 for each structure. Despite of the different brace geometry it is useful to note that, because of the common design method, the dynamic properties of the structural schemes are very close to each other. In fact, significant differences are due to the number of storeys and not to the bracing scheme. Record-to-record variability has been accounted for by considering 10 recorded accelerograms (Table 7) selected from PEER data base. Their average value matches approximately the linear elastic design response spectrum of Eurocode 8, for soil type A and 5% damping. In addition, each ground motion has been scaled to obtain the same value of the spectral acceleration, $S_a(T_1)$, corresponding to the fundamental period of vibration T_1 of the structure under examination (Table 6); successively $S_a(T_1)$ values have been progressively increased. The IDA analyses have been carried out by increasing the $S_a(T_1)/g$ value until the occurrence of structural collapse, corresponding to column or diagonal buckling or the attainment of the limit value of the chord rotation of structural members.

Incremental Dynamic Analyses results have been reported with reference both to the Link Plastic Rotation and to the Maximum Interstorey Drift Ratio (MIDR) considering the spectral acceleration ($S_a(T_1)/g$) as the seismic intensity measure. Plastic rotation demands are depicted

in Figure 14, Figure 15 and Figure 16 for the 4, 6 and 8 storey structures, respectively. In these figures the $Sa(T_1)/g$ value corresponding to the achievement of a plastic rotation equal to 0.08 rad (assumed as the target rotation) can be easily identified.

Table 6. First and third vibration mode period of buildings designed.

	4 STOREYS		6 STOREYS		8 STOREYS	
	T_1 (s)	T_3 (s)	T_1 (s)	T_3 (s)	T_1 (s)	T_3 (s)
K-scheme	1.00	0.45	1.38	0.56	1.80	0.67
D-scheme	1.01	0.44	1.42	0.56	1.87	0.67
V-scheme	1.00	0.42	1.40	0.51	1.74	0.59
Inverted Y-scheme	1.01	0.44	1.39	0.54	1.62	0.60

In addition, it is useful to consider that FEMA 356 provisions suggest limit values of the link plastic rotation demands equal to 0.11 rad and 0.14 rad with reference to the Life Safety (LS) and to the Collapse Prevention (CP) limit states, respectively. In particular, by comparing the average value of $Sa(T_1)/g$ corresponding to this last limit state it is possible to observe that, given the design approach, CP condition is achieved, first by the V-scheme structures and lastly by inverted Y-scheme for all the considered storey numbers. It means that, in the examined cases, the inverted Y-scheme is able to provide better seismic performances compared to the other schemes (Nastri, 2015).

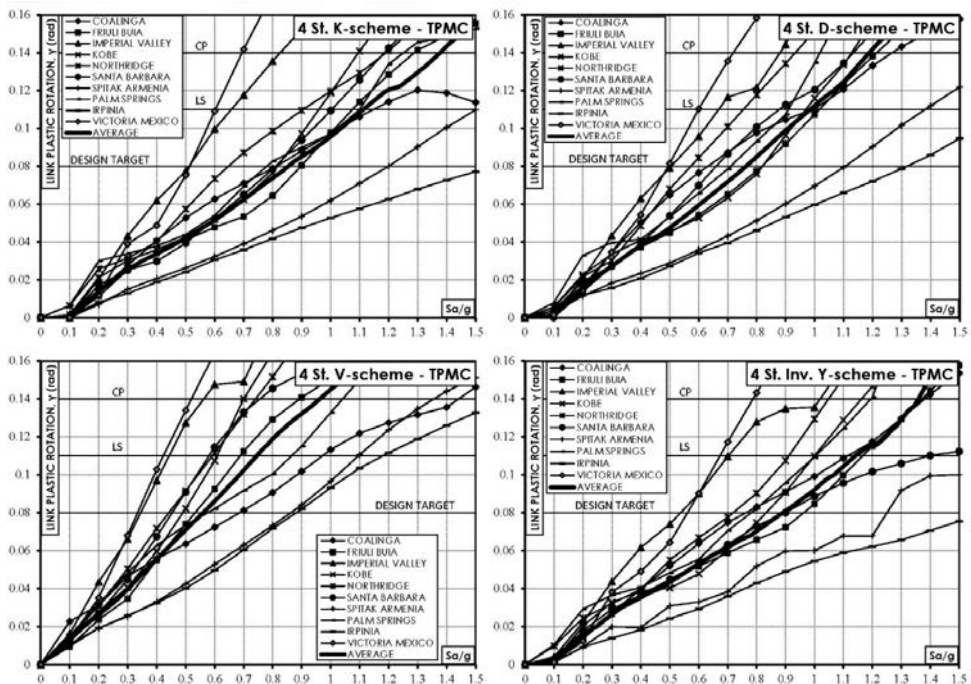


Figure 14. Maximum link plastic rotation versus spectral acceleration for the 4-storey structures.

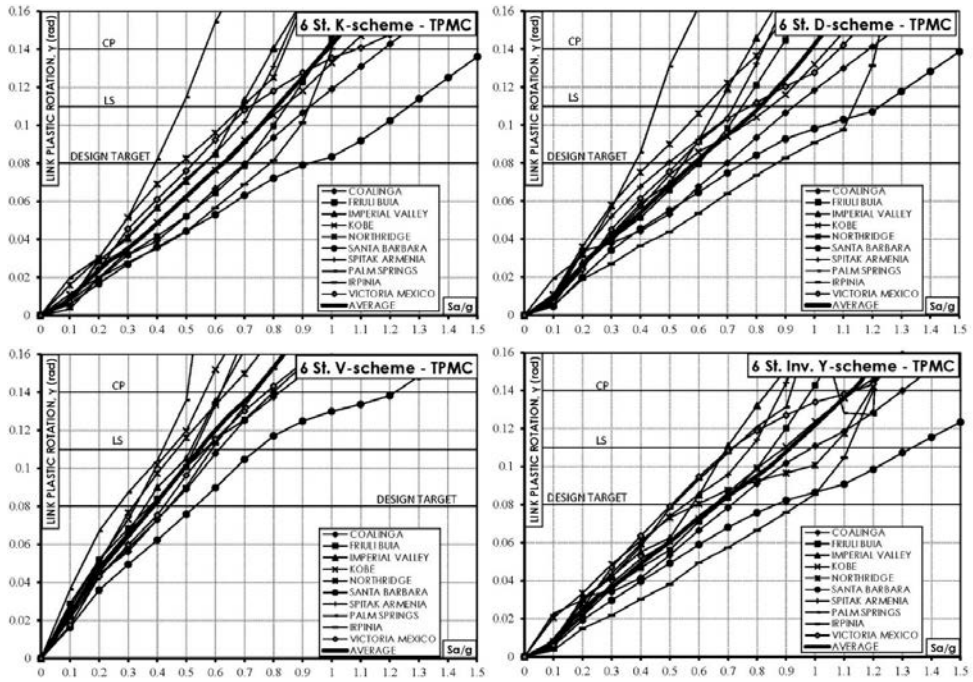


Figure 15. Maximum link plastic rotation versus spectral acceleration for the 6-storey structures.

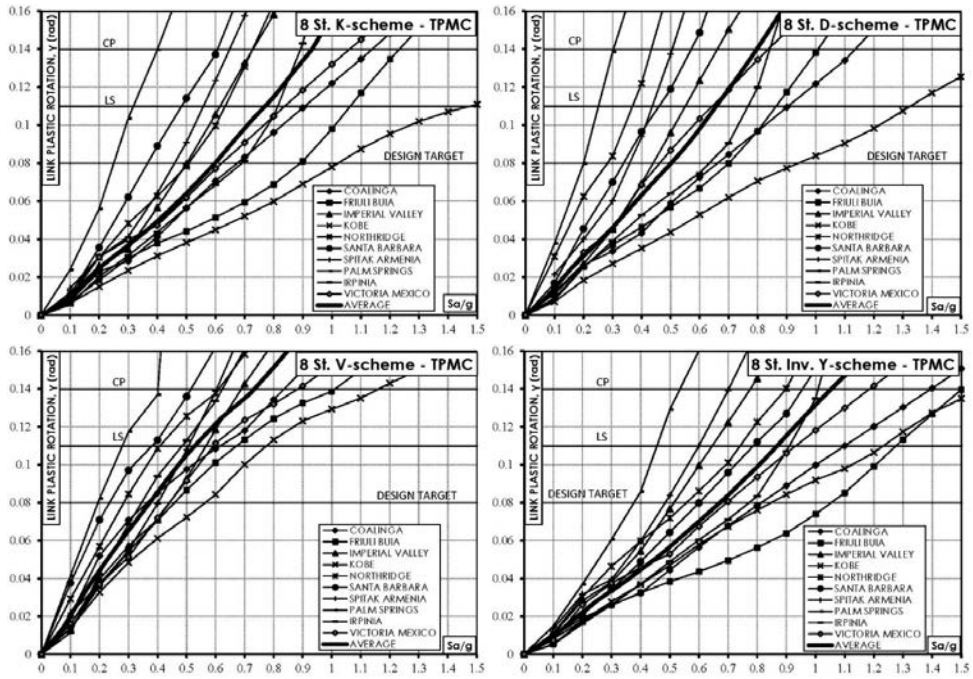


Figure 16. Maximum link plastic rotation versus spectral acceleration for the 8-storey structures.

Table 7. Selected Accelerograms.

Earthquake (record)	Component	Date	PGA/g	Length (s)	Step recording (s)
Victoria, Mexico (Chihuahua)	CHI102	1980/06/09	0.150	26.91	0.01
Coalinga (Slack Canyon)	H-SCN045	1985/05/02	0.166	29.99	0.01
Kobe (Kakogawa)	KAK000	1995/01/16	0.251	40.95	0.01
Spitak, Armenia (Gukasian)	GUK000	1988/12/17	0.199	19.89	0.01
Northridge (Stone Canyon)	SCR000	1994/01/17	0.252	39.99	0.01
Imperial Valley (Agrarias)	H-AGR003	1979/10/15	0.370	28.35	0.01
Palm Springs (San Jacinto)	PALMSPR/H08000	1986/07/08	0.250	26.00	0.005
Santa Barbara (Courthouse)	SBA132	1978/08/13	0.102	12.57	0.01
Friuli, Italy (Buia)	B-BUI000	1976/09/15	0.110	26.38	0.005
Irpinia, Italy (Calitri)	A-CTR000	1980/11/23	0.132	35.79	0.0024

Starting from this preliminary considerations that account for the behavior of braced part of the dual system, further remarks can be made. In particular, the ultimate limit state is always due to the attainment of ultimate plastic link rotation equal to 0.14 rad in a link element. Table 8, Table 9 and Table 10 provide $S_a(T_1)$ values corresponding to the ultimate condition achieved by 4, 6 and 8 storey structures, respectively. The $S_a(T_1)$ values leading to collapse are given for each selected ground motion and, in addition, also the average values are provided. In addition, being the analyzed structural system a dual system, it is useful to point out the influence of the MRF part by observing the Maximum Interstorey Drift Ratio (MIDR) curves (Figure 17, Figure 18 and Figure 19) that can be significant to highlight the achievement of maximum plastic rotation in the beam ends. These figures highlight that the average MIDR curves achieve the target value of 0.04 rad for average $S_a(T_1)$ values greater or almost equal to the collapse values reported in Table 8, Table 9 and Table 10. This confirms that the MRF part of MRF-EBF dual system really constitutes a supplementary fail safe system, as preliminarily discussed, whose contribution to the seismic performances of the structures become more and more important as the seismic intensity measure increases. However, the development of plastic hinges at beam ends can be anticipated by sharing different rates of the base shear between the EBF and the MRF parts of the seismic resistant scheme. As an example, ASCE 7-10 requires for a dual system that the moment frames shall carry at least 25% of the design seismic forces. It looks clear that many design solutions are possible corresponding to different sharing rates of the seismic design shear between the EBF part and the MRF part. This issue deserves specific investigations that have not been reported in this work for sake of shortness. Regarding the influence of the bracing scheme, whose investigation is the aim of this work, on the basis of the results obtained, it is possible to conclude that structures arranged with vertical link (Inverted Y-scheme) ever provide the best seismic performances. In fact, by comparing the ratio between the $S_a(T_1)$ values leading to the collapse of the Inverted Y-scheme structures with those occurring for the other bracing schemes, it can be observed that there is a maximum reduction in term of seismic performances (Figure 16) when the V-scheme is adopted.

Because of the influence of the bracing scheme on the seismic performances, on the basis of the results herein obtained, it seems quite rational, given the q-factor for the inverted Y-scheme, to propose a reduction factor equal to 0.90, 0.80 and 0.65 in the case of K-scheme, D-scheme and V-scheme, respectively, independently of the number of storeys. It is important to observe that the suggested reduction factors could be applied only in case of design procedures assuring, like TPMC, a collapse mechanism of global type.

In any case, in this work only 5 bays structures, with 4, 6 and 8 storeys, have been investigated so that additional analyses on different structural schemes with different number of bays should be carried out before arriving at more general conclusions. By the way, Y-

scheme EBFs are more performing not only in terms of seismic response, but also because the link member does not belong to the beam and therefore, can be easily substitute after a destructive seismic event.

Table 8. $S_a(T_1)$ values corresponding to the attainment of the collapse condition for the 4-storey structures.

$S_a(T_1)$				
Record	4 st. K-scheme	4 st. D-scheme	4 st. V-scheme	4-storey Inv. Y
Coalinga	1.90 g	1.25 g	1.45 g	1.45 g
Friuli, Italy	1.28 g	1.25 g	0.90 g	1.38 g
Imperial Valley	0.85 g	0.88 g	0.58 g	1.05 g
Irpinia, Italy	2.10 g	2.10 g	1.60 g	2.50 g
Kobe	1.10 g	1.15 g	0.70 g	1.15 g
Northridge	1.18 g	1.15 g	0.75 g	1.06 g
Palm Springs	1.25 g	1.02 g	1.02 g	1.20 g
Santa Barbara	1.15 g	1.15 g	0.75 g	2.10 g
Spitak Armenia	1.98 g	1.78 g	1.35 g	2.10 g
Victoria Mexico	0.68 g	0.70 g	0.55 g	0.78 g
Mean value	1.36 g	1.24 g	0.97 g	1.48 g

Table 9. $S_a(T_1)$ values corresponding to the attainment of the collapse condition for the 6-storey structures.

$S_a(T_1)$				
Record	6 st. K-scheme	6 st. D-scheme	6 st. V-scheme	6 st. Inv. Y-scheme
Coalinga	1.18 g	1.18 g	0.85 g	1.30 g
Friuli, Italy	0.95 g	0.85 g	0.80 g	0.98 g
Imperial Valley	0.80 g	0.77 g	0.65 g	0.85 g
Irpinia, Italy	1.00 g	1.20 g	0.75 g	1.10 g
Kobe	1.05 g	1.15 g	0.58 g	1.15 g
Northridge	0.86 g	0.82 g	0.65 g	1.28 g
Palm Springs	0.58 g	0.55 g	0.51 g	0.95 g
Santa Barbara	1.55 g	1.50 g	1.25 g	1.65 g
Spitak Armenia	0.83 g	0.85 g	0.65 g	0.88 g
Victoria Mexico	1.10 g	1.05 g	0.78 g	1.15 g
Mean value	0.99 g	0.99 g	0.75 g	1.13 g

Table 10. $S_a(T_1)$ values corresponding to the attainment of the collapse condition for the 8-storey structures.

$S_a(T_1)$				
Record	8 st. K-scheme	8 st. D-scheme	8 st. V-scheme	8 st. Inv. Y-scheme
Coalinga	1.15 g	1.15 g	0.85 g	1.40 g
Friuli, Italy	1.25 g	1.05 g	1.00 g	1.50 g
Imperial Valley	0.75 g	0.65 g	0.70 g	0.78 g
Irpinia, Italy	0.85 g	0.85 g	0.65 g	1.05 g
Kobe	1.88 g	1.65 g	1.05 g	1.55 g
Northridge	0.78 g	0.45 g	0.65 g	0.90 g
Palm Springs	0.40 g	0.30 g	0.42 g	0.55 g
Santa Barbara	0.62 g	0.58 g	0.52 g	0.96 g
Spitak Armenia	0.68 g	0.55 g	0.62 g	0.71 g
Victoria Mexico	1.05 g	0.85 g	0.88 g	1.20 g
Mean value	0.94 g	0.81 g	0.73 g	1.06 g

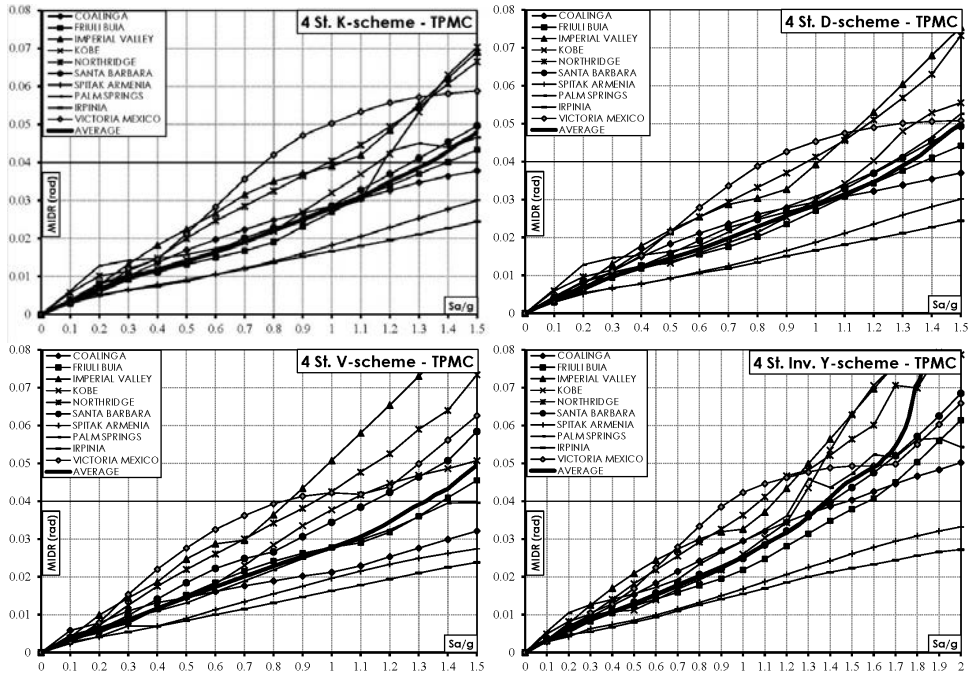


Figure 17. Maximum Interstorey Drift versus spectral acceleration for the 4-storey structures.

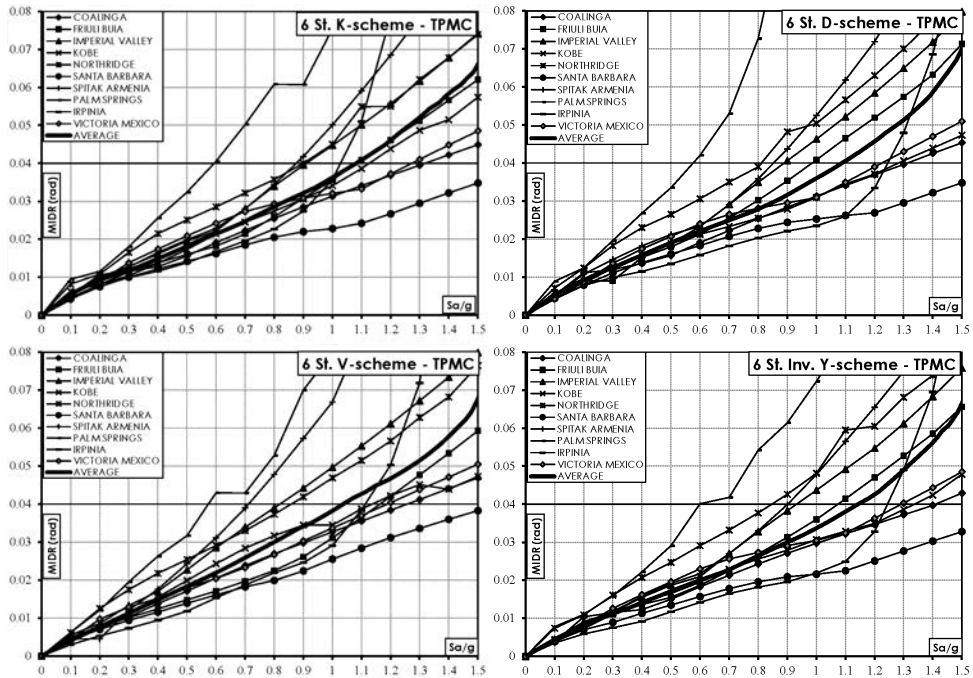


Figure 18. Maximum Interstorey Drift versus spectral acceleration for the 6-storey structures.

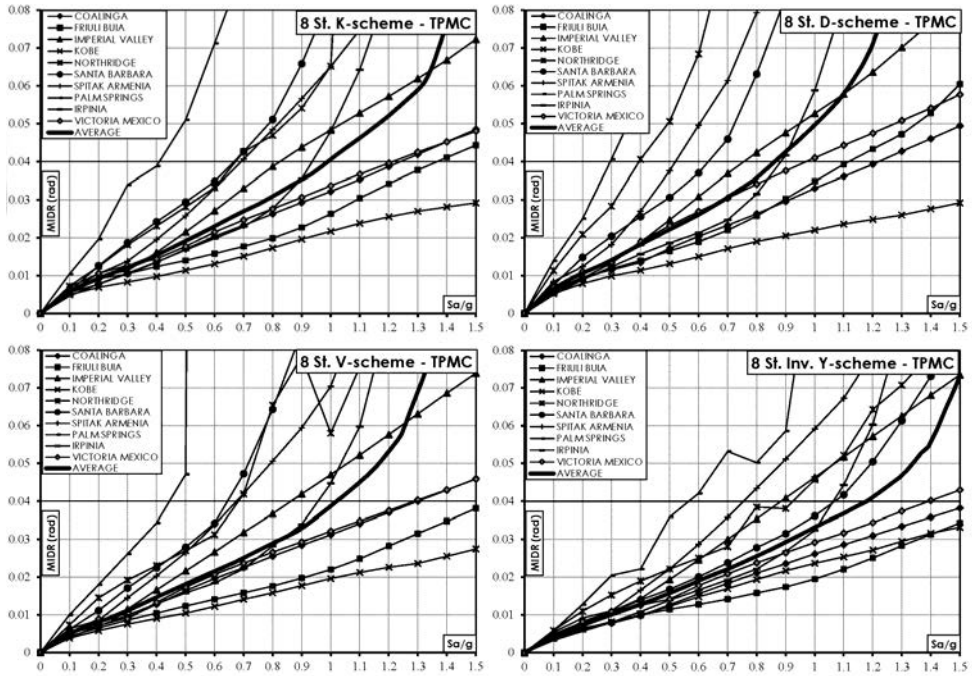


Figure 19. Maximum Interstorey Drift versus spectral acceleration for the 6-storey structures.

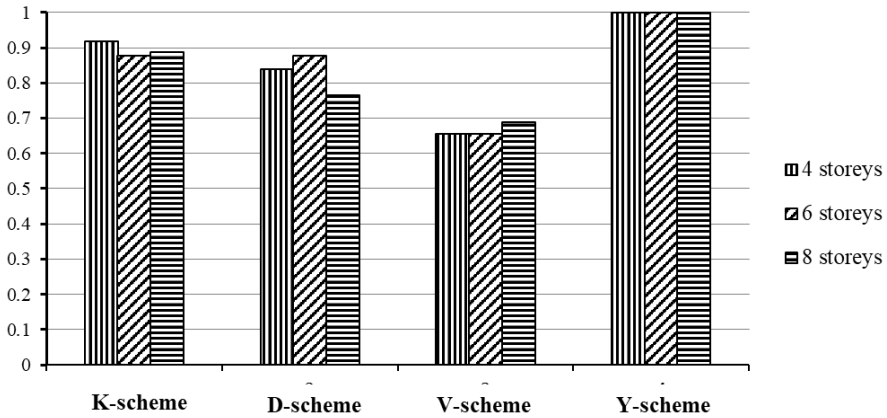


Figure 20. Structures designed by TPMC: $Sa(T_1)$ value leading to collapse normalized with reference to the value obtained in case of Y-scheme.

10 CONCLUSIONS

In this work the application of TPMC to MRF-EBF dual systems has been presented. In particular, by means of new considerations regarding the collapse mechanism typologies, a closed form solution has been provided, so that the unknown of the design problem, i.e. column sections at each storey, can now be derived also by means of hand calculations.

Aiming at the evaluation of TPMC accuracy, an adequate number of MRF-EBF dual systems have been designed. Push-over analyses have pointed out the accuracy of TPMC, as testified by the obtained plastic hinge distribution, which has resulted in perfect agreement with the global mechanism, and by the push-over curve whose softening branch tends to the mechanism equilibrium curve of the global mechanism. Therefore, the application of TPMC has led to the fulfilment of the design goal. Further investigations have been made by means of IDA analyses in terms of interstorey drift ratio and link plastic deformation demand. Structures whose braces are arranged according to the inverted Y-scheme have led, independently of the number of storeys, to the best seismic performances. In comparison with the inverted Y-scheme, the spectral acceleration leading to the collapse reduces on average of about 10%, 20% and 35% in case of K-scheme, D-scheme and V-scheme, respectively. Despite of this works investigates only 5 bays structures with 4, 6 and 8 storeys, it seems evident that a reduction of the q-factor should be suggested for the seismic design of eccentrically braced frames with V-scheme, K-scheme and D-scheme. However, additional analyses on different structural schemes with different number of bays should be carried out in order to provide a more robust proposal.

11 ACKNOWLEDGEMENTS

The research work herein presented has been partially supported by the grant agreement “DPC-RELUIS 2014-2016”. The financial support of the Italian Department for Civil Protection (DPC) is gratefully acknowledged.

12 REFERENCES

- Akiyama H. (1985). “Earthquake Resistant Limit State Design for Building” University of Tokyo Press, Tokyo.
- ASCE. (2010). “ASCE Standard 7-10: Minimum Design Loads for Buildings and Other Structures”, *American Society of Civil Engineers*.
- Balendra T., Sam M.T., Liaw C.Y., Lee S.L. (1991) “Preliminary studies into the behavior of knee braced frames subjected to seismic loading”, *Engineering Structures*, Vol. 13, Issue 1, pp. 67-74.
- Bertero V. V., Popov E. P. (1977). “Seismic behaviour of ductile moment-resisting reinforced concrete frames”, in *Reinforced Concrete Structures in Seismic Zones*, *ACI Publication SP-53*, American Concrete Institute, Detroit, pp. 247-291.
- Bruneau M., Uang C.M., Sabelli R.S.E. (2006). “Ductile Design of Steel Structures”, McGraw-Hill, 2011.
- Chao S.H., Goel S.C.: “Performance-Based Seismic Design of Eccentrically Braced Frames using target drift and yield mechanism as Performance Criteria”, *Engineering Journal*, Third Quarter.
- Conti M.A., Mastandrea L., Piluso V. (2009). “Plastic Design and Seismic Response of Knee Braced Frames”, *Advanced Steel Costructions*, Vol. 5, n.3 September, pp. 343-363.
- Dowrich D.J. (1977). “Earthquake Resistant Design”, *A Manual for Engineers and Architects*, Wiley, New York.
- Dusicka P., Itani A.M., Buckle I.G. (2004). “Evaluation of conventional and specialty steels in shear link hysteretic energy dissipators”, In: *Proceedings of 13th WCEE*, Paper No. 522.
- Dusicka P. (2004). “Hysteretic shear links utilising innovative steels for earthquake protection of long span bridges”, Ph.D. Dissertation, Reno, NV: University of Nevada.
- EN 1998-1. (2004). “Eurocode 8: Design of Structures for Earthquake Resistance – Part 1: general Rules, Seismic Actions and Rules for Buildings”, *CEN*.

- Engelhardt M.D., Popov E.P. (1989). "Behaviour of long links in eccentrically braced frames", Report N. UCB/EERC-89/01, *Earthquake Engineering Research Center*; University of California, Berkeley.
- Hera Publication P4001:2013. (2013). "Seismic Design of Eccentrically Braced Frames", *Earthquake Engineering*.
- Hjelmstad K.D., Popov E.P. (1983). "Cyclic behavior and design of link beams", *ASCE Journal of Structural Engineering*, Vol. 109, Issue 10, pp. 2387-2403.
- Hjelmstad K.D., Popov E.P. (1983). "Seismic behavior of active beam link in eccentrically braced frames", EERC Report No. 83-15, Berkeley: Earthquake Engineering Research Center, University of California.
- Kasai K, Popov E.P. (1986). "General behavior of WF steel shear link beams", *ASCE Journal of Structural Engineering*, Vol. 112, Issue 2, pp. 362-382.
- Kasai K., Han X. (1997a). "New EBF design method and applications: Redesign and analysis of US-Japan EBF. Proceedings of Stessa 97 – 2nd international conference on behaviour of steel structures in seismic areas.
- Kasai K., Han X. (1997b) "Refined Design and Analysis of Eccentrically Braced Frames", *Journal of Structural Engineering*, ASCE.
- Lee H.S. (1996). "Revised rule for concept of strong-column weak-girder design", *Journal of Structural Engineering*. ASCE, 122, 359D364.
- Longo A., Montuori R., Piluso V. (2012a). "Theory of Plastic Mechanism Control of Dissipative Truss Moment Frames", *Engineering Structures*, Vol. 37, pp. 63-75.
- Longo A., Montuori R., Piluso V. (2012b). "Failure Mode Control and Seismic Response of Dissipative Truss Moment Frames", *Journal of Structural Engineering*, Vol. 138, pp.1388-1397.
- Longo, A., Montuori R., Piluso V. (2012a) "Theory of plastic mechanism control for MRF-CBF dual systems and its validation." *Bulletin of Earthquake Engineering*, 1-31.
- Longo A., Montuori R., Nastri E., Piluso V. (2014b). "On the use of HSS is seismic Resistant Structures", *Journal of Constructional Steel Research*, Vol. 103, December, Pages 1-12.
- Malley J.O., Popov E.P. (1983). "Design consideration for shear links in eccentrically braced frames", EERC Report No. 83-24, Berkeley: *Earthquake Engineering Research Center*, University of California.
- Mastandrea L., Nastri E., Piluso V. (2013). "Validation of a Design Procedure for Failure Mode Control of EB-Frames: Push-over and IDA analyses", *The Open Construction and Building Technology Journal*, 7, 193-207, 2013.
- Mastrandrea L., Montuori R., Piluso V. (2003). "Shear-moment interaction in plastic design: eccentrically braced frames", STESSA 2003, *4th International Conference on Behavior of Steel Structures in Seismic Areas*, Naples, Italy, 9-12 June. Rotterdam: Balkema.
- Mastrandrea L., Piluso V. (2009). "Failure mode control of seismic resistant EB-frames", Plastic Design of Eccentrically Braced Frames, II: Failure Mode Control", *Journal of Constructional Steel Research*, pp. 1015-1028.
- Mazzolani F.M., Piluso V. (1996). "Theory and Design of Seismic Resistant Steel Frames", *E&FN Spon, an imprint of Chapman & Hall*.
- Mazzolani F.M., Piluso, V. (1997). "Plastic Design of Seismic Resistant Steel Frames", *Earthquake Engineering and Structural Dynamics*, Vol. 26, pp. 167-191.
- Montuori R., Nastri E., Piluso V. (2014a). "Rigid-plastic analysis and Moment-shear interaction for Hierarchy Criteria of Inverted Y EB-Frames", *Journal of Constructional Steel Research*, Vol. 95, April 2014, pp. 71-80.
- Montuori R., Nastri E., Piluso V. (2014b). "Theory of Plastic Mechanism Control for Eccentrically Braced Frames with inverted Y-scheme", *Journal of Constructional Steel Research*, Volume 93, pp. 122-135.
- Montuori R., Nastri E., Piluso V. (2014c). Theory of plastic mechanism control for the seismic design of braced frames equipped with friction dampers - *Mechanics Research Communications – Vol. 58*. pp. 112-123.

- Montuori R., Piluso V. (2000). "Design of Semi-Rigid Steel Frames for Failure Mode Control", *Moment Resistant Connections of Steel Frames: Design and Reliability*, London: E&FN Spon, Taylor & Francis Group, pp. 461-483.
- Montuori R., Piluso V. (1999). "L'Uso dei "Dog Bones" nella Progettazione a Collasso Controllato dei Telai Sismo-Resistenti", *XVII Congresso C.T.A. Italian Conference on Steel Construction*, Napoli, 3-5 Ottobre, vol. 1, pp. 301-310.
- Nistri E. (2015). "Theory of Plastic Mechanism Control for Eccentrically Braced Frames: Closed Form Solution", PhD Thesis.
- Neal B.G. (1961). "Effect of shear force on the fully plastic moment of an I-beam". *Journal of Mechanics and Engineering Science*, Vol. 3, Issue 3, pp. 258-268.
- Okazaki T., Arce G., Ryu H.C., Engelhardt M.D. (2004). "Recent Research on Link Performance in Steel Eccentrically Braced Frames", *13th World Conference on Earthquake Engineering, 13th WCEE*, Vancouver, Canada, August 1-6, Paper No. 302.
- Okazaki T., Engelhardt M.D., Drolias A., Schell E., Hong J.K., Uang C.M. (2009). "Experimental investigation of link-to-column connections in eccentrically braced frames", *Journal of Constructional Steel Research*, Vol. 65, pp. 1401-1412.
- Penelis G.G., Kappos A.J. (1997). "Earthquake-Resistant Concrete Structures", E&FN Spon, an imprint of *Chapman & Hall*.
- Park R. (1986). "Ductile Design Approach for Reinforced Concrete Frames", *Earthquake Spectra*, EERI, 2(3), pp. 565-619.
- Paulay T., Priestley M.J.N. (1995). "Seismic Design of Reinforced Concrete and Masonry Buildings", Wiley, New York.
- Pacific Earthquake Engineering Research Center, PEER Strong Motion Database, <http://peer.berkeley.edu/smcat>
- Piluso V., Montuori R., Troisi M. (2014). "Innovative structural details in MR-frames for free from damage structures", *Mechanics Research Communications*, Volume 58, June, 146-156.
- Piluso V., Nistri E., Montuori R. (2015). "Advances in Theory of Plastic Mechanism Control: Closed Form Solution for Mr-Frames", *Earthquake Engineering and Structural Dynamics*, 44 (7), pp. 1035-1054.
- Rai D.C., Wallace B.J. (1998). "Aluminium shear-links for enhanced seismic resistance", *Earthquake Engineering and Structural Dynamics*, Vol. 27, Issue 4, pp. 315-342.
- Roeder C.W., Popov E.P. (1978). "Eccentrically braced steel frames for earthquakes", ASCE, *Journal of Structural Division*, Vol. 104, Issue 3, pp. 391-412.
- Rosenblueth E. (1980). "Design of Earthquake Resistant Structures", *Pentech Press*, London.
- Wakabayashi M. (1986). "Design of Earthquake Resistant Buildings", *McGraw-Hill*, New York, p. 229.

SEISMIC-RESISTANT STEEL FRAMES WITH REINFORCED CONCRETE INFILL WALLS

Andrea Dall'Asta ^a, Graziano Leoni ^a, Francesco Morelli ^b, Walter Salvatore ^b,
Alessandro Zona ^a

^a *School of Architecture and Design, University of Camerino, Camerino, Italy,
andrea.dallasta@unicam.it; graziano.leoni@unicam.it; alessandro.zona@unicam.it*

^b *Department of Civil and Industrial Engineering, University of Pisa, Pisa, Italy,
francesco.morelli@dic.unipi.it; walter@ing.unipi.it*

ABSTRACT

Steel frames with reinforced concrete infill walls (SRCW) are an interesting seismic-resistant structural solution. However, an effective seismic design of SRCWs is no easy due to the current lack of specific capacity design rules that allow controlling the formation of a proper dissipating mechanism. In order to overcome such an issue, a ductile design procedure is presented in this chapter, leading to innovative SRCW systems where energy dissipation is expected to take place only in the vertical elements of the steel frame subjected mainly to axial forces. Experimental test results and nonlinear finite element analyses are presented to support the developed ductile design approach and highlight the potentialities of SRCWs.

KEYWORDS

Ductile design, earthquake resistant systems, experimental tests, hybrid systems, reinforced concrete infill walls.

1 INTRODUCTION

In earthquake-prone areas, steel-concrete composite and hybrid systems represent an optimal solution where the two materials work integrally to provide lateral strength and stiffness to meet the design objectives. These systems are particularly indicated when the design performances require not only an high level of lateral strength and ductility, fundamental for the life safety and collapse prevention requirements, but also a lateral stiffness able to minimize the damages to structural and non-structural elements in case of low-to-medium earthquakes (Morino, 1998) (Hajjar, 2002) (Deierlein and Noguchi, 2004) (Spacone and El-Tawil, 2004) (Zona *et al.*, 2008) (El-Tawil *et al.*, 2010) (Dall'Asta *et al.*, 2015) (Zona *et al.*, 2016) (Morelli *et al.*, 2016).

Steel frames with reinforced concrete infill walls (SRCWs) are a particular type of hybrid systems, in which the composite action between the reinforced concrete (r.c.) infill wall and the steel frame is assured by two main mechanisms, see Figure 1,: the direct interaction between the steel frame and the compression strut in the r.c. infill walls; the interaction between steel frames and the r.c. infill walls through friction and shear connectors. The former depends mainly on the steel frame and r.c. infill wall geometry, while the latter is strongly influenced by the number and distribution of the shear studs.

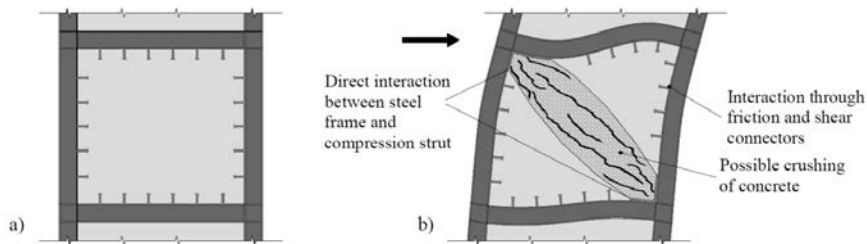


Figure 1. a) Traditional SRCW and b) schematization of the main steel frame - r.c. infill wall interaction mechanisms.

Three general categories of SRCWs can therefore be defined as a function of the shear studs distribution (El-Tawil *et al.*, 2010): integral infilled frames, characterized by connectors distributed along the interfaces between the frames and the infill walls; non-integral infilled frames are not provided with connectors; semi-integral infilled frames are intermediate configurations between integral and non-integral infilled frames.

The seismic behaviour of SRCWs has been the object of many theoretical and experimental studies over more than four decades. Test results of (Mallick and Severn, 1968) showed that the presence of shear connectors in the corner of the steel frame prevented the rotation of the infilled walls, increased the overall stiffness, and did not affect the lateral strength. Furthermore, integral infilled frames exhibited shear failure of the infill walls, while non-integral infilled frames were characterized by diagonal compression failure of the infill walls. (Liauw and Lee, 1977), (Liauw, 1979), and (Liauw and Kwan, 1985) studied the influence of the shear studs distribution along the steel frames through a series of static, dynamic, and cyclic tests on both integral and non-integral SRCWs. Test results showed that the presence of shear connectors along the entire interface between steel frame and infill walls determined an increment of global strength, stiffness, and energy dissipation capacity. In Japan, a series of cyclic tests was carried out by (Makino *et al.*, 1980) and (Makino, 1985) on one-third scale FSRCW specimens equipped with few studs having the primary purpose to prevent the out-of-plane collapse of the RC infills. These tests showed that infilled frames having columns bent about their strong axis had ductile behaviour comparable to that of typical bare steel frames. (Tong *et al.*, 2005) experimental investigation on PSRCWs highlighted that infill walls tended to develop a pattern of closely-spaced diagonal cracks, prior to any significant yield in the steel frame. The presence of reinforcing cages around the headed studs helped to avoid the concrete brittle failure modes. However, low-cycle fatigue of the headed studs became the main failure mode. Similar results on the importance of the reinforcing cages and on the behaviour of shear studs were obtained by (Saari *et al.* 2004). Their experimental tests showed that the axial tension greatly reduced the strength and deformation capacity of the studs. However, by providing confinement to the studs in the form of a reinforcement cage, the full strength and deformation capacity of the studs could be achieved, overcoming the effect of the nearby parallel edges of the infill wall. Not providing this confinement resulted in an unsatisfactory stud behaviour.

The review of the state of the art demonstrates how the intuitive idea of stiffening a steel frame with a RC infill is, in reality, rather difficult to be controlled because the actual resisting mechanism is affected by many variables. Ambiguity in the definition of the resisting mechanism is accompanied by a lack of capacity design rules able to produce a tailored hierarchy among the structural components. This situation is reflected by main design standards providing specific design rules for SRCWs, i.e. European Eurocode 8 (EN1998-1,

2004) and American AISC 341-05 (AISC, 2005). Specifically, Eurocode 8 considers SRCW systems to behave essentially as RC walls able of dissipating energy in the vertical steel sections and in the vertical reinforcements of the walls. In addition, the same detailing provisions provided for RC walls are repeated for SRCWs except for indications on the edge shear connections. AISC 341-05 permits to classify SRCWs as “special reinforced concrete shear walls composite with structural steel elements”, allowing the adoption of seismic response modification coefficients higher than those associated to the ordinary shear wall systems. In the case of non-encased boundary steel elements, the AISC standard assumes that the shear forces are carried only by the RC wall, while the entire gravity and overturning forces are carried by the steel frame in conjunction with the shear wall. However, also in this case, special indications for the formation of a proper dissipating mechanism are not provided.

Refined numerical analyses carried out on SRCWs (Dall'Asta *et al.*, 2015) designed according to the Eurocodes pointed out an unsatisfactory fragile behaviour due to the severe damage occurring to concrete long before yielding of the ductile elements. The failure mechanism is generally characterised by yielding of the steel frame concentrated mainly in the elements near the bottom of the wall (more specifically at the connections of the horizontal to the vertical parts). The plastic deformation on the concrete infill walls concentrates in a diagonal path clearly highlighted by the distribution of cracking. In addition, localized plastic deformations are also present near the corners of the infill walls due to the local action of the first studs of the horizontal and vertical elements. All these issues demonstrate how the idea, suggested by design standards, that SRCWs may behave as a RC shear walls is far from reality. The presence of boundary steel profiles leads rather to the formation of a unique diagonal strut within the RC infill wall contributing to the formation of a truss-like resisting mechanism.

Within this research, the attention is focused on an innovative SRCW, see Figure 2a). Such system is characterized by the presence of structural fuses, generally made placed within the vertical elements of the steel frame. The presence of such structural steel fuses allows the designer to obtain a prefixed ductile collapse mechanism, see Figure 2b), avoiding the crushing of concrete, and the presence the r.c. infill wall prevents possible buckling phenomena in the structural fuse and in the portion of steel frame in compression.

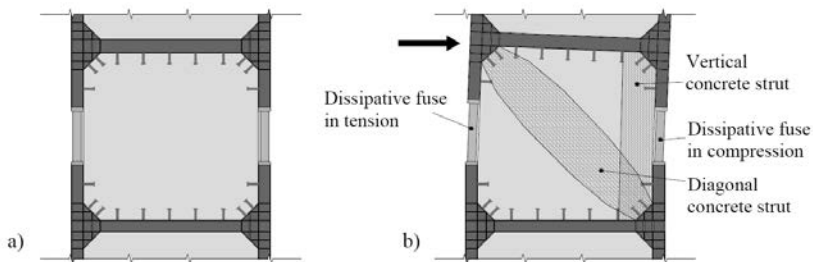


Figure 2. a) Innovative SRCW and b) schematic representation of the resisting mechanism.

The presence of shear studs connecting the infill wall and the steel frame is necessary to avoid out-of-plane rigid rotation of the wall itself and, depending on the number and characteristics of the shear studs, can activate different types of resisting mechanisms, as described in details in the following paragraph.

A specific capacity design procedure, able to assure the desiderated energy dissipation mechanism, is proposed consistently with the Eurocode 8 framework and explained in its

details. Finally, the results of an experimental campaign on two different two-thirds downscaled one-storey specimens are illustrated to provide insight into the influence of the shear studs distribution on the behaviour of the proposed SRCW system. More details about the dissipative SRCW can be found in (Dall'Asta *et al.*, 2017).

2 PROPOSED INNOVATIVE SRCW SYSTEM

2.1 Structural concept

As previously discussed, the behaviour of SRCWs may be very different from that assumed in the design because the resisting mechanism within the RC infill can only be roughly controlled. The idea that the system behaves as a RC shear wall as a whole, in which vertical steel elements act as reinforcements and contribute with axial forces to resist the overturning moments whereas the RC infill walls have to resist the storey shear, might be far from reality especially when not encased elements are adopted. In such cases, shear connectors spread at the wall edge strongly affect the behaviour of the system and the provision (usually required by design codes) that they have to resist the storey shear to be transmitted to the RC infill wall is not sufficient to ensure the formation of an inclined uniform compression field. Slip between the steel frame and the RC infill wall, in fact, produces a concentration of the forces at the wall corners that may be completely out of the designer control so that failure of shear connectors or concrete crushing typically occur well in advance with respect to yielding of the vertical elements. The basic idea of this paper is to design a system in which the objective resisting mechanism at the ultimate limit state is fostered by a suitable configuration of the elements; this allows to introduce a clear capacity design procedure that should lead to reliably ductile structural solutions.

The novel SRCW depicted in Figure 3a is proposed. Because the formation of a main diagonal strut within the RC infill wall cannot be avoided when yielding of the side steel element is enforced, the structural system should be conceived to properly control the compression field in the concrete. For this purpose, joints of the steel frame are shaped to support the diagonal strut formation, i.e. an inclined and appropriately stiffened plate permits force exchanges between the RC infill and the steel frame with an imposed effective contact area (Figure 3b). Accordingly, the infill wall, without the sharp corners, does not need to undergo significant slip for the formation of the diagonal strut. Shear connectors are not essential for the formation of such resisting mechanism but they are necessary only to avoid possible out-of-plan overturning of the infill wall.

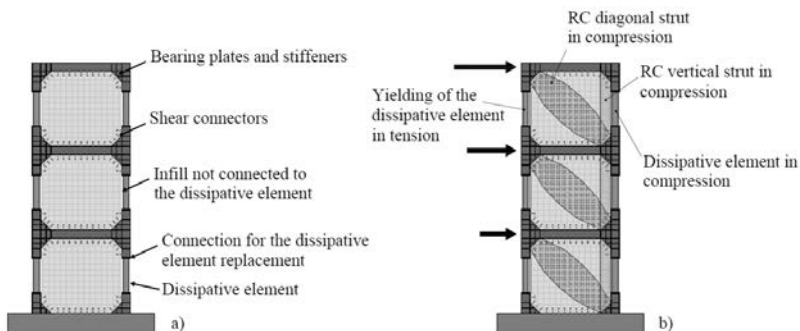


Figure 3. a) innovative SRCW systems; b) limit behaviour under seismic action of the innovative SRCW system.

In order to avoid secondary shear transfer mechanisms due to the interaction with the steel frame, the RC infill walls are not connected to the vertical steel elements. Such vertical elements are the dissipative fuses of the proposed system and energy dissipation is attained when their yielding in traction is activated whereas axial forces in compression are limited by the formation of vertical struts that act parallel to the compress side steel elements (Figure 3b). As the steel fuses are not connected to the RC infill walls, they may be replaced when damaged by a seismic event provided that suitable end connections are realised. Therefore, the proposed SRCW system behaves as a truss even from the very first lateral sways and, taking advantage from the stiffness of the concrete in compression and the energy dissipation capacity of the steel elements in tractions, represents a potentially efficient steel and concrete hybrid seismic-resistant structure.

2.2 Feasibility features

The construction of the proposed innovative SRCW does not involve particular difficulties in the shop prefabrication nor in the construction site where assemblage and concreting can be made by means of usual equipment and workmanship. The plant configuration of the required SRCWs can be arranged to accommodate functional and architectural needs, and can be profitably coupled with gravitational structures provided that rigid floors are suitably connected to them as usual in steel construction.

The steel side elements can be realised with hot rolled or hollow profiles. As these elements act as fuses for the system, they have to be designed in order to strictly fulfil strength verification limiting their over-strength and as well as to ensure that energy dissipation is uniformly activated among the adopted SRCWs and along their elevation. For this purpose, they could be realised with welded profiles using low-grade steels. As already mentioned these elements are not connected to the RC wall and, even if in principle no specific provisions are necessary, it is better to assure their cross section being compact, e.g. at least class 2 according to Eurocode 3 (EN1993, 2005).

The end connections of the ductile steel elements should be designed to remain in the linear range to permit the replacement of the ductile elements after seismic damage. End-plates connections should be preferred and the ductile elements should be connected to the split plate by means of full penetration welding. The adjacent vertical elements to which the ductile elements are connected should be over-strengthened; this can be assured by using a higher steel grade or by suitably enlarging the resisting cross section that should have width equal or greater than the infill wall thickness; for this purpose it can be advantageous using the same profile adopted for the horizontal beams.

Horizontal beams, including the stiffened joints and the shear connectors, necessary for the stability of the wall during a seismic event, can be entirely prefabricated in the shop by using hot rolled standard steel profiles. As it is better that their width is compliant with the wall thickness, HE series are usually preferable. However, when the wall thickness is higher than 300 mm (the max available width of HE profiles), welded sections may be also adopted instead of coupled elements.

As for the RC infill walls, detailing rules suggested by Eurocode 8 are not mandatory as the system is conceived as a lattice lateral resisting structure and it is not expected that energy dissipation takes place in wall critical regions. In addition to a double skin welded mesh placed to limit crack widths and complying with provisions for RC walls in non-seismic areas, reinforcements must be provided in order to prevent concrete crushing by means of a suitable confinement action. In particular, attention must be paid to regions in contact with the bearing plates where compression stress diffusion take place. For this purpose different reinforcement layouts may be used as suggested in the following section. It is important to

remark that the adoption of inclined confinement stirrups is possible only for thick walls due to the additional space required. The wall plays a role also in the case in which the steel side elements are not able to withstand compression forces due to the system overturning; in this case confinement of a side vertical region must be provided in order to guarantee the suitable strength.

Finally, shear connectors must be placed at the plates where the wall struts interact with the steel frame with the aim of avoiding out-of-plane collapses. In the case in which the wall has to bear a part of the compression, shear connectors must be welded at vertical elements in order to transmit forces from the frame to the wall. In this case it is important to remark that local failure mechanisms can be characterised by splitting of the wall. This mechanism can be controlled with suitable transverse reinforcements designed according to Eurocode 4 Part 2 (6.6.4 and Annex C) (EN1994, 2006) and by adopting stud connectors with suitable length.

3 DESIGN OF THE INNOVATIVE SRCW SYSTEMS

3.1 Details of the design procedure

As discussed in the previous section, the proposed SRCW should develop a resisting mechanism in which the steel elements of the frame are subjected mainly to axial forces and the concrete walls are characterised by the formation of diagonal struts (Figure 3b). A statically determinate truss model is considered to describe such a limit behaviour of the system. This scheme can be profitably used in a force-based procedure because the stress resultants in the elements do not depend on the dimension of members and because a capacity design is straightforward once the required strengths of the members are defined. The procedure hereafter described is articulated into 9 steps and follows a capacity design path leading to systems in which overall dissipative mechanisms can be developed.

Step 1: definition of the static equivalent lateral loads and calculation of the truss actions

A suitable distribution of lateral loads can be defined according to Eurocode 8 assuming a regular behaviour for the construction. The resulting base shear is derived from the seismic mass of the structure by considering the spectral acceleration corresponding to an estimated fundamental period. As usual, the design spectrum is reduced by a suitable behaviour factor q in order to account for the ductility of the system while designing the structure in the linear range. To a first approximation, the behaviour factor can be chosen as suggested for Type 1 composite walls (Eurocode 8, paragraph 7.3). Once the lateral force system is defined, forces in the elements of the lattice-like structure can be promptly evaluated.

Step 2: design of the cross sections of the ductile boundary elements in traction

Design of the steel fuses is carried out considering tensile forces evaluated in the previous step. Due to the formation of the diagonal strut in the RC wall, the element on the opposite side of the wall is subjected to a compression force that is less intense than the design traction force. For this reason, the fuse is not expected to undergo yielding in compression and a specific verification is carried out at Step 8 for what concern possible instability. In principle no specific provisions are necessary, it is better to assure the element cross section being compact, e.g. at least class 2 according to Eurocode 3.

Step 3: capacity design of the connection of the ductile elements and of the adjacent elements

The design of the connection of the ductile elements and of the adjacent elements is performed with the formula

$$R_d \geq 1.1\gamma_{ov}R_{fy} \quad (1)$$

suggested by Eurocode 8 (paragraph 6.5.5) where γ_{ov} is the over-strength coefficient of the element with plastic resistance R_{fy} of the connected dissipative member based on the design yield stress of the material.

Step 4: calculation of geometric over-strength factors

The over-strength factor Ω_i for the i -th dissipative steel side element is calculated as usual for steel structures by the ratio of the plastic resistance of the ductile element and its design force

$$\Omega_i = \frac{N_{pl,Rd,i}}{N_{Ed,i}} \quad (2)$$

The maximum over-strength Ω_i should not differ from the minimum value by more than 25% in order to guarantee yielding of the edge steel elements at the different levels. The same condition is adopted in the design of steel braced frames in order to avoid the formation of soft-storey and its influence investigated in a number of recent studies, e.g. (Rossi and Lombardo, 2007), (Elghazouli, 2010) (Zona *et al.*, 2012). The proposed SRCW system is less sensitive to the concentration of the deformations in a single storey, i.e. soft-storey formation, due to the presence of the non-dissipative RC infill walls. Hence, this design condition is not expected to be critical. Nevertheless, this check is useful to control the dissipation capacity along the building height allowing the system to be designed by selecting a reduced number of dissipation mechanisms exploiting a reduced level of ductility.

Step 5: calculation of axial forces in non-ductile elements by combining the effects of gravity loads with those of the seismic action suitably magnified

The non-ductile elements of the structure are the diagonal struts developed in the RC infill walls and the horizontal beams. The forces are calculated by a suitable increment of the seismic design component accounting for the material and geometric over-strength of the ductile elements with the usual formula

$$N_{Ed} = N_{Ed,G} + 1.1\gamma_{ov}\Omega N_{Ed,E} \quad (3)$$

where $\Omega = \min\{\Omega_i\}$.

Step 6: capacity design of the RC infill wall against concrete crushing

This step is crucial as it assures the good performance of the system that should not be affected by the wall failure (concrete crushing). As previously described, bearing plates are placed at the beam-to-column nodes to support the formation of the diagonal strut within the wall (Figure 4a). A fan shaped stress field is expected to form at the bearing plate; the effective width of the wall should be equal to the bearing plate width l_b at the diagonal ends whereas the effective width is imposed by a coefficient $\alpha > 1$ at mid diagonal. It is observed that in this region of the wall the concrete stress field is also characterised by transverse traction that reduces the relevant compression strength. The design formula

$$\left\{ 0.85 \frac{f_{ck}}{\gamma_c} t_w l_b; 0.85 \frac{f_{ck}}{\gamma_c} v \left(1 - \frac{f_{ck}}{250} \right) (\alpha t_w l_b) \right\} \geq N_{Ed,G} + 1.1\gamma_{ov}\Omega N_{Ed,E} \quad (4)$$

is derived from Eurocode 2 (paragraph 6.5); the second value of the strut strength takes into consideration the transverse tension ($v = 0.6$ may be assumed) whereas the first value considers a simple compression field. The two design parameters l_b and coefficient α can be determined with a trial procedure or by imposing a tentative value for α (e.g. $\alpha = 2$). The

bearing plate should then be proportioned and suitably stiffened to avoid stress localization in the concrete.

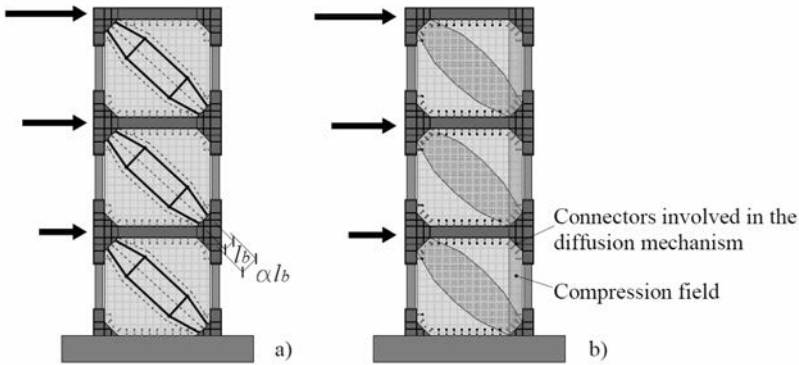


Figure 4. (a) diagonal struts within the infill walls; (b) compression fields involved to resist the axial force in the case lateral elements failed due to instability.

The wall reinforcements should be checked to guarantee the diffusive mechanism that depends on the choice of the parameter α ; for this purpose rules for partial discontinuity regions suggested in Eurocode 2 (paragraph 6.5.2) are considered. In this case, tractions to be resisted by reinforcements is evaluated by means of the formula

$$T = \frac{1}{4} \left(1 - \frac{1}{\alpha} \right) N_R \tag{5}$$

Two different reinforcement layouts may be adopted (Figure 5), the former is constituted by two sets of orthogonal reinforcements whereas the latter is constituted by a set of specific transverse (with respect to the strut direction) reinforcements. In the first case, vertical and horizontal reinforcements should fulfil the conditions

$$\frac{T^2}{f_{yd}^2} = A_{sl}^v + A_{sl}^h \qquad \frac{A_{sl}^h}{A_{sl}^v} = \frac{L}{h} \tag{6}$$

It is worth noting that the first reinforcement layout is simpler but possibly less stiff than the second, which instead requires a third order of reinforcements that can be placed only in the case of sufficiently thick walls.

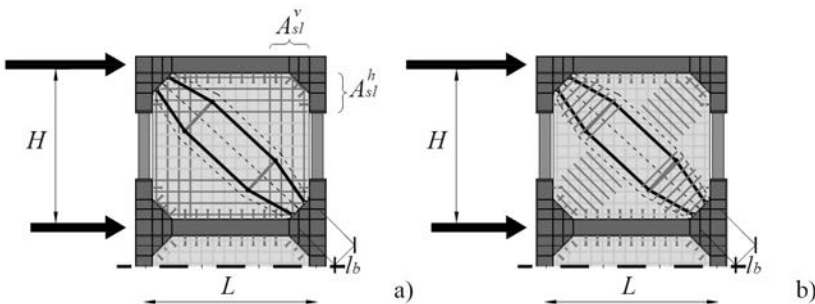


Figure 5. (a) reinforcements constituted by orthogonal rebar layout; (b) reinforcements constituted by additional stirrups.

Step 7: design of the beams in traction

These elements are designed to resist the magnified tensile axial forces calculated in step 5.

Step 8: check and possible re-design of the compressed edge elements

The ductile elements are checked for instability by using the formula

$$\frac{Af_y\chi}{\gamma_{M1}} \geq N_{Ed,G} + 1.1\gamma_{ov}\Omega N_{Ed,E} \quad (7)$$

The effective length of the element can be selected to be equal to the distance between the beam-to-column intersection nodes reduced by the real dimensions of the joint. In case the verification is not satisfied, it is expected that the adjacent strip of the concrete wall collaborates to bear the compression force (Figure 4b); in such a case, the design of the shear connection between the wall and the frame as well as the check of the vertical strut developing in the wall have to be carried out.

The shear connection is designed to involve an adjacent strip of the infill wall in resisting part of the compression force. In particular, this should be able to transmit the force in excess with respect to the bearing capacity of the ductile element given by

$$V_{Rd} \geq N_{Ed,G} + 1.1\gamma_{ov}\Omega N_{Ed,E} - \frac{Af_y\chi}{\gamma_{M1}} \quad (8)$$

In this case, the shear connection has to be placed at the vertical elements. It has to be designed by taking into account that possible splitting failure mechanisms of the wall might occur instead of the usual failures due to concrete crushing and yielding. For this purposes, rules suggested by Eurocode 4 Part 2 (paragraph 6.6.4 and Annex C) could be considered.

In the verification of the vertical strut developing in the wall, this element withstands the same force calculated from equation (8) and has to be suitably reinforced with confinement stirrups. The same detailing rules suggested in Eurocode 8 (paragraph 5.4.3.4.2) for RC walls might be adopted.

Step 9: calculation of the length of the dissipative elements, in order to ensure the compliance between local and global ductility

This is the second crucial point in the design as it permits a first control of the behaviour factor used in Step 1. The length of the dissipative elements can be evaluated assuming that: (i) the system achieves the plastic range with all the fuses simultaneously yielded, (ii) the steel has a perfectly plastic behaviour with a fixed ductility, and (iii) the equal displacement assumption is fulfilled. For this purpose, the formulas derived considering this simplified mechanisms (Figure 6) can be adopted.

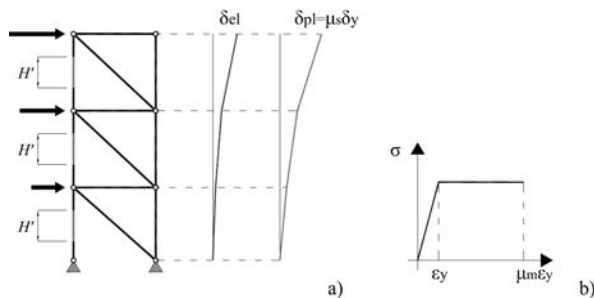


Figure 6. a) Elastic and plastic deformations of the SRCW; b) material stress-strain relationship.

Under the hypothesis that all the fuses have the same length H' , the following formula is obtained:

$$H' = \frac{(\mu_s - 1)}{(\mu_m - 1)} \frac{\delta_{el} L}{\varepsilon_y \sum_{i=1}^N (z_N - z_{i-1})} \quad (9)$$

where μ_s and μ_m are the ductility of the structure and of the material of the dissipative element respectively; the summation is extended only to the N elements that fall in the $\Omega \div 1.25\Omega$ range; δ_{el} is the structure elastic displacement evaluated for the static equivalent loading inducing the first yielding; δ_{pl} is the structure plastic displacement evaluated considering only the elements expected to yield.

It is worth to note that the statically determinate model depicted in Figure 6 can be profitably used also by considering more sophisticated assumptions involving the behaviour of the components. In particular, by introducing the hardening in the behaviour of the steel, it is possible to plot a simplified capacity curve of the system in which the development of the lateral-resisting mechanism can be controlled.

3.2 Applicability of the procedure

The efficiency of the proposed procedure for the design of feasible and safe SRCWs is assessed by considering a large set of cases defined by changing the wall aspect ratio, the number of storeys, and the base shear. 4-storey and 8-storey SRCWs, extracted from a regular building with interstorey height $h = 3.40$ m, are considered. The mass associated to each system is $200 \text{ kNs}^2/\text{m}$ for each floor. In order to investigate whether the system can be properly designed and at what extent the wall slenderness may compromise its efficiency, four different aspect ratios of the wall infills are considered, namely $w/h = 0.66, 1, 1.5$ and 2 (w is the wall width and h its height respectively); consequently, the overall aspect ratios of the SRCWs are $0.165, 0.25, 0.375$ and 0.5 , for 4-storey systems, and $0.083, 0.125, 0.188$ and 0.25 , for 8-storey systems, respectively. The systems are designed for three different base shears in order to cover low, medium, and high seismic intensities. As the design procedure is aimed at obtaining a global dissipative mechanism in which the lateral elements of the wall (ductile elements) may undergo yielding at each storey, four different design scenarios satisfying the condition $\Omega_{\max}/\Omega_{\min} \leq 1.25$ are considered namely: (1) all the ductile elements are designed to fulfil the optimal condition $\Omega_i = 1$; (2) half of the elements are optimal and the others are such that $\Omega_i = 1.25$; (3) one-fourth of the elements are optimal and the others are such that $\Omega_i = 1.25$; and (4) one ductile element is optimal and the other ones are such that $\Omega_i = 1.25$. Steel S235 is considered for the ductile elements whereas higher grades are considered for the non-ductile elements. Concrete C35/45 and steel B450 were used for RC infill, furthermore 8-storey systems were designed also for concretes C40/50 and C45/54. A total amount of 180 cases were completely designed. Due to space limitation, hereafter only a summary of the outcomes is reported.

Table 1 shows the results for the 4-storey systems. The design procedure behaves well for the selected with only some problems in the case of walls with aspect ratio 0.66 designed for the highest seismic intensity since the use of non-commercial profiles are needed for the non-ductile elements and the shear connection is not feasible with usual systems. It is noted that the four scenarios assumed for the regularity of the dissipative elements do not lead to different results.

In the case of 8-storey systems (Table 2) a very different picture can be observed. As expected, wall infills with aspect ratio 0.66 are not suitable for all the three selected levels of seismicity due to the very low aspect ratio 0.08 .

Table 1. Qualitative outcome of the design of 4 storey systems.

w [m]	w/h	w/h _{tot}	Seismic intens.	C35	
				Design	Remarks
2.25	0.66	0.17	Low	Y	
			Medium	Y	
			High	N	P, S
3.40	1.00	0.25	Low	Y	
			Medium	Y (*)	
			High	Y	
5.10	1.50	0.38	Low	Y	
			Medium	Y	
			High	Y	
6.80	2.00	0.50	Low	Y	
			Medium	Y	
			High	Y	
Remarks: Y = the system can be properly designed N = the system cannot be properly designed P = need of non-commercial profiles S = shear connection not feasible with usual systems					

Table 2. Qualitative outcome of the design of 8 storey systems.

w [m]	w/h	w/h _{tot}	Seismic intens.	C35		C40		C45	
				Design	Remarks	Design	Remarks	Design	Remarks
2.25	0.66	0.08	Low	N	P,B,S,W	N	P,B,S,W	N	P,B,S,W
			Medium	N	P,B,S,W	N	P,B,S,W	N	P,B,S,W
			High	N	P,B,S,W	N	P,B,S,W	N	P,B,S,W
3.40	1.00	0.13	Low	Y		Y		Y	
			Medium	Y		Y		Y	
			High	N	P,B,S,W	Y		Y	
5.10	1.50	0.19	Low	Y		Y (*)		Y	
			Medium	Y		Y		Y	
			High	N	P,B,S,W	Y		Y	
6.80	2.00	0.25	Low	Y		Y		Y	
			Medium	Y		Y		Y	
			High	N	P,B,S,W	N	P,B,S,W	Y	
Remarks: Y = the system can be properly designed N = the system cannot be properly designed P = need of non-commercial profiles S = shear connection not feasible with usual systems B = bearing plate for the formation of the diagonal strut not feasible W = wall thickness higher than 300 mm									

Problems are encountered in designing elements at the first three storey due to the need of using non-commercial profiles and to the fact that the wall is involved to resist compression axial forces in the vertical elements; this needs the definition of a shear connection system that cannot be properly designed. Furthermore, it is not possible to design the bearing plates needed for the concrete wall to withstand the diagonal compression field. In the case of wall infills with higher aspect ratio, the system can be designed only for low and medium seismicity level whereas the high seismicity case remains critical for the need of using non-commercial profiles. In an attempt to understand if the problem can be overcome by considering concrete with higher strength, SRCWs are redesigned by using concretes class C40 and class C45. Also in these cases the walls with the lowest aspect ratio cannot be properly designed.

The previous results are of course not exhaustive as the design of such systems could be refined in real cases adopting solutions that should be validated case-by-case. Nevertheless, they give the overall information that a feasible design is pursuable for the wall with overall aspect ratios higher than 0.15.

4 EXPERIMENTAL BEHAVIOUR OF THE INNOVATIVE SRCW SYSTEM

Results of an experimental campaign carried out on two two-third downscaled specimens are presented in order to: validate the predicted behaviour of the proposed SRCW, evaluate possible problems related to the realization of such system, and highlight the influence of different shear stud distributions along the steel frame perimeter. The specimens, respectively named "1" and "2" are shown in Figure 7.

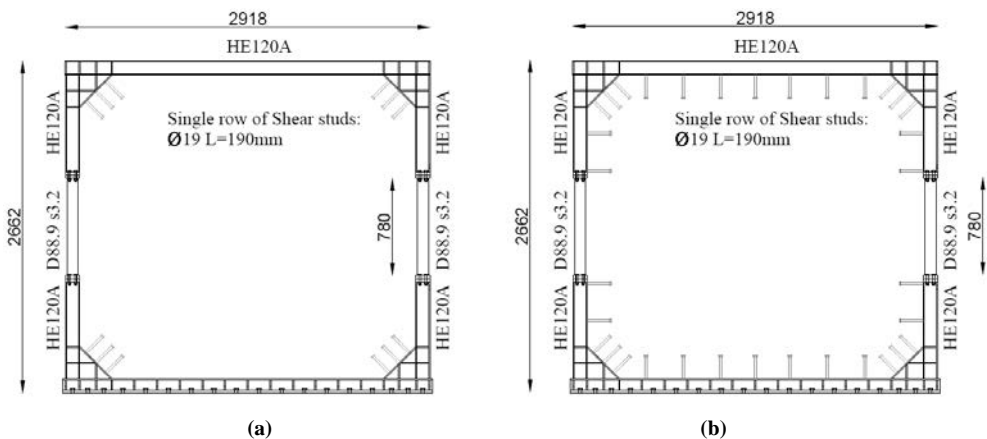


Figure 7. SRCW Steel frame specimens: (a) Specimen 1 with shear studs only in the corner; (b) Specimen 2 with shear studs all along the perimeter (excluded the dissipative zones).

Specimen 1 is characterized by the presence of shear studs only in the steel frame corner zones while specimen 2 has shear studs distributed all along the steel frame perimeter (excluded the dissipative zones). In both cases the RC wall is 12 cm thick and the reinforcement layout, shown in Figure 8, is made up of a couple, one for each side of the wall, of welded steel meshes 150 mm x 150 mm of diameter 8 mm bars, supplemental confining

reinforcement in the two vertical portions of the wall close to the dissipative elements, and open stirrups all along the upper and lower edges of the steel frame.

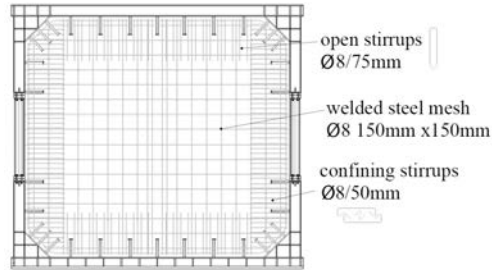


Figure 8. Concrete wall reinforcement layout of the two specimens.

4.1 Test setup

The SRCW specimen is bolted to a steel base firmly connected to the strong floor by means of an anchoring system and horizontal reaction system (Figure 9), while a lateral stabilizing system avoids transversal displacements of the wall. To distribute the external force applied by the jacks all along the upper beam of the steel frame, thus, avoiding the application of concentrated forces at one corner of the steel frame that could enforce the formation of particular resisting mechanisms on the specimen, a suitable system, shown in Figure 10, is used. The system is connected to the wall specimen by 10 friction connections and it is independent from the lateral supporting system, allowing so the free tensile deformation of the dissipative elements.

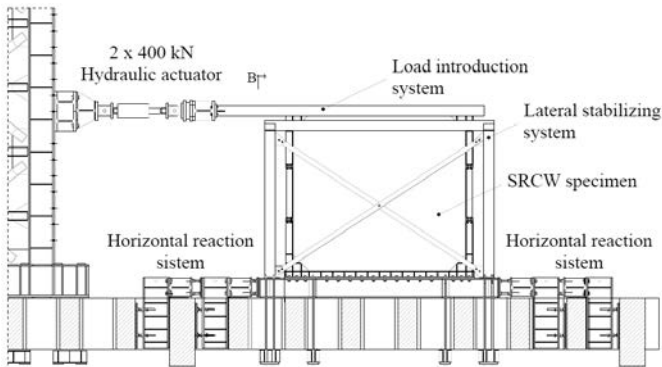


Figure 9. Global test setup.

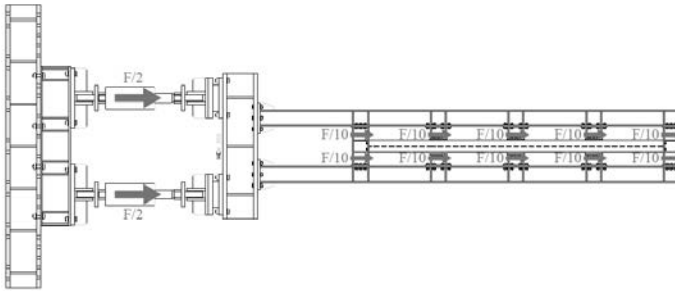


Figure 10. Loading distribution system.

The displacements of the wall, the force applied, the deformation of dissipative elements and of the load introduction system are recorded by several sensors placed as shown in Figure 11. The tests are carried out in displacement control and the displacement history imposed to the jacks end is reported, for both tests, in Figure 12. An initial maximum displacement equal to 20 mm is imposed cyclically in order to assess a displacement ductility equal at least to 3 (during the test a yield displacement equal to about 6 mm is observed). The imposed maximum displacement is then raised to about 30 mm.

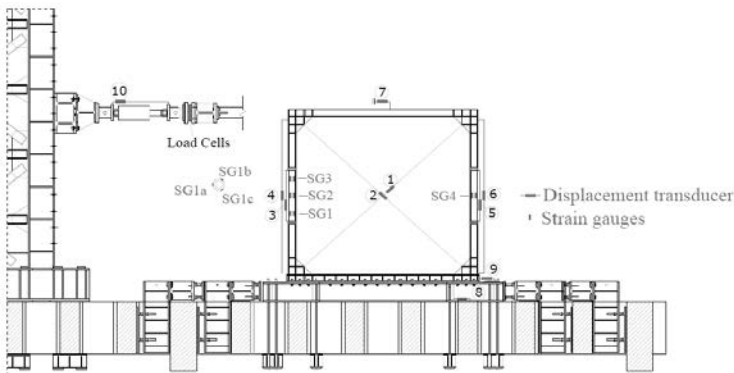


Figure 11. Sensors position.

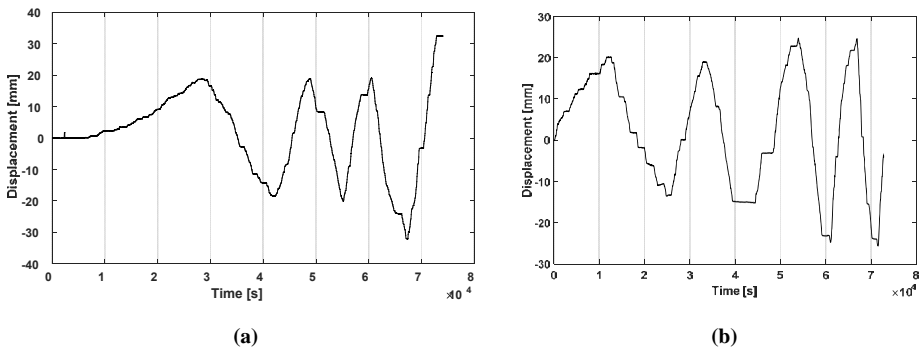


Figure 12. Loading history of tests on (a) Specimen 1 and (b) Specimen 2.

4.2 Experimental results

In Figure 13 the experimental cyclic behaviour of specimen 1 is shown. The first loading cycle highlights a relatively “fat” hysteretic behaviour, while pinching phenomena, with the maximum resistance that remains practically constant, is exhibited during the subsequent cycles. The first semi-cycle (Figure 13b) shows that the system is characterized by a behaviour very close to an ideal elastoplastic one with a displacement ductility equal, at least, to 3. At the end of the first unloading phase, the concrete wall exhibits practically no damage, exception made for a little detachment from the lateral steel boundary elements.

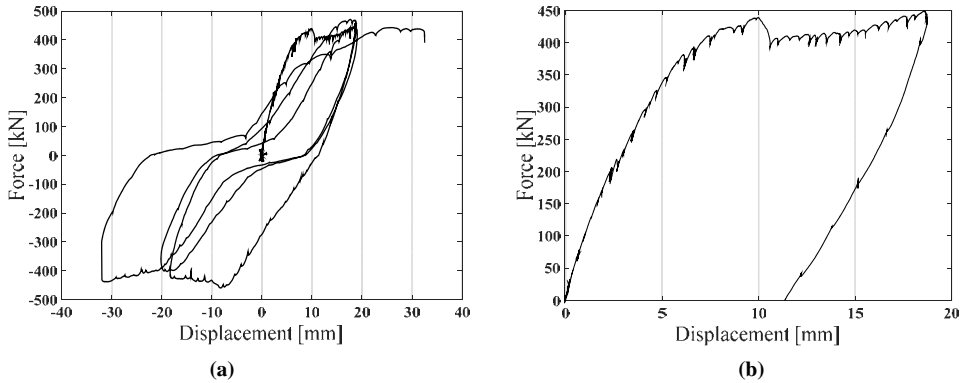


Figure 13. Specimen n.1: (a) cyclic force-displacement curve; (b) first loading and unloading phase.

During the cyclic test, specimen 1 shows the tendency to maintain some plastic deformation in the dissipative elements and vertical displacements (Figure 14) are accumulated in the lower interface between the steel frame and the infill wall. No cracks are detected within the concrete wall. It can be inferred that, mainly due to the low number of shear studs connecting the RC wall to the steel boundary elements, the wall behaves as a rigid body within the steel frame, avoiding any damage, except for the corner zones. Due to the continuous accumulation, cycle after cycle, of the vertical displacements in the lower edge, the force application point of the compressed concrete diagonal strut moves from the reinforced and stiffened steel corner, to the non-dissipative column of the steel frame, as schematically represented in Figure 15.

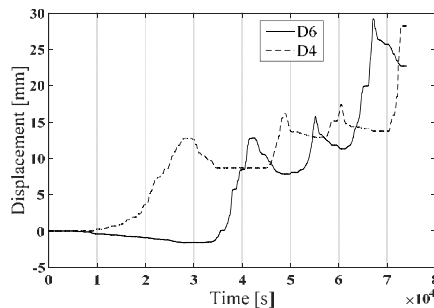


Figure 14. Vertical displacements of columns top recorded by sensors n.4 and n.6 (see figure 15) for Specimen 1.

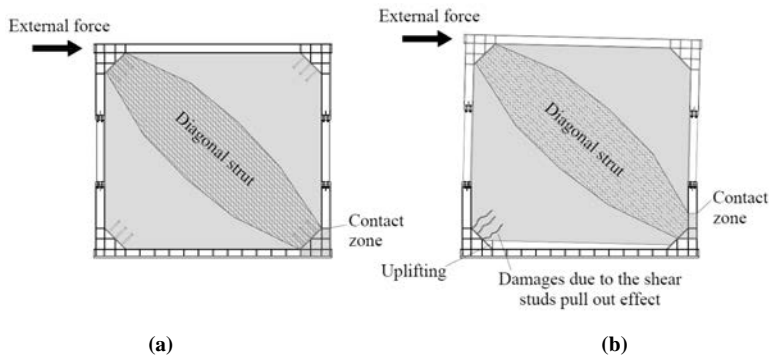


Figure 15. Specimen 1: (a) initial configuration; (b) configuration anticipating failure.

The change of the force application point causes the failure of the specimen due to an excessive shear deformation of the non-dissipative vertical steel element (Figure 16a). At the same time, the spalling of the concrete on the opposite lower corner of the infill wall and the complete detachment of the infill wall from the steel frame occurs (Figure 16b). Practically no other damages are visible within the RC wall.



Figure 16. Lower corners of Specimen 1 after failure: (a) shear failure of the non-dissipative zone and (b) spalling of the concrete and complete detachment by the steel frame.

Specimen 2 shows a behaviour similar to the one of specimen 1 as can be seen in Figure 17, with evident pinching phenomena but with an higher resistance. The diffused presence of the shear studs all along the perimeter of the steel frame allows the transmission of horizontal forces also through shear mechanism, as testified by the diffused diagonal cracking observed within the wall (Figure 18). The more efficient connection between the wall and the boundary steel elements causes the propagation of a main crack from the base of the dissipative element in tension, as illustrated in Figure 18, avoiding any detachment phenomena between the RC wall and the steel frame.

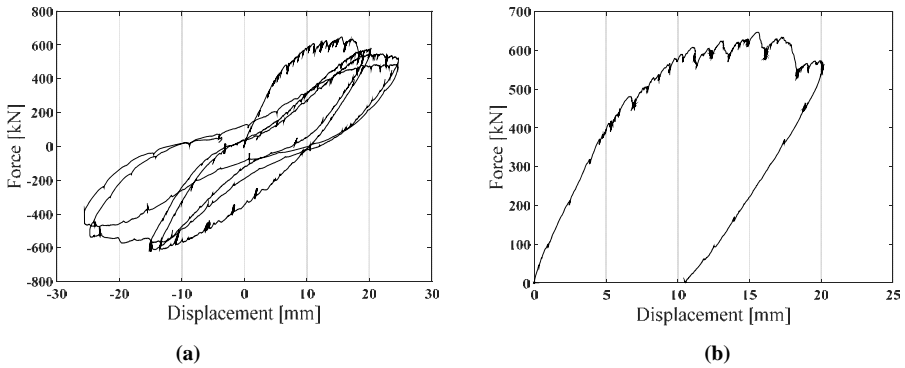


Figure 17. Specimen 2: (a) cyclic force-displacement curve; (b) first loading and unloading phase.

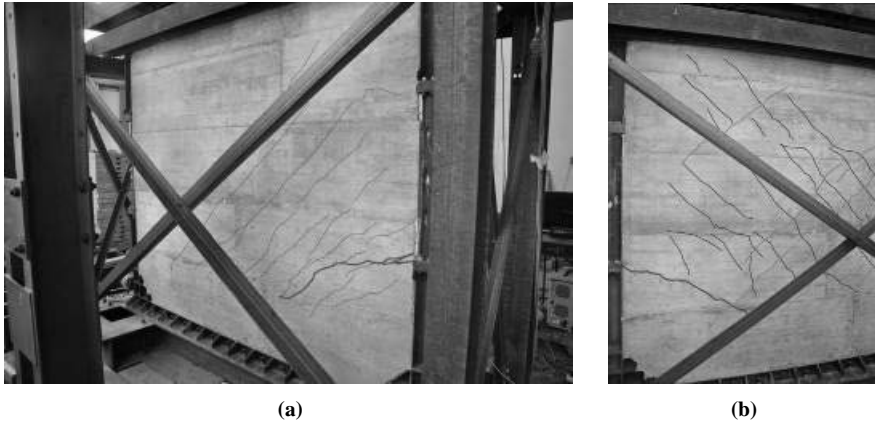


Figure 18. Specimen 2: cracking (a) at the end of the first unloading phase and (b) at the end of the first cycle (red line: main crack; blue lines: diffused cracking).

Specimen 2 shows, similarly to specimen 1, the tendency to accumulate some plastic deformations in the dissipative elements (Figure 19), but the resulting vertical displacement causes the gradual opening of the main cracks instead of the detachment of the wall from the lower edge of the steel frame. Due to the developed displacement, the vertical and horizontal reinforcing bars crossing the main crack break (Figure 20), causing the loss of some horizontal forces carrying capacity. After this break, the behaviour of Specimen 2 is very close to the one of Specimen 1: the RC wall acts as a rigid body within the steel frame originating a lattice brace resisting mechanism instead of a shear wall one.

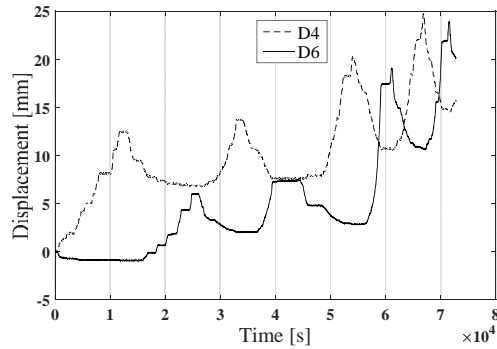


Figure 19. Vertical relative displacements of columns recorded by sensors n.4 and n.6 (see Figure 11) for Specimen 2.



Figure 20. Specimen 2 at the end of the test: (a) global view; (b) failure of the steel reinforcements in tension crossing the main crack.

The residual resistance of Specimen 2, after the breaking of the reinforcing bars, drops to a value very close to the resistance of Specimen 1, see Figures 13a and 17a, confirming the modification of the lateral resisting mechanism. The diffused presence of shear studs provides so an increasing of the initial lateral strength of the system with evident advantages for the whole structure, especially for the limitation of damages in case of low-to-moderate intensity earthquakes.

The experimental behavior of both specimens highlights the tendency of the system to accumulate vertical displacements during the cyclic loading: in Specimen 1 at the bottom interface between the steel frame and the RC wall while, in Specimen 2, in the main cracks that start from the bottom of the dissipative elements and propagate within the wall. In both cases, the presence of such vertical displacements, originated from the tensile effect related to the overturning moment, reduces the horizontal load carrying capacity of the system, due to the moving of the RC truss force application point, such as in Specimen 1, or to the tensile braking of the reinforcing bars and the consequent modification of the resisting mechanism, Specimen 2. In real applications, the presence of the gravity loads transmitted at the different levels of the structure by the floors should so bring positive effects on the resisting system, mitigating the formation of horizontal cracks within the wall, increasing the horizontal load carrying capacity and the re-centering one. Further researches are however needed to numerically and experimentally assess the influence of the vertical loads on both the system configurations.

5 CONCLUSIONS

In this paper a novel SRCW is presented, conceived on the basis of a simple statically determinate structural scheme where the RC walls work as diagonal struts and energy dissipation occurs in the vertical steel elements yielding in tension. A tailored capacity design procedure developed consistently with the Eurocode framework for seismic design is illustrated including a discussion the various steps. Nonlinear finite element analyses are used to validate the outcomes of the proposed design method for two case studies. The adopted numerical model includes a refined three-dimensional model as well as a simpler truss model that basically provided very similar results in terms of the global behaviour of the considered structural system. Afterwards, the behaviour of the proposed system is studied through an experimental campaign on two 2/3 downscaled specimens, characterized by a different shear stud distribution between the RC infills and the steel frame, i.e. shear studs only at the corners in specimen 1, shear studs distributed all along the non-dissipative steel boundary elements in specimen 2. The experimental tests for both specimens highlight the formation of the dissipative mechanism involving the yielding of the vertical dissipative elements, consistently with the design objectives. Good monotonic displacement ductility and cyclic pinching phenomena, a practically constant maximum resistance and a tendency to accumulate tensile plastic deformation on the dissipative elements are observed. Differences between the two shear stud distributions involve the damage distribution and failure modalities as well as the initial lateral stiffness of the system. Overall, both numerical and experimental results show the potentialities of the proposed SRCW system and the relevant ductile design approach for the development of more efficient steel frames with RC infill wall in seismic areas.

6 ACKNOWLEDGEMENTS

Support for this research from the European Commission, Research Fund for Coal and Steel, Steel Technical Group TGS 8 (RFSR-CT-2010-00025), is gratefully acknowledged.

7 REFERENCES

- AISC (2005), Seismic Provisions for Structural Steel Buildings, ANSI/AISC 341-05, March 9, American Institute of Steel Construction, Inc., Chicago, IL.
- Dall'Asta A., Leoni G., Zona A., Hoffmeister B., Bigelow H., Degée H., Braham C., Bogdan T., Salvatore W., Morelli F., Tsintzos P., Karamanos S.A., Varelis G.E., Galazzi A., Medici E., Boni P. (2015). "Innovative hybrid and composite steel-concrete structural solutions for building in seismic area - Final Report", EUR 26932 EN, European Commission, 2015. DOI:10.2777/85404.
- Dall'Asta A., Leoni G., Morelli F., Salvatore W., Zona A. (2017), "An innovative seismic-resistant steel frame with reinforced concrete infill walls", *Engineering Structures*, 141, pp. 144-158.
- Braga F., Morelli F., Salvatore W. (2015). "A Macroseismic approach for the evaluation of seismic Risk". J. Kruis, Y. Tsompanakis, B.H.V. Topping, (Editors), *Proceedings of the Fifteenth International Conference on Civil, Structural and Environmental Engineering Computing*, Civil-Comp Press, Stirlingshire, UK, Paper 91.
- Deierlein G.G., Noguchi H. (2004). "Overview of US-Japan research on the seismic design of composite reinforced concrete and steel moment frame structures". *Journal of Structural Engineering*, 130(2), pp. 361-367.
- Elghazouli A.Y. (2010). "Assessment of European seismic design procedures for steel framed structures". *Bulletin of Earthquake Engineering*, 8, pp. 65-89.

- El-Tawil S., Harries K., Fortney P., Shahrooz B., Kurama Y. (2010). "Seismic design of hybrid coupled wall systems: state of the art". *Journal of Structural Engineering*, 136, pp. 755-769.
- European Committee for Standardization, Eurocode 2 - Design of concrete structures - Part 1-1: General rules and rules for buildings. EN 1992-1-1, November 2005.
- European Committee for Standardization. Eurocode 3: Design of steel structures - Part 1-1: General rules and rules for buildings. EN1993-1-1, August 2005.
- European Committee for Standardization, Eurocode 4 - Design of composite steel and concrete structures - Part 2: General rules and rules for bridges. EN 1994-1, January 2006.
- European Committee for Standardization, Eurocode 8: Design of structures for earthquake resistance - Part 1: General rules, seismic actions and rules for buildings. EN 1998-1, December 2004.
- Hajjar J.F. (2002). "Composite steel and concrete structural systems for seismic engineering". *Journal of Constructional Steel Research*, 58, pp.703-723.
- Liauw T.C., Lee S.W. (1977). "On the behavior and analysis of multi-story infilled frames subject to lateral loading". *Proceedings of the Institute of Civil Engineering*, 63, pp. 641-56.
- Liauw T.C. (1979). "Test on multistory infilled frames subject to dynamic lateral loading". *ACI Journal*, 76, pp. 551-64.
- Liauw T.C., Kwan K.H. (1985). "Static and cyclic behaviors of multistory infilled frames with different interface conditions". *Journal of Sound Vibration*, 99, pp. 275-83.
- Makino M., Kawano A., Kurobane Y., Saisho M., Yoshinaga K. (1980). "An investigation for the design of framed structures with infill walls". *Proceedings of the seventh world conference on earthquake engineering*, vol. 4, pp. 369-72.
- Mallick D.V., Severn R.T. (1968). "Dynamic characteristics of infilled frames". *Proceedings of the Institute of Civil Engineering*, 39, pp.261-88.
- Morelli F., Manfredi M., Salvatore W. (2016). "An Enhanced Component Based Model of Steel Connection in a Hybrid Coupled Shear Wall Structure: Development, Calibration And Experimental Validation". *Computers and Structures*, 176, pp. 50–69.
- Makino M. (1985). "Design of framed steel structures with infilled reinforced concrete walls". Roeder CW, editor. *Composite and mixed construction*. New York (NY), ASCE, pp. 279–87.
- Morino S. (1998). "Recent developments in hybrid structures in Japan: research, design and construction". *Engineering Structures*, 20, pp. 336-346.
- Rossi P.P., Lombardo A. (2007). Influence of the link overstrength factor on the seismic behaviour of eccentrically braced frames. *Journal of Constructional Steel Research*, 63, pp. 1529-1545.
- Saari W.K., Hajjar J.F., Schultz A.E., Shield C.K. (2004). "Behavior of shear studs in steel frames with reinforced concrete infill walls". *Journal of Constructional Steel Research*, 60, pp.1453-1480.
- Spacone E., El-Tawil S. (2004). "Nonlinear analysis of steel-concrete composite structures: State of the art". *Journal of Structural Engineering*, 130, pp.159-168.
- Sun G., He R., Qiang G., Fang Y. (2011). "Cyclic behavior of partially-restrained steel frame with RC infill walls". *Journal of Constructional Steel Research*, 67, pp. 1821-1834.
- Tong X., Hajjar J.F., Schultz A.E., Shield C.K. (2005). "Cyclic behavior of steel frame structures with composite reinforced concrete infill walls and partially-restrained connections". *Journal of Constructional Steel Research*, 61, pp. 531-552.
- Zona A., Barbato M., Conte J.P. (2008). "Nonlinear seismic response analysis of steel-concrete composite frames". *Journal of Structural Engineering*, 134, pp. 986-997.
- Zona A., Ragni L., Dall'Asta A. (2012). "Sensitivity-based study of the influence of brace over-strength distributions on the seismic response of steel frames with BRBs". *Engineering Structures*, 37, 179-192.
- Zona A., Degeé H., Leoni G., Dall'Asta A. (2016). "Ductile design of innovative steel and concrete hybrid coupled walls". *Journal of Constructional Steel Research*, 117, pp.204-213.

SECTION 8

BRIDGES

SEISMIC BEHAVIOUR OF STEEL-CONCRETE COMPOSITE BRIDGE DECKS

Luigino Dezi ^a, Sandro Carbonari ^a, Andrea Dall'Asta ^b, Fabrizio Gara ^a,
Lucia Minnucci ^a

^a *Università Politecnica delle Marche, Dept. ICEA, Ancona, Italy,
l.dezi@univpm.it; s.carbonari@univpm.it; f.gara@univpm.it; l.minnucci@pm.univpm.it*

^b *University of Camerino, SAAD, Ascoli Piceno, Italy, andrea.dallasta@unicam.it*

ABSTRACT

The paper focuses on local problems relevant to the seismic response of steel-concrete composite bridge decks. In particular, the local mechanisms involved in the transferring of inertial forces from the slab to substructures are investigated with particular focus on the shear connection and the role of end cross beams. Firstly, open issues relevant to the seismic design and analysis of steel-concrete composite bridge decks are discussed and an overall state-of-art of the problem is depicted. Then, some case studies constituted by single span and two-spans I-shaped twin-girders and box girders steel-concrete composite bridges are selected and adopted to investigate local response of the decks subjected to seismic actions. Linear and non-linear applications are performed adopting different analysis methodologies in order to investigate stress resultants in the shear connection and to analyse the role of the end cross beams on the local transferring mechanisms of inertia forces; results of analyses on the selected case studies are shown and discussed.

KEYWORDS

Bridges, cross beams, load paths, local resisting mechanisms, seismic response, shear connection, steel-concrete composite bridge deck.

1 INTRODUCTION

Steel-concrete composite bridges represent a very common, economical, and efficient structural solution, especially for short and medium span lengths (Collings, 2005). These bridges are generally constituted by a continuous steel-concrete composite deck supported by reinforced concrete piers (Itani *et al.*, 2004). According to modern seismic codes (e.g. Eurocode 8), the composite deck is required to behave almost elastically, while piers usually provide the main seismic energy dissipation source, unless passive seismic protection techniques are adopted. The seismic performance of steel-concrete composite bridges has been extensively discussed in the literature and drawbacks, potentially leading to unsatisfactory seismic behaviours, have been highlighted by Astaneh-Asl *et al.*, Itani *et al.* and by Kawashima. Numerical investigations about potential causes of vulnerability have also been carried out, as in Padgett and DesRoches. Above works highlighted that steel-concrete composite bridges are very sensitive to earthquake loading and extensive damage can occur not only in the substructures, which can be designed to yield and dissipate the seismic energy, but also in the components of

the superstructure (steel-concrete composite deck and bearings), involved in carrying the seismic loads.

Furthermore, in the case of ductile piers, a special attention should be dedicated to the bridge transverse behaviour; in this case the deck is usually rigidly connected to piers and abutments through fixed bearings, steel plate stoppers or special links restraining the transverse displacements. This leads to a “dual load path” transverse behaviour, strongly involving the deck for the distribution of the transverse seismic inertia forces (Calvi, 2004; Tubaldi *et al.*, 2010; Tubaldi *et al.*, 2012; Tubaldi *et al.*, 2013). In particular, the transverse behaviour is characterized by the following two different mechanisms resisting the earthquake-induced inertia forces: (1) the inelastic load path constituted by the piers, designed to yield and dissipate energy; and (2) the elastic load path formed by the deck and the abutments, designed to remain elastic according to capacity design principles. During increasing horizontal loads the force transferred at the end supports (abutments) and the global transverse bending of the deck may become very demanding. Similar problems occur in the partially isolated bridges, when transverse fixed bearings are located at the abutments in order to avoid expensive bidirectional joints and to control the maximum transverse displacement (Tubaldi and Dall'Asta, 2011; Tubaldi and Dall'Asta, 2012).

The seismic design of bridges is generally organized in two levels: the former oriented to study the global dynamic response and to evaluate the stress resultants in the main components and the latter oriented to study the local behaviour of special components and to define the activated resisting mechanisms, considering their relevant influence on the global behaviour. Concerning the global response, a consolidated knowledge and a wide literature exists about the seismic behaviour of statically determined (simply supported) girders with regular geometry and regular substructures. In this case, simplified linear methods apply and a complete framework of design procedures is suggested by codes. On the contrary, the global seismic design of continuous composite bridges presents some open issues, like for example the effective dissipative properties of the whole system and the definition of design forces and over-strength factors to protect elastic mechanisms.

As the global response of the structure has been widely analysed in the literature, many local aspects are still little investigated. Local issues deserve attention in the design of steel-concrete composite bridges as they may affect the overall structural behaviour. In particular, over the seismic resistant supports, the role of diaphragms on seismic load paths has been little further explored though many steel bridges have reported damaged cross beams during recent earthquakes (Itani *et al.*, 2004; Dicleli and Bruneau, 1995; Bruneau *et al.*, 1996). Different cross beam typologies, each characterised by specific systems of connection with the longitudinal beams and substructure, are available, but only few works focus on the problem of damage of diaphragms and the relevant retrofitting techniques for existing bridges (Zahra and Bruneau, 1998 and 1999a,b). These works report that a dramatic change in the seismic behaviour may occur once an end diaphragm fractures (elongation of the bridge transverse periods has been observed with consequences on the deck displacements). It has been also found that the presence of intermediate diaphragms does not significantly influence the seismic performance of these types of bridges, in either the elastic or the inelastic range. Studies are necessary to investigate the resisting mechanisms associated to different diaphragm typologies and to define the relevant design forces.

Analogously, the shear connection (the most common and widespread steel-concrete connection in Europe as well as worldwide is constituted by headed stud shear connectors) is designed to withstand actions at non-seismic Ultimate Limit State, according to design formulas that are calibrated for monotonic one-directional actions (Viest, 1956; Ollgaard *et al.*, 1971; Lee *et al.*, 2005; Valente I., Cruz, P., 2009; Johnson, 2000) and are not suitable to

quantify capacity of studs subjected to cyclic bi-directional actions induced by earthquakes. Despite many Authors have contributed to the research concerning the behaviour of the stud shear connectors (Zona *et al.*, 2017), there is still a lack of knowledge regarding the seismic (i.e. low-cycle) behaviour of these elements.

The paper offers a contribution on the understanding of local load transfer mechanisms governing the seismic response of steel-concrete composite bridge decks. In particular, seismic forces acting on the shear connection and the role of end cross beams are analysed with reference to some case studies constituted by single span and two-spans I-shaped twin-girders and box girders bridges. Furthermore, different analysis methodologies (in the linear and non-linear field) are adopted to investigate stress resultants in the shear connection and to analyse the role of the end cross beams on the local transferring mechanisms of inertia forces from the deck to substructures.

2 STATE OF ART AND OPEN ISSUES

Continuous steel-concrete composite decks with short and medium spans represent a large part of bridges in Europe. The most widespread cross-section typologies are the twin girder solution with a concrete slab of constant or variable thickness, and the box-girder solution. Among the first cross-section type, I-shaped steel beams are generally employed, locally connected each other by I-shaped cross beams (transverse stiffeners) either not connected or directly-supporting the slab, depending on the width of the slab itself. In fact, for increasing slab width, this sectional typology may be still used if the main girders are interconnected by directly-supporting cross beams (Figure 1b). In some cases, the cross beam solution with cantilevers may be used to limit the girders spacing (Figure 1c).

Box girder composite bridges are less popular because they are more complex and expensive to build and maintain, but they are winning solutions for long span bridges, wide decks and high horizontal curvature. This solution may also be preferred to the previous one for aesthetic reasons. The simplest box girder deck is constituted by a concrete slab and a U-shaped steel frame (Figure 2a); the steel component is formed of longitudinal plates (flanges and webs that may be vertical or inclined) and of transverse elements (bulkheads at the supports, generally connected to the concrete slab and frames within the span). In the upper flanges the connection steel plates are soldered, while on the lower plates many steel profiles are employed to strengthen the web all along the deck to prevent buckling phenomenon. As for the previous typology, box girders can be provided along with directly supporting cross-beams with cantilevers (Figure 2b) or with propped cantilevers (Figure 2c).

The seismic design of bridges with composite steel-concrete decks is mainly oriented to the solution of global problems, governed by strength and ductility issues of the whole structure, and less attention is generally given to local problems of the deck that is generally designed with reference to vertical loads at Ultimate Limit States (ULSs). The deck is required to remain essentially elastic and the capacity is generally determined according to a conventional sectional analysis in which the deformability of the shear connection is neglected. According to Eurocode 8 Part 2, yielding of the deck is considered to be significant when it reaches the reinforcements of the concrete slab at a distance from its edge equal to the 10% of the slab width (or at the junction with the steel web, if it is closer to the edge). In the case of bridges with ductile behaviour, the check should be carried out assuming actions determined according to hierarchy rules.

Actually, transfer mechanisms of seismic horizontal forces from decks to substructures strongly involve the shear connection, which may undergo damage, as well as transverse diaphragm

systems (e.g. cross-beams, truss diaphragms). These mechanisms mainly develop at seismic resistant supports as demonstrated by damage suffered by diaphragm (cross beam) during recent earthquakes (Itani *et al.*, 2004; Dicleli and Bruneau, 1995; Bruneau *et al.*, 1996) (Figure 3a). With reference to the shear connection, headed studs represent the most employed solution for the shear connection in composite bridges (Figure 4). Studs of diameter 22 mm with a 25 mm diameter head of thickness 10 mm are generally used. As for the height, the most common dimension is 200 mm (lengths of 150, 175 or 225 are also used). Studs are usually located on the main girder top flanges and organized in rows. In the longitudinal direction, studs present different spacing, depending on the deck cross section and the design approach. If an elastic design is adopted, in mid-span sections (low shear actions), the studs spacing can reach 800 mm, while in hogging regions the studs spacing is far less and can be 200 mm.

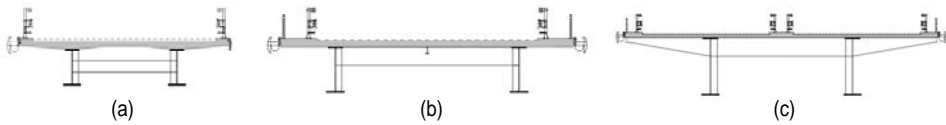


Figure 1. (a) Twin girder deck; (b) twin girder directly supporting cross-beams without cantilevers and (c) twin girder directly supporting cross-beam with cantilevers.

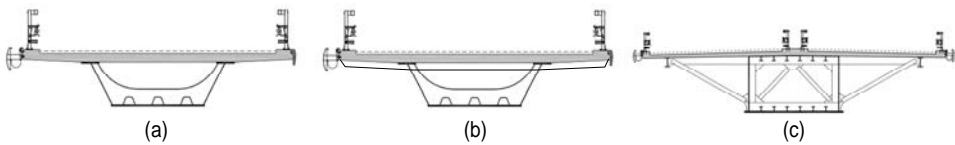


Figure 2. (a) Open box girder; (b) box girder directly supporting cross-beams with cantilevers and (c) box girder directly supporting cross-beam with propped cantilevers.

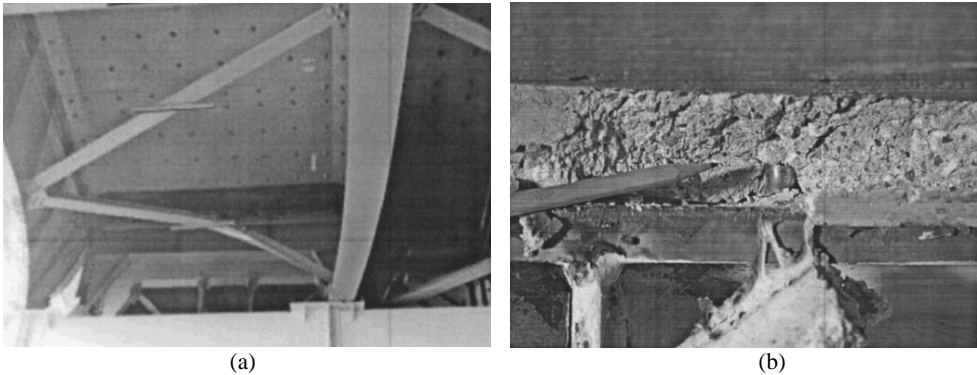


Figure 3. (a) Damage to end cross frames and girders during 1995 Kobe earthquake; (b) failure of shear connectors in bridge model during transverse cycling loading.



Figure 4. (a) Headed studs, (b) section view of connectors.

If the design is based on a plastic approach (recurring conditions required for both the main girders and the connection) studs spacing is almost constant along the girder top flange. In any case, the studs spacing must be compatible with the slab transverse reinforcements. The steel frame-slab connection is designed according to EN 1994-2 (and the relevant national appendices); this is based on forces acting at the ULS for vertical loads and the capacity of the studs is evaluated according to formulas suggested by the code that accounts for two possible failure mechanisms, associated to the static collapse of the stud and the concrete. Local transferring mechanisms developing at seismic resistant supports strongly involve the shear connection in proximity of cross frames and forces may exceed the connector capacity, as observed by Itani et al., 2004 (Figure 3b).

The transfer mechanisms of the inertial forces depend on the deck cross-section typology and on the deck static scheme at dynamic conditions. The typical bearing systems adopted for a single span and for a two-span bridge are shown in Figure 5. According to these schemes, which allow for thermal dilatations, longitudinal seismic actions are resisted by two supports while transverse actions are resisted by two supports for the single span bridge and by three supports for the two-span bridge.

2.1 Twin girders bridges

For twin I-shaped girder bridges, the path of transverse inertia forces at each seismic support should comply with those reported in Figure 6a and 6b for cross beams not connected or connected to the slab, respectively. The distribution of forces on the shear connection in the hogging sections of the deck may depend on the cross beam flexural stiffness. Furthermore, shear force and bending moment, the latter produced by eccentricity between inertia force and bearing reaction (Figure 7), could entail transverse sections significant local distortions.

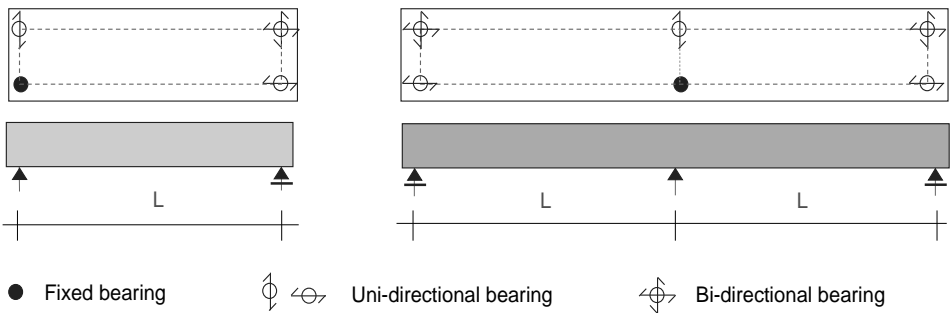


Figure 5. Typical bearing systems for single span and two spans bridges.

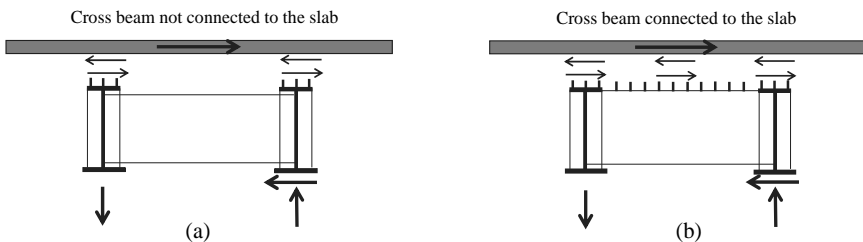


Figure 6. Transfer mechanism of transverse seismic actions for twin I-shaped girders with cross beams (a) not connected to the slab and (b) cross beams connected to the slab.

The distribution of forces on the shear connection in the hogging sections of the deck may depend on the cross beam flexural stiffness; shear force and bending moment, the latter produced by eccentricity between the inertia force and the bearing reaction, could entail significant local distortions of the cross section. When the transverse seismic force acts on the slab, the shear centre position is such that the inertial force induces a torque along the deck, balanced by the bi-flexion resistant mechanism that, depending on the cross-section typology, may develop further longitudinal shear forces in girders and in the shear connection. The girder in the fixed bearing seeks to lift up clockwise. Moving from the supports toward the mid-span, the deformation induced by the torque increases, as the rotation and the resulting girders up/down-lift are not prevented by the bearings. Finally, on the fixed bearing, the girder is subjected to the horizontal reaction due to equilibrium of the inertial force.

With reference to longitudinal seismic actions, the equilibrium condition reported in Figure 8 occurs for the single span and two span bridges, respectively. The actual distribution of forces acting on the shear connection depends on the slab-to-steel component axial stiffness ratio and a more significant effect is expected in correspondence of the fixed bearing. In addition, a constant shear action arises to equilibrate the bending moment induced by the eccentricity of inertia forces (mainly acting at the slab level) with respect to supports. The importance of this contribution depends on the girders height and the span length. Generally, by increasing the span length, the girders height increases, as well as the resultant of the inertia forces (because of the increasing masses); however, since the lever arm increases, general considerations are not possible.

2.2 Box-girder bridges

Concerning the box-girder transverse cross section, the typology shown in Figure 9 could be considered. For the seismic action acting in the transverse direction, a torque arises; this is balanced by the shear flows developing in the thin-walled box cross section (pure torque).

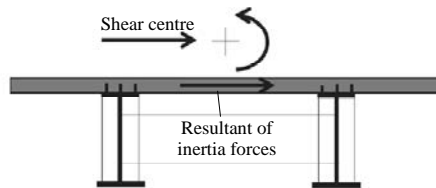


Figure 7. Shear centre and inertia forces resultant for a twin girders cross section.

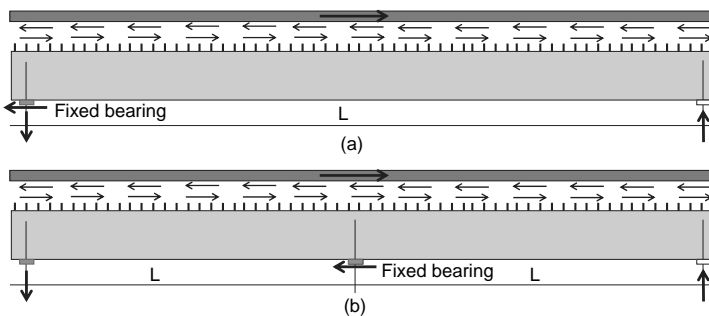


Figure 8. Transfer mechanism of transverse seismic actions for twin I-shaped girders for (a) single span and (b) two span bridges.

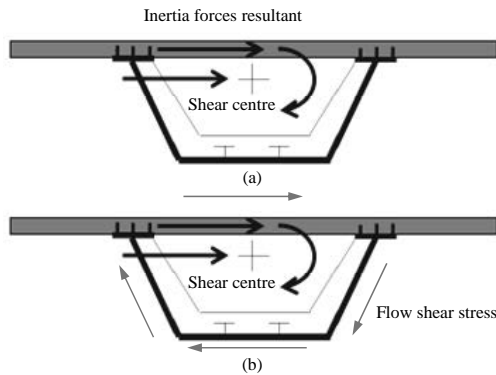


Figure 9. Transfer mechanism of transverse seismic actions for a typical box-girder structure: (a) distribution of the transverse seismic action and (b) flow shear stress.

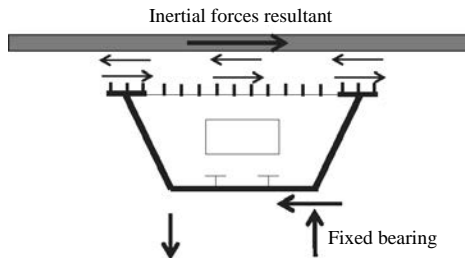


Figure 10. Local transfer mechanism of transverse seismic actions at the end sections.

Shear flows produces stresses that superimpose to the ones induced by the longitudinal global shear force due to vertical loads.

The torque induces a global rotation of the deck that increases moving from the bridge supports toward the mid-span, while deformations induced by the local transfer mechanism of inertial forces at supports are mitigated by the end diaphragms, which are generally directly connected to the slab through studs.

All previous observations apply to both single span and multi-span bridges.

2.3 Open issues

In previous paragraphs the qualitative behaviour of steel-concrete composite bridge decks subjected to longitudinal and transverse seismic actions has been presented, focusing on local problems induced in the shear connection and cross beams at supports. The significance of forces induced on the shear connection and studs as a consequence of the seismic actions has not been well addressed in the literature and studs are generally designed only referring to the ULS shear stress. From an overall point of view, during an earthquake, shear connection is stressed by cyclic forces acting along the longitudinal and transverse direction of the deck, due to the bi-directional seismic excitation, and by forces acting along the longitudinal direction, due to the vertical permanent loads. The shear connectors design formulas are calibrated for monotonic one-directional actions while earthquake produces cyclic bi-directional actions that superimpose to forces induced by vertical loads. Furthermore, the Safety verifications of the deck for seismic actions require the deck to remain essentially in the elastic range; connectors become inelastic more quickly than their rigid counterpart under moderate or strong earthquakes. Thus, even in the case shear forces at the connection level are lower with respect

to the design one (evaluated for vertical loads at ULS, dominated by traffic loads), an issue on the connection damage limitation arises (involving the definition of a service limit state for the shear connection). The Eurocode provides detailed information regarding the checks that enable to state that the deck is essentially in the elastic range only by considering the behaviour of the reinforcements neglecting the effect of the inelastic behaviour of the connection. No studies have been performed to support this assumption. Finally, the distribution of seismic shear forces on the steel frame-slab connection strongly depend on the transfer mechanisms of inertia forces from the deck to the substructures, which in turn depend on the deck cross-section typology and the cross beams at seismic resistant supports. Thus, the role of the end cross beams and the contribution of the pier deflection are worth to be investigated too.

The study of above issues cannot be performed exploding the beam approach for the deck modelling, currently largely adopted in the literature for the seismic evaluation or design of bridges. In fact, this approach does not allow the investigation of failures associated to local problems involved in the transfer mechanisms of inertia forces from the slab (where most of the bridge mass is located) to the steel components and substructures. The study of these problems needs advanced numerical finite element models able to account for the articulated geometry of the deck sections at supports and the interactions arising among the different parts of the composite structure (slab and steel girders).

3 CASE STUDIES

3.1 Cross section typologies and decks static schemes

The analysis of local problems of steel-concrete composite bridge decks subjected to seismic loads is performed with reference to some case studies constituted by single span and two-span bridges, characterised by a twin-girder and a box-girder steel-concrete composite deck. In particular, span lengths of 48 m are assumed and the static schemes reported in Figure 11 are considered. The deck restraints are defined to allow free elongations at service conditions and are not modified for the dynamic situation using lock-up devices. Thus, seismic actions in the transverse direction of the bridges are resisted by only one bearing at each support while a couple of bearings at only one support entrusts inertia forces in the longitudinal direction.

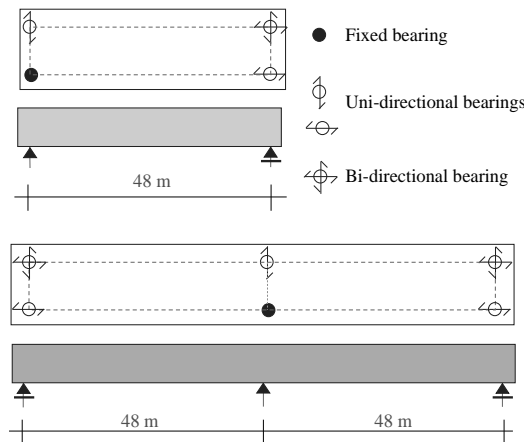


Figure 11. Deck static schemes for single span and two-span bridges.

Both the cross section typologies have a 12 m wide slab, with mean thickness of 0.30 m, while steel elements presents the geometry reported in Figure 12 and Figure 13 for the twin-girder and box-girder cross sections, respectively. The twin-girder cross section is composed by two 6 m spaced 2.4 m high steel I-shaped girders, connected by I-shaped 6 m spaced cross beams. Webs of longitudinal girders are stiffened in correspondence of cross beams by means of vertical plates, which are bigger above the supports in order to avoid the buckling of the web. The box-girder cross section is stiffened on the lower plate by T-shaped members to avoid the buckling at hogging regions subjected to negative bending moment. Stiffeners are continuous along the whole deck. Transverse diaphragms, directly connected to the slab, are provided at the seismic resistant supports while 6 m spaced stiffener plates not connected to the slab are placed longitudinally in mid-span sections.

Loads acting on the deck are schematically depicted in Figure 14 and reported in Table 1. The permanent structural loads are automatically defined as gravitational loads due to the masses of the model components. The permanent non-structural loads derive from the road pavement self-weight. Moving loads and wind are assigned according to the Italian NTC 2008. Finally, the seismic action is evaluated through some different method as illustrated in §3.3.

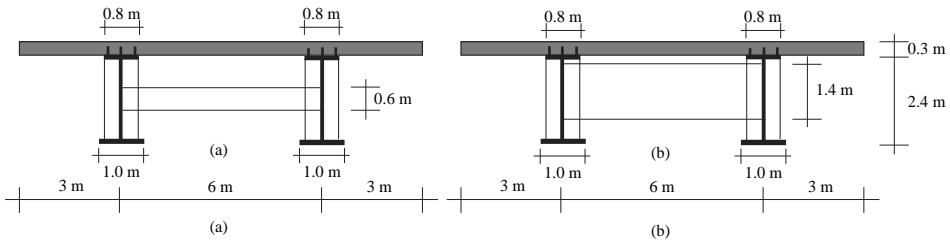


Figure 12. Twin-girder cross section geometry: (a) mid-span cross-section and (b) support cross-section.

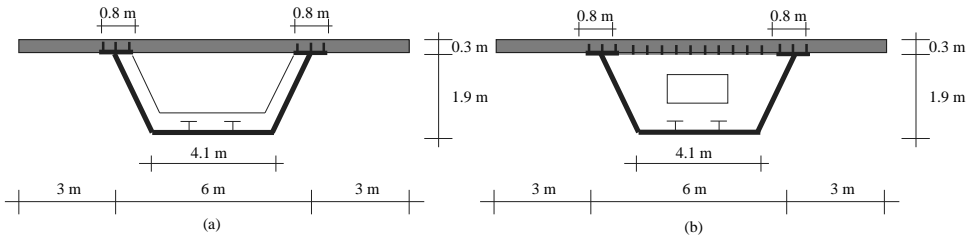


Figure 13. Box-girder cross section geometry: (a) mid-span cross-section and (b) support cross-section.

Table 1. Acting loads on the deck.

Type of Load	Intensity
Permanent structural Loads (G1)	(automatically defined from the model)
Permanent non-structural Loads (G2)	35 kN/m
Mobile Loads (Qm)	3 lanes
Vertical Wind (Qv)	8.92 kN/m
Transversal Wind (Qv)	9,13 kN/m
Seismic Action (E)	(see §3.3)

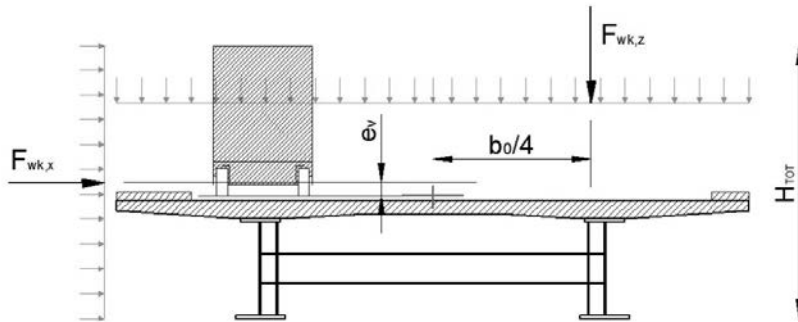


Figure 14. Accidental Loads (Moving Loads and Wind).

Actions have been combined for the deck verifications and the shear connection design according to the Ultimate Limit States defined by the Italian NTC 2008. Slab reinforcement ratio is 1% for mid span cross sections and 2% for cross sections at supports. The shear connection is constituted by 180 mm high-headed shear studs of diameter $\phi 22$ mm, organised in three rows and spaced 200 mm along the beam axis. According to the EC4, the shear capacity of the single stud is 109.5 kN.

At seismic condition, only actions and masses the permanent loads are assumed, according to the Italian NTC 2008. Total vertical loads for the seismic combination are about 140 kN/m, including self-weights. The bridge deck overall complies with requirements of EC8-2 for what concerns verifications at seismic conditions.

3.2 Structural modelling

As stated above, the equivalent beam approach, usually adopted for the modelling and analysis of bridge decks, is not able to capture local mechanisms assuring the transferring of inertia forces from the slab to substructures. Thus, for the analysis of local problems, complete 3-dimensional finite element models of the decks are developed exploiting potentials of the computer structural analysis program Straus7. All structural elements (plates of longitudinal steel girders, cross beams and stiffeners, as well as the concrete slab) are modelled through shell elements taking into account the actual position of their mid-planes. The mean dimension of the mesh is 0.2×0.2 m (Figure 15a). Materials are assumed to behave linearly with Young's modulus $E_s = 200000$ MPa and $E_c = 34000$ MPa for the steel and the concrete, respectively. Rigid constraints are used to account for the bearings dimensions, and restraints are applied to the master node of the constraints.

The shear connection is modelled with beam elements. The actual position of studs is considered (3 rows of connectors at the top plate of each longitudinal girder) (Figure 15b) and connectors are constituted by beam elements connecting the mid-plane of the top plate of the steel girder with the mid-plane of the concrete slab. In particular, each connector is modelled by two beam elements, one of short length in which the shear deformability is lumped and one with increased stiffness properties to simulate a rigid shear behaviour (Figure 16 a). In addition, both beam elements have a rigid flexural behaviour. Studs have a nonlinear shear behaviour defined according to the model of Ollgaard et al. (1971); an equivalent secant shear stiffness (at 40% of the maximum shear capacity) is also provided for the need of performing linear analyses (Figure 16b) in conjunction with nonlinear ones. In details, the following

expressions is used to relate the shear force of each stud t to his relevant slip d (Ollgaard *et al.*, 1971)

$$t = t_u (1 - e^{\beta d})^\alpha \tag{1}$$

where t_u is the maximum shear capacity of the stud and $\alpha = 0.558$, $\beta = 1$ are experimental parameters depending on the stud typology. The maximum shear value is defined as

$$t_u = \min(P_{Rd,a}, P_{Rd,b}) \tag{2}$$

where $P_{Rd,a}$ and $P_{Rd,b}$ are the ultimate shear resistance relet to the concrete and steel failures, respectively (NTC2008).

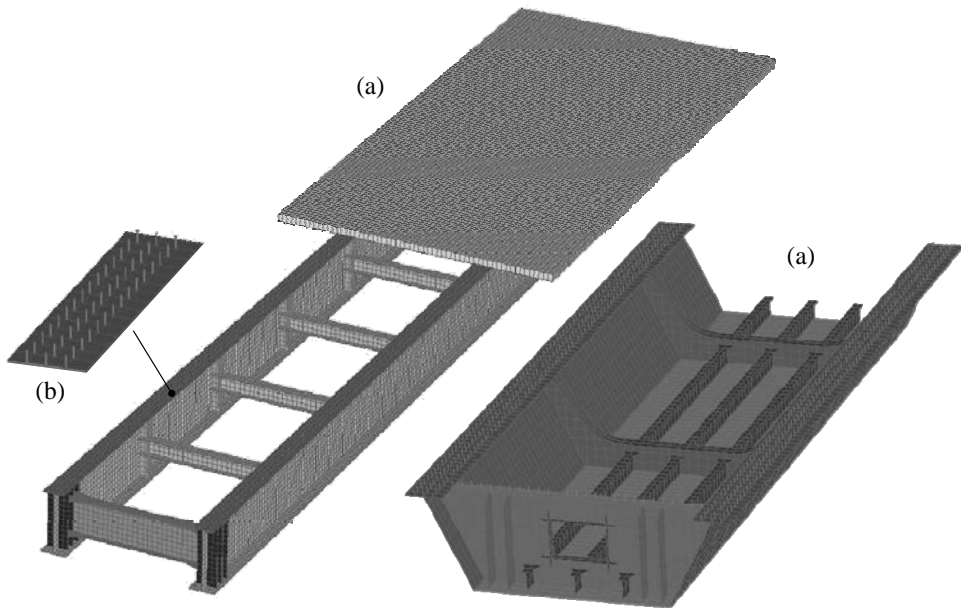


Figure 15. 3D finite element model of the bridge deck: (a) overall view, (b) detail of the studs modelling.

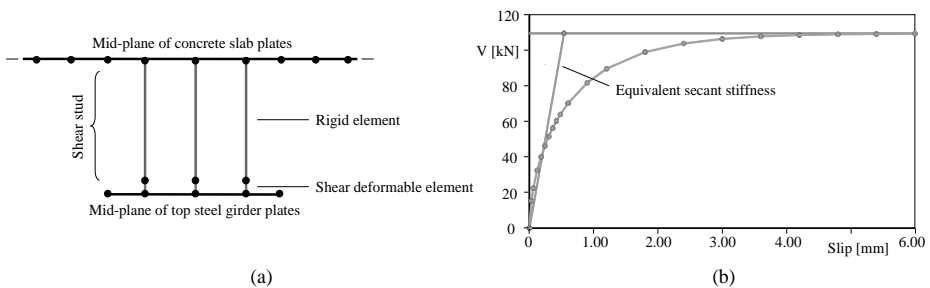


Figure 16. (a) Steel-concrete connection modelling; (b) shear force-slip relationship of the single stud.

3.3 Seismic action

In order to emphasize effects of seismic loads, bridges are assumed to be located in a high seismicity area characterised by a Peak Ground Acceleration (PGA) of 0.373 g, corresponding to a probability of exceedance of 10% in 100 years, which is assumed to be the bridges service life, for a type C soil profile. The pseudo-acceleration response spectrum, associated to the selected area, is reported in Figure 17.

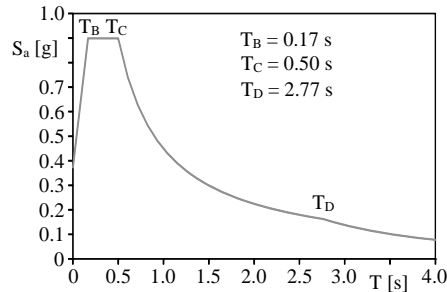


Figure 17. Pseudo-acceleration elastic response spectrum.

The seismic action effects have been studied with increasing complexity methods in order to highlight advantages or limits of the different approaches. Applications include linear and nonlinear static equivalent analyses, linear dynamic modal analyses and linear and nonlinear dynamic analyses through direct integration of the equations of motion. In the static equivalent analyses, the seismic actions are simulated through a mass proportional distribution of horizontal forces with intensity determined according to the highest pseudo-spectral acceleration (0.9 g, according to response spectrum of Figure 17 and the fundamental periods of the bridge deck).

Dynamic analyses using the response spectrum are performed considering 25 modes of vibration, necessary to involve the 85% of the whole deck mass (NTC2008). Finally, in the linear and nonlinear time history dynamic analyses 3 different artificial response spectrum-compatible time-histories are considered (Figure 18), as well as a set of seven real records, characterised by a mean spectrum that overall matches the reference one of the code (Figure 19). All the artificial accelerograms have a duration of 25 s, with a stationary part of 10 s. A Rayleigh damping is defined, calibrating stiffness and mass coefficients in order to get a 5% structural damping in correspondence of the first two vibration modes with the higher participating masses.

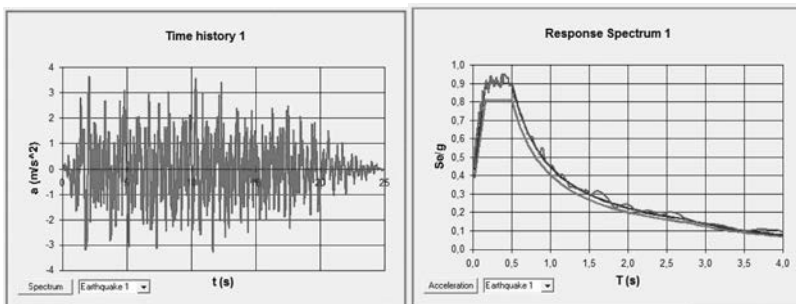


Figure 18. An example of artificial accelerogram and its compatible response spectrum.

All time histories of accelerations, especially the real records, have been pre-processed applying a third order polynomial baseline correction. All the analyses are performed considering the seismic action acting separately in the longitudinal and transverse direction of the deck.

Only single span bridges have been investigated through the direct integration dynamic analyses to conjugate the need of evaluating the effectiveness of simplified analysis approaches with the one of limiting the computational effort of the applications. Table 2 summarizes all the performed analysis for each case study.

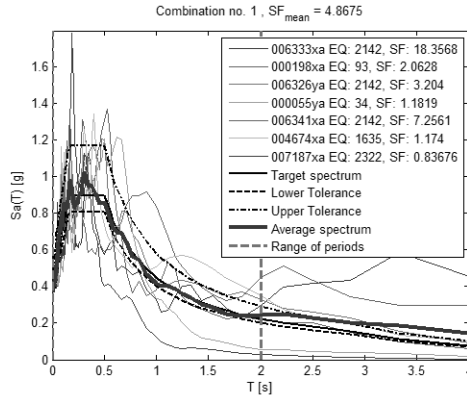
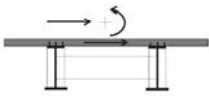
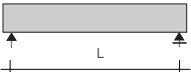

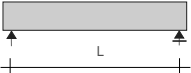
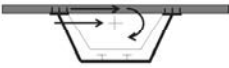



Figure 19. Selection of real earthquakes: elastic response spectra, average spectrum and target spectrum.

Table 2. List of the performed analyses on the selected models.

Cross section	Structural scheme	Seismic analyses
 Twin-girder cross section	 Single span bridge	<ul style="list-style-type: none"> • Linear static • Non-linear static • Linear dynamic • Time history (only transverse direction)
	 Two span bridge	<ul style="list-style-type: none"> • Linear static • Non-linear static • Linear dynamic
	 Single span bridge	<ul style="list-style-type: none"> • Linear static • Non-linear static • Linear dynamic • Time-history (only transverse direction)
 Box-girder cross section	 Two span bridge	<ul style="list-style-type: none"> • Linear static • Non-linear static • Linear dynamic

4 MAIN RESULTS

In this section, main results of seismic analyses performed on the selected case studies are reported. In particular, distributions of shear forces on the steel-concrete connection on the top plates of the longitudinal steel girders due to seismic loads acting in the longitudinal and transverse directions are presented and discussed. The significance of seismic induced shear forces on the steel-concrete connection is evaluated comparing results with those obtained for the ULS.

Results obtained for the simply supported bridge decks are firstly presented. For this case studies, the role of the cross beam on the local transferring mechanisms at supports is investigated with reference to the twin-girder bridge.

4.1 Twin-girder steel-concrete composite bridge decks

4.1.1 Single span deck

Figure 20 plots the transverse shear forces on the steel-concrete connection (obtained by summing forces acting in the three aligned connectors) along the top plates of the two steel girders due to the transverse seismic action. Results from linear static analyses are addressed in Figure 20a while those of nonlinear static applications are reported in Figure 20b.

It can be observed that the shear connection is almost unstressed along the whole beams, excepting for the end beam sections, about 2 m long, where transverse shear forces increase rapidly up to a maximum value in correspondence of the support that depends on the connection behaviour (linear or nonlinear). This result confirms that inertia forces, mainly acting on the concrete slab, travel on the slab itself, which is stiffer than the steel counterpart. As expected, shear forces from nonlinear analyses are lower with respect to those obtained from linear applications, as a consequence of the connection plasticization. However, the redistribution of forces appears to be confined in a limited beam end section.

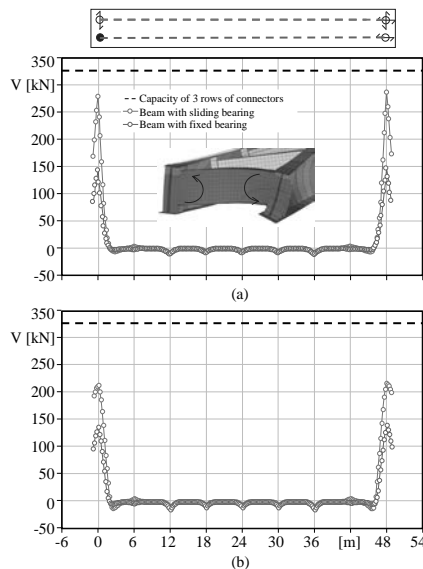


Figure 20. Distribution of transverse shear forces on the steel-concrete connection due to the transverse seismic action: (a) results of linear analysis and (b) results of nonlinear analysis.

The end cross beam plays an important role in distributing the transverse seismic inertia forces on the steel-concrete connections of the two steel girders. The local transfer mechanism, developing as a consequence of the un-symmetric boundary conditions, induces a significant distortion of the end cross sections with the cross beam deforming flexurally (Figure 21). The cross beam exerts recall forces on the steel girder with sliding bearing that limit the beam rotation and produce an increment of shear forces acting at the level of the steel-concrete connection.

Above observations hold for results from the other analysis approaches, as shown in Figure 22, which compares results from linear applications in terms of transverse shear forces in the shear connection of both longitudinal beams. Results from the static equivalent approach are in good agreement with those obtained from dynamic analyses for the shear connection at the end-support including the fixed bearing ($z = 0$ m) while at the opposite end support ($z = 48$ m) greater differences can be observed between results from static equivalent and dynamic analyses. By assuming results obtained from time history applications as “correct”, Table 3 reports the percentage error resulting from the use of the response spectrum and static equivalent approaches at both beam ends. It can be concluded that the maximum shear forces can be well captured by static equivalent applications.

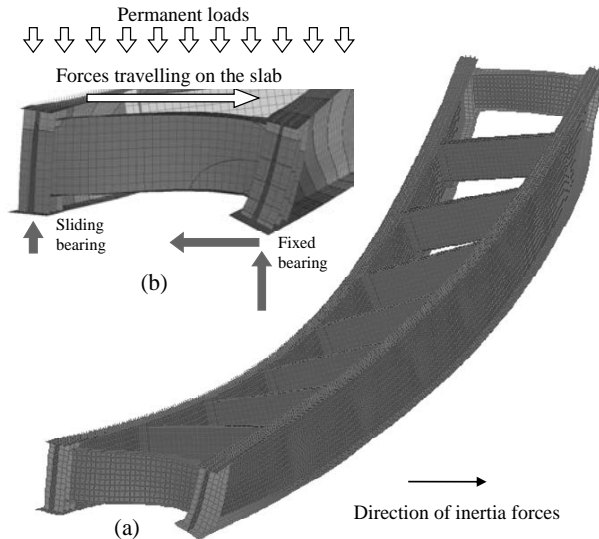


Figure 21. (a) Deformed shape of the simply supported deck subjected to transverse seismic action; (b) local transfer mechanism at supports inducing the cross-sections distortion.

Table 3. Percentage error with reference to time history analyses results in terms of maximum transverse force on the shear connection over the supports.

	Response Spectrum Analysis		Static Equivalent Analysis	
	Beam with Fixed Bearing	Beam with Sliding Bearing	Beam with Fixed Bearing	Beam with Sliding Bearing
Cross section at ($z = 0$ m)	1.61 %	3.57 %	2.05 %	2.88 %
Cross section at ($z = 48$ m)	2.2 %	1.1 %	24.9 %	25.7 %

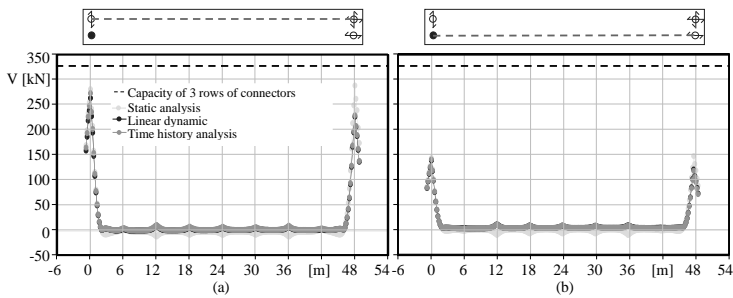


Figure 22. Comparison of distributions of transverse shear forces obtained from different analysis methods: (a) results for the beam with sliding bearing and (b) with the fixed bearing.

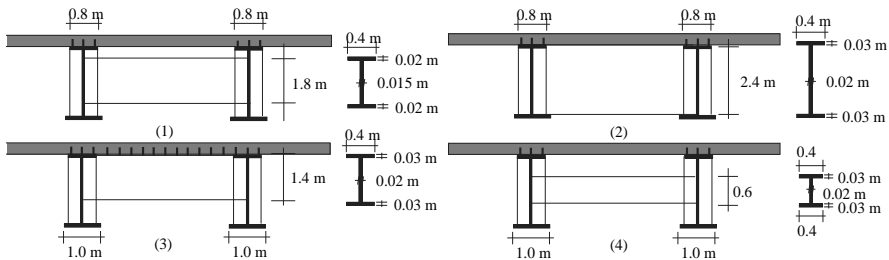


Figure 23. Considered cross-beams for the applications: end cross beams (1), (2) and (3) and middle-span cross beams (4).

In order to study the role of end cross beams on the load paths of seismically induced actions, three different typologies of end cross beams, schematically depicted in Figure 23, have been considered for the case study constituted by the single span twin-girder bridge. In particular, end cross beams not supporting the slab and characterised by an increasing flexural stiffness are considered, as well as a cross beam directly supporting the slab (i.e. connected to the slab through studs). Middle-span cross beams are the same for all cases. According to above observations concerning the analysis methodologies, the problem is investigated through static linear and nonlinear applications.

Figure 24 shows for both the linear and nonlinear applications the distribution of transverse forces in the shear connection for all the cases. As expected, shear forces attain their maximum values at the deck supports and overall reduces with respect to previous cases, due to the contribution of connectors over the top flange of the cross-beam. The distribution of shear forces for end cross beams (1) and (2) present the same trend, with maximum values attained at both deck supports. However, by increasing the flexural stiffness of the end cross beams, differences between shear forces resisted by connectors above the two longitudinal beams diminish; this is due to the limited flexural deformation of the stiff cross beams that mitigates the distortion of the end cross-section of the deck and reduces effects of the recall forces exerted on the longitudinal beam equipped with the sliding bearing. Distributions of transverse forces on the shear connection in the case of cross beams directly supporting the deck (3) deserve some comments. For cross beams directly supporting the deck, shear forces acting on the two longitudinal beams are opposite in sign, meaning that forces acting on the beam with the fixed bearing has the same sign of the applied seismic actions (Figure 24c). The distribution of forces in the shear-connection of the end cross beams is reported in Figure 25a for both the linear and nonlinear applications.

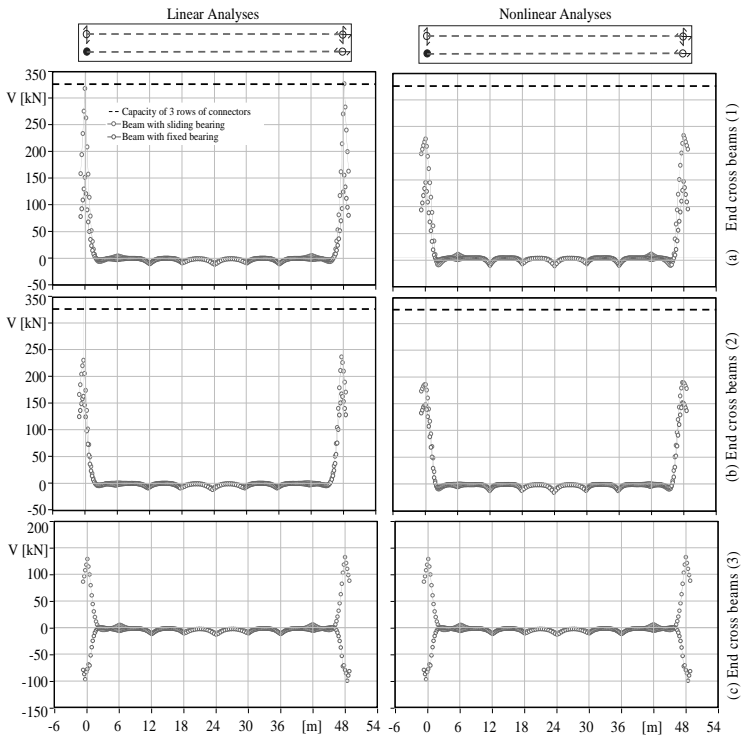


Figure 24. Distributions of transverse shear forces on the shear connection.

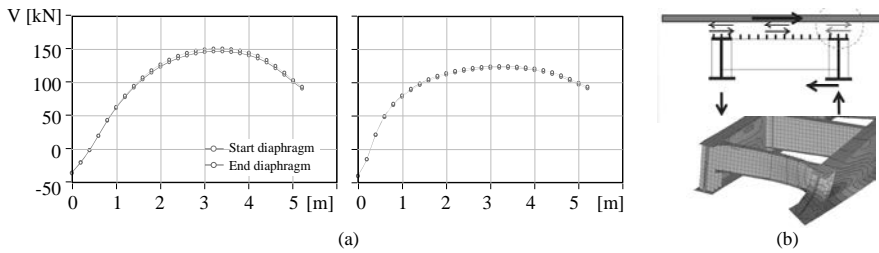


Figure 25. (a) Distribution of transverse forces on the shear connection of the end cross beams (3) and (b) schematic interpretation of the phenomenon.

Trend is due to the flexural deformation of the end cross beam that, being connected with the slab through studs, induces connectors over the top flange of the fixed girder to slip in the opposite direction with respect to the one suggested by the horizontal seismic force (Figure 25b).

Figure 26 shows the longitudinal shear forces on the steel-concrete connection along the top plates of the two steel girders due to the transverse seismic action. These are consequences of the overall flexural behaviour of the steel girders, produced by torsion resulting from the eccentricity of inertia forces with respect to the shear centre of the deck cross-section. For the sake of brevity, only results of linear applications are reported (in view of the relatively moderate induced forces). Differently from transverse shear forces, maximum longitudinal

shear forces on the steel-concrete connection are attained at a certain distance from the supports (about 2 m).

Finally, Figure 27 shows the absolute values of the resulting shear forces on the steel-concrete connection of the two steel girders, obtained from the vector sum of longitudinal and transverse shear forces induced by the transverse seismic action. Results from linear analyses are depicted in Figure 27a while those of nonlinear applications are reported in Figure 27b. The combined shear forces are compared with those acting at the ULS, resulting from the application of non-seismic loads (including traffic loads). It can be observed that maximum shear forces due seismic and non-seismic actions are attained at different locations.

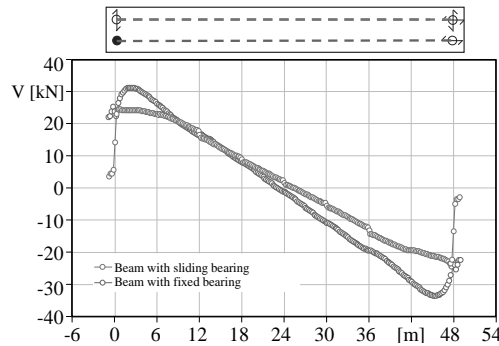


Figure 26. Distribution of longitudinal shear forces on the steel-concrete connection due to the transverse seismic action.

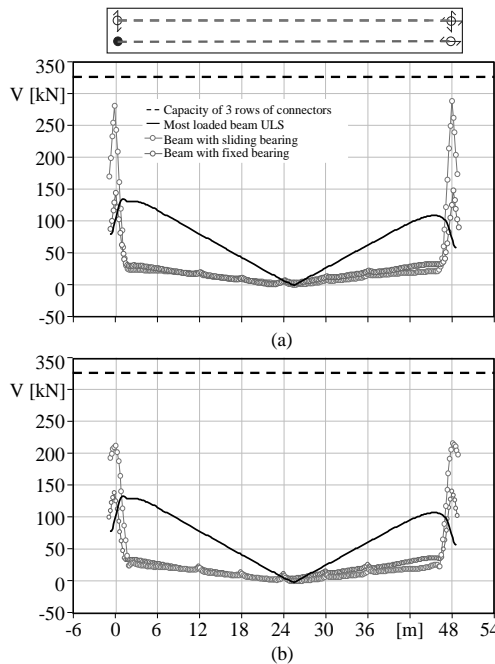


Figure 27. Distribution of total shear forces on the steel-concrete connection due to the transverse seismic action: (a) results of linear analysis and (b) results of nonlinear analysis.

Despite the shear connection capacity is never exceeded, shear forces due to transverse inertia forces are sensibly higher than those relevant to non-seismic actions (almost twice for the linear applications and 40% higher for the nonlinear applications), due to the high intensity of the seismic loads.

4.1.2 Two-span deck

Considerations relevant to the single span bridge hold for the three supports model of the twin-girder bridge. In this case, shear forces on the central support due to transverse seismic action are higher than those on the end supports, because of the increment of the deck masses, as can be observed from Figure 28. First applications are performed considering an infinite stiffness for the central pier.

Like for the simply supported deck, torsion resulting from the eccentricity of transverse inertia forces with respect to the shear centre of the deck cross section promotes the development of global bending moments and shear forces on the longitudinal beams and consequently on the shear connection. Figure 29 shows the absolute values of the total shear forces on the steel-concrete connection of the two steel girders, obtained from the vector sum of longitudinal and transverse shear forces induced by the transverse seismic action. Results from linear analyses are depicted in Figure 29a while those of nonlinear applications are reported in Figure 29b. The combined shear forces are compared with those acting at the ULS, resulting from the application of non-seismic loading (including traffic loads). Even in this case, maximum shear forces due seismic and non-seismic actions are attained at different locations.

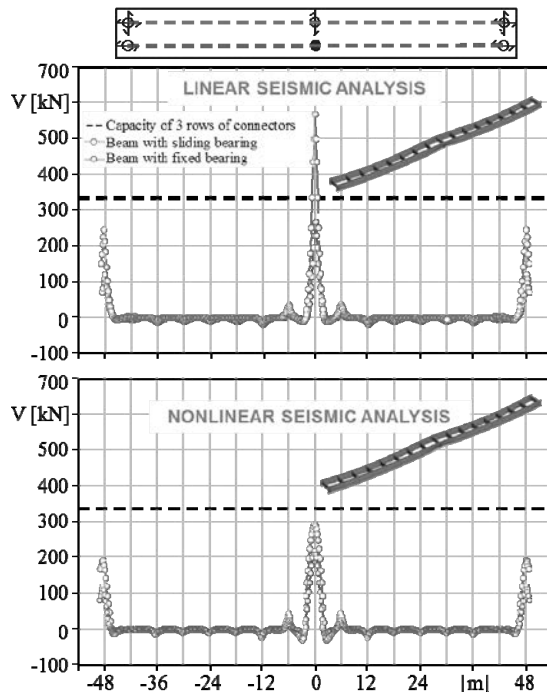


Figure 28. Transverse shear on studs induced by transverse seismic action from linear and non linear analyses.

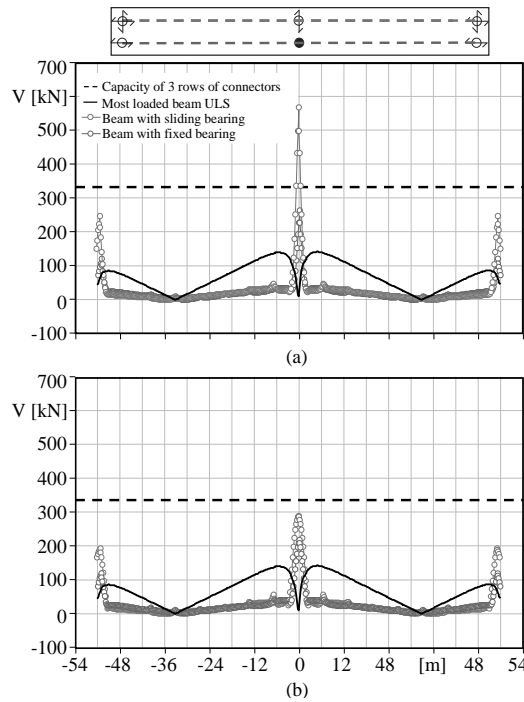


Figure 29. Distribution of total shear forces on the steel-concrete connection due to the transverse seismic action: (a) results of linear analysis and (b) results of nonlinear analysis.

It should be remarked that shear forces induced by non-seismic loads are almost the same for the single span and two-span bridges while effects of seismic actions are sensibly higher in the latter case, since the transfer mechanism of forces at the middle support requires the equilibrium of horizontal inertia forces relevant to two spans.

With reference to continuous decks, the stiffness of piers may significantly affect the behaviour of the structure and the local transferring mechanisms developing in the deck. In fact, as the pier stiffness reduces, the distribution of stress resultants in deck changes with consequences on the local transferring mechanisms (and on forces in the shear connection). The effects of the central pier stiffness on the local transferring mechanisms of the deck have been evaluated through linear static analyses. First applications are performed by only considering the translational stiffness of the pier (modelled through an extensional spring of stiffness k_t), disregarding the contribution of the bent rotation; then, a more realistic model, incorporating the pier has been considered in order to capture the coupled roto-translational behaviour of the central support.

Figure 30 reports transverse the overall shear forces on the shear connection of the two longitudinal girders for different horizontal stiffnesses of the middle spring. As expected, shear forces migrate from the central support to substructures by reducing the spring stiffness. In order to deepen this aspect, the real stiffness of the central support has been simulated by modelling the pier and adopting linear static analyses to investigate effects of different stiffnesses. Piers have a circular cross section with diameter $D = 2$ m and the pier cap is modelled with a beam with a rectangular cross section. Three different models have been considered characterised by different H/D ratio, where H is the height of the pier (Table 4).

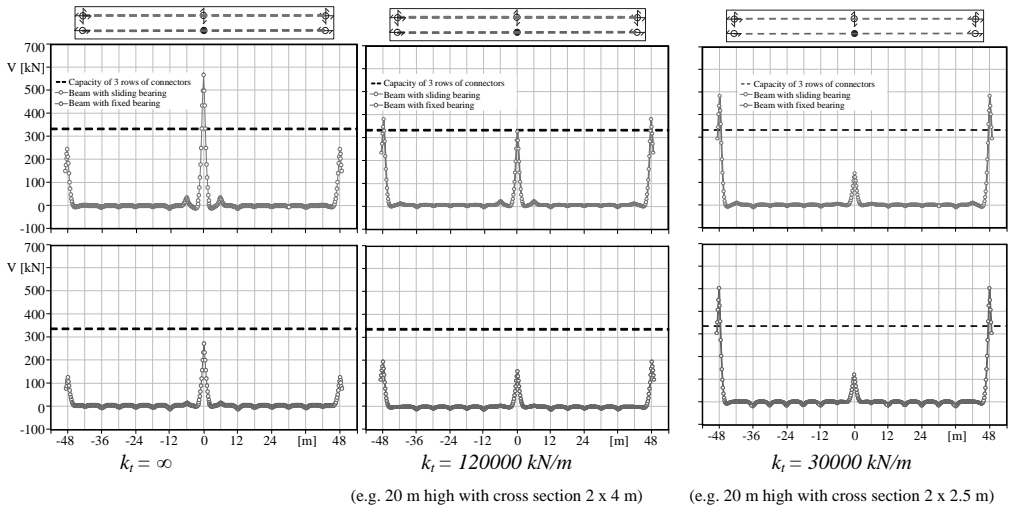


Figure 30. Resultant shear stress on the connection system from transverse seismic action for different support stiffness.

Table 4. *H/D* ratio values adopted for the modelling of the pile.

H/D	D [m]	H [m]
3	2,00	6,00
5		10,00
9		18,00

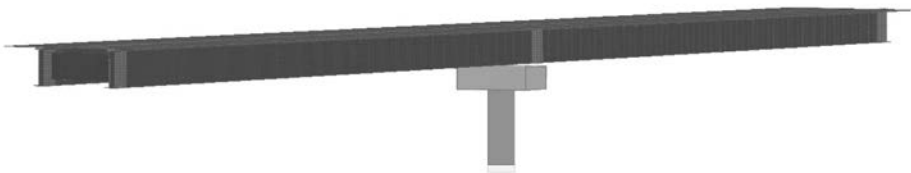


Figure 31. Two-span bridge model integrated with the 3D central pile structure.

Piers are modelled with beam elements; the pier bent is assumed to be rigid by artificially increasing the elastic modulus of the material. The mass of the pier bent is located in its centroid. The piers can undergo plastic deformations at the base through the development of a plastic hinge; this is modelled as a zero-link nonlinear link element, exploiting the software potentials. The moment-rotation relationship of the link accounts for the elastic deformation of the plastic hinge length that is modelled through a rigid element. Piers are assumed to behave elastically. Figure 32 shows resultants of shear forces in the three rows of studs over the top flanges of both longitudinal girders for the different *H/D* ratios considered in the applications.

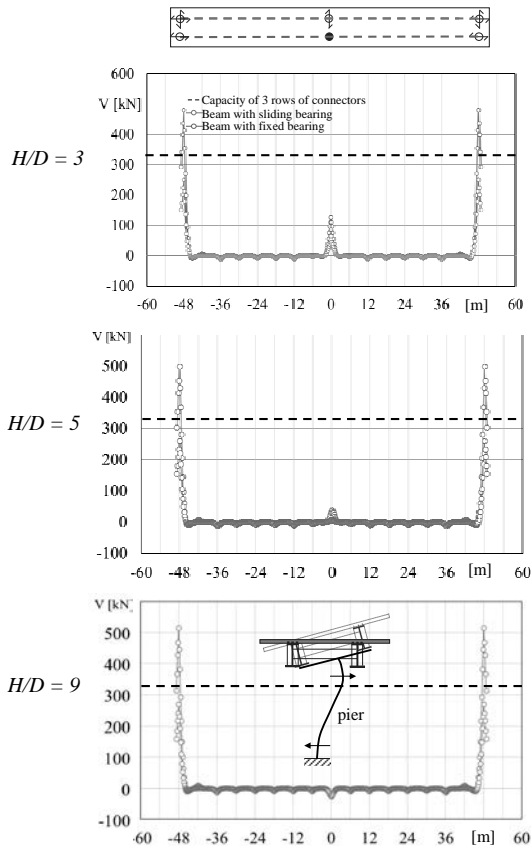


Figure 32. Transverse shear forces on the shear connection for different H/D .

According to the eccentricity of the deck shear centre with respect to the resultant of inertia forces (located at the concrete slab level) the deck cross sections at the middle support undergo overall rotations that are opposite with respect to those of the pier head induced by the horizontal seismic action. Consequently, the pier head rotation is partially restrained, depending on the ratio between the flexural stiffness of the deck and the pier. By increasing the pier slenderness, the deck rotation leads to modify the distribution of bending moments along the pier that is responsible for the change in sign of shear forces on the shear connection for $H/D = 9$.

4.2 Box-girder steel-concrete composite bridge decks

4.2.1 Single span deck

The analysis of the seismic response of box-girder decks subjected to earthquakes is performed, as for the twin-girder cross section typology, considering seismic actions acting separately in the longitudinal and transverse direction. Figure 33 shows the deck deformation under transverse seismic action: the torque determines clockwise rotation of the mid-span and the end cross section distortion.

Figure 34 shows the transverse shear forces due to transverse seismic actions obtained from linear and non-linear static analyses. As expected, shear forces from nonlinear analyses are lower with respect to those obtained from linear applications, as a consequence of the connection plasticization.

Furthermore, shear forces on the shear connection of the girder with sliding bearing (red curve) are bigger than the ones on the shear connection of the girder with the fixed support (blue curve), because of the recall forces exerted by the end cross beams. With respect to the twin-girder bridge, the shear connection of the box-girder bridge suffers lower shear forces, this is due to the contribution of the shear resisted by studs over the diaphragm's plate that is connected to the concrete slab.

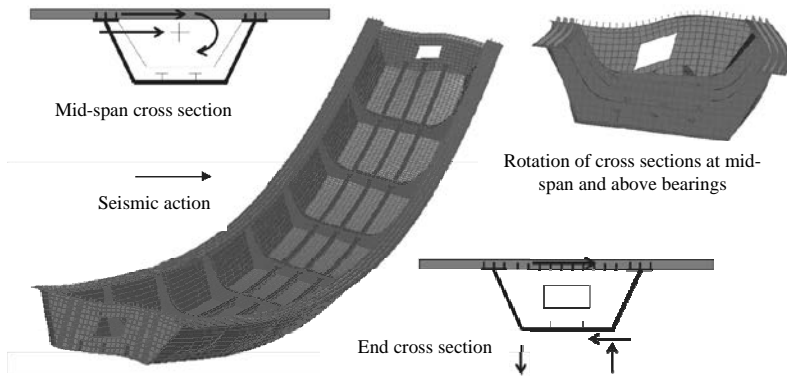


Figure 33. Deformed shape of the simply supported box-girder deck subjected to transverse seismic action; local transfer mechanism at supports inducing the cross-sections distortion.

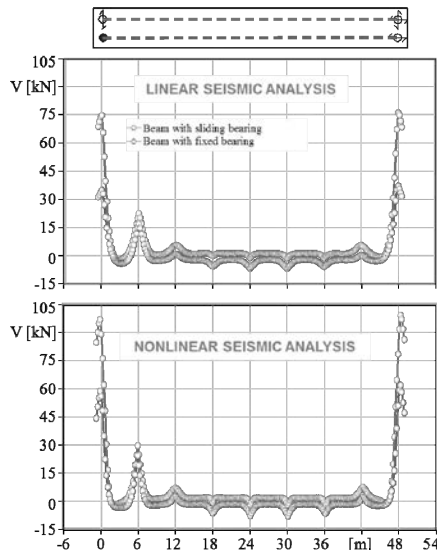


Figure 34. Resultant values of shear stress for transverse seismic action.

Figure 35 show the linear and non-linear behaviour of the shear connection over the support diaphragm; intensity of shear forces is comparable to that of longitudinal studs. Plasticization allows the redistribution of the stress so that the non-linear curve is more flat.

Results from the dynamic analysis reveal a good correspondence with the results of simplified methods. Linear dynamic and time history analyses determine higher values of shear forces with respect to static applications, on the shear connection in correspondence of the transverse diaphragms. Maximum shear forces are almost half the ones at supports (Figure 36). This increment is probably due to the contribution of higher vibration modes, which are neglected in the static analyses.

Transverse shear actions also induces longitudinal shear due to torque. Torsional effects are more evident near the supports, but it is worth to notice that maximum transverse shear values are not reached in the same location of the longitudinal ones (Figure 37).

Figure 38 shows the combination of the seismic and non-seismic longitudinal shear forces on the shear connection over the two box webs.

With reference to longitudinal seismic actions, Figure 39 shows longitudinal shear forces due to longitudinal seismic action, compared with forces induced by vertical loads. The intensity of the longitudinal shear forces induced by the seismic action has a minor relevance with respect to the transverse shear forces produced by the transverse seismic action.

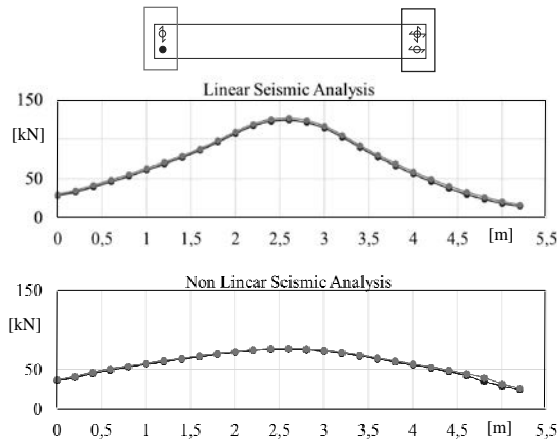


Figure 35. Transverse shear on the end cross beam diaphragm connection.

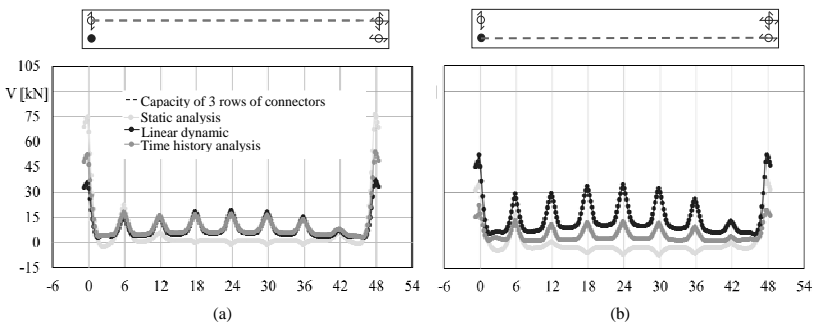


Figure 36. Comparison of distributions of transverse shear forces obtained from different analysis methods: (a) results for the beam with sliding bearing and (b) with the fixed bearing.

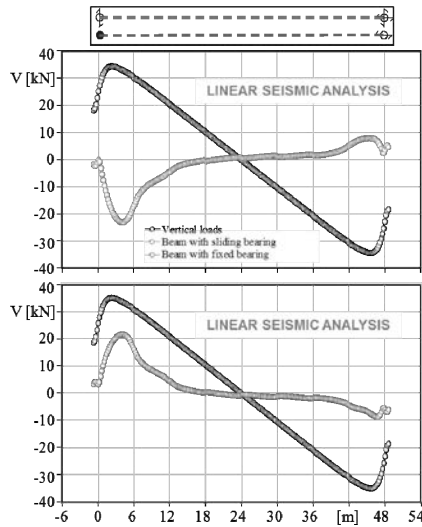


Figure 37. Longitudinal shear from transverse seismic action compared to the vertical loads stress.

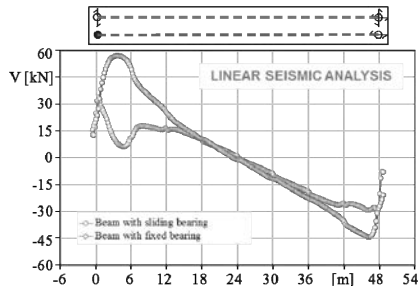


Figure 38. Resultant of longitudinal shear from transverse seismic action and vertical loads.

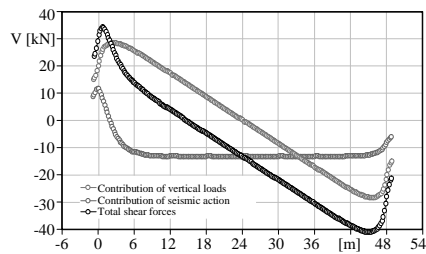


Figure 39. Longitudinal shear stress above the connection system.

4.2.2 Two span deck

Consideration relevant to the single span bridge also apply for the three support case. Shear forces on the middle support are higher than those on the end supports because of the increment of the deck masses.

With reference to seismic actions acting in the transverse direction of the bridge, Figure 40 shows the shear forces on studs on the two box webs.

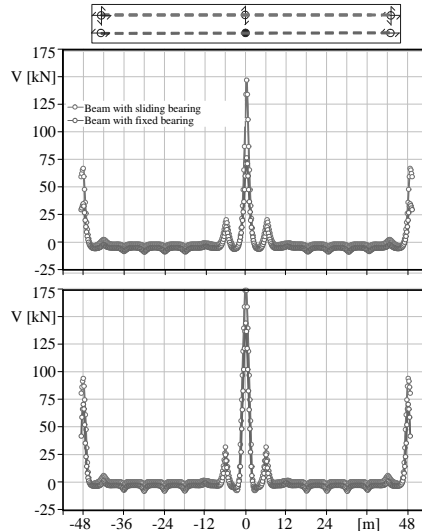


Figure 40. Transverse shear from transverse inertial forces acting on the shear connection.

Differently to the twin-girder typology, intensity of forces in correspondence of the middle support does not exceed the studs' capacity, due to the contribution of studs over the transverse diaphragm.

5 CONCLUSIONS

Local problems involved in the transfer mechanisms of inertia forces acting at the level of the concrete slab of typical steel-concrete composite bridge decks have been investigated in this work. In particular, the shear connection behaviour, usually designed with only reference to non-seismic loads at the ultimate limit state, is studied through applications to some case studies constituted by twin-girder and box-girder steel-concrete composite bridge decks characterised by different static schemes. Different analysis approaches are adopted, including linear and nonlinear static and dynamic analysis. The analysis of the distribution of longitudinal and transverse shear forces acting on studs demonstrates that the behaviour of the steel-concrete connection in proximity of cross frames at the seismic resistant restraints is not as easy to understand as expected, as it depends on the stiffness of the transverse cross frame and the flexural stiffness of the pier (for mid-span supports). Overall, transverse actions are concentrated at a limited number of studs and, for high intensity earthquakes, may exceed the connectors capacity.

With reference to the twin-girder cross section typology, the end cross beam plays an important role in distributing the seismic inertia forces on the shear connection of the two steel girders.

As a consequence of the un-symmetric boundary conditions, the end cross beams undergo a flexural deformation that is responsible for recall forces on the steel girder with sliding bearing. These forces limit the beam rotation and produce an increment of shear forces acting

at the level of the shear connection of the beam with sliding bearing. By increasing the flexural stiffness of the end cross beams, differences between shear forces resisted by connectors above the two longitudinal beams diminish, as effects induced by the flexural deformation of end cross beams reduce. For end-cross beams directly supporting the deck (i.e. connected to the slab through shear studs), the flexural behaviour of the end cross beams determines a local distortion of the beam with the fixed bearing that is responsible of forces in the shear connection having the same direction of the external seismic action.

Classical design methods and modelling strategies result inadequate to evaluate local problems relevant to the seismic behaviour of steel-concrete composite bridge decks. Applications demonstrate the need of sophisticated three dimensional finite element model. ON the contrary, simple static linear and nonlinear application revealed adequate to capture the actual distribution of shear forces on the shear connection resulting from more rigorous dynamic analysis, based on the direct integration of the equation of motion.

6 REFERENCES

- Astaneh-Asl, A., Bolt, B., McMullin, K. M., Donikian, R. R., Modjtahedi, D., and Cho, S. W. (1994). Seismic performance of steel bridges during the 1994 Northridge earthquake. Report No. UCB/CE-Steel-94/01, Dept. of Civil Engineering, Univ. of California, Berkeley.
- Bruneau, M., Wilson, J. W., and Tremblay, R. (1996). Performance of steel bridges during the 1995 Hyogo-ken Nanbu (Kobe, Japan) earthquake. *Canad. J. Civ. Engng.*, 23(3): 678-713.
- Calvi, G. M. (2004). Recent experience and innovative approaches in design and assessment of bridges. Proc., 13th World Conference on Earthquake Engineering, Vancouver, Canada, August 1–6, 2004, Paper No. 5009.
- Carbonari S., Gara F., Dall'Asta A., Dezi L. (2016) Shear connection local problems in the seismic design of steel-concrete composite decks – Lecture Notes in Civil Engineering (LNCE, volume 10) Proceedings of the Italian Concrete Days 2016. Springer. Editors: Marco Di Prisco, Marco Menegotto; pp. 341-354.
- Carbonari S., Minnucci L., Gara F., Dall'Asta A., Dezi L. (2017) The Role of End Cross-beams on the Distribution of Seismic Induced Shear Actions on the Shear Connection in Steel-Concrete Composite Bridge Decks - XXVI Giornate Italiane della Costruzione in Acciaio, 28-30 Settembre, 2017, Venezia, Italia.
- Collings, D. (2005). Steel-concrete composite bridges, Lon-don, Thomas Telford.
- Dall'Asta, A. 2001. Composite beams with weak shear connection. *International Journal of Solids and Structures*, 38(32-33): 5605-5624.
- Dicleli, M., Bruneau, M. (1995). Seismic performance of multispan simply supported slab-on-girder steel highway bridges. *Engineering Structures*, 17(1): 4-14.
- Earthquake Engineering Research Institute. (1990). Lorna Prieta earthquake reconnaissance report. Spectra. supplement to vol. 6, Oakland, Calif.
- Earthquake Engineering Research Institute. (1994). Northridge Earthquake Jan. 17, 1994, preliminary reconnaissance report. Oakland, Calif.
- EN1994. Design of composite steel and concrete structures. Part 1.1: General rules and rules for buildings, Brussels, Belgium.
- EN1998-2 - Design of structures for earthquake resistance Part 2: Bridges, Brussels, Belgium.
- Gara, F., Carbonari, S., Leoni, G., Dezi, L. 2014. A higher order steel-concrete composite beam model. *Engineering Structures*, 80: 260-273.
- Itani, A. M., Bruneau, M., Carden, L. P., and Buckle, I. G. (2004). Seismic behaviour of steel girder bridge superstructures. *J. Bridge Eng.*, 9(3): 243-249.

- Jara, J.M., Reynoso, J.R., Olmos, B.A. and Jara, M. (2015). Expected seismic performance of irregular medium-span simply supported bridges on soft and hard soils. *Engineering Structures*, 98(1): 174-185.
- Kawashima, K. (2010). Seismic damage in the past earthquakes, seismic design of urban infrastructure. Lecture note.
- Nielson, B.G., DesRoches, R. (2006). Influence of modeling assumptions on the seismic response of multi-span simply supported steel girder bridges in moderate seismic zones. *Engineering Structures*, 28(8): 1083-1092.
- Ollgaard, J., Slutter, R., Fisher, J. (1971). Shear strength of stud connectors in lightweight and normal-weight concrete. *AISC Engineering Journal*, 8:55-64.
- Padgett, J. E., and DesRoches, R. (2007). Sensitivity of seismic response and fragility to parameter uncertainty. *J. Struct. Eng.*, 133(12): 1710–1718.
- Priestley, M.J.N., Seible, F and Calvi, G.M. (1996). *Seismic design and retrofit of bridges*. John Wiley & Sons, Inc. USA.
- Ranzi, G., Zona, A. 2007. A steel-concrete composite beam model with partial interaction including the shear deformability of the steel component. *Engineering Structures*, 29(11): 3026-3041.
- Straus7 Software. Finite element analysis system. G+D Computing, Padova.
- Tubaldi, E., Barbato, M., Dall'Asta, A. (2010). Transverse seismic response of continuous steel-concrete composite bridges exhibiting dual load path. *Earthquakes Struct.*, 1(1): 21–41.
- Tubaldi E., Barbato M, Dall'Asta A. (2012). Influence of model parameter uncertainty on transverse response and vulnerability of steel-concrete composite bridges with dual load path. *ASCE Journal of Structural Engineering*, Vol.138(3), 363-374, DOI:10.1061/(ASCE)ST.1943-541X.0000456 (ISSN:0733-9445, e-ISSN:1943-541X).
- Tubaldi E., Dall'Asta A. (2011). A design method for seismically isolated bridges with abutment restraint. *Engineering Structures*, Vol.33(3), 786-795 (ISSN: 0141-0296).
- Tubaldi E., Dall'Asta A. (2012). Transverse free vibrations of continuous bridges with abutment restraint. *Earthquake Engineering and Structural Dynamics*, DOI:10.1002/eqe1190, Vol.41(9), 1319-1340 (ISSN: 0098-8847, eISSN: 1096-9845).
- Tubaldi E., Dall'Asta A., Dezi L. (2013). Reduced formulation for post-elastic seismic response of dual-load path bridges *Engineering Structures*, Vol.51, 178-187, DOI:10.1016/j.engstruct.2011.12.026, (ISSN: 0141-0296).
- Tubaldi E., Tassotti L., Dall'Asta A., Dezi L. (2014). Seismic response analysis of slender bridge piers. *Earthquake Engineering and Structural Dynamics*, Vol.43 (10), 1503-1519. (ISSN: 0098-8847, eISSN: 1096-9845).
- Zahrai, S.M. and Bruneau, M. (1998). Impact of diaphragms on seismic response of straight slab-on-girder steel bridges. *Journal of Structural Engineering*, 124(8): 938-947.
- Zahrai, S.M. and Bruneau, M. (1999) a. Ductile end-diaphragms for seismic retrofit of slab-on-girder steel bridges. *Journal of Structural Engineering*, 125(1): 71-80.
- Zahrai, S.M. and Bruneau, M. (1999) b. Cyclic testing of ductile end diaphragms for slab-on-girder steel bridges. *Journal of Structural Engineering*, 125(9): 987-996.
- Zona A, Leoni G, Dall'Asta A. (2017) Influence of the shear connection distribution on the behaviour of continuous steel-concrete beams. *The Open Civil Engineering Journal*, 17(11), 384-395.
- Zona, A., Ranzi, G. (2014). Shear connection slip demand in composite steel-concrete beams with solid slabs. *Journal of Constructional Steel Research*, 102: 266-281.

Finito di stampare nel mese di luglio 2018 per conto di Doppiavoce
presso Officine Grafiche Francesco Giannini & Figli S.p.A. – Napoli